

**The substrate specificity of N-end rule components from
*Arabidopsis thaliana***

Dissertation

zur Erlangung des
Doktorgrades der Naturwissenschaften (Dr. rer. nat.)

der

Naturwissenschaftlichen Fakultät I – Biowissenschaften –

der Martin-Luther-Universität
Halle-Wittenberg,

vorgelegt

von Frau Maria Katharina Klecker

geb. am 03.10.1986 in Marburg

Gutachter

Prof. Dr. Ingo Heilmann, Martin-Luther-Universität Halle-Wittenberg

Prof. Dr. Nico Dissmeyer, Universität Osnabrück

Prof. Dr. Frederica Theodoulou, Rothamsted Research, Harpenden

Verteidigung

18. Dezember 2019

Table of contents

Table of contents.....	I
Abbreviations	V
Summary	IX
Zusammenfassung.....	X
1. Introduction.....	1
1.1 Protein degradation in plants.....	1
1.1.1 Bulk protein degradation.....	1
1.1.2 Selective protein degradation – the 26S proteasome.....	1
1.1.3 Ubiquitin	2
1.1.4 Plant E3 ligases	4
1.2 The N-end rule pathway of protein degradation	7
1.2.1 Functions of the N-end rule pathway.....	9
1.2.2 Primary destabilizing amino acids and N-recognins.....	10
1.2.3 Secondary destabilizing N-termini	15
1.2.4 Tertiary destabilizing N-termini.....	16
1.3 Male gametogenesis in <i>Arabidopsis</i>	18
1.3.1 Regulation of pollen development.....	21
1.4 The phytohormone ethylene.....	26
1.4.1 Impact of ethylene on plant physiology	26
1.4.2 Ethylene signaling.....	28
1.5 The phytohormone cytokinin	32
1.5.1 Cytokinin during etiolation.....	33
2. Aims and scope of the thesis.....	35
3. Results	37
3.1 The genetic background in <i>prt1-1^{ts}</i> confers thermosensitivity of pollen development.....	37
3.1.1 The <i>prt1-1^{ts}</i> line is sterile at an elevated temperature	37
3.1.2 The thermosensitivity of <i>prt1-1^{ts}</i> is independent of the <i>PRT1</i> locus.....	38
3.1.3 The heat-induced sterility of <i>prt1-1^{ts}</i> is caused by a defect in male gametogenesis	40
3.1.4 Microspore to pollen transition at 28°C is affected in <i>prt1-1^{ts}</i>	43
3.1.5 Conditional male sterility of <i>prt1-1^{ts}</i> is likely a sporophytic trait	46
3.1.6 Several genes are differentially expressed in anthers of <i>prt1-1^{ts}</i>	47
3.2 PRT1 promoter activity.....	50
3.3 Biochemical characterization of the PRT1 protein.....	53

3.3.1	PRT1 acts as an E3 ubiquitin ligase <i>in vitro</i>	54
3.3.2	Both RING domains of PRT1 are required for autoubiquitination	56
3.3.3	The <i>in-vitro</i> substrate specificity of PRT1	59
3.3.4	PRT1 RING domains are not involved in substrate binding <i>in vitro</i>	62
3.3.5	<i>In-vitro</i> PRT1 binding to <i>Arabidopsis</i> peptide sequences.....	64
3.4	EIN2 is a potential <i>in-vivo</i> substrate for PRT1	66
3.4.1	EIN2 ^{C-term} is destabilized in a PRT1-dependent manner <i>in vivo</i>	67
3.4.2	Apparent molecular weight of EIN2 ^{C-term}	73
3.4.3	Physical interaction between EIN2 and PRT1 <i>in vivo</i>	73
3.4.4	Hypocotyl elongation in the dark is slightly increased in <i>prt1-1^{ts}</i>	76
3.4.5	Cytokinin-induced inhibition of hypocotyl elongation in the dark is impaired in <i>prt1-1^{ts}</i> and N119	78
3.4.6	Expression of EIN2 ^{C-term} confers signs of constitutive ethylene response in combination with the <i>prt1-1^{ts}</i> genotype	84
3.5	The substrate specificities of PRT6 and ATE1.....	86
3.5.1	The <i>in-vitro</i> substrate specificity of the UBR domain of PRT6	86
3.5.2	ATE1 arginylates acidic N-termini <i>in vitro</i>	90
4.	Discussion.....	93
4.1	A new temperature-dependent sterility phenotype.....	93
4.1.1	Potential origin of the sterility phenotype in <i>prt1-1^{ts}</i>	93
4.1.2	The thermosensitivity of <i>prt1-1^{ts}</i> reproduction.....	96
4.2	PRT1 acts as an E3 ligase <i>in-vitro</i> using both RING domains.....	103
4.3	The <i>in-vitro</i> substrate specificity of plant N-recognins	106
4.3.1	Determinants of N-degron recognition by PRT1	106
4.3.2	BB is an <i>in-vivo</i> substrate of PRT1	110
4.3.3	<i>In-vitro</i> substrate interactions of PRT6.....	112
4.3.4	<i>In-vitro</i> arginylation activity of ATE1	114
4.4	A potential role for PRT1 in EIN2 signaling.....	116
4.4.1	Physical interaction of EIN2 and PRT1.....	116
4.4.2	EIN2 ^{C-term} has low <i>in-vivo</i> protein stability	117
4.4.3	<i>In-vivo</i> stability of EIN2 ^{C-term} depends on PRT1 activity	118
4.4.4	EIN2 ^{C-term} degradation <i>in planta</i>	121
4.5	The genetic background of <i>prt1-1</i> lines confers cytokinin hyposensitivity in the dark	123
4.5.1	Sugar-dependence of cytokinin hyposensitivity in <i>prt1-1^{ts}/N119</i>	124
5.	Conclusions.....	128

6.	Materials and Methods	130
6.1	Plant growth conditions	130
6.2	Plant material	130
6.3	Hormone treatments.....	131
6.3.1	Triple response assays.....	131
6.3.2	Auxin treatments of inflorescences.....	132
6.4	Histological analyses.....	132
6.4.1	PEG embedment of flowers	132
6.4.2	Poly-L-Lys coating of sample slides	133
6.4.3	Safranin O/astra blue stainings of microsections.....	133
6.4.4	Preparations of microspore and pollen fractions.....	133
6.4.5	Pollen tube growth assays.....	133
6.4.6	GUS histological staining	134
6.5	Microscopy	134
6.6	Plasmid construction	135
6.6.1	Destination vectors.....	135
6.6.2	PRT1 expression vectors.....	136
6.6.3	EIN2 expression vectors	137
6.6.4	Further expression vectors.....	138
6.7	PCR.....	139
6.7.1	Standard PfuX7 polymerase PCR.....	139
6.7.2	Fusion PCR using PfuX7 polymerase	140
6.7.3	Standard Taq polymerase PCR	140
6.7.4	Plant genotyping.....	140
6.7.5	Site-directed mutagenesis.....	140
6.8	Reverse transcription and real-time PCR	141
6.8.1	Tissue collection	141
6.8.2	RNA extraction and reverse transcripion.....	141
6.8.3	Semi-quantitative RT-PCR.....	142
6.8.4	Quantitative PCR	142
6.9	Bacteria work and transformation protocols.....	143
6.9.1	Growth conditions.....	143
6.9.2	Preparation of competent <i>E. coli</i> cells.....	143
6.9.3	<i>E. coli</i> transformation	144
6.9.4	Preparation of electrocompetent <i>A. tumefaciens</i> cells.....	144

6.9.5	Transformation of <i>A. tumefaciens</i>	144
6.9.6	Plant transformation by floral dipping	145
6.10	Protein work	145
6.10.1	Plant protein extraction for Western blot.....	145
6.10.2	SDS-PAGE and Western blot.....	146
6.10.3	Immunodetection.....	146
6.10.4	Total protein stains.....	146
6.10.5	Expression and purification of recombinant proteins from <i>E. coli</i>	147
6.11	<i>In-vitro</i> autoubiquitination assays.....	148
6.12	X-peptide pull-down experiments.....	149
6.13	<i>In-vitro</i> arginylation assays.....	149
6.14	SPOT peptide arrays	150
6.14.1	SPOT peptide array synthesis	150
6.14.2	Side-chain deprotection	151
6.14.3	SPOT binding assays	152
6.14.4	Binding conditions for SPOT assays using His ⁶ MBP-PRT1	153
6.14.5	Binding conditions for SPOT assays using the PRT6 UBR box	153
6.14.6	SPOT membrane stripping.....	153
6.15	Protoplast work	153
6.15.1	Protoplast preparation	153
6.15.2	Maxi plasmid purification.....	154
6.15.3	Protoplast transfection.....	154
6.15.4	Cycloheximide and proteasome inhibitor treatments	155
6.15.5	Protein stability assays in protoplasts.....	155
6.15.6	Co-immunoprecipitation in protoplasts	155
6.16	Websites and software.....	156
7.	References.....	158
8.	Acknowledgments	211
9.	Appendix.....	212
9.1	Supplemental Figures and Tables.....	212
9.2	List of publications.....	234
9.2.1	Publications with contributions from this work.....	234
9.2.2	Further publications	234
9.3	Persönliche Daten	235
9.4	Erklärung	237

Abbreviations

ABA	Abscisic acid
ACC	1-Aminocyclopropane-1-carboxylic acid
APC/C	Anaphase-promoting complex/cyclosome
ATE	Arginyl-tRNA protein transferase
ATP	Adenosine triphosphate
ATPase	Adenosine triphosphatase
BA	N ⁶ -benzylaminopurine
BiFC	Bimolecular fluorescence complementation assay
BIR	BACULOVIRUS INHIBITOR OF APOPTOSIS PROTEIN REPEAT
BRCA1	BREAST CANCER 1
BTB	TRAMTRACK AND BROAD COMPLEX
C	Carboxy-
cDNA	complementary DNA
CDS	Coding sequence
CHX	Cycloheximide
Clp	Caseinolytic protease
COFRADIC	Combined fractional diagonal chromatography
Co-IP	Co-immunoprecipitation
Col-0	<i>Columbia-0</i>
CP	Core particle
DAPI	4',6-Diamidino-2-phenylindole
DDB	UV-DAMAGED DNA-BINDING
DHFR	Dihydrofolate reductase
DIAP1	INHIBITOR OF APOPTOSIS 1
DIC	N,N'-Diisopropylcarbodiimide
DMF	Dimethylformamide
DMSO	Dimethyl sulfoxide
DTT	Dithiothreitol
DUB	Deubiquitinating enzymes
E1	Ub activating enzyme
E2	Ub conjugating enzyme
E3	Ub ligase
e^K	Extension containing lysines (a peptide linker sequence derived from lacI)
ER	Endoplasmic reticulum
eto	Ethylene overproduction
GA	Gibberellic acid
gDNA	Genomic DNA
GFP	GREEN FLUORESCENT PROTEIN
GST	Glutathione S-transferase
GUS	β-Glucuronidase
HA	Hemagglutinin
HECT	HOMOLOGOUS TO E6-ASSOCIATED PROTEIN CARBOXYL TERMINUS
HIF-1α	HYPOXIA INDUCIBLE FACTOR 1α
HOBt	1-Hydroxybenzotriazole hydrate
Hyg	Hygromycin B
IAA	Indole-3-acetic acid

IPTG	Isopropyl β -D-1-thiogalactopyranoside
JA	Jasmonic acid
LB	Luria-Bertani (medium)
LEW	Lysis-Equilibration-Wash
MBP	MALTOSE BINDING PROTEIN
MES	2-(N-Morpholino)-ethane sulfonic acid
MetAP	Methionine aminopeptidase
MEX	MEKK1-related protein X
MHZ3	<i>MAO HUI3</i>
MS	Murashige & Skoog
N	Amino-
NAA	1-Naphthaleneacetic acid
NASC	Nottingham Arabidopsis Stock Centre
NAT	N-terminal acetyl transferases
Nedd8	Neural precursor cell expressed developmentally down-regulated 8
NMP	<i>N</i> -Methyl-2-pyrrolidone
NO	Nitric oxide
NRAMP	NATURAL RESISTANCE-ASSOCIATED MACROPHAGE PROTEIN
nsP4	RNA polymerase from Sindbis virus
OD	Optical density
ORF	Open reading frame
p62	Autophagy receptor required for selective macroautophagy in mouse
PAT	Phosphinothricin N-acetyltransferase
PBS	Phosphate buffered saline
PCNA	PROLIFERATING CELL NUCLEAR ANTIGEN
PCR	Polymerase chain reaction
PEB	Pollen extraction buffer
PEG	Polyethylene glycol
PHD	PLANT HOMEODOMAIN
PMSF	Phenylmethanesulfonyl fluoride
PVDF	Polyvinylidene fluoride
qPCR	Quantitative PCR
Rad18	RADIATION SENSITIVE 18
RBR	RING BETWEEN RING
RGS	REGULATOR OF G PROTEIN SIGNALING
RING	REALLY INTERESTING NEW GENE
RLK	Receptor-like protein kinase
RP	Regulatory particle
RPN	RP non-ATPase
RR	Response regulator
RT	Reverse transcription
RUB	RELATED TO UBIQUITIN
SCF	S-PHASE KINASE ASSOCIATED PROTEIN 1 (Skp1)-Cullin-F-box
SDS-PAGE	sodium dodecyl sulfate polyacrylamide gel electrophoresis
SPOT	Synthetic Peptides On membrane support Technique
SUMO	SMALL-UBIQUITIN-RELATED MODIFIER
TAILS	Terminal amine isotopic labelling of substrates
TBST	Tris-buffered saline containing Tween-20
TOE	target of ETO1

Ub	Ubiquitin
UBR	UBIQUITIN LIGASE N-RECOGNIN
UBR	UB LIGASE N-RECOGNIN
UFT	Ub Fusion Technique
UPR	Unfolded protein response
UPS	Ub proteasome system
Usp1	UBIQUITIN SPECIFIC PEPTIDASE 1
WT	Wildtype
YFP	YELLOW FLUORESCENT PROTEIN
Zn	Zinc
β-gal	β-Galactosidase

List of *Arabidopsis* genes that appear at least three times in the text or were experimentally addressed. AGI: *Arabidopsis* genome identifier.

Gene abbreviation	Name	AGI
ABCG1	<i>ATP-BINDING CASSETTE G1</i>	AT2G39350
ABCG16	<i>ATP-BINDING CASSETTE G16</i>	AT3G55090
ABCG20	<i>ATP-BINDING CASSETTE G20</i>	AT3G53510
ACS5	<i>ACC SYNTHASE 5</i>	AT5G65800
AFB1	<i>AUXIN SIGNALING F-BOX PROTEIN 1</i>	AT4G03190
AFB2	<i>AUXIN SIGNALING F-BOX PROTEIN 2</i>	AT3G26810
AFB3	<i>AUXIN SIGNALING F-BOX PROTEIN 3</i>	AT1G12820
AG	<i>AGAMOUS</i>	AT4G18960
AHK2	<i>ARABIDOPSIS HISTIDINE KINASE 2</i>	AT5G35750
AHK3	<i>ARABIDOPSIS HISTIDINE KINASE 3</i>	AT2G01830
ARF17	<i>AUXIN RESPONSE FACTOR 17</i>	AT1G77850
ARR4	<i>ARABIDOPSIS RESPONSE REGULATOR 4</i>	AT1G10470
ARR5	<i>ARABIDOPSIS RESPONSE REGULATOR 5</i>	AT3G48100
ARR6	<i>ARABIDOPSIS RESPONSE REGULATOR 6</i>	AT5G62920
ATE1	<i>ARGININE-TRNA PROTEIN TRANSFERASE 1</i>	AT5G05700
ATE2	<i>ARGININE-TRNA PROTEIN TRANSFERASE 2</i>	AT3G11240
ATL9	<i>ARABIDOPSIS TOXICOS EN LEVADURA 9</i>	AT2G35000
BB	<i>BIG BROTHER</i>	AT3G63530
BIG	<i>n/a</i>	AT3G02260
COI1	<i>CORONATINE INSENSITIVE 1</i>	AT2G39940
COP1	<i>CONSTITUTIVE PHOTOMORPHOGENIC 1</i>	AT2G32950
CRE1/WOL/AHK4	<i>CYTOKININ RESPONSE 1/WOODEN LEG/ ARABIDOPSIS HISTIDINE KINASE 4</i>	AT2G01830
CTR1	<i>CONSTITUTIVE TRIPLE RESPONSE 1</i>	AT5G03730
DA1	<i>"large" in Chinese1</i>	AT1G19270
DA2	<i>"large" in Chinese2</i>	AT1G78420
DAD1	<i>DEFECTIVE ANTHHER DEHISCENCE 1</i>	AT2G44810
EBF1	<i>EIN3-BINDING F BOX 1</i>	AT2G25490
EBF2	<i>EIN3-BINDING F BOX 2</i>	AT5G25350
EIL1	<i>EIN3-LIKE 1</i>	AT2G27050
EIN2	<i>ETHYLENE INSENSITIVE 2</i>	AT5G03280
EIN3	<i>ETHYLENE INSENSITIVE 3</i>	AT3G20770
EIN4	<i>ETHYLENE INSENSITIVE 4</i>	AT3G04580
ERS1	<i>ETHYLENE RESPONSE SENSOR 1</i>	AT2G40940

ETO1	<i>ETHYLENE-OVERPRODUCER 1</i>	AT3G51770
ETP1	<i>EIN2 TARGETING PROTEIN 1</i>	AT3G18980
ETP2	<i>EIN2 TARGETING PROTEIN 2</i>	AT3G18910
ETR1	<i>ETHYLENE RESPONSE 1</i>	AT1G66340
ETR2	<i>ETHYLENE RESPONSE 2</i>	AT3G23150
EXS/EMS1	<i>EXTRA SPOROGENOUS CELLS/EXCESS MICROSPOROCTES 1</i>	AT5G07280
FAD3	<i>FATTY ACID DESATURASE 3</i>	AT2G29980
FAD7	<i>FATTY ACID DESATURASE 7</i>	AT3G11170
FAD8	<i>FATTY ACID DESATURASE 8</i>	AT1G17420
GAPB	<i>GLYCERALDEHYDE-3-PHOSPHATE DEHYDROGENASE B SUBUNIT</i>	AT1G42970
HRE2	<i>HYPOXIA RESPONSIVE 2</i>	AT2G47520
HXK1	<i>HEXOKINASE 1</i>	AT4G29130
HYS	<i>HYPOCOTYL 5</i>	AT5G11260
IQD4	<i>IQ-DOMAIN 4</i>	AT2G26410
IRE1a	<i>INOSITOL-REQUIRING ENZYME 1a</i>	AT2G17520
IRE1b	<i>INOSITOL-REQUIRING ENZYME 1b</i>	AT5G24360
LOX3	<i>13-LIPOXYGENASE 3</i>	AT1G17420
MS1	<i>MALE STERILITY 1</i>	AT5G22260
MS2	<i>MALE STERILITY 2</i>	AT3G11980
MYB21	<i>MYB DOMAIN PROTEIN 21</i>	AT3G27810
MYB24	<i>MYB DOMAIN PROTEIN 24</i>	AT5G40350
n/a	<i>hypothetical protein containing AvrRpt2 consensus sequence VPxFGxW</i>	AT5G42070
NZZ/SPL	<i>NOZZLE/SPOROCTELESS</i>	AT4G27330
OPR3	<i>12-OXOPHYTODIENOATE REDUCTASE 3</i>	AT2G06050
PCO1	<i>PLANT CYSTEINE OXIDASE 1</i>	AT5G15120
PCO4	<i>PLANT CYSTEINE OXIDASE 4</i>	AT2G42670
PIF3	<i>PHYTOCHROME INTERACTING FACTOR 3</i>	AT1G09530
PME18	<i>PECTIN METHYLESTERASE 18</i>	AT1G11580
PP2A	<i>PROTEIN PHOSPHATASE 2A</i>	AT1G13320
PRT1	<i>PROTEOLYSIS 1</i>	AT3G24800
PRT6	<i>PROTEOLYSIS 6</i>	AT5G02310
PRT7	<i>PROTEOLYSIS 7</i>	AT4G23860
PUB4	<i>PLANT U-BOX 4</i>	AT2G23140
RAP2.12	<i>RELATED TO AP 2.12</i>	AT1G53910
RAP2.2	<i>RELATED TO AP 2.2</i>	AT3G14230
RBCL	<i>Large subunit of RuBisCO</i>	ATCG00490
RD21A	<i>RESPONSIVE TO DEHYDRATION 21A</i>	AT1G47128
RIN4	<i>RPM1-INTERACTING PROTEIN 4</i>	AT3G25070
SWEET8/RPG1	<i>SUGARS WILL EVENTUALLY BE EXPORTED TRANSPORTER 8/ RUPTURED POLLEN GRAIN 1</i>	AT5G40260
TIR1	<i>TRANSPORT INHIBITOR RESPONSE 1</i>	AT3G62980
TUB2	<i>TUBULIN BETA CHAIN 2</i>	AT5G62690
UBA1	<i>UB ACTIVATING ENZYME 1</i>	AT2G30110
UBC8	<i>UB CONJUGATING ENZYME 8</i>	AT5G41700
VRN2	<i>VERNALIZATION 2</i>	AT4G16845
YUC2	<i>YUCCA 2</i>	AT4G13260
YUC6	<i>YUCCA 4</i>	AT5G25620

Summary

The turnover rate of cellular proteins can be accelerated substantially by the proteolytic exposure of a destabilizing amino acid in ultimate N-terminal position. In eukaryotes, the selection and ubiquitination of such N-degrons is executed by certain E3 ubiquitin ligases, termed N-recognins. So far, two N-recognins have been identified in plants, called PROTEOLYSIS 1 (PRT1) and PRT6. They account for the destabilization of test substrates bearing aromatic and basic N-termini, respectively. During this decade, research has revealed functions of the PRT6-branch of the N-degron pathway (also termed N-end rule pathway) in plant development and stress response. However, substrate selection by components of the plant N-end rule is still barely investigated biochemically, and the role of PRT1 in plant physiology remains enigmatic. This work aimed at the establishment and application of *in-vitro* affinity approaches for the investigation of substrate selection by enzymes of the N-end rule pathway of *Arabidopsis thaliana*. To this end, synthetic peptide-based techniques were implemented for binding studies using recombinant proteins. This enabled the characterization of the substrate specificities exerted by PRT1, the UBR domain of PRT6 (UBR^{PRT6}), as well as one of the key enzymes generating destabilizing N-termini, ARGININE TRANSFERASE 1 (ATE1). In particular, a robust bead-based arginylation assay using synthetic peptides was set up that allowed for the first investigation of plant ATE1 substrate selection. This also revealed ATE1 to be capable of acting directly downstream of PLANT CYSTEINE OXIDASE activity *in vitro*. In order to approach substrate recognition by the two N-recognins, peptide arrays were synthesized and binding assays were established using both PRT1 and UBR^{PRT6}. This confirmed binding of both N-recognins to peptides exhibiting predicted target N-termini, and revealed contributions of the downstream peptide sequence. Unexpectedly, the presence of either Glu or Asp in second position of peptides bearing N-terminal Arg abolished binding of UBR^{PRT6}, questioning the proposed recognition of such ATE1 products by PRT6. Concerning PRT1, *in-vitro* autoubiquitination activity was shown for the first time within this work, proofing the capacity to act as an E3 ligase. Intriguingly, the ability to form poly-ubiquitin chains depended on the integrity of both RING domains of PRT1, whereas either RING domain was dispensable for binding of peptide substrates. Next to providing mechanistic insights, peptide library experiments facilitated the screening of putative endogenous substrate sequences for their eligibility as natural N-end rule targets. In doing so, the proteolytic fragments of both ETHYLENE INSENSITIVE 2 (EIN2), and the cell growth regulator BIG BROTHER, were discovered as potential physiological targets of PRT1. In support of the N-end rule antagonizing ethylene signaling, the C-terminal signaling fragment of EIN2 was found to be unstable in *Arabidopsis* protoplasts in an N-terminus- and PRT1-dependent manner. Phenotypical analyses of plants carrying the null allele *prt1-1* however revealed no substantial alterations of ethylene sensitivity attributable to PRT1 mutation. Instead, two independent traits were discovered that were caused by the genomic background of *prt1-1* plants. The first one, sterility at moderately elevated ambient temperature caused by post-meiotic developmental aberrations of male gametogenesis, might have established spontaneously during propagation of the line. In contrast, the second phenotype, hyposensitivity towards cytokinin during heterotrophic growth, was also present in a *prt1-1* progenitor line. Together, this work provides evidence for the conservation of target recognition by UBR and ATE enzymes between plants and other eukaryotes, but also finds plant-specific interactions for the type II N-recognin PRT1. These findings will help in the future to relate substrate N-termini and recognition pathways in plant cells.

Zusammenfassung

Die Abbaugeschwindigkeit zellulärer Proteine kann erheblich beschleunigt werden durch die proteolytische Freilegung einer destabilisierenden Aminosäure am N-Terminus der Peptidsequenz. In Eukaryoten wird die Erkennung und Ubiquitinierung solcher N-Degrone durch bestimmte E3 Ubiquitinligasen, bezeichnet als N-Rekognine, ausgeführt. Bis heute wurden zwei N-Rekognine in Pflanzen identifiziert, genannt PROTEOLYSIS 1 (PRT1) und PRT6. Sie sind für die Destabilisierung von Testsubstraten mit aromatischen, beziehungsweise basischen N-termini verantwortlich. Innerhalb dieses Jahrzehnts wurden Funktionen des PRT6-Zweiges des N-Degron-Weges (auch genannt *N-end rule*-Weg) für die pflanzliche Entwicklung und Stressantwort aufgeklärt. Jedoch blieb eine biochemische Charakterisierung der Substratelektion durch Komponenten der *N-end rule* bislang weitestgehend aus und die Rolle von PRT1 in der pflanzlichen Physiologie gibt noch immer Rätsel auf. Diese Arbeit hatte zum Ziel, *in-vitro* Affinitäts-Methoden zur Untersuchung der Substraterkennung durch Enzyme der *N-end rule* von *Arabidopsis thaliana* zu etablieren und anzuwenden. Zu diesem Ziel wurden Techniken basierend auf synthetischen Peptiden für Bindestudien anhand rekombinanter Proteine eingesetzt. Dies erlaubte die Charakterisierung der Substratauswahl durch PRT1, durch die UBR-Domäne von PRT6 (UBR^{PRT6}), sowie durch eines der Schlüsselenzyme zur Erzeugung destabilisierender N-Termini, ARGININ TRANSFERASE 1 (ATE1). Im Speziellen wurde ein robuster Assay zur Arginylierung von an Mikrokügelchen immobilisierten synthetischen Peptiden aufgebaut, der eine erste Erforschung der Substratelektion durch pflanzliche ATE1 ermöglichte. Dies offenbarte auch, dass ATE1 in der Lage ist, Produkte der Aktivität pflanzlicher Cystein-Oxidase (PCOs) direkt als Substrate zu nutzen. Um sich der Substraterkennung durch die zwei N-Rekognine anzunähern, wurden Peptid-Arrays synthetisiert und Bindestudien zur Untersuchung von PRT1 und UBR^{PRT6} etabliert. Dies bestätigte die Bindung beider N-Rekognine an Peptide mit den vorhergesagten Ziel-N-Termini und offenbarte außerdem die Bedeutung von Sequenzmerkmalen jenseits der N-terminalen Aminosäure für die Bindung. Unerwartet war dabei, dass die Gegenwart von Glu oder Asp an zweiter Position von Peptiden mit N-terminalem Arg eine Bindung von UBR^{PRT6} verhinderte, was die postulierte Erkennung solcher ATE1-Produkte durch PRT6 in Frage stellt. Bezüglich PRT1 wurde *in-vitro* Autoubiquitinierungsaktivität während dieser Arbeit zum ersten Mal gezeigt, wodurch die Fähigkeit zur Funktion als E3-Ligase bewiesen wurde. Interessanterweise war die Fähigkeit zur Bildung von Polyubiquitin-Ketten dabei abhängig von der Integrität beider RING-Domänen von PRT1, wohingegen jede einzelne RING-Domäne entbehrlich für die Bindung von Substratpeptiden war. Neben mechanistischen Einblicken ermöglichten die Experimente mit Peptid-Bibliotheken auch das *Screening* putativer endogener Substratsequenzen nach ihrer Eignung als natürliche Ziele der *N-end rule*. Im Zuge dessen wurden die proteolytischen Fragmente sowohl von ETHYLENE INSENSITIVE 2 (EIN2), als auch von BIG BROTHER, einem Regulator des Zellwachstums, als potentielle physiologische Ziele von PRT1 entdeckt. Zugunsten der Annahme, dass die *N-end rule* der Ethylen-Signalübertragung entgegenwirkt, wurde festgestellt, dass das C-terminale EIN2-Fragment in *Arabidopsis*-Protoplasten instabil war, in Abhängigkeit seines N-Terminus' und des *PRT1*-Gens. Phänotypische Analysen von Pflanzen mit dem Null-Allel *prt1-1* zeigten jedoch keine wesentlichen Änderungen der Ethylensensitivität, die auf *PRT1*-Mutation zurückzuführen wären. Stattdessen wurden zwei unabhängige Merkmale gefunden, die durch den genetischen Hintergrund der *prt1-1*-Pflanzen verursacht waren. Das erste Merkmal, Sterilität bei moderat erhöhter Umgebungstemperatur, verursacht durch post-meiotische Entwicklungsfehler der männlichen Gametogenese, könnte während der Vermehrung der Linie spontan aufgetreten sein. Dagegen war der zweite Phänotyp, Hyposensitivität gegenüber Cytokinin während heterotrophen Wachstums, auch in einer

Vorgängerlinie von *prt1-1* vorhanden. Insgesamt bietet diese Arbeit Belege für die Konservierung der Substraterkennung durch UBR- und ATE-Enzyme zwischen Pflanzen und anderen Eukaryoten, aber stellt auch pflanzenspezifische Interaktionen für das Typ-II-N-Rekognin PRT1 fest. Diese Erkenntnisse werden in Zukunft dabei helfen, Substrat-N-Termini und deren Erkennungswege in pflanzlichen Zellen miteinander zu verbinden.

1. Introduction

1.1 Protein degradation in plants

The continuous readjustment of the protein content in living cells is achieved by protein synthesis and degradation. It is due to this protein turnover that cells are able to grow, differentiate, divide, and adapt. Dynamic “cellular housekeeping” is especially important when an organism is as intimately associated with and subjected to its environment as a plant. Protein degradation ensures the removal of misfolded or damaged proteins, enables the recycling of amino acids, regulates stoichiometry between the subunits of protein complexes, attenuates signaling pathways, and abolishes gene function by eliminating proteins that are no longer needed (Vierstra, 1993). Impressively, the dimensions of protein turnover in plants are estimated to the replacement of half of the complete protein body within four to seven days (Buchanan et al., 2002b; Li et al., 2017b).

1.1.1 Bulk protein degradation

A large portion of protein degradation in cells is accomplished by non-specific proteolysis. In plants, non-specific proteases reside predominantly in the vacuole, an organelle that resembles the lysosome found in animal cells (Vierstra, 1993). In addition, organelles like mitochondria and chloroplasts harbor distinct proteolytic pathways that reflect their bacterial origin. In the vacuole, “bulk” protein which usually refers to aggregates of misfolded proteins, large protein complexes like ribosomes, or storage proteins, is degraded after delivery by several mechanisms that usually involve membrane encapsulation (Klionsky and Ohsumi, 1999; An and Harper, 2018). The main route for trafficking cytoplasmic contents to the lytic compartment is called macroautophagy, or short autophagy (Ohsumi, 2001). During autophagy, cytoplasmic components are engulfed by an isolation membrane that matures to a double-membrane-bounded compartment called an autophagosome. These compartments are able to fuse with the tonoplast and release the content for subsequent proteolytic breakdown. In plants, research has long focused on starvation-induced autophagy, and hence, the importance of this pathway for general protein degradation and nutrient recycling was emphasized (Bassham, 2009; Dong et al., 2017c). However, with the discovery of a complex machinery that allows for the tethering of specific target molecules to sites of autophagic vesicle formation, it was increasingly appreciated that autophagy can also operate highly selectively (Johansen and Lamark, 2011; Li and Vierstra, 2012). Some of the responsible adapter molecules appear to be conserved between eukaryotes and have also been described in plants (Tsukada and Ohsumi, 1993; Svenning et al., 2011; Kim et al., 2012).

1.1.2 Selective protein degradation – the 26S proteasome

While the importance of selective autophagy is being increasingly recognized, a distinct machinery present in the cytosol and nucleus was long known for its crucial role in the specific degradation of soluble and certain membrane-borne proteins (Voges et al., 1999; Finley, 2009; Vierstra, 2009). The 26S proteasome is a large (2.5 MDa) multi-subunit protein complex that contains a barrel-shaped core particle (CP) of 20 S in size with a broad-spectrum proteolytic activity. The eukaryotic CP is made

up of four stacked ring-shaped oligomers consisting each of seven peptide monomers (Groll et al., 1997; Yang et al., 2004). Within this structure, subunits $\beta 1$, $\beta 2$, and $\beta 5$ expose peptidase active sites towards the barrel-inside. Access to the proteolytic interior is restricted by a narrow pore formed by the α -subunits and is controlled by the 19 S regulatory particle (RP) that forms a cap on either one or both sides of the proteasome (Groll et al., 2000). Next to substrate entry, the RP is responsible for substrate selection and processing. Six AAA-ATPase (ATPase associated with diverse cellular activities ATPase) subunits cooperate to mediate the unfolding of substrates, trigger opening of the CP gate, and channel the peptide thread into the lytic core (Smith et al., 2007; Lander et al., 2012). Moreover, at least eleven additional non-ATPase subunits of the RP, including a number of RPN named proteins, are responsible for substrate recognition and regulation of the ATPases (Elsasser et al., 2002; Peth et al., 2009). Since some of these components appear to be reversibly associated with the holo-complex, proteasome activity is likely to be also adjustable (Thrower, 2000; Leggett et al., 2002). Consistently in plants, knock-down of individual RP subunits sometimes leads to specific, rather than pleiotropic phenotypes (Book et al., 2009). For example, mutation of RPN12a results in decreased sensitivity towards phytohormones of the cytokinin family (Book et al., 2009).

1.1.3 Ubiquitin

In eukaryotes, targeted protein degradation via the 26S proteasome, as well as distinct autophagic and endosomal pathways, is largely accounted for by a genetically expanded machinery that concentrates around a small protein called ubiquitin (Ub). Ub is a 76 amino acid (~8.5 kDa) protein of globular structure that can be post-translationally transferred to ϵ -amino groups of solvent-exposed lysine (K, Lys) residues on target proteins to serve as a covalent tag. Unconventionally, Ub attachment can also occur at either thiol or hydroxyl groups presented by cysteine (C, Cys) or serine (S, Ser)/threonine (T, Thr) side chains, respectively (Cadwell et al., 2005; Tait et al., 2007; Wang et al., 2007; Williams et al., 2007). A triad of enzyme classes, referred to as E1, E2, and E3, is responsible for the ATP-dependent attachment of Ub to substrate proteins, termed ubiquitination (or ubiquitylation). The successive processes that lead to target ubiquitination are: 1. Activation of the Ub terminal carboxyl group via the formation of an Ub-adenylate intermediate by an E1 (Ub activating) enzyme and subsequent thio-esterification with an E1-active site Cys (Haas and Rose, 1982; Haas et al., 1982). 2. Recruitment of an E2 (Ub conjugating) enzyme and transfer of Ub to a catalytic Cys of E2 (Hershko et al., 1983; Pickart and Rose, 1985; Haas et al., 1988). 3. Binding of the target protein by an E3 (Ub ligase) enzyme that either works as an adaptor to mediate direct transfer of Ub from E2 to the substrate, or accepts Ub from E2 in a transesterification reaction to subsequently catalyze the transfer to a substrate target site (Bartel et al., 1990; Reiss and Hershko, 1990; Hershko and Ciechanover, 1992; Scheffner et al., 1993; Pickart, 2001; Deshaies and Joazeiro, 2009). Finally, ubiquitination is reversible by the action of a large group of proteases, called deubiquitinating enzymes (DUBs) that recycle Ub by specific hydrolysis after glycine (G, Gly) 76 (Bachmair et al., 1986; Amerik and Hochstrasser, 2004). One example is RPN11 which hydrolyzes Ub chains as a component of the proteasomal RP (Verma et al., 2002). The combined activities of E1, E2, and E3 enzymes in the presence of adenosine triphosphate (ATP)/Mg²⁺ and Ub have been shown to be necessary and sufficient for the *in-vitro* reconstitution of target protein ubiquitination (Koepl et al., 1999), and for the attachment of Ub chains onto the E3 (autoubiquitination), the latter especially occurring in the absence of substrate (Lorick et al., 1999). Since the discovery of Ub in the late 1970s (Goldstein et al., 1975; Ciechanover et al., 1978, 1980b, 1980a; Wilkinson et al., 1980), the

significance of the system was increasingly recognized and Aaron Ciechanover, Avram Hershko, and Irwin Rose were awarded the Nobel Prize in Chemistry in 2004.

1.1.3.1 Ubiquitin modifications

Affecting virtually all aspects of cellular life (Weissman, 2001), ubiquitination is a posttranslational modification with extremely versatile features, and the information behind this protein tag was fittingly depicted as a molecular “code” that can translate into various distinct outcomes, including degradation (Komander and Rape, 2012; Yau and Rape, 2016). A single Ub molecule attached to a substrate protein is referred to as ‘mono-ubiquitination’ which can be restricted to one site, or can be repeated on several residues of the target protein (multi-mono-ubiquitination). Mono-ubiquitination has been associated with functions for intracellular trafficking (Haglund et al., 2003; Jura et al., 2006; Su et al., 2013; Wang et al., 2013b), complex-formation (Bienko et al., 2010; Ray et al., 2014), protein auto-inhibition (Hoeller et al., 2006), lysosomal/vacuolar degradation (Katzmann et al., 2001; Haglund et al., 2003; Spitzer et al., 2006), and transcriptional regulation (Pavri et al., 2006; Chandrasekharan et al., 2010; Chen et al., 2017b).

In addition to mono-ubiquitination, linear or even branched chains of Ub moieties can be created when any of the seven Lys present on Ub or the Ub amino-terminus (N-terminus) is used for the formation of an amide bond with the carboxy-terminal (C-terminal) Gly of another Ub molecule (poly-ubiquitination; Peng et al., 2003). Next to progressive E3 ligase activity, poly-ubiquitination can be accomplished by E4 Ub ligases that function to elongate Ub chains (Koegl et al., 1999; Hoppe et al., 2004; Huang et al., 2014). Among the possible sites for Ub-Ub linkage, Lys-48 is most frequently used for chain elongation in eukaryotes (Maor et al., 2007; Komander and Rape, 2012). Interestingly, Lys-27 linkage of Ub cannot be found in plants (Kim et al., 2013a), even though such chains have been detected in yeast (*Saccharomyces cerevisiae*) and mammals (Meierhofer et al., 2008; Xu et al., 2009). So far, the same holds true for linear (i.e., N- to C-terminus joined) Ub chains in plants (Walsh and Sadanandom, 2014). The species of a poly-Ub chain that is created on a substrate, referred to as the Ub linkage type, appears to be determined by the combined E2-E3 action, although the molecular mechanisms behind linkage-site choice are not very well understood (Eddins et al., 2006; Christensen et al., 2007; Suryadinata et al., 2014; Stewart et al., 2016).

As a consequence of different Lys residues used for Ub linkage, poly-Ub chains are structurally divergent. Deciphering the Ub code harnesses the fact that different types of Ub linkage lead to certain chain topologies which, in turn, are able to interact with distinct proteins that harbor Ub-interacting domains (Pickart and Fushman, 2004; Ye and Rape, 2009). Thus, poly-Ub tags feature a plethora of cellular outputs, including DNA repair (Hofmann and Pickart, 1999; Hoege et al., 2002; Wen et al., 2006), selective autophagy (Pankiv et al., 2007; Matsumoto et al., 2011), endosomal sorting for vacuolar degradation (Haglund et al., 2003; Lauwers et al., 2009; Gu and Innes, 2012; Yu et al., 2016), regulation of endoplasmic reticulum (ER)-associated protein degradation (Lemus and Goder, 2014), kinase modification (Davis and Gack, 2015), NF- κ B activation (Ikeda et al., 2011), and proteasomal degradation via K48, K11, and K29-linked poly-Ub chains (Hershko, 1988; Chau et al., 1989; Finley, 2009; Xu et al., 2009). The latter reflects the most prominent function of the poly-Ub tag. Generally in eukaryotes, a chain of K48-linked Ub molecules has high affinity to interact with the 26S proteasome when it exceeds a length of three monomers (Thrower, 2000). Thus, the K48-linked

poly-Ub tag leads to efficient degradation of a protein via the 26S proteasome, on condition that an unstructured region is provided within the ubiquitinated substrate to allow for unfolding initiation (Johnston et al., 1995; Inobe et al., 2011). Although other pathways exist for targeting the 26S proteasome (Erales and Coffino, 2014), poly-ubiquitination is by far the strongest signal for 26S proteasome binding. Hence, the machinery facilitating proteasomal degradation via ubiquitination is called the Ub proteasome system (UPS).

1.1.3.2 Ubiquitin-like proteins

Following the identification of Ub and its related machinery, a set of proteins has been discovered that act as post-translational modifiers and are similar to Ub in terms of structure and enzymatic mechanisms leading to their ligation; however their functions are distinct from Ub. Among these modifiers, the most-characterized ones in plants are SMALL-UBIQUITIN-RELATED MODIFIER (SUMO), RELATED TO UBIQUITIN (RUB, or Nedd8 in yeast and mammals), and AUTOPHAGY 8 (ATG8) and ATG12. SUMO typically participates in the modification of protein surfaces that are important for inter- or intramolecular interactions (van der Veen and Ploegh, 2012). In plants, SUMO often regulates the response to stresses, including tolerance towards heat and freezing (Kurepa et al., 2003; Miura et al., 2007; Zhang et al., 2017c). In contrast to the relative versatility of the SUMO tag, the major function of RUB appears to be the regulation of Cullin-subunit containing E3 ligases (see below), thus influencing plant hormone signaling and development (del Pozo and Estelle, 1999; Hakenjos et al., 2011). While SUMO and RUB have rather non-degradative functions, ATG8 plays a crucial role during autophagosome formation, and is recruited to the newly formed autophagosome by being conjugated to phosphatidylethanolamine in an ATG12-mediated manner (Ohsumi, 2001; Thompson et al., 2005; Klionsky, 2007; Fujioka et al., 2008; Chung et al., 2010). In addition, a series of Ub-fold or Ub-like modifier proteins have been described that often contain little sequence similarity outside of conserved β -grasp folds that are characteristic to Ub and all Ub-like proteins (Vierstra, 2012).

1.1.4 Plant E3 ligases

In plants, the group of genes encoding for E3 ligases has greatly expanded with more than 1,300 potential members in the *Arabidopsis thaliana* (hereafter referred to as *Arabidopsis*) genome (Smalle and Vierstra, 2004; Hua and Vierstra, 2011). E3 ligases outnumber all other components of the UPS, comprising 64 DUBs, 37 E2, and two E1 enzymes in *Arabidopsis* (Vierstra, 2009). This huge genetic effort might reflect the importance of rapid and specific protein degradation in an organism that 1) is subject to strongly differing environmental conditions (Willems et al., 2004), 2) depends as an autotroph on very efficient recycling of inorganic nutrients, and 3) is during most life stages not limited by energy supply for an ATP-consuming degradation system.

E3 ligases can be roughly classified into three groups (Stone et al., 2005): REALLY INTERESTING NEW GENE (RING), HOMOLOGOUS TO E6-ASSOCIATED PROTEIN CARBOXYL TERMINUS (HECT), and U-box. These groups are distinguished by their modes of action and the structures of their catalytic domains. Generally, HECT E3 enzymes are capable of catalyzing Ub ligation to a substrate after reception of Ub from E2 via transthiolation, whereas RING- and U-box based E3s act as an E2-target adaptor to

facilitate Ub transfer directly from the E2. Furthermore, a hybrid version named the RING BETWEEN RING (RBR) ligases were first identified in the human E3 ligase parkin and are represented in plants by four gene families, including the ARIADNE (ARI) E3s (Morett and Bork, 1999; Marín, 2010; Wenzel et al., 2011). RBR E3 ligases are composed of three RING-related domains and combine the classical RING function of binding the E2 within the first canonical RING domain with the formation of a HECT-type Ub-RING thioester via the third RING-like domain prior to substrate ubiquitination (Wenzel et al., 2011; Lechtenberg et al., 2016). The middle domain is called IN-BETWEEN-RING and, at least in parkin, is involved in autoinhibition (Trempe et al., 2013; Wauer and Komander, 2013; Gladkova et al., 2018). In order to undergo thioesterification with Ub, the C-terminal RING-domain in RBR ligases contains a conserved active-site Cys which is not Zn chelating, and resides in a stretch between the metal binding Cys residues 2 and 3 of the domain's primary sequence (Wauer and Komander, 2013; Dove and Klevit, 2017).

1.1.4.1 The RING domain

The RING domain is a secondary structure that serves for protein-protein interactions which in most cases enable the recruitment and activation of E2 enzymes (Lorick et al., 1999; Joazeiro and Weissman, 2000). Hereby, allosteric effects exerted by the RING domain cause the E2-Ub conjugate to adopt a closed conformation that is most suitable for the nucleophilic attack at the thioester bond by a substrate amino group (Budhidarmo et al., 2012; Stewart et al., 2016). Characteristically, the RING domain structure is stabilized by two zinc (Zn) ions that are coordinated by eight Cys/histidine (H, His) side chains (Freemont et al., 1991; Barlow et al., 1994). Since the amino acids chelating the Zn ions are not arranged in the same order as given by the primary peptide sequence, the inner structure forms a compact fold of two crossing β -strands sustained by one α -helix (Deshaies and Joazeiro, 2009; Budhidarmo et al., 2012). This "cross-brace" structure is the main distinction of a RING domain from the DNA-binding Zn finger. Different types of RING domains have been described based on the identity of the metal ligand amino acids and the number of interspacing residues. The most common types are the RING-HC (with a C3-H-C4 arrangement of the metal chelating residues in the primary peptide sequence) and the RING-H2 (C3-H2-C3) which mainly differ in the metal ligand at position five being either His or Cys (Stone et al., 2005; Deshaies and Joazeiro, 2009).

A modification of the RING finger primary sequence is the PLANT HOMEODOMAIN (PHD) domain with a C4-H-C3 arrangement of the metal chelating amino acids (Deshaies and Joazeiro, 2009). Although similar in terms of sequence, the PHD domain adopts a different fold than does the RING domain, and likely does not function in ubiquitination (Aravind et al., 2003). In contrast, the U-box domain has little sequence similarity with the RING domain, but folds to a similar structure by engaging charged and polar residues for Zn coordination (Aravind and Koonin, 2000; Ohi et al., 2003). Hence, U-box proteins are equally active in E2-assisted transfer of Ub to target proteins as RING E3 ligases (Koegl et al., 1999; Aravind and Koonin, 2000; Cyr et al., 2002). By now, a widespread array of functions has been attributed to PLANT U-BOX (PUB) proteins, with *Arabidopsis* counting 64 (Wiborg et al., 2008), and rice (*Oryza sativa*) 77 (Zeng et al., 2008) annotated members in their genomes. PUBs have been attributed a prominent role in defense (Durrant et al., 2000; Navarro et al., 2004; González-Lamothe et al., 2006; Yang et al., 2006; Trujillo et al., 2008), as well as in self-incompatibility (Gu et al., 1998; Stone et al., 1999, 2003), hormone response (Monte et al., 2003; Wang et al., 2017; Zhou et al., 2018), and other processes (Yee and Goring, 2009; Trujillo, 2017).

1.1.4.2 RING-type E3 ligases

RING-type E3s constitute a diverse class that can be further divided into single enzymes and composite E3s where the RING-containing protein acts as part of a complex (Stone et al., 2005). While simple RING-E3s comprise domains for both E2- and substrate binding, RING-type E3 complexes interact with the E2 via a RING-domain protein and rely on additional subunits for substrate interaction.

Differing in the domain composition, multiple different E3 complex types exist. Many are built on a scaffold protein family named cullin and contain the RING-H2 domain protein RING BOX 1, giving rise to the cullin-RING ligases that include the very prominent class of SCF (for \underline{S} -PHASE KINASE ASSOCIATED PROTEIN 1-Cullin-F-box) complexes (Willems et al., 2004). Substrate specificity of SCF complexes is provided by the identity of the associated F-box protein, a protein family encoded by almost 700 different loci in *Arabidopsis* (Gagne et al., 2002). This makes SCF E3s the most diverse group among the Ub ligases and it has manifested that probably every aspect of plant biology is affected by the action of SCF complexes (Hellmann and Estelle, 2002; Hua and Vierstra, 2011). To name a selection, F-box mediated protein degradation has been linked to development (Samach et al., 1999; Moon et al., 2004; Imaizumi, 2005; Schwager et al., 2007), circadian clock (Nelson et al., 2000; Somers et al., 2000), photomorphogenesis (Dieterle et al., 2001; Hoecker, 2005), and signaling of most plant hormones (jasmonic acid (JA): Xie et al. (1998), Yan et al. (2009); auxin: Gray et al. (1999), Dharmasiri et al. (2005a), Kepinski and Leyser (2005); gibberellins: Itoh et al. (2003), Sasaki et al. (2003); ethylene: Guo and Ecker (2003), Potuschak et al. (2003), Gagne et al. (2004), Qiao et al. (2009); strigolactones: Nelson et al. (2011); cytokinins: Kim et al. (2013b); brassinosteroids: Zhu et al. (2017); abscisic acid: Koops et al. (2011), Li et al. (2016)). In the cases of JA and auxin, the respective F-box proteins, namely CORONATINE INSENSITIVE 1 (COI1) and members of the TRANSPORT INHIBITOR RESPONSE 1/AUXIN SIGNALING F-BOX PROTEIN (TIR1/AFB) family, even act as the hormone receptors (Dharmasiri et al., 2005a, 2005b; Kepinski and Leyser, 2005; Yan et al., 2009). Here, target binding by TIR1 and COI1 is promoted by the respective hormone acting as a “molecular glue” (Tan et al., 2007; Sheard et al., 2010; Calderón Villalobos et al., 2012). This concept of hormone-mediated substrate reception is distinct from target recognition by many other F-box proteins that typically use phosphorylated residues of the substrate (Deshaies, 1999).

Next to F-box proteins, substrate recognition of multiple-subunit E3 ligases can be mediated by a BRIC A BRAC, TRAMTRACK AND BROAD COMPLEX (BTB) protein, or a UV-DAMAGED DNA-BINDING (DDB) protein. The accordingly named complexes (i.e., BTB and DDB complexes) each contain distinct cullin subunits (Vierstra, 2009). During ethylene biosynthesis, the BTB proteins ETHYLENE OVERPRODUCER 1 (ETO1) and the two paralogues ETO1-like 1 (EOL1) and EOL2 facilitate 26S proteasome-mediated degradation of 1-aminocyclopropane-1-carboxylic acid (ACC) SYNTHASE (ACS) in *Arabidopsis*, and likely in other plants, via binding to their C-terminal target of ETO1 (TOE) motif, thereby regulating a rate-limiting step in the production of this plant hormone (Wang et al., 2004; Yoshida et al., 2005).

Finally, the ANAPHASE-PROMOTING COMPLEX or the CYCLOSOME (APC/C) constitutes another multi-subunit E3 RING ligase conserved in eukaryotes that functions in the regulation of cell-cycle progression and mitosis-associated processes (Capron et al., 2003a). The APC/C is built on a scaffold protein called APC2 in yeast and vertebrates that is structurally related to cullin but cannot be regulated by Nedd8 (Tateishi et al., 2001; Capron et al., 2003a). As for APC2, *Arabidopsis* homologs

have been identified also for the target recognition elements of the APC/C that generally contain WD40-repeat domains (Capron et al., 2003a, 2003b). A feature of APC/C target molecules are often protein motifs called the destruction-box (D-box) and the KEN box (Glutzer et al., 1991; Pflieger and Kirschner, 2000).

In contrast to E3 complexes, simple RING-E3s contain all domains necessary for catalytic activity within one polypeptide. Nevertheless, it is increasingly recognized that many require the formation of homo- or heterodimers, or even oligomerization for E3 ligase activity or regulation (Poyurovsky et al., 2007; Deshaies and Joazeiro, 2009). This is in fact the case for both simple and multi-subunit E3s (Suzuki et al., 2000a; Yin et al., 2009), and several RING domain proteins even tend to spontaneously oligomerize in solution (Poyurovsky et al., 2007). Dimer and oligomer formation can occur via the RING domain itself (Poyurovsky et al., 2007; Liew et al., 2010; Feltham et al., 2011; Yudina et al., 2015), or via additional domains for protein-protein interactions (Printsev et al., 2014; Hu et al., 2017). The molecular consequences of E3 oligomerization are different, but they are usually involved in the regulation of enzyme activity. For example, multimer formation was found to be important for the activation of E3 ligase activity towards substrate molecules (Liew et al., 2010; Feltham et al., 2011; Yudina et al., 2015), for the regulation of E3-stability by activating autoubiquitination (Xie et al., 2002; Printsev et al., 2014; Furlan et al., 2017), and for increasing E3 processivity (Ranaweera and Yang, 2013; Hu et al., 2017).

A majority of the 469 predicted RING proteins encoded by the *Arabidopsis* genome contains additional domains that mediate protein-protein-interactions, including oligomerization, and enable for further individual functions (Stone et al., 2005). Among the various domain combinations possible, proteins with multiple RING domains are relatively scarce. In the study performed by Stone et al. (2005), only eight proteins with more than one RING domain were identified (excluding RBR ligases) in *Arabidopsis*. Five of these belong to the ORTHRUS (ORTH)/VARIANT IN METHYLATION protein family that, in mammals and likely also in plants, is involved in the maintenance of chromatin modifications (Kraft et al., 2008). For ORTH1 it was shown, using truncated and point-mutated protein versions, that either of the two RING domains can independently act in ubiquitination reactions (Kraft et al., 2008). However so far, the functional requirement for an additional RING domain was assessed for none of the eight multiple-RING containing candidates.

1.2 The N-end rule pathway of protein degradation

Selective protein degradation requires a feature of a target protein that is recognizable by an E3 ligase. Such a signal, called a degron (Varshavsky, 1991; Lucas and Ciulli, 2017), can be inherent to the protein sequence, like in the case of the before mentioned D- and KEN boxes, or the C-end degrons targeted by some cullin-RING ligases (Koren et al., 2018; Lin et al., 2018). On the other hand, a post-translational modification like a phosphorylation, or a small molecule-mediated interaction with adapter proteins (e.g., TIR1 and COI1), can recruit an E3 ligase and thereby pose instability on an otherwise long-lived protein. Strikingly, the first degron to be identified was both inherent to the protein sequence and required post-translational activation: It was found that different amino acids at the N-terminus of otherwise identical fusion constructs of *Escherichia coli* β -galactosidase dictated certain half-lives on this reporter when expressed in yeast, ranging from a few minutes to more than 20 hours (Bachmair et al., 1986). However, the destabilizing effect of certain amino acids depended

on the exposure of this residue as a free neo-N-terminus, rendering the sequence signal conditional. The relation between the identity of the N-terminal amino acid and the protein half-life was referred to as the “N-end rule” of protein degradation (Bachmair et al., 1986), and is more recently termed the N-degron pathway (Varshavsky, 2019).

These crucial observations were decisively facilitated by the implementation of a technique to genetically constitute non-native N-termini in cells. This approach is called the Ub Fusion Technique (UFT) (Bachmair et al., 1986; Varshavsky, 2005). Here, the reporter protein initiated by the requested N-terminus (X) is expressed as a chimeric gene with Ub at the 5' terminus. Upon translation of the Ub-X-reporter, the N-terminal Ub is reliably cleaved off the nascent polypeptide *in vivo* by the action of unknown DUBs. This cleavage occurs precisely after the last Gly residue of Ub, and is irrespective of the following amino acids, with the sole exception of proline (P, Pro) which appeared to be cleaved less efficiently (Bachmair et al., 1986; Bachmair and Varshavsky, 1989; Varshavsky, 2005).

Next to the destabilizing residue in ultimate N-terminal position, two more features of an N-terminus are required to provoke instability in eukaryotic cells: A properly spaced N-proximal Lys residue as well as structural flexibility and solvent exposure of the N-terminus allow for the E3 ligase-assisted attachment of Ub (Bachmair and Varshavsky, 1989). Such an N-terminal region that enables for proteolytic degradation was termed an N-degron (Varshavsky, 1991), and the enzymes responsible for N-degron selection were denoted N-recognins (Bartel et al., 1990) (Fig. 1).

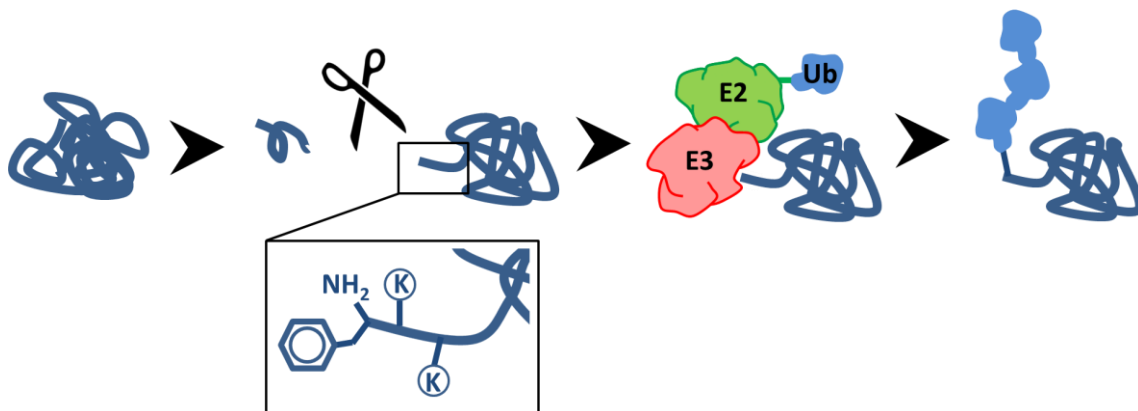


Fig. 1 | Generation of an N-degron and substrate recognition by N-recognins. Substrates for the N-end rule pathway are often created by peptidase activity (indicated by the scissors). In the depicted example, N-terminal phenylalanine is exposed as an N-degron at the new N-terminus of the proteolytic product. Enzymes that bind proteins harboring N-degrons and are required for their degradation are called N-recognins (red freeform). Canonical N-recognins in eukaryotes generally have an E3 ligase domain signature and act in Ub transfer for proteasomal degradation (Bartel et al., 1990; Varshavsky, 1996). Additionally, N-recognin-mediated target selection was also associated with autophagosome assembly (Kim et al., 2013d; Cha-Molstad et al., 2015, 2017; Jiang et al., 2016). A modified version of this figure was published in Mot et al. (2018).

The N-end rule was soon found to apply to both eukaryotes and bacteria, and at least a branch of the N-end rule likely exists also in archaea (Townsend et al., 1988; Bachmair and Varshavsky, 1989; Gonda et al., 1989; Tobias et al., 1991; Bachmair et al., 1993; Varshavsky, 2011). Although coinciding conceptually in both domains, eukaryotes and bacteria engage different mechanistic systems to execute N-end rule protein degradation: While eukaryotes have developed special E3 enzymes to target N-end rule substrates via the UPS, prokaryotes lack the Ub system and employ the ATP-dependent caseinolytic protease (Clp) system to target a distinct set of N-terminal amino acids as degradation signals (Tobias et al., 1991; Lupas and Koretke, 2003; Erbse et al., 2006; Schmidt et al.,

2009). A sequential homolog of the bacterial N-recognin ClpS was also identified in *Arabidopsis* chloroplasts (Nishimura et al., 2013). The presence of this ClpS1 designated homolog together with studies on protein stability (Apel et al., 2010), and N-termini abundances (Rowland et al., 2015; Bouchnak and van Wijk, 2019) in chloroplasts suggest that an N-end rule machinery of bacterial origin is also present in these organelles. Moreover, N-proteome analyses also indicate the prevalence of an N-end rule in mitochondria (Vögtle et al., 2009; Calvo et al., 2017), but mechanistic components are not described to date. With proteomic techniques like combined fractional diagonal chromatography (COFRADIC) and terminal amine isotopic labelling of substrates (TAILS) available today, scientists have also proven the strong overabundance of stabilizing in contrast to destabilizing N-terminal amino acids in cells of different systems, establishing the general validity of the N-end rule (Humbard et al., 2013; Lange and Overall, 2013; Plasman et al., 2013; Zhang et al., 2015b; Li et al., 2017b). The observation, however, that destabilizing N-termini are not fully absent from proteomes, supports the assumption that additional sequence features like flexibility and Lys-accessibility together with downstream amino acids influence the eligibility of an N-terminus as a degraon (Zhang et al., 2015b; Dissmeyer et al., 2018; Eldeeb et al., 2018b).

1.2.1 Functions of the N-end rule pathway

Consistent with an ancient origin, the N-end rule has been assigned overarching functions to date (reviewed in Varshavsky (2017, 2019)). Most of the described cases of N-end rule dependent degradation demonstrate the high amenability of N-degrons to activation by external cues. For example, a cryptic N-degron can be inactive as long as the protein is incorporated in a complex that shields the otherwise destabilizing N-terminus from recognition, giving rise to a mode of regulating complex stoichiometry (Shemorry et al., 2013). Next, a protein's N-terminus can be sensitive to chemical modifications that affects its eligibility as an N-degron. In this way the machinery can function as a sensory mechanism towards the modifying chemical reagent. Accordingly in higher eukaryotes, N-terminal Cys can be oxidized in the presence of oxygen and nitric oxide (NO), allowing for further enzymatic processing of the pre-degron to eventually expose a destabilizing N-terminus and trigger degradation of the sensor protein (Kwon et al., 2002; Hu et al., 2005; Lee et al., 2005). In this way, the mammalian REGULATOR OF G PROTEIN SIGNALING 4 (RGS4), RGS5, and RGS16 are conditionally unstable by means of their Cys-initiated mature N-terminus, thus impacting on cardiovascular development in an NO- and oxygen-sensing manner (Davydov and Varshavsky, 2000; Kwon et al., 2002; Hu et al., 2005; Lee et al., 2005). Moreover, oxygen- and NO-dependent degradation of Group VII ETHYLENE RESPONSE FACTOR (ERFVII) transcription factors mediates multiple aspects of plant physiology, including the response to low oxygen (hypoxia), the regulation of seed germination, stomatal closure (Holman et al., 2009; Gibbs et al., 2011, 2014a; Licausi et al., 2011; Vicente et al., 2019), and the immune response (Vicente et al., 2019; see section 1.2.4).

Intriguingly, an N-degron can also be exposed from virtually any cellular protein after peptidase processing. Consequently, the N-end rule was attributed various functions related to the removal of protease cleavage products. These functions include the regulation of apoptosis by the elimination of caspase-generated protein fragments (Ditzel et al., 2003; Piatkov et al., 2012a), the removal of neurodegeneration-associated protein fragments (Brower et al., 2013), the depletion of separase-cleavage products during chromatid segregation (Rao et al., 2001; Liu et al., 2016b), and the degradation of the autocleaved product of the UBIQUITIN SPECIFIC PEPTIDASE 1 (Usp1), a DUB that

functions in regulation of the DNA polymerase processivity factor PROLIFERATING CELL NUCLEAR ANTIGEN (PCNA). Thus, it appears that the N-end rule provides a versatile cellular tool that, during evolution, was easily recruited to fulfill new functions.

1.2.2 Primary destabilizing amino acids and N-recognins

Newly exposed protein N-termini can act as a destruction signal, but what determines the eligibility as an N-degron in eukaryotes? The observation that certain amino acids at the N-terminus conferred either long (more than 20 hours) or short (less than 30 minutes) half-lives to reporter proteins in yeast cells and mammalian cell extracts lead to the classification of amino acids into stabilizing and destabilizing residues (Bachmair et al., 1986; Gonda et al., 1989). Among the destabilizing ones, the basic (arginine (R, Arg), Lys, His) and the bulky hydrophobic (phenylalanine (F, Phe), leucine (L, Leu), tryptophan (W, Trp), tyrosine (Y, Tyr), and isoleucine (I, Ile)) trigger direct recognition and ubiquitination by E3 ligases and are therefore denoted primary destabilizing (Varshavsky, 1996; Fig. 2). While these determinants are axiomatic in yeast, the aliphatic residues Ile and Leu make exceptions in other eukaryotes. Specifically, both Ile and Leu conferred only intermediate instability to reporter constructs in tobacco (*Nicotiana benthamiana*) (Worley et al., 1998; Stary et al., 2003; Graciet et al., 2010), and Ile was considered a borderline case residue in mammals owing to its failure to act as an N-degron, but ability to interfere with the recognition of Phe-N-degrons in reticulocyte extracts (Gonda et al., 1989; Fig. 2).

Primary destabilizing residues are furthermore categorized into type I (basic) and type II (bulky hydrophobic), owing to their targeting by distinct enzymatic activities (Fig. 2; Reiss et al., 1988; Gonda et al., 1989; Bartel et al., 1990). The E3 ligases responsible for ubiquitinating the primary destabilizing residues in eukaryotes are mostly characterized by the presence of an approximately 70-residue Zn-finger-like domain called the UB LIGASE N-RECOGNIN (UBR) box (Tasaki et al., 2005). In yeast, destabilization of all primary N-degrons is governed by a single gene which encodes the RING-type E3 ligase Ubr1p (Bartel et al., 1990). By contrast, the mammalian genome harbors seven UBR box containing genes, designated UBR1-UBR7 (Kwon et al., 1998; Kwon et al., 2001; Tasaki et al., 2005). Like yeast Ubr1p, all mammalian UBR proteins except for UBR4 also contain domains signaling Ub ligase activity. In *Arabidopsis*, *PROTEOLYSIS 6 (PRT6)* encodes an N-recognin closely related structurally to yeast Ubr1p and mammalian UBR1, UBR2, and UBR3 in that it contains the UBR box, a RING domain, and a predicted C-terminal autoinhibitory domain (Fig. 3; Kwon et al., 2002; Garzón et al., 2007; Tasaki et al., 2012). It was shown that PRT6 mediates the degradation of type I N-end rule substrates in *Arabidopsis* (Garzón et al., 2007). A homolog of the *Arabidopsis* gene was also found in barley (*Hordeum vulgare L.*), indicating that the gene is conserved in plants (Mendondo et al., 2016).

Excluding also PRT6, *in-vitro* affinity for N-degrons was confirmed only for yeast Ubr1p, as well as for mammalian UBR1, UBR2, UBR4, and UBR5 (Bartel et al., 1990; Tasaki et al., 2005, 2009). In UBR proteins, the UBR box is essential for N-recognin activity. However, a UBR box alone is only sufficient for binding to type I primary destabilizing residues. Recognition of type II substrates requires the presence of an additional domain, called the N-domain (Tasaki et al., 2009). It is present in Ubr1p, UBR1, and UBR2, enabling these N-recognins to target both type I and type II substrates (Kwon et al., 2003; Tasaki et al., 2005). Eukaryotic N-domains exhibit significant similarity to the *E. coli* N-recognin

ClpS which mediates the targeting of all bacterial primary destabilizing residues, comprising Leu, Phe, Trp, and Tyr (Erbse et al., 2006). In ClpS, substrate selectivity is achieved by a deep hydrophobic binding pocket that fully engulfs the ligand amino acid. Ligand binding is further supported inside the binding cleft by hydrogen bonds to the α -amino group as well as to the amide bonds of the first and second substrate residues (Wang et al., 2008a; Roman-Hernandez et al., 2009; Schuenemann et al., 2009).

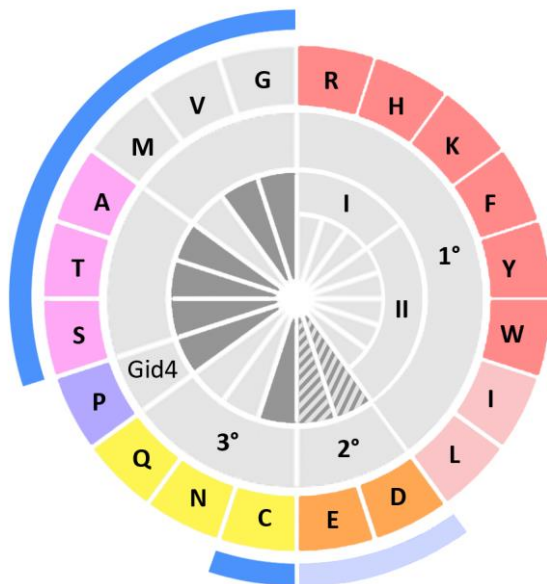


Fig. 2| The N-end rule in eukaryotes. Indicated are amino acids at the protein N terminus, their modifications, and effects on protein stability. **Red:** Primary (1°) destabilizing amino acids comprise basic (“type I”) and bulky hydrophobic (“type II”) residues. Among the latter, Ile and Leu (**light red**) are fully destabilizing in yeast, intermediary destabilizing in plants, and Ile is not a destabilizing N-terminus in mammals. **Orange:** Secondary (2°) destabilizing residues are ligated to Arg prior to their targeting by N-recognins. **Yellow:** Tertiary (3°) destabilizing residues can be processed into 2° by enzymatic and/or chemical modifications *in-vivo*. **Violet:** In yeast, Pro at N-terminal position 1 or 2 can be targeted for ubiquitination by Gid4 or Gid10 in certain sequence contexts (Chen et al., 2017a; Melnykov et al., 2019). In other organisms, the stability effect of N-terminal Pro is unclear due to the low DUB cleavage efficiency of the Ub-Pro fusion. **Magenta:** Ala, Thr, and Ser are stable in plants and yeast, but unstable in

rabbit reticulocyte extracts; they are potential substrates of the Ac/N-end rule (Eldeeb et al., 2018b). **Grey amino acids** are conditionally destabilizing depending on the penultimate amino acid and/or N^α-acetylation (Gibbs et al., 2014b; Kim et al., 2014; Xu et al., 2015). In yeast it was shown that N-terminally formylated Met can also target for degradation in the cytosol of eukaryotic cells (Kim et al., 2018a). Here, formyl-Met was found to be the product of a mitochondrial formyltransferase that was retained in the cytosol upon a starvation stimulus. Furthermore, the human proteins ZYG11B and ZER1 are substrate adaptors of Cullin E3 complexes targeting substrates with N-terminal Gly (Timms et al., 2019). **Dark grey inner sections:** These residues allow for initiator-Met excision when present at the second position (Giglione et al., 2015). For Met-Asp and Met-Glu (**hatched**), the only known cases of N-terminal Met removal are mammalian cytoplasmic β -actin and γ -actin, respectively (Van Damme et al., 2011). **Blue outer bar:** These N-termini are subject to N^α-acetylation; however, Gly-acetylation is observed relatively rarely (Hwang et al., 2010a; Lee et al., 2016). For Glu and Asp (**light blue outer bar**), N^α-acetylation refers only to the iMet-cleaved N-termini of mammalian cytoplasmic β -actin and γ -actin (Van Damme et al., 2011). For further references see main text. The figure was modified from Eldeeb and Fahlman (2014).

An exception from the rule that type II N-recognin activity of UBR box proteins requires the N-domain is mammalian UBR4, an extraordinarily large protein with multiple functions (Parsons et al., 2015; Kim et al., 2018c, 2018b). Although lacking the N-domain, UBR4 exhibited binding affinity towards both Arg and Phe-initiated peptides in pull-down assays (Tasaki et al., 2005). UBR4 has homologous genes in plants and flies. In *Arabidopsis*, the homolog is called BIG for its protein size of ~560 kDa and was attributed a function in PIN1 localization for polar auxin transport during light signaling (Gil et al., 2001; Yamaguchi et al., 2007; Guo et al., 2013), as well as the regulation of the circadian period (Hearn et al., 2018), and the regulation of JA pathways (Zhang et al., 2019), but N-recognin activity of BIG has not been shown to date. However notably in the light of UBR4 binding of type II N-degrons in an N-domain independent way, BIG contains three Zn-finger domains, one of which is characterized as a ZZ domain (Fig. 3; Gil et al., 2001). The ZZ domain is a eukaryotic cross-brace Zn finger motif that complexes two Zn ions employing four to six Cys and two His/Ser residues

(Ponting et al., 1996; Legge et al., 2004). Among other functions of ZZ domains from different proteins (Legge et al., 2004), the domain was shown to act as a structural equivalent to the UBR box in mouse p62 (or Sequestosome-1) which is an autophagic adaptor (Cha-Molstad et al., 2017; Kwon et al., 2018). Here, the ZZ domain facilitated binding to both type I and aromatic (Phe, Trp, Tyr) type II N-degrons by p62.

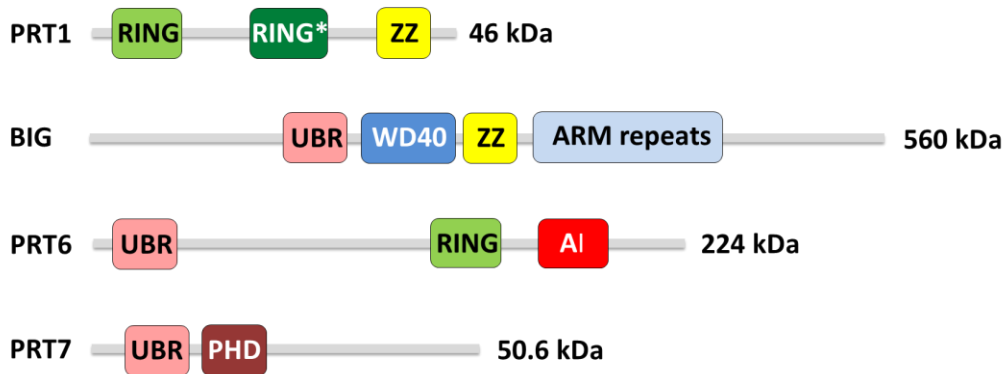


Fig. 3| Domain structures of *Arabidopsis* putative and confirmed N-recognins. The *Arabidopsis* genome harbors three genes containing a UBR box signature, called BIG, PRT6, and PRT7. Of these, PRT6 ubiquitinates substrates that present type I (Arg, His, Lys) N-degrons. The E3 ligase responsible for the degradation of type II (Phe, Tyr, Trp) substrates is PRT1 which lacks the UBR domain and has no homolog in eukaryotes outside of the plant kingdom. BIG and PRT7 were proposed to potentially function as additional N-recognins due to the presence of the UBR box. **RING**, RING finger; **RING***, modified domain containing RING and C₃H-type Zn fingers; **ZZ**, Zn finger binding two Zn ions; **UBR**, UBR box; **WD40**, domain with β -propeller architecture that functions in protein-protein or protein-DNA interactions; **ARM repeats**, ARMADILLO repeats implicated in signal transduction processes; **AI**, predicted autoinhibitory domain; **PHD**, plant homeodomain finger. The figure was modified from Tasaki et al. (2012) and domain information of BIG and PRT7 was obtained from the InterPro protein sequence analysis tool at <https://www.ebi.ac.uk/interpro>.

Next to *PRT6* and *BIG*, a third gene containing a UBR box signature was found in the *Arabidopsis* genome, denoted *PRT7* (AT4G23860) because of its closest homology to mammalian UBR7 (Fig. 3; Garzon et al. 2007, Taloji 2011, Tasaki et al 2005). Like UBR7, *PRT7* is a PHD finger protein and was therefore suggested to function as an adaptor protein for N-end rule substrate ubiquitination (Fig. 3). However, neither in the case of UBR7 nor *PRT7* a role in the N-end rule has been proven so far.

Five non-UBR box containing N-recognins were described in eukaryotes with largely unrelated domain structures. These include the above mentioned p62 in mouse that is not involved in the UPS but directly links N-end rule recognition to autophagosome targeting (Cha-Molstad et al., 2017; Ji et al., 2019). Another non-UBR N-recognin might be the caspase inhibitor *Drosophila* INHIBITOR OF APOPTOSIS 1 (DIAP1). This RING E3 ligase is subject to N-end rule dependent regulation itself (Ditzel et al., 2003; Tasaki et al., 2012), and was proposed to act as an N-recognin towards alanine- (Ala, A) initiated pro-apoptotic substrates (Green et al., 2004; Ditzel and Meier, 2005). In DIAP1, substrate interactions depend on either of its two BACULOVIRUS INHIBITOR OF APOPTOSIS PROTEIN REPEAT domains. Next, the human proteins ZYG11B and ZER1 act as adaptors within cullin2-based RING E3 complexes to target substrates with N-terminal Gly (Timms et al., 2019).

Finally, the *Arabidopsis* gene *PRT1* was identified as the plant E3 ligase responsible for the degradation of aromatic type II N-end rule substrates using a mutant screen (Bachmair et al., 1993; Potuschak et al., 1998; Stary et al., 2003). The domain architecture of *PRT1* is unprecedented by

other N-recognins and the gene is specific to dicot plants with putative homologs existing in algae, moss, and monocots (Fig. 3; Graciet et al., 2010). The three Zn fingers present in the 46 kDa protein are one canonical RING domain, one composite RING domain containing Zn fingers of the RING and C₃H-type, and a ZZ domain in the C-terminal part of the protein (Potuschak et al., 1998; Tasaki et al., 2012). The activities of PRT1 and PRT6 together account for the destabilizing effect of type I and aromatic type II N-terminal residues in plant cells (Stary et al., 2003; Garzón et al., 2007). However, the aliphatic type II residues Leu and Ile also conferred at least intermediate instability when exposed at a protein's N-terminus in plants (Worley et al., 1998; Stary et al., 2003; Graciet et al., 2010), and in the case of Leu it was shown that this is independent of *PRT1/6* (Garzón et al., 2007). This led to the postulation that plants might possess at least one more active N-recognin (Stary et al., 2003; Garzón et al., 2007; Graciet et al., 2010).

The ubiquitination machineries targeting type I and II N-degrons, and Pro-initiated degrons, are also referred to as the Arg/N-end rule pathways and Pro/N-end rule pathway, respectively (Fig. 4), in order to distinguish them from another branch of the system that recognizes N-terminally acetylated degrons. The latter Ac/N-end rule pathway depends on the acetylation of α -amines by ribosome-associated N-terminal acetyl transferases (NATs) (Hwang et al., 2010b; Lee et al., 2016). Indeed, N ^{α} -acetylation is a prevailing modification in eukaryotic proteomes, with 80-90 percent of human proteins, and 72 percent of the protein body in a plant cell being affected (Bienvenut et al., 2012; Drazic et al., 2016). In contrast to primary destabilizing residues of the Arg/N-end rule, NAT substrates can be created via N-terminal Met excision through the action of methionine aminopeptidases (MetAPs) (Giglione et al., 2015). Although the impact of N ^{α} -acetylation on protein stability has been questioned recently (Kats et al., 2018), loss of NAT function causes multiple phenotypic effects in plants, including pathogen resistance, constitutive abscisic acid (ABA) signaling entailing drought tolerance, and embryo lethality (Gibbs, 2015; Linster et al., 2015; Xu et al., 2015).

1.2.2.1 The N-recognin PRT1

Published in 1993, the first approach towards the isolation of N-recognins from a multicellular organism was conducted using an elaborate genetic screen for *Arabidopsis* mutants impaired in the N-end rule (Bachmair et al., 1993). Andreas Bachmair and colleagues expressed a reporter construct of dihydrofolate reductase (DHFR) that conferred resistance towards the drug methotrexate, but was constitutively short-lived *in planta* due to the exposure of N-terminal Phe by means of the UFT (Bachmair et al., 1993). A mutagenized population of this "4H" denoted transgenic *Arabidopsis* line yielded a complementation group of six seedlings with methotrexate resistance and the locus was referred to as *prt1*. Within these individuals, *prt1-1* was shown to contain higher protein levels of DHFR. The according gene was later mapped to a RING- and ZZ-finger containing open reading frame (ORF) and the gene was designated *PRT1* (Potuschak et al., 1998). Final proof of *PRT1* encoding a plant N-recognin was provided by the heterologous expression of *PRT1* in yeast *ubr1 Δ* and reconstitution of the ability of these cells to degrade reporter proteins initiated by aromatic (but not aliphatic or basic) residues (Stary et al., 2003). The specificity of PRT1 for aromatic N-termini was further supported *in planta* by the comparison of protein steady-state levels of reporters with different N-termini stably expressed in the *prt1-1* mutant or wildtype (WT) background (Stary et al., 2003; Garzón et al., 2007).

Although PRT1 is overall sequentially unrelated to any other N-recognin, Potuschak et al. (1998) noted that the 410 amino acids peptide shows weak similarity to a protein from *S. cerevisiae*, RADIATION SENSITIVE 18 (Rad18p). This E3 Ub ligase is involved in post-replication DNA repair and targets the sumoylated form of PCNA for mono-ubiquitination (Bailly et al., 1997; Hoege et al., 2002). As does PRT1, Rad18p exhibits more than one Zn finger, including a canonical RING domain and a RAD18-type Zn finger that was implicated in DNA-binding (Jones et al., 1988a). However, the CCHC-type motif found in the Rad18-Zn finger does not occur in any of the PRT1 domains (Potuschak et al., 1998) which all contain eight potential Zn ligand residues (i.e., Cys or His). Indeed interesting in the light of PRT1 resemblance is the notion that Rad18p operates as a heterodimer in complex with Rad6p (Bailly et al., 1997; Potuschak et al., 1998; Miyase et al., 2004; Notenboom et al., 2007), a Ub conjugating enzyme (Jentsch et al., 1987) essential for N-end rule dependent degradation in yeast (Dohmen et al., 1991). Rad6p homologs exist in *Arabidopsis* (Sullivan et al., 1994; Zwirn et al., 1997), but so far, no particular E2 enzyme has been linked to N-end rule degradation in plants, nor have PRT1-E2 interactions been reported.

Since the RING domains are less likely to be involved in specific N-degron recognition, it was speculated that the ZZ domain (assigned to residues 303-370 of the PRT1 amino acid sequence by Legge et al. (2004)) could mediate substrate recognition (Stary et al., 2003). This assumption was strengthened by Tasaki et al. (2005) who found weak resemblance between the ZZ domain of PRT1 and parts of the UBR box motif. Finally, the recent structure resolution of the ZZ domain of p62 in complex with several N-degrons again emphasized the potential of PRT1's ZZ sequence for N-degron substrate binding (Kwon et al., 2018). In p62, the key residue aspartic acid (D, Asp) 129 formed a hydrogen bond with the α -amino group of the substrate and was essential for substrate interaction. This residue was found to be conserved in the UBR box as well as in the ZZ domain of PRT1 by Asp-312 (Kwon et al., 2018). Furthermore, according to the authors, the hydrophobic side chains of Val-316 and/or Ile-333 in PRT1 might correspond to p62's Ile-127 which helps to properly orient the side chain of the substrate's N-terminal residue on the binding surface. Nevertheless, biochemical evidence for the contribution to substrate recognition by any of the Zn fingers found in PRT1 is lacking to date.

Even though PRT1 was found to be conserved in the plant kingdom and also in Chromalveolata (Graciet et al., 2010), there are only few reports on phenotypic consequences of the loss of PRT1 function. The plant line with the null allele *prt1-1* lacks obvious growth phenotypes under normal conditions (Bachmair et al., 1993). When investigating the role of the N-end rule during germination and seedling establishment in *Arabidopsis*, Holman et al. (2009) rejected a contribution of PRT1 during these developmental stages. In their studies, *prt1* mutants exhibited WT-like sensitivity towards ABA in germination assays, and, in contrast to *prt6* mutants, were not impaired by exogenous sucrose. Interestingly, increased susceptibility towards several plant pathogens was reported for almost all N-end rule mutants in *Arabidopsis*, including *prt1-1* (de Marchi et al., 2016). The study comprised plant infection analyses using *Sclerotinia sclerotiorum*, *Botrytis cinerea*, *Erysiphe cruciferarum*, and virulent as well as avirulent strains of *Pseudomonas syringae*. Interestingly, in the case of *prt1-1*, the response towards the necrotrophic fungus *B. cinerea* was normal, in contrast to infection by the necrotroph *S. sclerotiorum*, indicating distinct defense mechanisms against relatively similar pathogens. Notably, some of the results obtained by de Marchi et al. (2016) were recently contradicted by another study that proposed higher resistance of N-end rule mutants towards *P. syringae* virulent and avirulent strains (Vicente et al., 2019). However, *prt1-1* plants were not included in this latter study. The overall mild phenotypes of the *prt1-1* mutant plant are

surprising, assuming a potentially high number of PRT1 substrates generated by proteolytic activity in the cell (Venne et al., 2015; Dissmeyer et al., 2018), and given the dramatic effect of the mutation on the stability of artificial N-end rule reporters which contradicts gene redundancy. Thus, the physiological role of the gene and molecular functions on the substrate level might become apparent only under more specific conditions than previously applied.

1.2.3 Secondary destabilizing N-termini

Some N-terminal amino acids confer short half-lives to proteins even though these residues are not targeted directly by N-recognins (Varshavsky, 1992). This phenomenon was attributed to enzymatic processing of N-termini already early during the discovery of the N-end rule pathway, prompted by the observation that the degradation of such proteins required tRNA (Ciechanover et al., 1985; Bachmair et al., 1986; Ferber and Ciechanover, 1987). Conserved among eukaryotes, arginyl-tRNA protein transferases (ATEs) catalyze the tRNA-dependent ligation of Arg to free α -amines of negatively charged residues such as glutamic acid (E, Glu) and Asp (Ciechanover et al., 1988; Elias and Ciechanover, 1990). With Arg being a primary destabilizing residue, this renders Glu and Asp ultimately destabilizing as well, establishing the term of secondary destabilizing N-termini within a hierarchical concept of the N-end rule (Fig. 2,4).

Little is known mechanistically about the reaction catalyzed by ATEs. Due to the usage of preactivated arginyl-tRNA, the reaction is independent of ATP (Wang et al., 2011a). It was proposed that the linkage occurs in a way comparable to the ribosomal reaction by the formation of a peptide bond between the N-terminally exposed amino group of the substrate protein and the carboxyl group of the Arg-tRNA (Soffer and Hoehinshi, 1969; Wang et al., 2014). However, arginylation of ϵ -carboxyl groups on internal residues within proteins, as well as self-arginylation was also reported (Wang et al., 2011a, 2014).

Post-translational arginylation appears to be a relatively frequent feature of eukaryotic proteomes (Wong et al., 2007; Saha and Kashina, 2011). One ATE gene encoding a single isoform of the enzyme was found in yeast (Balzi et al., 1990), and in the moss *Physcomitrella patens* (Schuessele et al., 2016), whereas evolutionarily higher eukaryotes express several isoforms from splicing variants (Kwon et al., 1999; Rai and Kashina, 2005), or, in the case of plants, from different genes (Yoshida et al., 2002). In *Arabidopsis*, the genes encoding the two isoforms ATE1 and ATE2 together account for the full arginylation activity of a protein extract towards an artificial substrate with N-terminal Glu, with *ATE1* providing the much stronger contribution (Graciet et al., 2009). Loss of function of these genes, particularly in combination, entails a series of specific phenotypes in *Arabidopsis*, including delayed leaf senescence (Yoshida et al., 2002), increased sensitivity towards ABA during germination (Holman et al., 2009), decreased apical dominance and changes in leaf and shoot morphology that are promoted by short-day conditions, namely a more frilled and stronger serrated leaf shape and reduced cell elongation in the stem (Graciet et al., 2009), upregulation of genes associated with the low-oxygen (hypoxia) response in an age-dependent way (Gibbs et al., 2011; Licausi et al., 2011; Giuntoli et al., 2017), defects in skoto- and photomorphogenesis (Abbas et al., 2015), and reduced levels of glucosinolates and of the phytohormone JA (here, methyl JA was detected) (de Marchi et al., 2016). JA refers to a class of lipid-derived phytohormones that regulate many aspects of plant development by integration of endogenous and environmental signals, most prominently from biotic

interactions (reviewed in Huang et al. (2017b)). Most of the *ate1 ate2* phenotypes are paralleled by a mutation in the *PRT6* gene, consistent with PRT6 being the E3 ligase responsible for the ubiquitination of ATE products. This phenotypic congruency between *ate1 ate2* and *prt6* also indicates that the main function of plant ATEs is associated with N-end rule degradation, even though mid-chain arginylation might also be catalyzed.

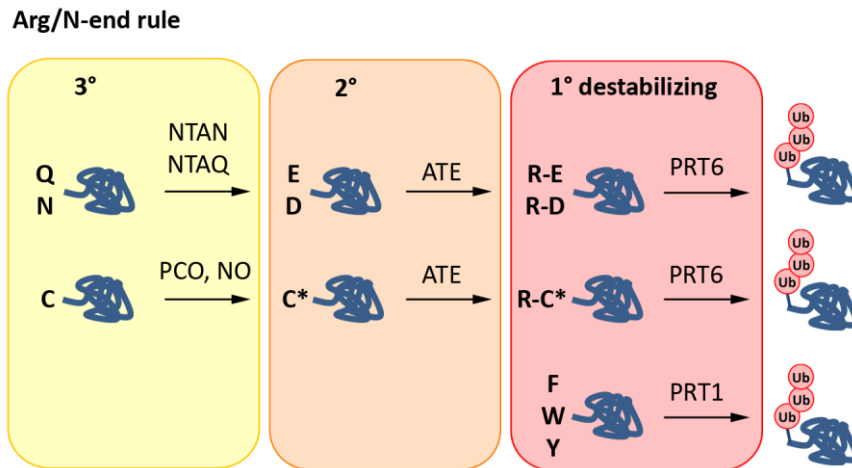


Fig. 4| Structure of the plant Arg/N-end rule. Tertiary (3°) and secondary (2°) destabilizing residues at a protein N-terminus can be transformed into primary (1°) ones by enzymatic processing. The 3° Gln and Asn are deamidated by N-terminal amidases that are specific for either residue (NTAQ and NTAN, respectively) to yield secondary Glu or Asp. N-terminal Cys as a 3° residue is oxidized by PLANT CYSTEINE OXIDASES (PCOs) using oxygen as a co-substrate, in a manner that requires NO *in vivo*. Cys sulfenic acid (C*), together with Glu and Asp, constitute substrates to arginyl-tRNA protein transferases (ATEs) that catalyze the addition of Arg to the N-terminus of the polypeptide. Finally, Arg functions as a type I 1° residue that is recognized and ubiquitinated by the E3 ligase PRT6. In contrast, substrates of the E3 ligase PRT1 are characterized by aromatic N-termini. Here, no progenitor substrates have been identified that would result from enzymatic processing other than peptidase cleavage. Nevertheless, PRT1 and PRT6 activity are both included within the framework of the Arg/N-end rule.

1.2.4 Tertiary destabilizing N-termini

Of the *ate*-mutant phenotypes described above, the constitutive expression of hypoxia-related genes is best understood on the molecular level. A condition of low oxygen availability within plant tissues can occur inside of dense or metabolically active tissues, such as seeds or meristems, or it arises from an external restriction of gas exchange caused by flooding or waterlogging (Drew, 1997; Bailey-Serres and Voesenek, 2008). A rapid acclimation to oxygen limitation counteracting an energetic crisis upon respiratory restriction is crucial for plant survival. Additionally, hypoxia is suggested to function as a developmental signal (Abbas et al., 2015; Weits et al., 2019). Oxygen- and NO sensing in plants is mediated by the N-end rule pathway (Gibbs et al., 2011, 2014a; Licausi et al., 2011). This is achieved by the ability of ATEs to recognize and arginylate Cys at the N-terminus of key transcription factors, but on condition of prior oxygen- and NO-dependent Cys oxidation to Cys-sulfenic acid (CysO₂H) or Cys-sulfonic acid (CysO₃H) (Hu et al., 2005; Gibbs et al., 2011, 2014a; Licausi et al., 2011; Fig. 4). The requirement of Cys-oxidation for ATE-mediated arginylation defines Cys as a tertiary destabilizing residue in mammals and plants.

The plant transcription factors that are controlled by the presence of oxygen and NO in an N-end rule determined way belong to the ERFVIIIs (Gibbs et al., 2011, 2014a; Licausi et al., 2011). There are five members in *Arabidopsis*: RELATED TO AP 2.12 (RAP2.12), RAP2.2, RAP2.3, HYPOXIA RESPONSIVE 1 (HRE1), and HRE2 (Nakano et al., 2006). They were shown to confer hypoxia responses and to improve plant survival under low-oxygen stress (Hinz et al., 2010; Licausi et al., 2010; Lin et al., 2019). Moreover, ERFVIIIs mediate NO-regulation of germination, stomata closure and hypocotyl elongation, as well as sensitivity to exogenous sugars, and storage protein breakdown (Holman et al., 2009; Gibbs et al., 2014a; Zhang et al., 2018c, 2018b). ERFVIIIs are characterized by an N-terminal region that is conserved across plant species over approximately 13 residues, and, spanning all genomes investigated, almost exclusively starts with methionine (M, Met)-Cys (Hinz et al., 2010; Licausi et al., 2010). Using *Arabidopsis* as the model system, it could be proven that ERFVII stability in air depends on the Cys in penultimate N-terminal position, or on *prt6* mutation, whereas upon hypoxic conditions RAP2.12 and HRE2 are stable also in the WT genotype (Gibbs et al., 2011; Licausi et al., 2011). Given these data together with the constitutive expression of ERFVII target genes in *prt6* and *ate1ate2* mutant plants, it was established that the ERFVII transcription factors are processed by MetAPs following translation, N-terminally oxidized at Cys-2 in normoxia, resulting in ATE-catalyzed arginylation, and subsequent PRT6-mediated ubiquitination, eventually suppressing the hypoxic response in oxygen-sufficient conditions. In contrast, under oxygen deprivation, ERFVIIIs are stabilized by the absence of Cys-oxidation, are released from their membrane-tethered binding partner by a yet unknown mechanism, and accumulate in the nucleus to trigger expression of hypoxia-response genes. However, stabilization of any ERFVII proteins in the *ate1 ate2* double mutant has not been shown so far, although constitutive nuclear localization of RAP2.12 was observed in this genetic context (Licausi et al., 2011). This is in contrast to VERNALIZATION 2 (VRN2) which is not a member of the ERFVIIIs, but exposes N-terminal Met-Cys as an oxygen-sensitive N-degron (Gibbs et al., 2018). Protein levels of VRN2 were increased in both *prt6* and *ate1 ate2* mutants, and it was shown that this subunit of POLYCOMB REPRESSIVE COMPLEX 2 (PRC2) improves hypoxia resistance of *Arabidopsis* roots under cold conditions (Gibbs et al., 2018). Next to the ERFVIIIs and VRN2, LITTLE ZIPPER 2 (ZPR2) is a Met-Cys-initiated regulatory protein, abundance of which is controlled by hypoxia via the PRT6-branch of the *Arabidopsis* N-end rule pathway (Weits et al., 2019). It was shown that within the hypoxic niche of shoot meristems, N-end rule control of ZPR2 protein levels is involved in the regulation of stem-cell activity and, hence, plant development.

In contrast to higher eukaryotes, Cys is stabilizing as an N-terminal residue in yeast, suggesting that Cys oxidation might not take place in yeast cells (Bachmair and Varshavsky, 1989). This phenomenon was attributed to the lack of NO synthase genes in the organism. However, this explanation is insufficient after Cys oxidation has been discovered in plants where the existence of NO synthases is also under debate (Santolini et al., 2017), and given the finding that significant levels of NO can arise from other sources such as nitrate reductase (Yamasaki and Sakihama, 2000; Planchet et al., 2005; Astuti et al., 2016; Santolini et al., 2017). Hence, Cys oxidation was considered an enzymatic rather than uncatalyzed reaction, involving further enzymes that might be unique to higher eukaryotes (Kwon et al., 2002). Consistently, a protein family comprising five members were identified as the enzymes responsible for N-terminal Cys-oxidation of ERFVIIIs in *Arabidopsis* and termed PLANT CYSTEINE OXIDASEs (PCO1–5) (Weits et al., 2014). Mutation of *PCO1* and *PCO2* resulted in constitutive expression of hypoxia response genes and stabilized the RAP2.12 protein in normoxic conditions (Weits et al., 2014), whereas overexpression of either gene impaired survival of submergence in the dark. *PCO* transcripts were themselves upregulated upon hypoxia, whereby

induction of *PCO* genes depended on the functionality of the respective gene, indicating a feedback mechanism of *PCO* activity on their own transcript levels. Moreover, it was shown that purified *PCOs* were able to oxidize N-terminal (but not internal) Cys on di- and penta-peptides in an O_2 -consuming manner (Weits et al., 2014). The dependence of the reaction on molecular oxygen as a co-substrate and the target specificity prompted the authors to postulate *PCOs* as the long sought-after direct oxygen sensors in plants. The mechanism was proposed to be the plant-specific N-end rule equivalent of the mammalian oxygen sensory system: Here, internal Pro residues of the HYPoxIA INDUCIBLE FACTOR 1 α (HIF-1 α) are oxidized by prolyl-hydroxylases, enabling the recognition and ubiquitination of the transcriptional activator complex HIF by a cullin-based E3 complex (Wang et al., 1995; Maxwell et al., 1999; Lando et al., 2003).

Unlike Cys which is only destabilizing as an N-terminus in higher eukaryotes (see above), glutamine (Gln, Q) and asparagine (Asn, N) are tertiary destabilizing residues yielding ATE substrates in all eukaryotic systems investigated so far (Fig. 2; Bachmair et al., 1986; Gonda et al., 1989; Baker and Varshavsky, 1995; Ditzel et al., 2003; Graciet et al., 2010). Although these residues prohibit for initiator-Met excision when present in the second position, Gln- and Asn-starting fragments were shown to be generated by protease activity and to constitute N-end rule substrates. This was exemplified by the 15 kDa autocatalytic cleavage fragment of mammalian Usp1 that starts with Gln (Piatkov et al., 2012b), as well as for the Asn-initiated caspase product of *Drosophila* DIAP1 (Ditzel et al., 2003; compare to section 1.2.2). N-terminal processing of Gln- and Asn-starting fragments is performed by N-terminal amidases (NTAs). In yeast, Nta1 indifferently deamidates both residues (Baker and Varshavsky, 1995), whereas mammals and plants contain specific enzymes for each N-terminus, denoted NTAN1 and NTAQ1 for Asn and Gln, respectively (Grigoryeva et al., 1996; Wang et al., 2009a; Graciet et al., 2010; Vicente et al., 2019). Little is described on specific phenotypic consequences of *NTA* deletion. However in mice, homozygous knock-out of *NTAN1* resulted in physically normal, but socially recessive individuals (Kwon et al., 2000). In *Arabidopsis*, a function of NTAQ1 in basal pathogen resistance was recently proposed (Vicente et al., 2019), and a fragment of a putative AAA-type ATPase starting with Gln was reported to be deamidated and subsequently arginylated in *P. patens* (Hoernstein et al., 2016).

1.3 Male gametogenesis in *Arabidopsis*

The life cycle of most angiosperm plants culminates in the production of a hermaphroditic flower that gives rise to male and female gametophytes (Gifford and Foster, 1989). The female gametophyte is formed in the ovary of the carpel and is retained at the sporophytic organism. The male gametophyte, in contrast, develops into a passively mobile entity, the pollen grain, that produces two gametes, the sperm cells. Although many flowering plants, including *Arabidopsis*, are able to undergo self-fertilization, dispersal of the pollen grains and subsequent cross-fertilization is mostly responsible for gene flow between populations and works as a major driver of plant evolution (Scheepens et al., 2012). Hence, evolutionary success of a plant species strongly depends on male gametophyte fitness.

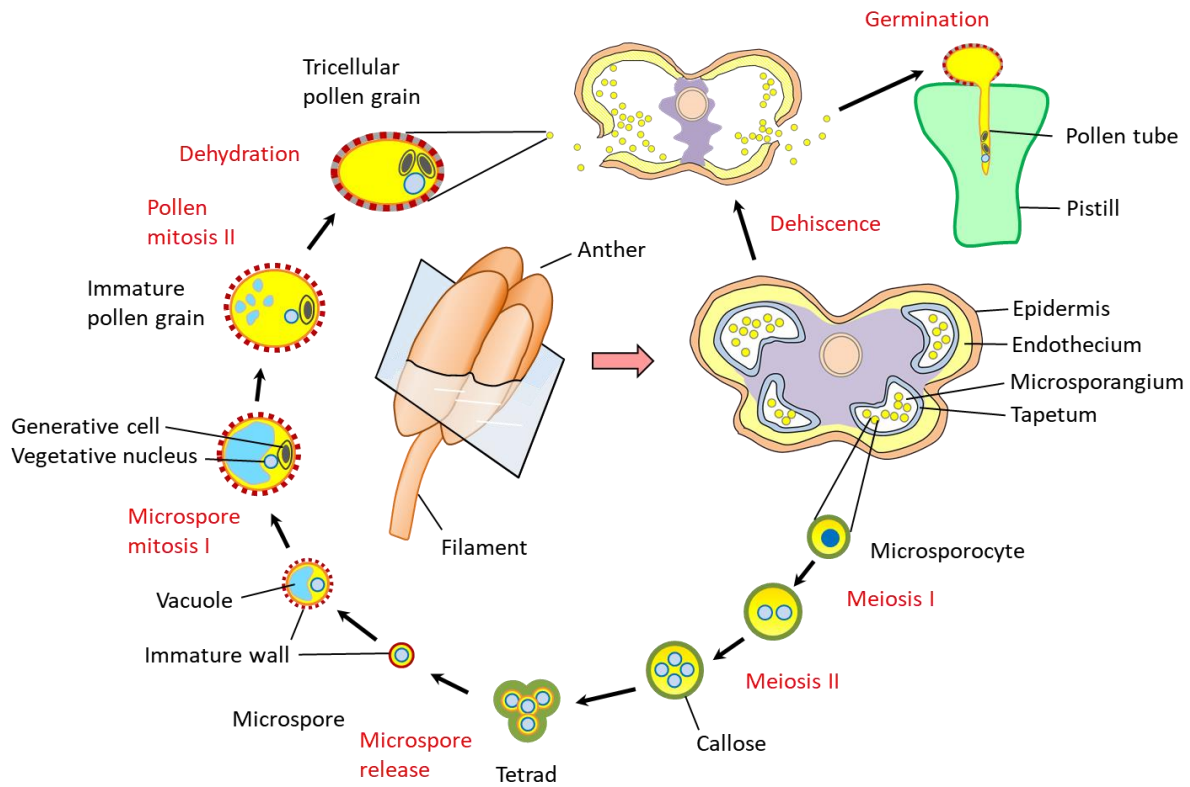


Fig. 5 | Development of the male gametophyte in angiosperms. The stamen consists of filament and anther and is the site of male gametogenesis in flowering plants. Each of the four anther lobes contains one microsporangium that is surrounded by a sporophytic tissue, the tapetum. The four microsporangia are connected by the connective (violet), while the anther wall is formed by an outer epidermis, an inner cell layer called endothecium, and a middle layer (not shown). The gametophytes originate from diploid microsporocytes which undergo two meiotic divisions to form haploid cells clustered inside a callose-bound structure, called a tetrad. Upon tapetal callase activity, the four cells are released into the microsporangium as microspores. The microspores are surrounded by a microfibrillar polysaccharide matrix, the primexine, which is already encrusted by a scaffold of sporopollenin, called the sexine, composed of bacula (red) and later also tecta. An asymmetric mitosis yields a bicellular structure composed of a large vegetative nucleus and a generative cell that, depending on the plant species either within the anther or during pollen tube growth, undergoes a second mitosis to give rise to a tricellular pollen grain. Microspore and pollen maturation further include vacuolization, size increment, pollen wall maturation, and final dehydration. Dehiscence requires a degenerative program that culminates in the breakage of the stomium area of the epidermis. Upon contact with the stigma of the female reproductive organ (pistil), the pollen grain rehydrates. During germination, the pollen tube protrudes through apertures of the pollen wall to deliver the two sperm cells to the embryo sac. For details and references, see main text. The figure was inspired by Goldberg et al. (1993) and Buchanan et al. (2002a).

In all plants, male reproductive processes initiate with the formation of stamen primordia in the third whorl of the flower meristem prior to the production of carpel primordia (Goldberg et al., 1993). This is regulated by a network of homeotic genes and a central MADS-box transcription factor, NOZZLE/SPOROCTELESS (NZZ/SPL), in *Arabidopsis* (Goldberg et al., 1993; Schiefthaler et al., 1999; Yang et al., 1999; Ito et al., 2004; Liu et al., 2009), but differences exist in monocots (Walbot and Egger, 2016). Early during flower development, the stamen primordia differentiate into the stem-like filament and the anther tissues (Fig. 5). The anther is a four-lobed compartment that is built up by a number of highly specialized cell types with generative and non-generative fates. At least four cell types can be distinguished that belong to the sporophytic part of the anther (from outside to inside): Epidermis, endothecium, middle layer, and tapetum (Goldberg et al., 1993). Of these, the epidermal cell layer and the subjacent endothecium make up most of the anther wall. Next to structural

support, the function of the endothecium involves secondary thickening and lignocellulosic deposition during final anther maturation which is required for anther opening, termed dehiscence (Wilson et al., 2011). Moreover, the endothecium was recently found to contribute to the production of very-long-chain fatty acid lipids via expression of *ECERIFERUM 2 (CER2)* and particularly *CER2-LIKE 2 (CER2L2)*, a function that is essential for pollen rehydration prior to germination on the stigma (Zhan et al., 2018).

Each of the four anther lobes contains a microsporangium (also: pollen sack or locule) inside of which the gametophytes are produced (Fig. 5). The sporophytic cell layer enclosing the microsporangium is called the tapetum. Tapetal cells are in direct contact with the germ cells and are separated from the endothecium only by a thin middle layer with mainly structural and some regulatory functions (Mascarenhas, 1990; Goldberg et al., 1993; Cecchetti et al., 2017). The nutritive locular fluid inside the microsporangia is secreted by the tapetum (Pacini et al., 1985). High rates of nucleic acid and protein biosynthesis inside the tapetum, together with the requirements for locular fluid production, bring about an extremely high energy demand of tapetum cells. Hence, this tissue is particularly sensitive to starvation conditions induced by adverse conditions (Liu and Dickinson, 1989; Parish et al., 2012).

One of the first tasks of the tapetum during gametogenesis is the production of callase required for postmeiotic microspore release (Stieglitz, 1977). Since callase is stored in the vacuoles prior to secretion, tapetum vacuolization is observed in a fashion strictly coordinated with the progression of gametogenic meiosis (Sanders et al., 1999; Wu and Yang, 2005; Wan et al., 2010). During later development, the tapetum provides pollen wall components to the inside of the microsporangia, including pigments and precursors for complex structural polymers such as sporopollenin (Heslop-Harrison, 1962; Pacini et al., 1985; Piffanelli et al., 1998; Wang et al., 2018b). Sporopollenin makes up the major component of the extraordinarily resistant outer pollen wall layer, the exine (Bedinger, 1992; Piffanelli et al., 1998). The exact chemical composition of this terpene-based biopolymer remains cryptic, but it is assumed to contain phenolics, aromatics, and long-chain-fatty acids (Piffanelli et al., 1998; Ariizumi and Toriyama, 2011). During later stages of pollen development, the tapetum undergoes programmed cell death, and releases cytoplasmic content to the inside of the locule upon disintegration (Bedinger, 1992; Sanders et al., 1999). This provides further lipids, lipid precursors, flavonoids, and proteins to the developing pollen grains and deposits the lipoidal tryphine layer for final pollen wall maturation (Wu et al., 1997; Hsieh and Huang, 2007; Parish and Li, 2010).

The development of the male gametophyte initiates with the emergence of a diploid microsporocyte (or pollen mother cell) from a sporogenous progenitor cell that also gives rise to a tapetal initial cell (McCormick, 1993; Fig. 5). After two meiotic divisions of the microsporocyte, a tetrad of haploid cells is held together by a wall of callose. These cells are released by tapetal callase activity as uninucleate, free microspores, and are surrounded by remnants of a transiently occurring primexine wall previously embedded in callose (Ariizumi and Toriyama, 2011; Shi et al., 2015). This immature microspore wall is already equipped with sporopollenin-based incipient baculae and tecta. These will later form the extremely resistant sexine layer of pollen exine, a scaffold for pollen coat assembly and the cause of species-specific pollen patterning at the mature stage (McCormick, 1993; Ariizumi and Toriyama, 2011; Quilichini et al., 2014). In a two-phase view of plant male gametogenesis, all cell types of the anther are established at the end of the second meiosis, terminating phase one, and the development switches from a specification- to a rather maturation and dehiscence program

(Goldberg et al., 1993). Soon after release from the tetrads, the spherical microspores start to enlarge and the nucleus moves towards the cell periphery, a process that is accompanied by increasing microspore vacuolization (Bedinger, 1992). At day five after meiosis, an asymmetrical mitosis occurs that produces two cells: A vegetative cell arrested in G1 with highly active chromatin and a much smaller, generative cell that is engulfed by the vegetative cell and is considered as transcriptionally almost inactive (Mascarenhas, 1990; Twell, 1992; McCormick, 1993, 2004; Da Costa-Nunes and Grossniklaus, 2004). Both cells remain surrounded by the microspore wall and the bicellular structure is termed a pollen grain from this stage (Mascarenhas, 1990). Subsequent final pollen maturation includes the production of starch granules, assembly of the strongly hydrophobic pollen coat (or tryphine), deposition of the intine (i.e., the cellulosic innermost layer of the pollen wall), fortification of the nexine called basal layer of the exine, as well as profound dehydration of the pollen grain to an extent dependent on the plant species (Bedinger, 1992; Franchi et al., 2002; Shi et al., 2015).

Pollen grain release, or dehiscence, is timely regulated to optimize either for cross- or self-fertilization (Wilson et al., 2011). Anther opening is achieved by a program consisting of endothecium expansion and lignification, accompanied by the degeneration of a cell layer that separates the two adjacent locules, resulting in a bilocular anther, and ultimate breakdown of a specialized epidermal region that is called “stomium” (Wilson et al., 2011). In all angiosperms, the generative cell undergoes a second mitosis, yielding two sperm cells and one vegetative cell nucleus per pollen grain (McCormick, 1993; Fig. 5). In most cases, this occurs within the growing pollen tube during stigma-pollen interaction. However, in grasses and crucifers (including *Arabidopsis*), the second mitosis of the generative cell takes place already in the anther before dehiscence (McCormick, 2004). The production of pollen with two sperm cells allows for the double fertilization that is characteristic to all flowering plants and gives rise to both embryo and endosperm (Russell, 1992). The delivery of the two sperm cells to the female gametophyte via the pollen tube completes pollen development.

1.3.1 Regulation of pollen development

During anther development, the processes of the sporophyte and the gametophyte are tightly coordinated to allow for faithful gametogenesis (Sanders et al., 1999; Ma, 2005). As a consequence, anther morphology as seen by light microscopy serves as a reference to subdivide gametogenesis into distinct stages. In *Arabidopsis*, 15 anther stages have been ascribed (Sanders et al., 1999), and were found to be largely transferable to other species, with differences concerning for example the timing of tapetal programmed cell death (Fernández Gómez et al., 2015; Browne et al., 2018). Benchmarks of this developmental program include the appearance of pollen mother cells (stage 5), the onset of meiosis (stage 6), the release of microspores (stage 8), the initiation of tapetum degeneration (stage 10), pollen mitotic divisions and endothecium thickening (stage 11), and anther dehiscence at anthesis, the state of flower maturity (stage 13) (Sanders et al., 1999).

An intricate regulatory genetic network is responsible for the development of the male gametophyte, including 607 transcription factors that are transcribed in the course of pollen development and an estimate of 4 to 11 percent of the *Arabidopsis* genome being specifically expressed in pollen (Honys and Twell, 2004; Rutley and Twell, 2015). Investigating male gametophyte molecular functions is challenging, since mutations that affect the gametophyte directly can only be maintained as

heterozygotes, and – in contrast to sporophytic mutations – hardly penetrate to the next generation. An exception is given with mutations that express only conditionally. Identification of gametophytic mutations was nevertheless achieved by, for example, screening mutant collections for segregation ratio distortions, or 4',6-diamidino-2-phenylindole (DAPI) staining of pollen from mutagenized populations (Park et al., 1998; Procissi et al., 2001; McCormick, 2004). Mutants identified by such studies include *duo* (Durbarry, 2005), *sidecar pollen* (Chen and McCormick, 1996), *gemini pollen* (Park et al., 1998), *germ unit malformed*, and *male germ unit displaced* (Lalanne and Twell, 2002), which affect mitotic progression, disturb cell identity adaption upon asymmetric mitosis, affect migration of germ cells, or abolish spatial association of the germ cell with the vegetative cell. Moreover, specific components of the cell cycle control are required for progression through microspore mitoses, including the F-box protein F-BOX-LIKE 17 that mediates degradation of the cyclin-dependent kinase inhibitors KIP-RELATED PROTEIN 6 (KRP6) and KRP7 (Kim et al., 2008; Liu et al., 2008; Gusti et al., 2009; Takatsuka et al., 2015).

Despite progress in male gametophyte research is increasingly facilitated by cell-specific large scale analytic techniques (Borg et al., 2009; Zhang et al., 2017d), sporophytic anther development is much better understood at the molecular level. As one major regulator, the homeotic gene and MADS-box transcription factor AGAMOUS (AG) not only acts upstream of NZZ/SPL in stamen and carpel specification, but also controls later stages of anther development, affecting filament elongation, anther morphology, pollen maturation, and dehiscence (Ito et al., 2004, 2007). The Leu-rich repeat receptor kinase EXTRA SPOROGENOUS CELLS/EXCESS MICROSPOROCTES 1 (EXS/EMS1) controls archesporial cell number, and mutation of the respective gene results in the absence of tapetum, while too many microsporocytes are produced (Canales et al., 2002; Zhao et al., 2002; Jia et al., 2008). These microsporocytes fail to undergo cytokinesis. Next to EXS/EMS1, a plethora of receptor-like protein kinases (RLKs) is engaged in the processes controlling anther cell identity and maturation, underlining the essence of cell-cell communication for synchronizing tissue development during gametogenesis (Cai and Zhang, 2018). Likely downstream of NZZ/SPL and EXS/EMS1, a series of transcription factors mediate developmental progression of the tapetum, each being essential for male fertility. These include the basic-helix-loop-helix transcription factors DYSFUNCTIONAL TAPETUM 1 (DYT1) and ABORTED MICROSPORE (AMS), as well as the PHD transcription factor MALE STERILITY 1 (MS1). While gametophyte development is already impaired during meiotic cytokinesis upon *DYT1* mutation (Zhang et al., 2006), microspore abortion occurs after release from the tetrads in *ams* and *ms1*, due to premature vacuolization and degeneration of the tapetum (Wilson et al., 2001; Sorensen et al., 2003).

Mutations that specifically affect exine formation primarily concern metabolic, rather than signaling enzymes. *SUGARS WILL EVENTUALLY BE EXPORTED TRANSPORTER 8/RUPTURED POLLEN GRAIN 1* (*SWEET8/RPG1*) encodes a sugar transporter located at the plasma membrane of microsporocytes and the tapetum during meiotic stages (Guan et al., 2008; Chen et al., 2010b). It is required for proper callose deposition and primexine development (Sun et al., 2013). Consequently, in the *rpg1* mutant, sporopollenin deposits randomly on the microspores, resulting in microspore degeneration and male sterility (Guan et al., 2008; Sun et al., 2013). Eight genes have been reported to contribute to the synthesis of sporopollenin precursors in *Arabidopsis*, and all of them are expressed in the tapetum (Wang et al., 2018b). Mutations in most of these genes, and also in the presumptive sporopollenin transporter ATP-BINDING CASSETTE G26 (ABCG26), dramatically compromise male fertility (Aarts et al., 1997; Morant et al., 2007; de Azevedo Souza et al., 2009; Grienberger et al., 2010; Kim et al., 2010; Kuromori et al., 2011). Among the sporopollenin biosynthesis genes, *MS2* is

probably the most thoroughly investigated one. It encodes for a fatty acyl reductase that converts palmitoyl acyl carrier protein into a C16:0 fatty alcohol (Chen et al., 2011b). Loss of *MS2* function leads to severe defects in the exine structure, and pollen from *ms2* plants collapse during maturation (Aarts et al., 1997; Dobritsa et al., 2009; Chen et al., 2011b).

Most of the phytohormones, comprising auxin, JA, gibberellic acid (GA), cytokinins, ethylene, and brassinosteroids, have been implicated in the regulation of male fertility (Kieber et al., 1993; Park et al., 2002; Huang et al., 2003a; Cheng et al., 2004; Cecchetti et al., 2008; Ye et al., 2010; Dobritsch et al., 2015). Their effects on stamen development will be outlined in the following, with focus on JA, auxin, and GA which have the strongest reported effect on male gametogenesis in *Arabidopsis*.

1.3.1.1 Jasmonic acid

The before mentioned role of AG in late anther development was attributed in parts to the activation of the gene DEFECTIVE ANther DEHISCENCE 1 (*DAD1*) (Ito et al., 2007). *DAD1* encodes for a phospholipase A1 that catalyzes an initial step in JA biosynthesis during anther development, the release of α -linolenic acid from plastidial lipids desaturated by FATTY ACID DESATURASE 3 (*FAD3*), *FAD7*, and *FAD8* (McConn and Browse, 1996; Ishiguro et al., 2001). In the *dad1* T-DNA insertion mutant line, JA and methyl JA levels are reduced by almost 80 percent compared to the WT in flower buds (Ishiguro et al., 2001). Although otherwise phenotypically normal, *dad1* is male sterile and exhibits delayed anther dehiscence and inviable pollen (Ishiguro et al., 2001). Gametophyte development is compromised in this mutant at postmitotic stages. This is in agreement with an important role of JA during late stamen development in *Arabidopsis* and a peak of JA concentrations in flowers immediately before anther dehiscence (Nagpal et al., 2005; Song et al., 2013). As for *dad1*, a male-sterile phenotype was described for *Arabidopsis* lines with mutations in many of the genes involved in JA biosynthesis or signaling, including the triple mutant *fad3 fad7 fad8* (McConn and Browse, 1996), the double mutant of the 13-LIPOXYGENASE (*LOX*) genes *LOX3* and *LOX4* (Caldelari et al., 2011), the ALLENE OXIDE SYNTHASE (*AOS*) gene (Park et al., 2002; Von Malek et al., 2002), the gene encoding the peroxisomal 12-OXOPHYTODIENOATE REDUCTASE 3 (*OPR3*) (Sanders et al., 2000; Schaller et al., 2000; Stintzi and Browse, 2000), and the signaling mutant *coi1* (Feys et al., 1994; Xie et al., 1998). *COI1* encodes the F-box protein (Xie et al., 1998; Xu et al., 2002) that serves as the JA (JA-Ile) receptor (Katsir et al., 2008b; Fonseca et al., 2009; Yan et al., 2009), and triggers JA responses by destabilization of the JA ZIM-domain (JAZ) transcriptional repressors (Chini et al., 2007; Thines et al., 2007; Yan et al., 2007). As direct targets of JAZ proteins, the R2R3-MYB transcription factors MYB21, MYB24, and MYB57 mediate JA responses in stamens (Mandaokar et al., 2006; Cheng et al., 2009; Song et al., 2011; Qi et al., 2015; Huang et al., 2017a). Consistently, the T-DNA null mutant *myb21-1* is also infertile and the phenotype is exacerbated by additional mutation of *MYB24* (Mandaokar et al., 2006). As for *coi1* and in contrast to JA biosynthesis mutants, sterility of *myb21-1* or *myb21 myb24* cannot be rescued by exogenous JA application (Sanders et al., 2000; Stintzi and Browse, 2000; Mandaokar et al., 2006). However, there are some further phenotypical differences between the JA mutant lines concerning the manifestation of male sterility. For example, *dad1* shows delayed but successful filament elongation, but fails to produce viable pollen (Ishiguro et al., 2001). In contrast, the major cause of the sterility of *myb21-1* appears to be the complete failure of filament elongation, since the pollen produced is viable (Mandaokar et al., 2006). For *coi1* mutants, a combination of short filaments and inviable pollen was reported (Feys et al., 1994; Ellis and Turner,

2002). Thus, JA signaling in *Arabidopsis* stamens appears to have specialized outputs, potentially depending for example on the source of JA and the tissue of perception (Jewell and Browse, 2016). Furthermore, two members of the ABCG transporter family, ABCG1 and ABCG16, were found to be required for postmeiotic microspore development (Yadav et al., 2014; Yim et al., 2016). The *abcg1 abcg16* double mutant displayed abnormalities in the tapetal cells, defects in pollen mitosis, and failed to form nexine and intine layers (Yim et al., 2016). Lipidic and phenolic compounds that constitute sporopollenin precursors were speculated as the potential cargo for these transporters. However interestingly, a more recent report attributed a function to ABCG16 as a JA-Ile transporter for cellular export and nuclear import, required for activating JA signaling (Li et al., 2017c).

JA biosynthetic and signaling pathways are conserved in other plant species, and JA is involved in the regulation of reproductive development in plants others than *Arabidopsis* (Li et al., 2004; Katsir et al., 2008a; Yan et al., 2012). However, the specific function and timing of JA action during flower development differs considerably between species (Li et al., 2001b, 2004; Acosta et al., 2009; Cai et al., 2014; Dobritsch et al., 2015). For example, a JA insensitive mutant of tomato (*Solanum lycopersicum*) is sterile and produces pollen of low viability, but the main cause of the sterility is an arrest of embryo maturation, apparently caused by a defect of the female gametophyte (Li et al., 2001b, 2004).

1.3.1.2 Gibberellic acid

JA biosynthetic genes, namely *DAD1* and *LOX1*, are upregulated by another plant hormone, GA, in *Arabidopsis* (Cheng et al., 2009). Since also *AG* is required in this pathway (Ito et al., 2007), and GA-deficient mutants show reduced *AG* expression (Yu et al., 2004), GA might actually act upstream of both *AG* and JA in filament elongation and anther growth (Cheng et al., 2009). Aside, or prior to regulating JA synthesis, GA operates during relatively early stages of anther development (Hu et al., 2008). Thus, GA synthesis or signaling mutants in *Arabidopsis* and other species exhibit an arrest of gametogenesis already before or during mitoses (Jacobsen and Olszewski, 1991; Izhaki et al., 2002; Cheng et al., 2004; Griffiths et al., 2006; Hu et al., 2008). Furthermore, GA controls pollen tube growth (Singh et al., 2002; Chhun et al., 2007), and in rice, also tapetum development is aberrant in GA-deficient and -synthesis mutants (Aya et al., 2009).

1.3.1.3 Auxin

Auxin, predominantly indole-3-acetic acid (IAA), controls most aspects of plant development by regulating cell proliferation, expansion, and differentiation (Chapman and Estelle, 2009; Vanneste and Friml, 2009; Zhao, 2010; Korver et al., 2018). Auxin distribution and occurrence in stamens has been thoroughly investigated (Aloni et al., 2006; Feng et al., 2006; Cecchetti et al., 2008, 2013). It accumulates in the sporophytic tissues of the anther and in the filament during premeiotic stages, and peaks during meiosis in the anther, including microspores, whereas the activity of an auxin reporter in the filament is low at this stage. During microspore maturation, auxin levels are highest in the microspores and the tapetum. After mitoses, auxin is almost not detected in the anthers anymore, but it is highly abundant at the upper filament and anther-filament procambium. Auxin is required for filament elongation, timing of endothecium lignification and dehiscence, and microspore

mitotic progression during male gametogenesis. This was first inferred from the phenotypes of plants mutated in the *YUCCA* (*YUC*) genes, encoding flavin monooxygenases that catalyze the rate-limiting step of auxin biosynthesis from Trp (Zhao et al., 2001; Cheng et al., 2006). Among the eleven *YUC* members, *YUC2* and *YUC6* are most specifically expressed in stamens (Cheng et al., 2006; Cecchetti et al., 2008). The double mutant *yuc2 yuc6* exhibits short filaments, delayed anther maturation, and is almost completely sterile due to an arrest of microspore development before mitosis (Cheng et al., 2006; Yao et al., 2018). The expression of *YUC2* and *YUC6* in anthers is paralleled by the genes encoding the auxin receptor F-box proteins TIR1 and AFB1-3 (Cecchetti et al., 2008). The quadruple mutant *tir1 afb1 afb2 afb3* produces fertile flowers, but anther development occurs precociously. Next, filaments of the receptor quadruple mutant are shorter than in the WT which is here nevertheless compensated for by a likewise reduction in pistil length (Cecchetti et al., 2008). Almost the same phenotype is also observed upon simultaneous mutation of the genes *MULTIDRUG RESISTANCE 1* and its homolog *P-GLYCOPROTEIN 1*, a genetic situation which disturbs auxin basipetal distribution (Noh et al., 2001). The premature anther dehiscence in *tir1 afb2 afb3* was ascribed to early expression of *MYB26*, as well as a twofold increase in JA levels in flower buds compared to WT, coinciding with significantly higher than WT transcript levels of *DAD1* and *OPR3* at the mitotic stage (Cecchetti et al., 2013). However contrarily, AUXIN RESPONSE FACTOR 7 (ARF7) and ARF8 were shown to contribute to the activation of JA synthesis genes, including *LOX2*, *AOS*, and *OPR3*, and JA levels were strongly reduced in the respective double mutant plants (Nagpal et al., 2005). Hence, auxin might regulate JA biosynthesis differentially throughout several stages of flower maturation in order to coordinate stamen developmental processes. Revealing yet another process that is subject to auxin-mediated regulation during male gametogenesis, a mutation in *ARF17* entails male sterility that is caused by abnormal callose biosynthesis during tetrad formation, and subsequent failure to deposit primexine and exine (Mallory et al., 2005; Yang et al., 2013). These microspores become vacuolated and are degraded after release from the tetrads. Yang et al. (2013) could show that ARF17 directly binds to the promoter of *CALLOSE SYNTHASE 5*, a gene essential for tetrad callose synthesis (Dong et al., 2005).

1.3.1.4 Other phytohormones

Brassinosteroids and their growth-promoting effect were first discovered and isolated from oilseed rape (*Brassica napus* L.) pollen (Grove et al., 1979). Mutations affecting brassinosteroid synthesis and signaling in *Arabidopsis* result in pleiotropic phenotypes, including severe dwarfism, delayed flowering, photomorphogenesis in darkness, and male sterility (Szekeres et al., 1996; Choe et al., 1998; Bouquin et al., 2001; Li et al., 2001a; Kim et al., 2005; Ariizumi et al., 2008; Xing et al., 2013). Sterility in these mutants is mainly caused by reduced filament elongation, abnormal tapetum and microspore development, and defects in primexine and exine formation preventing pollen dispersal upon dehiscence (Ariizumi et al., 2008; Ye et al., 2010). Moreover, brassinosteroids were shown to promote pollen tube growth (Szekeres et al., 1996; Vogler et al., 2014). The effects of brassinosteroids on anther development were partially explained by direct regulation of anther gene expression, including the promoters of *NZZ/SPL*, *MS1*, and *MS2*, by the central transcription factor of the brassinosteroids signaling pathway, BRI1-EMS SUPPRESSOR 1 (BES1) (Ye et al., 2010).

Evidence for the involvement of cytokinin signaling in male gametogenesis arises mostly from the phenotypes of higher order mutants of cytokinin receptors. Simultaneous mutation in three of the

ARABIDOPSIS HISTIDINE KINASEs (AHK), *ahk2-1 ahk3-1 ahk4-1*, leads to defects in several organs, but structurally regular flowers which are nevertheless male sterile (Nishimura et al., 2004). Analysis of the triple mutant *cytokinin response1-12 (cre1-12) ahk2-2tk ahk3-3* revealed a sporophytic function of cytokinin perception, since the mutant showed incomplete tapetum degeneration and failed to dehisce (Kinoshita-Tsujimura and Kakimoto, 2011). Furthermore, it was reported that a reduction of cytokinin levels by genetic engineering greatly diminished the amount of pollen produced in *Arabidopsis* (Werner et al., 2003), and yielded male-sterile maize (*Zea mays*) plants upon a similar approach (Huang et al., 2003a). Recently, it was also presented that exogenous treatment of *B. napus* with the synthetic cytokinin N⁶-benzylaminopurine (BA) affected filament elongation and anther maturation (Zuñiga-Mayo et al., 2018).

Ethylene is not described to be directly involved in stamen development in *Arabidopsis*, although ethylene-dependent regulation of anther dehiscence has been proposed (Scott et al., 2004; Wilson et al., 2011). These postulations are mostly driven by the observation that in *Solanaceae*, ethylene plays an important role for the progression through the second phase of anther development, facilitating dehiscence and pollen release (Rieu et al., 2003; Dobritsch et al., 2015). In these species, JA was found to prohibit premature anther dehiscence by repressing ethylene gene expression (Dobritsch et al., 2015).

1.4 The phytohormone ethylene

1.4.1 Impact of ethylene on plant physiology

Gaseous ethylene is the smallest molecule among the phytohormones and its signaling function has an ancient origin that is conserved back to charophyte algae (Ju et al., 2015). Acting throughout the plant life cycle, ethylene regulates seed dormancy and germination, impacts differentially on growth and morphology, triggers organ senescence, and signals during biotic and abiotic stress conditions (Bleecker and Kende, 2000). Of huge agronomical importance is the capacity of ethylene to regulate organ abscission and fruit ripening of crops such as apples, tomatoes, and bananas (Harvey, 1928; Bleecker and Kende, 2000; Payasi and Sanwal, 2010). The dramatic effect that ethylene can exert on plant growth and morphology is prominently demonstrated in an assay using dark-grown seedlings. Here, the absence of light causes germinating seedlings to adopt the typical etiolated morphology (i.e., skotomorphogenesis), including a massively elongated hypocotyl, small and closed cotyledons, lack of chlorophyll production, and formation of an apical hook that is believed to protect the cotyledons during passage through the soil (Fig. 6A; McNellis and Deng, 1995; von Arnim and Deng, 1996; Josse and Halliday, 2008). The impact of ethylene during skotomorphogenesis was first observed in seedlings of pea (*Pisum sativum*) more than a century ago: Treatment with illumination gas triggered a growth inhibition, stem swelling, and hypocotyl bending towards horizontal growth, a phenomenon that was referred to as the “triple” response (Fig. 6A; Neljubov, 1901; Beyer, 1976).

In etiolated *Arabidopsis* seedlings, the response to ethylene was found to be slightly different, comprising inhibition of root and hypocotyl elongation, hypocotyl and root radial swelling, and an exaggeration of the apical hook curvature (Fig. 6A; Ecker, 1995). Deployment of the triple response assay in forward genetic screens of *Arabidopsis* has enabled the identification of at least 16 loci associated with ethylene production or perception (Bleecker et al., 1988; Guzmán and Ecker, 1990;

Van Der Straeten et al., 1993; Kieber et al., 1993; Roman et al., 1995; Lehman et al., 1996; Chao et al., 1997; Sakai et al., 1998; Solano et al., 1998; Alonso et al., 1999; Alonso and Ecker, 2001).

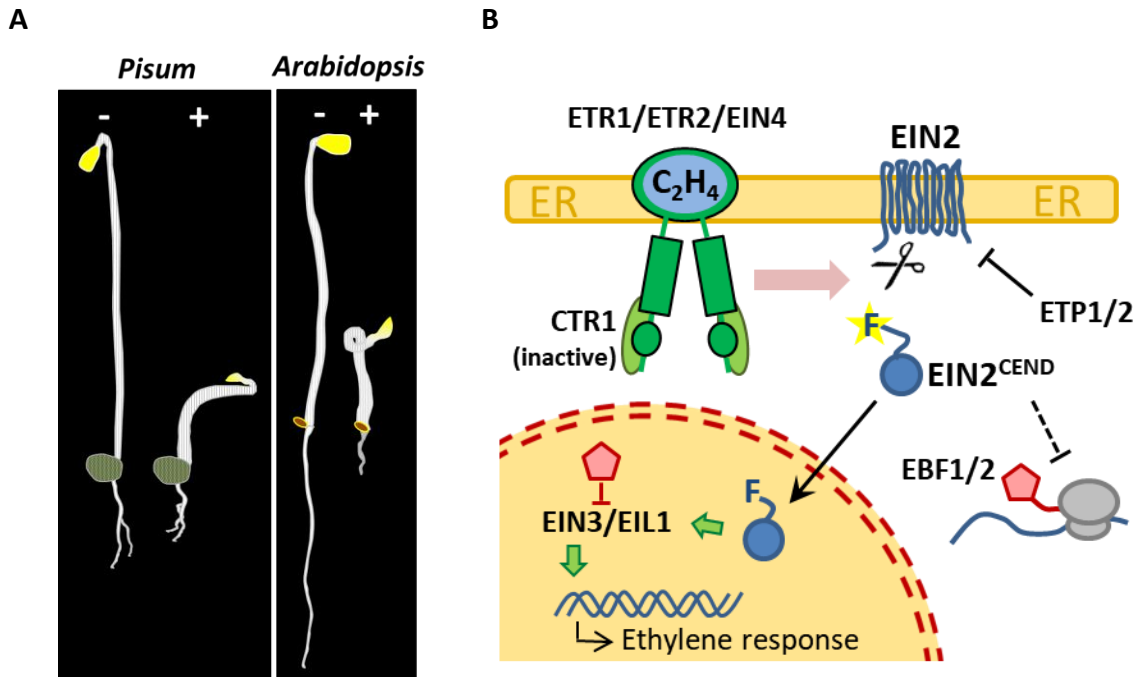


Fig. 6 | Ethylene modulates plant growth and morphology through a complex signaling network. A, The triple response assay monitors the changes in morphology that are elicited by ethylene during dark-growth of dicotyledonous seedlings. In control conditions (-), seedlings exhibit elongated hypocotyls and modest apical hook formation; in contrast, upon supplementation with ethylene gas or the ethylene precursor substance ACC (+), hypocotyl and root elongation are repressed, stem and root swelling is induced, and agravitropic growth behavior is triggered that takes different shapes depending on the plant species. These changes occur in a dose-dependent manner. **B,** Ethylene (C₂H₄) is perceived in the ER membrane by binding to homo-dimeric receptors such as ETR1, ETR2, and EIN4. The C-terminal His kinase-like domains and receiver domains of these receptors interact with the Raf-like kinase CTR1 that targets the cytosolic C-terminal domain of the ER-resident protein EIN2 in the absence of ethylene. Upon hormone binding to the receptors, phosphorylation of EIN2 is abolished, resulting in the cleavage of EIN2 by an unknown endopeptidase, and release of a soluble signaling fragment initiated by Phe-646 of EIN2, denoted as EIN2 CEND. In the cytosol, EIN2 CEND interferes with translation of the F-box proteins EBF1 and EBF2 which are responsible for ubiquitination of the ethylene response transcription factors EIN3 and EIL1. Additionally, EIN2 migrates to the nucleus and facilitates EIN3/EIL1 function on target promoters. Full-length EIN2 protein is itself negatively regulated by the F-box proteins ETP1 and ETP2.

Consistent with cotyledon and root shortening within the triple response of etiolated seedlings, ethylene was characterized as a general inhibitor of growth (Dubois et al., 2018), and it was found that this effect was due to ethylene action mainly at the site of the epidermis (Vaseva et al., 2018). In line with this view, mutations that impair ethylene signaling often result in larger rosettes and bigger leaf area of *Arabidopsis* plants (Guzmán and Ecker, 1990; Feng et al., 2015; Rai et al., 2015). The increase in leaf area was explained by an increase in both cell number and size when ethylene signaling is blocked (Feng et al., 2015; Rai et al., 2015). Conversely, *Arabidopsis* lines that exhibit ethylene overproduction (*eto*), or have constitutively active ethylene responses, show dwarf phenotypes (Guzmán and Ecker, 1990; Kieber et al., 1993; Qu et al., 2007; Rai et al., 2015). Moreover, ethylene was reported to be associated with osmotic stress-induced cell cycle arrest (Skirycz et al., 2011), and to inhibit cell proliferation of the root meristem cooperatively with cytokinin (Street et al., 2015).

On the other hand, various studies have also established a growth-stimulating effect of ethylene, depending on the treatment conditions, the tissue of perception, or the plant species. For example, when grown in the dark, rice coleoptile growth is promoted by ethylene, in contrast to what is seen in dicotyledonous seedlings (Yin et al., 2015). Furthermore, deepwater rice varieties are adapted to withstand flooded conditions using an escape strategy through ethylene-induced internode elongation via SNORKEL 1 and SNORKEL 2 transcription factors (Hattori et al., 2009). Similarly, in the semi-aquatic dicot plant *Rumex palustris*, ethylene is the primary signal for submergence-induced petiole elongation (Voeselek et al., 1990) which is mediated by responses including cell-wall acidification and induction of expansin genes (Vreeburg et al., 2005). Next, differential growth behavior, such as the formation of the apical hook, depends on ethylene-induced cell elongation: Using *Arabidopsis* lines carrying mutant alleles of *HOOKLESS 1*, it was shown that ethylene modifies the spatial expression patterns of auxin-responsive genes likely through histone modifications, resulting in differential growth of the hypocotyl (Lehman et al., 1996; Liao et al., 2016). In parallel, enhanced auxin biosynthesis is assumed to mediate ethylene induced inhibition of root cell expansion (Swarup et al., 2007).

Furthermore in *Arabidopsis*, the hypocotyl growth repression that is observed within the triple response, is reversed when seedlings are exposed to ethylene in the light. Here, hypocotyl growth is promoted upon ethylene treatment, mainly via cell expansion (Smalle et al., 1997). The opposing effects of ethylene in the light and in the dark are mediated by differential signaling events around the transcription factors ETHYLENE INSENSITIVE 3 (EIN3) and EIN3-LIKE 1 (EIL1), which are central to ethylene gene activation (Chao et al., 1997; Chang et al., 2013; Yu and Huang, 2017). Two of their direct target genes, *ERF1* and *PHYTOCHROME INTERACTING FACTOR 3* (*PIF3*), respectively repress and promote hypocotyl elongation (Solano et al., 1998; Leivar et al., 2008; Zhong et al., 2012). Under normal air conditions, *ERF1* protein level is destabilized in the dark (Zhong et al., 2012; Cheng et al., 2017), whereas *PIF3* is unstable in the light (Ni et al., 2014), as is *EIN3* (Shi et al., 2016b). It is only upon ethylene-dependent *EIN3* activation (i.e., protein accumulation, see below), that the protein levels of *ERF1* and *PIF3* are elevated above a critical functional concentration under the respective conditions, ultimately triggering the respective changes in hypocotyl elongation (Zhong et al., 2012). Additionally, *EIN3* activity facilitates the light-repressed nuclear localization of the E3 ligase CONSTITUTIVE PHOTOMORPHOGENIC 1 (*COP1*), thus destabilizing the *COP1*-target HYPOCOTYL 5 (*HY5*) which represses hypocotyl elongation in the light (Osterlund et al., 2000; Yu et al., 2013). These effects furthermore underlie positive feedback, since ethylene destabilizes two F-box proteins that target both *EIN3* and *PIF3*, partly in an *COP1*-dependent manner (Guo and Ecker, 2003; Potuschak et al., 2003; An et al., 2010a; Li et al., 2015; Shi et al., 2016a; Dong et al., 2017b). Together, ethylene signaling results in a stunning variety of physiological consequences, depending on the plant species, the tissue of perception, and the environmental context. An intricate network of downstream effectors and massive crosstalk with other signaling pathways, first of all with auxin, is in charge to mediate finely tuned responses.

1.4.2 Ethylene signaling

Ethylene is produced in plant cells from S-adenosylmethionine in a two-step mechanism via the intermediate ACC (reviewed in Yang and Hoffman (1984)). The first step releases ACC and 5-methylthioadenosine, and is catalyzed by ACSs encoded by a multi-gene family with twelve members

in *Arabidopsis* (Sato and Theologis, 1989; Van der Straeten et al., 1990, 1992; Yamagami et al., 2003). Due to a strict regulation of ACS activity on the transcript- and post-transcriptional level (reviewed in Wang et al. (2002a), and continued in Chae et al. (2003), Wang et al. (2004), Schellingen et al. (2014), Lee et al. (2017), and Lee and Yoon (2018)), this reaction is rate-limiting for ethylene biosynthesis in most plant cells (Yang and Hoffman, 1984; Van de Poel et al., 2012). While 5-methylthioadenosine is salvaged back to Met in the further course of the Yang cycle (Wang et al., 1982; Miyazaki and Yang, 1987), ACC is metabolized to ethylene in the presence of oxygen and ascorbate by ACC oxidases (Hamilton et al., 1991; Spanu et al., 1991; Ververidis and John, 1991; Dong et al., 1992; Zhang et al., 2004).

As a gas, ethylene does not depend on transport mechanisms to diffuse throughout plant tissues and within cells (Alonso and Stepanova, 2004). In all plants analyzed so far, it is perceived by a set of structurally related receptors located in the ER membrane and the Golgi apparatus (Chen et al., 2002; Dong et al., 2008; Grefen et al., 2008; Merchante et al., 2013). The ethylene receptor gene family contains five members in *Arabidopsis*: ETHYLENE RESPONSE 1 (ETR1), ETHYLENE RESPONSE SENSOR 1 (ERS1), ETR2, ERS2, and EIN4 (Bleecker et al., 1988; Chang et al., 1993; Hua et al., 1995, 1998; Sakai et al., 1998; Ju and Chang, 2012). The different isoforms act redundantly, but also contribute distinctively to ethylene signaling outputs (Merchante et al., 2013). In *Arabidopsis*, ETR1 and ERS1 appear to have a predominant function (Hall and Bleecker, 2003; Wang et al., 2003; Qu et al., 2007; McDaniel and Binder, 2012). Sequence differences exist between the receptor isoforms, but all show a similar modular composition (reviewed in Chang and Shockey (1999)): N-terminally, ethylene receptors contain a transmembrane domain that is responsible for ethylene binding (Schaller and Bleecker, 1995; Hall et al., 2000; O'Malley et al., 2005), and interaction with upstream regulators (Dong et al., 2010; Shi et al., 2016c). High-affinity ethylene binding is achieved by the membrane-spanning portion through the employment of a copper cofactor, facilitating effective cellular concentrations of ethylene in the nanomolar range (Rodríguez et al., 1999). Next, a cytosolic GAF (cGMP-specific phosphodiesterases, adenylyl cyclases, and FhIA) domain mediates receptor homo- and hetero-dimerization (Gao et al., 2008; Grefen et al., 2008; Chen et al., 2010c). The cytosolic C-terminus harbors a His protein kinase-like domain that confers *in-vitro* His kinase activity to ETR1 and ERS1, whereas ETR2, ERS2, and EIN4 might be kinase inactive or exhibit Ser/Thr kinase specificity (Gamble et al., 1998; Wang et al., 2003; Moussatche and Klee, 2004). ETR1, ETR2, and EIN4 are furthermore equipped with a terminal receiver domain, making these isoforms most similar to bacterial two-component His kinase systems (Fluhr, 1998; Chang and Shockey, 1999). In fact, the requirement of receptor autokinase activity for ethylene signaling is ambiguous (Hall and Bleecker, 2003; Wang et al., 2003; Voet-Van-Vormizeele and Groth, 2008; Hall et al., 2012; Kamiyoshihara et al., 2012). However, the His kinase-like and receiver domains of ETR1 and ERS1 were shown to be necessary for the interaction with downstream signaling components (Clark et al., 1998; Gao et al., 2003; Qu and Schaller, 2004; Scharein et al., 2008; Bisson et al., 2009; Bisson and Groth, 2010), and His kinase activity of ETR1 is required for growth recovery following ethylene signaling (Binder et al., 2018).

Among the cytosolic interactors of ethylene receptors, the Raf-like kinase CONSTITUTIVE TRIPLE RESPONSE 1 (CTR1) is the primary target of the ethylene signal (Fig. 6B; Kieber et al., 1993; Hua et al., 1995; Chao et al., 1997; Clark et al., 1998). In the absence of ethylene, the CTR1 kinase domain is kept active by the interaction with the receptor His kinase-like and receiver domains, and thereby inhibits downstream signaling events (Kieber et al., 1993; Clark et al., 1998; Gao et al., 2003; Huang et al., 2003b). Hence, CTR1 as well as the ethylene receptors are negative regulators of the ethylene

response, and inactivation of CTR1 results in constitutive ethylene signaling (Kieber et al., 1993; Hua and Meyerowitz, 1998; Qu et al., 2007).

When active, CTR1 phosphorylates the cytosolic portion of ETHYLENE INSENSITIVE 2 (EIN2), the key positive regulator of the ethylene response (Chen et al., 2011a; Ju et al., 2012; Qiao et al., 2012). So far, *EIN2* is the only known gene that causes complete loss of ethylene sensitivity upon knock-out, and it is conserved in green algae and the plant kingdom (Roman et al., 1995; Alonso et al., 1999; Jun et al., 2004; Travella et al., 2006; Ju et al., 2015). The 141 kDa protein locates to the ER membrane with its N-terminal domain comprising twelve transmembrane helices (amino acids 1-461 of 1294), and the remaining part protrudes to the cytosol (Alonso et al., 1999; Bisson et al., 2009). Although the integral membrane domains resemble NRAMP (Natural resistance-associated macrophage protein) metal ion transporters, there is no evidence for metal transport activity of EIN2 (Alonso et al., 1999). The sequence of the C-terminus is plant specific and does not show domain signatures known from other proteins (Alonso and Ecker, 2001; Wen et al., 2012). However, the C-terminus contains a nuclear localization signal that also associates with the His kinase-like domain of ethylene receptors (Qiao et al., 2012; Wen et al., 2012; Bisson and Groth, 2015).

It is understood that upon ethylene binding to the receptors, CTR1 is inactivated potentially by steric changes (Mayerhofer et al., 2012), preventing phosphorylation of the cytosolic EIN2 portion on Ser-645 and/or Ser-924 (Fig. 6B; Chen et al., 2011a; Ju et al., 2012; Qiao et al., 2012). This renders EIN2 subject to proteolytic cleavage by an unknown protease, and the C-terminal half of the protein, referred to in the literature as EIN2 CEND, is released to the cytosol and nucleus (Ju et al., 2012; Qiao et al., 2012; Wen et al., 2012). The precise cleavage site was assigned to Ser-645 by mass spectrometric analysis, resulting in a C-terminal fragment initiated by Phe-646 (i.e., amino acids 646-1294; Qiao et al., 2012, 2013). Once detached from the membrane, the major molecular function of EIN2 CEND appears to be the activation of EIN3-like transcription factors (Chao et al., 1997; Alonso et al., 1999; Guo and Ecker, 2003; Potuschak et al., 2003; An et al., 2010a; Li et al., 2015; Merchante et al., 2015). These trigger downstream responses mainly via binding to the promoters of APETALA2/ERF transcription factors (Solano et al., 1998; Zhang et al., 2011b; Chang et al., 2013). Notably, in etiolated seedlings, it was evident that ethylene also provokes a rapid short-term growth inhibition that requires EIN2, but is independent of EIN3/EIL1 activity (Binder et al., 2004b, 2004a). It is not understood how this response is mediated mechanistically.

The protein level of EIN2 is kept at a relatively low level under normal conditions, since EIN2 is targeted for proteasomal degradation by the F-box proteins EIN2 TARGETING PROTEIN 1 (ETP1) and ETP2 (Qiao et al., 2009). Upon ethylene signaling, ETP1/2 are destabilized on the protein level themselves, consequently enhancing EIN2 signaling capacity (Qiao et al., 2009). Accordingly, knock-down of *ETP* mRNA resulted in EIN2 hyper-accumulation and constitutive ethylene responses (Qiao et al., 2009). How ETP protein abundance is regulated is not known. Interestingly, it was shown in rice that *MAO HUI3* (*MHZ3*) interacts with the OsEIN2 NRAMP-like domain in the ER membrane, and antagonizes EIN2 ubiquitination (Ma et al., 2018a). Here, loss of *MHZ3* function resulted in ethylene insensitivity during etiolation of rice coleoptiles. However, the rice genome appears not to contain homologs of *ETP* genes (Ma et al., 2018a).

1.4.2.1 Molecular functions of EIN2

There are at least two ways how EIN2 influences EIN3 and EIL1 activity: First, EIN2 CEND is translocated to the nucleus where it facilitates EIN3 binding to its promoter targets. This is at least partially achieved by EIN2 CEND regulating the levels of HISTONE 3 acetylation at K14, K23, or K9 at EIN3 target sites by interaction with the active-chromatin associated EIN2 NUCLEAR-ASSOCIATED PROTEIN 1 (Zhang et al., 2017a, 2018a). Second, next to the nuclear localization, EIN2 CEND was observed to also form pronounced foci in the cytoplasm, indicating a cytoplasmic function (Qiao et al., 2012; Wen et al., 2012). This function of EIN2 CEND in the cytoplasm includes, or constitutes, the negative regulation of the protein levels of two F-box proteins, EIN3-BINDING F-BOX (EBF1) and EBF2, which in turn target EIN3 and EIL1 for Ub mediated degradation (Guo and Ecker, 2003; Potuschak et al., 2003; Gagne et al., 2004; An et al., 2010a). Shut-down of EBF1/2 protein levels during ethylene signaling is accomplished by EIN2 in two ways: First, proteasomal degradation of the F-box proteins is triggered in an EIN2-dependent manner (An et al., 2010a). Second, EIN2 interacts with a 5'-3' exoribonuclease, called EIN5, in order to target *EBF1/2* mRNA to cytoplasmic processing bodies and the RNA decay pathway based on *UP-FRAMESHIFT SUPPRESSOR 1* (*UPF1*), *UPF2*, and *UPF3* (Li et al., 2015; Merchante et al., 2015). Interestingly, the C-terminal NLS of EIN2 was found to be essential for both its nuclear and the cytosolic functions (Ju et al., 2012; Qiao et al., 2012; Wen et al., 2012; Li et al., 2015). Moreover, EBF2, and to a lesser extent EBF1 were also reported to be transcriptionally induced by ethylene in an EIN2- and EIN3-dependent manner, likely as part of a negative feedback loop (Potuschak et al., 2003).

All ethylene responses downstream of EIN3/EIL1 are thought to depend on the translocation of EIN2 CEND from the ER membrane to the nucleus and cytosol (Merchante et al., 2015). Consistently, expressions of the EIN2 C-terminal fragment alone was sufficient to constitutively activate a number of ethylene responses (Alonso et al., 1999; Qiao et al., 2012; Wen et al., 2012). Namely, it was described that transgenic expression of EIN2 CEND resulted in growth retardation and reduced fertility due to the protrusion of the gynoecium prior to flower opening (Alonso et al., 1999; Qiao et al., 2012; Wen et al., 2012). Moreover, when expressed in *ein2-5* mutant plants, EIN2 CEND reconstituted the light-dependent hypocotyl elongation response to ethylene, as well as the induction of *PLANT DEFENSIN 1.2* gene expression upon JA or paraquat treatment which is blocked by *EIN2* mutation (Penninckx et al., 1998; Alonso et al., 1999). However, not all phenotypes that are entailed by *EIN2* mutation could be rescued by expressing *EIN2 CEND* alone. Most strikingly, EIN2 CEND fails to complement the triple response in *ein2* mutants (Alonso et al., 1999). Moreover, there are several phenotypes linked to *ein2* mutation which were not addressed in the studies using transgenic *EIN2 CEND*. For example, alleles of *EIN2* have emerged from genetic screens for the sensitivity of root growth towards auxin transport inhibition (Fujita and Syono, 1996), for cytokinin resistance of root growth in the light (Su and Howell, 1992; Cary et al., 1995; Kurepa et al., 2014), for ABA sensitivity (Beaudoin et al., 2000; Ghassemian et al., 2000), and for delayed leaf senescence (Oh et al., 1997; summarized in Alonso and Ecker (2001)). Consistent with delayed senescence, later flowering was also described for *ein2* mutants (Guzmán and Ecker, 1990; Feng et al., 2015). Furthermore, *ein2* plants were found to be more susceptible to infection by pathogens such as *P. syringae* pv. *tomato*, and *B. cinerea* (Bent et al., 1992; Thomma et al., 1999; Alonso and Ecker, 2001; Geraats et al., 2002). When grown in the light, *ein2* was hypersensitive to glucose in the growth medium (Cheng et al., 2002), and *ein2-5* showed altered gene expression upon phosphate starvation (Kwon et al., 2011; Lei et al., 2011). Finally, *ein2-5* and *ein3-1 eil1-1* plants were described to be

hypersensitive towards cadmium exposition (Abozeid et al., 2017), whereas reports on *EIN2* requirement for the perception of mechanical stimuli are ambiguous (Johnson et al., 1998; Okamoto et al., 2008; Braam, 2013). The multitude of effects triggered by a loss of *EIN2* activity is in line with the various consequences of ethylene signaling, as well as a growing number of *EIN2*-interacting factors being recognized (see above).

1.5 The phytohormone cytokinin

The phytohormone class of cytokinins regulates plant growth and development at nearly all stages, most prominently by impacting on cell division and differentiation. The class comprises mostly adenine derivatives with an isoprenoid side chain at the N⁶ position of the purine, with zeatin-type cytokinins being the predominant form in higher plants (Mok and Mok, 2001; Gajdošová et al., 2011). Much less abundant than isoprene-conjugated purines, and potentially restricted to a limited number of species, are cytokinins with aromatic side chains (Jones et al., 1996; Strnad, 1997; Mok and Mok, 2001). Despite their rather marginal occurrence, aromatic variants are biologically equally active, and the synthetic aromatic cytokinin BA, together with kinetin (N⁶-(2-furfuryl)-aminopurine), are most widely used in biotechnology due to their high *in-vivo* stability and ease production (Scott and Liverman, 1956; Galuszka et al., 2007; Podlešáková et al., 2012).

First identified and isolated from maize kernels (Netien et al., 1951; Letham, 1973) and coconut milk (Mauney et al., 1952; Miller et al., 1955, 1956), cytokinins were named with respect to their ability to promote the growth and division of cultured plant cells in an auxin-dependent manner (Skoog and Miller, 1957). Using tobacco (*Nicotiana tabacum*) BY-2 cell cultures, endogenous levels of cytokinin were shown to oscillate during the cell cycle, thus controlling cell cycle progression dose-dependently (Redig et al., 1996; Hartig and Beck, 2005). Next to their role in cell proliferation, the two hormones have opposing effects on apical dominance (Wickson and Thimann, 1958; Jones et al., 1988b; Shimizu-Sato et al., 2009), as well as on the cell fate in root and shoot meristems, including the establishment of the apical-basal axis during embryogenesis (Werner et al., 2001; Higuchi et al., 2004; Nishimura et al., 2004; Dello Ioio et al., 2007, 2008; Müller and Sheen, 2008; Pernisova et al., 2009; Ruzicka et al., 2009). In the shoot, cytokinins promote cell proliferation, whereas they inhibit growth and partly induce differentiation in the root, both processes being antagonized by auxin crosstalk (Su et al., 2011). Further processes governed by cytokinin signaling include chloroplast development (reviewed in Cortleven and Schmölling (2015)) and leaf senescence (Mothes and Engelbrecht, 1963; Van Staden et al., 1988; Balibrea Lara et al., 2004), the development of the female gametophyte (Pischke et al., 2002; Deng et al., 2010; Cheng et al., 2013; Yuan et al., 2016), and the gynoeceium (Marsch-Martínez et al., 2012; Zúñiga-Mayo et al., 2014; Müller et al., 2017), seed production (Ashikari et al., 2005; Bartrina et al., 2011; Li et al., 2011; Zhang et al., 2012b; Zhao et al., 2015), and development of the vasculature (Mähönen et al., 2006; Nieminen et al., 2008; Han et al., 2018).

Trans-zeatin-type cytokinins are produced from adenine nucleotides by the subsequent action of isopentenyltransferases (Kakimoto et al., 2001; Takei et al., 2001, 2004a; Sun et al., 2003), cytochrome P450 enzymes hydroxylating the isoprenoid side chain (Takei et al., 2004b), and LONELY GUY family enzymes liberating the free base active form from the cytokinin ribotides (Kurakawa et al., 2007; Kuroha et al., 2009). The levels of active cytokinins are reduced reversibly or irreversibly by

glycosylation (Brzobohaty et al., 1993; Hou et al., 2004; Spíchal et al., 2004), or cytokinin oxidase mediated cleavage of the N⁶-side chain (Werner et al., 2001, 2006; Schmülling et al., 2003).

Cytokinin sensing occurs via a classical multistep phosphorelay system, a His-Asp phosphorylation cascade resembling bacterial two-component signal transmission (Kakimoto, 1996; D'Agostino and Kieber, 1999; Hwang and Sheen, 2001). In the plant system, the cytokinin signal is perceived by receptor kinases containing both His kinase and receiver domains. Phosphate is subsequently transferred to a His phosphotransfer protein that migrates into the nucleus and ultimately serves as the phospho-donor for autophosphorylation of a response regulator (RR) (Hwang and Sheen, 2001; Mok and Mok, 2001; Punwani and Kieber, 2010). All steps are performed by members of multigene families in *Arabidopsis* (Hwang et al., 2002; Riefler et al., 2006; Müller and Sheen, 2007) and other plants (Ito and Kurata, 2006; Pareek et al., 2006; Du et al., 2007; Pils and Heyl, 2009). *Arabidopsis* cytokinin receptors (AHK2, AHK3, and AHK4/CYTOKININ RESPONSE 1/WOODENLEG) reside mostly at the ER membrane (Caesar et al., 2011; Lomin et al., 2011; Wulfetange et al., 2011), with the cytokinin-binding CHASE (cyclase- and His kinase-associated sensing extracellular) domain facing the ER lumen (Caesar et al., 2011). However, signaling from the plasma-membrane is also argued for (Zürcher et al., 2016), and the exact site of cytokinin perception is under debate (Romanov et al., 2018). Downstream of AHKs, there are six *Arabidopsis* His Phosphotransferases (AHPs) (Suzuki et al., 2000b; Hwang et al., 2002; Tanaka et al., 2004; Mähönen et al., 2006). AHP1-5 act redundantly as positive regulators of cytokinin signaling (Hutchison et al., 2006), whereas AHP6 is repressed transcriptionally by cytokinin and negatively regulates the system (Mähönen et al., 2006). As terminal phosphate acceptors, *Arabidopsis* RRs (ARRs) translate the cytokinin signal into context-dependent transcriptional responses (Brandstatter and Kieber, 1998; Imamura et al., 1999; Hwang et al., 2002; Lohrmann and Harter, 2002). The *Arabidopsis* gene family of bacterial-type RRs comprises 23 members, 21 of which were associated with cytokinin signaling and are divided into type-A and type-B ARR (Lohrmann and Harter, 2002; Pils and Heyl, 2009). Type-B ARR (ARR1, 2, 10-14, 18-21) contain both phospho-receiver and DNA binding/transactivation domains and mediate the primary transcriptional response to cytokinin (Sakai et al., 2000, 2001; Kazuo Hosoda et al., 2002; Mason et al., 2005; Argyros et al., 2008; Ishida et al., 2008). In contrast to *type-B* ARRs, *type-A* ARR genes (ARR3-9, 15-17) are rapidly induced by cytokinin application (Brandstatter and Kieber, 1998; Taniguchi et al., 1998; D'Agostino et al., 2000). Lacking domains for DNA interaction, type-A ARRs dampen the transcriptional response to cytokinin by a mechanism that is not known, but depends on phospho-transfer to their receiver domains (Imamura et al., 1999; To et al., 2004, 2007). How ARR function is coordinated to induce the multiple outcomes of cytokinin signaling is poorly understood, but apparently involves massive hormonal cross-regulation (Xie et al., 2018).

1.5.1 Cytokinin during etiolation

Many phytohormones impact on skotomorphogenesis of seedlings. Next to ethylene exposure (see above), JA (Zheng et al., 2017), cytokinin (Chory et al., 1994), as well as inhibition of GA (Alabadí et al., 2004) or brassinosteroids biosynthesis (Li et al., 1996; Szekeres et al., 1996; Asami et al., 2000), and inhibition of auxin transport (Schwark and Schierle, 1992; Friml et al., 2002; Vandenbussche et al., 2010) promote aspects of photomorphogenesis in the dark. In the case of cytokinin application, the morphological changes during etiolation comprise the full induction of a triple response (Chory et al., 1994; Vogel et al., 1998b; Hansen et al., 2009). This effect is at least partially due to cytokinin-

induced stimulation of ethylene biosynthesis (Liebermann, 1979; Cary et al., 1995; Vogel et al., 1998b), which occurs downstream of ARR1, 2, 10, and 12 (Hansen et al., 2009). ARR-induced ethylene production is largely accomplished by the type-2 ACS enzymes ACS5 and ACS9 (Vogel et al., 1998b, 1998a; Chae et al., 2003; Hansen et al., 2009; Lee et al., 2017). Cytokinin, as well as micromolar levels of brassinosteroids (Vogel et al., 1998b; Woeste et al., 1999b; Chae et al., 2003; Wang et al., 2004; Hansen et al., 2009; Lee et al., 2017), and to a lesser extent also GA and auxin (Woeste et al., 1999a; Lee et al., 2017), positively regulate ACS activity by increasing their protein stability. A distinct and conserved sequence signature in the ACS C-termini determines their stability (Yoshida et al., 2005). In case of the subgroup of type-2 ACSs, the presence of the TOE motif is conserved in dicots and monocots, and confers recognition by ETO1 family proteins that mediate degradation via the 26S proteasome (Woeste et al., 1999b; Wang et al., 2004; Yoshida et al., 2006; Christians et al., 2009). Consistently, overexpression of ETO1 restores hypocotyl elongation of etiolated seedlings in the presence of kinetin (Wang et al., 2004). Phosphorylation of ACS5 by CASEIN KINASE 1.8 was shown to enhance the interaction with ETO1 and thus to increase ACS5 turnover (Tan and Xue, 2014). On the other hand, ACS proteins of both type-2 and type-3 were stabilized by the interaction with 14-3-3 proteins, partly by 14-3-3-mediated destabilization of ETO1/EOLs (Yoon and Kieber, 2013). However, cytokinin and brassinosteroids were able to partly increase type-2 ACS protein levels post-transcriptionally even when the C-terminal TOE degrons were mutated (i.e., *eto2* and *eto3* alleles of ACS5 and ACS9, respectively), indicating a level of regulation that is independent of ETO1/EOLs (Chae et al., 2003; Hansen et al., 2009; Yoon and Kieber, 2013). One potential mechanism might be the regulation of homo- and hetero-dimerization which was shown to influence kinetics and stability of ACS isoforms (Yamagami et al., 2003; Tsuchisaka and Theologis, 2004a, 2004b; Lee et al., 2017).

Since cytokinin responses are mediated considerably by ethylene biosynthesis and signaling, mutations of *EIN2* lead to cytokinin resistance under dark (Cary et al., 1995; Hansen et al., 2009) and illuminated conditions (Su and Howell, 1992). However, ethylene mutants are not completely insensitive to cytokinin application, as *ein2* root and hypocotyl elongation in dark were both inhibited by roughly 10-25 percent of control growth in media containing 0.1-10 μM BA, in comparison to 40-60 percent inhibition of WT seedling elongation (Cary et al., 1995; Hansen et al., 2009). Moreover, cotyledon expansion in the dark was triggered to similar extents in WT and *ein2-1* mutant seedlings by the presence of 3 μM BA, indicating a direct role of cytokinin during photomorphogenesis (Cortleven et al., 2018). Also, simultaneous application of BA and the ethylene signaling inhibitor silver nitrate failed to fully restore hypocotyl elongation of WT plants (Cortleven et al., 2018). Hence, cytokinin impacts on the morphology of etiolated seedlings also independently of ethylene. Evidence was presented supporting that this response might be mediated by the regulators of photomorphogenesis COP1, DE-ETIOLATED 1, and CYTOKININ INSENSITIVE4/COP10 (Vogel et al., 1998a; Cortleven et al., 2018), which all act to enable activation of a CUL4-based E3 ligase complex towards substrates such as HY5 (Yanagawa et al., 2004; Chen et al., 2006, 2010a). Mutants of these genes show constitutive photomorphogenic phenotypes, but fail to further reduce hypocotyl length when subjected to cytokinin (Cortleven et al., 2018). HY5 itself appears not to be involved in cytokinin-induced hypocotyl shortening in the dark, and how the COP1 complex might regulate cytokinin induction of photomorphogenesis is not yet understood (Cortleven et al., 2018).

2. Aims and scope of the thesis

In the past, genetic approaches have revealed multiple components of the *Arabidopsis* N-end rule pathway, as well as their involvement in developmental and stress-related processes. In the case of the type I Arg/N-end rule, enzymatic cascades have been defined, and distinct protein targets were identified. However, the physiological function of the type-II pathway remained largely unknown, and no endogenous substrates had been assigned to the type-II N-recognin PRT1 till the beginning of this work. Furthermore, contrasting to the situation of N-degron research in other systems, a biochemical characterization of the substrate specificity of plant N-end rule recognition elements is lacking so far. Thus, urgent questions concerning substrate recognition and the selectivity of the plant N-end rule pathways have remained unanswered. Importantly, the knowledge on N-recognin substrate binding determinants could also help to substantiate or reject previously proposed interactions between enzymes of the N-end rule pathway and potential target proteins.

In the frame of this work, two different routes were taken in order to gain a deeper understanding of the substrate specificity of plant N-end rule components, and to furthermore decipher the physiological role of the *PRT1* gene: First, a reverse-genetic approach was conducted on a mutant line bearing the *prt1-1* null allele. It was anticipated that a phenotypical characterization of the *prt1-1* mutant would help to attribute biological functions to this Ub E3 ligase. Indeed, two developmental abnormalities were identified in *prt1-1* which were, however, both caused by the genetic background of the lines tested, and were independent of the *prt1-1* allele. The first phenotype expressed as complete male sterility conditional for high temperature, which was investigated morphologically, histologically, and on the level of gene expression. The second phenotype constituted hyposensitivity to cytokinin in the dark and might provide valuable genetic resources for future studies on heterotrophic growth during seedling establishment. To enable a phenotypical characterization of the *prt1-1* mutant in the future, backcross lines were generated that separate the *prt1-1* allele from both phenotypic alterations.

The second strategy employed within this work was to establish and perform *in-vitro* techniques for the robust investigation of the physical interaction of N-recognins and ATE1 with artificial peptide substrates in a large scale. This should allow for the identification of sequence determinants of substrate interactions, and for the screening of potential physiological substrates. It was ultimately aimed to validate the results obtained from *in-vitro* studies in living cells.

For the purpose of investigating ATE substrate selection, a novel pull-down based arginylation assay engaging artificial peptides and radiolabeled Arg-tRNA was set up that is highly responsive, specific, and time efficient. With this in hands, Arg-transfer to canonical ATE substrate N-termini was proven for *Arabidopsis* ATE1. Moreover, in collaboration with Mark White¹ and Emily Flashman¹, oxidation of a Cys-initiated peptide substrate by PCOs and subsequent ATE1-mediated Arg-transfer were reconstituted *in vitro*.

In order to study substrate recognition by the N-recognins, peptide array binding assays were established with libraries of artificial N-termini that were generated by SPOT peptide array synthesis. Both the N-recognin PRT1 and the UBR domain of PRT6 were exposed to this binding assay system. This revealed affinity for the predicted N-terminal amino acids, and deeper insight was gained into

¹ University of Oxford, Oxford OX1 2JD, United Kingdom

downstream sequence requirements indicating a high degree of selectivity featured by both enzymes. In the case of PRT1, it was furthermore aimed to exploit peptide binding assays to address the requirements of two RING domains in substrate recognition, as well as catalytic activity. This showed dispensability of both individual domain functions for substrate interaction, whereas either domain proved to be necessary for *in-vitro* autoubiquitination activity of this E3, hinting at an unusual reaction mode performed by PRT1. Finally, to test for interactions with proposed *in-vivo* substrates, artificial peptides mimicking endogenous substrate candidates were furthermore exposed to both N-recognins in the binding assays. This confirmed physical interaction of PRT6 with peptides mimicking the mature N-termini of ERFVII transcription factors, but not to the post-proteolysis-N-termini of RIN4. For PRT1, affinity for two potential endogenous substrates was observed, one of them being the Phe-646 initiated fragment of EIN2. To address a potential role of PRT1 in EIN2 signaling, EIN2 CEND stability and its dependency on PRT1 was assessed *in vivo* using transient expression of protein variants in *Arabidopsis* protoplasts, and phenotypic consequences were addressed in stably transformed plant lines.

3. Results

3.1 The genetic background in *prt1-1^{ts}* confers thermosensitivity of pollen development

Despite the high impact of the *prt1-1* allele on the stability of an N-end rule reporter construct, and the apparent lack of any homologous sequences of the *PRT1* gene in the *Arabidopsis* genome, hardly any physiological consequences have been attributed to *PRT1* mutation so far. Hence, the biological function of *PRT1* remained elusive. Developmental differences between the *prt1-1* mutant and WT plants, or alterations in the stress response of *prt1-1*, however, could eventually lead to the identification of *PRT1*-dependend degradation pathways. Here, a reverse-genetic approach was undertaken on a line bearing the null allele *prt1-1*, in order to link a potential phenotype caused by the mutation to a biological function of this E3 ligase.

3.1.1 The *prt1-1^{ts}* line is sterile at an elevated temperature

Upon the search for stress-related phenotypes, it was observed that the *prt1-1* line that was established in the laboratory (hereafter referred to as *prt1-1^{ts}*; see Fig. 50 for the origin of the plant line) completely failed to produce any seeds when grown at an elevated ambient temperature of 28°C, a condition that readily allowed seed production of the WT (Fig. 7B). This sterility effect was

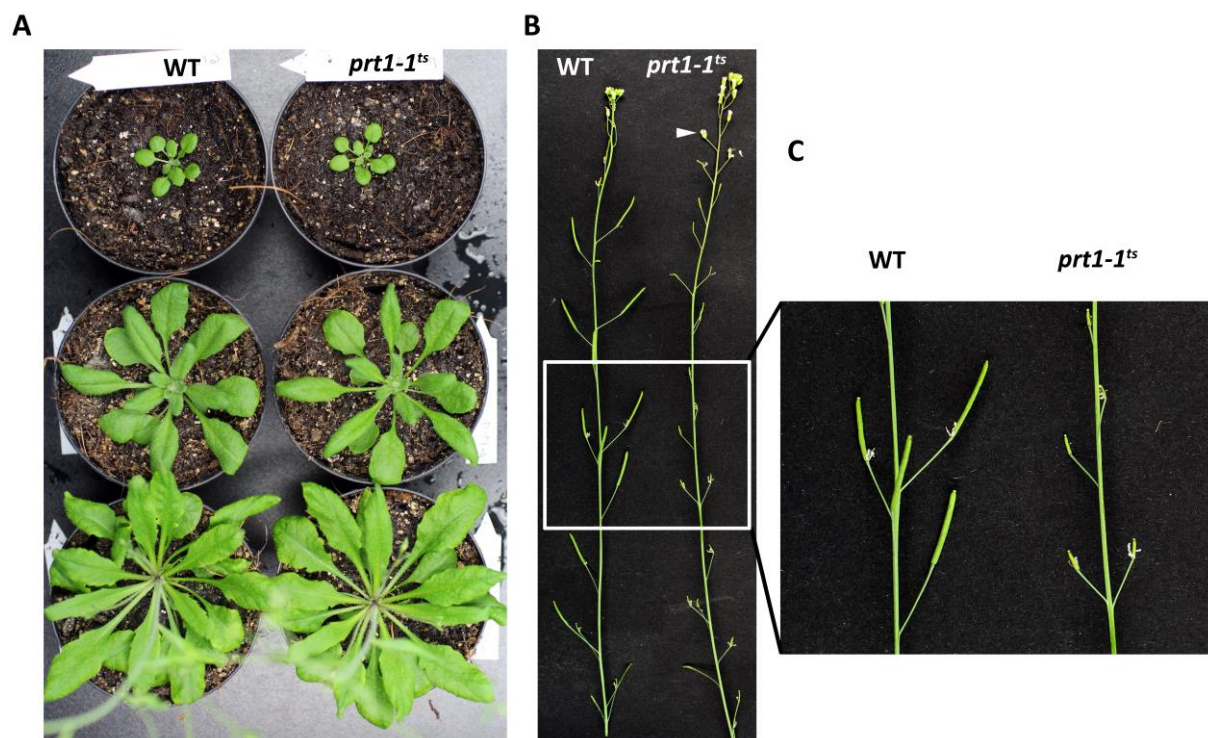


Fig. 7 | Development and sterility of the *prt1-1^{ts}* mutant at 28°C. **A**, Growth phenotype of *prt1-1^{ts}* (right) during vegetative development at 28°C and 55-65 percent relative air humidity, compared to the WT (left). Top to bottom: representative plants at the ages of 21, 32 or 42 days, respectively. **B**, Primary inflorescences from representative plants of WT and *prt1-1^{ts}* grown at 28°C and 55-65 percent relative air humidity. The failure by *prt1-1^{ts}* to produce siliques is accompanied by a delayed abscission of the petals (arrowhead). **C**, Magnification of the excerpt from B. Instead of siliques, unfertilized pistils are observed on *prt1-1^{ts}* inflorescences at 28°C.

highly specific to the condition of mild heat since growth at a lower temperature (19-23°C) restored full fertility of *prt1-1^{ts}* (Fig. S1A). The failure of *prt1-1^{ts}* to develop seeds at 28°C furthermore entailed a delayed abscission of the petals (Fig. 7B). In contrast, WT and mutant were indistinguishable at any stage of development during vegetative growth at 28°C (Fig. 7A, S2); and neither the time of flowering nor the formation of the generative shoot system were affected during mild heat.

Moreover, no differences to WT were detected when heterozygous *prt1-1^{ts}* [+/-] plants were tested for silique formation at 28°C (Fig. S1B), indicating that the sterility might potentially be caused by a genetic locus with recessive inheritance. When sterile plants were transferred from 28°C to lower temperatures (20°C), newly formed flowers developed normally and immediately gave rise to viable seeds (data not shown). Thus, *prt1-1^{ts}* was found to be specifically impaired in reproduction under acute mild heat.

3.1.2 The thermosensitivity of *prt1-1^{ts}* is independent of the *PRT1* locus

In order to test if the temperature-induced sterility of the *prt1-1^{ts}* line depended on the loss of *PRT1* activity, it was attempted to complement the phenotype with an intact copy of the *PRT1* gene. To this end, the *prt1-1^{ts}* line was stably transformed with different constructs of the *PRT1* coding sequence (CDS), and the transgenic lines were tested for their fertility under the restrictive condition of 28°C. However, no complementation of the sterility phenotype was observed in any of the tested transgenic lines (data not shown). These included T2 lines (i.e., the first segregating progeny) overexpressing a C-terminally triple hemagglutinin- (3HA) tagged *PRT1* CDS sequence under control of the strong constitutive 35S promoter from the cauliflower mosaic virus (*p35S::PRT1-3HA*), as well as T3 lines expressing N-terminal *PRT1* CDS fusions of either 3HA or GREEN FLUORESCENT PROTEIN (GFP) under control of an endogenous promoter construct (*proPRT1^{ΔCTCT}::3HA-PRT1* and *proPRT1^{ΔCTCT}::GFP-PRT1*). Of note, during one early experiment, fertility was observed for at least five T2 lines with single insertions of *proPRT1^{ΔCTCT}::mGFP5:PRT1* derived from independent transformation events (data not shown), but the effect was not seen in the next generation and the result failed to be reproduced by later experiments. Thus, it is possible that a potential malfunction of the phytocabinet caused this effect.

It was furthermore sought to test the *PRT1* dependence of the phenotype by the assessment of additional alleles conferring loss of *PRT1*-function. To this end, six T-DNA lines with insertions into the *PRT1* gene were ordered at the *Nottingham Arabidopsis Stock Centre* (NASC) and termed *prt1-2*, *prt1-7*, *prt1-8*, *prt1-9*, *prt1-10*, and *prt1-11* (Fig. S3). Of these lines, none exhibited sterility under the elevated temperature condition (Fig. S4). Importantly, while only *prt1-2*, *prt1-7*, *prt1-9*, and *prt1-11* were derived from the *Columbia-0* (Col-0) genomic background, as was *prt1-1*, only *prt1-7*, *prt1-9*, and *prt1-11* were found to actually contain a T-DNA insertion into *PRT1*. Moreover, transcript analysis revealed the presence of *PRT1* transcript downstream of the insertion sites in all three of these lines, indicating that *PRT1* function was probably not lost in these plants (Fig. S5).

Since transgenic complementation of the phenotype or reproduction through additional loss-of-function alleles was not achieved, it could not be excluded that a locus other than *PRT1* was causal for the temperature-sensitive fertility of *prt1-1^{ts}*. Thus, the mutant line *prt1-1^{ts}* (♀) was backcrossed

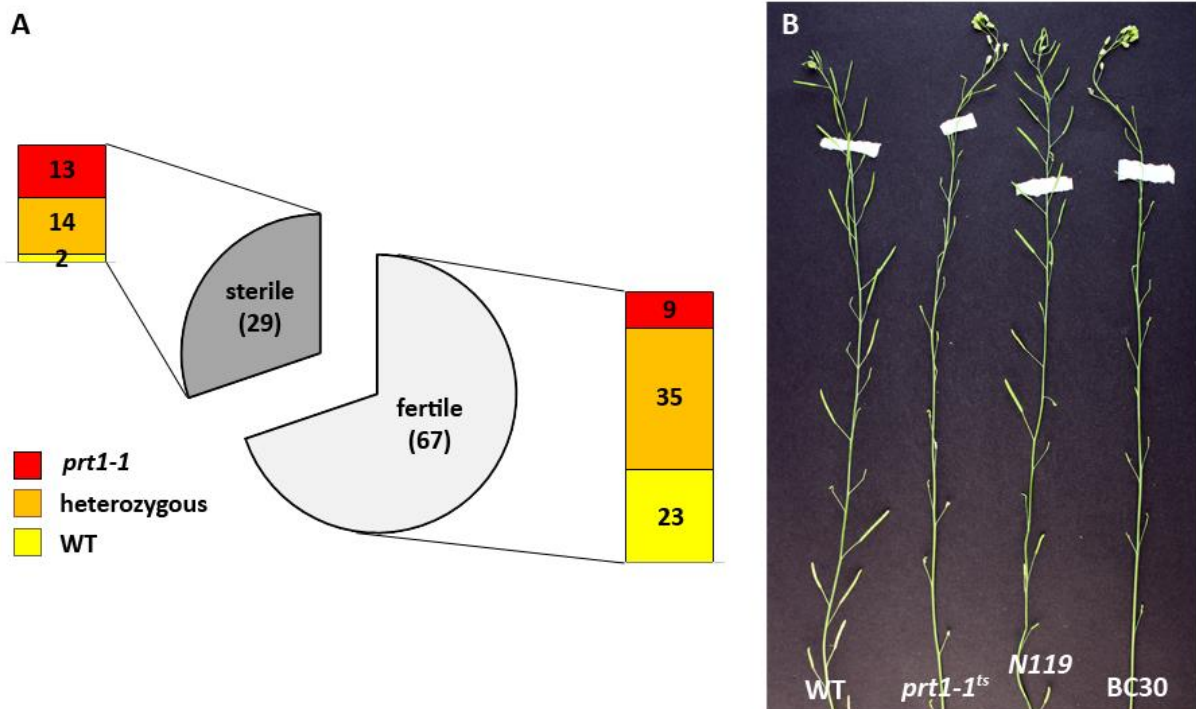


Fig. 8 | The temperature-dependent sterility phenotype segregates independently of the *PRT1* locus. A, The *prt1-1^{ts}* line was backcrossed to the WT (♂) and F2 progeny was scored for fertility at 28°C and PCR-genotyped for the *PRT1* locus. All three possible genotypes were found among both sterile and fertile plants with an enrichment of the *prt1-1* allele within the group of sterile plants. **B,** Inflorescence phenotypes of different plant lines grown at 28°C. Representative individuals for each line are shown. Genotypes are: WT; *prt1-1^{ts}*; N119 (the original *prt1-1* line deposited at NASC); and BC #30, a descendant of a backcross line that was sterile at 28°C and was homozygous for the WT *PRT1* locus.

to the WT (♂) in order to test for co-segregation of the phenotype with the *prt1-1* allele. Within the segregating F2 generation, 29 out of 96 individuals failed to produce seeds at 28°C (Fig. 8A), representing 30 percent of the tested progeny. This segregation pattern varied from, but was best explainable by a Mendelian monogenic recessive inheritance. Importantly, among the 22 plants homozygous for *prt1-1* (23 percent of all plants), 9 individuals were fertile at the restrictive temperature condition. The group of 28°C-sterile F2 progeny, however, was composed in almost equal shares of plants homozygous and heterozygous for the *prt1-1* allele, and even comprised two plants that were genotyped as WT for the *PRT1* locus (Fig. 8). The fact that the temperature-dependent phenotype could be genetically separated from the *prt1-1* allele strongly indicated that a different genetic locus accounted for the phenotype.

The group of sterile assessed individuals was enriched for the *prt1-1* allele (Fig. 8A), indicating linkage disequilibrium between the putative second-site locus responsible for the phenotype and the *PRT1* locus. This assumption was supported by Chi² analysis (at <http://www.socscistatistics.com> on 12/13/2107). Here, H₀ (independent distribution of both categories, sterility and *prt1-1* genotype) could be rejected by a level of significance at $p \leq 0.01$. Assessment of the frequency of recombination events between the *PRT1* locus and the putative second site within the group of sterile plants revealed

$$r = 18 \text{ (WT alleles)} / 58 \text{ (total alleles)} = 31 \text{ percent,}$$

where r is the recombination frequency.

By definition, this frequency determines both loci to be linked (i.e., likely arranged in *cis* on a chromosome) (Bonhomme et al., 1999). Calculating the map distance (D) using the Kosambi function (Koornneef and Stam, 1992) gave

$$D = 25 * \ln [(100 + 2 * 31) / (100 - 2 * 31)] = 36 \text{ cM.}$$

This recombination frequency and hence the genetic distance can be assumed to be rather overestimated: During phenotyping for the sterility effect, a false-positive result (i.e., a heterozygous or WT plant did not produce siliques) was much more likely than a false-negative (i.e., a mutant plant did produce siliques), since silique formation on *prt1-1^{ts}* plant was hardly ever observed, while poor seed production occasionally occurs on WT plants exposed to high temperature stress. This might also explain the unusual segregation ratio of 30 percent sterile plants.

When comparing the classical *Arabidopsis* genome map (Meinke et al., 1998) to the *Arabidopsis* Genome Initiative sequence map (both received from The *Arabidopsis* Information Resource (TAIR), www.arabidopsis.org), the genetic distance of 36 cM translated to a physical distance on chromosome number 3 of roughly 8.5 Mio basepairs (bp) downstream or 11 Mio bp upstream of the *PRT1* locus. A search for genes associated with male gametophyte development (by means of expression or functional data) was conducted using the sequence annotations on TAIR. A total of 21 genes were identified in a 2.6 Mio bp range surrounding the region upstream of the *prt1-1* locus, and 18 genes in a 2.4 Mio bp range surrounding the region 11 Mio bp downstream of the *prt1-1* locus (Fig. S6, Tab. S1). Among these, *ABCG16* (AT3G55090) was a potential candidate for being mutated in a temperature-dependent sterile mutant (see introduction, chapter 1.3.1.1). Hence, the *ABCG16* locus (885 bp upstream of ATG to 145 bp downstream of the stop codon) was sequenced from *prt1-1^{ts}* genomic DNA; however, no sequence divergence from WT was detected (data not shown).

The *prt1-1^{ts}* line established in the laboratory was received by Nico Dissmeyer^{1,2} personally from Prof. Andreas Bachmair³ in 2004. It was therefore asked whether the fertility phenotype was also inherent to the *prt1-1* line deposited at NASC by A. Bachmair in 1991. In contrast to *prt1-1^{ts}* which had been backcrossed four times to Col-0 in the laboratory of A. Bachmair, the reference line at the stock center contains the transgenic reporter construct 4H which confers resistance to hygromycin B (Hyg) (see Fig. 50). This line *prt1-1/4H* is listed at NASC with the code N119 and will hereafter be referred to as N119. When N119 was grown at 28°C, normal silique formation was observed (Fig. 8B). Taken together, this supported the conclusion that the *prt1-1* allele was not causing the temperature-sensitive sterility phenotype of the *prt1-1^{ts}* line, but that instead a genetically linked alteration had apparently occurred in the genome subsequent to the generation of line N119.

3.1.3 The heat-induced sterility of *prt1-1^{ts}* is caused by a defect in male gametogenesis

Conditional male sterility constitutes a plant trait that is of high economic potential (Saxena and Hingane, 2015; Zhao et al., 2017). Moreover, mutant alleles affecting reproductive fitness under high temperature can also lead to the identification of new adaptive mechanisms employed by plants to

¹ Leibniz Institute of Plant Biochemistry, 06120 Halle (Saale), Germany

² University of Osnabrück, 49074 Osnabrück, Germany

³ University of Vienna, 1010 Vienna, Austria

reproduce in a warmer than optimal environment. Thus, in order to find the cause of the thermosensitivity of *prt1-1^{ts}* reproduction, flower development was examined in more detail. When flowers of WT and mutant plants grown at 28°C were compared, no morphological differences were observed up to late stages of development (Fig. 9). Consistent with previous reports (Sakata et al., 2010), filament elongation was slightly reduced by the elevated temperature in both WT and *prt1-1^{ts}*, but elongation was sufficient in both genotypes to bring the stamen into proximity with the stigma (Fig. 9, stages 13/15). However, at the transition from stage 12 to 13, concomitantly with flower opening, differences between WT and *prt1-1^{ts}* became visible concerning anther development: While the anthers of the WT appeared slightly swollen short before pollen dehiscence, no changes in size were observed with the mutant anthers and no pollen was released even from mature flowers of *prt1-1^{ts}* (Fig. 9, stages 13/15).

Flower stages

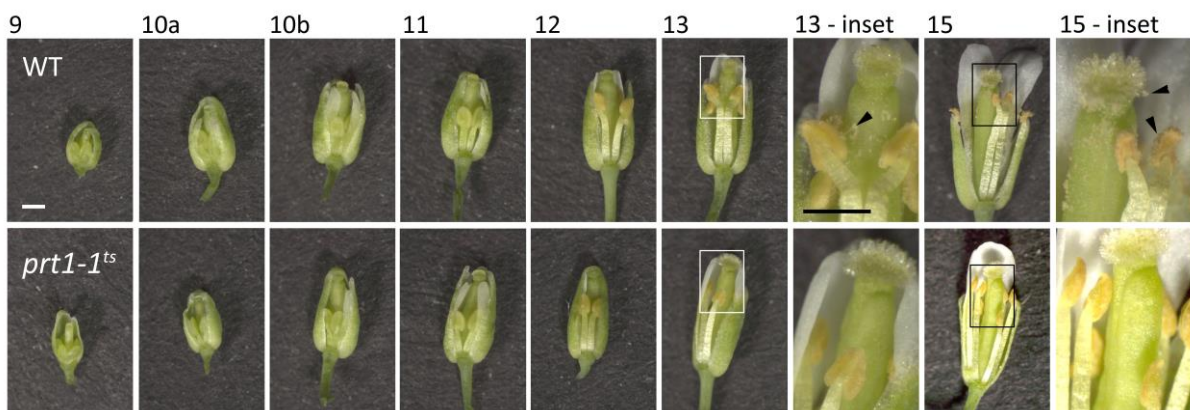


Fig 9 | Flower development during late stages in WT and *prt1-1^{ts}* at 28°C. WT and *prt1-1^{ts}* mutant plants were grown at 28°C and 55-60 percent air humidity. Sepals and petals were removed partially to show interior organs. Flower stages were assigned according to Smyth et al. (1990) and Wang et al. (2011b). Note: Flower stages do not match anther stages according to Sanders et al. (1999) which are referred to in Fig. 13. **Stages 13/15:** Pollen grains visible on anthers, pistil, and stigma of the WT are indicated by arrowheads. Panels “13 - inset” and “15 - inset” show magnifications of the previous panels. Scale bars 0.5 mm; the black scale bar applies to all inset images, the white scale bar to all remaining images.

In order to test whether the temperature-dependent sterility in *prt1-1^{ts}* was indeed caused by an anomaly in stamen development rather than a defect of the ovules, *prt1-1^{ts}* plants grown at 28°C were emasculated before anther maturity and pollen grains of WT plants grown under the same conditions were applied to the mutant stigmata. After the cross-pollination, plants were returned to the elevated ambient temperature condition. In this way treated pistils of *prt1-1^{ts}* readily developed WT-like siliques and produced viable seeds, while untreated flowers of the same plant remained sterile (Fig. 10A). This result strongly indicated that the integrity of the female flower parts was not affected in mutant plants.

As described above, heterozygous plants remained fertile at elevated temperature (Fig. S1B). To determine if the homozygous *prt1-1^{ts}* genotype conferred thermosensitivity to embryo development, siliques of *prt1-1^{ts}* [+/-] plants grown at 28°C were examined for seed abortion. However, heterozygotes contained a full set of normal appearing seeds (Fig. 10B), confirming that the defect in *prt1-1^{ts}* fertility emerges earlier during reproduction than at embryogenesis, most likely at the stage of male gametogenesis.



Fig. 10| *prt1-1^{ts}* plants are not defective in female gametogenesis or embryogenesis at 28°C. **A**, WT pollen is able to complement the fertility phenotype of the *prt1-1^{ts}* line. WT or *prt1-1^{ts}* plants were grown at 28°C before and after emasculating single flowers of the mutant and pollinating them with pollen from WT plants. Selfed WT (left) and cross-pollinated mutant flowers (*prt1-1^{ts}* x Col-0) developed into siliques, while untreated pistils of the same *prt1-1^{ts}* plants remained sterile. **B**, Plants heterozygous for the *prt1-1* locus produce seeds at 28°C without observable seed abortion.

Provided a defect in male gametogenesis of *prt1-1^{ts}* at mild heat, it would be possible that the line exhibited impaired male fitness already at control temperature which might be too marginal to display at seed setting. Thus, gametophyte vitality of plants grown at 23°C was assayed with respect to pollen tube growth at 25°C in the light, a standard condition for pollen tube growth assays. Additionally, prolonged tube growth was assessed with additional 14 hours incubation in the dark at 22°C. No differences were visible in either timing or extend of pollen tube growth of the mutant compared to WT pollen for both growth durations (Fig. 11), confirming that the phenotype was tightly restricted to the elevated temperature cue or suggesting an effect that does not reflect in pollen germination capacity.

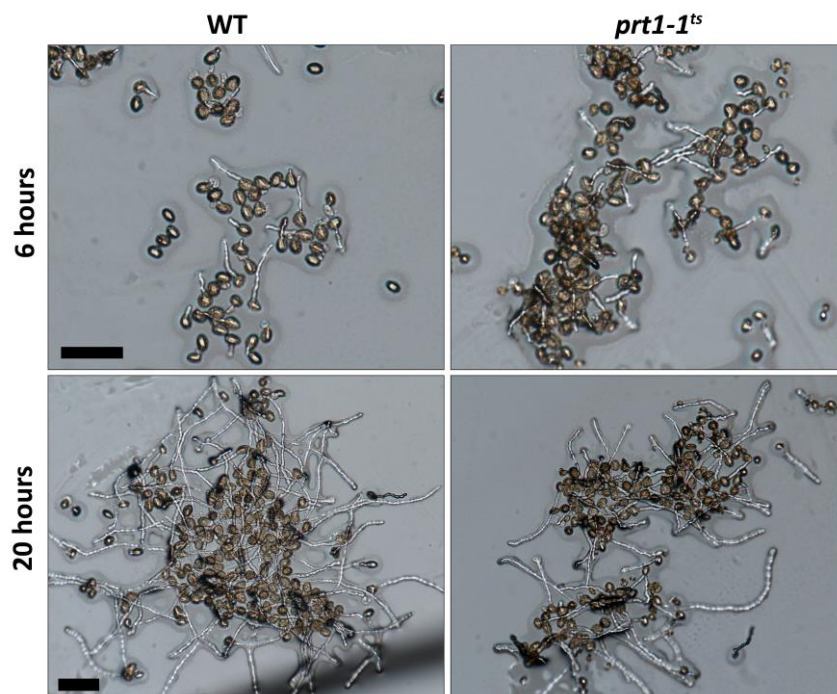


Fig. 11| Pollen tube growth is not affected in *prt1-1^{ts}*. Pollen of the two genotypes was harvested from plants growing at 23°C, transferred to pollen germination medium, and incubated in a wet chamber. Samples were kept for 6 hours at 25°C in the light and for additional 14 hours in the dark at 22°C (i.e., 20 hours of tube growth) before pictures were taken. Scale bars: 100 μ m.

Notably, it was observed during backcross experiments between WT and *prt1-1^{ts}* performed at control temperature (22°C), that the transmission of the *prt1-1* allele was slightly reduced: In two independent experiments, allele penetration of *prt1-1* was 48.4 percent (n = 96) and 48.6 percent (n = 107), respectively. Thus, there might be a slight effect on gametophyte fitness caused either by the *prt1-1* allele itself, or the linked second locus. This effect on gametophytic performance is present already under control conditions, but might conceivably be augmented at higher temperatures.

3.1.4 Microspore to pollen transition at 28°C is affected in *prt1-1^{ts}*

The observed failure by *prt1-1^{ts}* to release mature pollen grains raised the question whether dehiscence by the anthers or pollen development was impaired in the mutant during modest heat. To address the latter possibility, a microspore and pollen fraction was prepared from whole flowers before anthesis of WT and mutant grown at 28°C.

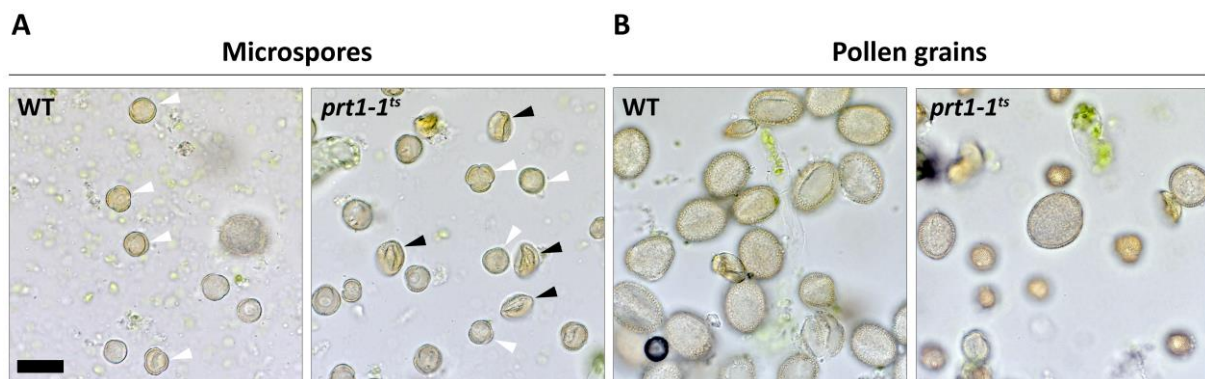


Fig. 12 | Microspores of *prt1-1^{ts}* collapse during the development into pollen grains. Bright field images are shown. Isolations of male gametes were performed on flowers of WT and *prt1-1^{ts}* plants grown at 28°C. Both populations, microspores and pollen grains, were contained in the same fractions, but were visible at different focal planes. **A**, Normal microspores are found in both WT and mutant (white arrowheads), but mutant flowers additionally contain a high number of collapsed pollen grains (black arrowheads). **B**, While mature pollen grains are highly abundant in WT preparations, they are hardly present in preparations from mutant flowers, and the ones that can be found in one mutant sample appear of different shape (smooth, spherical) and sizes compared to the WT. Scale bar: 25 μ m (applies to all images).

Microspore analysis revealed that both microspores and pollen grains were present in the mutant flowers (Fig. 12). However, while microspores were similarly abundant in preparations from mutant and WT flowers (Fig. 12A), mature pollen grains were extremely scarce in the mutant fractions and of irregular size (Fig. 12B). Moreover, in contrast to WT, microspore fractions of the mutant additionally contained a high number of collapsed immature pollen grains (Fig. 12A). This indicated that pollen development was disturbed in the mutant at the stage of microspore to pollen transition. Consistently, DAPI staining of chromatin in meiotic anthers performed by Paul E. Grini¹ on *prt1-1^{ts}* plants grown at 28°C showed that mutant microspores progressed through meiosis and tricellular pollen was found in these flowers, however with lower abundance than in WT flowers (Fig. S7).

To investigate in more detail which stage of pollen development was aberrant in the *prt1-1^{ts}* mutant plants under elevated temperature, microsections of anthers from different flower stages were

¹ University of Oslo, 0316 Oslo, Norway

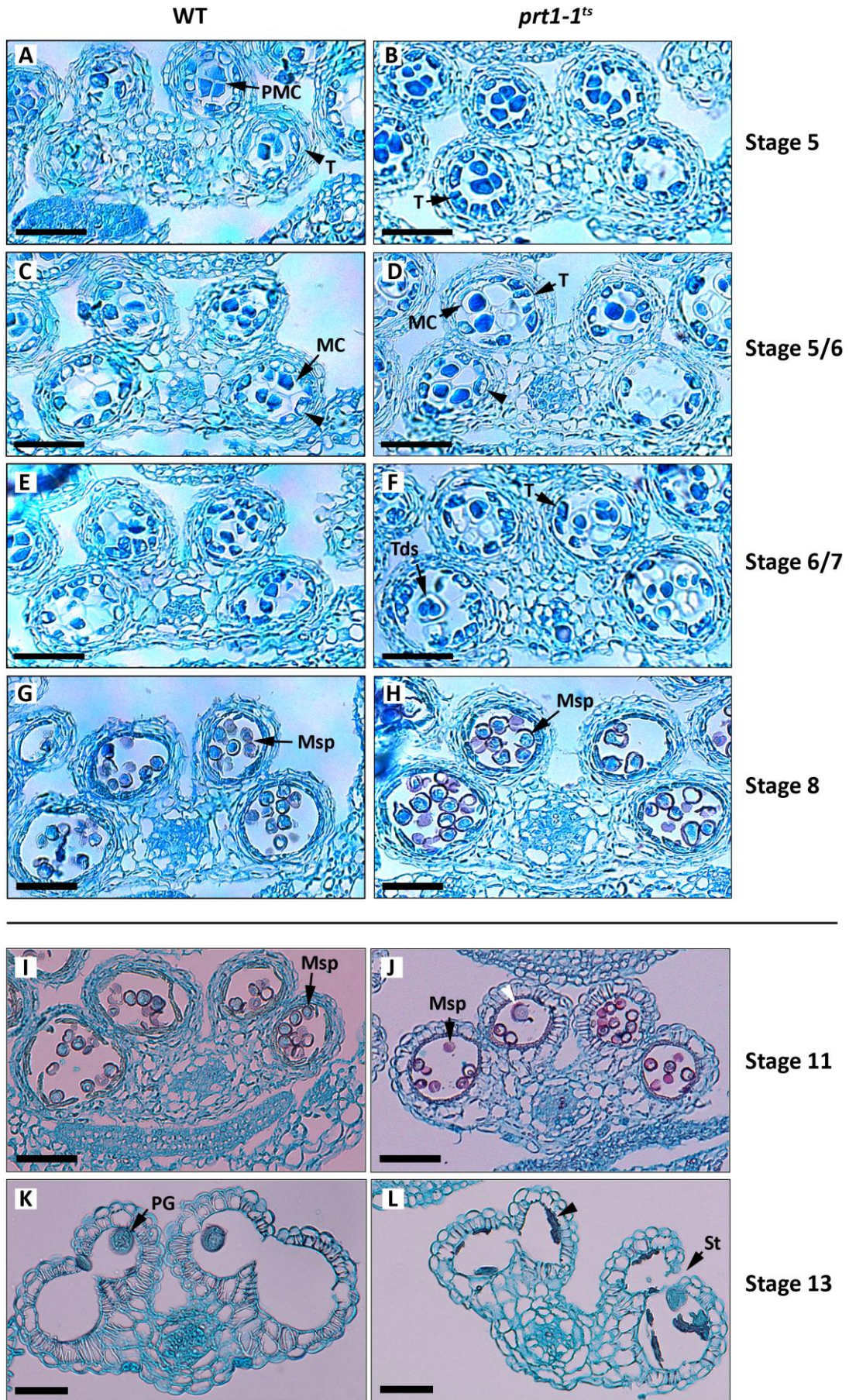


Fig. 13| Male gamete development in *prt1-1^{ts}* and WT at mild heat. Bright field images of transverse sections (4 μm) of anthers from closed flowers (A to H) and flowers short before (I, J), and at anthesis (K, L) are shown. Specimens were counterstained using astra blue and safranin O. Anthers from WT (A, C, E, G, I, K) and *prt1-1^{ts}* mutant plants (B, D, F, H, J, L) grown at 28°C ambient temperature and 55-65 percent relative air humidity were analyzed. **A-F**, WT and mutant microsporocytes during and after meioses are visible as well as tetrads (**tds**). Slightly enlarged and vacuolated tapetum cells (**T**) occurring at early stages in both WT and mutant are marked by arrowheads in C and D. **G, H**, Anthers at the stage of or shortly after microspore release from tetrads are depicted (stage 8). **I, J**, Free microspores are visible at the stage of pollen mitotic divisions (stage 11). An enlarged microspore, or premature pollen grain visible inside of a locule from *prt1-1^{ts}* is indicated by a white arrowhead. **K, L**, Anthers at anthesis are shown. Mature pollen grains have been released from WT anthers. Collapsed pollen deposits attached to the inner locule wall of the mutant anther are highlighted by a black arrowhead. **PMC**, pollen mother cell/premeiotic cell/microsporocyte; **T**, tapetum; **MC**, meiotic cell; **Tds**, tetrads; **Msp**, microspore; **PG**, pollen grain; **St**, stomium. Scale bars: 50 μm . Anther stages according to Sanders et al. (1999).

prepared. In these images, microsporangia and contained gametes appeared normal up to late stages (Fig. 13), confirming the results of the gamete isolation. The transition from microsporocytes to tetrads was passed through apparently normally, indicating that the *prt1-1^{ts}* genotype still allowed for the accomplishment of meiosis at modest heat. Occasionally, slightly enlarged and vacuolated tapetal cells were visible at premature stages (Fig. 13C, D); but such cells were found within both WT and mutant microsporangia and were likely a result of the mild heat stress, or microscopic artefacts.

Tapetal cells were still visible at the tetrad stage of mutant anthers (Fig. 13F), coinciding with the WT development, and further confirming that tapetum development was probably not impaired in *prt1-1^{ts}*. Next, microspore release from the tetrads was fulfilled in the mutant as in the WT (Fig. 13G, H). At this stage (anther stage 8), the tapetum is described to be at the most expanded cell stage under normal conditions (Sanders et al., 1999; Browne et al., 2018). However, both WT and mutant investigated at 28°C exhibited larger tapetal cells at the tetrads stage (stage 7). This slightly accelerated tapetum degradation, together with the previous observation of vacuolated tapetal cells already at stage 5/6, probably reflects the general effect of mild heat on tapetum development (Parish et al., 2012; Rieu et al., 2017). Blatant differences, however, between WT and mutant anthers became apparent short before anthesis, when microspores undergo mitosis and maturation into pollen grains: Here, the majority of microspores did not enlarge in the mutant sample (Fig. 13H, J), but were found to have completely collapsed in the sporangia of open flowers, manifested by shrunken depositions at the inner wall of the locule (Fig. 13L). An intermediate state between free microspores and collapsed pollen was hardly observed, suggesting that the breakdown occurred rather rapidly.

Broken stomia, in contrast, were found in mature anthers of *prt1-1^{ts}* as well as WT, suggesting that dehiscence was not affected in *prt1-1^{ts}* (Fig. 13K, L). Strikingly, in anther microsections of *prt1-1^{ts}* at stage 11, when WT sporangia contained exclusively microspores, some pollen grains were observed that were larger in size and of spherical shape (Fig. 13J, 14). The large size of these microspores could reflect an increased DNA content as observed upon meiotic defects (Zamariola et al., 2013), or asynchronous development with the remaining microspores in the locules. Interestingly, the affected gametes obviously escaped from collapse at the restrictive temperature (Fig. 12B, 13L). However, since silique formation was hardly ever observed on *prt1-1^{ts}* at 28°C, these pollen grains were probably inviable, or too few in number to accomplish efficient fertilization.

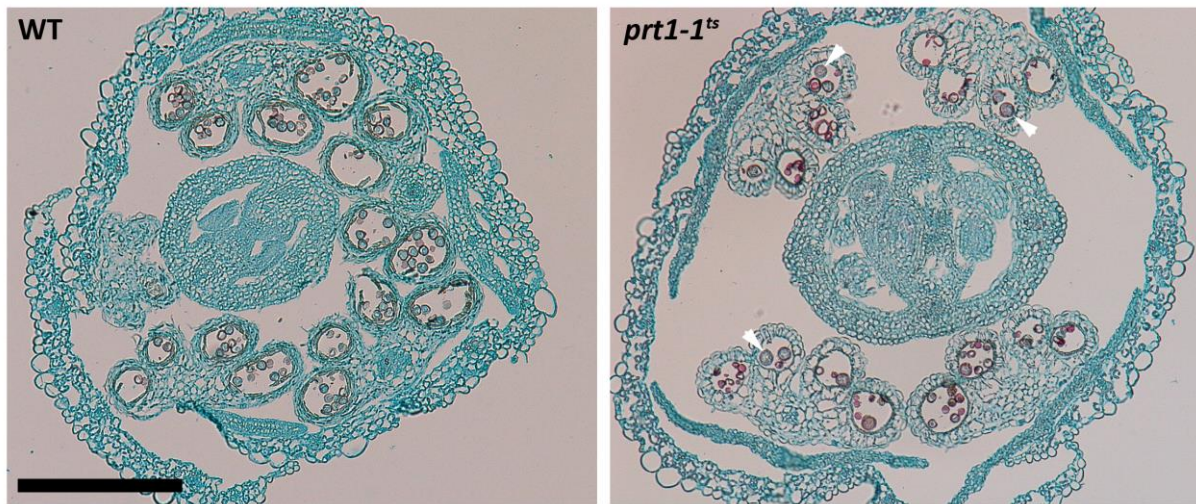


Fig. 14 | Occurrence of larger and spherical pollen grains in *prt1-1^{ts}* at 28°C. Bright field images of transverse sections (4 μ m) through flowers of anther stage 11 of WT and *prt1-1^{ts}* grown at 28°C are shown. Sections were stained with astra blue and safranin O. Individual pollen grains of *prt1-1^{ts}* that are larger and of spherical shape are highlighted by white arrowheads. Images are the same magnification. Scale bar: 200 μ M.

In the mutant, stainability of microspore walls by safranin O increased before collapse, which was not observed on WT anthers (Fig. 13H, J, 14). Since safranin O stains phenolic polymers such as lignin (Wanner, 2010; Ferreira et al., 2017), this might indicate higher contents of polyphenols in the mutant cell walls, potentially indicating lignification. It was reported that anomalies in tryphine composition led to male sterile phenotypes that could be rescued by growth at high air humidity (Koornneef et al., 1989). To test whether pollen collapse upon elevated temperature in *prt1-1^{ts}* was also a consequence of aberrations in pollen wall formation, plants were matured at 100 percent air humidity (established by covering the plants with a transparent bag). But no silique formation was observed upon these treatments (Fig. S8), suggesting that microspore desiccation or failure to re-hydrate might not be the reason for male sterility of *prt1-1^{ts}*.

Taken together, *prt1-1^{ts}* exhibited a defect in male gametogenesis under elevated temperature, manifesting at the transition from microspores to pollen grains. The vast majority of microspores arrested after release from the tetrads and eventually collapsed at anthesis. However, some *prt1-1^{ts}* microspores obviously underwent pollen mitoses since tricellular pollen grains were observed and some pollen grains escaped from collapse. Moreover, individual gametes were found in microsections and microspore preparations which were of irregular size and shape, indicating asynchronous development or abnormal DNA contents of these microspores.

3.1.5 Conditional male sterility of *prt1-1^{ts}* is likely a sporophytic trait

Problems in male gametogenesis can either arise from a malfunction of the maternal (sporophytic) tissues or from defects inherent to the mutant gametes. Hence, the fact that heterozygous plants exhibited WT-like silique formation at the elevated temperature (Fig. 10B, S1) could be explained by two scenarios (Fig. 15): 1. In heterozygous anthers, only gametes with the WT allele reach maturity at 28°C, which is still sufficient pollen amount to confer WT-like fertility (i.e., the mutation affected the gametophyte). 2. Heterozygous anthers developed WT-like because half gene dose in the sporophytic tissue was sufficient to support normal gametophyte development of both WT and mutant gametes (i.e., the mutation affected the sporophyte). When the genetic locus causing the

sterility phenotype is known, both scenarios can be distinguished by performing a backcross of the WT to a heterozygous father and genotyping of the progeny.

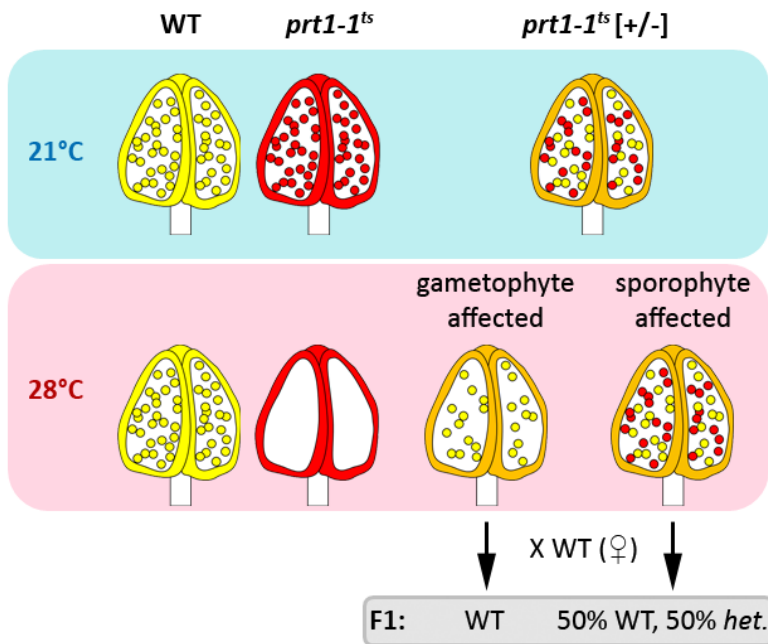


Fig 15| Principle of trait analysis to differentiate sporophytic and gametophytic manifestation of a recessive male sterility phenotype. The model depicts sporophytic (anther) and gametophytic (pollens) tissues at permissive (here: 21°C) and restrictive (here: 28°C) conditions. The color code of the anthers indicates the presence of a specific allele (here: *prt1-1^{ts}*), with yellow signaling the WT genotype (homozygous or haploid), red the mutant genotype (homozygous or haploid), and orange indicating a heterozygous situation (*prt1-1^{ts} [+/-]*). When heterozygous plants are backcrossed as the father to WT plants under restrictive conditions, all F1 descendants have the WT genotype in a gametophytic

trait situation, while a mutation affecting the sporophyte leads to half WT, half heterozygous progeny. Anther pictograms were adapted from Sanders et al. (2000).

Since the mutation causing the phenotype in *prt1-1^{ts}* was not known, genetic linkage to the *prt1-1* allele was exploited for the experiment. Two independent crossing experiments of WT × *prt1-1^{ts} [+/-]* performed at 28°C yielded 41 percent ($n = 17$) and 45 percent ($n = 44$) of plants heterozygous for the *prt1-1* allele among the F1 generation. Given a recombination frequency of maximal 31 percent (see chapter 3.1.2), a gametophytic manifestation of the phenotype-causing mutation would statistically require that not much more than 31 percent of the progeny are heterozygous for the *prt1-1* allele, while 50 percent would be expected for a sporophytic trait. Thus, the mutant allele transmitted in a way more supporting a sporophytic trait causing the sterility of *prt1-1^{ts}*.

3.1.6 Several genes are differentially expressed in anthers of *prt1-1^{ts}*

Both sporophytic anther parts and pollen rely on an intricately regulated genetic network for faithful gametogenesis and pollen release (Becker et al., 2003; Wijeratne et al., 2007; Pearce et al., 2015; Li et al., 2017a). Aberrations of anther development that cause male sterility often cause misexpression of regulated genes (Wijeratne et al., 2007). Hence, in order to narrow down the cause of the male sterility in *prt1-1^{ts}*, the expression of a number of genes was assessed using quantitative reverse transcription polymerase chain reaction (qRT-PCR) on WT and mutant anthers (samples included also residues of the filaments attached) of flower stages 11 to 13 (i.e., postmeiotic anther stages) grown at 28°C. Here, target genes were chosen that were relevant to pollen development by means of hormone signaling or synthesis, carbohydrate metabolism, or pollen exine formation.

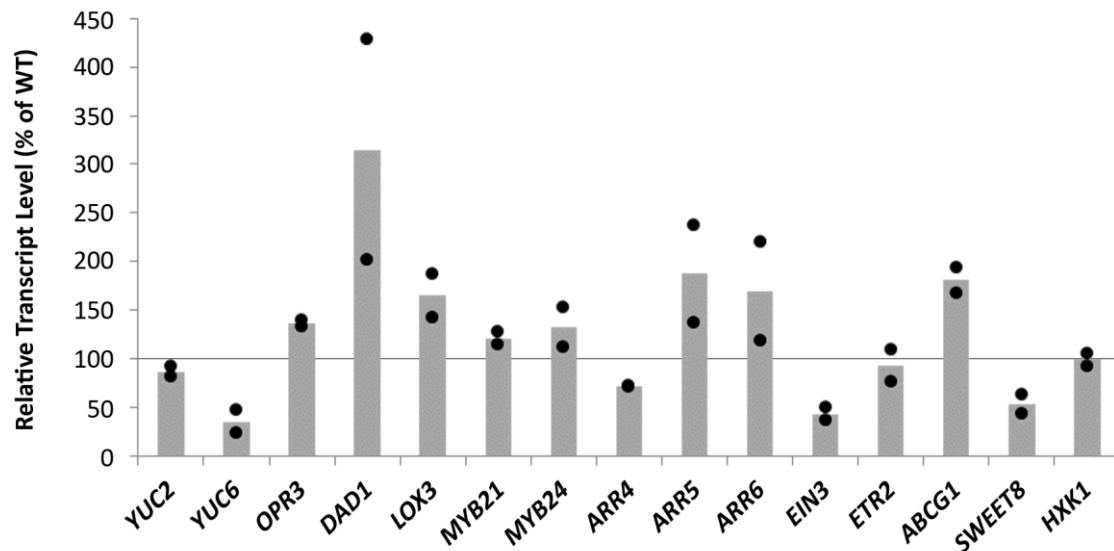


Fig. 16] Marker gene expression of *prt1-1^{ts}* anthers at mild heat in comparison to the WT. Plants of WT or *prt1-1^{ts}* mutant genotype were grown at 28°C. At a plant age of 7-8 weeks, anthers at flower stages 11 to 13 were collected and pooled from about 50 plants per genotype and experiment. Two independent experiments were conducted, comprising each two technical replicates. Transcript levels were calculated relative to the expression of the housekeeping gene *PP2A* and expressed as a percentage of the WT values. Bars represent the means between both experiments. The mean values calculated from the technical replicates of both individual experiments are depicted as dots.

Of the transcripts investigated, a trend was observed in the mutant anthers towards a slightly higher expression of JA biosynthesis genes such as *OPR3*, *DAD1*, and *LOX3* compared to the WT (Fig. 16). Of these, *DAD1* was most upregulated in the mutant, albeit displaying quite high deviation between the two biological replicates. Despite increased JA biosynthetic gene expression, the transcription factor genes *MYB21* and *MYB24*, which are known to be induced by JA in stamens (Mandaokar et al., 2006), were found to be only marginally elevated in *prt1-1^{ts}* mutant anthers (Fig. 16).

The auxin biosynthetic genes *YUC2* and *YUC6* were reported to be expressed in early differentiating anther tissues, throughout the microspores and until the early pollen stage (Cecchetti et al., 2008). Crucially, in a study performed by Sakata et al. (2010), both transcripts were found to be reduced by ~60 (*YUC2*) and ~75 (*YUC6*) percent in anthers of the premeiotic to meiotic stage upon three days of heat stress. Hence, *YUC2* and *YUC6* transcript levels were also investigated in Col-0 and *prt1-1^{ts}* anthers of postmeiotic stages at elevated temperature. Here, the relative transcript level of *YUC2* was found to be comparable between both genotypes (Fig. 16). In contrast, *YUC6* transcript was clearly less abundant in the mutant *prt1* compared to the WT (Fig. 16), indicating reduced contribution of this gene to auxin biosynthesis in *prt1-1^{ts}* under warm temperatures. Of note, in contrast to *YUC2*, promoter activity of *YUC6* was also strongly observed in mature pollen grains by the use of promoter::GUS constructs (Cheng et al., 2006). In the experiment performed within the work presented here, the fraction of mature pollen grains was obviously reduced in mutant anther preparations for qRT-PCR. Thus, it could not be fully ruled out that the apparent downregulation of *YUC6* was an artefact caused by the lower abundance of mature pollen grains in the mutant anther samples. However, RNA in situ hybridizations (Cecchetti et al., 2008), as well as GFP fusions of *YUC2* and *YUC6* coding sequences (CDS) (Yao et al., 2018), did not support higher transcript abundance of *YUC6* at the mature pollen stage, but showed co-expression of both genes throughout anther tissues and stages. Thus, to address the possibility that the sterility phenotype was caused by depressed auxin biosynthesis, mutant plants grown at 28°C were repeatedly sprayed with a solution containing

the synthetic auxin 1-naphthaleneacetic acid (NAA) and examined for silique formation. In a previous work, such a treatment was able to rescue defects in anther development of Col-0 plants induced by high temperature conditions (31°C or 33°C) (Sakata et al., 2010). However, reconstitution of silique formation was not achieved by this treatment (data not shown). Hence, reduced auxin biosynthesis is unlikely to be the major cause of the temperature sensitivity in *prt1-1^{ts}*.

There is growing evidence for the participation of cytokinins in the regulation of stamen development (Huang et al., 2003a; Werner et al., 2003; Nishimura et al., 2004; Kinoshita-Tsujimura and Kakimoto, 2011; Zuñiga-Mayo et al., 2018). Strikingly, the phenotype observed for *prt1-1^{ts}* resembled to some extent the effect reported for a mutant of the *PUB4* gene: The mutant line *Atpub4* was described to be male sterile in a temperature-dependent manner, since plants were infertile at 22°C, whereas partial fertility was restored when plants were grown at 16°C (Wang et al., 2013a). In this mutant, the tapetum degenerated incompletely, leading to abnormal exine structures and failure to dehisce. *PUB4*, together with *PUB2*, were later shown to be involved in cytokinin signaling (Wang et al., 2017). Thus, *PUB4* establishes a potential link between cytokinins and the temperature adaptation of male reproduction. To investigate whether cytokinin signaling was affected in *prt1-1^{ts}* anthers at the restrictive temperature, *type-A ARR* genes were included in the transcript analysis of *prt1-1^{ts}* stamens. In order to obtain robust reporters of cytokinin signaling, *ARR5* and *ARR6* were chosen for the high responsiveness of their transcripts towards cytokinins, and *ARR4* for its relatively high basal expression levels (D'Agostino et al., 2000; Rashotte et al., 2003; To et al., 2004). Differential expression between *prt1-1^{ts}* and WT was observed for all three *type-A ARR*s (Fig. 16). Interestingly, while transcript levels of *ARR5* and *ARR6* were increased in the mutant anthers, indicating a slight increase in cytokinin levels in anthers of *prt1-1^{ts}*, a slight downregulation of *ARR4* was detected in comparison to the WT (Fig. 16).

Transcriptional induction of the ethylene signaling components *EIN3* and *ETR2* was reported to also be part of the early response to cytokinin sensing (Brenner et al., 2005). When analyzing anthers grown at elevated temperature, downregulation of *EIN3* transcript, but not of *ETR2*, was observed in *prt1-1^{ts}*, again demonstrating a more complex deregulation of cytokinin-related gene expression in the mutant anthers. Notably, while both genes have major functions in ethylene signaling, only *ETR2* expression was described to be induced by ethylene (Hua et al., 1998; Ellison et al., 2011), whereas *EIN3* transcript levels are unaffected by ethylene treatment (Chao et al., 1997). Thus, given that *ETR2* mRNA levels were unchanged in *prt1-1^{ts}* anthers compared to the WT at high temperature, ethylene levels were potentially unchanged in the mutant anthers, or only slightly elevated. In contrast, downstream signaling via *EIN3* appeared to be affected in *prt1-1^{ts}* stamens, potentially through attenuated cytokinin signaling.

ABCG half-transporters are involved in the deposition of suberin at tissues with barrier functions, and *ABCG1*, in particular, is important for pollen exine and intine formation (Yadav et al., 2014; Yim et al., 2016). Consistent with the increased staining of phenolic compounds on *prt1-1^{ts}* microspores that was visible in anther thin sections at stage 11 (Fig. 13), *ABCG1* transcript was upregulated in these stamens as compared to the WT (Fig. 16).

Similar to *ABCG1*, the hexose transporter *SWEET8/RPG1* is essential for exine pattern formation and pollen viability, by facilitating proper callose deposition and primexine formation (Guan et al., 2008; Chen et al., 2010b; Sun et al., 2013). Highest expression of *SWEET8* is seen in the tapetum and microspores at the meiotic stage (5/6) (Guan et al., 2008). Within this work, in samples of post-

meiotic anthers at mild heat stress, *SWEET8* transcript was also detected to relatively high amounts: In the WT, transcript levels relative to the housekeeping gene *PROTEIN PHOSPHATASE 2A (PP2A)* were comparable to *YUC2* values in both experiments (Tab. S2). Interestingly, a reduction of the transcript level of *SWEET8* was detected in *prt1-1^{ts}*, suggesting reduced metabolic activity associated with exine maturation. In contrast, *HXX1* – encoding for a protein with glucose sensor function (Moore et al., 2003; Ramon et al., 2008) – is most expressed in stamens of flowers at stage 12 according to publicly available expression data (*Arabidopsis* eFP Browser; Schmid et al., 2005; Winter et al., 2007). Thus, *HXX1* expression should be relatively high in the samples that were collected for this experiment. Furthermore, *HXX1* transcript is responsive to exogenously supplied sugars as indicated by microarray expression data available at *Genevestigator* (experiment IDs AT_00639, AT_00650, and AT_00313). *HXX1* was found to be transcriptionally unchanged in anthers between WT and *prt1-1^{ts}* (Fig. 16), supporting that both samples (WT and mutant) contained predominantly anthers of the targeted stage. Moreover, constant *HXX1* levels might indicate that sugar availability was not altered in *prt1-1^{ts}* anthers.

In summary, the mutant line *prt1-1^{ts}* was found to be male sterile conditional on a moderately elevated ambient temperature, but the phenotype was caused by a second site genetic alteration which was genetically linked to *PRT1*. The cause of the male sterility of *prt1-1^{ts}* was most likely microspore abortion occurring after meiotic divisions. The mutant line exhibited differential expression of genes related to hormonal pathways, most clearly of JA biosynthesis and cytokinin signaling, but also of genes associated with pollen wall biosynthesis. These findings are in accordance with a postmeiotic defect in microspore development of *prt1-1^{ts}*, since JA signaling predominantly affects later stages of anther development, and also cytokinin appears to act mainly during postmeiotic stages of microspore maturation (Kinoshita-Tsujimura and Kakimoto, 2011).

3.2 PRT1 promoter activity

Information on the expression pattern of the *PRT1* promoter and the localization of the PRT1 protein could help to unravel the gene's physiological role. To this end, stably transformed *Arabidopsis* lines were created that expressed the β -glucuronidase (*GUS*) reporter gene under the control of the *PRT1* promoter or of the *ARABIDOPSIS TOXICOS EN LEVADURA 9* promoter (*proATL9*) as a control. *ATL9* encodes for an E3 Ub ligase involved in plant immunity (Deng et al., 2017).

Because of amplification difficulties, the *PRT1* promoter could only be obtained as a sequence lacking CTCT in a 65 bp repetitive sequence that starts 10 bp upstream of the start codon. The resulting construct is therefore referred to as *proPRT1^{ACTCT}*.

At the seedling stage, in the vast majority of the 49 *proPRT1^{ACTCT}::GUS* T2 lines examined, no GUS signal (Fig. 17A) or a weak signal restricted to vascular tissues (Fig. 17B) was detected. Individual lines exhibited relatively strong staining at the shoot and root apices (Fig. 17C), indicating promoter activity at meristematic regions. Notably, signal strength variation observed between T2 lines were likely due to different numbers of T-DNA insertions, since T2 lines with the strongest reporter expression exhibited little to no segregation on selective medium (including lines 26 and 40 shown in Fig. 17C and 17B, respectively). In contrast, *GUS* expressed from *proATL9* reported uniform expression in seedling roots of all tested T2 and T3 lines (Fig. 17D). Here, staining in the root was strongest in the central portion of the primary root, starting at the site of emergence of the first

lateral root down to the end of the root hair zone. In more developed seedlings (age 14 days) and more expanded root systems, staining of the lateral roots was at least as strong as of the primary root (Fig. 18). At this age, the root tip was also stained in many lines (Fig. 18B). Expression of *ATL9* in the seedling root is consistent with microarray data publicly available at the *Arabidopsis eFP Browser*. The finding however conflicts with recent work from Deng et al. (2017) who reported *proATL9::GUS* activity at this seedling stage predominantly in vasculature, hypocotyl, leaves, petioles and stems.

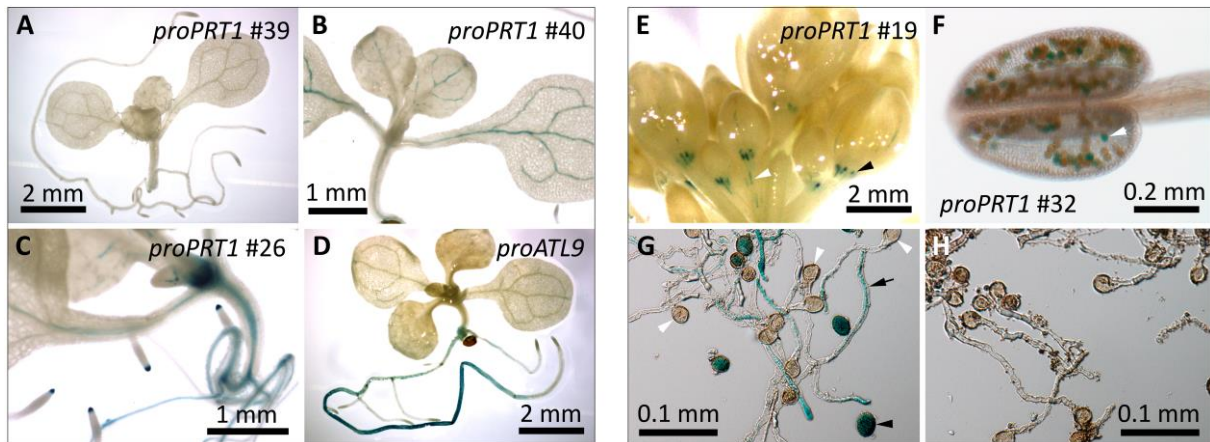


Fig. 17 | Promoter activity of the *PRT1* gene and control genes in *GUS* reporter lines. Histochemical analysis of β -glucuronidase (*GUS*) activity in *promoter::GUS* expressing *Arabidopsis* lines. **A-D**, *GUS* activity in 10 days old seedlings transformed with *proPRT1^{ACTCT}::GUS* (**A-C**) or *proATL9::GUS* (**D**). **A-C**, *PRT1* expression in seedlings of independent transformation events is below the detection level (**A**), weakly detected in vascular tissues (**B**), or localized to shoot and root apices (**C**); **D**, *proATL9::GUS* confers *GUS* activity restricted to the root in seedlings. **E-H**, Expression of *proPRT1^{ACTCT}::GUS* in single-T-DNA-insertion lines (**E**, **F** and **H**) or (**G**) *proIQD4::GUS* (the plant line was kindly provided by K. Bürstenbinder) in reproductive tissues. **E**, *proPRT1^{ACTCT}::GUS* expression in inflorescences is seen at the base of young flowers (black arrowhead), and in pedicles (white arrowhead). **F**, *GUS* staining in individual pollen grains (arrowhead) of dehiscent anthers was detected in at least three independent T2 lines, including the depicted line 32, but could not be detected in T3 lines. **G**, **H**, *GUS* activity in germinating pollen. **G**, *proIQD4::GUS* yields signals in pollen tubes (black arrow) and mature pollen grains (black arrowhead), but not in germinating pollen grains (white arrowheads). **H**, No *GUS* activity was detected in germinating pollen or pollen tubes of *proPRT1^{ACTCT}::GUS* expressing lines (T3).

In flowers of single-T-DNA-insertion lines of *proPRT1^{ACTCT}::GUS* expressing plants, reporter activity was detected predominantly in a stripe-like pattern potentially coinciding with vasculature at the base of young flowers, i.e. the junction between pedicle and young petals (Fig. 17E). This signal was restricted to flowers younger than approximately stage 10-11. Less frequently, staining was seen in the pedicle or stem vasculature (Fig. 17E). The signal at the young flower base was observed in three independent lines with single insertions of the T-DNA in the T2 as well as in the T3 generations. Furthermore, *GUS* staining of individual pollen grains of dehiscent anthers was observed in three independent transgenic lines of *proPRT1^{ACTCT}::GUS* in the T2 generation (Fig. 17F), but could not be detected in T3 lines anymore. Of note, *PRT1* transcript abundance is reported to have a maximum in mature pollen grains according to the data available at the *Arabidopsis eFP Browser*.

In order to test if *proPRT1^{ACTCT}* was active in germinating pollen grains or pollen tubes, pollen germination assays and subsequent *GUS* stainings were performed. Here, no expression of *GUS* from *proPRT1^{ACTCT}* could be detected (Fig. 17H). However, *GUS* activity was readily detected in pollen tubes and mature pollen grains, but not in germinating pollen, when *GUS* expression was driven by the *IQ-DOMAIN 4* promoter (Fig. 17G; *proIQD4::GUS*; stable transgenic lines were kindly provided by

Jakob Quegwer¹ and Katharina Bürstenbinder¹ and the line was previously published in Bürstenbinder et al. (2017)).

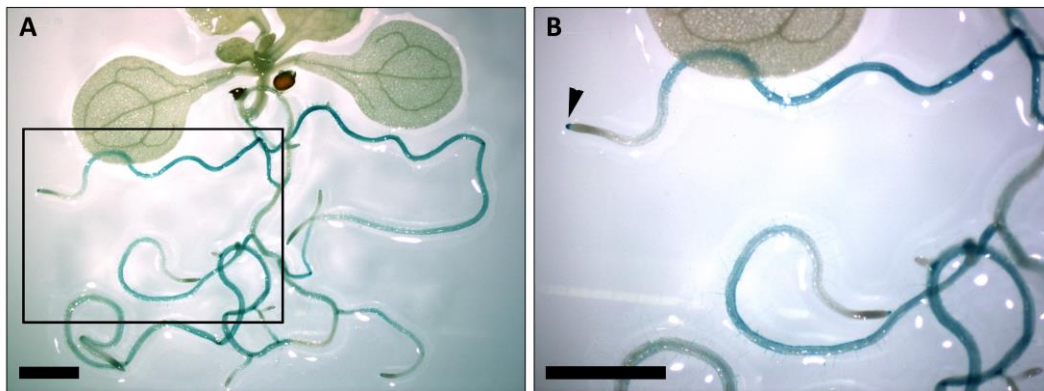


Fig. 18 | Expression pattern of the *ATL9* promoter in seedling roots at 14 days age. GUS reporter activity was analyzed in T3 lines stably transformed with *proATL9::GUS*. **A**, In branched root systems, promoter activity was observed in lateral roots as well as the younger part of the primary root. **B**, Magnification of A. Next to the maturation and root hair zones, GUS signal in the root tip was also observed in some, but not all T3 lines (arrowhead). Scale bars: 1 mm.

Because of the deletion of four nucleotides in the *PRT1* promoter sequence, the functionality of the construct was confirmed by RT-PCR analysis of transgenic mRNA produced from *proPRT1^{ΔCTCT}* in two different stable transgenic contexts: Plant lines in the *prt1-1^{ts}* genetic background expressed either the *PRT1* CDS as a GFP-tagged variant where Cys-29 of PRT1 had been replaced by Ala (see chapter 3.3.2), or the coding sequence for the WT protein with a triple hemagglutinin (HA) tag.

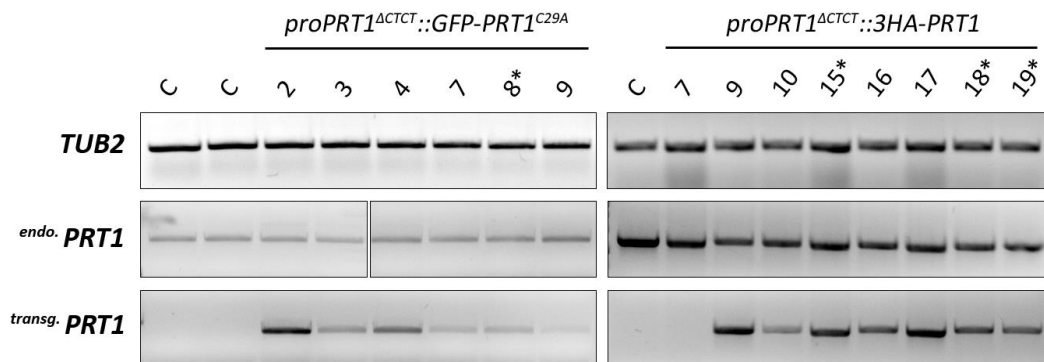


Fig. 19 | *PRT1* transcript is expressed from the *proPRT1^{ΔCTCT}* promoter construct. *Arabidopsis* lines of the *prt1-1^{ts}* mutant genotype were stably transformed with either *proPRT1^{ΔCTCT}::GFP-PRT1^{C29A}* or *proPRT1^{ΔCTCT}::3HA-PRT1* and transcript analysis was performed by semi-quantitative RT-PCR. Transcript of the endogenous *PRT1* gene was targeted by amplification priming in the 5' UTR that was absent from the *PRT1* transgenic sequence. Transgenic transcript was amplified starting in the sequence of the affinity tag. For the experiment using GFP-*PRT1^{C29A}* lines in the left panel, flower material of T2 lines was analyzed and PCR cycle numbers were the same for amplification of both the housekeeping gene *TUBULIN BETA CHAIN 2 (TUB2)* and the *PRT1* targets. In the case of 3HA-*PRT1* lines in the right panels, samples were derived from seedling material and amplification cycles were adjusted to yield similar amplicon levels for *TUB2* and *PRT1* sequences. Lines with single T-DNA insertions are marked by an asterisk. **C**, Control (untransformed *prt1-1^{ts}*); **endo-*PRT1***, endogenous *PRT1*; **transg-*PRT1***, transgenic *PRT1*.

¹ Leibniz Institute of Plant Biochemistry, 06120 Halle (Saale), Germany

Of these transgenic lines, random T2 lines were selected for transcript analysis. In almost all cases, transgenic *PRT1* transcript was detected (Fig. 19). The levels of expression varied between lines, but were roughly comparable to the levels of the endogenous mRNA, especially in the cases of transformants with potential single insertions of the T-DNA which was determined by segregation on selective medium. This data indicated that neither the activity of the cloned *PRT1* promoter, nor the stability of the transgenic transcript was affected by the deletion in the downstream promoter sequence.

During RT-PCR (Fig. 19), as well as qRT-PCR (Fig. S5), signals for the endogenous *PRT1* transcript were overall low for both flower (Fig. 19) and leaf material (Fig. 19, S5), and suggested a weak expression of the endogenous promoter of *PRT1*, confirming what was concluded from the GUS reporter analyses. Moreover, recombinant protein in transgenic *PRT1*-expressing lines could not be detected by immunoblot analysis against the GFP- or the HA tag, respectively, in any genetic context, even after enrichment via immunoprecipitation (data not shown). In fact, PRT1 immunoblot detection failed in stable transgenic lines (all in the *prt1-1^{ts}* genomic background) expressing *p35S::PRT1-3HA*, *proPRT1^{ΔCTCT}::3HA-PRT1*, *proPRT1^{ΔCTCT}::GFP-PRT1*, and *proPRT1^{ΔCTCT}::GFP-PRT1^{C29A}*. The extremely difficult recovery of PRT1 protein from transgenic lines despite detectable transcript levels indicated that the protein exhibited low stability *in planta*.

It was aimed to confirm the results for *PRT1* expression patterns obtained from the GUS reporter system by transgenic lines stably expressing *eGFP* under control of the *PRT1* promoter construct (*proPRT1^{ΔCTCT}::eGFP*). Yet, no fluorescent signal corresponding to GFP was detected in any of the examined transgenic lines either at the seedling stage, in anthers, or in pollen grains. The same was true for the plant lines expressing the translational fusions of GFP-PRT1 or GFP-PRT1^{C29A} (data not shown).

The findings presented here showed that the *PRT1* promoter has overall low activity with a predominance to vascular and apical tissues of seedlings and to the basis of young flowers. Interestingly, the young flower basis is a region with potentially high proliferating activity (Ichihashi et al., 2011; Ichihashi and Tsukaya, 2015). This, together with the observation of promoter activity in apical tissues of some reporter lines, suggests a role for *PRT1* at certain meristematic cells.

3.3 Biochemical characterization of the PRT1 protein

Until the beginning of this work, the function of the *PRT1* gene was investigated exclusively by means of genetic approaches. Hereby it was shown that the gene is necessary for the degradation of reporter constructs bearing type II N-degrons in plants, and that heterologous expression of *PRT1* confers instability to such constructs in yeast. However, the cellular environment in these genetic experiments might provide additional unknown factors which are required for PRT1 activity, thus obscuring details of the enzymatic function of PRT1. Furthermore, the determinants for substrate recognition by PRT1 were assessed only to the level of the very N-terminal amino acid of a flexible linker at the N-terminus of a test substrate. Therefore, we sought to characterize the PRT1 protein in more detail using recombinantly expressed purified protein *in vitro*.

3.3.1 PRT1 acts as an E3 ubiquitin ligase *in vitro*

Bioinformatical analysis identifies two putative RING domains within the PRT1 protein sequence, and the *PRT1* gene was associated with protein stability and ubiquitination events in plants (Potuschak et al., 1998; Stary et al., 2003), leading to the hypothesis that it acts as an Ub ligase. However, *in-vitro* ubiquitination activity of purified PRT1 had never been shown, and the reported *in-vivo* dependency of test substrate instability on the presence of PRT1 could still be explained by PRT1 functioning as an adaptor molecule, rather than a catalyst. Hence, in order to test if PRT1 acts as an E3 ubiquitin ligase *in vitro*, an *Escherichia coli* clone carrying *PRT1* fused N-terminally with an eightfold His-tag in combination with the MALTOSE BINDING PROTEIN (MBP) tag (^{His}MBP-PRT1; kindly provided by Christin Naumann¹) was used for protein expression and purification (Fig. S9). To investigate if the recombinant protein featured E3 activity *in vitro*, an autoubiquitination assay was set up engaging *Arabidopsis* UB ACTIVATING ENZYME 1 (UBA1) and UB CONJUGATING ENZYME 8 (UBC8) as E1 and E2 enzymes, respectively (purified 6His-UBA1 and 6His-UBC8 were kindly provided by Marco Trujillo^{1,2} and Augustin Mot^{1,3}). UBC8 constitutes a promiscuous E2 enzyme that is active with various RING-type E3 ligases (Kraft et al., 2005), and therefore was a good candidate to function in combination with PRT1. UBA1 is supposed to act redundantly with the second E1 enzyme in *Arabidopsis*, UBA2, since they exhibit very similar expression patterns and the recombinant enzymes showed the same *in-vitro* capacity for Ub activation (Hatfield et al., 1997). The combined use of UBA1 and UBC8 in autoubiquitination assays employing plant E3 ligases was established previously (Stegmann et al., 2012), and the same fusion constructs were applied in this work as published by Stegmann and coworkers.

In the performed assay, E3 autoubiquitination becomes apparent by the formation of higher molecular weight protein species, which are seen as a smear of Ub signal upon immunoblot. In the presence of ATP, Ub, E1, E2, and PRT1 enzyme, the formation of protein species of intermediate to high molecular weight was detectable with an anti-Ub antibody (Fig. 20A). When instead of the PRT1 fusion protein the protein tag (^{His}MBP) alone was added to the reaction, no ubiquitination smear appeared in the immunoblot, showing that PRT1 protein was responsible for the catalysis of the Ub ligation. Since no additional substrate protein was provided for Ub transfer in the assay, it was concluded that the observed high-molecular weight signals represented mainly poly-Ub chains as a result of autoubiquitination. This was supported by the signals obtained from an antibody against the His tag, where the band corresponding to the unmodified species of the E3 were weaker in those samples showing an ubiquitination smear in the anti-Ub blot (Fig. 20). However, approaches using the anti-His antibody failed to detect modified versions of ^{His}MBP-PRT1. This might be due to differences in sensitivity between the two antibodies, as well as to the fact that each ubiquitinated E3 species contained only one molecule of ^{His}MBP-PRT1, but increasing amounts of Ub epitopes with higher order modified species.

Furthermore, when PRT1 was added to activated UBC8 enzyme (i.e., in the presence of Ub, ATP and E1), the formation of di- and tri-ubiquitinated species of the E2 was strongly enhanced compared to the same reaction lacking PRT1 (Fig. 20A). This indicated that the presence of PRT1 augmented the

¹ Leibniz Institute of Plant Biochemistry, 06120 Halle (Saale), Germany

² University of Freiburg, 79104 Freiburg, Germany

³ Babeş-Bolyai University, Cluj-Napoca RO-400028, Romania

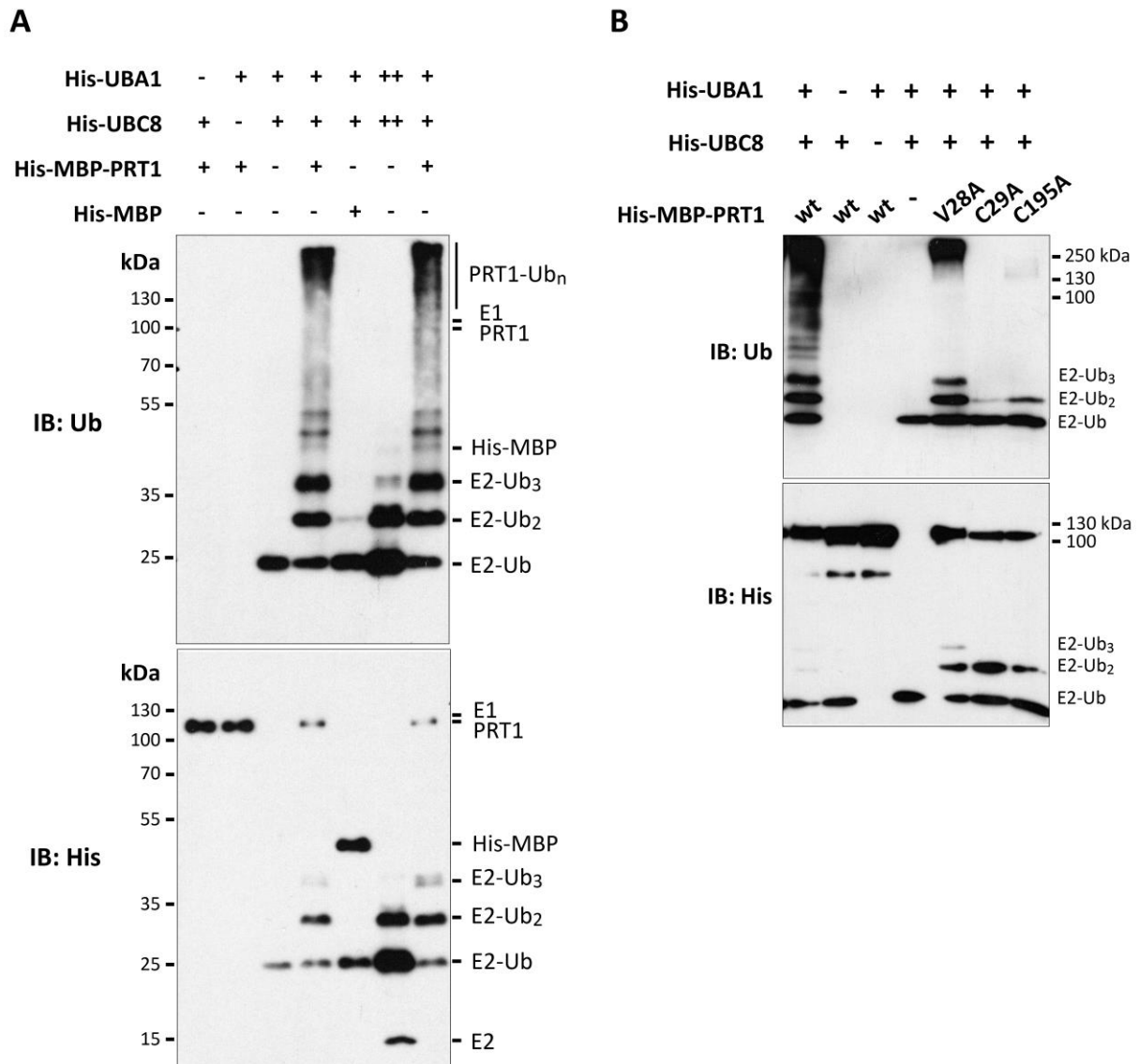


Fig. 20 | PRT1 acts as an E3 Ub ligase *in vitro* by engaging both RING1 and RING2. **A**, Recombinant PRT1, UBA1 and UBC8 proteins were combined with ATP and Ub, as indicated. The reaction was performed for 3 hours at 30°C, and the samples in the endpoint reaction states were subjected to SDS-PAGE followed by immunoblotting with anti-Ub or anti-His antibodies, respectively. E1 and E2 enzymes were provided at standard (+) or ten-fold (++) concentrations. Poly-Ub chains on substrate proteins (e.g., PRT1 itself: PRT1-Ub_n) is visible in the immunoblot using anti-Ub antibody (P4D1). **B**, Endpoint autoubiquitination as described in A but involving mutant versions of PRT1 with amino acid changes to Ala of Val-28 (RING1), Cys-29 (RING1), or Cys-195 (RING2).

ability of the E2 to multi-mono-ubiquitinate itself, or that the E3 used the E2 as a substrate. In contrast, the autocatalysis of E2 in combination with HisMBP alone was marginal (Fig. 20A). This finding was consistent with the assumption that the presence of a RING domain is able to activate E2 enzymes of the mammalian Ube2D family, which is homolog to *Arabidopsis* UBC8 (Scheffner et al., 1994; Stewart et al., 2016), towards reaction with Lys (Ozkan et al., 2005; Wenzel et al., 2011; Stewart et al., 2016). Interestingly, the same effect on E2, but no autoubiquitination, was observed when purified PRT7 (Fig. S9), a PHD-finger protein-like protein with potential N-end rule adapter function (Garzón et al., 2007; Talloji, 2011), was subjected to the autoubiquitination reaction (Fig. S10). This indicated that the increased formation of ubiquitinated E2 species were the result of

enhanced autocatalysis performed by the E2, which is apparently also facilitated by the presence of a PHD domain *in vitro*.

Notably, ^{His}MBP-PRT7 exhibited a considerably higher migration pattern in sodium dodecyl sulfate polyacrylamide gel electrophoresis (SDS-PAGE) than would be expected from the molecular weight of the protein (~130 kDa apparent vs. 96.5 kDa calculated; Fig. S9). However, the protein band at 130 kDa was excised from an SDS polyacrylamide gel, and the identity of PRT7 was confirmed by mass spectrometry with a sequence coverage of 81 percent (data not shown; unpublished results by Wolfgang Hoehenwarter¹ and Petra Majovsky¹).

Together, the result showed for the first time that PRT1 1) is active as an E3 Ub ligase catalyzing the reaction of poly-Ub chain formation, 2) is able to cooperate with UBC8 *in vitro*, and 3) is enzymatically active as an N-terminally tagged version.

3.3.2 Both RING domains of PRT1 are required for autoubiquitination

The domain structure of PRT1 is characterized by the presence of two RING finger domains and one ZZ domain (Fig. 3). Because one RING is normally sufficient for the activity of RING E3 ligases, and the ZZ domain was presumed to work as a protein-protein interaction site rather than being involved in catalysis (Stary et al., 2003; Mogk et al., 2007), it was asked whether both RING finger domains are required for PRT1's autoubiquitination activity.

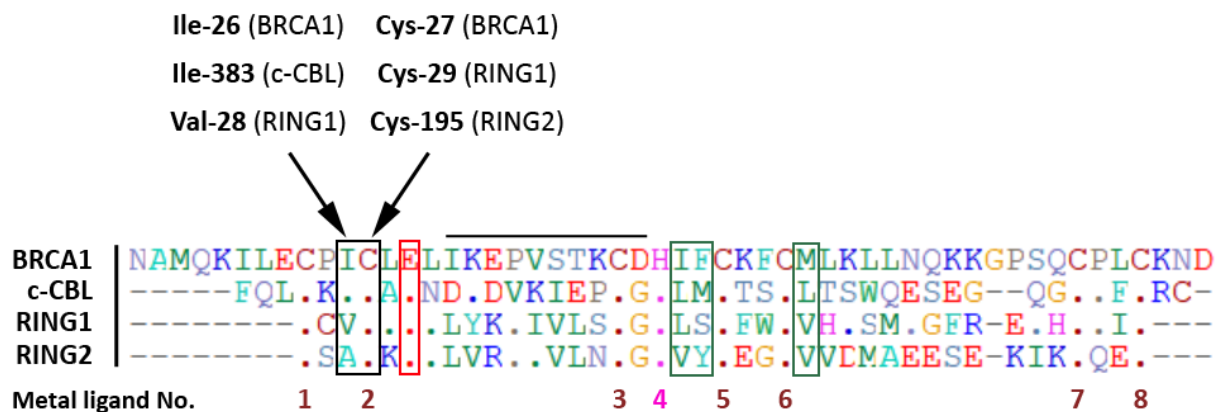


Fig. 21 | Alignment of the amino acid sequences of the PRT1 RING domains with human E3 RING domains of the C3HC4 type. The alignment with human BRCA1 and c-CBL with the PRT1 RING domains shows conservation of all eight potential metal coordinating (ligand) residues (Cys and His, numbered below), characterizing the RING domains of PRT1 as of the C3HC4 type. Residues that were previously found to be important for the catalytic activity of these human E3 ligases (Zheng et al., 2000; Brzovic et al., 2003; Stone et al., 2005), and were therefore selected for mutation at the respective PRT1 RING sites, are highlighted with arrows. The red box indicates a conserved negatively charged residue and dark green boxes highlight conserved hydrophobic residues. The stretch between metal ligands 2 and 3 which shows divergence between the human and the *Arabidopsis* sequences is marked by a black bar above. The following amino acid (aa) sequences are presented: BRCA1 aa18-67, c-CBL aa378-421, PRT1_RING1 aa26-65, and PRT1_RING2 aa192-231. A dot indicates conservation of the amino acid as compared to the uppermost (BRCA1) sequence.

¹ Leibniz Institute of Plant Biochemistry, 06120 Halle (Saale), Germany

To address this, it was aimed to identify residues of PRT1 that, when mutated, could be expected to have a significant impact on catalytic activity. To this end, the amino acid sequences of the two RING domains of PRT1 were aligned to the RING finger domains of the well characterized human E3 ligases BREAST CANCER 1 (BRCA1) and c-CBL (referred to hereafter as BRCA1^{RING} and c-CBL^{RING}). These human RING domains were chosen because they are of the C3HC4 type, as it is the case for both RING domains of PRT1 (referred to hereafter as RING1 and RING2).

The alignment of the four RING domains showed relatively low conservation between the *Arabidopsis* and the human sequences apart from the metal coordinating residues (Fig. 21). Divergence between the human RING domains and the PRT1 domains was found particularly within the stretch between the second and the third metal ligand, particularly a loss of negatively charged residues in the PRT1 domains (Fig. 21, black bar). Interestingly, RING2, but not RING1, was furthermore enriched in negative charges throughout the second half of the domain.

For both BRCA1 and c-CBL, it was reported that mutating the hydrophobic residue preceding metal ligand 2 completely abrogated E3 activity *in vitro* (Zheng et al., 2000; Brzovic et al., 2003; Stone et al., 2005). This effect was attributed to the disruption of the E2 interface. In the case of BRCA1, the mutation of the respective Ile-26 to Ala, a smaller but likewise hydrophobic residue, was sufficient to prohibit autoubiquitination activity (Brzovic et al., 2003). Interestingly, in RING2, Ala occurs naturally at this position. This allowed speculation that in PRT1, RING1 but not RING2 might be responsible for the E2 interaction. To test this, the hydrophobic valine (V, Val) 28 of RING1, which aligns with BRCA1 Ile-26 (Fig. 21), was mutated to Ala (PRT1^{V28A}). In order to furthermore address the contribution of the individual RING domains to PRT1 activity, two more mutants were created with Cys to Ala mutations at the position of the second metal ligand of either of the two domains (referred to as PRT1^{C29A} and PRT1^{C195A} for RING1 and RING2 mutations, respectively). These mutations were expected to massively disturb the integrity of the affected RING domain, and it was shown previously that mutation of the respective Cys residue in other RING E3 ligases abolished RING domain function (Lorick et al., 1999; Brzovic et al., 2003).

All three mutant proteins could be expressed to equal amounts in *E. coli* (Fig. S11). However, purification efficiency via Ni-NTA column was rather poor, as was the case already for the WT protein, and translational abrogation products were co-purified with high efficiency (Fig. S9). Moreover, especially the Cys mutants showed a tendency to aggregate upon higher concentration even as a fusion with the highly soluble MBP-tag (data not shown). This could be a consequence of protein misfolding due to the disturbed domain structure.

Nevertheless, recombinant protein of all three mutated variants could be recovered at sufficient amounts for further *in-vitro* experiments. When subjected to the autoubiquitination reaction, all three PRT1 mutant variants exhibited compromised activity, differing in the degree of impairment (Fig. 20B). The V28A mutant, with a change that was expected to highly impact on E2 interaction, but to preserve overall structural integrity of the protein, was still capable of forming Ub chains of high molecular weight onto itself as well as it produced higher ubiquitinated species of the E2 enzyme (Fig. 20B). A strong reduction of activity of PRT1^{V28A} compared to the WT protein was most apparent at the disappearance of Ub conjugates of intermediate molecular weight (Fig. 20B). Such products were easily detected in the WT reaction and might represent ubiquitinated species of protein contaminants present in the reaction or of translational abrogation products of the E3 itself that were co-purified. Interestingly, detection of ubiquitination products of intermediate molecular

weight with PRT1^{V28A} could be restored by omitting reducing agents during SDS sample preparation (Fig. S12), indicating that these reaction products of PRT1^{V28A} might represent thioesterified E2-poly-Ub conjugates, rather than covalently ubiquitinated species. Nevertheless, the fact that the activity of PRT1^{V28A} was not abolished completely as it was the case for the respective mutant of BRCA1, suggests that this hydrophobic residue was not as crucial for E2 interaction of PRT1, or Ala at this position is able to partially fulfill the same function in RING1.

In contrast to Val-28, a single amino acid exchange of the metal coordinating Cys following Val-28 fully abolished autoubiquitination activity of PRT1 (Fig. 20B, S12). Hence, the integrity of the first RING domain was indispensable for PRT1 activity, even if RING2 was intact. Moreover, the appearance of a di-ubiquitinated E2 signal was marginal upon reaction with PRT1^{C29A} (Fig. 20, S12), and resembled incubation with the His⁶MBP control only. Thus, the first RING domain of PRT1 was also required for the above mentioned effect of RING domain proteins on E2 activation. This finding would be in accordance with the assumption that in PRT1, RING1 is most responsible for mediating the interaction with the E2 enzyme.

Disturbance of RING2 via mutation of Cys-195 also impaired PRT1 autoubiquitination activity severely (Fig. 20B, S12), showing that both RING domains are mechanistically involved in the reaction. However, although PRT1^{C195A} exhibited strongly repressed autoubiquitination activity, this mutant still enabled the production of some higher molecular weight ubiquitinated species, visible as the formation of a faint smear starting roughly 30 kDa higher than unmodified His⁶MBP-PRT1 (Fig. 20B, S12). Furthermore, next to residual ubiquitination activity, PRT1^{C195A} still triggered pronounced double- and triple-ubiquitination of the E2, consistent with retained E2 interaction capability of this mutant (Fig. 20B, S12). Hence, the second RING domain of PRT1 appeared to fulfill an additional role required for PRT1-mediated Ub ligation. So far, the requirement of more than one RING domain for E3 activity is known exclusively for RBR ligases (Wenzel et al., 2011). Here, interaction with the E2 is mediated by a canonical RING domain, and a second, C-terminal RING-like domain accepts Ub via a transient thioester in a HECT-like fashion (Wenzel et al., 2011; Riley et al., 2013). Given the requirement of two RING domains for the autoubiquitination activity of PRT1, a RBR-like mechanism of action could be proposed. However, none of the three Zn fingers present in PRT1 aligns well with the conserved RING2 domain of the RBR E3 ligase parkin which undergoes thioesterification with Ub (Riley et al., 2013; Fig. S13). Particularly the sequence divergence within the region preceding the catalytic Cys of parkin contradicts PRT1 acting as a RBR E3 ligase, since this region shows homology within the family of RBR E3 ligases (Eisenhaber et al., 2007). However, it is possible to align most of the Cys and His residues of PRT1 RING1 and RING2 to the sequence of RING2 from parkin (Fig. S13). Therefore, it was considered that the faint Ub smear seen with PRT1^{C195A} might contain thioesterified variants of PRT1, suggesting an HECT- or RBR-like mechanism of action for PRT1 that involves conjugation of Ub to RING1. To address this, it was tested whether the product of PRT1^{C195A} autoubiquitination would be increased when the protein was denatured in the absence of a reducing substance. However, ubiquitination products formed by PRT1^{C195A} were not sensitive to treatment with the reducing agent dithiothreitol (DTT), ruling out the possibility that they represented E3~Ub-thioesters (Fig. S12).

The finding that disturbance of RING1, but not RING2 resulted in a complete disruption of PRT1's autoubiquitination activity and E2 activation, indicated that RING1, rather than RING2, might be most responsible for E2 interaction. Additionally, RING2 was found to further support catalytic activity of PRT1 in another, almost equally important manner.

3.3.3 The *in-vitro* substrate specificity of PRT1

All work published on the substrate specificity of PRT1 was performed *in vivo* using reporter proteins as degradation targets that were equipped with either of two artificial N-terminal amino acid sequences (Bachmair and Varshavsky, 1989; Bachmair et al., 1993; Potuschak et al., 1998; Stary et al., 2003; Garzón et al., 2007). First, the N-terminal sequence used as a bait to isolate the *prt1-1* allele was initiated by Phe, followed by Arg-Ser and a subsequent 12 residue Gly stretch (FRS-[G]₁₂-RG...) (Bachmair and Varshavsky, 1989; Potuschak et al., 1998). This N-terminus was also employed by Stary et al. (2003) for Ub protein-reference constructs containing DHFR that were expressed in plants. Second, for complementation assays expressing *PRT1* in *Δubr1* mutant yeast cells, a β-galactosidase (β-gal) reporter was applied (Stary et al., 2003). Here, the reporter contained a 40 amino acids N-terminal extension derived from the *E. coli* Lac repressor (IacI), as a consequence of the cloning strategy that was originally applied to construct the reporter (Bachmair and Varshavsky, 1989). This linker sequence (X-HGSGAWLLPVSLVKRK...) was termed e^K (extension [e] containing Lys [K]; Varshavsky, 2005). The disordered character of e^K was considered to confer segmental mobility to the N-terminal region of the reporter protein, thus enabling the linker to serve as an N-degron, together with the provision of properly spaced Lys residues for Ub transfer (Bachmair and Varshavsky, 1989). For previous investigation of PRT1, e^K was applied as the N-terminus of a β-gal test substrate in yeast (Stary et al., 2003), as well as for Phe-initiated GUS reporters expressed *in planta* by Garzón et al. (2007). Finally, a short variation of e^K, derived from the N-terminus of a novel DHFR construct called K2, was expressed for exploiting PRT1-mediated degradation by Faden et al. (2016, 2019). K2 provides the N-terminal sequence F-HGSGI-MVRPLNCIVA, where the latter part (MVRP...) represents the N-terminus of WT DHFR.

Based on a BLAST search, peptides similar to e^K or FRS-poly-Gly cannot be found in the *Arabidopsis* proteome (albeit blasting the sequence YRSGGGGG yielded 3 protein hits; the respective identifiers are AT3G60110, AT2G21660, and AT4G39260). Thus, the N-terminal sequences that have been used to investigate PRT1 activity so far are not suitable for the prediction of potential *in-vivo* targets of this N-recognin. To unravel the physiological role of the degradation of type II N-end rule substrates in plants, however, it would be of major interest to identify those protein targets of PRT1. Hence, it was decided to investigate in more detail which features of a peptide sequence next to the aromatic N-terminus specifically confer binding by this N-recognin.

To this end, the synthesis of SPOT (for Synthetic Peptides On membrane support Technique) peptide arrays was chosen to perform comprehensive binding assays with recombinant ^{His}MBP-tagged PRT1. SPOT membranes are arrays of artificial peptides on a cellulose surface where each peptide sequence is individually concentrated within a defined region ("spot") with a diameter of about 4 mm. Protein binding to these sequences can be assessed by incubation of the recombinant protein of interest with the peptide array and subsequent immunodetection following Western blotting (see materials and methods, Fig. 53). The intensity of the Western blot signal at each "spot" roughly correlates with the dissociation constant of the tested protein and the respective peptide ligand (Weiser et al., 2005). Hence, the signal intensities can be used as a relative measure of protein affinity when comparing peptide sequences. Furthermore, since the local peptide concentration within each spot can be considered to be extremely high, the method especially allows for the detection of protein interactions that are transient or of low affinity (Hilpert et al., 2007; Klecker and Dissmeyer, 2016). In the frame of this work, automated synthesis of SPOT peptide arrays was set up at the IPB using existing protocols, and binding assays using recombinant N-recognins were

established. Applying robot-supported methodology, arrays of 17-mer peptides of defined sequences with a free (i.e., not acetylated) N-terminus were covalently linked to a PEG-functionalized cellulose support via a C-terminal Gly (residue No. 17). The application of SPOT assays in the context of plant enzymes had to my knowledge not been attempted before.

In a first approach it was asked if recognition of aromatic N-termini by PRT1 was also influenced by the amino acid in penultimate position of the N-terminus (referred to as position 2), and if binding depended on the overall subsequent peptide sequence. For this purpose we designed a SPOT membrane that comprised two different primary sequences that were previously applied in the context of N-recognins. These peptide sequences were e^K and the N-terminus of the *Sindbis virus* RNA polymerase nsP4, the latter representing an authentic type II-N-degron that was used as a reporter for N-recognin activity in the mouse system (de Groot et al., 1991; Tasaki et al., 2005). Both e^K and nsP4 were represented on the SPOT membrane setup with two different amino acids in position 2 of the N-terminus: Gly or Lys (instead of the WT His) in the case of e^K, and Ile (conforming to the WT sequence) or Lys in the case of nsP4 (Fig. 22). Each of these four sequences was synthesized with all 20 N-terminal amino acids.

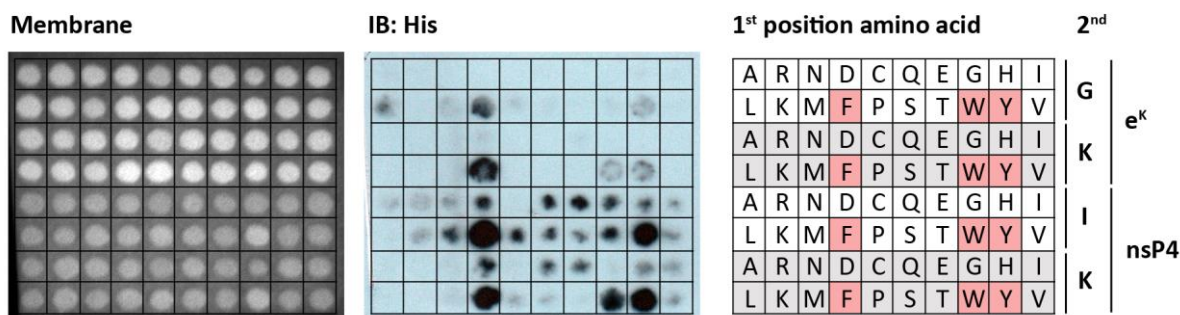


Fig. 22] PRT1 binds peptides with aromatic N-termini with different strength depending on the subsequent amino acids. A SPOT peptide array was performed using His-MBP-PRT1 as recombinant purified protein. The peptides synthesized on the membrane are visualized by UV light (left). PRT1 was bound to the membrane and subsequently transferred to a polyvinylidene fluoride (PVDF) membrane using Western blotting. The tagged protein was detected using anti-His-tag antibody (center). The scheme on the right side depicts the amino acid sequences present on the membrane. These differ in their N-terminus (1st position amino acid; aromatic amino acids are highlighted in red), and the penultimate residue (2nd), as well as in the subsequent 15 amino acid sequence which is either e^K (XZ-GSGAWLLPVSLVKRG), or nsP4 (XZ-FSTDTGPGHLQKKS). The image is representative for two independent experiments using different membranes and different protein batches. An excerpt of a replicate of this experiment was published in Dong et al. (2017a).

In the SPOT assay, sequences with aromatic N-termini were most robustly bound by PRT1 (Fig. 22), with Phe and Tyr both tending to cause a stronger interaction than Trp. Overall, the nsP4 sequence yielded stronger signals for PRT1 binding than e^K, even when peptides with identical amino acids in positions 1 and 2 of the N-terminus were compared. For instance, Lys-Tyr-e^K gave a weaker signal than Lys-Tyr-nsP4. This suggested that amino acids downstream of the very N-terminus most likely also contributed to PRT1 interaction. Interestingly, the influence of the tested amino acids in position 2 was less pronounced, but a hydrophobic residue in penultimate position of nsP4 (XI-nsP4) supported more promiscuous binding of PRT1 than a basic one (XK-nsP4) *in vitro*, meaning less dependency on the aromatic N-terminus. However, it should be noted that overall binding to all tested e^K and nsP4 peptides was rather weak and the Western blot had to be approached with highly sensitive detection reagents (i.e., enhanced chemiluminescence substrates of femtogram sensitivity). In contrast, binding to peptides with non-aromatic N-termini was negligible when using sequences

with higher binding potential and more stringent detection measures (see below: Fig. 25, 26). Such weak signals as seen for non-aromatic N-termini of nsP4 might actually represent artefacts of the *in-vitro* binding system. Of note, ^{His}MBP alone, or ^{His}MBP-PRT7 did not give rise to Western blot signals in the binding assay (data not shown).

In order to confirm the peptide array results, an X-peptide pull-down assay was set up where 12-mer synthetic peptides of a derived e^K sequence (with deletion of His in position 2 of the original e^K sequence) were coupled to avidin-agarose beads via a C-terminal biotin modification. Here, peptide synthesis was performed doing batch synthesis on solid-phase resin by Carolin Müller^{1,2} and Tom Grossmann^{1,2}.

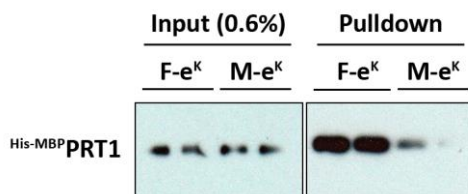


Fig. 23 | Recombinant PRT1 binds to aromatic N-termini in an X-peptide pull-down system. ^{His}MBP-PRT1 was subjected to a pull-down assay using C-terminally biotinylated 12-mer peptides of the e^K-derived sequence X-GSGAWLLPVSG, with X = F or M, that were coupled to avidin-agarose beads. Shown is the immunoblot following SDS-PAGE using anti-His-tag antibody.

As observed in the SPOT assay, ^{His}MBP-PRT1 was pulled down in the bead-based system preferentially by peptides with Phe in the starting position (Fig. 23). However, the interaction was rather weak and did not withstand rigorous washing steps, confirming on the one hand a low affinity of PRT1 to the modified e^K sequence, and on the other hand the strong binding potential of the peptide array, where washing did not significantly impact on the amount of bound PRT1.

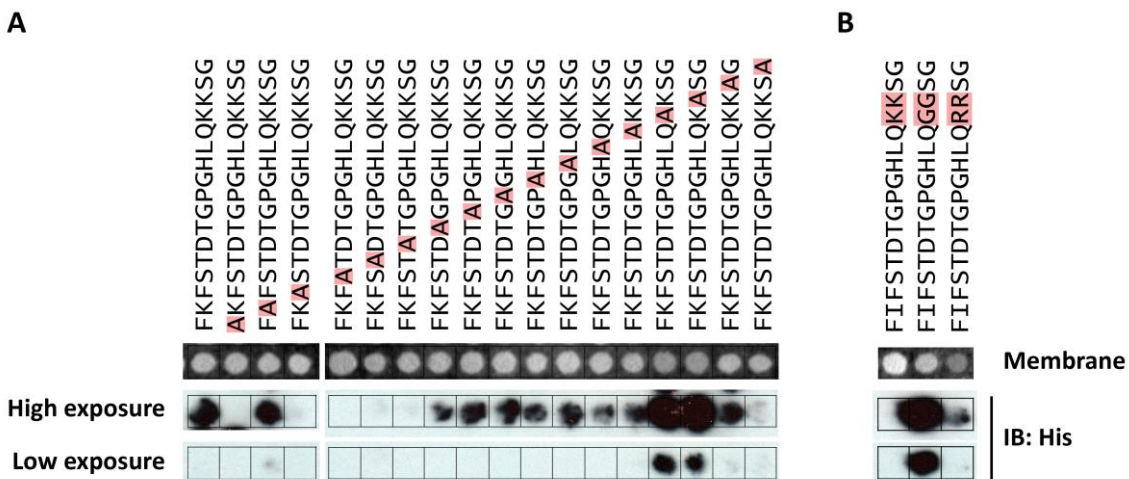


Fig. 24 | The first six amino acids and Lys 14 and 15 influence the *in-vitro* affinity of PRT1 for nsP4. Shown are sections from a SPOT peptide assay carrying variants of the nsP4 peptide sequence and employing recombinant ^{His}MBP-tagged PRT1 as the binding partner. Peptide sequences are annotated as starting from N-terminus (bottom) to C-terminus (top). A and B are membrane sections derived from the same experiment. The membrane without protein as seen in UV light is presented in the top row, and Western blot detections of ^{His}MBP-PRT1 using anti-His tag antibody are shown in the bottom rows. **A**, Ala walk through a derived nsP4 sequence. The amino acid that has been replaced by Ala is highlighted in red. **B**, Substitution of Lys in the C-terminal region (highlighted in red) of the original nsP4 sequence by Gly or Arg. The images are representative of two independent experiments using two different membranes.

¹ Chemical Genomics Centre of the Max-Planck Society, 44227 Dortmund, Germany

² VU University Amsterdam, 1081 HV Amsterdam, The Netherlands

In order to gain further insight into the effect of downstream N-terminal amino acids of a PRT1 peptide ligand, an array was designed in which each residue of the nsP4 peptide sequence was individually exchanged for Ala (Fig. 24A). Consistent with the previous findings, the substitution of amino acids subsequent to the N-terminus had a marked influence on PRT1 binding. The first six amino acids, bearing mostly polar or hydrophobic side chains in the case of nsP4, but also one acidic residue (Asp), diminished PRT1 binding substantially when they were replaced by Ala. The only striking exception was the amino acid in second position, a Lys residue in the test sequence, since binding capacity of PRT1 was hardly affected by the Lys to Ala substitution. Moreover, replacement of one of the Lys residues in positions 14 and 15 markedly improved binding of PRT1 (Fig. 24A). The apparently deleterious effect of Lys in the sequence of a PRT1 ligand peptide was rather counterintuitive, since the E3 ligase is expected to rely on the presence of Lys residues close to the binding site for the attachment of Ub.

The influence of the distal Lys residues was further addressed using variants of the N-terminal nsP4 sequence that contained Ile (instead of Lys) in position 2, corresponding to the WT version of nsP4 (Fig. 24B). Here, the two distal Lys residues were replaced simultaneously by either Gly, a residue with a small neutral sidechain, or Arg, a residue that is positively charged like Lys, but is not ubiquitinatable (Hershko, 1988). Interestingly, PRT1 was pulled down by far most efficiently when both Lys residues were replaced by Gly (Fig. 24B). Mutation of the distal Lys residues of nsP4 to Arg also improved the affinity of the peptides towards PRT1, but the effect was less pronounced compared to the GG-variant. Strikingly, in this experiment (Fig. 24B), binding of PRT1 to the WT nsP4 sequence that robustly and reproducibly pulled down PRT1 in the previous membrane context (Fig. 22), was not detectable. This was likely a consequence of the proximity of the much better binding GG-variant. The observation hints towards a bias in SPOT assay results that is caused by ligand competition between closely located spots (Weiser et al., 2005).

Taken together, next to the aromatic N-terminus, polar or hydrophobic side chains within the first six amino acids of a peptide's N-terminus appeared to be most decisive in terms of PRT1 interaction. As an exception of this, the impact of the penultimate N-terminal residue appeared to be modest in the here tested sequence contexts. Moreover, the elimination of positive charges in the C-terminal part of a 17-mer peptide generally improved binding capacity of PRT1 *in vitro*, but Lys residues in this region proved to particularly weaken the interaction.

3.3.4 PRT1 RING domains are not involved in substrate binding *in vitro*

After having established an assay for PRT1 substrate binding, it was asked if any of the two RING domains was involved in peptide substrate recognition. To address this question, the previously introduced PRT1 protein variants with mutations in either RING1 or RING2 were subjected to SPOT assay experiments. For this purpose, an improved and more robustly binding peptide array setup was designed. These membranes contained, next to the previously employed descendant of nsP4, the K2 N-terminal sequence. Derivatives of this sequence had facilitated strong *in-vitro* interaction with PRT1 in binding assays performed by Frederik Faden¹ (Faden, 2017).

¹ Leibniz Institute of Plant Biochemistry, 06120 Halle (Saale), Germany

Consistent with the assumption that PRT1's ZZ domain rather than either of the RING domains is responsible for substrate interaction, none of the two RING mutants showed considerable differences in binding preference to the peptides presented on the SPOT membrane as compared to the WT (Fig. 25). For all three protein variants, binding strength to the K2 sequence was stronger than to the nsP4 sequence. Notably, there was a mild trend observable that the mutant variants, especially PRT1^{C195A}, bound stronger to the K2 sequence than did WT PRT1, whereas binding to the nsP4 sequences was slightly reduced for the mutant proteins.

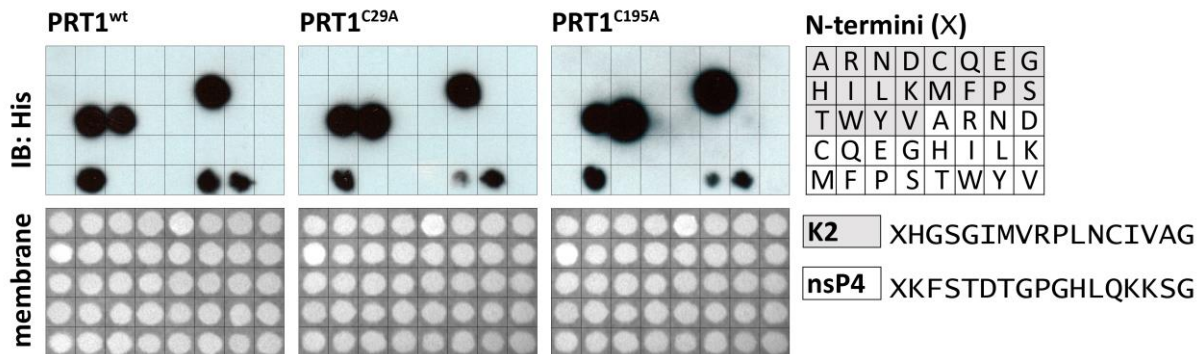


Fig. 25 | Neither of the RING domains of PRT1 is involved in substrate recognition *in vitro*. SPOT assays with peptide arrays comprising peptides of the indicated sequences K2 (grey background in the right panel) and nsP4 (white background) with varying N-terminal amino acids (X) were performed using recombinant ^{His}MBP tagged versions of PRT1 WT protein, or mutants in RING1 (C29A) or RING2 (C195A). Depicted are immunodetections following Western blot using anti-His-tag antibody (top), and membrane images taken in UV light without protein added (bottom). Images of WT and C29A binding are representative of 2 and 3 experiments, respectively. The experiment using the C195A version was not replicated due to technical issues.

Inferring from the results described above, strong binding of PRT1 to K2 could be explained by the lack of Lys residues in the K2 sequence. However, additional differences in the physicochemical properties exist between the Phe-His-K2 sequence compared to the Phe-Lys-e^K and Phe-Lys-nsP4 sequences that might contribute to PRT1 affinity: First, hydrophobicity does not appear to correlate with PRT1 affinity, since both K2 and e^K are overall hydrophobic peptides, while nsP4 is predicted to exhibit good water solubility (according to the Innovagen Peptide Property Calculator on <https://pepcalc.com/>). This also implies that the propensity of a peptide to expose from the cellulose matrix into the aqueous medium is not alone decisive for PRT1 binding in the peptide assay. In contrast, the positive net charge of the peptides at neutral pH increases with decreasing PRT1 binding capacity, being K2 (1) < nsP4 (2.1) < e^K (3) (Innovagen Peptide Property Calculator). Thus, a close to neutral net charge might improve the binding of an N-degron by PRT1, provided that a bulky hydrophobic amino acid is in the ultimate position. Potentially, this would also explain why substituting Asp-6 in nsP4 abolished PRT1 binding (Fig. 24A), since this increased the positive net charge of the peptide.

Importantly, PRT1^{C29A} and PRT1^{C195A} binding to the SPOT membrane also showed that, despite being catalytically compromised, these mutant proteins were not generally inactive. This indicated that the overall protein structures were obviously not misfolded, although mutation of the metal chelating Cys residues likely affected the structure of the respective RING domains.

3.3.5 *In-vitro* PRT1 binding to *Arabidopsis* peptide sequences

The final goal of deciphering the specificity determinants for PRT1 substrate recognition would be the identification of natural targets. Thus, it was aimed to create a SPOT membrane presenting peptides that mimic potential physiological substrates of PRT1. This should be used to screen these candidates for their capacity to bind PRT1 *in vitro*.

Based on published data, at least two proteins are known to reveal aromatic amino acids after physiologically occurring peptidase cleavage in *Arabidopsis*. These proteins are EIN2 (Qiao et al., 2012), and BIG BROTHER (BB). The RING-type E3 ligase BB limits organ growth by restricting the duration of cell proliferation (Disch et al., 2006). During the period of this work, the peptidase DA1 (“DA” for Chinese “large”) was identified as a physiological substrate of BB by a group of scientists in the laboratories of Yunhai Li¹ and Michael Bevan². Next to BB, a second RING E3 ligase, called DA2, was also found by Bevan and coworkers to target DA1. Crucially, ubiquitination of DA1 resulted in the activation of this endopeptidase and DA1-mediated cleavage of both BB and DA2 as part of a feedback-mechanism. In the case of BB, this released a 188 amino acid C-terminal fragment initiated by Tyr (denoted Y61-BB) that was destabilized compared to a Met-initiated variant in a cell-free rabbit reticulocyte system. Contributing also PRT1-binding assays using YK-initiated nsP4 sequences from this work (a replicate of the SPOT assay shown in Fig. 22), BB was published as the first physiological PRT1 substrate in collaboration with our group (Dong et al., 2017a).

Additional hints for potential PRT1-target proteins are provided by a proteomic screen performed on N-end rule mutants by Majovsky et al. (2014). Here, GLYCERALDEHYDE-3-PHOSPHATE DEHYDROGENASE B SUBUNIT (GAPB, AT1G42970), and RESPONSIVE TO DEHYDRATION 21A (RD21A, AT1G47128) were found to be more abundant in *prt1-1* than in the WT, although the predicted neo-N-termini after peptidase cleavage do not reveal type-II N-degrons in these cases. In contrast, levels of PECTIN METHYLESTERASE 18 (PME18; AT1G11580) were found to be increased in another N-end rule mutant, *prt6-3*, but PME18 likely exposes Phe after signal peptide removal (Naumann, 2017), thus conceptually qualifying as a potential PRT1 ligand.

Finally, the gene with the identifier AT5G42070 codes for an unknown protein that contains a presumptive cleavage site for the bacterial effector protease AvrRpt2 with the consensus sequence VPxFGxW (Chisholm et al., 2005). AvrRpt2-mediated cleavage behind Gly-100 would release a 64 amino acid peptide that is initiated by Trp. Hence, the neo-N-terminus of this protein was also considered a potential target for PRT1 (N. Dissmeyer, personal communication). The sequences of the C-terminal proteolytic fragments of RPM1-INTERACTING PROTEIN4 (RIN4) were present on the membrane as controls, as were versions of the RAP2.12 N-terminal peptide.

Two different arrays were synthesized that comprised the respective neo-N-terminal peptides of these proteins. Each sequence was included as variants carrying different N-terminal amino acids in order to provide additional controls.

¹ CAS Centre of Excellence in Molecular Plant Biology, Chinese Academy of Sciences, Beijing 100101, China

² John Innes Centre, Norwich NR4 7QA, United Kingdom

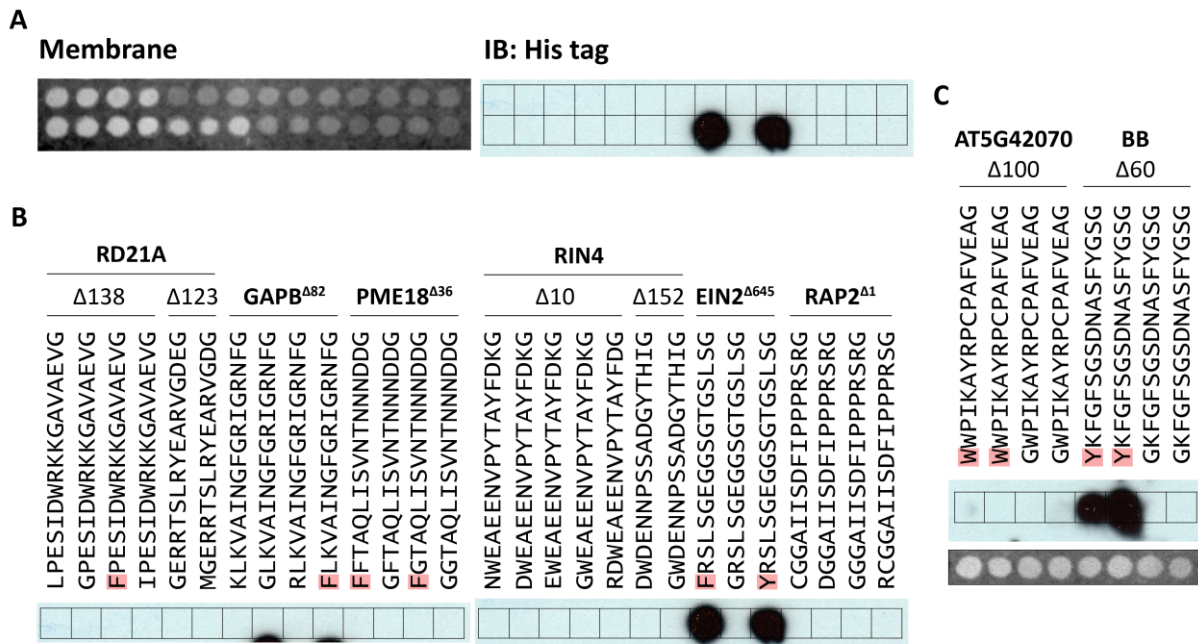


Fig. 26 | The C-terminal peptidase cleavage products of EIN2 and BB constitute potential PRT1 targets. Recombinant ^{His}MBP-PRT1 was incubated with SPOT peptide arrays presenting the neo-N-termini of several proteins which are supposed to be subject to protease cleavage *in planta*. **A**, Overview of the SPOT membrane shown in B. Left: as seen in UV light; right: immunoblot using anti-His antibody. **B**, ^{His}MBP-PRT1 binding was detected with the neo-N-terminus (Δ645) of EIN2 in a manner dependent on the aromatic N-terminus, but not with versions of RD21A, GAPB, PME18, or RIN4. The presented peptides represent N-terminal variations of sequences predicted to be produced by protease cleavage *in planta*. Δx indicates that x amino acids are removed N-terminally from the native protein sequence to give rise to the presented peptide sequence. Aromatic N-termini are highlighted in red. C-terminally, Gly was added for synthesis reasons. **C**, Immunoblot (top) and UV-seen membrane (bottom) of a SPOT assay using recombinant ^{His}MBP-PRT1 on the neo-N-termini of the putative AvrRPT2 substrate encoded by AT5G42070 and BB. The hydrophobic residues marked in red correspond to the WT sequences. **A** and **B** show an experiment representative for three independent experiments using different membranes. The experiment shown in **C** was not repeated.

Of all tested sequences, only the EIN2 and BB neo-N-termini facilitated binding of PRT1 (Fig. 26). The signal strength was in both cases comparable to the well-binding K2 sequence and was very specific for an aromatic amino acid at the N-terminus (Fig. 26), with Phe and Tyr representing the natural neo-N-termini of cleaved EIN2 and BB, respectively. Consistent with previous findings concerning the preference of PRT1, both EIN2 and BB peptides lack Lys in the distal parts of their N-termini and the 17-mer N-terminal peptides are overall uncharged at neutral pH. Of interest, Lys in position 2 did obviously not interfere with PRT1 binding in the BB sequence context. Strikingly, just like K2, both EIN2 and BB bear a protonatable residue in second position (K2: His-2; EIN2: Arg-2; BB: Lys-2), prompting the requirement of a basic residue in this position for optimal PRT1 binding. It is furthermore interesting that especially the FRS-starting EIN2 peptide resembles the artificial FRS-poly-Gly sequence which was initially used for the identification of PRT1 (Bachmair et al., 1993). Both sequences, EIN2 and BB, are also rich in Gly and Ser, confirming the requirement of flexibility and solvent exposure for an N-terminal linker to function as an N-degron. Finally, of all peptides tested for PRT1 binding, the EIN2 sequence featured the highest number of disorder-promoting amino acids (according to Dunker et al. (2001)).

In summary, *in-vitro* binding of PRT1 showed high specificity of this N-recognin for aromatic N-termini. Furthermore, it was concluded that the amino acids subsequent to the very N-terminus

have a high influence on a peptide's capacity to interact with PRT1. Here, a flexible, slightly polar, and overall electrically neutral linker with a positively charged residue in second position appeared to be most favorable for an N-terminus to act as a degron for PRT1. The neo-N-termini of EIN2 and BB match these requirements and exhibited high affinity for PRT1 *in vitro*, suggesting that they might be recognized by PRT1 in a physiological context. Consistently, in the case of BB, *in-vivo* degradation via PRT1 could be published in collaboration with Dong et al. (2017a).

3.4 EIN2 is a potential *in-vivo* substrate for PRT1

Ethylene signaling in *Arabidopsis* and other plants is tightly linked to the processing and stability of the key regulator EIN2. Activation of EIN2 signaling involves proteolytic cleavage that results in the liberation of a C-terminal fragment starting with Phe-646 (referred to in the literature as EIN2 CEND). According to the plant N-end rule, this fragment should have a short half-life and might be targeted by PRT1. Using peptide arrays, it was confirmed that PRT1 directly bound to the N-terminus of EIN2 CEND in a manner dependent on the ultimate amino acid Phe (Fig. 26). Thus, it was asked whether this interaction takes place in a physiological context.

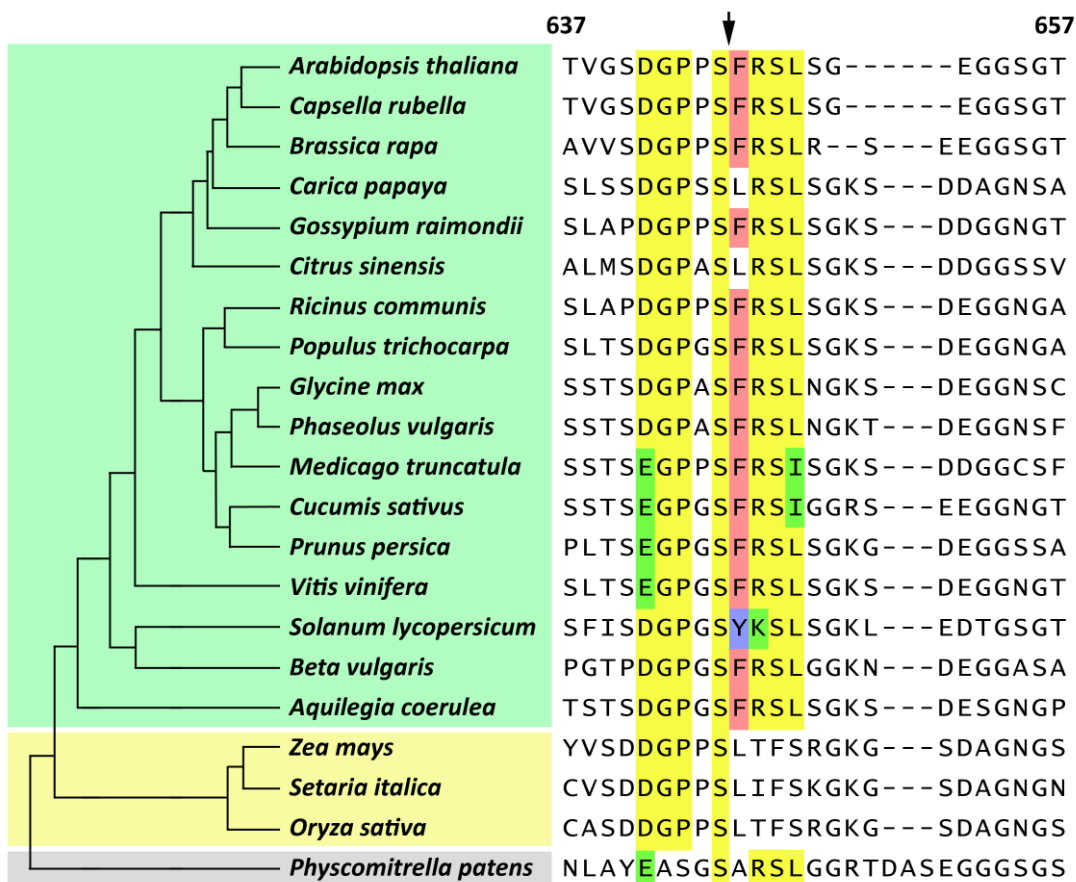


Fig. 27 | Conservation of the sequence around the *bona fide* cleavage site of EIN2. An alignment of putative homolog protein sequences to *Arabidopsis* EIN2 at amino acids 637-657 is presented. Species were selected as representatives of different taxa, including eudicots (green), monocots (yellow), and moss (grey). A conserved region around the *bona fide* cleavage site (indicated by the arrowhead) is highlighted in yellow, with sequence variations in green. The conservation of an aromatic residue following the cleavage site is indicated in red (Phe), and blue (Tyr). The cladogram was adapted from Liu et al. (2016a).

To assess whether a potential N-end rule-mediated degradation of EIN2 CEND could be relevant also in other plant species, sequence conservation of the neo-N-terminus of EIN2 was analyzed across selected species. As noted before (Chen et al., 2011a; Ju et al., 2012; Qiao et al., 2012), Ser-645 preceding the *bona fide* cleavage site of EIN2 was conserved across all species investigated (Fig. 27). Interestingly, the motif Φ -RSL (where Φ represents a hydrophobic residue) following Ser-645 was also strongly conserved among eudicots (Fig. 27). Variations of the *Arabidopsis* sequence FRSL at this position were found in *Medicago truncatula* and *Cucumis sativus* (FRSI), *Solanum lycopersicum* (YKSL), and a Leu starting variant (LRSL) was detected in both *Carica papaya* and *Citrus sinensis* (Fig. 27). Outside of the *Brassicaceae*, a Lys (or Arg, in *Cucumis sativus* and *Physcomitrella patens*) insertion was furthermore present at position seven of the potential neo N-terminus. The high degree of conservation around the EIN2 cleavage site likely reflects the requirements for the conserved interactions of EIN2 with signaling components such as CTR1 (Ju et al., 2015), and/or the unknown protease responsible for EIN2 CEND release. However, the preferred occurrence of an aromatic N-terminus (Phe, Tyr) followed by a basic amino acid in penultimate position would conceptually also allow for interaction with a PRT1 homolog in most eudicot species, suggesting that N-end rule targeting of EIN2 might potentially be of general relevance in plants. In the following, I was asking whether such an interaction between PRT1 and EIN2 CEND takes place in *Arabidopsis in vivo*, and if it had physiological consequences.

3.4.1 EIN2^{C-term} is destabilized in a PRT1-dependent manner *in vivo*

In *Arabidopsis* cells, release of EIN2 CEND occurs upon receptor binding of ethylene. In order to track EIN2 CEND stability *in vivo*, the EIN2⁶⁴⁶⁻¹²⁹⁴ fragment was expressed, mimicking a situation of constitutive cleavage. Approaches to express the EIN2 C-terminal cleavage fragment in *Arabidopsis* have been undertaken before (e.g., Alonso et al. (1999), Qiao et al. (2012), Wen et al. (2012); see also discussion, section 4.4.4). However, all constructs were designed larger or smaller than it would result from cleavage before Phe-646. Moreover, previous EIN2 CEND constructs were initiated by Met as a requirement for translation initiation, thereby ignoring the fragment's true N-terminus Phe and eluding a potential influence of the N-end rule on the protein. In this work, expression of EIN2⁶⁴⁶⁻¹²⁹⁴ with its post-cleavage neo-N-terminus was achieved by application of the UFT. Exposure of the N-terminal Phe is mediated here by the DUB-dependent co-translational removal of the N-terminal Ub moiety from the Ub-EIN2⁶⁴⁶⁻¹²⁹⁴ fusion protein (Bachmair et al., 1986; Bachmair and Varshavsky, 1989; Varshavsky, 2005). The resulting EIN2⁶⁴⁶⁻¹²⁹⁴ fragment is referred to in the following as EIN2^{C-term}, to clearly distinguish it from the EIN2 CEND constructs that have been published before.

EIN2^{C-term} ubiquitination by PRT1 would imply its subsequent degradation and should reflect in decreased protein stability of EIN2^{C-term} *in vivo*. Thus, to test for its stability in plant cells, Ub-EIN2^{C-term} variants were expressed in *Arabidopsis* protoplasts under control of the *UBQ10* promoter. C-terminal YELLOW FLUORESCENT PROTEIN (YFP) was chosen as an affinity tag since previous work had proven its compatibility with EIN2 function (Qiao et al., 2012). To ensure that N-terminally fused Ub was cleaved of the EIN2^{C-term} peptide faithfully in the overexpression system, Met-initiated EIN2^{C-term} without Ub fusion was also cloned. The migration of this construct during SDS-PAGE was indistinguishable from the Ub fusion constructs starting with either Phe or Gly (Fig. S14, 34), confirming the efficient removal of the Ub moiety from the UFT constructs.

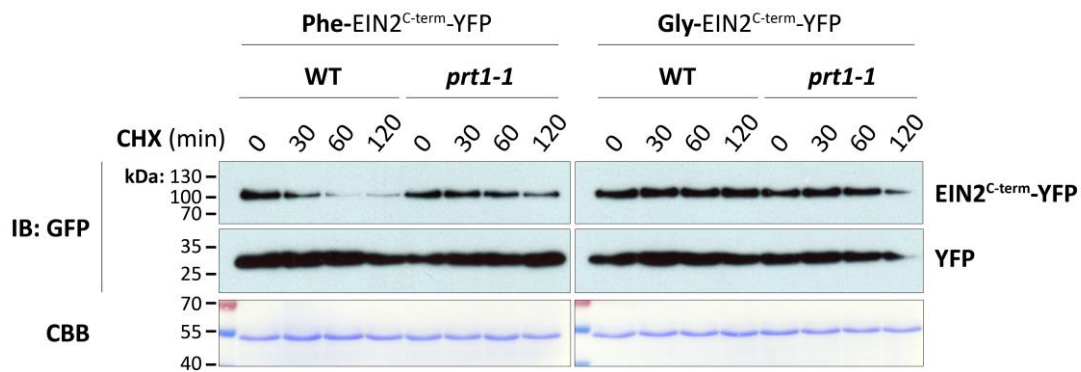


Fig. 28 | The stability of EIN2^{C-term} depends on its hydrophobic N-terminus in plant cells. Variants of EIN2^{C-term}-YFP were transiently expressed in *Arabidopsis* WT or *prt1-1* (line N119) protoplasts as Ub fusion constructs with either Phe or Gly at the N-terminus after de-ubiquitination. A plasmid for YFP-expression alone was co-transfected and detected on the same Western blot membrane as an internal control for transfection efficiency, protoplast viability, gel loading, and immunodetection. All constructs were driven by the *UBQ10* promoter. Samples were taken before (0 min) and at 30, 60, and 120 min after addition of the translation inhibitor cycloheximide (CHX). Total proteins were extracted and subjected to immunoblot analysis. Coomassie Brilliant Blue (CBB) unspecific protein stains of the membranes are shown as additional loading control. The figure is representative of three independent experiments.

Protein stability of the fusion proteins was chased after inhibition of protein synthesis with cycloheximide (CHX), and assessed by immunoblot (Fig. 28). A plasmid carrying YFP alone was co-transfected as a control. When the Phe-starting EIN2^{C-term} (Ub-Phe-EIN2^{C-term}-YFP) was expressed in WT protoplasts, protein abundance of the fusion protein in comparison to YFP decreased strongly within 2 hours after the addition of CHX (Fig. 28). In contrast, in the mutant genotype *prt1-1*, Phe-EIN2^{C-term}-YFP remained relatively stable (Fig. 28). Crucially, when Phe at the N-terminus of EIN2^{C-term} was replaced by Gly, protein stability was high in both genotype backgrounds (Fig. 28). This finding was consistent with the observation that Phe to Gly mutation at position 1 of the EIN2^{C-term} peptide abolished PRT1 interaction *in vitro* (chapter 3.3.5, Fig. 26). These results show that rapid degradation of EIN2^{C-term} depended on N-terminal Phe and the presence of *PRT1*, indicating that *PRT1* might recognize and ubiquitinate EIN2^{C-term} *in vivo*.

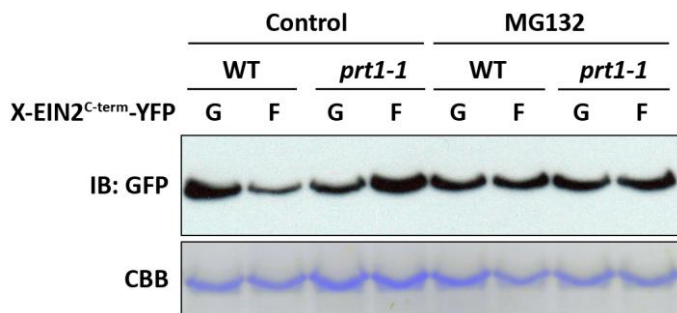


Fig. 29 | Destabilization of F-EIN2^{C-term} is Ub-dependent. *proUBQ10::Ub-X-EIN2^{C-term}* was transiently expressed in protoplasts as Ub fusions exposing either X= Gly or Phe after DUB cleavage. Protoplasts were treated with MG132 (50 μM) or DMSO (control) for 3.5 hours before harvest and extraction of total protein. Line *prt1-1^{ts}* was used as the *prt1-1* mutant line.

Next to the lower stability of Phe-EIN2^{C-term}-YFP compared to the Gly-starting variant, in most experiments the steady state levels of Phe-EIN2^{C-term}-YFP protein in the WT genetic background was lower than G-EIN2^{C-term}-YFP, and also lower in WT than in the *prt1-1* mutant background (Fig. 29, 33, S14). To investigate if this difference in protein level was accounted for by Ub dependent degradation, cells were treated with the proteasome inhibitor MG132. Indeed, proteasome inhibitor treatment abolished the difference in protein levels between Phe- and Gly-EIN2^{C-term} in WT

protoplasts as well as between WT and mutant genotypes (Fig. 29). Thus, N-terminus specific degradation of EIN2^{C-term} appeared to be Ub dependent.

No further increase of the protein level was observed upon MG132 treatment for Gly initiated EIN2^{C-term}-YFP (Fig. 33). This is noteworthy because next to a potential influence of the N-end rule on EIN2^{C-term} stability, EIN2 is targeted for degradation by the F-box proteins ETP1 and ETP2 (Qiao et al., 2009). However, Qiao et al. (2009) have shown ETP1/2-dependent accumulation of EIN2 only for the full-length protein. Moreover, it was observed during studies in rice, that Ub-dependent degradation of OsEIN2 requires the N-terminal Nramp-like domain of EIN2 (Ma et al., 2018a). Thus, EIN2^{C-term} might not represent a target for ETP1/2 ubiquitination. This is also in line with the result presented here that EIN2^{C-term} destabilization was solely dependent on the N-terminus. Nevertheless, functionality of the proteasome inhibitor treatment in this system was confirmed in collaboration with the group of Angelika Mustroph¹ by assaying another target of Ub-dependent degradation (Fig. S15; the expression clone was kindly provided by Judith Bäumler¹ and Angelika Mustroph). Hence, the data presented here support the idea that EIN2^{C-term} is no subject to Ub dependent degradation, other than via the N-end rule.

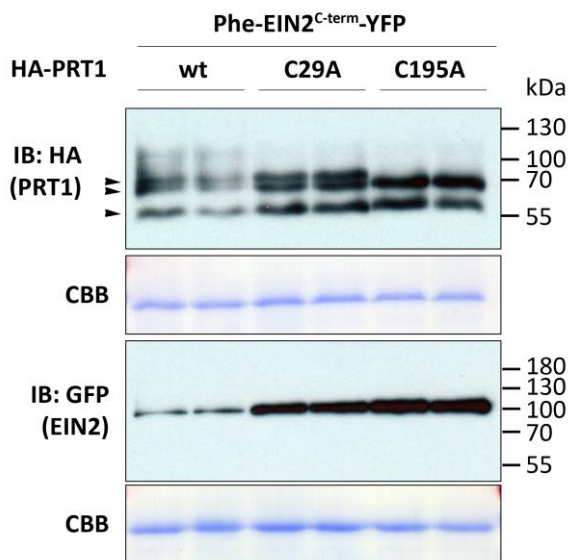


Fig. 30 | EIN2^{C-term} instability depends on PRT1 activity. Phe-exposing EIN2^{C-term}-YFP was transiently co-expressed with variants of 3HA-PRT1 in *Arabidopsis prt1-1^{ts}* protoplasts. Samples of whole-cell lysates were subjected to SDS-PAGE in duplicates. Two gels were loaded with the same samples, one of which was developed with anti-HA antibody following Western blot, and the other one with anti-GFP antibody. The respective CBB stains are shown below each antibody detection. 3HA-PRT1 is expected at an apparent molecular weight of 50 kDa, EIN2^{C-term}-YFP at 98 kDa. Arrowheads indicate potential mono- (58 kDa), di- (67 kDa), and tri- (75 kDa) ubiquitinated species of 3HA-PRT1.

It was further asked whether EIN2^{C-term} destabilization depended on PRT1 activity. To test this, PRT1 and its RING domain mutants were co-expressed with the EIN2^{C-term}-YFP construct in the *prt1-1^{ts}* mutant background. Since an N-terminal tag did not interfere with PRT1 function *in vitro*, the protein was cloned with an N-terminal triple-HA affinity tag. Strikingly, EIN2^{C-term}-YFP levels were markedly reduced when co-expressed with the WT sequence of PRT1 compared to either of the two RING mutants C29A and C195A (Fig. 30). Since both RING mutants were (nearly) inactive in autoubiquitination assays, this coincided with PRT1 activity being necessary for EIN2^{C-term}-YFP destabilization. The result of EIN2^{C-term}-YFP destabilization by overexpression of active PRT1 was also obtained when expressing and detecting EIN2^{C-term} with a C-terminal Myc-tag (Fig. S16). Thus, EIN2^{C-term} instability coincided with the presence of active PRT1, further substantiating that PRT1 might be responsible for EIN2^{C-term} ubiquitination.

¹ University of Bayreuth, 95447 Bayreuth, Germany

While detection of transgenic PRT1 protein had failed for stably transformed *Arabidopsis* lines (see chapter 3.2), an immunoblot signal for 3HA-tagged PRT1 was obtained from the transient overexpression system in protoplasts (Fig. 30). As would be expected based on their impaired autoubiquitination activity, the RING mutants showed higher abundance than the WT protein (Fig. 30). Interestingly, the HA-fusion proteins migrated in SPD-PAGE in at least two bands, the lowest of which still exceeding the calculated molecular weight of 3HA-PRT1 by circa 8 kDa, the next one by roughly 18 kDa, which would coincide with a mono-ubiquitinated and a di-ubiquitinated species, respectively. A smear of higher molecular weight species was also detected, the intensity of which varied between experiments (Fig. 30, 34). The potentially mono- and di-ubiquitinated species were particularly increased in the RING mutant versions of PRT1 (Fig. 30), indicating that the failure to autoubiquitinate *in vitro* did not preclude potential mono- and di-ubiquitination *in vivo*. Strikingly, a third band that would coincide with a triple ubiquitinated species was absent in PRT1^{C195A}, but not PRT1^{C29A} (Fig. 30), although the latter variant was stronger impaired during *in-vitro* autoubiquitination assays (Fig. 20B). In the later course of this work, PRT1 variants were also transiently overexpressed in protoplasts as fusions with N-terminal GFP. In contrast to the 3HA-fusion proteins, these constructs appeared as one prominent band in the immunoblot (Fig. 31B). Here, only a faint smear of moderately increased molecular weight species was apparent which was restricted to the WT variant, and no obvious difference in the abundances of WT and the point mutants was detected (Fig. 31B). Since GFP-fused PRT1 was bigger than 3HA-PRT1, mono- and di-ubiquitinated species might not have separated to a visible extent upon SDS-PAGE. Given that 3HA-PRT1 facilitated the destabilization of EIN2^{C-term}-YFP (Fig. 30), this might however represent the more functional fusion construct compared to GFP-PRT1. As N-terminal GFP fusions, both the GFP-PRT1 and GFP-PRT1^{C29A} overexpression constructs appeared to localize to the cytosol and nucleus in protoplasts (Fig. 31A, S17).

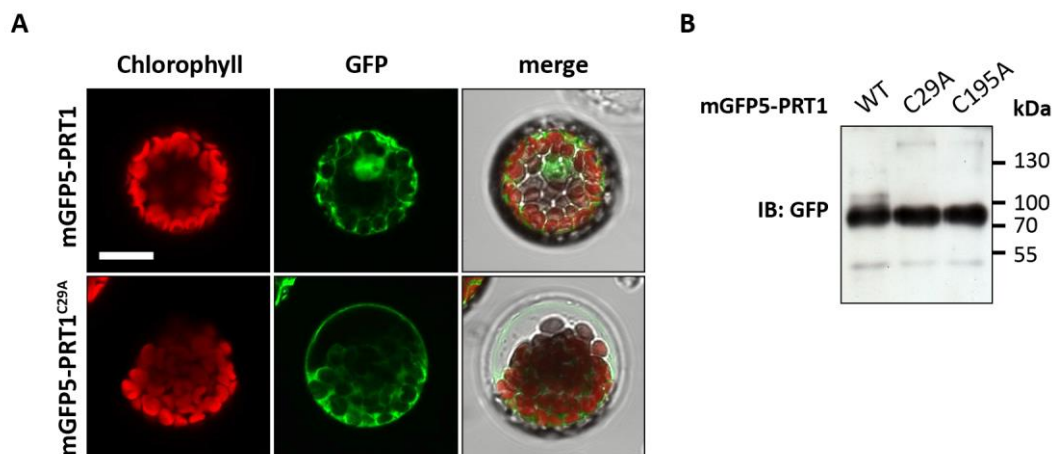


Fig. 31 | Transient expression of N-terminally GFP-tagged PRT1 in *Arabidopsis* protoplasts. Protoplasts of the *prt1-1^{ts}* genotype were transfected with expression plasmids carrying WT and mutant (PRT1^{C29A}, PRT1^{C195A}) CDS variants of *mGFP5-PRT1* under the control of the *UBQ10* promoter. Cells were incubated overnight before microscopy (A), and assessment of protein abundance by immunoblotting (B). **A**, Representative cells expressing GFP-PRT1 or GFP-PRT1^{C29A} are shown. Scale bar: 16 μ m. **B**, Immunodetection of GFP-PRT1 variants from protoplasts using anti-GFP antibody (JL-8). GFP-PRT1 is expected at an apparent molecular weight of 73 kDa.

In order to test for EIN2 stability in plant lines under more physiological conditions, two stable transgenic lines carrying C-terminally tagged variants of EIN2 were investigated. Of these, a line

overexpressing EIN2-7HA in the *ein2-1* mutant background (kindly provided by Thomas Potuschak¹) failed to complement the triple response phenotype of *ein2-1* and was not used further. The other line carried a transgene with the *EIN2* genomic locus sequence fused to eGFP downstream of an *EIN2* promoter construct in the *ein2-5* mutant background (kindly provided by Markus Grebe^{2,3} and Yoshihisa Ikeda²). This line fully complemented the *ein2-5* phenotype in the triple response assay (data not shown). Here, full-length *EIN2* could be detected when using a urea-based extraction buffer (Fig. 32A). This transgenic line was introgressed into the *prt1-1* mutant background and analyzed for EIN2-eGFP abundance in the presence or absence of the ethylene precursor molecule ACC. However, no accumulation of EIN2 CEND, and even a slight reduction of full-length EIN2-eGFP protein levels were observed in the *prt1-1* background compared to the *PRT1* WT genotype or a pooled batch of seedlings segregating for *prt1-1* (Fig. 32). Importantly, upon ACC treatment, processing of the EIN2

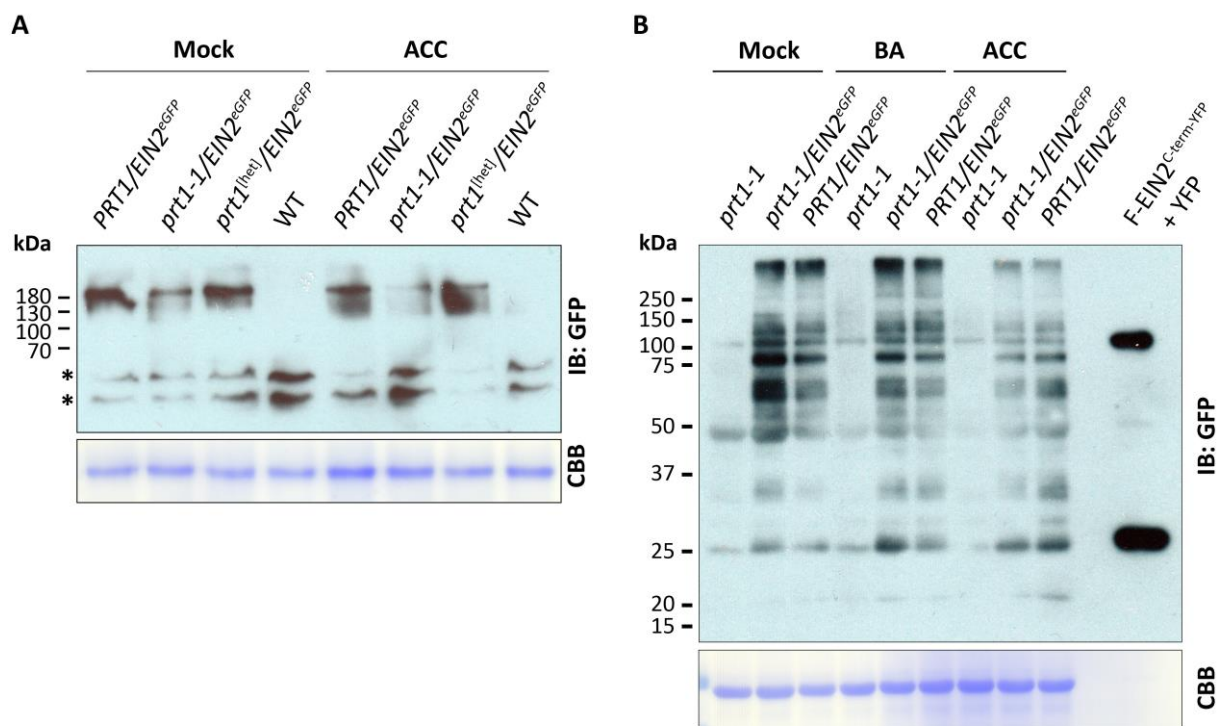


Fig. 32 | EIN2 levels in transgenic seedlings of the *prt1-1* background. Transgenic lines stably expressing *proEIN2::genEIN2-eGFP* were kindly provided by M. Grebe and Y. Ikeda and crossed into the *prt1-1* mutant background. Whole-seedling protein extracts were subjected to SDS-PAGE and immunodetection using anti-GFP antibody. **A**, Seedlings of the indicated genotypes were transferred to agar plates containing 10 μ M ACC or a mock solution at the age of 7 days. Material was harvested after additional 2 days and subjected to urea-based protein extraction. The genotype description "*prt1*^{het}" refers to the pooled, segregating progeny of a line heterozygous for the *prt1-1* allele. Asterisks denote unspecific reactions of the antibody. **B**, Seedlings of the indicated genotypes were grown for 5 days on agar plates before transfer to agar medium containing 1 μ M BA, 1 μ M ACC, or a mock solution. After additional 3 days of growth, seedlings were harvested and subjected to RIPA-buffer based protein extraction. For SDS-PAGE, a control was loaded to the last lane as a reference for the protein size of the *EIN2*^{C-term} fusion protein: Here, 2 μ l of protoplast extract containing *EIN2*^{C-term}-YFP and YFP alone that had been transiently co-expressed under control of the *UBQ10* promoter, were applied to the lane. Full-length *EIN2*-eGFP is expected at 168 kDa, *EIN2* CEND-eGFP at 97 kDa, *EIN2*^{C-term}-YFP at 98 kDa, YFP at 27.4 kDa.

¹ Institut de Biologie Moléculaire des Plantes du CNRS, Strasbourg, France

² Umeå University, Umeå, Sweden

³ University of Potsdam, Potsdam-Golm, Germany

protein was not observed in any of the samples and full-length EIN2 levels were not increased, as would be expected from ethylene signaling processes taking place. This indicated that ACC supplementation might not be sufficient to stimulate the ethylene signaling cascade, including stabilization of the full-length protein and appearance of the cleaved C-terminal fragment. This observation was in contrast to what was shown by Qiao et al. (2009), but consistent with the results obtained with EIN2-GFP by Wen et al. (2012).

Cytokinin is known to trigger ethylene production in etiolated seedlings (Liebermann, 1979; Cary et al., 1995; Vogel et al., 1998b). Since ACC had failed to elicit EIN2 cleavage in transgenic *Arabidopsis* seedlings (Fig. 32A), and ethylene gassing was not established at our institute, the synthetic cytokinin BA was employed as an alternative ethylene-inducing signal. To better solubilize membrane fractions during the preparation of protein extracts, a different buffer system (RIPA buffer) was used. Since it was reported by Qiao et al. (2013) that EIN2 tended to fragment upon harsh conditions of protein sample preparation, protein extracts were incubated at only 68°C for 15 minutes prior to SDS-PAGE, instead of boiling. Nevertheless, this procedure led to the detection of a multitude of bands in the transgenic lines expressing EIN2-eGFP when probing for the GFP tag (Fig. 32B). Of these bands, one matched the size of the EIN2^{C-term}-YFP product expressed from protoplasts, a sample of which was loaded as a control (eGFP and YFP are very similar to each other in terms of the calculated molecular weight, with 27 kDa and 27.4 kDa, respectively). However, a corresponding band was also detected in untransformed seedlings and therefore likely constituted a cross-reaction of one of the antibodies (Fig. 32B). Overall, no differences in the protein band pattern could be observed between BA- or ACC-treated and control seedlings, indicating that EIN2 processing was not induced by either treatment. Likewise, no difference in band patterns, and no reproducible difference in band strengths, was observable between the seedlings expressing EIN2-eGFP in the WT or in the *prt1-1* mutant backgrounds (Fig. 32B). This data suggested that PRT1 did not impact significantly on the EIN2 protein levels in whole seedling extracts under the conditions tested within the frame of this work.

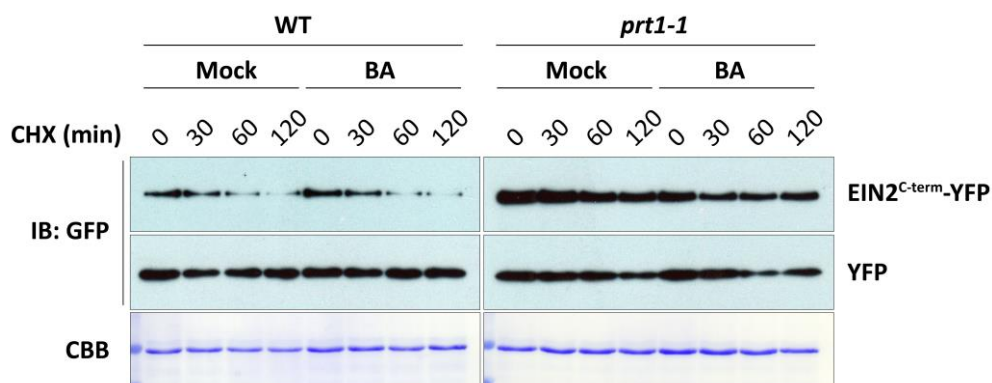


Fig. 33 | EIN2^{C-term} stability is not influenced by the presence of cytokinin during transient expression. EIN2^{C-term}-YFP (expressed as Ub fusion to expose N-terminal Phe) was transfected in *Arabidopsis* protoplasts of WT or *prt1-1* mutant genotype (line N119). YFP alone was co-transformed with all samples as a control. All constructs were driven by the *UBQ10* promoter. During overnight incubation for plasmid expression, 0.5 μM of the synthetic cytokinin BA or a vehicle control were included in the protoplast suspension medium. The next day, CHX treatments were conducted to follow protein stability dynamics. Samples were taken before (0 min) and at 30, 60, and 120 min after addition of CHX. Total proteins were extracted and subjected to immunoblot analysis.

To test a potential effect of BA on PRT1-dependent EIN2^{C-term} degradation, stability of EIN2^{C-term}-YFP was assayed during transient expression in protoplasts in the presence or absence of 0.5 μM BA in the protoplast medium. Here, EIN2^{C-term}-YFP protein abundance was not influenced in the WT by the presence or absence of 0.5 μM BA in the protoplast medium (Fig. 33). In the *prt1-1* mutant background, EIN2^{C-term}-YFP was more stable than in the WT, as was observed before. This was also unaffected by the presence of BA, confirming that EIN2^{C-term}-YFP abundance during BA signaling was not regulated in a *PRT1*-independent manner (Fig. 33). Thus, *PRT1*-dependent degradation of transiently expressed EIN2^{C-term}-YFP was concluded to be unaffected by exogenous supply of cytokinin – and also ACC (Fig. S14) – in *Arabidopsis* protoplasts. In summary, PRT1 was identified as a factor regulating the abundance of an EIN2 fragment initiated by Phe-646, in a transient expression system. However, loss of *PRT1* function did not lead to visible changes in EIN2 protein abundance in light-grown transgenic seedlings.

3.4.2 Apparent molecular weight of EIN2^{C-term}

In the past, the migration behavior of EIN2 CEND in SDS-PAGE has raised a debate on the true cleavage site of EIN2 (Cooper, 2013; Qiao et al., 2013). In my hands, the EIN2^{C-term}-YFP constructs all migrated about 5-10 kDa higher in SDS-PAGEs than it would be expected from the calculated molecular weight of 98 kDa when comparing to the protein standard (PageRuler™ Prestained Protein Ladder, Thermo Fisher Scientific) (Fig. S14, 28, 30, 34, 35). Notably, when compared to a different protein standard (Precision Plus Protein™ Dual Color Standard, BIO-RAD), the fragment migrated at the expected height (Fig. S18). This marker, on the other hand, gave rise to underestimations of the size of a second protein, the large subunit of RuBisCO (RBCL), with a calculated molecular weight of 53 kDa and an apparent molecular weight of less than 50 kDa as compared to the BIO-RAD protein standard (Fig. S18). This discrepancy of RBCL molecular weight was not observed when using the PageRuler™ protein standard (e.g., Fig. 28, S14). Hence, the PageRuler™ protein standard that showed a slightly larger apparent molecular weight of EIN2^{C-term}-YFP than calculated, but estimated RBCL subunit correctly, should allow for a better comparison with previous studies.

3.4.3 Physical interaction between EIN2 and PRT1 *in vivo*

Direct binding between the N-terminal 16 amino acids of EIN2^{C-term} and PRT1 was observed *in vitro* (Fig. 26, chapter 3.3.5). To investigate the biological relevance of this interaction, it was asked whether a physical association could also be detected in plant cells. To test this, constructs for a bimolecular fluorescence complementation assay (BiFC, or split-YFP) were created. Here, a fusion construct comprising 3HA-Ub^{K29,48R}-EIN2^{C-term}-3HA-YFP^C (YFP^C referring to the C-terminal half of YFP) was co-transfected in *Arabidopsis* protoplasts with PRT1-YFP^N (this plasmid was kindly provided by C. Naumann), both under control of the strong *UBQ10* promoter. A plasmid for expression of cytoplasmic and nuclear mCherry (kindly provided by Giulia Furlan¹ and M. Trujillo) was also co-transfected as an expression control. Conceptually, if protein-protein interactions take place in this assay, the fluorophore YFP is reconstituted and fluorescence is emitted. Since BiFC assays can notoriously lead to false-positive results due to the tendency of the YFP halves to self-assemble

¹ Leibniz Institute of Plant Biochemistry, 06120 Halle (Saale), Germany

(Horstman et al., 2014), the construct 3HA-Ub^{K29,48R}-G-EIN2^{C-term}-3HA-YFP^C was included as a negative control. Indeed, a weak signal of corresponding wavelength with cytosolic or endoplasmic localization was detected in protoplasts (Fig. S19). However, this was not exclusive to mCherry expressing cells, indicating that the weak signal was likely not derived from YFP assembly. Confirming this assumption, the signal was seen in both G-EIN2^{C-term} and F-EIN2^{C-term} combinations.

Given that PRT1 interaction with EIN2^{C-term} would conceptually lead to the degradation of EIN2^{C-term}, it was conceivable that the BiFC signal intensity derived from PRT1 interaction with F-EIN2^{C-term} was too low to be distinguished from the background signal. Next, a C-terminally tagged fusion of PRT1 might not support substrate binding, given that the putative substrate binding ZZ domain of PRT1 (Stary et al., 2003) is also located at the C-terminus. Hence, BiFC constructs were created for expression of both WT and V28A-mutated N-terminally YFP^N-3HA-tagged PRT1 variants (YFP^N-3HA-PRT1 and YFP^N-3HA-PRT1^{V28A}), reasoning that catalytic impairment of PRT1^{V28A} (see Fig. 20B, S12) would prevent degradation of EIN2^{C-term} upon a potential interaction with PRT1. Additionally, EIN2 expression constructs were recloned to lack the 3HA-tags (Ub^{K29,48R}-G/F-EIN2^{C-term}-Myc-YFP^C). However, no fluorescence signal was detected that matched the emission spectrum of YFP upon expression of any combination (data not shown). Since both PRT1 and EIN2^{C-term} were found to exhibit rather low *in-vivo* stability, YFP complementation derived from the interaction of these two constructs might not lead to signal intensity high enough to be visualized by microscopy. Alternatively, expression of a K29,48R-mutated Ub sequence in the corresponding EIN2^{C-term} UFT constructs, and consequent release of high amounts of mutated Ub upon DUB-dependent cleavage, might be toxic to the cells, and could have been detrimental to the interaction assay. Taken together, an interaction between PRT1 and EIN2^{C-term} could not be detected in BiFC assays.

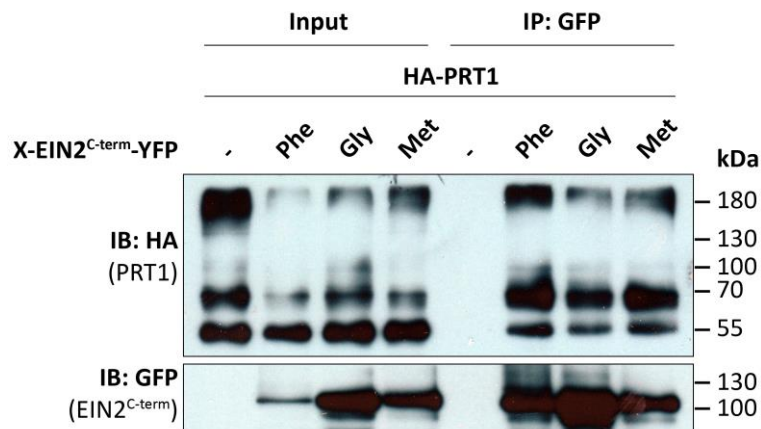


Fig. 34 | EIN2^{C-term} physically interacts with PRT1 in *Arabidopsis* protoplasts. Under control of the *UBQ10* promoter, 3HA-PRT1 was transiently co-expressed with variants of EIN2^{C-term}-YFP in *Arabidopsis* protoplasts of the *prt1-1^{ts}* genotype. N-termini of the EIN2^{C-term} constructs were created by Ub-fusions (X= Phe, Gly) or translation initiation via the start codon (X= Met). After overnight expression, GFP-fused protein was immunoprecipitated (GFP-Trap[®]_A, Chromotek) and samples were subjected to SDS-PAGE and immunoblot. 3HA-PRT1 is expected at a molecular weight of 50 kDa, but migrates as a band pattern and high molecular weight smear as seen before. EIN2^{C-term}-YFP is expected at 98 kDa.

Thus, a co-immunoprecipitation (co-IP) approach was taken to alternatively test for a physical interaction of EIN2^{C-term} and PRT1, expressing the previously employed EIN2^{C-term}-YFP UFT constructs containing the WT Ub sequence. EIN2^{C-term}-YFP strongly pulled down 3HA-PRT1, when both constructs were transiently co-expressed in *Arabidopsis* protoplasts under control of *proUBQ10* (Fig. 34). However, in contrast to the observations *in vitro*, this interaction did not depend on an aromatic

amino acid at the N-terminus of EIN2^{C-term}: *In-vivo* pull-down of 3HA-PRT1 was achieved for EIN2^{C-term} constructs initiated by either Phe, Gly, or Met (the last one was not expressed as a Ub-fusion, but Met served as the translation initiation signal in this construct; Fig. 34).

Notably, when a small protein like YFP alone was co-expressed with PRT1, no interaction with PRT1 was detected for YFP, while N-terminus-independent co-IP of PRT1 by EIN2^{C-term} persisted (Fig. S20). These observations, together with the rather low solubility of recombinant PRT1 proteins upon expression in *E. coli*, prompted me to assume that a phenomenon like co-aggregation, rather than specific protein-protein interactions, might have been responsible for the pull-down.

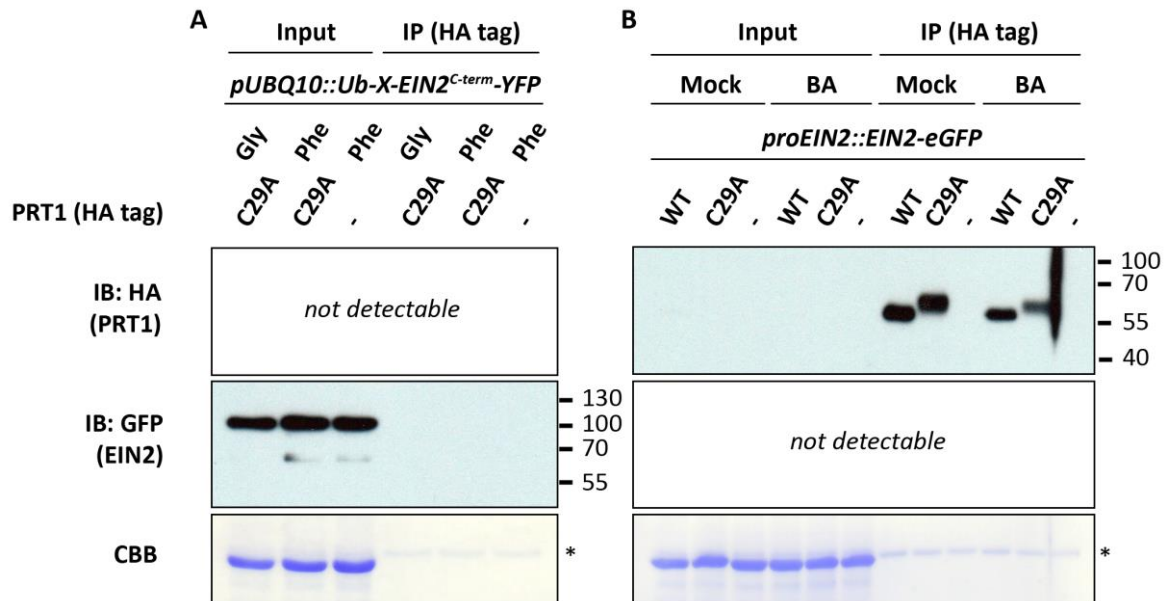


Fig. 35 | Co-immunoprecipitation attempts of EIN2^{C-term} and PRT1 under low expression conditions. In order to circumvent potential unspecific co-aggregation between the EIN2 and PRT1 proteins during immunoprecipitation from *Arabidopsis* protoplast cells, 3HA-PRT1 (A), or both constructs (B) were expressed under the control of the *EIN2* promoter conferring low expression levels. **A**, Ub-X-EIN2^{C-term}-YFP constructs under control of the *UBQ10* promoter were co-transfected together with *proEIN2::3HA-PRT1^{C29A}* (**C29A**) in *prt1-1* protoplasts. X denotes the N-terminus of EIN2^{C-term} after DUB cleavage and is either Gly or Phe. After overnight expression, 3HA-fused protein was immunoprecipitated (Anti-HA-Agarose, Sigma-Aldrich), and subjected to SDS-PAGE. For immunodetection, anti-HA tag primary antibody in combination with Protein A-HRP was applied to minimize the labelling of IgG heavy chain (asterisk in CBB). EIN2^{C-term}-YFP is expected at 98 kDa. **B**, Procedure like in A, but instead of co-transfecting EIN2^{C-term} constructs, protoplasts were prepared from transgenic lines in the *prt1-1* mutant background stably expressing full-length *EIN2-eGFP* under control of the *EIN2* promoter (line received from M. Grebe and Y. Ikeda and crossed into *prt1-1^{ts}*). Protoplasts of this line were transfected with *proEIN2::PRT1* constructs encoding *PRT1* either as a CDS-based 3HA-PRT1^{C29A} variant (**C29A**), or as the genomic WT sequence with C-terminal 3HA tag (**WT**: genPRT1-3HA). After transfection, protoplasts were treated with 0.05 μ M BA or a mock solution, and subjected to IP after overnight expression. Asterisks mark the CBB label of IgG heavy chain in the IP fractions, which are not to be confused with RubisCO large subunit in the input samples. 3HA-PRT1 (or PRT1-3HA) is expected at an apparent molecular weight of 50 kDa.

Since high protein concentrations can promote protein aggregation (Lebediker and Danieli, 2014), it was subsequently attempted to express PRT1 under a weak promoter, thereby also approximating more physiological conditions. The *EIN2* promoter was chosen for weak expression of *PRT1*, because it confers low but constitutive and ubiquitous expression in vegetative rosette leaves according to the *Arabidopsis* eFP Browser. However, when *proEIN2::3HA-PRT1^{C29A}* (the mutant was chosen for its catalytic inactivity *in vitro*) was co-transfected with *proUBQ10::Ub-EIN2^{C-term}-YFP* constructs in

protoplasts, PRT1^{C29A} fusion protein was not detectable (Fig. 35A), potentially due to suppression of plasmid-resided *proEIN2* by co-transfection with the much stronger *proUBQ10* (or, potentially, due to an unknown negative-feedback effect of high levels of EIN2^{C-term} on the *EIN2* promoter). Thus, transgenic lines stably expressing *proEIN2::genEIN2-eGFP* (received from M. Grebe and Y. Ikeda) in the *prt1-1* genomic background were used for protoplasting and transfection with *PRT1* constructs driven by the *EIN2* promoter. Here, the *PRT1* WT sequence was expressed either as the genomic locus region including introns and 5' untranslated region (UTR) with a C-terminal 3HA-tag (*genPRT1-3HA*), or as the previously introduced CDS-based *3HA-PRT1^{C29A}*. Moreover, protoplasts were subjected to 50 nM BA during overnight expression in order to trigger ethylene production, and consequently EIN2 cleavage. While PRT1 protein was not detected in whole cell lysates (i.e., input fractions) of these protoplasts, it was readily extracted by IP (Fig. 35B). However, no co-IP of EIN2 CEND-eGFP was achieved by this approach and total EIN2-eGFP levels in the stably transformed plant line were too low to be detected in input fractions of the protoplast lysates. Co-IP was also unsuccessful when both partners (*3HA-PRT1^{C29A}* and EIN2^{C-term}-YFP) were transiently co-expressed from the *EIN2* promoter in the presence or absence of BA, or when YFP-fused protein was targeted for IP, instead of the HA-tagged partner (data not shown).

Interestingly, under the low-expression conditions, the double-band appearance as well as the higher molecular weight species of 3HA-tagged PRT1 were absent (Fig. 35B), indicating that overexpression might have caused these observations. Moreover, PRT1 expressed as *genPRT1-3HA* exhibited faster migration in SDS-PAGE than *3HA-PRT1^{C29A}*, but both were larger than would be expected for an unmodified version. In the case of *3HA-PRT1^{C29A}*, a mono-ubiquitinated form could explain the observed protein size of roughly 58 kDa (Fig. 35B). Thus, either the genomic locus information (5' untranslated region (UTR) and introns), or the orientation of the affinity tag had an influence on the protein outcome (whereas it is unlikely that the size shift was caused by the mutation in RING1: Among the CDS versions, neither *3HA-PRT1* (Fig. 30), nor *GFP-PRT1* (Fig. 31B) constructs exhibited differences in apparent molecular weight between WT and C29A proteins when compared directly).

In summary, an *in-vivo* physical interaction between PRT1 and EIN2^{C-term} clearly attributable to specific protein interactions as opposed to protein co-aggregation could not be demonstrated. Next to the possibility that PRT1 might not interact with EIN2 *in vivo*, this might be caused by a failure to establish the right culture or assay conditions to trigger and maintain interaction, or by the dissociation of the interaction complex during IP procedures due to low binding affinity as it was observed *in vitro* during X-peptide pull-down assays (Fig. 23).

However, instability of EIN2^{C-term} clearly depended on the presence of functional PRT1, UPS function, and Phe on the N-terminus of EIN2^{C-term}, which is a canonical substrate recognition signal of PRT1. These latter results strongly argued that PRT1 ubiquitinates EIN2^{C-term} *in vivo*.

3.4.4 Hypocotyl elongation in the dark is slightly increased in *prt1-1^{ts}*

So far, direct *in-vitro* peptide-protein interactions between EIN2^{C-term} and PRT1 were demonstrated in this work and it was observed that PRT1 activity led to N-terminus specific destabilization of EIN2^{C-term} upon transient overexpression in protoplasts. Given these results it was assumed that EIN2^{C-term} might be a substrate for PRT1 in a physiological context. To test for a potential involvement of *PRT1* in EIN2-dependent signaling, the *prt1-1* mutant was subjected to the triple response assay. Here, the

sensitivity of seedlings towards the specific effects of ethylene during etiolation is tested. In *Arabidopsis*, these effects include: 1. The inhibition of hypocotyl and root elongation, 2. hypocotyl thickening, and 3. exaggeration of the apical hook curvature (Bleecker et al., 1988; Guzmán and Ecker, 1990).

In the triple response assays, no differences were noticeable between WT and *prt1-1^{ts}* mutant seedlings in terms of hypocotyl thickening and apical hook formation at any concentration of ACC tested (Fig. 36A, S21). The same was true for hypocotyl and root elongation upon ACC concentrations as high as or higher than 10 μM (Fig. 36A, B). In contrast, a plant line carrying the *ein2-5* knock-out allele (containing also a transgenic *DR5::GUS* reporter construct) did not show apical hook formation and was unaffected by the ACC treatments in terms of hypocotyl and root growth, confirming that the observed effects on WT and *prt1-1^{ts}* were indeed caused by the supplemented ACC (Fig. 36B). Of

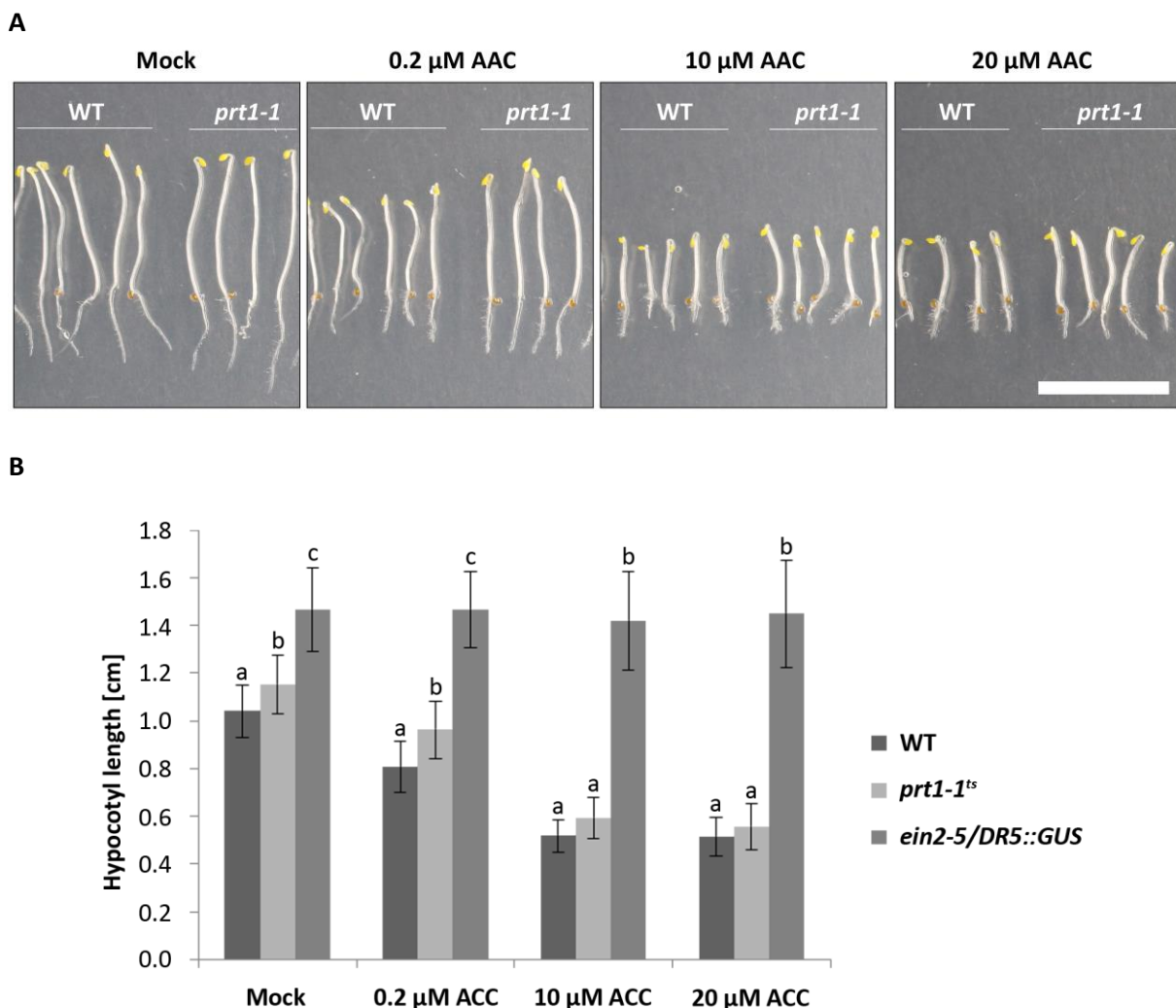


Fig. 36 | Dose response of the *prt1-1^{ts}* mutant to ACC during etiolation. For the triple response assay, seeds were aligned on sucrose-supplemented agar medium containing ACC or a mock supplement (0.005% ethanol), and stratified in the dark for 5 days. Before etiolation, germination was facilitated by 6 hours incubation at room temperature in the light. Subsequently, plates were kept vertically in the dark for 87 hours before examination. **A**, Representative seedlings of WT and *prt1-1^{ts}* etiolated at different ACC levels are depicted. Scale bar 1 cm. **B**, Quantification of hypocotyl lengths of all seedlings from the experiment exemplified in A. $n \geq 78$; whiskers indicate standard deviations. For statistical analysis, each treatment group was tested individually: Shapiro-Wilk normality tests, followed by one-way ANOVA and Tukey HSD; $p \leq 0.001$.

note, the *ein2-5/DR5::GUS* line showed longer hypocotyls even under mock conditions compared to the WT and *prt1-1* mutants (Fig. 36, S21), even when seed batches were raised and matured in parallel. This was consistent with previous reports on the *ein2-5* phenotype (Alonso et al., 1999).

Although *prt1-1^{ts}* responded normally towards moderate to high levels of ACC, differences between WT and mutant were detected at a concentration of 0.2 μ M. Here, *prt1-1^{ts}* exhibited slightly longer hypocotyls (and roots) than WT plants (Fig. 36, S21). The difference was measurable to statistical significance upon large sample numbers. Interestingly, a marginally longer hypocotyl growth in darkness compared to the WT was repeatedly observed for *prt1-1* mutants under mock conditions (Fig. 36B), an effect that was also measurable to statistical significance exclusively under large sample numbers. This might be caused by a lower sensitivity towards endogenous levels of ethylene (reflecting what was seen for *ein2-5*), but also raises the question whether the effects observed upon low ACC dosage were indeed due to the ethylene precursor supplement, or were rather the continuation of a preexisting effect.

Compromised sensitivity of *prt1-1^{ts}* plants towards ACC would be counter-intuitive when assuming a function of PRT1 in EIN2^{C-term} degradation. Nevertheless, from the results obtained by triple response assays, it was concluded that PRT1-targeting EIN2 is unlikely to contribute substantially to dampening ethylene responses during scotomorphogenesis, and that *PRT1* might slightly impact on dark-induced seedling growth in an ethylene-dependent or independent manner.

3.4.5 Cytokinin-induced inhibition of hypocotyl elongation in the dark is impaired in *prt1-1^{ts}* and N119

Next to its crucial function in ethylene signaling, considerable hormonal crosstalk converges around the axis of the EIN2 protein. Resistance to root growth inhibition by cytokinin is one of the most prominent phenotypes caused by an *ein2* null allele. It was considered that PRT1 targeting EIN2 might play a role in this pathway, rather than during the triple response to ACC.

To check the role of *PRT1* in cytokinin signaling, inhibition of shoot and root growth by BA was assayed. However, no difference was observed concerning size, root length, or greening of plantlets upon BA between the WT and *prt1-1^{ts}* (Fig. 37), or *prt1-1* homozygous backcross lines that produced siliques at 28°C (Fig. S22). In contrast, both the *ein2-1* and the *ein2-5* alleles conferred near insensitivity of root growth to 0.1 μ M BA in the medium, and root growth of the *ein2* mutant lines was also much less affected than WT or *prt1-1^{ts}* seedlings in the presence of 0.5 μ M BA (Fig. 37).

Next, to test if *prt1* mutation affected cytokinin sensitivity in the dark, the triple-response-like effect of BA on etiolated seedlings was assessed. For these and all further experiments, the *ein2-1* allele was used for comparison instead of *ein2-5/DR5::GUS*, since it lacked the reporter construct. Moreover, the *ein2-5* allele leads to a frameshift between the eighth and ninth transmembrane helix of the N-terminal NRAMP-like domain of EIN2, whereas *ein2-1* introduces a stop codon in the hydrophilic part well behind the NRAMP-like domain, after amino acid number 555 (Alonso et al., 1999). Hence, the *ein2-1* mutant line potentially still contains a truncated version of EIN2 comprising the N-terminal NRAMP-like domain which was shown to contribute to some aspects of EIN2 signaling, and is certainly required for responses upstream of CEND signaling (see introduction).

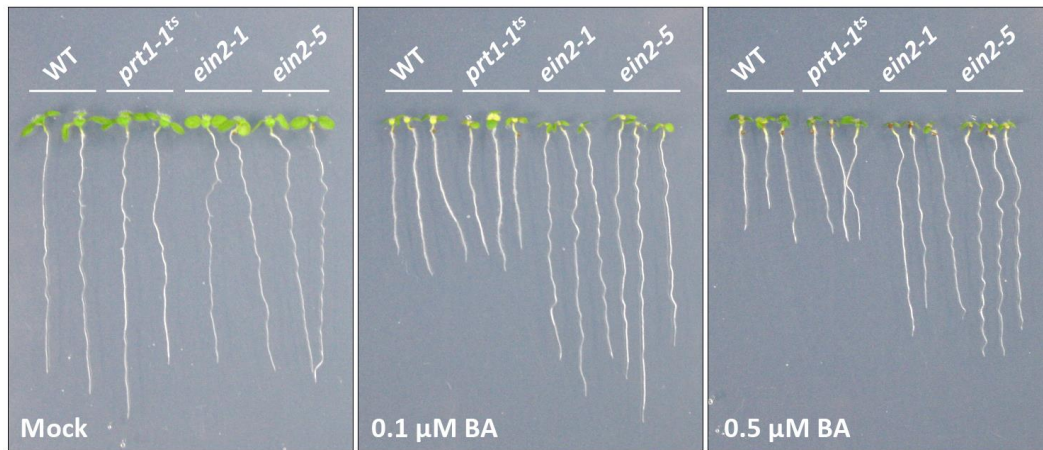


Fig. 37 | Shoot and root inhibition of *prt1-1^{ts}* seedlings by cytokinin. Seeds of the indicated genotypes were placed on sugar-supplemented agar medium containing 0.1 μ M BA (cytokinin), 0.5 μ M BA, or a mock solution (0.006% dimethyl sulfoxide (DMSO)). After stratification for 5 days, plates were transferred to 22°C and the plants were grown for 8 days under a long-day light regime (16/8). Pictures were taken of representative seedlings derived from one out of four independent experiments, each comprising at least 12 plants per genotype and growth condition. Note: The *ein2-5* genotype refers to the line harboring also the *DR5::GUS* construct (NASC ID: N16707).

Given that *PRT1*-function would potentially affect only the C-terminal part of EIN2, the *ein2-1* line was considered the better comparison for these experiments. For both *ein2-1* and *ein2-5*, full germination capacity could only be reached upon extensive seed after-ripening for several months. This effect of ethylene mutants was described before (Bleecker et al., 1988; Beaudoin et al., 2000; Bentsink and Koornneef, 2008). However, in contrast to previous reports (Beaudoin et al., 2000), in my hands stratification did not break the prolonged seed dormancy of freshly matured *ein2* seeds.

To test for their capacity for induction of the triple response to cytokinin, plants of the WT, *prt1-1^{ts}*, *ein2-1*, and double mutant *prt1-1 ein2-1* (hereafter referred to as *prt1 ein2*) genotypes were subjected to different concentrations of BA during germination in the dark.

Interestingly, *prt1-1^{ts}* showed a pronounced loss of sensitivity towards BA treatment in the triple response assay as compared to the WT (Fig. 38). In fact, *prt1-1^{ts}* lines exhibited up to 30 percent longer hypocotyls than the WT when etiolating on medium containing BA. Next to hypocotyl growth, root inhibition by cytokinin also appeared to be slightly reduced in *prt1-1^{ts}* lines, but this effect was much less evident (Fig. 38A). Concerning hypocotyl length, the strongest effect was observed upon an intermediate BA concentration of 1 μ M. Under these conditions, the mean hypocotyl lengths of *prt1-1^{ts}* were about 90 percent of those of *ein2-1*, while the difference between *prt1-1^{ts}* and *ein2-1* got stronger upon higher levels of BA. No difference was measurable between *ein2-1* and the *prt1 ein2* double mutant, although the *ein2-1* mutation did not confer full insensitivity to BA. Moreover, cotyledon opening was occasionally observed in the *prt1-1^{ts}* line upon BA treatment (Fig. 38A). Induction of cotyledon opening in the dark, particularly in the presence of BA, is characteristic of ethylene-insensitive mutants, since WT plants require much higher BA levels to induce cotyledon opening (Chory et al., 1994; Wei et al., 1994; Hansen et al., 2009; Cortleven et al., 2018).

The *prt1-1^{ts}* line was previously found to exhibit sensitivity to elevated temperatures caused by the genomic background of the line. To address the possibility that the BA-related phenotype was also induced by the second locus, the line N119 was subjected to triple response assays. This line also contains the *prt1-1* allele, but lacks the temperature-dependent sterility trait (Fig. 8B).

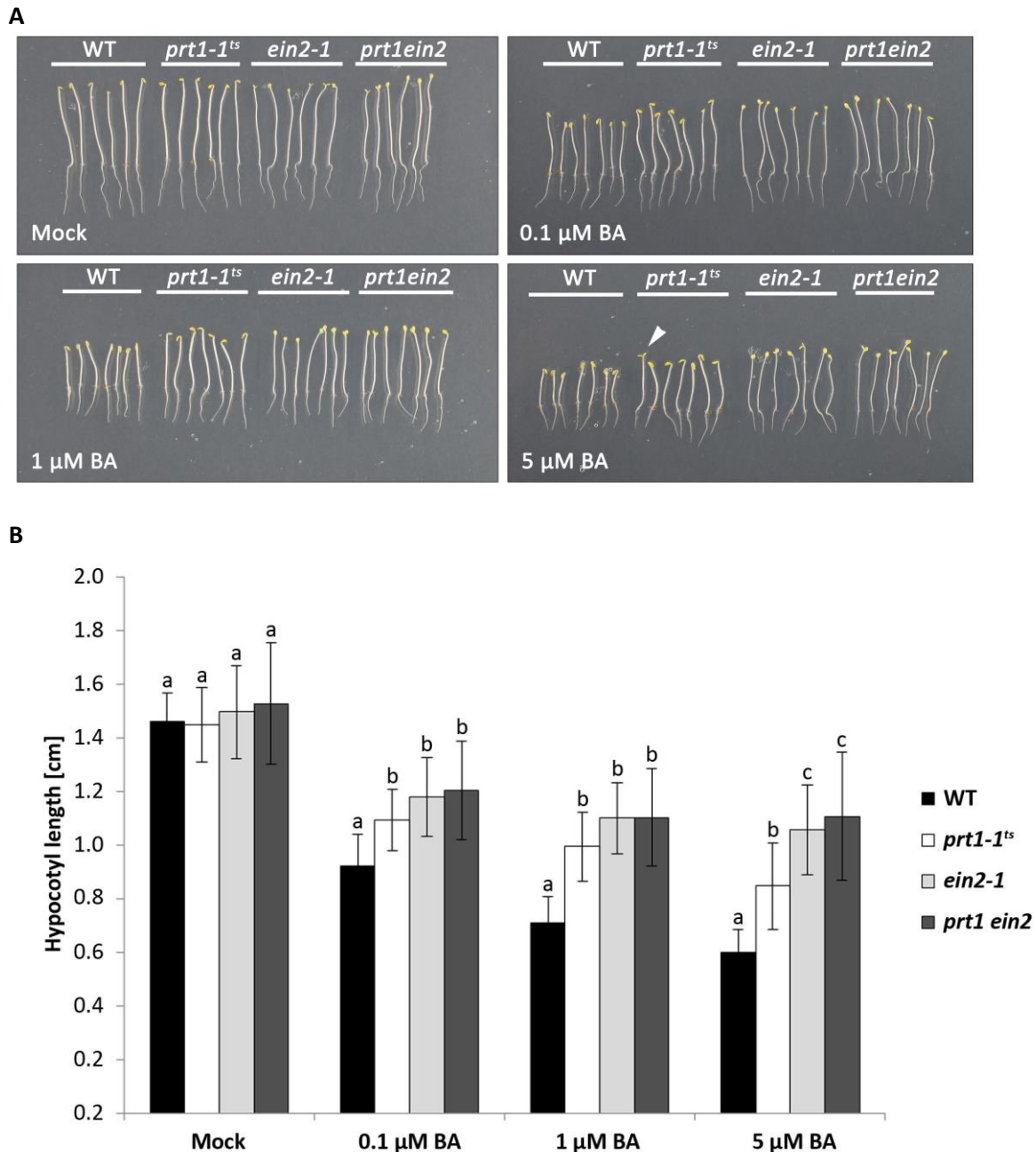


Fig. 38| The *prt1-1* mutant displays decreased sensitivity towards cytokinin during etiolation. Seeds of the indicated genotypes were transferred to sucrose-supplemented agar plates containing different concentrations of BA or a mock additive (0.03% DMSO), chilled for 5 days in the dark, subjected to illuminated conditions at 22°C for 9 hours and subsequently kept in the dark. Hypocotyl lengths were measured after 87 hours of dark growth. **A**, Pictures show representative seedlings at different concentrations of BA. The arrowhead indicates a seedling of *prt1-1^{ts}* with open hypocotyls. **B**, Quantifications of hypocotyl lengths of all individuals from the experiment exemplified in A. $n \geq 30$; whiskers indicate standard deviations. For statistical analysis, each treatment group was tested individually: Shapiro-Wilk normality tests, followed by one-way ANOVA and Tukey HSD; $p \leq 0.001$.

While the effect of ACC on N119 during etiolation was minor, like previously observed for *prt1-1^{ts}*, hypocotyl lengths of N119 were markedly increased in comparison to the WT upon 1 μM BA (Fig. 39). Hypocotyls of N119 in the presence of 1 μM BA were at least 25 percent longer than WT, resembling the effect detected for *prt1-1^{ts}*. This indicated that the higher resistance to BA treatment during etiolation in *prt1-1* lines was likely not accounted for by the genetic locus that triggered male sterility at elevated temperature.

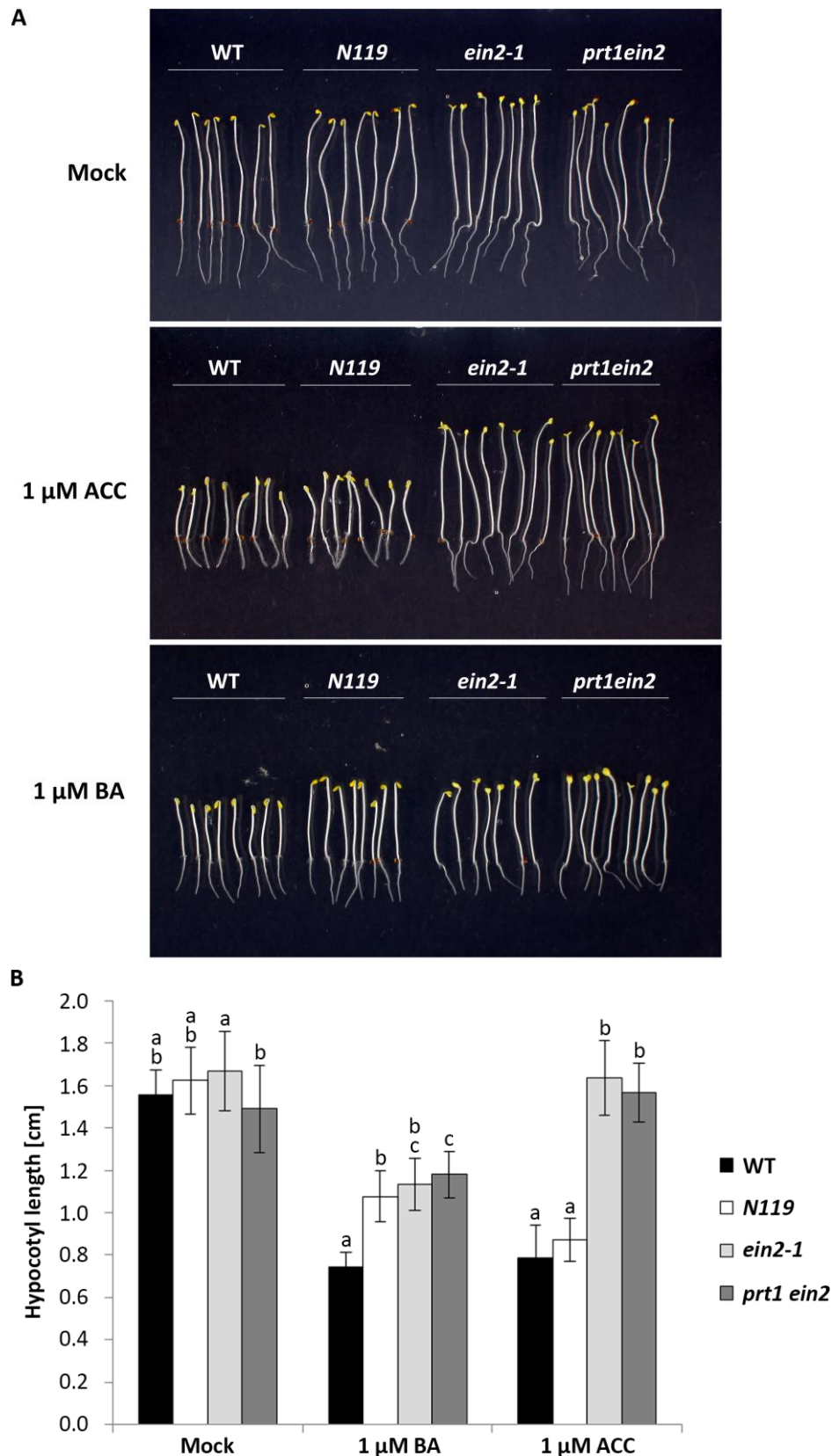


Fig. 39| Inhibition of hypocotyl elongation by BA, but not by ACC, is also impaired in the *prt1-1* line N119. Seedlings of the WT, the 28°C-fertile *prt1-1* line N119, *ein2-1*, and the double mutant *prt1 ein2* were placed on media containing 1 μM BA and mock (0.001% ethanol), 1 μM ACC and mock (0.006% DMSO), or mock supplements only (0.001% ethanol and 0.006% DMSO). After 5 days stratification, plates were transferred to 22°C and exposed to light for 8 hours before etiolation for another 88 hours. **A**, Representative seedlings were aligned for photographing. **B**, Quantification of hypocotyl lengths of all seedlings from the experiment

exemplified in A. $n \geq 32$; whiskers indicate standard deviations. For statistical analysis, each treatment group was tested individually: Shapiro-Wilk normality tests, followed by one-way ANOVA and Tukey HSD; $p \leq 0.001$.

Since interplay between ethylene, cytokinin, and sugar signaling had been reported (Gibson et al., 2001; Yanagisawa et al., 2003; Price et al., 2004; Franco-Zorrilla et al., 2005; Hartig and Beck, 2006; Laxmi et al., 2006; Kwon et al., 2011; Das et al., 2012), it was asked whether the supplementation with exogenous sucrose during heterotrophic growth in the dark contributed to the BA hyposensitive phenotype of the *prt1-1* mutant seedlings. In fact, in the absence of sucrose in the medium, inhibition of hypocotyl elongation by BA was much stronger than previously observed upon sugar supplementation in N119 (Fig. 40), as well as *prt1-1^{ts}* (Fig. S23), and approached WT levels. In the presence of additional sucrose, hypocotyl lengths of N119 were decreased by about 35 percent by 1 μ M BA compared to mock treatment (Fig. 39, 40). In contrast, without sugar supplement, the hypocotyl elongation of N119 plants was decreased by about 50 percent (Fig. 40). WT plants, by comparison, showed a reduction of hypocotyl elongation by about 55 percent, independently of whether sugar was added to the medium or not. The BA sensitivity of *ein2-1* was also marginally influenced by sucrose supplementation, with 28 and 32 percent inhibition of hypocotyl elongation on sucrose-supplemented or basal medium, respectively (Fig. 40). Thus, exogenous sucrose provided by the growth medium apparently counteracted the effect of BA in N199 and *prt1-1^{ts}* mutant plants.

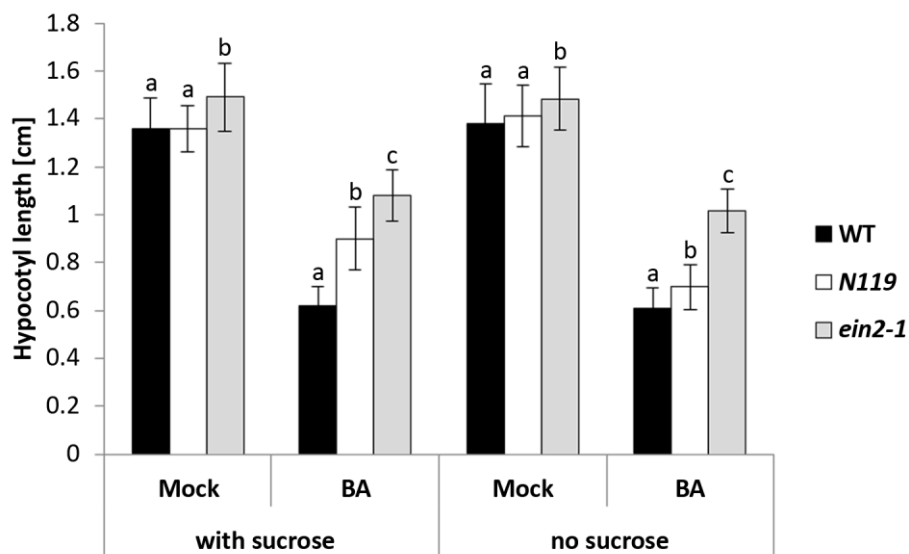


Fig. 40 | BA-resistance of hypocotyl repression in the *prt1-1* mutant line N119 is sugar-dependent. The triple response to BA was assayed with or without sugar supplementation of the medium using seedlings of WT, the *prt1-1* genotype N119, and *ein2-1*. Seeds were placed on agar-containing plates with BA (1 μ M) or mock (0.006% DMSO) addition, and 0.5 % sucrose or without sugar addition. After a 5 day period of dark stratification, seeds were illuminated at 22°C for 9 hours and subsequently incubated in the dark for additional 87 hours. $n \geq 29$; whiskers indicate standard deviations. For statistical analysis, each treatment group was tested individually: Shapiro-Wilk normality tests, followed by one-way ANOVA and Tukey HSD; $p \leq 0.001$.

Of note, in contrast to what was described previously (Zhang et al., 2010; Kushwah and Laxmi, 2014), hypocotyl-elongation under control conditions was not promoted considerably by the presence of 0.5% sucrose in the growth medium in any of the lines tested. This was potentially due to the experimental setup, since previous assays evaluated seedlings at the age of 8 days (Zhang et al., 2010; Kushwah and Laxmi, 2014), while hypocotyls were assessed at the fourth day after stratification during this work.

3.4.5.1 Cytokinin hyposensitivity is not caused by the *prt1-1* allele

Hyposensitivity towards cytokinin in the triple response assay was observed in this work for two related lines carrying the *prt1-1* allele, namely N119 and *prt1-1^{ts}*. In order to test whether *PRT1* was required for the cytokinin response, transgenic lines expressing *PRT1* under control of a *PRT1* promoter construct in the *prt1-1^{ts}* genomic background (compare to Fig. 19) were subjected to the triple response assay.

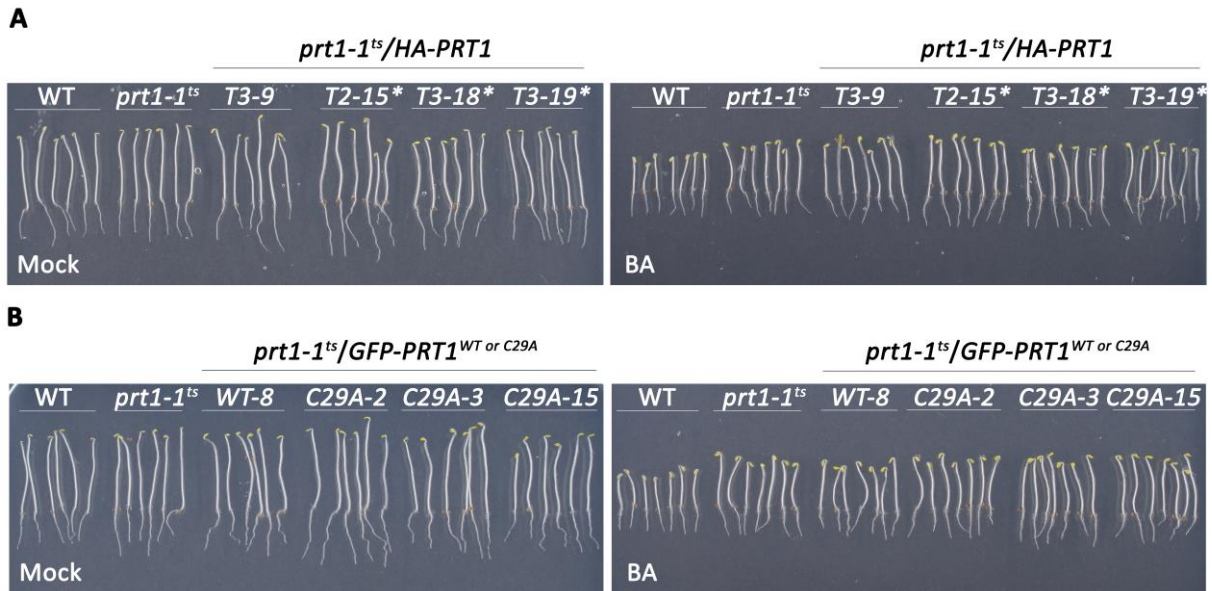


Fig. 41| Expression of an N-terminally tagged PRT1 coding sequence does not complement the BA hyposensitivity of *prt1-1^{ts}* in the triple response assay. Seeds were transferred to sucrose-supplemented agar plates containing 1 μ M BA or mock (0.006% DMSO). Triple response was assayed after 5 days stratification, 8 hours light exposure at 22°C and subsequent 87 hours dark incubation of the vertical plates. Representative seedlings were aligned for photography. **A**, Next to WT and *prt1-1^{ts}*, T2 (line 15) or T3 (all others) lines expressing N-terminally 3HA-tagged *PRT1* under control of the endogenous promoter (*proPRT1^{ACTCT}*) in the *prt1-1^{ts}* mutant background were assayed. Asterisks indicate lines with single insertions of the T-DNA. **B**, T3 lines in the *prt1-1^{ts}* background carrying N-terminally GFP-tagged variants of the *PRT1* coding sequence were subjected to the triple response assay. Line WT-8 contained *PRT1* as the WT sequence, whereas the other lines harbored the *PRT1^{C29A}* sequence with a mutation in RING1 leading to *in-vitro* autoubiquitination inactivity.

When assaying T2 and T3 transgenic lines bearing either N-terminally 3HA-tagged or GFP-tagged *PRT1* fusion constructs, complementation of the cytokinin hyposensitive phenotype of *prt1-1^{ts}* was not observed for any of the lines (Fig. 41). This strongly indicated that the loss of *PRT1* function was not causal for the phenotype, even though it cannot be excluded that the N-terminal tag interfered with *PRT1*'s function in this particular case. To further address this possibility, backcross lines derived from a cross between *prt1-1^{ts}* (female) and Col-0 WT (male) plants were included in the analysis. These lines, designated BC #68 and BC #85, exhibited WT-like fertility at 28°C while carrying the *prt1-1* allele homozygously (data not shown).

Both tested *prt1-1* backcross lines had lost the cytokinin hyposensitive phenotype of reduced hypocotyl inhibition observed for *prt1-1^{ts}* and N119 in the triple response assay (Fig. 42, S23). Opposing the progenitor lines, one of the backcross lines, BC #68, even exhibited a faint reduction of dark-induced hypocotyl growth in the presence of both sucrose and BA (Fig. 42). However, this very mild effect was not measurable to statistical significance during replication of the experiment and was not seen for the backcross line BC #85. A previously observed occasional opening of the

cotyledons in response to BA was likewise lost in the backcross lines (Fig. S23). Based on these results, it was concluded that loss of *PRT1* function does not affect the sensitivity towards BA during etiolation. Notably, the cytokinin hyposensitive phenotype was not observed in the backcross line BC #30 which was sterile at 28°C (Fig. 8) but carried the WT *PRT1* allele homozygously (Fig. S23). This indicated that the two phenotypes, high temperature sterility and cytokinin hyposensitivity in the dark, were genetically independent and were caused by different alterations in the genetic background of both the *prt1-1^{ts}* and N119 lines.

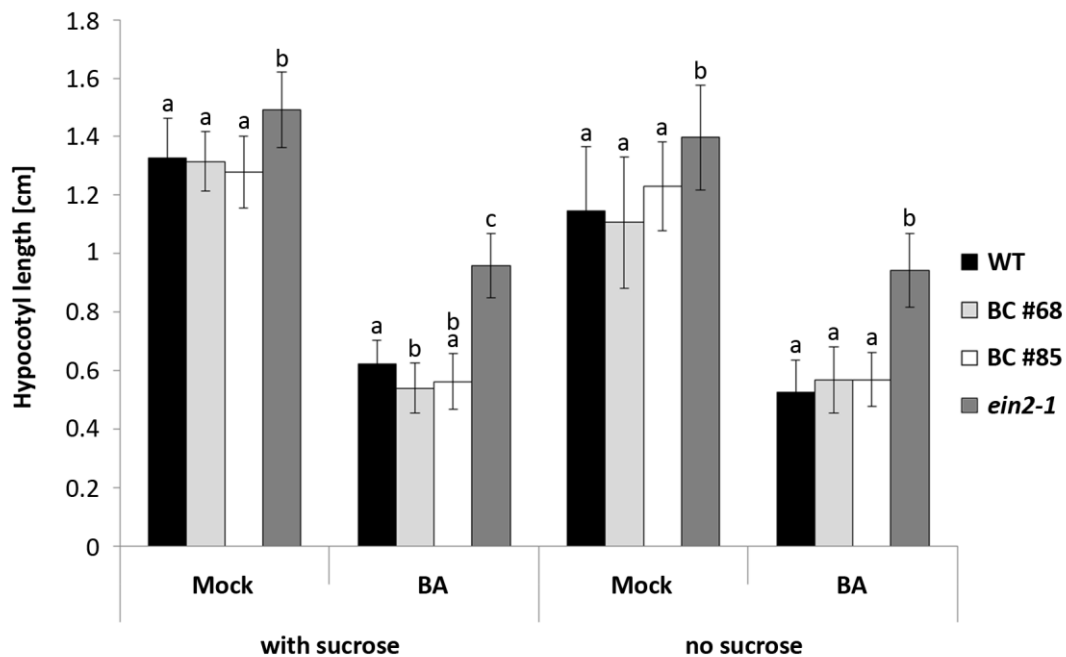


Fig. 42 | Cytokinin hyposensitivity does not depend on the *prt1-1* allele. The triple response to cytokinin (1 μ M BA) in the presence or absence of sucrose was analyzed using two *prt1-1* backcross lines, in comparison to the WT and *ein2-1* mutant genotype. Backcross lines BC #68 and #85 were derived from a cross *prt1-1^{ts}* X Col-0 and were homozygous for the *prt1-1* locus, but exhibited WT-like fertility at 28°C. F4 seeds were used in the assay. The experiment was performed as described in Fig. 40. $n \geq 35$; whiskers indicate standard deviations. For statistical analysis, each treatment group was tested individually: Shapiro-Wilk normality tests, followed by one-way ANOVA and Tukey HSD; $p \leq 0.001$.

3.4.6 Expression of EIN2^{C-term} confers signs of constitutive ethylene response in combination with the *prt1-1^{ts}* genotype

Previous work had shown that expression of EIN2 CEND failed to rescue the lack of a triple response in *ein2-5* mutants (Alonso et al., 1999). However, these transgenic constructs were expressed as simple ORFs initiated by Met. Hence, the gene products differed from the proposed endogenous EIN2 proteolytic fragment at least in the N-terminal residue. In order to test whether N-terminal Phe was required for CEND activity, the Ub fusion construct *proEIN2::Ub-EIN2^{C-term}-YFP* was introduced into the *ein2-1* mutant background by *Agrobacterium*-mediated transformation. Transgenic lines of the T3 generation were subjected to the triple response assay using ACC or BA as the stimulus.

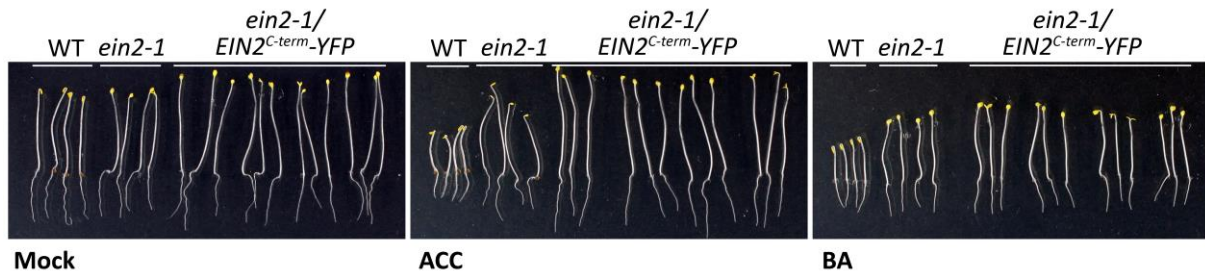


Fig. 43 | Expression of *EIN2^{C-term}-YFP* does not complement the lack of a triple response in *ein2-1*. Transgenic lines stably expressing *proEIN2::Ub-EIN2^{C-term}-YFP* in the *ein2-1* genomic background were subjected to the triple response assay together with untransformed WT and *ein2-1* seedlings. The triple response of etiolated seedlings was triggered by growth on agar medium containing 1 μ M ACC, 1 μ M BA, or a vehicle control. Representative seedlings were aligned for photography. Next to WT and *ein2-1* seedlings, transgenic T3 lines #5, #16, #18, and #19 derived from independent transformation events (each three seedlings are aligned from left to right in each panel) are shown. All images were taken at the same magnification.

As was reported for CEND, *EIN2^{C-term}-YFP* did not reconstitute a triple response of the *ein2-1* mutant plants (Fig. 43). Moreover, at the rosette stage, the transgenic lines were phenotypically indifferent from *ein2-1* also under normal growth conditions (Fig. 44). The latter was surprising since expression of CEND had been reported to be sufficient to trigger ethylene-responsive phenotypes in the light (Alonso et al., 1999; Qiao et al., 2012; Wen et al., 2012). It was reasoned that *PRT1*-dependent destabilization of the Phe-initiated *EIN2^{C-term}* could prevent the emergence of constitutive ethylene-signaling phenotypes in these lines. Hence, the construct was transformed into the *prt1-1^{ts}* mutant background and single-insertion lines were selected on the basis of the segregation ratio on selective medium.



Fig. 44 | *EIN2^{C-term}-YFP* expression triggers morphological defects and early flowering in the *prt1-1^{ts}* genomic background. Growth morphology of six weeks old plants under long-day (16/8) conditions is depicted for WT, *prt1-1* mutant line N119, *ein2-1*, and transgenic lines expressing *proEIN2::Ub-EIN2^{C-term}-YFP* in the genomic background of *ein2-1* or *prt1-1^{ts}*. Each three different transgenic T3 lines (*ein2-1* background) or T2 lines (*prt1-1^{ts}* background) derived from independent transformation events are shown.

Indeed, *prt1-1^{ts}* stably expressing *EIN2^{C-term}-YFP* exhibited growth retardation phenotypes at various degrees, and flowered earlier than WT or untransformed *prt1-1* mutant plants (Fig. 44). Furthermore, *prt1-1^{ts}/EIN2^{C-term}-YFP* lines produced only few seeds. The low fertility was partly caused by a protrusion of the pistil before flower maturity (Fig. 45) which was not observed on untransformed *prt1-1* mutant plants (Fig. 45, compare also to Fig. 9 for the line *prt1-1^{ts}*). However, not all transgenic flowers exhibited projected pistils; a strong protrusion was observed on average for one flower per inflorescence, and hence other factors likely contributed to the low fertility of these plants. This was consistent with overall abnormal flower morphology, including a rather small size of the flower buds, as well as occasional shortening of individual sepals and petals (Fig. 45).



Fig. 45| Expression of *EIN2^{C-term}-YFP* leads to abnormal flower morphology in the *prt1-1^{ts}* genomic background. Flowers of untransformed WT and *prt1-1* mutant (line N119) plants were compared to transgenic lines expressing *proEIN2::Ub-EIN2^{C-term}-YFP* in the genomic background of *ein2-1* or *prt1-1^{ts}*. Flowers of each three different T3 lines (*ein2-1* background) or T2 lines (*prt1-1^{ts}* background) derived from independent transformation events are shown. *EIN2^{C-term}-YFP* expressing *prt1-1^{ts}* lines frequently exhibited protruded pistils already before flower opening (arrowhead), and occasionally shortened sepals and petals (arrow). Scale bar: 1 mm.

The phenotypes observed for *prt1-1^{ts}/EIN2^{C-term}-YFP* transgenic lines strongly indicated aspects of constitutive ethylene signaling in these plants, since similar phenotypes were described for CEND expressing lines before (Alonso et al., 1999; Qiao et al., 2012; Wen et al., 2012). The fact that these effects of *EIN2^{C-term}* were not observed in the *PRT1* WT (*ein2-1* mutant) background, supports the hypothesis that *EIN2^{C-term}* is destabilized in a *PRT1*-dependent manner *in planta*. This was in line with the results obtained from protoplast experiments (chapter 3.4.1). It was attempted to correlate the phenotypic results with the levels of the YFP-fusion protein in the transgenic plants. However, no transgenic protein was detectable in neither *ein2-1*, nor *prt1-1^{ts}* genetic backgrounds by Western blot and probing with the anti-GFP antibody. This was likely due to the low expression level of the *EIN2* promoter.

Together, *in-vitro* and *in-vivo* evidence obtained during this work indicates that a C-terminal fragment of *EIN2* resulting from proteolytic cleavage before Phe-646 is destabilized by *PRT1* activity. The destabilization is most likely caused by proteasomal degradation after *PRT1*-mediated Ub transfer. In agreement with this hypothesis, binding of *PRT1* to peptides mimicking the liberated *EIN2* neo-N-terminus could be observed *in vitro*. *PRT1*-dependent decrease of *EIN2* signaling does not appear to contribute substantially to ethylene signaling in the dark, but potentially affects other aspects of ethylene signaling, such as growth inhibition and determination of flower morphology.

3.5 The substrate specificities of PRT6 and ATE1

3.5.1 The *in-vitro* substrate specificity of the UBR domain of PRT6

Next to *PRT1*, the second *bona fide* N-recognin of *Arabidopsis* is *PRT6* which is acting in the recognition of arginylated N-degrons (Garzón et al., 2007). Because of the sequence homology of *PRT6* to yeast Ubr1 and the conservation of the UBR domain, it was furthermore suggested that *PRT6* could also recognize the remaining type I destabilizing residues Lys and His. However, like in the case of *PRT1*, a direct interaction of *PRT6* with any substrate was not shown so far. Hence, the sequence requirements for a peptide-*PRT6* interaction were analysed using the SPOT system.

Purified protein of the N-terminally Glutathione S-transferase- (GST) tagged UBR domain comprising amino acids 119-189 of PRT6 (hereafter referred to as UBR^{PRT6}) was kindly provided by Hongtao Zhang¹ and Frederica Theodoulou¹.

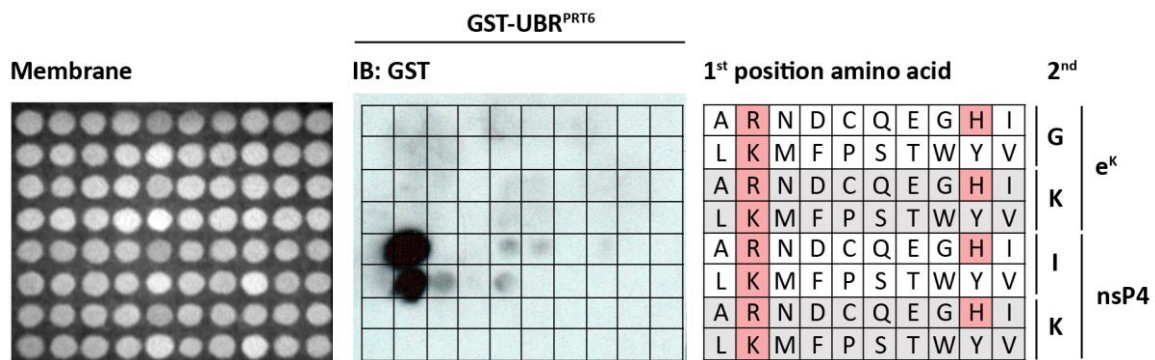


Fig. 46 | The UBR domain of PRT6 binds to Arg- and Lys-initiated peptides in a manner dependent on subsequent amino acids. The UBR domain of PRT6 comprising amino acids 119-189 was obtained from H. Zhang and F. Theodoulou as a purified N-terminal GST fusion protein and subjected to a SPOT assay with 17-mer peptides of e^K- and nsP4-derived sequences with varying amino acids in the N-terminal positions 1 and 2. Peptides present on the membrane were visualized by UV light (left), and UBR protein bound during the assay was detected by immunoblot using anti-GST antibody (center). A schematic representation of the peptide sequences is given on the right side. Type I primary destabilizing residues are highlighted in red. The immunoblot is representative of two independent experiments using different membranes.

When this protein was incubated with a SPOT membrane containing variants of the nsP4 and e^K sequences, it was found to bind only to N-termini with Arg and Lys in the first position, but not His (Fig. 46). In contrast to PRT1, the binding of GST-UBR^{PRT6} to type I residues was facilitated only by the nsP4 backbone, and only when Ile was the amino acid in second position (Fig. 46). Notably, Ile in second position represents the WT variant of nsP4.

The first identified *in-vivo* targets of N-end rule components in plants were members of the ERFVII group transcription factors (Gibbs et al., 2011; Licausi et al., 2011), and ATE1/2- and PRT6-dependent degradation of RAP2.12 and HRE1/2 was evidenced genetically. Since biochemical studies were missing, it was decided to investigate this interaction using SPOT assays. Indeed, when GST-UBR^{PRT6} was incubated with a SPOT membrane presenting peptides that corresponded to the MetAP-processed and arginylated N-terminus of RAP2.12 (the sequence of which is conserved in RAP2.2 up to Ser-16; hereafter denoted RAP2 sequence), specific pull-down of GST-UBR^{PRT6} was observed (Fig. 47). Interestingly, this was not the case for a sequence mimicking the deamidation-arginylation product of the Asn-11 starting fragment of RIN4 (Fig. 47A). This N-terminus is created *in vivo* by proteolytic cleavage of the 211 amino acid long RIN4 at two distinct sites by the protease AvrRpt2, releasing both the Asn-11-starting, and an Asp-153-starting fragment (Axtell and Staskawicz, 2003; Chisholm et al., 2005; Takemoto and Jones, 2005). Both fragments were proposed to be subject to N-end rule dependent degradation (Takemoto and Jones, 2005). The Δ152 C-terminal fragment of RIN4 was not synthesized as an Arg-initiated peptide on this membrane setup due to spatial limitations. However, an arginylated variant mimicking the considerably longer middle fragment of RIN4 (corresponding to the Δ10 peptide) was included in the assay and, crucially, was not recognized by GST-UBR^{PRT6} (Fig. 47A). Thus, the SPOT assay results contradicted the previously proposed interaction between PRT6 and the RIN4 middle fragment.

¹ Rothamsted Research, Harpenden AL5 2JQ, United Kingdom

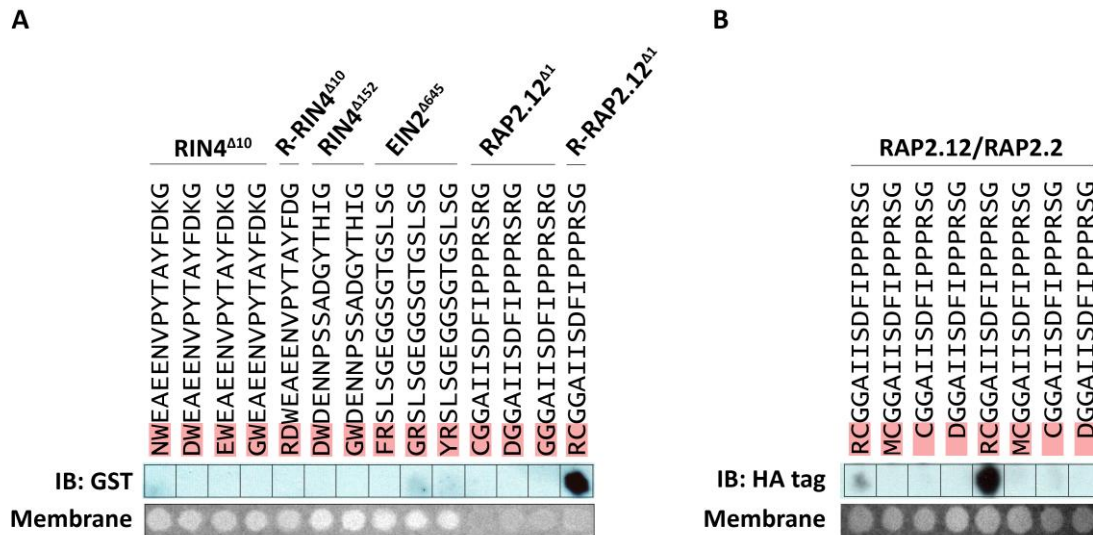


Fig. 47 | A PRT6 fragment containing the UBR box binds to the arginylated N-terminal peptide of ERFVII transcription factors, but not the RIN4^{A10} proteolytic fragment. Immunoblots of SPOT peptide assays using anti-GST (A) or anti-HA tag (B) antibodies are depicted together with images of the blank SPOT membrane seen in UV light (bottom rows). Amino acids at the peptide's N-termini that were varied between otherwise identical peptides are highlighted in red. **A**, Recombinantly expressed GST-UBR^{PRT6} (obtained from H. Zhang and F. Theodoulou) was incubated with a SPOT membrane presenting peptides corresponding to variants of the neo-N-termini of RIN4, EIN2, and RAP2.12 which are conditionally produced in plant cells. The experiment was performed twice with the same result using different replicates of the peptide membrane. **B**, A fragment of PRT6 comprising amino acids 1 to 193 was expressed from *E. coli* with an N-terminal GST- and a C-terminal simple HA tag. Purified fusion protein was incubated with a SPOT membrane containing variants of the conserved N-terminal peptide of the ERFVII transcription factors RAP2.12 and RAP2.2. The experiment was performed four times independently with comparable results using different membranes, one of which (the one seen in the figure) was derived from an independent synthesis batch.

SPOT-membrane bound peptides pulled down GST-UBR^{PRT6} with overall relatively low affinity. Hence, it was aimed to test the interaction with a larger portion of the PRT6 protein. For this purpose, a C-terminally truncated version of PRT6 comprising amino acids 1-193 with a C-terminal simple HA tag (received from Pavel Reichman¹) was subcloned to be expressed as an N-terminal fusion with GST. Even though the purification efficiency of this construct from *E. coli* cells was low, and purifications contained high amounts of GST alone (Fig. S24), the recombinant protein proved to be applicable to SPOT assays. When GST-PRT6¹⁻¹⁹³-HA was incubated with peptides representing the RAP2 N-terminus, binding was observed exclusively for the Arg-Cys starting variants mimicking the ATE-processed form, as previously observed for GST-UBR^{PRT6} (Fig. 47). In contrast, incubation with GST alone (purified GST protein was received from H. Zhang and F. Theodoulou) did not lead to detectable signals (data not shown). However, again only weak binding to RC-starting ERFVII N-termini was detected, and the pull-down efficiency for both PRT6 fragments varied between experiments (Fig. 48), and even within the same membrane (Fig. 47B). Of note, the RAP2 sequence appeared rather difficult to synthesize, as reflected by low signal intensities in UV light, even when compared to EIN2 sequences with similar contents of aromatic amino acids (Fig. 47A). A potentially low synthesis efficiency of RAP2 might be due to a high number of residues such as Ile which are considered to cause synthesis problems (Bacsa et al., 2008). Notably, an alternative explanation for weak UBR binding to Arg-Cys-starting peptides in the SPOT system could be the lack of Cys oxidation in these peptides.

¹ Leibniz Institute of Plant Biochemistry, 06120 Halle (Saale), Germany

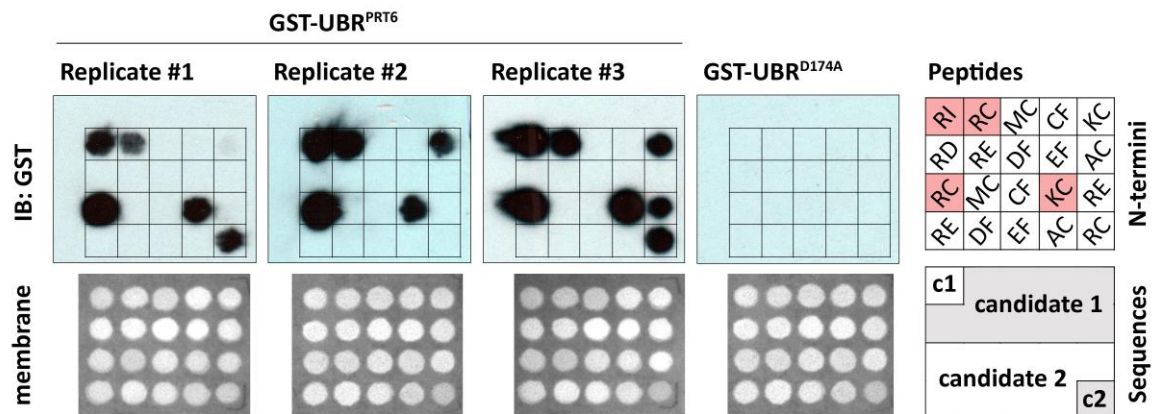


Fig. 48 | The UBR box of PRT6 binds to peptides mimicking the processed N-termini of two MC-starting proteins in an N-terminus dependent manner. Purified GST-tagged UBR domain from PRT6 or a mutated version (both proteins were kindly provided by H. Zhang and F. Theodoulou) were incubated with SPOT membranes that presented variants of the 17 amino acid N-termini of two different MC-initiated substrate candidates. The figure depicts Western blot detections of the fusion proteins using anti-GST antibody (top), as well as the blank membrane as seen in UV light (bottom). The scheme on the right side indicates the N-terminal amino acids in position 1 and 2 of the peptides (top) together with the arrangement of the peptide backbones (bottom). The sequences of “candidate 1” and “candidate 2” are confidential. Additionally, two control sequences were synthesized (c1 being nsP4-derived with RIFSTDTGPGHLQKKSG, and c2 represents the arginylated N-terminus of RAP2.12 with RCGGAIISDFIPPPRSG). The experiment was performed three times independently using different membranes. Due to observed variation between the replicates, all three immunoblots are shown in the figure. Peptides that caused a signal in the immunoblot within all three experiments are highlighted in red. The mutated UBR variant was included on a parallel membrane each time. Of these, one representative experiment is shown.

In the next step, binding of GST-UBR^{PRT6} to other Met-Cys starting proteins was tested, since this N-terminus conceptually allows for the enzymatic production of an arginylated N-degron *in vivo*. Here, two sequences were chosen in collaboration with F. Theodoulou. These sequences had been identified as potential *in-vivo* substrates of PRT6 (unpublished results by F. Theodoulou). The two sequences were synthesized on SPOT membranes as sets of peptides with varying N-termini together with nsP4 and RAP2 as control sequences. It was found that both candidate sequences produced clear signals for GST-UBR^{PRT6} binding when the first amino acid was either Arg or, with lower signal intensities, Lys (Fig. 48). In contrast, a UBR^{PRT6} variant containing an Asp to Ala mutation at position 174 (purified protein was kindly provided by H. Zhang and F. Theodoulou) showed no detectable binding (Fig. 48). Regarding the interaction with the WT protein, candidate 2 gave rise to stronger signals with UBR^{PRT6} than candidate 1 did, even though the two peptides differ only in 3 amino acids in the C-terminal part. This might, however, have been due to a better accessibility of candidate 2 since the concerning amino acids likely improved flexibility of this peptide, compared to candidate 1.

Since ATEs arginylate N-terminal Glu and Asp in mammals and yeast (Gonda et al., 1989; Kwon et al., 2002), it was also asked whether an Arg-Glu initiated peptide would support binding by the plant PRT6. However, peptides initiated by these amino acids did not yield reliable signals for UBR^{PRT6}-binding when presented on the SPOT membrane (Fig. 48), as it was observed before for the RD-starting RIN4^{Δ10} sequence (Fig. 47). This was even more surprising since, as mentioned above, the Arg-Cys variants of the same peptide backbones interacted robustly with UBR^{PRT6} within the same experiment (Fig. 48), even despite of the fact that they deviated from the naturally occurring protein version by the lack of Cys oxidation. Hence, it could be concluded from the results obtained with SPOT assays, that UBR^{PRT6} did not target synthetic peptides mimicking ATE products derived from

Glu- and Asp-starting substrates. In contrast, interaction of UBR^{PRT6} with peptides mimicking the processed N-termini of ERFVII transcription factors could be confirmed by these experiments.

3.5.2 ATE1 arginylates acidic N-termini *in vitro*

Based on genetic evidence, ATE1 and ATE2 were accounted responsible for the N-terminal arginylation of ERFVII transcription factors prior to their recognition by PRT6 (Gibbs et al., 2011; Licausi et al., 2011). It was argued that oxidation of the demethylated Cys-starting peptide triggers recognition and arginylation of ERFVII members by the ATEs under aerated conditions, ultimately repressing the hypoxic response in plants. Additionally, it was shown that arginylation activity of a protein extract prepared from *Arabidopsis* seedlings towards a test substrate, Glu-starting α -lactalbumin, depended on an intact *ATE1*, and to a much lesser extend *ATE2* gene (Graciet et al., 2009). However, whether ATEs use the RAP2 N-terminus as a substrate and whether this relies on the oxidation of the free Cys was never proven on a biochemical level. Moreover, the state of oxidation of the N-termini remained unclear. Finally, for α -lactalbumin arginylation, it was unknown whether arginylation by ATEs depended on additional cofactors or upstream events occurring in the cell extract.

To address these questions, ATE1 (the CDS was obtained as a Gateway Entry clone from C. Naumann) was subcloned into an expression vector giving rise to a fusion protein with an N-terminal hexa-His-tag, which was purified from *E. coli* (Fig. S24). Using this protein, a new *in-vitro* arginylation assay was set up deploying artificial peptides as substrates, which was, in contrast to previous peptide-based approaches (Song et al., 2014), independent of reverse-phase column-based purification of the peptides. In our assay, 12-mer C-terminally biotinylated peptides were incubated with ATE1 in an arginylation reaction involving radiolabeled Arg and subsequently coupled to avidin-agarose (the peptides were synthesized by C. Müller and T. Grossmann). After removal of unreacted radiolabel by thorough washing steps, bead-coupled peptides were subjected to liquid scintillation counting in order to assess the incorporation of radioactive Arg.

Using this method, Arg incorporation by ATE1 into peptides of the RIN4 ^{Δ 11} (X-WEAEENVPYTA) and RAP2 ^{Δ 2} (X-GGAIISDFIPP) (corresponding to the conserved N-termini in RAP2.2, RAP2.12, and HRE2) sequences was observed with no marked differences between the two sequences, but with strong dependence on the peptide's N-terminus (Fig. 49). Consistent with findings from mammalian and yeast ATEs, both RIN4 and RAP2 were readily arginylated by the *Arabidopsis* ATE1 when Asp was exposed at the N-terminus, whereas only a very weak signal was detected when the peptide contained Gly in the first position. Notably, the RAP2 N-terminus contains an internal Asp residue in the middle part of the 12-mer peptide used in this assay, and RIN4 carries three internal Glu residues. The fact that Gly starting variants of these peptides did hardly facilitate Arg incorporation by ATE1 in our system indicates that midchain arginylation might be of minor importance in case of the plant enzyme, in contrast to what has been reported for mouse ATE1 (Wang et al., 2014).

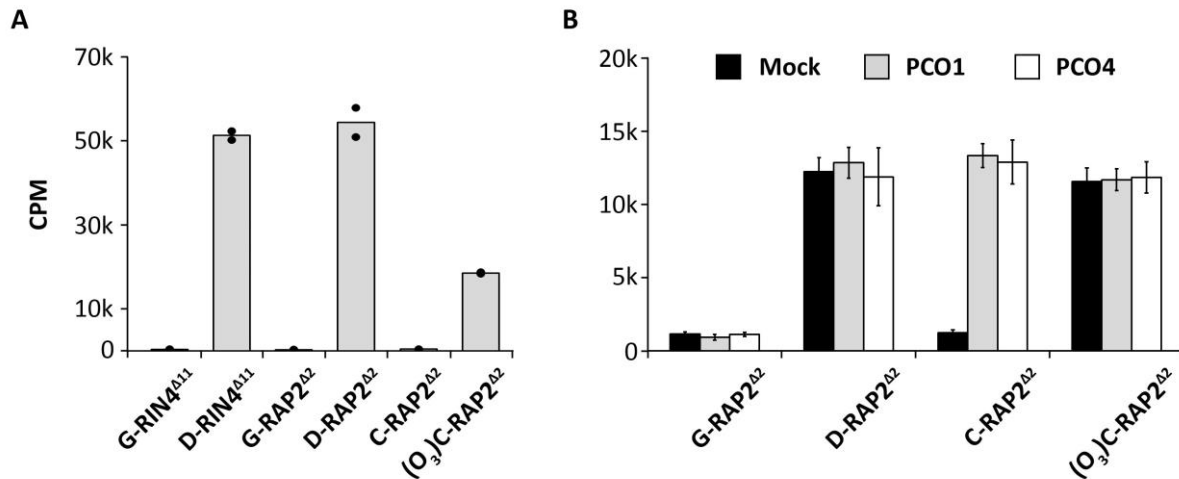


Fig. 49 | Arginylation of peptide substrates by ATE1 depends on an acidic side chain in the peptide N-terminus and can occur downstream of PCO action. *In-vitro* arginylation by purified 6xHis-tagged ATE1 using artificial 12-mer peptide variants of the sequences X-RIN4^{Δ11} (X-WEAEENVPYTA) and X-RAP2^{Δ2} (X-GGAIISDFIPP) (which is conserved in RAP2.2, RAP2.12, and HRE2) was assayed by scintillation measurement of incorporated radiolabeled Arg. All peptides were C-terminally functionalized by (PEG)-K-(biotin) for avidin pull-down. X=Gly, Asp, Cys, or (O₃)-Cys (sulfonic acid). **A**, Artificial peptide variants of the RIN4^{Δ11} and RAP2^{Δ2} sequences were subjected to an arginylation reaction including recombinant ATE1 and radiolabeled Arg-tRNA. ¹⁴C-Arg incorporation was assessed by liquid scintillation counting (CPM: Counts per minute). The reaction mixture included 100 mM DTT. The experiment was performed twice independently, data points indicate the values of each independent replicate, and bars are the means of both experiments. The dataset was published in Goslin et al. (2019). **B**, Arginylation of X-RAP2^{Δ2} peptides was performed as described in A, but in the presence of 1 mM DTT, and including recombinant PCO1 or PCO4 as indicated. A control was performed in the absence of PCO (mock). Mean values with standard deviations are presented. n=3 independent experiments using two different purification batches of ATE1. The data from this figure (panel B) was published in White et al. (2017).

Crucially, RAP2 was not used as a substrate by ATE1 when present as the Cys-starting sequence that mimics the MetAP-processed endogenous version in the absence of oxidation (Fig. 49). In contrast, a peptide starting with Cys sulfonic acid ((O₃)Cys) was arginylated by ATE1 *in vitro*, proving the requirement of Cys oxidation for ATE1-mediated arginylation (Fig. 49A). Interestingly, the arginylation reaction, as judged from total scintillation counts, was less efficient, with almost half the scintillation count values, when offering the (O₃)C-RAP2 sequence compared to the D-RAP2 substrate (Fig. 49A). However, no difference in the reaction efficiency was observed between D-RAP2 and (O₃)C-RAP2 sequences under less reducing conditions (1 mM DTT (Fig. 49B) compared to 100 mM DTT (Fig. 49A)). Here, both peptides yielded lower signals than previously observed for D-RAP2. Thus, reducing conditions apparently activated ATE1 towards the Asp-starting peptide substrate. Alternatively, reducing conditions might have promoted ATE1 activity in general, but the presence of (O₃)C-RAP2 counteracted this effect.

Next, in collaboration with Mark White¹ and Emily Flashman¹ it was asked whether processing of a Cys initiated peptide by PCO1 and PCO4 would enable subsequent modification by ATE1. PCO4, which is in contrast to PCO1 not induced upon hypoxia (Weits et al., 2014), represents the catalytically most potent isoform (White et al., 2018). PCO1 and PCO4 purifications were kindly provided by M. White and E. Flashman. It had previously been established by the collaborators that these recombinant proteins were capable of N-terminal oxidation of a 10-mer RAP2 peptide (CGGAIISDFI), producing Cys-sulfinic acid in an *in-vitro* system.

¹ University of Oxford, Oxford OX1 2JD, United Kingdom

When PCO1 or PCO4 were included in the ATE1 activity assay, Arg incorporation into the Cys-RAP2 peptide was robustly detected at high levels (Fig. 49B). Crucially, as seen before (Fig. 49A), the same peptide was not modified by ATE1 in the absence of PCO. PCO-independent arginylation was again observed upon application of a peptide that contained chemically oxidized Cys ((O₃)C-RAP2). Since the reaction product of PCO, however, is Cys-sulfinic acid, ATE1 appears to be indiscriminative between these two oxidation states of Cys, at least under the conditions tested here.

Together, the findings presented here were consistent with the suggestion that oxidation is a prerequisite for Cys-initiated N-termini to be used as an arginylation substrate by ATE1 in plants. The result constitutes the first *in-vitro* evidence for an enzymatic cascade of N-end rule components acting on an ERFVII group member and proves that PCO action, in the absence of NO, is sufficient for the generation of a secondary destabilizing residue according to the N-end rule.

4. Discussion

The N-end rule pathway of protein degradation is an extremely versatile cellular mechanism for controlling the abundances of specific proteins in prokaryotes and eukaryotes. While the Ac/N-end rule and the type I branch of the Arg N-end rule have been the focus of plant research during the last decade, the type II branch for the degradation of bulky hydrophobic N-termini has been marginally investigated to date. This is also due to the fact that only a single component of this branch, the N-recognin PRT1, has been affiliated with this type of protein degradation in plants. Here I presented a biochemical characterization of the PRT1 protein, as well as new insights into the substrate selectivity of other components of the plant N-end rule. Moreover, phenotypic analysis of derived *prt1-1* mutant lines revealed two physiological abnormalities that were inherited independently of each other and of the *PRT1* locus, indicating second-site modifications in the genome of this mutant line.

4.1 A new temperature-dependent sterility phenotype

4.1.1 Potential origin of the sterility phenotype in *prt1-1^{ts}*

Investigation of the *prt1-1^{ts}* mutant line within the course of this work lead to the discovery of a sterility trait that was conditional for a moderately elevated temperature of 28°C. Using a backcross population, it was affirmed that this phenotype did not depend on the *prt1-1* allele and was likely associated with an unknown, second locus on chromosome three. Importantly, the original seed stock of the *prt1-1* line, listed at NASC as N119, did not exhibit this temperature-dependent phenotype. A timeline describing the origins of N119 and *prt1-1^{ts}* is presented in Fig. 50. Although N119 is in the Col-8 genomic background and was backcrossed to Col-0, it is unlikely that the phenotype is a consequence of the converged genomes of Col-8 and Col-0, since these are considered genetically identical germ plasm stocks according to TAIR (germ plasm number CS60000). Hence, it is conceivable that a spontaneous mutation has occurred during propagation of *prt1-1^{ts}* at a genetic locus that affects plant fertility, which allele has subsequently become homozygous during further propagation, and has remained unnoticed so far due to the conditionality of the phenotypic manifestation.

The rate of spontaneous mutations in *Arabidopsis* is estimated to 7×10^{-9} per site per generation (Ossowski et al., 2010), implicating almost one mutation per genome and generation, provided a genome total of roughly 135 Mbp (TAIR). It is furthermore estimated that 62 percent of all *Arabidopsis* genes are expressed throughout male gametophyte development in the spores (Honys and Twell, 2004), and mutations of these potentially affect pollen development. Numerous additional genes are required for proper development of the sporophytic part of the anther. In light of this, it appears justifiable to assume the existence of a second site mutation affecting gametogenesis in *prt1-1^{ts}*. The observed phenotype, male sterility at mild heat, constitutes a trait that potentially offers agronomic applicability. Provided a genome mutation as the cause of the phenotype, the line *prt1-1^{ts}* may furthermore facilitate the discovery of a genetic locus associated with a new mechanism of temperature adaptation in *Arabidopsis* reproduction. Alternatively, it is possible that the line bears a new temperature-sensitive allele of a gene with general importance for male gametogenesis. Such temperature-sensitive gene variants are rare in plants and have the potential to simplify the

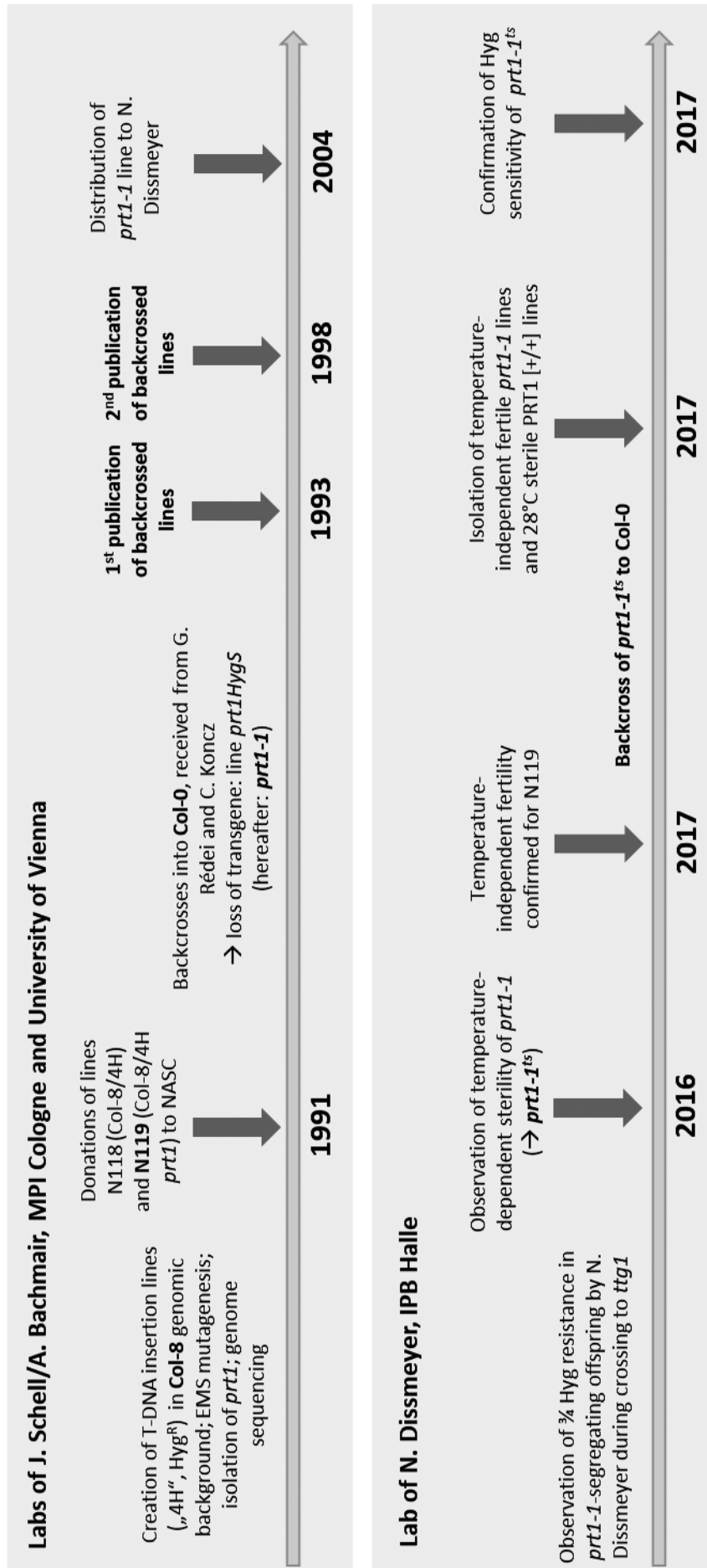


Fig. 50 | Origin of the *prt1-1^{ts}* mutant line. The timeline indicates events during the generation of the line and observations made during the course of this work. The *prt1-1* allele was generated by A. Bachmair, F. Becker, and J. Schell by EMS mutagenesis of a transgenic population carrying the Ub-F-DHFR reporter construct conferring methotrexate resistance to an N-end rule defective mutant. A hygromycin (Hyg) resistance marker was present on the T-DNA for selection of transgenic lines. The genome of the mutant line *prt1* was sequenced to identify the site of the mutation causing methotrexate resistance, and the mutant (N119), together with the WT reference (Col-8/4H; N118), were subsequently donated to NASC. Before publication (Bachmair et al., 1993; Potuschak et al., 1998), the line was backcrossed four times (personal information from A. Bachmair) into the Col-0 background and a Hyg sensitive line *prt1HygS* (hereafter: *prt1-1*) was established. The line *prt1-1* was distributed to N. Dissmeyer who initially observed a segregating phenotype of Hyg resistance during a cross to *ttg1*. In 2016, the temperature-dependent sterility was observed for the first time leading to the designation *prt1-1^{ts}*. N119 was hereafter ordered from NASC and the line was found to lack the sterility phenotype. Another backcross of *prt1-1^{ts}* to Col-0 resulted in the separation of the phenotype and the *prt1-1* genotype. Hyg sensitivity was re-assessed for *prt1-1^{ts}* and was found to be indistinguishable from WT.

investigation of traits that otherwise lead to lethality or sterility. Together, if a backside mutation is causal for the observed phenotype, it would be of great interest to identify the locus associated with the sterility in *prt1-1^{ts}*. A number of potential gene candidates is provided in table S1, and a detailed discussion of the phenotype is given below. Efforts towards genome sequencing of *prt1-1^{ts}* are currently ongoing in the laboratory of A. Bachmair in collaboration with N. Dissmeyer, and may reveal a genetic cause of the phenotype.

Next to spontaneous mutation, a polymorphism could have been introduced during EMS mutagenesis, and could have co-segregated during backcrossing of *prt1-1*. However, since the progenitor line N119 did not show the sterility phenotype, this scenario would require another factor suppressing the phenotype in N119. Although it might be possible that a third mutated locus, or the transgene itself, affects the outcome of the mutation in N119, this would be the least parsimonious explanation.

In contrast, an epigenetic cause of the sterility phenotype could be taken into consideration as an alternative explanation. Environmental factors such as stress situations are known to trigger epigenetic changes that can progress through several generations (Paszkowski and Grossniklaus, 2011; Lämke and Bäurle, 2017; Begcy and Dresselhaus, 2018). In rice, large-scale posttranslational modifications of histone 3 during male gametogenesis are regulated by MEIOSIS ARRESTED AT LEPTOTENE1 (MEL1), an Argonaute protein, and mutants of the *MEL1* gene are sterile with aberrant tapetum and pollen mother cell histology (Nonomura et al., 2007; Liu and Nonomura, 2016). Furthermore, Ma et al. (2018b) showed that high temperature caused a disruption in genome methylation in anthers of the high-temperature sensitive cotton (*Gossypium hirsutum*) cultivar H05, but not in the tolerant line 84021. In the sensitive H05, exposure to one week of high temperature entailed defects in endothecium secondary thickening, and microspore abortion (Min et al., 2014). This defect in male fertility of H05 upon high temperature stress could be attributed to reduced genome methylation by Ma et al. (2018b). Next to differences in methylation patterns, the two cultivars exhibited contrasting changes in the expression of genes involved in the RNA-directed DNA methylation pathway upon high temperature, with lower expression of such genes in the sensitive H05, and upregulation in the tolerant 84021 (Ma et al., 2018b). Sterility of H05 was additionally linked to disordered sugar metabolism in the anthers, and suppression of DNA methylation upon heat stress was shown to impact on starch hydrolysis (Ma et al., 2018b). Taken these results together, the temperature-dependent male sterility of the cotton cultivar H05 described by Ma et al. (2018b) obviously resembles the phenotype observed for *prt1-1^{ts}*. It is conceivable that in *prt1-1^{ts}*, stress conditions during propagation in the greenhouse have incidentally caused epigenetic alterations that resulted in the male sterile phenotype. Such a trait could probably segregate in a ratio approximating Mendelian rules, if stable epigenetic modifications at a distinct locus would be responsible for the phenotype.

However, no phenotype comparable to *prt1-1^{ts}* was raised in any other line propagated under the same conditions in the laboratory. Thus, it is tempting to consider a scenario where inactivation of *PRT1* actually facilitated the emergence of epigenetic alterations at a second locus in the *prt1-1^{ts}* line. A number of circumstances would support an involvement of *PRT1* itself in epigenetic regulation. First, *PRT1* expression was seen in pollen, a site of high epigenetic activity (Calarco et al., 2012; Gutierrez-Marcos and Dickinson, 2012), during promoter-GUS analysis (Fig. 17F), and high *PRT1* transcript abundance in mature pollen grains is recorded by publicly available expression data bases such as the *Arabidopsis* eFP Browser, or FlowerNet (Pearce et al., 2015), and is supported by the

transcriptome analysis performed by Wang et al. (2008b). Notably however, some mRNAs accumulate in mature pollen grains and are stored until translation during pollen germination (Mascarenhas, 1990; Bedinger, 1992); transcript abundance in mature pollen grains might therefore not necessarily reflect a direct function of the protein product in this tissue. Second, implication of N-end rule components in epigenetic regulation is already exemplified by UBR2, one of the N-recognins for type I and type II N-degrons in mammals. UBR2 mono- and poly-ubiquitinates histone 2 and other chromatin-associated proteins, and is engaged in transcriptional gene silencing and the DNA damage response (An et al., 2010b, 2012). Third, next to the RBR E3 ligases and PRT1, only seven more proteins are found in the *Arabidopsis* genome that contain more than one RING domain (Stone et al., 2005), and five of these are implicated in chromatin methylation (Kraft et al., 2008). Fourth, the similarity of the PRT1 protein to the yeast DNA repair enzyme Rad18p raised early speculations on a respective function of PRT1 (Potuschak et al., 1998). A role in DNA repair was later rejected for PRT1 by studies in yeast (Stary et al., 2003), and DNA binding by Rad18p was found to depend on its N-terminal SAP domain rather than the RING domain which shows homology to PRT1 (Notenboom et al., 2007). However, chromatin association of PRT1 was never examined. Finally, FlowerNet analysis indicates that PRT1 expression pattern clusters together and is strongly correlated with the expression of *ATRX* (AT1G08600), a gene involved in histone H3 deposition (Duc et al., 2017). Mutation of *atrx* leads to reduced pollen content of otherwise normal anthers, while combination with a mutation in the H3.3 chaperone gene *HIRA* results in extreme growth retardation and sterility (Duc et al., 2017). To unravel a potential involvement of *PRT1* in epigenetic regulation during pollen development, it would be interesting to see if *PRT1* genetically interacts with *ATRX* or *HIRA* in a double mutant situation. Furthermore, it might be worth testing whether the RNA-directed DNA methylation pathway is misregulated in *prt1-1^{ts}* upon high temperature, as it is the case in the cotton cultivar H05.

4.1.2 The thermosensitivity of *prt1-1^{ts}* reproduction

4.1.2.1 Post-meiotic defects in *prt1-1^{ts}* pollen development

Reproductive organs of plants, and pollen in particular, are most sensitive to high temperature stress, causing crop failure already at conditions of mild heat (Hedhly et al., 2009; Zinn et al., 2010; De Storme and Geelen, 2014; Mesihovic et al., 2016; Rieu et al., 2017). Heat stress is primarily caused by changes in membrane fluidity and protein folding, cytoskeleton stability, and chromatin structure, as well as accelerated metabolic processes (Bitá and Gerats, 2013). In *Arabidopsis*, the number of seeds per silique was shown to gradually decrease with increasing temperature, even within a temperature range generally considered favorable for the growth of *Arabidopsis* (Ibañez et al., 2017). In this work, a heritable trait in a descendant of the *Arabidopsis prt1-1* line was identified which conferred complete sterility at an elevated ambient temperature of 28°C, where WT plants readily produced siliques. Using reciprocal crosses, as well as histological analyses, it was shown that male reproduction was likely affected in the line *prt1-1^{ts}* at a post-meiotic stage (Fig. 9, 10, 12, 13, 14). Microspore development was found to arrest under the elevated temperature after separation from the tetrads, when the majority of the microspores stopped enlargement and eventually collapsed (Fig. 12, 13). Due to pollen abortion, the anthers were indehiscent, but stomium breakage took place (Fig. 13), indicating that the dehydration process essential for anther opening (Pacini et al., 2006) was not affected. This is noteworthy since the processes leading to anther dehiscence are commonly

prevented by heat shock treatment of WT *Arabidopsis* plants in a manner dependent on high air humidity (Kim et al., 2001).

Major defects in pollen development of *prt1-1^{ts}* were observed following separation of the microspores from tetrads, indicating that the cells succeeded to pass through meiosis (Fig. 13, S7). However, the observation that larger and spherical microspores occurred in *prt1-1^{ts}* anthers prior to or concomitant with collapse (Fig. 12, 14) indicated that DNA segregation might be affected in the mutant gametocytes at high temperature. Likewise, a mutation in *SHUGOSHIN1 (SGO1)* which is required for centromere cohesion during meiosis caused reduced fertility with collapse of a portion of the pollen grains, while other pollen grains were larger than normal, correlating with higher DNA contents (Zamariola et al., 2013). Given that *SGO1* resides in a region roughly 36 cM upstream of *PRT1* which would match the observed recombination frequency between the *prt1-1* allele and the sterility phenotype (Fig. S6), this gene constitutes a promising target for sequence analysis in the mutant.

4.1.2.2 A potential defect of the pollen wall in *prt1-1^{ts}*

The phenotype seen in *prt1-1^{ts}* coincided strikingly with the temperature-independent effect described for the *abcg1 abcg16 abcg20* triple mutant (Yadav et al., 2014). Here, normal flower and microspore development was observed up to flower stage 12, at which state the microspores collapsed (Yadav et al., 2014). In *abcg1 abcg16 abcg20*, this was accompanied by the retraction of the cytoplasm from the cell wall visible in transmission electron microscopy. Notably, the *abcg1 abcg16 abcg20* mutant was not completely sterile but showed a severe reduction in pollen produced. Yim et al. (2016) furthermore described defects in pollen mitoses for the *abcg1 abcg16* double knock-out, which possibly occurred also in *prt1-1^{ts}*, given that tricellular pollen was rarely detected in this line grown at 28°C. The similarity of the phenotypes suggests that the pollen wall, particularly the nexine layer, might be affected in *prt1-1^{ts}* as it is the case in *abcg1 abcg16 (abcg20)*. In fact, it would be interesting to test whether one of the single mutants of the ABCG transporters would also confer temperature-dependent defects in male fertility, since this was not assessed to my knowledge. High temperature was reported to induce an increase in pollen wall thickness in quinoa (*Chenopodium quinoa*) (Hinojosa et al., 2018), indicating that adaptations of the pollen wall composition could particularly contribute to thermotolerance of the gametes.

The transcript level of *ABCG1* was furthermore found to be upregulated in *prt1-1^{ts}* anthers compared to the WT (Fig. 16), confirming that processes of pollen wall biogenesis might be disturbed in *prt1-1^{ts}*. Due to its location on chromosome three and the phenotypic similarities between *prt1-1^{ts}* and *abgc* mutants, the *ABCG16* locus of the *prt1-1^{ts}* line was sequenced within this work and found to be the WT sequence. Notably, the *ABCG16* and *ABCG20* genes reside close to each other on chromosome three (Fig. S6). *ABCG20* is suggested to have its major function at the root endodermis (Yadav et al., 2014); however, its mutation clearly adds to the sterility phenotype in the *abcg1 abcg16 abcg20* triple mutant (Yim et al., 2016). Thus, a mutation of *ABCG20* in *prt1-1^{ts}* could also potentially be causal of the temperature-dependent sterility phenotype. Loss of function of this gene might in turn activate the expression of *ABCG1* via a feedback mechanism, which would explain the increased transcript level measured in *prt1-1^{ts}* anthers. Transcript analyses of *ABCG16* and *ABCG20* in the mutant anthers, as well as sequencing the *ABCG20* locus, would serve to address these possibilities.

In line with a generally high temperature sensitivity of pollen wall biogenesis via the vulnerability of the tapetum cells (Parish et al., 2012), it was recently described that loss of function of *THERMOSENSITIVE GENIC MALE STERILE 10* (*TMS10*) led to temperature-dependent male sterility at 28°C in two different cultivars of rice, whereas simultaneous knock-out of the close homolog *TMS10-LIKE* (*TMS10L*) caused constitutive sterility under both 22°C und 28°C (Yu et al., 2017). *TMS10* and *TMS10L* encode Leu-rich repeat receptor-like kinases of unknown function. Yu et al. (2017) showed that they are required for timely tapetum degeneration at elevated temperature, and sterility of the *tms10* mutant is caused by a lack of primexine and reduced sporopollenin deposition on the microspore surface. As seen with *abcg1 abcg16 abcg20* and *prt1-1^{ts}*, pollen grains of *tms10* collapse before anthesis (Yu et al., 2017).

In accordance with a potential aberration of pollen wall development in *prt1-1^{ts}*, mutant pollen walls were stronger stainable with safranin O than WT microspores short before microspore degeneration was observed in *prt1-1^{ts}* (Fig. 13, 14). This observation hints at an increased abundance of phenolic polymers on *prt1-1^{ts}* microspore surfaces, potentially reflecting lignification. Hypothetically, it could also be possible that a lack of other structures, such as the lipidic tryphine (Piffanelli et al., 1997; Mariani and Wolters-Arts, 2000), would make polyphenolic compounds, including sporopollenin, more accessible to staining in the mutant. Mutants unable to synthesize the long chain fatty acid derivatives required for the production of tryphine waxes exhibit male sterility due to defects in rehydration upon pollen-stigma interaction (Preuss et al., 1993; Aarts et al., 1995; Hülkamp et al., 1995; Jenks et al., 1995; Wolters-Arts et al., 1998; Fiebig et al., 2000; Chen et al., 2003; Jessen et al., 2011; Zhan et al., 2018). Such mutant pollen is viable, but succeeds to germinate only on the condition of high ambient air humidity. However, since *prt1-1^{ts}* pollen maturation at elevated temperature was affected already at earlier stages, and pollen germination efficiency of *prt1-1^{ts}* plant grown at normal temperature was not decreased (Fig. 11), it is rather unlikely that tryphine production is specifically affected in this line.

In *abcg1 abcg16*, as well as in *tms10*, several layers of the pollen wall, including intine and nexine (*abcg1 abcg16*), or primexine and (consequently) overall exine (*tms10*), are aberrant due to defects in tapetal development (Yadav et al., 2014; Yim et al., 2016; Yu et al., 2017). For further analysis of *prt1-1^{ts}*, it would be required to test if the pollen wall of *prt1-1^{ts}* is indeed similarly defective, and if so, if this applies to several, or to a distinct structure of the pollen wall. Since no alterations in tapetum development were observed by histological analysis in *prt1-1^{ts}* (Fig. 13), it would be anticipated that potential defects might be more specific than in the previously reported mutants.

The *Arabidopsis* *RPG1/SWEET8* gene encodes a sugar transporter located in the tapetum and microspores and is required for primexine deposition (Guan et al., 2008; Sun et al., 2013). The single mutant *rpg1*, and to a stronger extend the double mutant *rpg1 rpg2*, show severely reduced male fertility at control temperature, and microspore development phenocopies *prt1-1^{ts}* grown at 28°C. The phenotypic similarities between *prt1-1^{ts}* and *rpg1 rpg2* also include the observation that the few individual microspores which manage to escape from collapse appear abnormally enlarged at the mature stage (Fig. 13, 14; Guan et al., 2008). Interestingly, *SWEET8* transcript was found to be reduced by 50 percent at 28°C in *prt1-1^{ts}* anthers in comparison to the WT (Fig. 16). A downregulation of sugar transport activity and potentially related processes at 28°C might thus at least partially explain the sterility of *prt1-1^{ts}*. It was previously reported that alterations of the carbohydrate metabolism occur during high temperature stress in plant reproductive tissues. For example, sugar metabolism was shown to be downregulated on the transcript level of vacuolar

invertase by continuous mild heat in microspores of tomato (Sato et al., 2006). Furthermore, moderate temperature elevation leads to a decrease in the starch content of developing tomato pollen, and reduced pollen viability (Pressman et al., 2002). Interestingly, this was accompanied by an increase in soluble sugars of the locular fluid (Pressman et al., 2002). A downregulation of genes encoding microspore-located sugar transporters such as *SWEET8* in *Arabidopsis* might potentially explain this discrepancy.

High temperature rapidly induces the accumulation of unfolded proteins and causes ER stress (Niu and Xiang, 2018). Coherently, signaling components of the unfolded protein response (UPR) mediate part of the temperature sensing in plants (Che et al., 2010; Deng et al., 2011; Niu and Xiang, 2018). Given the high secretory activity of tapetum cells, ER stress particularly compromises tapetal performance. In line with this, simultaneous mutations in *INOSITOL-REQUIRING ENZYME 1a* (*IRE1a*) and *IRE1b*, which disrupt RNA splicing within the signaling of the UPR, lead to temperature-dependent male sterility in *Arabidopsis* (Deng et al., 2011, 2016; Nagashima et al., 2011). While developing normally at control temperature, the *ire1a ire1b* mutant fails to produce seeds at an elevated temperature of 27.5°C (Deng et al., 2016). Defects under the restrictive temperature include the production of a more highly vacuolated tapetum which degenerates incompletely, followed by aberrant deposition of the pollen coat. Consequently, the majority of pollen grains adhere to each other and to the anther wall, while some of the microspores collapse before maturation (Deng et al., 2016). The importance of the UPR for plant fertility was furthermore supported by transcriptome analyses showing that UPR-associated genes are enriched among reproductive tissue-specific genes upregulated by heat stress (Zhang et al., 2017b). Thus, the UPR constitutes another link between above optimal temperatures and pollen wall integrity, and aspects of the UPR might also be affected in *prt1-1^{ts}*, although the phenotype varies from *ire1a ire1b* by the absence of tapetum abnormalities and microspore aggregation.

Notably, temperature signaling via the UPR (Che et al., 2010), as well as via PIF4 and auxin (Ibañez et al., 2017, 2018) were also dependent on brassinosteroid signaling, and mutations in brassinosteroid synthesis and signaling can lead to male sterility (see introduction). However, male sterility of such mutants is caused by reduced filament length (Choe et al., 1998; Kim et al., 2005; Xing et al., 2013), failure of pollen tube elongation (Szekeres et al., 1996), or transient defects in exine formation (Ariizumi et al., 2008), but not by pollen abortion. Moreover, growth retardation is usually associated with the inhibition of brassinosteroid pathways. This obviously differs from the phenotype observed in *prt1-1^{ts}*, and brassinosteroid signaling is therefore less likely to be the primary cause of the temperature-dependent sterility of this line.

In general, it would be exciting to clarify whether adjustments of the pollen wall specifically contribute to thermoprotection of pollen grains. Such adaptations of male gametogenesis towards abiotic stress conditions have been described for changes in ambient humidity (Firon et al., 2012). Several cellular adaptations of post-meiotic anthers characteristic to heat stress, such as the induction of heat shock proteins and reactive oxygen species scavenging mechanisms, were also described which are usually effective to maintain tapetum function (Parish et al., 2012; Rieu et al., 2017). Identification of the genetic basis of *prt1-1^{ts}* temperature-dependent sterility lacking obvious aberrations of tapetum development could lead to additional mechanisms enabling anthers to cope with modest heat stress.

4.1.2.3 Hormonal alterations in stamen of *prt1-1^{ts}* at 28°C

Transcript analysis performed with *prt1-1^{ts}* anthers at 28°C revealed several genes associated with hormone biosynthesis or signaling to be differentially expressed as compared to the WT (Fig. 16). Such hormonal alterations could to some extent explain the developmental differences observed for mutant and WT microspores at high temperature. On the other hand, hormone pathways could be secondarily affected on the transcript level by a perturbation of pollen development caused by metabolic changes. Since anther developmental programs are tightly coordinated with the differentiation of the gametes (Sanders et al., 1999; Cecchetti et al., 2004; Ma, 2005), stalling of pollen grain maturation might well impact on the transcript levels of hormone-related genes.

Upon transcript analysis of the auxin biosynthetic genes *YUC2* and *YUC6*, a clear downregulation of *YUC6*, but not *YUC2* was observed in high-temperature exposed anthers of *prt1-1^{ts}* compared to WT gene expression (Fig. 16). While *yuc2 yuc6* double mutants are male sterile, knock down of *YUC6* alone is not expected to trigger developmental phenotypes (Cheng et al., 2006), although the performance of single mutants at elevated temperatures has, to my knowledge, not been tested. Furthermore, *yuc2 yuc6* sterility is primarily caused by premature endothecium lignification and tapetum degeneration (Cheng et al., 2006; Cecchetti et al., 2008), following defects in microspore development as early as pollen mitosis I (Yao et al., 2018). Characteristically, filament elongation is also strongly reduced in *yuc2 yuc6* mutants (Cheng et al., 2006). Similarly, heat-stress induced decrease of endogenous auxin levels impairs plant fertility due to shortening of the filament and microspore abortion beginning at the time of microspore release from the tetrads (Sakata et al., 2010). These effects of auxin inhibition differ from the phenotype observed in *prt1-1^{ts}* upon mild heat, since no acceleration of the dehiscence program (i.e., tapetum degeneration and endothecium lignification) was obvious in *prt1-1^{ts}* (Fig. 13), and filament elongation was not further reduced as compared to the WT (Fig. 9). Next, microspore abortion initiated slightly later in *prt1-1^{ts}* at 28°C than in the cases of auxin deficient mutants at control temperature, probably at the time or even after mitosis II (Fig. 13, S7). Hence, it is rather unlikely that downregulation of auxin biosynthesis at the level of *YUC6* transcript caused male sterility in the *prt1-1^{ts}* mutant. Pertinently, exogenous application of auxin to *prt1-1^{ts}* flowers did not rescue fertility (data not shown), in contrast to what was reported for heat-stress induced sterility of WT flowers (Sakata et al., 2010). However notably, exogenous auxin application was equally not sufficient to rescue fertility of *yuc1 yuc2 yuc6* mutants (Cheng et al., 2006), leaving the possibility that temporally regulated auxin biosynthesis might be essential for a rescue effect in *prt1-1^{ts}* as it was suggested for *yuc1 yuc2 yuc6* (Cheng et al., 2006). Moreover supporting that auxin signaling might at least partly explain the *prt1-1^{ts}* phenotype, auxin signaling via *ARF17* was also shown to be essential for primexine and exine formation, and loss of function of *ARF17* leads to similar phenotypes as in *prt1-1^{ts}*, accompanied by only slightly reduced filament length (Yang et al., 2013). Thus, it cannot be ruled out that disturbed auxin signaling causes sterility of *prt1-1^{ts}* at 28°C.

Concerning the downregulation of *YUC6*, this phenomenon however could be linked with the observed moderately increased transcript levels of JA biosynthetic genes, since it was reported that the auxin perception mutants *afb1-3* and *tir1 afb2 afb3* also showed upregulated expression of *DAD1* and *OPR3* in flower buds (Cecchetti et al., 2013). However, at later anther stages, which were targeted during sample preparation for *prt1-1^{ts}* transcript analysis, auxin appears to rather positively regulate JA biosynthetic gene expression (Song et al., 2013; see introduction, chapter 1.3.1.3). Notably moreover, in *prt1-1^{ts}*, increased gene expression particularly of *DAD1* did not reflect in

significantly stronger expression of *MYB21* and *MYB24* in *prt1-1^{ts}* anthers, as would be expected from enhanced JA biosynthesis (Mandaokar et al., 2006). However, adequate MYB-gene expression is crucial for faithful stamen development (Huang et al., 2017a), and likely underlies strict regulation. Thus, whether auxin or JA levels are altered in *prt1-1^{ts}* anthers at 28°C, remains to be determined experimentally.

Strikingly, of all JA mutant phenotypes described (see introduction, chapter 1.3.1.1), the *dad1* mutant most closely resembles the *prt1-1^{ts}* phenotype at 28°C, including normally elongated filaments, and normal microspore development up to flower opening, but failure to produce viable pollen grains (Ishiguro et al., 2001). Coincidentally, within this work *DAD1* was also the gene that (although highly variable between reproductions of the experiment) showed the strongest upregulation in expression in *prt1-1^{ts}* anthers as compared to the WT, while the two other tested JA biosynthetic genes, *OPR3* and *LOX3*, were less affected (Fig. 16). *DAD1* expression in stamens is believed to be highest in the filament, which is considered the actual site of JA production in the stamen (Sanders et al., 2000; Ishiguro et al., 2001), and only a faint expression can be detected in the anther (Jewell and Browse, 2016). Since anthers are not devoid of, but contain rather few plastids (Clément, 2001), JA synthesis in the filament might also be the logical consequence of precursor availability. The fact that JA synthesis in the anther is of minor importance however raises the question why *DAD1* might be differentially regulated in anthers of *prt1-1^{ts}* at all. Interestingly, linolenic acid, the product of *DAD1* enzymatic activity, was found to be critical specifically for pollen development (McConn and Browse, 1996). Routaboul et al. (2012) furthermore showed that the knock-out of *fad3 fad7 fad8*, disrupting biosynthesis of the galactolipid precursor for linolenic acid (McConn and Browse, 1996), resulted in decreased tolerance towards long-term, but not short-term, high temperature stress. The temperature-sensitivity of the JA-deficient triple mutant was not rescued by the exogenous delivery of JA, indicating that it might be the trienoic fatty acid, not the hormone product, which confers thermotolerance. This finding was also surprising since a general function of JA signaling in basal thermotolerance of *Arabidopsis* was described before (Clarke et al., 2009). It is compelling to speculate that potentially increased *DAD1* activity in the *prt1-1^{ts}* mutant anthers might serve to provide linolenic acid in order to compensate for a defective process in lipid metabolism, and thus to protect cellular membranes in the anther, or the pollen coat from ongoing thermal damage. Notably, a decrease in lipid unsaturation upon heat stress was previously associated with thermosensitivity of *Sorghum* pollen (Djanaguiraman et al., 2018). Furthermore, linolenic-acid containing phospholipids make up more than 90 percent of the total extraplastidial phospholipids in wheat pollen, but decreased to 80 percent upon high temperature stress (Narayanan et al., 2018). This differed from the situation in leaves, where linolenic acid-containing phospholipids were less prominent. However, there is no indication that *DAD1* transcript upregulation might be part of the response to long-term heat stress in the *Arabidopsis* WT, although *FAD3* and *FAD8* transcript levels were doubled in transcriptomic data from a recent study investigating the response of *Arabidopsis* pollen to one week of alternating temperature stress (Rahmati Ishka et al., 2018). Comparison of *DAD1* and *FAD* transcription in WT anthers at normal temperature and long-term heat, together with lipid analyses of anthers, would help to address a potential function of linolenic acid in pollen adaptation to high-temperature induced stress.

Although several lines of evidence suggest the involvement of ethylene in the high temperature response of plants (Larkindale, 2002; Frank et al., 2009; Jegadeesan et al., 2018; Jin et al., 2018), ethylene levels were likely unaffected in *prt1-1^{ts}* anthers at 28°C, as judged from the unchanged expression of the ethylene-inducible (Hua et al., 1998; Ellison et al., 2011) *ETR2* gene. In contrast,

expression of the type A ARRs *ARR4*, *ARR5*, and *ARR6* indicated a perturbation of cytokinin signaling in this mutant (Fig. 16). Concerning cytokinin signaling, it should be taken into account that a hyposensitivity towards cytokinin in the triple response assay was later detected for *prt1-1^{ts}*, which was independent genetically from the 28°C sterility (see chapter 3.4.5). Hence, it is difficult to decipher whether the alterations in cytokinin gene expression seen in the anther of *prt1-1^{ts}* were associated with the sterility phenotype, or rather driven by an independent genetic locus. It would be crucial to compare anther gene expression of *prt1-1^{ts}* at normal and high temperature, in order to address a potential involvement of cytokinin signaling in the sterility phenotype. The observed repression of *EIN3*, which is known to be induced by cytokinin (Brenner et al., 2005), but unaffected transcriptionally by ethylene treatment (Chao et al., 1997), in *prt1-1^{ts}* anthers would coincide with reduced cytokinin signaling in the *prt1-1^{ts}* mutant. *EIN3* repression in turn might be responsible for the observed upregulation of some ARRs, such as *ARR5* (Shi et al., 2012). Of note, differential regulation of type A ARRs in response to heat shock in *Arabidopsis* pollen was also observed within an RNA-Seq experiment performed by Rahmati Ishka et al. (2018). Here, a slight but significant downregulation of *ARR4* and *ARR7*, and a 2.5-fold upregulation of *ARR9* were detectable in heat-shocked WT pollen compared to control temperature. It is therefore conceivable that differential expression of ARRs in *prt1-1^{ts}* represents an exaggeration of the heat shock response that occurs in the WT at higher temperatures.

Interestingly, mutation of *PUB4*, encoding an E3 ligase that acts redundantly with *PUB2* (Wang et al., 2017), results in pronounced cytokinin hyposensitivity of light-grown as well as etiolated seedlings, and entails temperature-dependent male sterility (Wang et al., 2013a, 2017). Both phenotypes, cytokinin hyposensitivity and reduced male fertility, are shared by a mutant defective in the genes *EXTRA-LARGE G PROTEIN 1 (XLG1)*, *XLG2*, and *XLG3*, and all three XLGs were shown to interact with *PUB2* and *PUB4* (Wang et al., 2017). Although the combination of the phenotypes coincidentally resembles the situation found in *prt1-1^{ts}*, there are some major differences concerning the manifestation of male sterility. *Pub4* is infertile at a control temperature of 22°C, but silique formation is partially restored upon growth at 16°C (Wang et al., 2013a). In contrast to *prt1-1^{ts}*, *pub4* and *pub2 pub4* mutants exhibit hypertrophy and delayed senescence of the tapetum at the restrictive temperature, and fail to dehisce due to adherence of the pollen grains to the locules (Wang et al., 2013a, 2017), thus mimicking in part the UPR deficient phenotypes (see above). The pollen produced by *pub4/pub2 pub4* is furthermore misshaped, but viable, and hand-pollination produces normal seeds. Finally, *pub2 pub4* exhibited pronounced resistance towards exogenous cytokinin application already under light-grown conditions (Wang et al., 2017), which was not observed for *prt1-1^{ts}* (Fig. 37). These differences to the phenotypes of *prt1-1^{ts}*, and the fact that sterility and hormone insensitivity of *prt1-1^{ts}* were separable genetically, indicate that different pathways are likely affected in *prt1-1^{ts}* and the *pub* mutants.

The data presented here suggests that a so far unknown mechanism potentially affecting pollen wall development might underlie the defect in male gametogenesis of *prt1-1^{ts}*. In the future, this could provide new insights into the stress response of plant reproduction, or lead to the identification of new genetic targets for the development of hybrid crops.

4.2 PRT1 acts as an E3 ligase *in-vitro* using both RING domains

The *PRT1* gene was previously shown to reconstitute poly-ubiquitination of a test substrate in N-end rule deficient *ubr1Δ* yeast cells (Stary et al., 2003), providing indication that the enzyme is capable of acting as an E3 ligase in cells. Using *in-vitro* autoubiquitination assays with recombinant purified proteins, it was shown within this work that PRT1 is indeed not only required, but sufficient for catalyzing Ub transfer in the presence of E1, E2, and ATP (Fig. 20). Since biochemical studies on PRT6 are still missing to date, this is also the first demonstration of *in-vitro* Ub ligase activity of a plant N-recognin.

In the autoubiquitination assays performed here, UBC8 was engaged as the E2 enzyme. UBC8 constitutes a close homolog to the mammalian Ube2D family (Girod et al., 1993; Scheffner et al., 1994; Stewart et al., 2016) whose members are promiscuously active with diverse E3 enzymes and indiscriminate for Ub linkage sites (Brzovic et al., 2006; Zhang et al., 2011a; Stewart et al., 2016). Promiscuity towards RING and U-box containing E3s was also observed for UBC8 (Stone et al., 2005; Turek et al., 2018), and it is very likely that there are different E2 enzymes acting on PRT1 *in vivo*, potentially even in a context-dependent manner. Notably, high protein concentrations in ubiquitination assays can facilitate unspecific interactions, and E2-E3 pairing *in vitro* must hence be carefully interpreted (Turek et al., 2018). Nevertheless, it is noteworthy that the human MEKK1-related protein X (MEX), an E3 ligase with testis-specific expression, is similar to PRT1 in that it contains two RING domains and a ZZ domain (Nishito et al., 2006). Interestingly, MEX was autoubiquitinated specifically through members of the Ube2D family (UbcH5a and UbcH5c), but not by other tested E2s, *in vitro* (Nishito et al., 2006). Although MEX exhibits further domains at the N- and C-termini, a truncated fragment comprising only the two RING and the central ZZ domain was sufficient for the interaction with UbcH5a during co-immunoprecipitation from co-transfected cells (Nishito et al., 2006). Thus, the domain structure of PRT1 potentially allows for the interaction with UBC8 also *in vivo*.

However, in order to reveal a cellular function of PRT1, it would be interesting to know which E2 enzymes specifically cooperate with this E3 *in vivo*, and where this interaction takes place. The Ub-linkage specificity conferred by PRT1-E2 interactions *in vivo* would provide initial information on this question. The fact that recombinantly expressed test substrates were destabilized by the presence of an intact PRT1 gene *in planta* (Potuschak et al., 1998; Stary et al., 2003; Garzón et al., 2007) indicates that PRT1 ubiquitinates its substrates to target them for degradation. Whether degradation occurs via the UPS, implying mostly K48-linked poly-Ub chains (Thrower, 2000), or rather the endocytic pathway via K63 chains or multi-mono-ubiquitination (Haglund et al., 2003; Lauwers et al., 2010; MacGurn et al., 2012), is still an open question. Proteasome inhibitor treatment was shown here to increase the abundance of a constitutively expressed PRT1 substrate in *Arabidopsis* protoplasts, to an extent that approached the effect of *PRT1* mutation, or replacement of the N-terminal hydrophobic residue of the substrate (Fig. 29). This hints towards a role of PRT1 within the UPS, implying K48-linked Ub-ligation. However, use of proteasome inhibitors can also indirectly affect other Ub-dependent processes such as autophagy, due to rapid depletion of cellular Ub pools (Mimnaugh et al., 1997; Hanna et al., 2003). The determination of the Ub-linkage specificity conferred by PRT1, for example by the use of linkage type-specific anti-Ub antibodies on artificial PRT1 substrates that have been purified from cell extracts after proteasome inhibition, would help to decipher the specific purpose of PRT1-mediated ubiquitination.

Crucially, it could be shown using point mutated variants that *in-vitro* autoubiquitination activity of PRT1 depends on both RING domains (Fig. 20B), whilst overall structural integrity of the mutant proteins was confirmed by peptide binding assays (Fig. 25). The requirement of two RING domains for autoubiquitination of an E3 ligase was, to my knowledge, observed for the first time outside of the RBR class of proteins. Since PRT1 lacks a domain homologous to the RING2 domain of RBR ligases (Eisenhaber et al., 2007; Riley et al., 2013; Fig. S13), it is unlikely that PRT1 acts via an RBR-like mechanism. However, to exclude the formation of a thioester linkage between PRT1 and Ub during the autoubiquitination reaction, the initial stages of the reaction, when thioester products of RBR activity would still outweigh isopeptide linkages, would have to be assayed in the presence or absence of reducing agents (Wenzel et al., 2011). Additionally, the activities of E3 ligases other than RBR or HECT are specifically abolished when a catalytic residue of the E2 required for E2~Ub Lys reactivity (N77 in UBCH5C) is mutated (Wenzel et al., 2011). Hence, to exclude a similar mechanism for PRT1, it would be of interest to assay its activity with a UBC8 variant mutated in the homologous residue (i.e., N77 also in UBC8).

Of the few E3 ligases comprising more than one RING domain outside of RBRs in *Arabidopsis*, mutational studies have been performed with ORTH1 (Kraft et al., 2008). Here, point mutants as well as truncations of either of the RING domains retained most *in-vitro* autoubiquitination activity (Kraft et al., 2008). Similarly, replacement of metal chelating Cys residues of either RING domain by Ser in MEX only slightly compromised autoubiquitination activity of the human protein (Nishito et al., 2006). Thus, PRT1 autoubiquitination in concert with UBC8 might represent a new mechanism of Ub ligation performed by a RING enzyme.

The observation that PRT1 is able to ubiquitinate itself furthermore suggests a mechanism for self-regulation, since autoubiquitination activity of E3 enzymes can lead to proteasomal degradation (Galan and Peter, 1999; Nishito et al., 2006; Printsev et al., 2014; Furlan et al., 2017). Interestingly, a PRT1 fusion construct expressed in *Arabidopsis* protoplasts migrated as double to triple bands accompanied by a faint smear of higher molecular weight species in SDS-PAGE which would coincide with mono- and higher order ubiquitination *in vivo* (Fig. 30). While the potentially mono- and di-ubiquitinated variants were observed independently of RING mutations, a band corresponding to tri-ubiquitinated 3HA-PRT1 was lost upon mutation of the second RING domain (Fig. 30), and a faint smear of higher molecular weights was furthermore seen especially upon expression of the WT sequence of *PRT1* (Fig. 30, 31B). Consistent with a minor role of mono- and di-ubiquitination in protein degradation (see introduction), only the presence of the higher molecular weight species coincided with decreased PRT1 protein levels *in vivo* (Fig. 30). Thus, auto-poly-ubiquitination by PRT1 might depend on functional RING domains also *in vivo*. In contrast, mono- and di-ubiquitination of PRT1 are obviously achieved *in vivo* when either of the two RING domains is mutated (Fig. 30). Hence, these modifications might be the result of the interaction with another E2 enzyme than UBC8 which does not depend on the integrity of both domains, or PRT1 could be target to mono- and di-ubiquitination by other Ub ligases *in vivo*. Surprisingly, formation of the tri-ubiquitinated version *in vivo* was only abolished upon mutation of the second RING domain (Fig. 30), which constitutes the more degenerated RING domain, and is unlikely to mediate E2 interaction as judged from the sequence information (e.g., the presence of Ala-194 in RING2 instead of a larger hydrophobic residue, Fig. 21), and based on the fact that residual autoubiquitination was observed in the respective mutant *in vitro* (Fig. 20B, S12). Thus, RING2 might offer a different platform for regulation of PRT1. This could be dimerization or binding of further interaction partners. Interestingly, protein sequence analysis on InterPro (<https://www.ebi.ac.uk/interpro/>) identified RING2 of PRT1 as a LisH-

dimerization motif-Zn finger, supporting the hypothesis that PRT1 might be capable of dimerization. Of note, whether the higher migration pattern in SDS-PAGE of PRT1 expressed in protoplasts actually corresponded to ubiquitinated variants, a different modification, or to unusual SDS-loading properties of the fusion proteins, cannot be unequivocally concluded from the results obtained within this work and would have to be determined analytically, i.e. by mass spectrometry. However, regulation of an E3 ligase by mono-ubiquitination would not be unusual and should be considered as a possibility for PRT1.

When comparing the sequences of the PRT1 RING domains to the RING domains of the well-studied human BRCA1 and c-CBL, some differences were seen. The amino acids spacing metal ligand 2 and 3 in both RING domains of PRT1 were depleted of acidic residues (Fig. 21). This feature is shared by the RING domains of the human and yeast Rad18 proteins and make up part of the sequence homology observed between PRT1 and Rad18p (Barlow et al., 1994; Potuschak et al., 1998; Stary et al., 2003). As in BRCA1 and c-CBL, the conserved hydrophobic residue preceding metal ligand 2 of human Rad18 (Ile-27) was shown to be important for the interaction of Rad18 with the E2 (Huang et al., 2011). Interestingly, the replacement of this residue of Rad18 by Ala reduced *in-vitro* ubiquitination activity, but did not abolish it (Huang et al., 2011), very similar to what was seen for V28A replacement in PRT1 (Fig. 20B), and differing from the situation with BRCA1 and c-CBL (Zheng et al., 2000; Brzovic et al., 2003; Stone et al., 2005). Thus, Rad18 and PRT1 might actually share mechanistic properties for E2 interaction, indicating that the observed sequence similarity might be of some functional importance after all.

Importantly, Rad18 was also found to appear as a double band in Western blots from human cells, corresponding to non- and mono-ubiquitinated species, whereas higher order species were detected during *in-vitro* autoubiquitination assays (Miyase et al., 2004). Moreover, poly-ubiquitination of Rad18 in cells was observed upon proteasome inhibition, indicating differential regulation of Rad18 by ubiquitination (Miyase et al., 2004). In fact, immunodetection of high-molecular weight species of PRT1 was exclusively observed upon overexpression (Fig. 30, 31B, 34), which could mimic a situation of proteasome inhibition, in terms of E3 protein overabundance. In contrast, expression under the control of a very weak promoter resulted in a single band potentially corresponding to a mono-ubiquitinated version (Fig. 35B). In the case of Rad18, it was suggested and evidence was provided that dimer formation at high nuclear concentrations of Rad18 allows for mono-ubiquitination, which in turn causes Rad18 re-localization from the nucleus to the cytoplasm (Miyase et al., 2004). PRT1 likely localized to the cytoplasm and nucleus in the overexpression situation (Fig. 31A). This was independent of the integrity of the first RING domain, as was the formation of potential mono- and di-ubiquitinated forms (Fig. 30). It would be worth testing whether the single band occurrence seen with PRT1 under low promoter expression exhibits differential localization as compared to the strong promoter, and whether isolations of different cellular fractions would yield distinct species of PRT1.

Notably, self-association was also reported for MEX, in a manner dependent on the protein fragment containing RING- and ZZ domains (Nishito et al., 2006). Given the similar domain organization of PRT1 and MEX, this might indicate the conceptual ability of PRT1 to form dimers or oligomers. In order to test PRT1 for its ability to self-associate, reciprocal pull-downs of differently tagged *E. coli*-expressed PRT1 variants (N-terminal^{His}MBP or GST) were attempted during this work. However, the experiment was obstructed by the severe tendency of all PRT1 variants to aggregate, hampering to distinguish specific protein-protein interactions (data not shown). Creation of RING double mutants of PRT1, and

of variants mutated in the ZZ domain, as well as reciprocal pull-downs from plant cells under lower expression conditions, might reveal further regulatory mechanisms acting on PRT1 *in vivo*.

In summary, the results obtained here show that PRT1 acts as an E3 ligase that might be subject to posttranslational regulation. This implies that timely PRT1 action might be required under specific conditions in the plant, and hyperactivity is prevented by cellular mechanisms.

4.3 The *in-vitro* substrate specificity of plant N-recognins

The substrate binding properties of the two cognate plant N-recognins, with focus on PRT1, were investigated using recombinantly expressed fusion proteins on peptide arrays. These experiments demonstrate for the first time a direct physical association of plant N-recognins with substrate peptides. Previous work has proven the applicability of peptide arrays in the context of mammalian, yeast, and bacterial N-end rule related substrate recognition using peptides of up to 13 amino acids in length (Choi et al., 2010; Hwang et al., 2010a; Kim et al., 2014; Wadas et al., 2016; Colombo et al., 2018; Wang et al., 2018a). Hence, with 17-mer peptides immobilized on a cellulose membrane support, this work employs the longest peptide sequences that were used so far for N-degron peptide binding assays. Notably, the overall hydrophilicity of a peptide sequence was not predictive for N-recognin binding in the assays presented here, since some among the sequences that bound well to PRT1 (e.g., peptides “K2” and the BB neo-N-terminus) exhibited an overall hydrophobic character, independently of the N-terminal aromatic amino acid. Thus, it is not to be assumed that solvent exposure and protrusion from the membrane of these longer sequences were limiting protein interactions simply in terms of accessibility. Strong interactions of the peptides with the membrane support would be furthermore unexpected since the membranes used for array synthesis were functionalized with polyethylene glycol (PEG) as a linker scaffold for peptide coupling, strongly promoting peptide flexibility and hydration during the assay. Hence, given the large number of peptide sequences that can be tested in parallel with each SPOT peptide array, it can be assumed that N-terminus selection of PRT1 and the UBR box of PRT6 can be suitably monitored by the SPOT assay experiments.

4.3.1 Determinants of N-degron recognition by PRT1

PRT1 substrate selection depends on the exposure of bulky hydrophobic N-degrons, as was shown by the isolation of the *prt1-1* null allele using a type II-N-degron bearing reporter construct, and by subsequent analyses (Bachmair et al., 1993; Potuschak et al., 1998; Stary et al., 2003; Garzón et al., 2007). However, sequence properties determining recognition by PRT1 beyond the very N-terminal amino acid and the general requirements of N-degrons remained unknown. Here, using peptide binding assays, the high specificity of PRT1 for bulky hydrophobic N-terminal residues was confirmed *in vitro*. Neither of the two RING domains was required for this binding behavior (Fig. 25), and it remains to be determined whether the ZZ domain is required, or even sufficient for the interaction, or whether the two RING domains are able to complement each other for substrate binding.

Peptide binding assays furthermore revealed a pronounced influence of the more downstream amino acids on PRT1 binding, consistent with what was seen for other N-end rule components (Erbse

et al., 2006; Xia et al., 2008; Choi et al., 2010; Matta-Camacho et al., 2010; Wadas et al., 2016). When sequentially replacing the amino acids of the nsP4 sequence that interacted with PRT1 in the WT version, it was found that the first six amino acids were most important for PRT1 binding (Fig. 24A). Next to the bulky hydrophobic N-terminal residue, these included amino acids with polar side chains (Ser-4, Thr-5) which might be required for the mobility of the peptide, in accordance with what was acknowledged before as a requirement for a functional N-degron (Bachmair and Varshavsky, 1989). In line with this, the sequences of EIN2 and BB which showed very good PRT1 binding, were likewise rich in Gly and Ser residues, consistent with the assumption that the combination of these residues will increase flexibility of a peptide linker sequence (Van Rosmalen et al., 2017).

Interestingly, another hydrophobic residue (Phe-3) was furthermore found within the first six amino acids of nsP4 that proved to be important for PRT1 binding, and especially the well-binding BB sequence was also rich in aromatic residues. This indicates that the substrate binding pocket of PRT1 might be relatively hydrophobic and large. In the case of *E. coli* ClpS, it was proposed that a deep hydrophobic pocket mediates selection of bacterial N-degrons (starting Phe, Leu, Trp, or Tyr), potentially involving an induced-fit mechanism (Wang et al., 2008a; Schuenemann et al., 2009; Kwon et al., 2018). A similar mechanism might also apply to PRT1 substrate binding. Alternatively, the PRT1 binding pocket itself could be rather small, and hydrophobic residues might be required to properly position the substrate N-terminus on the PRT1 surface. Of interest in this context, when comparing the ZZ domains of p62 and PRT1, Kwon et al. (2018) noted the presence of additional hydrophobic residues in the PRT1 ZZ domain when compared to the binding pocket of p62. Investigation of the PRT1 crystal structure in complex with a substrate peptide would help to test whether such hydrophobic residues of PRT1 are specifically involved in positioning PRT1-substrates in the binding pocket.

Notably, throughout the peptide sequences tested for PRT1 interaction, the three best binding sequences, K2 and the neo-N-termini of EIN2 and BB, all exhibited a low net charge at neutral pH, owing to an overall low number of charged residues. This is in contrast to the $\Delta 138$ N-terminus of RD21A which, despite of a neutral net charge, contains a rather high number of charged amino acids, and could not bind PRT1 detectably even when Phe was in N-terminal position (Fig. 26B). It is possible that differently charged amino acids within a peptide sequence interfere with PRT1 binding because they impose a rather rigid peptide structure. The preference of PRT1 for N-termini with low net charges was furthermore supported by the observation that replacement of distal Lys residues (Lys-14 and Lys-15) of nsP4 by Ala or Gly strongly promoted pull-down of PRT1 by this peptide (Fig. 24), whereas replacement by another positively charged amino acid, Arg, had only a modest effect (Fig. 24B). Moreover, the positively charged Lys-2 was the only residue among the first six amino acids of a tested substrate peptide, substitution of which did not dampen PRT1 binding. The preference of low net-charged N-termini by PRT1 differs from *E. coli* ClpS substrate binding, where a preference for N-termini with positive net charge was reported (Erbse et al., 2006).

Finally, despite of the apparent preference for low net charges, all three PRT1 binders (K2, EIN2, BB) contained a protonatable residue in penultimate position. Interestingly, this was accompanied by the occurrence of a negatively charged residue in more downstream position, namely Glu-7 and Asp-9 in EIN2 and BB, respectively, although this co-occurrence of positive and negative charges is also likely to decrease structural flexibility. Consistent with the presence of negatively charged residues in peptides that bound well to PRT1, replacement of Asp-6 in nsP4 also weakened the interaction (Fig.

24A). Potentially, this negative charge compensates for the positive charge in position 2 to restore neutral net charge.

Together, based on the binding studies performed with peptide arrays it can be concluded that a 17-mer N-terminal peptide optimal for PRT1 recognition is characterized by 1) an aromatic N-terminal residue; 2) a protonatable residue in penultimate position; 3) a negatively charged residue in a central position; 4) a high number of Gly and Ser residues providing segmental mobility; and 5) preferentially additional hydrophobic residues throughout the sequence.

4.3.1.1 Distal Lys residues in the N-terminus of a PRT1 substrate

The results obtained here concerning Lys in penultimate position of a PRT1 substrate peptide are rather contradictory. On the one hand, the neo-N-terminus of BB which proved to be a very good ligand for PRT1 *in vitro*, bears a Lys residue in position 2, indicating that Lys at this position is advantageous for binding. This is also in agreement with the assumption that a protonatable residue in penultimate position of a peptide substrate increases PRT1 affinity. On the other hand, replacement of Lys-2 by Ala in the nsP4 sequence did not diminish PRT1 binding, or even improved pull-down of the N-recognin slightly (Fig. 24A). It would have to be tested whether Lys in second position is only beneficial in certain sequence contexts, for example when contributing to a neutral net charge as in the case of BB, or if binding of PRT1 to the BB sequence would be even improved upon replacement of Lys-2.

In contrast, Lys in the distal part of an N-terminal substrate sequence (Lys-14 and Lys-15 of nsP4) clearly decreased PRT1 binding compared to Ala in this position (Fig. 24). This was surprising since E3 ligase action depends on the presence of Lys residues for Ub transfer. One explanation for this observation could be the idea that N-recognins act by scanning the substrate sequence for a ubiquitination site, eventually allowing for substrate release (Eldeeb et al., 2018a). Although Ub was not provided in the SPOT assays performed here, it is conceivable that the absence of Lys in a sequence leads to longer dwell times of the E3 at the peptide during a process of sequence scanning, resulting in higher steady-state protein levels at the peptide spot. In disagreement with this idea however, optimal Ub transfer to a substrate by an N-recognin appears to occur considerably more downstream of the substrate's N-terminus than residue number 15 (Bachmair and Varshavsky, 1989). Hence, a potential process of sequence scanning by PRT1 would likely target more distal parts of the substrate protein, and dwell time effects on 17-mer artificial peptides might be negligible. In contrast, the simpler conclusion for the observation that PRT1 pull-down was augmented upon replacement of distal Lys residues would be that Lys in a downstream peptide sequence decreased PRT1 affinity. In fact, this hypothesis would be directly in line with observations made by (Bachmair and Varshavsky, 1989). Here, replacement of Lys-15 in the e^K N-degron linker sequence by Arg even improved the efficiency of the linker to act as a type II N-degron in yeast. This effect was however position specific, since K17R mutation led to a significant reduction in N-degron efficiency, prompting the authors to propose the requirement of properly spaced Lys residues for degron function (Bachmair and Varshavsky, 1989). Bachmair and Varshavsky (1989) inferred a competition mechanism between the two Lys residues of e^K at position 15 and 17 for a binding site at the N-recognin, and suggested that degron efficiency might be decreased when Lys-15 is occupying this binding site as compared to Lys-17.

These considerations would suggest that decreased affinity, rather than shortened dwell time of PRT1 at the peptide, explains the lower protein signals at the Lys-containing compared to the Lys-deleted peptide sequences. However, in the experiment presented in Fig. 24B, PRT1 occupancy was also strongly increased upon replacement of all Lys residues in nsP4 (i.e., Lys-15 and Lys-16), in a manner only partially independent of the positive charge elimination (Fig. 24B). This contradicts the explanation that competition effects between the Lys residues are responsible for a binding effect. Instead, the result obtained here suggests that 1) positive charge in the distal region of a substrate's N-terminus interferes with PRT1 binding, and 2) Lys in this region furthermore conflicts with the stability of the association between PRT1 and a peptide ligand by a yet unknown mechanism.

4.3.1.2 PRT1 substrates bear a protonatable residue in position 2

All three peptide sequences that were found to interact strongly with PRT1 in SPOT peptide assays (i.e., K2, and the neo-N-termini of EIN2 and BB) contained a protonatable residue in penultimate position. Remarkably, also all of the previously employed artificial substrates used to address PRT1 activity *in vivo*, i.e. for capturing the *prt1-1* allele (Bachmair et al., 1993; Potuschak et al., 1998), as well as for subsequent studies (Stary et al., 2003; Garzón et al., 2007; Faden et al., 2016), harbored a protonatable residue in second position. The experiments obtained from SPOT assay experiments now suggest that the affinity of PRT1 might in fact be strongest towards substrates initiated by aromatic N-termini followed by a basic amino acid. Notably, in a proteomics approach, Majovsky et al. (2014) found that some substrates of the type I branch of the N-end rule were also modestly enriched upon loss of *PRT1* function, indicating that PRT1 also slightly contributes to the degradation of these proteins. The assumption that the PRT1 binding pocket prefers peptides with positive charge close to the N-terminus would potentially explain this observation. Compellingly, this finding also implies the possibility that the genetic screen performed by Bachmair et al. (1993) might have actually resulted in the identification of a specialized N-recognin targeting type II N-degrons with a protonatable second residue. This would lead to the conclusion that other substrates with aromatic neo-N-termini might remain unstable upon loss of function of *PRT1*, and would allow the postulation of the existence of further N-recognins with type II specificity in *Arabidopsis*. Alternatively, the specificity for basic amino acids in second position might be a common feature among type II N-recognins, given that also several ClpS proteins showed preferential binding to peptides with positively charged amino acid in penultimate position during SPOT assay experiments (Erbse et al., 2006; Stein et al., 2016).

There are three proteins from other organisms than *Arabidopsis* known to confer binding preferentially to aromatic, rather than branched hydrophobic N-degrons. These are the ZZ domain of mammalian p62 (Cha-Molstad et al., 2017; Kwon et al., 2018), the ClpS2 N-end rule substrate adaptor of *Agrobacterium tumefaciens*, and ClpS1 from *Synechococcus elongatus* (Stein et al., 2016). Comparison of PRT1 and p62 substrate binding is worthwhile given that these two are the only known N-recognins engaging a ZZ domain for substrate interaction. Kwon et al. (2018) investigated the crystal structure of the ZZ domain of p62 in complex with different N-degrons. Thereby they also noted structural homology of the p62 ZZ domain with the one from PRT1, including the conservation of an Asp residue responsible for binding of the substrate's α -amino group (Kwon et al., 2018). Given that p62 has the strongest affinity towards Arg-initiated degrons which is a type I residue (Kwon et

al., 2018), it would be also conceivable that preference of PRT1 towards substrates with a positive residue in second position reflects an evolutionarily old feature of the ZZ domain.

Interestingly, many α -proteobacteria and also cyanobacteria contain an additional ClpS protein, and the variants from *A. tumefaciens* and *S. elongatus* were shown to be specific for aromatic N-degrons (Stein et al., 2016), as is PRT1. Moreover, like PRT1, all ClpS proteins investigated so far exhibit a preference for positively charged residues in position 2 (Erbse et al., 2006; Stein et al., 2016). In contrast, the N-terminus of the known natural substrate of p62, BiP, is of highly acidic nature (Chamolstad et al., 2015). Hence, although sequentially different, the PRT1 binding pocket might actually have specialized to function similarly to the bacterial ClpS domain (Erbse et al., 2006; Stein et al., 2016). While *E. coli* ClpS does not discriminate between aromatic amino acids and Leu in N-terminal position, the examples of *A. tumefaciens* ClpS2 and *S. elongatus* ClpS1 show that sequence variations of ClpS can principally lead to specificity for aromatic amino acids. It would be interesting to learn if such specialized ClpS proteins show structural analogy to PRT1, and if PRT1 and these ClpS proteins have evolved in parallel to perform similar substrate binding reactions.

With the criteria for PRT1-binding determined above, it is possible to predict whether a neo-N-terminus, once proteolytically exposed, principally qualifies as a substrate for PRT1. The uncertainty of *in-planta* generated N-terminal sequences however renders the search for potential substrate candidates difficult. While a growing number of studies provides information on the steady-state N-terminal proteome of *Arabidopsis* (Tsiatsiani et al., 2013; Rowland et al., 2015; Li et al., 2017b; Willems et al., 2017), data on the unstable N-terminome is still limited, and to date has mostly addressed the type I substrate branch of the *Arabidopsis* N-end rule (Majovsky et al., 2014; Zhang et al., 2015b, 2018b). The analysis of proteomes upon proteasome inhibition using methods suitable for the identification of endogenously created N-termini, such as COFRADIC and TAILS, could help in the future to provide the information needed for the identification of plant N-end rule substrates outside of the oxygen- and NO-dependent pathway.

4.3.2 BB is an *in-vivo* substrate of PRT1

The RING E3 ligase BB, in cooperation with and also independently of the peptidase DA1, antagonizes cell proliferation and promotes cell expansion and senescence by destabilizing downstream signaling components largely independently of phytohormones (Disch et al., 2006; Li et al., 2008; Du et al., 2014; Peng et al., 2015; Vanhaeren et al., 2017a). In doing so, BB and DA1 regulate the sizes of leaf-like organs, root meristems, and seeds, and promote leaf senescence (Li et al., 2008; Xia et al., 2013; Cattaneo and Hardtke, 2017; Vanhaeren et al., 2017b).

The cooperative action of DA1 and BB implies poly-ubiquitination of DA1 by BB, resulting in DA1 peptidase activation towards cellular substrates (Dong et al., 2017a). In parallel to BB, DA2 is a second RING E3 ligase capable of ubiquitination and activation of DA1 (Xia et al., 2013; Dong et al., 2017a). Following ubiquitination of DA1, both BB and DA2 are subject to DA1-mediated proteolysis themselves, and their cleavage products are rapidly degraded (Dong et al., 2017a). In the case of BB, the cleavage site behind Ala-60 releases a 35 kDa C-terminal fragment initiated by Tyr-61 (denoted Y61-BB), thus qualifying as a PRT1 substrate (Dong et al., 2017a). It was shown by the lab of N. Dissmeyer that Y61-BB was degraded in a rabbit reticulocyte lysate depending on the N-terminal amino acid, as well as on proteasome function (Dong et al., 2017a). Furthermore, a fusion of Y61-BB

and the firefly luciferase protein expressed in *Arabidopsis* protoplasts demonstrated that Y61-BB stability, assessed from normalized luciferase activity, depended on the N-terminus and on an intact PRT1 gene *in vivo* (Dong et al., 2017a). In the frame of this thesis, a direct and strong physical interaction of recombinant PRT1 with peptide sequences corresponding to the N-terminus of Y61-BB was furthermore shown by *in-vitro* peptide binding experiments (Fig. 26C), adding to the evidence that the cleaved C-terminal fragment of BB constitutes the first described *in-vivo* substrate of PRT1.

In fact, a role of PRT1 within the network controlling meristem activity coincides with the promoter activity observed with *PRT1*-promoter GUS fusions (Fig. 17). Although GUS activity was very weak in the reporter lines, and the majority of lines did not show any signal, some staining was observed in a few instances in the vasculature of young leaves, at shoot and root apices, and at the base of young flowers (Fig. 17). This expression pattern matches largely with promoter activity and transcript localization of BB which was described in the shoot and root meristems, developing vasculature, young leaf primordia and young flower meristems (Disch et al., 2006).

Destabilization of Y61-BB by PRT1 raises the question of the physiological relevance to this degradation. Although the cleavage product Y61-BB comprises three quarters of the native protein sequence, including BB's C-terminal RING domain, it was shown that this fragment is not capable of rescuing the large-petal phenotype of a *da1 bb* double mutant upon overexpression (Dong et al., 2017a). Thus, it is unlikely that PRT1-mediated degradation is required to remove BB function after peptidase cleavage. This would be also in agreement with the lack of any phenotypes in the *prt1-1* mutant associated with aberrant BB function, i.e. altered petal, sepal, or seed size, changes in flower biomass, stem diameter, or in timing of senescence (Disch et al., 2006; Li et al., 2008; Vanhaeren et al., 2017a).

Yet, the Y61-BB fragment expressed *in planta* by (Dong et al., 2017a) carried N-terminally an additional Met arising from the translational start site. It was seen in cell-free assays using both reticulocyte or *Arabidopsis* seedling lysates, that M-Y61-BB was also highly unstable, in contrast to a Gly-starting variant (Dong et al., 2017a). Interestingly, this was unaffected by proteasome inhibitor treatment in the mammalian system, whereas proteasome inhibition abolished M-Y61-BB degradation in the seedling extracts. Degradation of a MY-starting substrate would be in accordance with the idea that Met can serve as an N-degron when a bulky hydrophobic residue is in the second position, as shown in yeast (Kim et al., 2014). Although it is not clear if this branch of the N-end rule exists in higher eukaryotes, rapid M-Y61-BB degradation in cell extracts suggests that low stability of this construct could be responsible for the failure to complement the *da1 bb* phenotype upon stable expression in this mutant line. Thus, to clarify whether the C-terminal cleavage product of BB is still functional, it will be crucial to test for the *da1 bb* phenotype complementation by a stable Gly-initiated variant.

Accumulation of Y61-BB, either by *prt1-1* mutation or expression of a stable variant, could have different consequences depending on the functionality of this construct. Provided that Y61-BB is fully functional, this could lead to a situation mimicking constitutive BB activity. However, BB overexpression was shown to cause severe growth retardation (Dong et al., 2017a), and the absence of any related phenotype in *prt1-1* argues against this scenario. In contrast, a fragment with impaired function might compete with uncleaved BB for interaction with DA1 or other proteins, and could cause a dominant-negative phenotype. In this case, PRT1-mediated degradation would ensure the continuous responsiveness of BB signaling. Although this would also ask for a phenotypical

consequence of *PRT1* mutation, it is possible that BB-related phenotypes of *prt1-1* are rather mild in the single mutant. Hence, to evaluate potential phenotype alterations triggered by the accumulation of Y61-BB in a *prt1* mutant situation, it would be interesting to see if the *prt1-1* allele has additional effects in the background of a DA1 overexpressing line, where proper BB function might be more essential.

As a third option, efficient degradation of Y61-BB via PRT1 might be required irrespectively of the enzymatic functionality of this fragment, if accumulation to low levels would be toxic to the cell. This could be the case, for example, if the cleaved fragment is misfolded and prone to aggregation. In this case, PRT1 activity would contribute to the cellular disposal of this protease product, and protect from ER stress. Such a role of PRT1 might not even be restricted to Y61-BB, but could be a general function of this E3 ligase in the protein quality control.

4.3.3 *In-vitro* substrate interactions of PRT6

Destabilization of MC-initiated substrates, particularly of the ERFVIs, by PRT6 is well established genetically (Garzón et al., 2007; Gibbs et al., 2011, 2014a, 2018; Licausi et al., 2011; Majovsky et al., 2014; Abbas et al., 2015; Zhang et al., 2018b). However, in contrast to mammalian and yeast UBR proteins, direct substrate interaction and specificity have not been studied for this plant N-recognin. Here, truncated versions of PRT6 containing the UBR domain were applied to the SPOT array system in order to approach PRT6 substrate specificity.

Importantly, peptide arrays confirmed binding of UBR^{PRT6} to a peptide sequence mimicking the arginylated N-terminus of Met-1 excised RAP2.12 (and RAP2.2) in an N-terminus dependent manner (Fig. 47). Moreover, the N-terminal sequence of nsP4 was accepted as a binding ligand by UBR^{PRT6} with pull-down efficiency comparable to or even higher than the RAP2 sequence (Fig. 46, 48). Since nsP4 was shown to constitute an N-end rule substrate in rabbit reticulocyte extract (de Groot et al., 1991), and to interact with UBR box proteins from mouse (Tasaki et al., 2005), this indicates the functional conservation of the UBR boxes from *Arabidopsis* and mammals. Consistent with such conservation, investigation of the N-terminus specificity of UBR^{PRT6} furthermore revealed a slight preference for binding to Arg-initiated peptides over Lys-starting ones, whereas His-initiated peptides were not bound in the SPOT assay system (Fig. 46). Similar observations were made with SPOT peptide arrays engaging the UBR box of yeast UBR1 (Choi et al., 2010). Choi et al. (2010) furthermore confirmed decreasing UBR affinity towards Arg < Lys < His N-degrons using isothermal titration calorimetry, proving that the signal intensities seen in SPOT assays correlated with the substrate binding affinity of the UBR. The low affinity towards His-substrates, although recapitulated by yeast UBR1 (Choi et al., 2010), and human UBR2 (Matta-Camacho et al., 2010), is surprising given the low stability of His-initiated test substrates in both plants (Graciet et al., 2010) and yeast (Bachmair and Varshavsky, 1989). In mammalian cell extracts, however, a lower destabilizing effect of N-terminal His as compared to Arg and Lys was reported (Gonda et al., 1989). It will be interesting to learn from future experiments if full-length PRT6 is required to bind all three type I residues with high affinity. However, whether the stability of His-initiated substrates actually depends on an intact *PRT6* gene has not been published so far.

SPOT array binding profiles of UBR^{PRT6} also confirmed a strong influence of the second amino acid of the substrate sequence on UBR^{PRT6} affinity, since nsP4 was only recognized when Ile was in

penultimate position, but not Lys (Fig. 46). This observation again agrees with reports on other UBR box proteins (Choi et al., 2010; Matta-Camacho et al., 2010). For yeast UBR1 it was found using SPOT assays that any hydrophobic residue was accepted at the second position of an RXAAA peptide (Choi et al., 2010). This was explained by a rather indeterminate positioning of the second residue side chain inside of a hydrophobic pocket of UBR1 (Choi et al., 2010). Among the non-hydrophobic residues, only Pro completely prevented binding of UBR1 when present in second position.

As was observed with UBR^{PRT6} (Fig. 47, 48), Cys in second position was also relatively suitable for peptide binding of UBR1 (Choi et al., 2010). This property of UBR^{PRT6} is on the one hand in accordance with the fact that endogenous substrates of PRT6 (Gibbs et al., 2011; Licausi et al., 2011), as well as mammalian UBR1 and UBR2 (Hu et al., 2005; Lee et al., 2005) bear Arg-Cys-starting N-termini. On the other hand, in both plants and mammals, the true *in-vivo* N-degrons of these substrates do not contain Cys, but Cys-sulfonic acid ((O₃)Cys) in second position. Hence, it appears that the UBR domain, in contrast to ATEs (see below), does not discriminate between these two states of the penultimate residue. Alternatively, binding affinity towards an Arg-(O₃)Cys peptide might be even stronger than what was seen for Arg-Cys peptides.

Interestingly, Arg-starting peptide substrates with either of the acidic residues Asp or Glu were less favored by yeast UBR1 (Choi et al., 2010). Likewise, Glu- or Asp-starting sequences of candidate 1 and 2 sequences (Fig. 48), or the Arg-Asp starting sequence mimicking the processed RIN4 middle fragment (Fig. 47) were not bound by UBR^{PRT6}. This is remarkable in the light of Asp- and Glu-starting N-degrons, next to oxidized Cys starting ones, being canonical substrates for ATE-mediated arginylation (Kwon et al., 1999; Hu et al., 2006; Graciet et al., 2009; Wadas et al., 2016). Accordingly, and in contrast to the yeast and plant UBR proteins, a tetrapeptide of the sequence RXFS exhibited the highest affinity towards the UBR boxes of human UBR1 and UBR2 in isothermal titration calorimetry when Asp was the residue in second position (Matta-Camacho et al., 2010). It is therefore possible that ATE-products from Asp- and Glu-starting peptides in both plants and yeast actually escape UBR-mediated recognition. *In vivo*, this might even apply to animals as well, since here the only evidenced endogenous Asp- or Glu-starting ATE substrates are the human chaperones BiP, calreticulin, and protein disulphide isomerase which are recognized by the N-recognin and autophagic adaptor p62 after arginylation, rather than any of the UBR proteins (Cha-Molstad et al., 2015). Similarly, the RIN4 cleavage product starting Asn-11 which is unstable and was proposed to be degraded according to the N-end rule (Takemoto and Jones, 2005), might actually be destabilized in a PRT6-independent way. Indeed, even N-terminus independent instability of both C-terminal RIN4 fragments was recently reported in (Goslin et al., 2019), as the result of a collaboration involving also the Dissmeyer laboratory.

Notably, variability was observed for UBR^{PRT6}-binding to R-RAP2^{Δ1} sequences between experiments (Fig. 48), and even within the same experiment (Fig. 47B). Next to the general possibility that the lack of Cys-2 oxidation might have decreased pull-down efficiency exerted by this peptide, the relatively low synthesis efficiency of the RAP2 was already taken into consideration (see chapter 3.5.1). Furthermore, it was discussed by others that SPOT membrane topology can lead to differential binding of sequentially identical peptide spots at different locations on the membrane (Weiser et al., 2005). However, during this work, hardly any other peptide sequence exhibited a comparable extend of technical variability as observed for RAP2 peptides. It should therefore be noted that also the triple Pro motif of RAP2 could have influenced the interaction with UBR^{PRT6}, given that Pro exhibits

random cis-trans isomerization in artificial peptides, whereas cis-trans configuration of this amino acid in native proteins is strictly determined (Wedemeyer et al., 2002).

In summary, SPOT peptide arrays confirmed UBR box-mediated binding of PRT6 to genetically predicted substrate peptides starting with Arg or Lys, when either Cys or Ile were present in position 2 of the N-terminus. Here, the interaction with RC-starting peptides did not depend on Cys-2 oxidation. Interestingly, the affinity of UBR^{PRT6} towards peptides with an acidic residue (Asp, Glu) in second position which mimic certain products of ATE activity, was very low. This also applied to the RD-starting RIN4^{Δ11} fragment which was previously suggested a substrate of the Arg/N-end rule pathway.

4.3.4 *In-vitro* arginylation activity of ATE1

ATE1 and ATE2 act redundantly within the *Arabidopsis* N-end rule machinery to control a plethora of physiological processes (Domitrovic et al., 2017). Whilst the substrate specificities of mammalian ATEs have been investigated *in vitro* (Wang et al., 2011a, 2014; Wadas et al., 2016), very few enzymatic data were available for plant ATEs (Graciet et al., 2009). During this work, first insights into ATE1 substrate selectivity were gained after the establishment of a new peptide-based assay, allowing for rapid and highly reproducible assessment of enzyme substrate usage.

In the peptide assays, arginylation of peptides corresponding to sequences from both RIN4 and RAP2 by ATE1 was shown (Fig. 49). While arginylation of the ERFVII N-termini through ATEs was genetically evidenced by numerous preceding publications (Gibbs et al., 2011, 2014a, 2015, 2018; Licausi et al., 2011; Weits et al., 2014; Abbas et al., 2015; Riber et al., 2015; Giuntoli et al., 2017), the interaction of ATEs with the RIN4 proteolytic middle fragment was only anticipated (Takemoto and Jones, 2005). The finding that deamidated RIN4^{Δ10} peptide functions as a substrate for ATE1 *in vitro*, strengthens the possibility that this interaction takes place also in a cellular context, although downstream processing via PRT6 might be less likely (see chapter 4.3.3).

Importantly, substrate acceptance of ATE1 strictly depended on the peptide's N-terminus, since only Asp- and (O₃)Cys-initiated variants were modified by ATE1, whereas Gly and Cys did not allow for arginylation (Fig. 49A). These results are in accordance with the canonical ATE substrate specificity (Kwon et al., 1999, 2002; Hu et al., 2005, 2006; Gibbs et al., 2014b), proving the conservation of ATEs between eukaryotes. In contrast, arginylation of Gly or Cys as non-canonical N-termini as previously reported (Wong et al., 2007; Rai et al., 2008; Zhang et al., 2012a, 2015a) is not supported by the results obtained here with *Arabidopsis* ATE1, consistent also with the results from peptide assays with mouse ATE1 (Wadas et al., 2016). Similarly, during the experiments described here, internal arginylation of artificial peptides by ATE1 was negligible, given that incorporation of radiolabel was marginal with the Gly starting peptide variants of either RIN4 or RAP2, although acidic residues were present in both sequences. This is likewise in agreement with the study performed by Wadas et al. (2016), and was supported *in vivo* by the findings of Hoernstein et al. (2016).

Arginylation specifically of the α -amino group of a polypeptide, as seen during this work, would be explainable by a reaction mechanism performed by ATE1 that is analog but reverse to the ribosome reaction (Fig. S25), as was previously postulated (Wang et al., 2014). Here, the tRNA-born amino acid would provide the activated C-group to be attacked by the target protein's N-group, resulting in the

formation of a standard peptide bond. In contrast, side-chain arginylation to occur would suggest the formation of an anhydride intermediate between the two acid groups of the tRNA-Arg and the side chain Asp, due to the lack of a nucleophile N-terminus, as was also proposed by (Wang et al., 2014). The latter reaction mechanism might be less likely to occur in the light of the results obtained here.

However notably, without one exception (Wang et al., 2018a), previous reports on both non-canonical N-terminus arginylation and midchain arginylation were based on either whole protein substrates, or *in-vivo* analyses (Eriste et al., 2005; Wong et al., 2007; Saha et al., 2011; Wang et al., 2011a, 2014; Zhang et al., 2012a, 2015a). Thus, the possibility remains open that such modifications can occur 1) on proteins rather than short peptide substrates, 2) in a cofactor-assisted manner, or 3) under certain cellular conditions.

Furthermore, although major differences exist between the downstream sequences of RIN4 (D-WEAEENVPYTA) and RAP2 (D-GGAIISDFIPP), end point arginylation efficiency of both sequences was comparable in the experiments presented here (Fig. 49A). This hints at a minor importance of the downstream sequence for ATE1 substrate selection. However, previous peptide library experiments with mouse ATEs have shown that the downstream sequence clearly influenced arginylation efficiency, and a marked impact particularly of the amino acid in position 2 was attested (Wadas et al., 2016; Wang et al., 2018a). Interestingly, among the amino acids tested in position 2 of an Asp starting peptide substrate, Trp and Gly (which are present in RIN4 and RAP2, respectively) exhibited similar amenability as arginylation substrates in the peptide array experiments performed by Wadas et al. (2016). Hence, the comparable results obtained for D-RIN4 and D-RAP2 might also be coincidental.

Crucially, the arginylation assay established within this work also allowed for the first *in-vitro* reconstitution of the sequential action of PCO and ATE enzymes on artificial peptides derived from a natural substrate. Hereby it was demonstrated that processing of a Cys-starting peptide by PCOs is sufficient to render the peptide a fully accepted substrate of ATE1 (Fig. 49B). It was shown by our collaborators that PCOs are cysteinyl dioxygenases that produce N-terminal Cys-sulfinic acid ((O₂)-Cys) (White et al., 2017)). In the *in-vitro* arginylation assays, PCO-supplemented reactions with Cys-starting peptides yielded the same levels of ¹⁴C-Arg incorporation as did the chemically produced Cys-sulfonic acid peptide without addition of PCO (Fig. 49B). Using reactions without radiolabel, it was confirmed by LC-MS analysis that the peptides produced in the presence of both PCO and ATE1 indeed carried Cys-sulfinic acid preceding the N-terminal Arg (White et al., 2017). Hence, ATE1 appears to be indiscriminant between the two oxidation products of Cys.

Through PCO-mediated peptide processing, Arg transfer by an ATE enzyme to (O₂)-Cys starting substrates was also evidenced within this work, and it was previously proposed that a transiently occurring (O₂)-Cys N-terminus might structurally best mimic an Asp or Glu side chain, which are well-established residues for ATE recognition (Kwon et al., 2002; Lee et al., 2005). Considering structural resemblance of the Asp side chain, it was also pointed out by Mike Schutkowski¹ during personal communication that phosphorylated hydroxyl groups on protein N-termini might be recognized by ATE enzymes as well. A number of proteins have been discovered that likely bear phosphorylated Ser or Thr residues at their mature N-termini (Sugiyama et al., 2008; Reiland et al., 2009). During preliminary experiments, peptides representing the phosphorylated or unmodified N-termini of

¹ Martin Luther University Halle-Wittenberg, 06108 Halle (Saale), Germany

three of these proteins (ARA4/AT2G43130, DWARF1/AT3G19820, and AHK2/AT5G35750 (Sugiyama et al., 2008)) were subjected to the arginylation assay using ATE1. However, no Arg transferase activity was detected for these peptides (data not shown). Nevertheless, arginylation of phosphorylated N-termini is an intriguing suggestion and it will be worth testing in the future whether this can take place *in vivo*, or whether this can be catalyzed by other ATE enzymes.

Notably, NO was not included in the reaction mixtures for PCO-mediated Cys oxidation of RAP2 peptides, nor were the enzymes pretreated for Cys nitrosylation, and the reaction depended merely on the presence of PCOs and oxygen in the solution (Fig. 49B; White et al. (2017)). The fact that it was still possible to produce a functional tertiary N-degron that was further processed by ATE1 indicates that these steps can be conducted fully enzymatically. This was surprising since destabilization of ERFVII transcription factors in normoxia depends on nitrate reductase activity and NO in plants (Gibbs et al., 2014a). Furthermore, oxidation and subsequent arginylation of Cys-starting 8-mer peptides by mouse ATE1 was also successfully reconstituted *in vitro* through application of NO, instead of PCOs (Hu et al., 2005). Concerning the response to low oxygen, both NO- and PCO-mediated oxidation are likely reinforced upon hypoxia, given that NO levels rise under these conditions (Sasidharan et al., 2018), and PCOs are induced on the transcript level (Mustroph et al., 2009, 2010; Weits et al., 2014). These reactions might dampen the hypoxic response, or prepare for the re-aeration conditions. However, whether NO and PCO pathways can act in parallel, or influence each other in a physiological context, remains elusive to date.

4.4 A potential role for PRT1 in EIN2 signaling

Although EIN2-independent aspects of the ethylene response are known (Kim et al., 2013c; Bakshi et al., 2018; Binder et al., 2018), EIN2 processing and re-localization remains at the hub of ethylene signaling. The gene has been in the focus of intense research since its discovery (Alonso et al., 1999), and latest studies have helped understanding its dual function in transcriptional and translational regulation (Li et al., 2015; Merchante et al., 2015; Zhang et al., 2017a, 2018a). Nevertheless, crucial questions regarding EIN2 signaling remain unresolved. For example, it is still not clear why expression of the C-terminal half alone confers only a subset of ethylene responses, whereas other developmental defects resulting from *ein2* mutation are not complemented by *EIN2 CEND* expression. Next, while the stability of full-length EIN2 was thoroughly investigated (Qiao et al., 2009, 2012; Wen et al., 2012), nothing is known about the post-signaling fate of cleaved EIN2 CEND. This is remarkable, given that rapid removal of EIN2 CEND can be considered essential for both relief from the signal and maintaining ethylene responsiveness. The work presented here provides evidence for an N-end rule dependent destabilization of Phe-initiated EIN2⁶⁴⁶⁻¹²⁹⁴ (termed EIN2^{C-term}) via PRT1.

4.4.1 Physical interaction of EIN2 and PRT1

Using peptide binding assays, it was found that purified PRT1 strongly and specifically bound to an artificial peptide that mimicked the neo-N-terminus of EIN2 resulting from cleavage between Ser-645 and Phe-646 (Fig. 26). Given that PRT1 probably localizes to the cytosol and nucleus (Fig. 31) which represent the sites of EIN2 CEND action, this opens up the possibility that the interaction takes place also *in vivo*.

In order to test for an interaction between PRT1 and EIN2^{C-term} in plant cells, BiFC constructs were co-transfected into *Arabidopsis* protoplasts, but failed to show an N-terminus dependent physical association of EIN2^{C-term} and PRT1 (Fig. S19, and data not shown for YFP^N-3HA-PRT1^{V28A} constructs). To test for an *in-vivo* interaction using a different method, it was therefore attempted to pull-down N-terminally tagged PRT1 by EIN2^{C-term} variants in a co-IP approach. Indeed, EIN2^{C-term} variants efficiently captured PRT1 when both partners were expressed from a strong promoter (Fig. 34, S20). However, no specificity for the N-terminal amino acid of EIN2^{C-term} was observed for this interaction, and the pull-down was abolished when *PRT1*, or both *PRT1* and *EIN2^{C-term}* were expressed under the control of a weaker promoter (Fig. 35). Thus, it cannot be excluded that the pull-down observed under strong expression conditions was rather due to unspecific protein co-aggregation, especially since recombinant PRT1 exhibited a pronounced tendency to aggregate *in vitro*. In conclusion, further experiments will be required to unambiguously test for a potential *in-vivo* interaction of EIN2^{C-term} and PRT1. This could be co-IP experiments using stably transformed lines expressing ubiquitination inactive variants of *PRT1* together with *EIN2^{C-term}*. Additionally, treatment of these lines with ethylene gas might be a prerequisite, or also a prohibition, to establish a stable interaction. Alternative protein-interaction assays, such as yeast-two-hybrid, isothermal titration calorimetry, or split-luciferase, might furthermore be of choice for further studies.

4.4.2 EIN2^{C-term} has low *in-vivo* protein stability

After withdrawal of an ethylene signal, rapid recovery of *Arabidopsis* seedlings to pre-treatment growth rates is observed within 90 minutes (Binder et al., 2004b, 2004a), and this is achieved partly independently of the downstream transcriptional cascade via EIN3/EIL1 (Binder et al., 2018). Protein stability of the EIN2 signaling fragment is an obvious target for the efficient abolishment of the ethylene response. Within this work, it was shown that EIN2^{C-term} exhibits low stability when expressed in WT *Arabidopsis* protoplasts. Precisely, the bulk of the protein was reduced to low levels upon inhibition of translation within one to two hours which matches also the duration of the growth recovery phase (Fig. 28, 33). Thus, the data presented here identify rapid turnover of the cleaved EIN2 C-terminus as a previously unknown potential negative regulator of ethylene signaling. This suggests that the ethylene response may also be fine-tuned by control of EIN2^{C-term} stability, next to already defined negative-regulatory mechanisms that act on different levels of the signaling network (Guo and Ecker, 2003; Potuschak et al., 2003; Gagne et al., 2004; Resnick et al., 2006; Christians et al., 2008; Gao et al., 2008; Grefen et al., 2008; Gao and Schaller, 2009; Xu et al., 2014; Rai et al., 2015; Shakeel et al., 2015).

Next to low stability of EIN2^{C-term} in *Arabidopsis* protoplasts, it was observed that EIN2^{C-term} did not accumulate to high steady-state levels (Fig. 28, 29, 33, 34, S14). Nevertheless, it has to be assumed that the active pool of EIN2^{C-term} is strictly protected from depletion in order to allow for full and even dose-dependent activation of the ethylene signaling cascade. This can be concluded from several studies that have reported constitutive ethylene signaling phenotypes upon perturbation of EIN2 post-translational regulation, where EIN2^{C-term} obviously escaped from cellular degradation also under ethylene-depleted conditions. First, a severe constitutive ethylene response phenotype is triggered by the *ctr1-1* allele (Kieber et al., 1993). The primary consequence of this mutation is believed to be the abolishment of EIN2 phosphorylation, resulting in EIN2 accumulation (Qiao et al., 2009, 2012), and constitutive membrane release of the EIN2 C-terminus (Ju et al., 2012; Qiao et al.,

2012). Next, in the study performed by Qiao et al. (2009), two F-box proteins, ETP1 and ETP2, were identified that target full-length EIN2 for proteasomal degradation. Consistent with this function, microRNA-mediated knock-down of *ETP1/2* mRNA also resulted in hyper-accumulation of EIN2 full-length protein. In the transgenic knock-down lines, this was accompanied by constitutive ethylene responses as seen in *ctr1-1* (Qiao et al., 2009), although it is not fully clear why accumulation of the full-length EIN2 protein initiates the signaling cascade. It was first argued by Ju et al. (2012) who also observed constitutive ethylene response phenotypes upon overexpression of the *EIN2* genomic sequence, that excess EIN2 could escape CTR1-mediated phosphorylation resulting in membrane release of the C-terminus and the onset of signaling.

In all of these studies, constitutive ethylene response phenotypes were observed indicating that EIN2^{C-term} is obviously not unstable “enough” to abolish EIN2 signaling following perturbation of upstream regulation, even in the absence of ethylene. This might be reconcilable with the idea of EIN2^{C-term} instability by the fact that in all the mentioned cases, genetically induced accumulation of EIN2 full-length protein was preceding downstream EIN2^{C-term} signaling, potentially causing an overload of the machinery in charge of EIN2^{C-term} degradation. This hypothesis can also be carefully applied to explain the strong constitutive ethylene responses that resulted from native-promoter driven expression of *EIN2* mutated in Ser-924 (Ju et al., 2012), given that Ser-924 phosphorylation is likely to interfere with ETP1/2 interaction (Ju et al., 2012; Qiao et al., 2013), and can therefore be assumed to also trigger EIN2 accumulation. However, this has to be tested experimentally, and protein levels of this mutant version of EIN2 were not addressed by Ju et al. (2012). Nevertheless, based on the above summarized observations, it appears that a potential new pathway controlling the level of EIN2^{C-term} after membrane release is regulated to prevent abolition of ethylene signaling.

Ju et al. (2012) first directly suggested a role of EIN2 phosphorylation in the regulation of EIN2 turnover via ETP1/2. Given that no phosphatase was identified so far that would antagonize CTR1 activity, a primary role of ETP1/2 in recycling phosphorylated EIN2 would be extremely convincing, and might be a prerequisite of maintaining the cell in a signal-sensitive state. Notably however, the interaction of ETP1/2 with EIN2 occurs at the EIN2 C-terminus (Qiao et al., 2009). In fact, a potential role of these F-box proteins in controlling also the level of cleaved EIN2 CEND was never disproven, and would be worth testing, especially since data on the cellular localization of ETP1/2 is missing. In this context and in general, it would be furthermore interesting to test whether phosphorylatable sites within the EIN2 C-terminus (e.g., Ser-924) are important for the stability of the cytosolic fragment in the protoplast assay, either via ETP1/2 or other pathways. Finally, a physical interaction of EIN2⁵¹⁶⁻¹²⁹⁴ with components of the COP9 signalosome was reported by Christians et al. (2008), offering another so-far unexplored potential link of ethylene to light signaling via COP1 (Wang et al., 2009b). The *eer5-1* mutation which affects a putative component of the COP9 signalosome, induces partial ethylene hypersensitivity downstream of EIN2 (Christians et al., 2008). To date, the molecular function of this interaction is not known. Given the phenotype of the *eer5-1* mutant, it might also be worth testing if EIN2 CEND stability depends on this gene.

4.4.3 *In-vivo* stability of EIN2^{C-term} depends on PRT1 activity

Remarkably, upon transient overexpression, EIN2^{C-term} degradation depended on both PRT1 activity (Fig. 28, 30, 33), and the nature of its N-terminal amino acid (Fig. 28, S14). This strongly indicates

degradation of EIN2^{C-term} through PRT1 by means of the N-end rule. Inhibition of proteasome activity gave rise to protein levels of EIN2^{C-term} comparable to those caused by *prt1* mutation, or replacement of the N-terminal Phe by a stabilizing residue (Fig. 29), hinting at ubiquitination as the mode of destabilization exerted by PRT1. To unequivocally confirm PRT1-dependent ubiquitination of EIN2^{C-term}, immunoprecipitated protein from WT and *prt1-1* mutant cell extracts would have to be detected with the anti-Ub antibody in a next step. Within this work, *in-vitro* ubiquitination of EIN2^{C-term} variants by recombinant PRT1 was not achieved, since purifications of recombinant EIN2^{C-term} were extremely poor (data not shown).

PRT1-dependent stability of EIN2^{C-term} was not altered by the addition of BA to the protoplast medium which is assumed to trigger ethylene production (Fig. 33), indicating that N-end rule-mediated degradation was acting constitutively on EIN2^{C-term} under the conditions of the protoplast assay. However, it was not assessed within this work whether *Arabidopsis* protoplasts exhibited ethylene signaling already under the applied control conditions. Given that ethylene signaling is activated within the wounding response (Cheong et al., 2002; Delessert et al., 2004; Savatin et al., 2014), it can actually be assumed that this was the case. Therefore, assaying the stability of EIN2^{C-term} in protoplasts in the presence of ethylene receptor inhibitors such as silver ions or 1-methylcyclopropene (Schaller and Binder, 2017) might reveal a potential regulation of PRT1 activity by ethylene.

Presuming PRT1-dependent degradation of EIN2^{C-term} under physiological conditions, ethylene hypersensitive phenotypes caused by *PRT1* mutation would be expected, especially those which were previously associated with increased EIN2 CEND abundance. The latter include a reduction in rosette size, abnormal morphology of the gynoecium and low fertility, increased expression of ethylene regulated genes such as *GLUTATHIONE S-TRANSFERASE PHI 2* (At4g02520) and *ETHYLENE-RESPONSIVE ELEMENT BINDING PROTEIN* (At3g16770), as well as an elongated hypocotyl of seedlings germinated on low nutrient media in constant light (Alonso et al., 1999; Wen et al., 2012). However, so far no morphological differences of adult plants were observed for the original and backcrossed *prt1-1* lines compared to the WT, whereas hypocotyl lengths of nutrient depleted seedlings and ethylene gene expression will have to be determined using genomically clean mutant lines of *prt1*. Interestingly, a very mild increment in hypocotyl length was attested for *prt1-1^{ts}* compared to WT seedlings when grown in the dark, which was significant upon higher sample numbers (Fig. 36). Such a phenotype would be explainable by a lower sensitivity towards endogenous levels of ethylene, although additional experiments using backcrossed lines and independent alleles, as well as complementation studies, will be necessary to exclude a contribution of the genetic background of *prt1-1^{ts}* that also conferred cytokinin hyposensitivity (see chapter 3.4.5). Nevertheless, it should be considered that a potential *prt1-1*-dependent failure to discard low basal levels of cleaved EIN2^{C-term} could also activate the mechanisms that lead to desensitizing of plants towards low levels of ethylene (Hua and Meyerowitz, 1998; Resnick et al., 2006; Rai et al., 2015; Binder et al., 2018). In this scenario, *PRT1* mutation could ultimately result in reduced, rather than enhanced ethylene responses in the mutant. Expression analyses of members of the *AUXIN REGULATED GENE INVOLVED IN ORGAN SIZE* (*ARGOS*) family (Rai et al., 2015) might help to estimate the level of basal ethylene desensitization in *prt1* mutant plants. Alternatively, continuous low above normal levels of ethylene were also seen to slightly increase the hypocotyl growth of etiolated *Arabidopsis* seedlings (Hua and Meyerowitz, 1998). Thus, longer hypocotyls of *prt1-1* mutants in the dark might also be directly explainable by a failure to dampen endogenous ethylene signaling on the level of EIN2^{C-term}.

Apart from the considerations made above, *PRT1* mutation preventing the degradation of EIN2^{C-term} would actually not be expected to impact considerably on the onset of signaling upon perception of the hormone. In contrast, resetting the signal after withdrawal of ethylene is more likely compromised by increased stability of the signaling fragment. Hence, failure of EIN2^{C-term} degradation should express in the timing and/or duration of the growth recovery phase following ethylene treatment. To test this, experiments assaying the growth response of *prt1-1^{ts}* seedlings upon an ethylene signal followed by withdrawal of ethylene were performed by David Bullock¹ in the laboratory of José Alonso¹ in collaboration with N. Dissmeyer. However, no changes were observed for *prt1-1^{ts}* compared to the WT (unpublished results). Nevertheless, growth recovery kinetics might obviously be linked to EIN2^{C-term} stability, and it will be worth to reassess the impact of *PRT1* in this process using independent lines lacking cytokinin hyposensitivity. A potential interference of cytokinin signaling in this context is particularly critical since B-type ARR_s were implicated in the ethylene growth recovery (Binder et al., 2018).

The protein pool of EIN2^{C-term} was not reduced to undetectable levels in *Arabidopsis* protoplasts of the WT genotype (Fig. 28, 33). This might be explained by exceedance of the degradation capacity in the overexpression situation, as discussed above. However notably, released EIN2 CEND encounters different fates, including both nuclear and cytosolic functions (Li et al., 2015; Merchante et al., 2015; Zhang et al., 2017a). Cytosolic tasks of EIN2 CEND involve the localization to processing bodies (Li et al., 2015; Merchante et al., 2015). Furthermore, the requirement of the EIN2 C-terminal NLS for interaction with the ethylene receptor ETR1 (Bisson and Groth, 2015) indicates that cleaved EIN2 CEND may also fulfill another function at the ER membrane. Crucially, in both cases, the local environment and/or conformation of EIN2 CEND could potentially interfere with recognition of EIN2 CEND by components mediating its degradation. Thus, an alternative explanation for incomplete EIN2^{C-term} degradation seen in protoplasts might be inaccessibility of a portion of EIN2^{C-term} to PRT1-mediated degradation due to its association with processing bodies and/or the ER membrane. In this case, PRT1 might be in charge to reduce the pool of “unengaged” EIN2^{C-term}, rather than contributing to the abolition of the ethylene signal. Notably, high levels of free EIN2^{C-term} would bear a particular risk to the cell, given that this soluble fragment lacking CTR1 phosphorylation might even act as a competitive inhibitor of CTR1 activity, thus enforcing auto-amplification of the ethylene signal. Therefore, it should also be tested whether EIN2^{C-term} stability in *prt1-1* is particularly critical in situations of increased signaling, for example in combination with the weak allele *ctr1-10* (Yu and Wen, 2013), or upon knock-out of either of the *ETP* genes. Here, an aggravation of the *ctr1-10* and *etp* phenotypes in the respective double mutant situations would hint at a role for PRT1 in reducing high pools of cleaved EIN2^{C-term}. Similarly, *prt1-1* mutation might bring about additive phenotypes with transgenic expression of *proEIN2::EIN2^{S645A}* which alone likewise triggered mild ethylene responses in the WT (Ju et al., 2012).

The functions of the EIN2 cleavage products are diverse and not fully understood. Certainly, accumulation of EIN2^{C-term} alone does not trigger all ethylene responses, indicating a so far unknown role for the N-terminal part remaining in the ER membrane (Alonso et al., 1999; Ma et al., 2018a). However, there is a range of phenotypes caused by *EIN2* mutation, complementation of which by EIN2 CEND has not been addressed so far (see above). Any of these responses might potentially be affected by loss of PRT1 function as well, and N-degron-dependent degradation of EIN2^{C-term} could be restricted to certain tissues and conditions. Some ethylene-related stress conditions have already

¹ North Carolina State University, Raleigh, North Carolina, USA

been applied on the *prt1-1* mutant in different contexts and revealed no aberrant phenotypes. These include the sensitivity towards ABA during germination (Holman et al., 2009), and susceptibility towards the necrotrophic fungus *B. cinerea* (de Marchi et al., 2016). Thus, further experiments will be required to reveal the physiological function of N-end rule-mediated degradation of EIN2^{C-term}.

4.4.4 EIN2^{C-term} degradation *in planta*

In stably transformed plant lines, EIN2^{C-term} expression triggered constitutive ethylene response phenotypes only in the *prt1-1* genetic context, strengthening the hypothesis that PRT1 targets EIN2^{C-term} also in intact plants (Fig. 44, 45). Interestingly, *ein2-1* mutant plants expressing EIN2^{C-term} were indistinguishable phenotypically from untransformed *ein2-1* lines, indicating that EIN2^{C-term} function was effectively abolished in the presence of an intact *PRT1* gene. This observation differed from what was seen during protoplast experiments, where low steady-state levels of EIN2^{C-term} were persistent also in the WT. This discrepancy between EIN2^{C-term} stability in protoplasts and the lack of EIN2^{C-term} function in transgenic *ein2-1* plants is likely due to the lower expression strength in the transgenic lines compared to *UBQ10*-promoter driven expression in the protoplast system. As argued before, the capacity of PRT1-mediated ubiquitination might be limiting for EIN2^{C-term} degradation under conditions of EIN2 CEND hyper-accumulation. In support of a generally limited capacity of PRT1 action, it should be noted that the *prt1-1* mutant allele was also isolated using a stability reporter expressed from the relatively weak nopaline synthase promoter (Bachmair et al., 1993). Thus, limited PRT1 capacity could adequately explain the apparent contradiction of PRT1-mediated EIN2^{C-term} instability on the one hand, and numerous reported observations of constitutive ethylene signaling triggered by EIN2 full-length accumulation on the other hand (Kieber et al., 1993; Qiao et al., 2009, 2012; Ju et al., 2012; Wen et al., 2012).

Elimination of EIN2^{C-term} signaling in a *PRT1* WT genomic background under endogenous expression conditions however raises the question how ethylene signaling is permitted in the presence of the hormone. One hypothesis would be that ethylene-mediated accumulation of EIN2 upon ethylene perception (Qiao et al., 2009) results in levels of cleaved EIN2 CEND which override PRT1-mediated ubiquitination. This would ask for a cooperative role of PRT1 and ETP1/2 in EIN2^{C-term}-degradation under ethylene-depleted conditions. In this scenario, ETP1/2 action would contribute to the degradation of the (erroneously or basally cleaved) C-terminal fragment of EIN2. Such cooperative degradation would have to be assumed since EIN2 is not induced transcriptionally during ethylene signaling (Alonso et al., 1999; Qiao et al., 2009), but the entire pool of EIN2^{C-term} produced from an *EIN2* promoter construct was obviously readily depleted in the presence of a WT *PRT1* allele, as judged from the absence of constitutive ethylene responses in these lines (Fig. 44, 45). Addressing the impact of *ETP1/2* mutation on EIN2^{C-term} stability in protoplasts will be crucial to test this hypothesis of PRT1 and the F-box proteins acting cooperatively. Alternatively, PRT1 action on EIN2^{C-term} could be subject to additional regulation, with mechanisms in place to antagonize PRT1-mediated ubiquitination upon ethylene perception. Therefore, a future challenge will be to investigate the interactions and co-localization of EIN2^{C-term} and PRT1, including their dependences on stimuli, developmental stages, cell types, and post-translational modifications (e.g., Ser-924 phosphorylation), using stable transgenic lines. The identification of specific ethylene-related phenotypes of *prt1* mutants, as outlined above, will additionally help to narrow down appropriate conditions and tissues to be used for these analyses.

Importantly, due to the lack of phenotype complementation in the *ein2-1* mutant by expression of *EIN2^{C-term}*, evidence is missing so far that *EIN2^{C-term}* is generally functional in a *PRT1* WT genotype. Therefore, another priority for subsequent studies will be to test for specific EIN2 CEND responses of this transgenic line in the *ein2-1* mutant background, such as hypocotyl elongation in nutrient starved conditions, or the induction of defense genes like *PLANT DEFENSIN 1.2* in response to JA (Alonso et al., 1999). A failure of *EIN2^{C-term}* to rescue these responses in *ein2-1* would be critical, since this would open up the possibility that a Phe-646 starting fragment is not the right signaling compound produced in plants, but rather constitutes an artificial degron recognized by PRT1. Indeed, cleavage of EIN2 at this specific site has been a matter of debate (Cooper, 2013; Qiao et al., 2013). In previous studies, different variants of *EIN2 CEND* have been expressed in plants, including *EIN2⁴⁶²⁻¹²⁹⁴* (Alonso et al., 1999), *EIN2⁵¹⁶⁻¹²⁹⁴* (Christians et al., 2008), *EIN2⁶³⁸⁻¹²⁹⁴* (Qiao et al., 2012), *EIN2⁴⁵⁹⁻¹²⁹⁴* (Wen et al., 2012), and *EIN2⁶⁵⁴⁻¹²⁷²* (Li et al., 2015). Functionality of all of these constructs was demonstrated by means of the ability to induce specific responses. Evidence for the precise cleavage site between Ser-645 and Phe-646 was provided by a targeted mass spectrometric approach: Here, after treating plants with ethylene, Qiao et al. (2012) quantitatively detected the peptide *EIN2⁶³⁰⁻⁶⁴⁵* which cannot be produced by sole tryptic digest but requires an endogenous proteolytic event giving rise to the C-terminus. Concerns about the correctness of this result were raised from the absence of this peptide in a different (notably: untargeted) proteome analysis (Chen et al., 2011a; Cooper, 2013). Moreover, it was criticized that *in-planta* processed EIN2 C-terminal fragments migrated higher in SDS-PAGE than calculated from the molecular weight of a Phe-646 initiated product (Qiao et al., 2012; Cooper, 2013). Precisely, Qiao et al. (2012) observed a molecular weight discrepancy of about 10 kDa increase that was seen in immunodetections of C-terminal cleavage products of both endogenous EIN2 and an N-terminally fused YFP variant. Strikingly, concerning the latter fusion construct, a very similar behavior in SDS-PAGE was seen within this work for both Met-initiated *EIN2⁶⁴⁷⁻¹²⁹⁴-YFP* and (Phe-initiated) *EIN2^{C-term}-YFP* produced by UFT upon protoplast expression (Fig. 30, 34, 35, S14). Thus, expressing a UFT construct of *EIN2^{C-term}-YFP* which is identical to the proposed *in-vivo* cleavage product of EIN2-YFP serves as *in-vivo* proof for previous postulations (Qiao et al., 2013) that properties of the EIN2 protein (such as post-translational modifications or SDS-binding behavior), rather than an alternative size of the proteolytic product, are responsible for the unexpected migration in SDS-PAGE.

Exposure of Phe-646 of EIN2 *in vivo* would be decisive for PRT1-mediated degradation, as evidenced by *in-vitro* peptide binding and stability assays expressing *EIN2^{C-term}* variants initiated by stabilizing amino acids in protoplasts. Thus, the uncertainty of the true cleavage site constitutes a major flaw to the postulation of PRT1-mediated degradation of EIN2 CEND. However, the imperative requirement of Phe exposure for EIN2-targeting by PRT1 may also serve to finally proof cleavage at this particular site: Having established a robust assay to track *PRT1*-dependent *EIN2^{C-term}* degradation in protoplasts, the system can now be applied to transiently express the constitutively cleaved variants of full-length EIN2 harboring Ser to Ala mutations at residues 645 and/or 924 (Ju et al., 2012; Qiao et al., 2012). If the resulting C-terminal fragment is also destabilized in protoplasts in a *PRT1*-dependent manner, this would be strong evidence for *in-vivo* proteolysis of EIN2 between Ser-654 and Phe-646.

Plants respond to ethylene within a stunningly wide range of concentrations (Chen and Bleeker, 1995; Hua and Meyerowitz, 1998; Chang, 2016). While it is assumed that the high responsiveness is facilitated at the level of the ethylene receptors (Hua and Meyerowitz, 1998; Gao et al., 2008; Grefen et al., 2008; Chen et al., 2010c), *Arabidopsis* also reacts quantitatively to doses of ethylene (Bleeker et al., 1988), and the signaling output of EIN2 is obviously also gradual. One mechanism to balance

ethylene signaling downstream of the receptors appears to be N-end rule dependent degradation of the EIN2 CEND signaling molecule. In previous studies, stability determinants of EIN2 CEND have escaped attention, probably due to the use of constructs of *EIN2 CEND* giving rise to inaccurate N-termini for transgenic expression. Likewise, screens for interaction partners of EIN2 such as the yeast-two-hybrid approach performed by Qiao et al. (2009) must have missed a potential interaction with components of the N-end rule since proper cleavage of EIN2 is not expected to occur in yeast cells. The work presented here provides first evidence that EIN2 indeed contains a potential N-degron that could be important to fine-tune ethylene responses in plants.

4.5 The genetic background of *prt1-1* lines confers cytokinin hyposensitivity in the dark

Upon the search for alterations in the ethylene response of *prt1-1* mutant lines, it was observed that etiolated seedlings of these lines exhibited decreased sensitivity towards exogenously applied BA, a synthetic cytokinin (Fig. 38, 39). During a backcross experiment, it was possible to obtain *prt1-1* homozygous lines that were undistinguishable from the WT in terms of dark-induced hypocotyl elongation in the presence of cytokinin, and the phenotype can therefore be considered a result of the genetic background of the tested lines. Given that the cytokinin hyposensitivity was present in both *prt1-1^{ts}* and the progenitor line N119, it is likely that the phenotype resulted from a second-site mutation that had been introduced during the EMS mutagenesis that gave rise to the *prt1-1* allele (Bachmair et al., 1993). Since the backcross experiment was performed in order to screen for the presence of a different phenotype (male sterility at high temperature) which also segregated independently of the cytokinin hyposensitivity (Fig. S23), no line is available at the moment that shows the cytokinin phenotype in the absence of the *prt1-1* allele. Therefore, it cannot be fully excluded at this point that the combined effect of *PRT1* mutation and a second-site locus is responsible for the observed cytokinin hyposensitivity of *prt1-1^{ts}/N119*. However, given that transgenic expression of N-terminally tagged PRT1 variants under control of an endogenous promoter fragment did not complement the cytokinin hyposensitivity of *prt1-1^{ts}* (Fig. 41), it is rather unlikely that the *prt1-1* allele contributed to this phenotype.

The cytokinin hyposensitivity was mainly pronounced at the level of hypocotyl growth inhibition by BA. Interestingly, cotyledon opening was also sporadically observed on *prt1-1^{ts}* and N119 lines in response to BA (Fig. 38, S23). This hinted at compromised ethylene signaling as the cause for reduced hypocotyl inhibition in these lines, since reduced sensitivity to cytokinin independently of ethylene would rather prevent precocious cotyledon opening (Chory et al., 1994; Hansen et al., 2009; Cortleven et al., 2018). In this case, it would be assumed that the affected locus is involved in signaling dependent on EIN2. Consistent with this assumption, the ability of *prt1-1^{ts}/N119* to inhibit hypocotyl elongation by BA was similar to the *ein2-1* mutant, with a slightly higher responsiveness of *prt1-1^{ts}/N119* compared to *ein2-1* (Fig. 38, 39). Crucially, the response to exogenous ACC was normal in *prt1-1^{ts}/N119* during etiolation (Fig. 39), suggesting that the signal transduction from cytokinin to ethylene might be compromised in dark-grown seedlings of *prt1-1^{ts}/N119*. Since the regulation of ACC production by cytokinins is still poorly understood, the emergence of a new allele affecting this process would provide a valuable resource for future studies. For example, the transcriptional targets of B-type ARR1s that mediate stabilization of ACS enzymes are still elusive (Hansen et al., 2009), and cytokinin was proposed to affect ACS stability through more than one pathway, meaning also

independently of *ETO1/EOLs* (Chae et al., 2003). Next, it is not known whether and how cytokinins might directly impact on 14-3-3 action in *ETO1/EOLs* regulation (Yoon and Kieber, 2013). Including also upstream B-type ARR regulation, all of these processes might potentially be affected by the genetic locus in the background of *prt1-1^{ts}/N119*.

Notably, a number of mutants were previously identified that exhibited inability to produce the triple response specifically in the presence of cytokinin (Vogel et al., 1998b, 1998a). One of these *cytokinin insensitive (cin)* denoted mutants was mapped to the locus of *ACS5*. Therefore, testing the genomic sequences of both *type-2 ACS* genes in the *prt1-1^{ts}/N119* background would be recommendable prior to further experiments. Additionally, the mutation in the *prt1-1^{ts}/N119* background might be allelic with any of the remaining *cin* mutants identified by (Vogel et al., 1998a). Notably, while the phenotype observed in *prt1-1^{ts}/N119* rather suggests a disturbance in ethylene signaling, this would still have to be tested by the assessment of ethylene production, or ACS protein abundance in etiolated seedlings of these lines. Alternatively, misregulation of photomorphogenesis can also result in specific cytokinin-insensitive phenotypes in the dark, and especially the *COP10 (cin4)* locus should be considered in this respect (Vogel et al., 1998a; Cortleven et al., 2018).

4.5.1 Sugar-dependence of cytokinin hyposensitivity in *prt1-1^{ts}/N119*

Intriguingly, the resistance to cytokinin-induced hypocotyl inhibition in the dark observed on *prt1-1^{ts}/N119* was dependent on the presence of sucrose in the growth medium. This observation allows two scenarios for explanation: First, the genetic background of *prt1-1^{ts}/N119* interferes with an inhibitory effect that sucrose exerts on cytokinin-mediated repression of hypocotyl elongation. Second, sucrose promotes photomorphogenesis and this effect is enhanced by cytokinin in a manner dependent on the *prt1-1^{ts}/N119* genotype. Given the known crosstalk between sucrose and cytokinin signaling pathways which will be discussed in the following, the first scenario probably explains the phenotype better.

Sucrose provided exogenously to the growth medium promotes the hypocotyl growth of etiolated *Arabidopsis thaliana* seedlings (Zhang et al., 2010; Kircher and Schopfer, 2012). This effect is specific to sucrose and its constituents glucose and fructose (Zhang et al., 2010), and is dose-dependent since concentrations higher than ~30 mM are inhibitory to seedling dark growth (Kircher and Schopfer, 2012; Kushwah and Laxmi, 2014). Several links have previously been established between sugar and cytokinin signaling. Prominently, the glucose signaling incompetent allele of *HXK1*, *glucose insensitive2 (gin2)*, displays hypersensitivity to cytokinin for shoot regeneration from hypocotyl explants (Moore et al., 2003). Cytokinin signaling mutants on the other hand were shown to be hypersensitive to sugar-induced growth inhibition in the light (Franco-Zorrilla et al., 2005), whereas mutants with constitutive cytokinin responses are more resistant (Moore et al., 2003). This might be mediated via ethylene signaling since ethylene insensitivity and constitutive signaling were also found to induce sugar hypersensitivity and resistance, respectively (Zhou et al., 1998; Gibson et al., 2001; Cheng et al., 2002). In contrast to that, cytokinins act synergistically with sucrose in the regulation of anthocyanin synthesis (Das et al., 2012), a process which is apparently antagonistic to ethylene signaling, since *ein2-1* showed increased anthocyanin accumulation in response to sucrose (Kwon et al., 2011).

In line with the cytokinin hypersensitive phenotype of *gin2*, glucose induces EIN3/EIL1 degradation in a HXK1-dependent manner in protoplasts of maize and *Arabidopsis* (Yanagisawa et al., 2003), and *EIN3/EIL1* transcription was repressed by glucose in sugar-depleted (i.e., dark-incubated) *Arabidopsis* seedlings (Price et al., 2004). Given this relationship, the phenotype of increased hypocotyl growth upon BA and sucrose in *prt1-1^{ts}/N119* could be explained by altered HXK1 function (Fig. 51). However, an increased activity of HXK1 for *EIN3/EIL1* repression would have to be assumed in this scenario, and this would have to be cytokinin-specific. Thus, this explanation would be rather little parsimonious. HXK1-induced *EIN3* repression was assayed by (Yanagisawa et al., 2003) using a luciferase-based reporter system in maize protoplasts, which might be possible to adapt to *Arabidopsis* protoplasts in the presence or absence of cytokinins in order to address a potential effect of the *prt1-1^{ts}/N119* genetic background.

Cytokinins also interact with sugar signaling in regulating the expression of several D-type cyclins to control cell cycle progression (Richard et al., 2002; Riou-Khamlichi et al., 2002; Hartig and Beck, 2006). However, given that dark-induced hypocotyl elongation is mainly achieved via cell expansion, rather than cell division (Gendreau et al., 1997), cell cycle regulation by cytokinin is not expected to impact highly on seedling growth during etiolation.

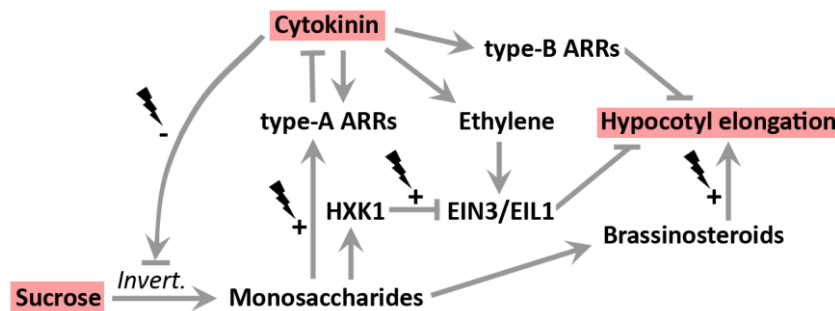


Fig. 51| Connections between sugar and cytokinin signaling and potential implications of the genetic background of *prt1-1^{ts}/N119*. Sucrose from the medium enters root cells either by the subsequent action of cell wall invertases (*Invert.*) and hexose transporters, or by sucrose transporters and vacuolar invertases (Veillet et al., 2016). Of these two pathways, the first one is regulated by cytokinin (Balibrea Lara et al., 2004; Hartig and Beck, 2006), but the effect in hypocotyls of dark-grown *Arabidopsis* seedlings is not clear. In etiolated seedlings, sugars promote hypocotyl elongation via brassinosteroid signaling (Zhang et al., 2015c). Glucose is sensed in the cell primarily by HXK1 (Moore et al., 2003) which represses EIN3/EIL1 in protoplasts and dark-adapted seedlings (Yanagisawa et al., 2003; Price et al., 2004). Next, type-A ARRs are transcriptionally induced by glucose in dark-adapted seedlings establishing another antagonistic link between sugar and cytokinin (Kushwah and Laxmi, 2014). For cytokinin-mediated repression of hypocotyl elongation, ethylene-dependent and –independent pathways via type-B ARRs were furthermore described (refer to the introduction for details). Processes that might potentially be affected by the *prt1-1^{ts}/N119* genetic background causing sucrose-dependent resistance to hypocotyl inhibition by the cytokinin BA during etiolation are indicated by a lightning symbol and +/- for a presumptively promoting or inhibiting effect, respectively.

Importantly, cytokinin signaling also directly impacts on sucrose metabolism by regulating the expression of extracellular invertases required for sugar uptake, but the effect of the regulation differs between tissues and plant species (Balibrea Lara et al., 2004; Hartig and Beck, 2006). Unfortunately, the nature of this regulation has not been addressed in etiolated *Arabidopsis* seedlings so far. Notably, a repressive effect of cytokinin on extracellular invertases was observed in tobacco (*Nicotiana tabacum*) root cell culture (Hartig and Beck, 2006), and a defect in cytokinin-

mediated repression of sugar uptake in *Arabidopsis* roots would be consistent with increased sucrose-promotion of hypocotyl elongation in *prt1-1^{ts}/N119*. Thus, to test whether extracellular sucrose metabolism is affected in *prt1-1^{ts}/N119* during etiolation in the presence of cytokinin, it would be necessary to analyze whether the phenotype is still observed upon application of glucose in this assay.

Transcript analyses in dark-incubated seedlings furthermore revealed an up-regulation of type-A ARR by glucose, suggesting a direct mechanism of cytokinin repression by sugar (Kushwah and Laxmi, 2014). Indeed, a type-A ARR sextuple mutant showed markedly reduced hypocotyl growth promotion by one percent glucose during etiolation compared to the WT (Kushwah and Laxmi, 2014). As in the case of HXK1 function, a gain of glucose-mediated type-A ARR activation would be required to explain the phenotype of *prt1-1^{ts}/N119*. Transcript analyses of type-A ARRs in etiolated seedlings of *prt1-1^{ts}/N119* would help to address this possibility.

The enhancing effect of sucrose on hypocotyl elongation during etiolation was found to depend mainly on brassinosteroid signaling in *Arabidopsis* seedlings (Zhang et al., 2010, 2015c). This is consistent with brassinosteroids promoting hypocotyl growth via the transcription factor BRASSINAZOLE-RESISTANT1 (BZR1) exclusively in the dark (Wang et al., 2002b; He et al., 2005). Given that BZR1 action is tightly linked to PIF4 (Oh et al., 2012), and PIF genes were described to govern seedling growth responses to sucrose (Stewart et al., 2011), it is likely that PIF signaling is also involved in this pathway. Thus, it would be worth testing whether *prt1-1^{ts}/N119* exhibits a brassinosteroid hypersensitive phenotype in the triple response, and whether the combination of cytokinin treatment with inhibitors of brassinosteroid biosynthesis restores WT-like growth patterns.

Since altered brassinosteroid signaling in *prt1-1^{ts}/N119* would open up the question why cytokinin is required to produce the phenotype, growth regulation might be more complex in this mutant. Synergistic effects occur between brassinosteroid and auxin signaling in hypocotyl elongation in the light and dark (Nemhauser et al., 2004; Oh et al., 2014). Conceivably, a slightly altered auxin response in *prt1-1^{ts}/N119* could become visible only upon exposure to the antagonist cytokinin. In fact, an analysis of cytokinin-glucose crosstalk during etiolation also revealed that cytokinin repression of hypocotyl elongation depended on *AUXIN RESISTANT 2/IAA7 (AXR2/IAA7)*, a repressor of auxin-inducible gene expression (Kushwah and Laxmi, 2014). However, glucose-dependent growth promotion was not affected in the respective mutant, and neither were other auxin signaling mutants like *tir1*, *axr1*, or *axr3* (Kushwah and Laxmi, 2014), indicating that sucrose induces hypocotyl growth during etiolation directly via brassinosteroids, and supporting that auxin and brassinosteroids can act independently in hypocotyl growth regulation (Reed et al., 2018). However, to further decipher how exogenous sucrose impacts specifically on cytokinin signaling during etiolation, it would be interesting to test if *prt1-1^{ts}/N119* shows hypersensitivity to auxin in the triple response, and whether this is promoted by sucrose.

To date, many aspects of cytokinin hormonal crosstalk have been investigated, and cytokinin signal integration with metabolic cues is increasingly recognized also in crop research (Corot et al., 2017; Jarret et al., 2018; Lupi et al., 2019). The fact that darkness and sugar supply constitute rather paradox signals in plants, would actually suggest colliding adaptational pathways. Changes in the genetic background of the *prt1-1^{ts}/N119* lines might help to understand in the future how these signals are nevertheless integrated in plants to allow for optimal growth even under unconventional conditions. However, given that two independent phenotypes were identified in the *prt1-1^{ts}* mutant

line within this work, these findings also urge the question whether previous efforts towards the identification of physiological processes associated with the *PRT1* gene might have been hampered by the masking of respective phenotypes in the currently sole available mutant line, due to the impact of background mutations.

5. Conclusions

The plant N-end rule pathway regulates physiological processes through context-dependent protein degradation. In recent years, much attention was paid to the regulation of MC-starting members of the ERFVII group of transcription factors which become destabilized through N-terminal processing by the subsequent action of MetAPs, ATEs, and PRT6. Within this work, new insight was gained into the substrate recognition determinants of ATE1 and PRT6, and first evidence was provided for the N-end rule-targeting of endopeptidase cleavage products by the type II N-recognin PRT1.

During a phenotypical characterization of the *prt1-1* mutant, alterations of the genetic background of this line became apparent with complex physiological implications. First, a defect in male gametogenesis of the descendant line *prt1-1^{ts}* was attested that was conditional for a moderately elevated temperature and resulted in complete sterility of the plant. Morphological and histological analyses revealed that pollen development was impaired after the post-meiotic release of microspores. Progression of microspore degeneration in *prt1-1^{ts}* resembled the defects observed in mutants with tapetum malfunctions, or impaired sister chromatid cohesion during meiosis. Alterations in the gene expression of several plant hormones, as well as genes involved in cell wall maturation, confirmed that microspore to pollen transition was affected at various levels in *prt1-1^{ts}*. Next, a hyposensitivity to cytokinin was observed during etiolation caused by the genetic background of *prt1-1* mutant lines. The phenotype is unprecedented in its conditionality on exogenously provided sucrose, and might be induced by a misregulation of cytokinin crosstalk with ethylene and other plant hormones. Both (independent) phenotypes found in the background of *prt1-1* mutant lines could provide valuable genetic resources for future investigations of plant reproduction, or development under stress conditions. On the other hand, in the light of the observations described here, phenotypes previously attributed to the *prt1-1* mutation might require re-assessment using independent alleles.

Using peptide-based approaches, *in-vitro* substrate specificity was furthermore assessed for components of the Arg/N-end rule of *Arabidopsis*. In SPOT peptide arrays, a physical interaction of the PRT6 UBR domain with peptides mimicking the arginylated N-terminus of members of the ERFVII transcription factors was demonstrated. Binding assays furthermore confirmed functional conservation of UBR^{PRT6} with UBR domains from mammals and yeast in terms of substrate specificity, but potentially excluded recognition of the proteolytic middle fragment of RIN4 by PRT6. In contrast, *in-vitro* arginylation of artificial peptides by ATE1 was proven for sequences mimicking both the neo-N-termini of ERFVII transcription factors, and RIN4. Crucially, it could be shown that ATE1 is able to act directly downstream of PCOs on Cys-initiated substrate peptides *in vitro*, confirming PCOs at the top of a fully enzymatic oxygen sensing cascade.

As opposed to PRT6, little is known on the second plant N-recognin, PRT1, which targets type II N-degrons. Within this work, E3 Ub ligase activity was confirmed for PRT1 by the *in-vitro* reconstitution of autoubiquitination. Strikingly, ubiquitination depended on both RING domains of PRT1, suggesting a mechanism distinct from other E3s with multiple RING domains. In peptide binding assays, substrate specificity of PRT1 was furthermore deciphered hinting at similarity with the binding mode performed by certain ClpS proteins. Intriguingly, *in-vitro* peptide binding indicated strong affinity of PRT1 towards the neo-N-termini of both the organ growth regulator BB, and the ethylene signaling component EIN2, which are produced by endopeptidase activities in physiological contexts. In the case of EIN2, *PRT1*-dependent degradation of the respective protein fragment, EIN2^{C-term}, could be

proven in *Arabidopsis* protoplasts. The destabilization of EIN2^{C-term} furthermore depended on the nature of its N-terminal Phe, consistent with an N-end rule mediated interaction. While physiological consequences of EIN2^{C-term} accumulation caused by *PRT1* mutation remain to be identified, constitutive expression of EIN2^{C-term} brought about signs of ethylene signaling in plants of the *prt1-1* mutant genotype. So far, how EIN2 signaling is abolished to terminate ethylene responses was not known. The work presented here suggests that the N-end rule via PRT1 contributes to releasing the cell from signaling following hormone perception.

6. Materials and Methods

6.1 Plant growth conditions

Plants were grown on a steamed (3 h, 90°C) soil mixture composed of a clay substrate with coco fibers (Einheitserde® CL Ton Kokos, Cat.-No. 10-00800, Einheitserdewerke Patzer, Gebr. Patzer, Sinntal, Germany), and 25% (w/w) Vermiculite (2/3 mm grain size, Cat.-No. 29.060220, Gärtnereibedarf Kammlott, Erfurt, Germany). For plant propagation in the greenhouse, 300-400 g/m³ of the insecticide mixture Exemptor (10% (w/w) Thiacloprid; Hermann Meyer, Rellingen, Germany) were added. Seeds were spread on soil and dark incubated for three days of stratification at 4°C prior to transfer to phytochambers (Johnson Controls, Milwaukee, USA) with growth conditions set to 21°C and 60% relative air humidity at a short day light regime (8 h light, 16 h dark; light intensity 90-107 µE). After 10-15 days, plants were pricked, and either kept at the same short-day growth conditions, or transferred to growth cabinets (models AR-66L2 or AR-66L3; Percival Scientific, Perry, USA) with a long-day light regime (16 h light, 8 h dark; 113-173 µE), 55-65% relative air humidity, and temperatures specified for each experiment. For propagation, plants were transferred to a temperature-controlled (19°C) greenhouse.

For seedling analyses, seeds were surface-sterilized by exposure to chlorine gas produced from a 2:1 mixture of sodium hypochlorite solution (12% Cl; Carl Roth, Karlsruhe) and 37% hydrochloric acid (VWR International, Radnor, USA) in a closed container for 35-45 min. Sterilized seeds were placed in petri dishes on solidified 1x strength Murashige & Skoog (MS) media containing 4.4 g/l MS salts including vitamins (Cat.-No. M0222.0025; Duchefa Biochemie, Haarlem, Netherlands), 0.8% phyto agar (Cat.-No. P1003; Duchefa Biochemie), 0.5% (w/v) sucrose, 0.05% (w/v) 2-(N-Morpholino)-ethane sulfonic acid (MES) (Carl Roth), and KOH to pH = 5.6-5.8. The plates were sealed with Leukopor® tape (BSN medical; Hamburg, Germany), and stratified in the dark at 4°C for 2-4 days. Subsequently, plates were transferred to phytochambers with a long-day light regime (90-95 µE), and a 21°C temperature set point.

6.2 Plant material

If not indicated otherwise, Col-0 (CS60000) was used as the WT and was provided by N. Dissmeyer. A list of the used mutant genotypes is presented in Tab. 1. The sequences of oligonucleotide primers used for genotyping are presented in Tab. S3. For genotyping the *prt1-1* allele, primers prt1-1_fw and prt1-1_rev were used, and the 180 bp PCR product was subjected to *Mnl*I (Cat.-No. FD1074; Thermo Fisher Scientific, Waltham, USA) digestion yielding a 144 bp in the WT situation which is prevented by the *prt1-1* allele. A 3.6% agarose (Cat.-No. A8963; AppliChem, Darmstadt, Germany) gel was employed for electrophoretic separation of the products. For genotyping *prt1-2*, primers PRT1_UTR_fw and PRT1_Exon3_rev were used to amplify the WT sequence, and primer combinations of PRT1_UTR_fw with SALK_LB, SALK_LB2, and RB_SALK were tested to amplify the T-DNA. For *prt1-7*, the WT sequence was amplified using PRT1_UTR_fw/PRT1_Exon3_rev, and the T-DNA fragment using SAIL_LB1/PRT1_Exon3_rev. *prt1-9* was genotyped with PRT1_upstream_fw/PRT1_Exon1_rev (WT sequence) and SAIL_LB1/ PRT1_Exon3_rev (T-DNA). For *prt1-11*, primers PRT1_upstream_fw/PRT1_Exon1_rev (WT sequence) and PRT1_upstream_fw/SALK_LB (T-DNA) were used.

Genotyping of *ein2-1* (N3071) using primers *ein2-1_dCAPS_fw* and *ein2-1_dCAPS_rev* was described previously (Resnick et al., 2006), and for restriction of the *BsrBI* site, *Mbil* (Cat.-No. FD1274, Thermo Fisher Scientific) was employed. The restriction products were separated by 3.6%-agarose gel electrophoresis.

The *prt1 ein2* double mutant was created by crossing *prt1-1^{ts}* (female) and *ein2-1* (male). Next, the transgenic line carrying *pSL34::proEIN2::genEIN2-eGFP* (where *genEIN2* denotes the genomic locus sequence of *EIN2*) was received from Y. Ikeda and M. Grebe, and crossed into the *prt1-1^{ts}* mutant background. Due to the presence of the transgene, it was not possible to screen for homozygosity of the *ein2-5* allele, but the presence of the mutant allele was confirmed by PCR.

For genotyping the *ein2-5* locus, primers *ein2-5_wt_fw/ein2-5_rev* were applied to amplify the WT sequence, and *ein2-5_del_fw/ein2-5_rev* to amplify the mutant (Δ CATGACT) sequence. Both reactions were performed with a primer annealing temperature of 60°C. Reactions to amplify the EIN2-eGFP transgene were primed using *EIN2_Exon7_fw* and *eGFP_rev*.

Tab. 1 | Mutant genotypes used in this work. NASC ID, NASC identifier; AGI, *Arabidopsis* genome identifier; Alt. name, Alternative name.

NASC ID	AGI	Name	Alt. name	Background	Source
N/A	AT3G24800	<i>prt1-1/ prt1HygS</i>	N/A	Col-0	A. Bachmair
N119	AT3G24800	4H Proteolysis	4H <i>prt1-1</i>	Col-0	NASC
N586253	AT3G24800	SALK_086253	<i>prt1-2</i>	Col-0	NASC
N876723	AT3G24800	SAIL_772_D04	<i>prt1-7</i>	Col-0	NASC
N851857	AT3G24800	WiscDsLox340E05	<i>prt1-8</i>	Ler	NASC
N870226	AT3G24800	SAIL_20_H03	<i>prt1-9</i>	Col-0	NASC
N/A	AT3G24800	FLAG_496F01 / FLAG_533F12	<i>prt1-10</i>	Ws-4	INRA-IJPB Versailles
N665056	AT3G24800	SALK_127481C	<i>prt1-11</i>	Col-0	NASC
N3071	AT5G03280	ethylene insensitive	<i>ein2-1</i>	Col	NASC
N16707	AT5G03280	<i>ein2-5</i> DR5:GUS	N/A	Col	NASC
N/A	N/A	<i>pSL34::proEIN2::genEIN2- eGFP</i>	N/A	<i>ein2-5</i>	Y. Ikeda/M. Grebe

6.3 Hormone treatments

6.3.1 Triple response assays

ACC stock solutions were prepared at 10 mM in 10% aqueous ethanol and stored at -20°C. Surface-sterilized seedlings were aligned on standard MS agar plates including ACC (Cat.-No. A3903; Sigma-Aldrich, St. Louis, USA) at the concentrations indicated in the experiment, or a corresponding volume of mock solution (10% aqueous ethanol). In the case of BA treatments within triple response assays, BA (Cat.-No. A7685,0001; AppliChem) was added to the medium at the indicated concentrations

from a 1 mg/ml stock solution in 25% aqueous DMSO (which was prepared freshly from a 4 mg/ml BA stock solution in DMSO stored at -20°C). 25% aqueous DMSO was applied as the mock solution. Where applicable, sucrose was excluded from the medium during BA experiments. Seeds were stratified in the dark at 4°C for 5 days, transferred to control growth conditions (21°C, 90-95 µE) in vertical position for 6 to 9 hours, and subsequently wrapped in aluminum foil, and grown vertically in the dark for additional 87 to 88 hours.

For BA treatments of seedlings in the light, the indicated amounts of BA were included in MS growth medium containing agar. Seeds were stratified for 5 days at 4°C in the dark, and subsequently grown vertically for 8 days under control conditions (21°C, 90-95 µE).

6.3.2 Auxin treatments of inflorescences

Auxin treatments of flowers were performed as described by Sakata et al. (2010). WT and *prt1-1^{ts}* mutant plants were grown at 28°C. Three to five days after opening of the first flowers, inflorescences were sprayed with an aqueous solution of 1 µM NAA (Cat.-No. N0640; Sigma-Aldrich) and 0.1% (v/v) DMSO. This was made from a freshly prepared stock solution of 1 mM NAA in DMSO. In order to test for rescue by auxin application, a single application event and observation for two weeks was performed as described by Sakata et al. (2010), as well as repeated spraying every two to three days during three weeks.

6.4 Histological analyses

6.4.1 PEG embedment of flowers

PEG embedment of flowers was performed according to Hause et al. (1996) and Isayenkov et al. (2005). Of each WT and *prt1-1^{ts}* mutant plants, more than ≥15 adult flowers, or three to four young inflorescences (for younger flower stages) grown at 28°C were harvested into 5 ml glass vials containing 4% para-formaldehyde (Cat.-No. 104005; Merck Millipore) and 0.1% Triton X-100 in phosphate buffered saline (PBS) (135 mM NaCl; 3 mM KCl; 1.5 mM KH₂PO₄; 8 mM Na₂HPO₄; pH 7.0-7.2), and vacuum infiltrated for 15 minutes. After an incubation time of 2 hours at room temperature to allow for fixation, the samples were washed twice 15 minutes with PBS under rotation. Samples were subsequently dehydrated by washing steps in PBS containing gradually increasing proportions of ethanol (30 min in 10% ethanol, 60 min in 30% ethanol, 60 min in 50% ethanol, overnight in 70% ethanol, 30 min in 90% ethanol, 30 min in 100% ethanol) under rotation and room temperature. This was followed by 30 min incubation in ethanol at 55°C. Subsequent PEG 1500 (Cat.-No. 807489; Merck Millipore) embedment was performed at 55°C by each 1 hour subsequent incubations in PEG solutions containing 25% (w/v), 50%, and 75% PEG in ethanol. Finally, the solution was replaced by pure liquefied PEG and the samples were incubated for 1 hour, and subsequently 1 hour without vial lids at 55°C. The samples were hardened at room temperature overnight, and the vials containing specimens were stored with closed lids at 4°C until use. The PEG-embedded specimens (blocks) were sectioned to slides of 4 µm using a HM 325 rotary microtome (Microm™, Thermo Fisher Scientific™), and transferred to poly-L-Lys coated microscope slides (see below).

6.4.2 Poly-L-Lys coating of sample slides

Clean microscope slides (Cat.-No. 1879; Carl Roth) were covered with 60 µl of poly-L-Lys solution (Cat.-No. P8920; Sigma-Aldrich), and two slides were apposed face-to-face in order to allow spreading of the liquid film. After incubation for 45 min at room temperature, the slides were separated in a water bath, placed vertically in a rack, washed 3 times 5 min with water and dried at room temperature for subsequent storage at 4°C.

6.4.3 Safranin O/astra blue stainings of microsections

Each 100 µl of 0.5% aqueous safranin O solution (Cat.-No. 12284; Armin Baack, Schwerin, Germany) and astra blue solution in 2% tartaric acid (Cat.-No. 11812; Armin Baack) were mixed and applied to a microscope slide bearing specimens. This was carefully covered with another microscope slide to disperse the liquid, and incubated for 5 minutes at room temperature. Unspecific dye was washed off in an ethanol bath, followed by a PBS bath. Samples were covered with PBS containing 50% glycerol, and sealed with a cover glass using nail polish.

6.4.4 Preparations of microspore and pollen fractions

Microspores and pollens were prepared according to Borges et al. (2012). In brief, young inflorescences containing closed flower buds (approximately 20 ml) were harvested and gently ground with mortar and pestle in 10 ml of pollen extraction buffer (PEB) (10 mM CaCl₂; 2 mM MES, pH 7.5; 1 mM KCl; 1% (w/v) H₃BO₃ (w/v) (Cat.-No. 50765; Euromedex, Souffelweyersheim, France); 10% (w/v) sucrose). The extract was filtered through Miracloth (Calbiochem, Merck Millipore), and transferred to 15 ml conical tubes for centrifugation at 800 RCF, 5 min. The pellet containing microspores and pollen grains was resuspended in 500 µl of PEB. Samples of this suspension were transferred to microscope slides for analysis. Microspores and mature pollen grains appeared in different focus areas.

6.4.5 Pollen tube growth assays

Analysis of pollen fitness by *in-vitro* germination was performed using a protocol that was modified from (Fan et al., 2001). Here, an agar-solidified germination medium was prepared in a petri dish by mixing 1% (w/v) Phytoagar (Duchefa) with pollen germination medium (5 mM MES, pH 5.8 using Tris; 0.5 mM KCl; 10 mM CaCl₂; 0.8 mM MgSO₄; 1.5 mM H₃BO₃; 10 µg/ml myo-inositol (Cat.-No. 57570; Fluka, now: Sigma-Aldrich); 16.6% (w/v) sucrose; 3.65% sorbitol). The agar-suspension was heated up to 100°C for 2 minutes, and a thin layer was poured into a petri dish using 1.5 to 2.25 ml per dish. After the medium had chilled, pollen was transferred to the plates by brushing dehiscent anthers over the sticky surface. The petri dishes were placed in a transparent wet chamber, and incubated in the light at 28°C for 6 hours or overnight.

For GUS staining of germinated pollen, the protocol was further modified according to Li (2011). Here, 20 to 50 freshly opened flowers were collected into 1.5 ml tubes, and desiccated at room

temperature for 30 minutes. Subsequently, 1 ml of modified pollen germination medium (containing only 5% sucrose and 15% PEG4000) was added to the samples and pollen was released by vortexing at maximal speed for 1 minutes. After centrifugation at 500 RCF and room temperature for 5 min, the supernatants including floating flowers were removed, and the pollen pellets were resuspended in 1 ml of germination medium by vortexing. Pollen was subsequently germinated by overnight incubation at 25°-28°C.

6.4.6 GUS histological staining

GUS staining of plant material was performed according to Kim et al. (2006). Here, seedlings or plant organs grown under control conditions were harvested into 6-well microtiter plates containing ice-cold harvesting solution (90% (v/v) aqueous acetone). After harvesting, samples were washed once with 100 mM sodium phosphate buffer (NaH₂PO₄/Na₂HPO₄; pH 7.0), and subsequently vacuum infiltrated for 30 minutes in GUS staining solution (100 mM sodium phosphate buffer, pH 7.0; 1 mM K₄[Fe(CN)₆]; 1 mM K₃[Fe(CN)₆]; 1 mM X-Gluc (obtained from X-Gluc DIRECT on <https://www.x-gluc.com/>); 0.1% (v/v) Triton X-100). For GUS staining of germinated pollen grains, the germination medium was removed from the reaction tubes containing germinated pollen, and was directly replaced by GUS staining solution for vacuum infiltration. Plant organs, seedlings, or pollen samples were subsequently incubated in GUS staining solution at 37°C for 4 hours (reporter lines with *proATL9::GUS*), or overnight (samples derived from other GUS-reporter lines). For destaining and fixation, the staining solution was replaced by fixation solution (90% (v/v) ethanol; 10% (v/v) acetic acid), and the samples were incubated for 4 hours under rotation at room temperature. During the incubation time, the fixation solution was replaced once. For storage and analysis, samples were transferred to 70% (v/v) aqueous ethanol.

6.5 Microscopy

GUS stained seedlings were analyzed using a Stemi 2000-c stereo microscope (Carl Zeiss, Oberkochen, Germany) in combination with an AxioCam ICc 3 (Carl Zeiss) camera and a TV2/3" C 0,63X 1069-414 (Carl Zeiss) camera adapter. AxioVision Release 4.7 (Carl Zeiss) was used as the software.

For the microscopy of flower and anther thin sections, flowers (Fig. 9), siliques (Fig. 10), and pollen tubes, an AZ100 stereo microscope (Nikon Instruments, Tokyo, Japan) with a Digital Sight DS-U3 camera controller (Nikon) was used in combination with a DS-Fi1c camera (Nikon), and a 0.6x camera adapter (Nikon). The NIS-Elements software (Nikon) was applied as the software.

For microscopy of protoplasts and seedling roots or pollen of transgenic plant lines, a LSM 780 confocal microscope (Carl Zeiss) equipped with a LD C-Apochromat 40x/1.1 W Corr M27 objective (Carl Zeiss) in combination with the ZEN2.3 SP1 Rel. 14.0.0.0 software (Carl Zeiss) was used. The following excitation and emission settings were applied: GFP: EX488 nm, EM496-524 nm; YFP: EX488 nm, EM510-560 nm; mCherry: EX594 nm, EM600-640 nm.

For imaging microspore preparations, an Axioplan 2 imaging microscope (Zeiss) was used with the AxioCam MRm camera (Zeiss) and ZEN software (Zeiss).

6.6 Plasmid construction

Cloning success was monitored by endonuclease digestion using at least two independent restriction enzymes, and following PCR amplification steps, sequences were checked by external sequencing at Eurofins Scientific (Brussels, Belgium). If not indicated otherwise, cloning was performed in *E. coli* strains Dh5 α or Top10. All primer sequences used for cloning purposes are listed in Tab. S4.

Most constructs were created by use of the Gateway™ technology (Invitrogen, Thermo Fisher Scientific, Waltham, USA). To this end, a PCR product flanked by attB-sites was amplified by PfuX7 Polymerase (Nørholm, 2010), and purified from an agarose gel using the GeneJET Gel Extraction Kit (Cat.-No. K0832; Thermo Fisher Scientific). Plasmids were purified using the GeneJET Plasmid Miniprep Kit (Cat.-No. K0502; Thermo Fisher Scientific), and DNA concentrations were measured with a plate-reader photospectrometer (Infinite F200 PRO; Tecan, Männedorf, Switzerland). BP and LR reactions were performed with Gateway™ BP Clonase™ II Enzyme mix (Cat.-No. 11789020; Thermo Fisher Scientific) and Gateway™ LR Clonase™ II Enzyme mix (Cat.-No. 11791100; Thermo Fisher Scientific) according to the manufacturer's instructions, but with half total reaction volumes and additional reductions of the respective clonase enzyme mixes. The composition of the BP and LR reaction mixtures is presented in Tab. 2.

Tab. 2 | Compositions of BP and LR reaction mixtures. TE buffer: 10mM Tris-HCl, pH 8.0; 1mM EDTA.

BP reaction		LR reaction	
attB-PCR product (7.5-75 ng)	0.5-3.5 μ l	Entry Clone (25-75 ng)	0.5-3.5 μ l
pDONR vector (150 ng/ μ l)	0.5 μ l	Destination Vector (150 ng/ μ l)	0.5 μ l
TE buffer	to 4 μ l	TE buffer	to 4 μ l
BP clonase II enzyme mix	0.5 μ l	LR clonase II enzyme mix	0.25 μ l

Following overnight incubation at room temperature (22°C), 0.5 μ l of Proteinase K (provided with the clonase enzyme kits) was added to the reactions, the mixture was incubated for 0.5-3 hours at 37°C, cooled down on ice, and subsequently transformed into *E. coli* cloning strains.

6.6.1 Destination vectors

All promoter constructs were cloned to yield Destination vectors containing the Gateway™ cassette (GW) behind the promoter sequence by replacing the *Ascl/XhoI* fragment of pAM-PAT-ProCDKA;1-GW (*Addgene* plasmid #79750; Nowack et al., 2006). Ligation was performed using T4 DNA Ligase (Cat.-No. EL0011; Thermo Fisher Scientific) according to the manufacturer's instructions. The promoter sequences of *PRT1*, *ATL9*, and *EIN2* were amplified from Col-0 genomic DNA (gDNA) using primers proPRT1_fw/proPRT1_rev, proATL9_fw/proATL9_rev, and proEIN2_fw/proEIN2_rev, respectively. The final vector pAM-PAT-proPRT1 ^{Δ CTCT}-GW (lacking CTCT in the 3' region of the promoter due to amplification problems of a repetitive sequence) is listed on *TAIR* with the stock number CD3-2396.

To construct pAM-PAT-ProUBQ10 GW (*Addgene* #79751), a plasmid that contained the *UBQ10* promoter (generated and kindly provided by Stefan Pusch¹ (Pusch et al., 2011)) was used as a template to amplify the *UBQ10* promoter sequence using the primer pair

¹ German Cancer Research Center, 69120 Heidelberg, Germany

(proUBQ10_fw/proUBQ10_rev). The PCR product was subsequently cloned into the *Ascl*/*Xho*I sites of pAM-PAT-ProCDKA;1-GW (Addgene plasmid #79750; Dissmeyer and Schnittger (2011)), yielding pAM-PAT-ProUBQ10 GW (Addgene #79751). All destination vectors were cloned using *E. coli* DB3.1.

6.6.2 PRT1 expression vectors

For expression of *PRT1-3HA* from *p35S*, a Gateway® Entry Clone containing the CDS of *PRT1* plus a 17 bp Kozak sequence (GCTTAGCCGCCATGGGA) upstream of ATG was provided by C. Naumann, and recombined with pAM-PAT-p35S::GW-3HA (Bernoux et al., 2008). Primers used by C. Naumann to amplify the BP product were PRT1_kozak_ss and PRT1new_as.

3HA-PRT1 was constructed by fusion PCR. To this end, the 3HA-tag was amplified using primers Fw_HA and Rev_HA-PRT1 from plasmid pENTR-K2-GUS (obtained from F. Faden), and *PRT1* was amplified from plasmid pAM-PAT-p35S::PRT1-3HA using Fw_PRT1 and Rev_PRT1+stop. Subsequently, fusion PCR of both PCR products was conducted using primers Fw_attB1-HA and Rev_attB2-PRT1. The fusion product was used in a BP reaction with pDONR 201 (Invitrogen) to yield pEN-3HA-PRT1, and the BP product was used in LR reactions with pAM-PAT destination vectors bearing the requested promoter sequences (i.e., pAM-PAT-ProUBQ10 GW, pAM-PAT-proPRT1^{ΔCTCT}-GW, and pAM-PAT-proEIN2-GW). pEN-3HA-PRT1 was furthermore subjected to site-directed mutagenesis to obtain pEN-3HA-PRT1^{V28A}, pEN-3HA-PRT1^{C29A}, and pEN-3HA-PRT1^{C195A} (see below, chapter 6.7.5).

PRT1 was also cloned as the genomic locus sequence including the 5' UTR followed by a C-terminal quadruple-Gly linker and a 3HA-tag. For this purpose, the *genPRT1* sequence was amplified from gDNA with primers attB1-genPRT1_fw and HA-genPRT1_rev, and the 3HA-tag was obtained from pEN-3HA-PRT1 using primers genPRT1-HAT_fw and attB2-HAT_rev. Due to amplification problems which were already encountered during amplification of the *PRT1* promoter, the sequence of *genPRT1* in the final vector contained a deletion of "CT" within a repetitive sequence of the 5' UTR. Fusion-PCR was performed with attB1-genPRT1_fw and attB2-HAT_rev. The PCR product was recombined into pDONR 201 and subsequently subjected to LR reaction with pAM-PAT-proEIN2-GW.

To create *GFP-PRT1* expression vectors, *mGFP5* was amplified including a C-terminal Ser-Ala linker from pEarleyGate 103 (Earley et al., 2006) using primers attB1_mGFP5_fw and mGFP5_rev, and *PRT1* was amplified from pEN-3HA-PRT1 (WT, C29A, or C195A) with primers GFP-PRT1_fw and Rev_PRT1+stop. Subsequent fusion-PCR employed primers attB1_mGFP5_fw and Rev_attB2-PRT1, and these products were used in BP reactions with pDONR 201. LR reactions were performed with pAM-PAT-proUBQ10 GW or pAM-PAT-proPRT1^{ΔCTCT}-GW Destination Vectors.

For BiFC assays, a plasmid for expression of C-terminally YFP^N-tagged *PRT1* (pUBC-YFP^N-PRT1) was kindly provided by C. Naumann. Alternatively, pEN-3HA-PRT1 and pEN-3HA-PRT1^{V28A} were recombined with pUBN-YFP^N-Dest (Grefen et al., 2010), to obtain WT and V28A variants of pUBN-YFP^N-3HA-PRT1.

For expression of *PRT1* with N-terminal 8xHis^NMBP tag in *E. coli*, an Expression Clone carrying the *PRT1* CDS with a 5' recognition sequence of the Tobacco Etch Virus (TEV) protease in pVP16 (Clontech Laboratories, Mountain View, USA) was provided by C. Naumann (Naumann et al., 2016). For the

production of the mutated variants of *PRT1*, an Entry Clone containing the *PRT1* CDS with the TEV recognition sequence at the 5' end (pEN-TEV-PRT1) was received from C. Naumann (cloning of this Entry Clone is described in Mot et al. (2018)), and was subjected to site-directed mutagenesis (see below). The modified Entry Clones were recombined with pVP16. For N-terminal GST-tagged variants, the same Entry Clones were recombined with pDEST™15 Vector (Invitrogen). For expression of PRT1 variants from pVP16, *E. coli* BL21 (DE3) was used as the expression strain, and pDEST™15 constructs were expressed in *E. coli* Rosetta™ 2(DE3)pLysS (a kind gift of M. Trujillo).

6.6.3 EIN2 expression vectors

To express a UFT construct of EIN2⁶⁴⁶⁻¹²⁹⁴ with a C-terminal Myc-YFP^C tag, a plasmid containing the sequence of a synthetic codon-optimized Ub (Faden et al., 2016) with Lys to Arg exchanges at positions K29 and K48 fused to the CDS of EIN2⁶⁴⁶⁻¹²⁹⁴ (pEN-Ub^{K29,48R}-EIN2⁶⁴⁶⁻¹²⁹⁴) was kindly provided by C. Naumann, and used as a PCR template. Primers attB1-Ub and EIN2-myc_rev were used for amplification. The Myc-tag was amplified from vector pE-SPYNE-GW (Schütze et al., 2009) using primers EIN2_myc_fw and attB2_Myc_noS, and both PCR fragments were fused by PCR using primers Ub_fw and Myc_rev. Subsequently, an adapter PCR primed by attB1_Ub and attB2_Myc_noS was conducted, and the product was subjected to BP reaction with pDONR 201, to yield pEN-Ub^{K29,48R}-EIN2⁶⁴⁶⁻¹²⁹⁴-Myc. Phe-646 (TTC) of EIN2⁶⁴⁶⁻¹²⁹⁴ was subsequently changed to Gly (GGT) by site-directed mutagenesis (see below), and both Entry Clones (containing EIN2⁶⁴⁶⁻¹²⁹⁴ or Gly-EIN2⁶⁴⁷⁻¹²⁹⁴) were recombined with pUBC-YFP^C-Dest (Grefen et al., 2010).

To create the BiFC construct pUBC-YFP^C-3HA-Ub^{K29,48R}-EIN2^{C-term}-3HA, an Entry Clone was first constructed by PCR fusion of 3HA (amplified from a plasmid containing the K2 construct (Faden et al., 2016) using primers Kozak-HAT_fw/HAT_rev_1), and Ub^{K29,48R}-EIN2⁶⁴⁶⁻¹²⁹⁴ (amplified from pEN-Ub^{K29,48R}-EIN2⁶⁴⁶⁻¹²⁹⁴ using primers Ubiq_fw/EIN2-KpnI-Ascl_rev; primer EIN2-KpnI-Ascl_rev leads to the 3' addition of sequential *KpnI* (FD0524, Thermo Fisher Scientific) and *Ascl* restriction sites). Fusion PCR was performed using primers Kozak-HAT_fw/EIN2-KpnI-Ascl_rev. The fusion PCR product was subjected to an adapter PCR using attB1_Kozak/attB2_EIN2, and recombined into pDONR 201 to yield pEN-3HA-Ub^{K29,48R}-EIN2⁶⁴⁶⁻¹²⁹⁴-KpnI-Ascl. This Entry Clone was used in mutagenesis PCR to create pEN-3HA-Ub^{K29,48R}-Gly-EIN2⁶⁴⁷⁻¹²⁹⁴-KpnI-Ascl. Both constructs were subsequently ligated with KpnI-3HA-Ascl (including a [Gly-Ala]₂ linker in front of the 3HA sequence) which was amplified from K2 using primers GAGA-HAT_fw/HAT_rev2. Ligation was performed using T4 DNA Ligase (Cat.-No. EL0011; Thermo Fisher Scientific) according to the manufacturer's instructions, and resulted in Phe- and Gly variants of pEN-3HA-Ub^{K29,48R}-EIN2^{C-term}-3HA. These Entry Clones were recombined with pUBC-YFP^C-Dest to create the final constructs. In an alternative BiFC assay, the above described plasmid variants of pUBC-YFP^C-Ub^{K29,48R}-EIN2^{C-term}-Myc were used.

For Ub-EIN2^{C-term}-YFP constructs, the CDS of EIN2⁶⁴⁶⁻¹²⁹⁴ was amplified from pEN-Ub^{K29,48R}-EIN2⁶⁴⁶⁻¹²⁹⁴-Myc using primers ss_UBQ_EIN2 and YFP-EIN2_rev. The CDS of a synthetic codon-optimized Ub (without any amino acid exchanges) was amplified from a plasmid containing the K2 construct (Faden et al., 2016) using primers attB1_Ub and as_UBQ_EIN2. YFP was obtained from pEarleyGate 101 (Earley et al., 2006) by applying primers EIN2-YFP_fw and attB2-YFP. All three PCR products were combined in a reaction for fusion PCR using primers attB1-Ub and attB2-YFP. The product was recombined into pDONR 201, and subjected to Phe⁶⁴⁶ (TTC) to Gly (GGT) mutation to yield both pEN-

Ub-EIN2⁶⁴⁶⁻¹²⁹⁴-YFP and Ub-Gly-EIN2⁶⁴⁷⁻¹²⁹⁴-YFP (or: EIN2^{C-term}-YFP and Gly-EIN2^{C-term}-YFP). To construct pEN-Met-EIN2⁶⁴⁷⁻¹²⁹⁴-YFP (or: pEN-Met-EIN2^{C-term}-YFP), the sequence of EIN2⁶⁴⁷⁻¹²⁹⁴-YFP was amplified from pEN-Ub-EIN2⁶⁴⁶⁻¹²⁹⁴-YFP using primers attB1-Met-EIN2 and attB2-YFP, and subjected to a BP reaction with pDONR 201. All three Entry Clones were recombined with pAM-PAT-ProUBQ10 GW. pEN-Ub-EIN2⁶⁴⁶⁻¹²⁹⁴-YFP and Ub-Gly-EIN2⁶⁴⁷⁻¹²⁹⁴-YFP were furthermore introduced into pAM-PAT-proEIN2-GW.

6.6.4 Further expression vectors

The *PRT7* expression vector was created by Taq DNA polymerase-mediated amplification of the *PRT7* CDS with primers PRT7_CDS_fw and PRT7-attB2 from complementary DNA (cDNA) of Col-0. Subsequently, an adapter PCR was conducted using primers adapter_TEV and PRT7-attB2 to add the TEV protease recognition sequence, as well as the attB1 site to the 5' end of the amplicon. This product was introduced into pDONR 201 by BP reaction, and into pVP16 for *E. coli* BL21 (DE3) expression with N-terminal His⁶MBP-tag by LR reaction.

An Entry clone containing the CDS of ATE1 was created by C. Naumann using primers ATE1_pos2_ss and ATE1_as for amplification from cDNA. For *in-vitro* studies within this work, this Entry Clone was used in a LR reaction with pDESTTM17 Vector (Invitrogen) for N-terminal fusion with a hexa-His tag. The construct was expressed from *E. coli* BL21-CodonPlus[®] (DE3)-RIL.

PCO1 and PCO4 with N-terminal hexa-His tag were provided as purified enzymes by M. White and E. Flashman (White et al., 2017).

For UBR^{PRT6} expression, an Entry Clone containing the CDS of PRT6¹⁻¹⁹³ with N-terminal TEV recognition sequence and C-terminal simple HA-tag was provided by P. Reichman. This was included in a LR reaction with pDESTTM15 for N-terminal GST fusion. The construct was transformed into *E. coli* BL21-CodonPlus[®] (DE3)-RIL. In contrast, purified recombinant GST-PRT6¹¹⁹⁻¹⁸⁹ was provided by H. Zhang and F. Theodoulou.

To create pEN-YFP, the sequence of YFP was amplified from pEN-Ub-EIN2⁶⁴⁶⁻¹²⁹⁴-YFP using primers attB1-YFP and attB2-YFP, and the product was recombined into pDONR 201. LR into pAM-PAT-ProUBQ10 GW yielded pAM-PAT-ProUBQ10::YFP.

A plasmid containing mCherry was co-transformed as a control during BiFC experiments. The respective plasmid was kindly provided by G. Furlan and M. Trujillo as a vector containing mCherry for cytoplasmic and nuclear localization (Furlan et al., 2017). The plasmid for expression of YFP with a plastidial localization signal (Fig. S19) was provided by C. Naumann.

To create the GUS reporter constructs, an Entry Clone containing the GUS CDS was provided by N. Dissmeyer (IPB, Halle Saale), and originally obtained from Bekir Ülker¹. This Entry Clone was recombined with Destination vectors pAM-PAT-proPRT1^{ΔCTCT}-GW and pAM-PAT-proATL9 (see above). The vector for expression of GUS under control of the promoter of *IQD4* was kindly provided by J. Quegwer and K. Bürstenbinder and was previously published in Bürstenbinder et al. (2017).

¹ Institute of Cellular and Molecular Botany, University of Bonn, 53115 Bonn, Germany

For expressing eGFP from the *PRT1^{ACTCT}* promoter, pEN-L1-F-L2 (Karimi et al., 2007) was recombined with pAM-PAT-proPRT1^{ACTCT}-GW.

6.7 PCR

All PCRs were performed using Labcycler machines (SensoQuest; Göttingen, Germany). dNTPs were purchased as a set (Cat.No. R0182; Thermo Fisher Scientific), mixed to an aqueous stock solution containing 10 mM of each nucleotide, and stored at -20°C in aliquots. Primer oligonucleotides were purchased from Eurofins Scientific (Brussels, Belgium), diluted to an aqueous stock solution of 10 μM, and stored at -20°C. PCR products were visualized by agarose gel electrophoresis, using a TAE (40 mM Tris-Cl; 1 mM EDTA; 20 mM Acetate; pH 8.2 to 8.6) buffered solution of 1-4% agarose containing 1 μl/100 ml SERVA DNA Stain G (Cat.-No. 39803; Serva Electrophoresis, Heidelberg, Germany).

6.7.1 Standard PfuX7 polymerase PCR

For cloning purposes, if not indicated otherwise, home-made PfuX7 (Nørholm, 2010) was applied in PCR steps as the polymerase. PCR was performed in combination with the Phusion HF Buffer (Cat.-No. F518L; Thermo Fisher Scientific), and was set up according to the manufacturer's instructions for Thermo Fisher Scientific Phusion High-Fidelity DNA Polymerase (i.e., 1x Phusion HF Buffer; 0.2 mM dNTPs (each); each 0.5 μM primer oligonucleotides; 1% (v/v) PfuX7 solution). As the template, 1 μl of gDNA or cDNA, or 5-10 ng of plasmid DNA were applied per 20 μl total reaction volume. For amplifying products longer than 1,000 bp, 1 M betaine (Cat.-No. 14290; Sigma-Aldrich) was included in the reaction mixture. Cycling conditions for PfuX7 PCR are given in Tab. 3. For amplifying promoter sequences, the temperature during the extension step was lowered to 68°C. For attB-site adapter PCRs, a standard PfuX7 PCR was conducted, or a two-step protocol was followed which is described online by the European Molecular Biology Laboratory (EMBL) (https://www.embl.de/pepcore/pepcore_services/cloning/cloning_methods/gateway/2step/).

Tab. 3 | Thermal profiles used for PCR reactions.

Standard PfuX7 PCR			Fusion PfuX7 PCR			Taq PCR		
98°C	1 min		98°C	1 min		96°C	2 min	
98°C	15 sec		98°C	15 sec		96°C	30 sec	
[T _m]-4°C	30 sec	32x	46°C	45 sec	5x	[T _m]-5°C	45 sec	32x
72°C	30-90 sec/kbp		72°C	60-90 sec/kbp		72°C	60-90 sec/kbp	
72°C	10 min		98°C	15 sec		72°C	10 min	
			54°C	45 sec	30x			
			72°C	60-90 sec/kbp				
			72°C	10 min				

6.7.2 Fusion PCR using PfuX7 polymerase

The reaction mixtures for PfuX7-catalyzed Fusion PCRs were set up as described for standard PfuX7 PCRs, but additionally contained 1 M betaine. PCR products purified from agarose gels were included in the reaction as templates at concentrations of 0.1-1 ng/($\mu\text{l} \cdot 100 \text{ bp}$), and a molar ratio of 1:1 to 1:10. A two-step cycling program was applied (Tab. 3), except for the PCR performed to fuse the 3HA-tag with genPRT1 which was performed using a standard PfuX7 cycling program.

6.7.3 Standard Taq polymerase PCR

Home-made Taq was employed as the polymerase during semi-quantitative RT-PCRs, for screening bacterial colonies, and for cloning of the *PRT7* CDS. The reaction mixture for Taq-PCR included: 2 mM Tris-Cl (pH 8.7); 5 mM KCl; 0.2 mM MgCl_2 ; 0.1 mM dNTPs (each); 0.2 μM primer oligonucleotides (each); 1% (v/v) Taq polymerase. For semi-quantitative RT-PCRs and *PRT7* cloning, the template was 1 μl of the 20 μl reverse transcription product containing 1 μg RNA in a total PCR volume of 25 μl . For cycling conditions, refer to Tab. 3. In the case of semi-quantitative RT-PCRs, only 30 sec of initial denaturation were applied, whereas for screening *E. coli* colonies, 3 min initial denaturation were used.

6.7.4 Plant genotyping

Plant genotyping was performed in a slightly modified version of the “TaqMulti” protocol that was previously described (Dissmeyer and Schnittger, 2011). In detail, 500 μl of “Magic buffer” (Tab. 4) were added to a young leaf and ground in a bead mill (28 Hz, 2.5 min) (MM400; Retsch, Haan, Germany). The cell debris was pelleted by centrifugation for 10 min at >13,000 RCF, and the supernatant was used as the template in a PCR reaction (Tab. 4).

Tab. 4 | PCR conditions for “TaqMulti” genotyping of fresh *Arabidopsis* leaves (Dissmeyer and Schnittger, 2011). Both “Magic buffer” and TaqMulti buffer were autoclaved and stored at 4°C for several months.

Reaction mixture	[μl]	TaqMulti Thermal Profile			"Magic buffer"	
		Temp.	[min]			
H₂O	19	95°C	∞		Tris-Cl, pH 7.5	50 mM
TaqMulti buffer [10x]	2.5	95°C	00:30		NaCl	300 mM
dNTPs [10 mM each]	0.5	[T _m]-4°C	00:45	35x	sucrose	300 mM
Taq	0.5	72°C	1.5/kbp		TaqMulti buffer (10x)	
Primers (each) [10 μM]	0.5	72°C	10:00		Tris-Cl (pH 8.7)	200 mM
Template	1.5	15°C	∞		KCl	500 mM
Total volume	25				MgCl_2	20 mM
					Xylene cyanol FF	1.5 g/l
					Orange G	1.5 g/l

6.7.5 Site-directed mutagenesis

Primers used for PCR-based site-directed mutagenesis are given in Tab. S5. To create PRT1^{V28A} (GTT \rightarrow GCG) in pEN-TEV-PRT1 and pEN-3HA-PRT1, a mutagenesis PCR using primers PRT1_V28A_fw and PRT1_V28A_rev was conducted on the respective Entry Clones according to Edelheit et al. (2009), but including 1 M betaine in the reaction mixture and using PfuX7 polymerase. In brief, two reaction

mixtures of 25 µl total volume were prepared containing 1.6 µM of either forward or reverse primer oligonucleotides in a solution of 1x Phusion HF Buffer; 1 M betaine; 0.2 mM dNTPs; 2% (v/v) PfuX7; 500 ng plasmid template. Cycling was performed as 98°C/3 min; 18 cycles of [98°C/30 sec; 55°C/30 sec; 72°C/5 min]; 72°C/10 min. The PCR products were mixed and subjected to a 10 min-annealing program with a stepwise temperature decrease from 95°C to 37°C. The annealed product was digested by *DpnI* (Cat.-No. FD1703; Thermo Fisher Scientific) over night, and 4 µl of the product were transformed into *E. coli* Dh5α. Mutagenesis success was monitored by digestion with *Bsh1236I* (Cat.-No. FD0924; Thermo Fisher Scientific). PRT1^{C29A} (TGC → GCT) and PRT1^{C195A} (TGT → GCT) in pEN-TEV-PRT1 and pEN-3HA-PRT1 were produced accordingly, using primers PRT1_C29A_fw/PRT1_C29A_rev, and PRT1_C195A_fw/PRT1_C195A_rev, respectively. In the case of C195A, the mutation was visualized by *DdeI* (Cat.-No. ER1881; Thermo Fisher Scientific) digestion. Since no restriction enzyme was available to screen for the C29A mutation, these clones were checked by sequencing.

pEN-Ub^{K29,48R}-Gly-EIN2⁶⁴⁷⁻¹²⁹⁴-Myc was created from pEN-Ub^{K29,48R}-EIN2⁶⁴⁶⁻¹²⁹⁴-Myc by a one-step mutagenesis protocol engaging primers EIN2_F646G_fw and EIN2_F646G_rev (TTG → GGT). Here, a standard PfuX7 PCR reaction was set up containing both forward and reverse primers, and 300 ng of plasmid template. The reaction was performed using the same cycling conditions as described for the prior mutagenesis procedure. After *DpnI* digestion, 4 µl of the product were transformed into *E. coli* Dh5α. Phe-646 to Gly mutations were monitored by sequencing. Using the same strategy, pEN-Ub-Gly-EIN2⁶⁴⁷⁻¹²⁹⁴-YFP was prepared from pEN-Ub-EIN2⁶⁴⁶⁻¹²⁹⁴-YFP.

6.8 Reverse transcription and real-time PCR

6.8.1 Tissue collection

Leaf, flower, or seedling material was harvested into tubes containing two metal beads and immediately frozen in liquid nitrogen. Frozen plant material was ground to a fine powder in a bead mill prior to use.

For the collection of anthers, whole inflorescences of WT and *prt1-1^{ts}* genotypes growing at 28°C were harvested into 50 ml tubes containing ice-cold ethanol, and vacuum-infiltrated for 30 min. After infiltration, flowers were stored in ethanol at -20°C for several weeks. Using a stereo microscope, anthers of flower stages 11-13 were subsequently manually selected and transferred to a screw cap tube containing 700 µl ice-cold ethanol and 10-15 ceramic beads. Anthers were collected until a yellowish precipitation was clearly visible at the bottom of the tube, corresponding to roughly 500 anthers. The closed tubes were stored at -20°C. Anthers were subsequently lyophilized overnight using an *Alpha 1-4 LDplus* lyophilizer (Martin Christ Gefriertrocknungsanlagen, Osterode, Germany), and the dried material was homogenized using a tissue homogenizer (Item No. 03119-200-RD000; Precellys 24; Bertin Technologies, Montigny-le-Bretonneux, France).

6.8.2 RNA extraction and reverse transcription

RNA extraction was performed using the TRIsure™ reagent (Cat.-No. BIO-38032; Bioline, London, UK), and according to the manufacturer's instructions, but at half reagent volumes. The purity of the RNA

was assessed by absorbance measurements at 260 nm and 280 nm, and RNA integrity was checked by agarose gel electrophoresis. 1-3 µg of RNA were applied to cDNA synthesis for semi-quantitative RT-PCRs, and 1 µg of RNA for qPCR. In order to remove contaminating DNA from RNA samples, DNase I (Cat.-No. EN0521; Thermo Fisher Scientific) digestion was performed prior to reverse transcription according to the manufacturer's instructions. Reverse transcription was conducted using RevertAid Reverse Transcriptase (Cat.-No. EP0441; Thermo Fisher Scientific), or RevertAid H Minus Reverse Transcriptase (Cat.-No. EP0452; Thermo Fisher Scientific). During the procedure, instructions for the latter reverse transcriptase were followed (i.e., including RiboLock™ RNase Inhibitor (Cat.-No. EO0381; Thermo Fisher Scientific) in the reaction).

6.8.3 Semi-quantitative RT-PCR

Standard Taq PCRs were set up for semi-quantitative RT-PCRs, and the products were subjected to 1% agarose gel electrophoresis. For amplifying the *TUB2* gene in Fig. 19, primers TUB2_fw/TUB2_rev were used. Endogenous *PRT1* was targeted using primers PRT1_UTR_fw/PRT1_FL_rev (Fig. 19, left panel), or Fw_PRT1/PRT1_rev (Fig. 19, right panel). Transgenic *GFP-PRT1^{C29A}* was amplified using primers attB1_mGFP5_fw/PRT1_Exon3_rev, and transgenic *3HA-PRT1* with primers FW_HA/PRT1_rev. The respective primer sequences are summarized in Tab. S6.

6.8.4 Quantitative PCR

Maxima SYBR Green Master Mix (Cat.-No. K0251; Thermo Fisher Scientific) was engaged for qPCR and used according to the manufacturer's instructions (using 0.9 µM of each forward and reverse primers), but at a total volume of 10 µl per reaction and using triple amounts of the reference dye solution (i.e., 15 µl of "ROX solution" in 2x master mix). As the template, 1.5 µl of the 1:10 diluted cDNA synthesis product was included in the reaction mixture. Primers were designed to fit the recommendations of the Maxima SYBR Green Master Mix. All used qPCR primer sequences are included in Tab. S7, and primer melting curves were monitored as a quality control step after each run. qPCRs were performed using a MX3005P qPCR system (Stratagene, San Diego, USA). The thermal profile used is depicted in Tab. 5.

Tab. 5 | Thermal profile for qPCR reactions.

Temp.	min:sec	
95°C	10:00	
95°C	00:15	40 cycles
64°C	01:00	
95°C	01:00	
55°C	00:30	
95°C	00:30	

Reactions were performed as duplicates. Transcript levels were calculated from mean values relative to the expression of the housekeeping gene *PP2A*. If not indicated otherwise, relative transcript levels were calculated as

$$RTL = 1000 * 2^{-(\Delta CT)},$$

where ΔCT is defined as

$$\Delta CT = CT_{\text{Target gene}} - CT_{PP2A}.$$

6.9 Bacteria work and transformation protocols

6.9.1 Growth conditions

E. coli strains were grown on MacConkey medium containing agar (Difco Laboratories, Detroit USA), or in Luria-Bertani (LB) liquid medium (Cat.-No. X968; Carl Roth). *E. coli* cells were allowed to grow at 21-37°C. Media used for *A. tumefaciens* GV3101-pMP90RK were either LB, or YEB (all reagents purchased from Carl Roth, for 1 liter of YEB medium: 5g sucrose, 5 g pepton, 5 g beef extract, 1 g yeast extract, 2 mM MgSO₄), containing 1.5% (w/v) plant agar (Duchefa Biochemie) if applicable. For selection, media were supplemented with antibiotics at concentrations presented in Tab. 6.

Tab. 6 | Antibiotics used and concentrations applied to growth media.

Antibiotic/ Herbicide	Manufacturer	Cat.-No.	Final concentration [µg/ml]	Solvent used to prepare 1000x stock solution
Bacteria				
Ampicillin	Sigma-Aldrich	A9518-5G	100	H ₂ O
Carbenicillin	Duchefa Biochemie	C0109.0025	50	H ₂ O
Chloramphenicol	Carl Roth	3886.2	34	Ethanol
Gentamycin	Duchefa Biochemie	G0124.0001	25	H ₂ O
Kanamycin	AppliChem	A1493,0005	50	H ₂ O
Rifampicin	Duchefa Biochemie	R0146.0005	50	DMSO
Streptomycin	Carl Roth	0236.2	50	H ₂ O
Plants				
Kanamycin	AppliChem	A1493,0005	50	H ₂ O
Phosphinothricin, glufosinate	Toronto Research Chemicals (North York, Canada)	G596959	10	H ₂ O
Basta®	Bayer	n/a	1/1,000 (v/v)	tap water
Hygromycin	Duchefa Biochemie	H0192.0001	20,35	supplied as solution 407 mg/ml

6.9.2 Preparation of competent *E. coli* cells

Cells of *E. coli* were made chemically competent for heat-shock mediated transformation with plasmid DNA using CaCl₂ as previously described (Mandel and Higa, 1970; Hanahan, 1983). In brief, 400 ml of LB medium were inoculated with 4 ml of an overnight culture of the respective *E. coli* strain, and the culture was allowed to grow until an optical density at 600 nm (OD₆₀₀) of 0.3 to 0.45 was reached. After chilling down on ice, each 100 ml of cells were pelleted in 50 ml conical tubes at 4,000 RCF and 4°C for 10 to 15 min. Each pellet was first washed in 10 ml of sterile, ice-cold 0.1 M CaCl₂ solution. Subsequently, cells were resuspended in 2 ml of 0.1 M CaCl₂, and the suspension was mixed with 2 ml of 60% aqueous glycerol. Cell suspensions were aliquoted to 100 µl, frozen in liquid nitrogen, and stored at -80°C until use.

6.9.3 *E. coli* transformation

E. coli cells were transformed by heat shock with plasmid DNA using a standard method (Froger and Hall, 2007). In brief, 50 µl of competent cells were thawed on ice, and 5-50 ng of plasmid DNA were added. After 20 to 30 min incubation on ice, cells were subjected to 42°C using a thermoblock (Cat.-No. T3317; Sigma-Aldrich) for 75 seconds, cooled down on ice, and mixed with 250 µl of LB medium. After incubation at 37°C and 850 rpm for 1 to 2 hours, cells were plated on selective agar plates.

6.9.4 Preparation of electrocompetent *A. tumefaciens* cells

To render *A. tumefaciens* GV3101-pMP90RK cells competent for electro-transformation, 200 ml of YEB medium containing antibiotics (rifampicin, kanamycin) were inoculated at 1:50 using an overnight culture of the cells, and grown to $OD_{600} = 0.5$. Each 50 ml of the culture were pelleted in conical tubes by centrifugation at 4,000 RCF and 4°C for 10 min, and incubated for 10 min on ice. Subsequently, three consecutive washing steps were performed using the following solutions: 1) 25 ml of 1 mM HEPES (pH 7.5); 2) 10 ml of 1 mM HEPES (pH 7.5), 10% (v/v) glycerol; 3) 5 ml of the same solution as used before. Finally, the cells were resuspended in 1 ml (per tube) of aqueous 10% (v/v) glycerol, aliquoted to 50 µl, frozen in liquid nitrogen, and stored at -80°C until use.

6.9.5 Transformation of *A. tumefaciens*

Competent *A. tumefaciens* cells were thawed on ice, and gently mixed with 2 µl of plasmid DNA solution (containing up to 800 µg of DNA). Subsequently, the cell suspension was transferred to an electroporation cuvette with 2 mm gap size (Cat.-No. 732-1136; VWR International) that was precooled at -20°C. Electroporation was performed with a Gene Pulser (Bio-Rad Laboratories, Hercules, USA) at a capacity of 25 µF, voltage of 2.5 kV, and resistance of 400 Ω for 2 seconds. Immediately after electroporation, 750 µl of ice-cold YEB medium was added, the cells were transferred to 1.5 ml reaction tubes, and incubated on a thermoshaker at 28°C/850 rpm for 4 hours. Cells were subsequently plated on selective plates in aliquots of 10 µl, 100 µl, and residual bacterium suspension, and incubated at 28°C for 48 to 72 hours. To check colonies for the presence of the plasmid, a quick test was performed by pelleting 500 µl of an overnight culture (8,000 RCF; 2 min), washing the pellet in 500 µl of distilled water, resuspension of the pellet in 150 µl of distilled water, incubation at 95°C for 10 min, and removal of cell debris by centrifugation for 15 min at 8,000 crf. Of the supernatant, 5 to 10 µl were used in a Taq PCR to amplify the transgene. To confirm transformation success, plasmid DNA was purified from 3 ml of an overnight culture of the transformed *Agrobacterium* using the GeneJET Plasmid Miniprep Kit (Cat.-No. K0502; Thermo Fisher Scientific), and retransformed into an *E. coli* cloning strain to finally check the plasmid purified from *E. coli* by endonuclease digestion.

6.9.6 Plant transformation by floral dipping

Agrobacterium-mediated transformation of *Arabidopsis* plants was performed using the floral dip method (Bent and Clough, 1998) with a few modifications. In brief, a 500 ml overnight culture (YEB medium containing antibiotics) of *Agrobacterium* carrying the requested plasmid was supplemented with 25 g household sugar, and incubated in a shaker at 28°C for 30 minutes. Prior to floral dipping, 100 µl of Silwet L-77 were mixed with the culture. For plant infection, inflorescences of flowering plants were immersed into the bacteria suspension under some rotation. Subsequently, plants were oriented horizontally, and incubated in the dark for 16 to 24 hours. The plants were then uprighted and grown under normal (greenhouse) conditions. Seeds were harvested after at least four weeks after floral dipping and spread on soil. For selection of transformants, seedlings were sprayed every 3 to 4 days starting from the emergence of the first true leaves with a dilution of 1 ml Basta® (Bayer, Leverkusen, Germany) per liter tap water. Resistant plants (T1 generation) were pricked and seeds of the next generation (T2) were screened for segregation patterns on agar plates containing phosphinothricin.

6.10 Protein work

6.10.1 Plant protein extraction for Western blot

For the purposes of SDS-PAGE and Western blot, extracts of plant total soluble proteins were prepared either by a urea-based extraction system, or using RIPA buffer. For both purposes, plant material was collected into 2 ml reaction tubes containing two metal beads, frozen in liquid nitrogen, and ground in a frozen state with a bead mill for 90 seconds at 28 Hz.

For urea-extraction, 450 µl of freshly prepared pre-warmed (42°C) “Lyse & Load” buffer (8 M Urea; 50 mM Tris-Cl, pH 6.8; 5 mM DTT; 30% (v/v) glycerol; 4% (w/v) SDS) were applied per 22 mg of ground seedling material. The mixed suspension was incubated on a thermoblock at 42°C for 20 to 25 minutes, and directly loaded onto a SDS polyacrylamide gel.

RIPA buffer (50 mM Tris-Cl, pH 7.6; 150 mM NaCl; 20 mM NaF (S7920, Sigma-Aldrich); 10 mM Na₄P₂O₇; 1 mM DTT; 1 mM EDTA; 0.5 mM EGTA; 1% (v/v) Nonidet® P40 BioChemica (Cat.-No. A1694; Applichem); 0.5% (w/v) deoxycholate sodium salt; 1x cOmplete™ protease inhibitor cocktail (Cat.-No. 04693132001; Roche, Basel, Switzerland)) was prepared on the day of use from a 2x stock solution containing all reagents but protease inhibitors and DTT, which were added from frozen stocks. For protein extraction, 100 to 400 µl of ice-cold RIPA buffer were added per 20 mg of ground seedling material (400 µl were applied during the experiment presented in Fig. 32). After addition of RIPA buffer, the samples were directly transferred to a thermoblock shaking at 850 rpm and 4°C and incubated for 30 to 60 minutes. Subsequently, cell debris was removed by single or, if necessary, double centrifugation for 10 minutes, ≥14,000 RCF, 4°C.

Upon attempts to detect PRT1 fusion proteins from transgenic plant lines, variations of this protocol were applied: Instead of using a bead mill, up to 500 mg of plant material was ground using mortar and pestle during some experiments, and RIPA buffer was added upon grinding. The mixture was allowed to defreeze slowly upon further grinding, and the liquefied suspension was subjected to centrifugation as stated above.

6.10.2 SDS-PAGE and Western blot

Protein extracts were mixed with 5x SDS sample buffer (0.25 M Tris-Cl, pH 6.8; 50% (v/v) glycerol; 10% (w/v) SDS; 0.5 M DTT) to a final strength of 1 to 1.5, and denatured either at 95°C for 5 to 10 minutes, or at 68°C for 15 to 20 min. SDS polyacrylamide gels were cast, and SDS-PAGE was performed using the Mini-PROTEAN® Electrophoresis System (Bio-Rad Laboratories). Resolving gels were prepared containing 8 to 15% of acrylamide (Cat.-No. 3029.1; Carl Roth), 375 mM Tris-Cl (pH 8.8), 0.01% (w/v) SDS, 0.1% (w/v) APS, and 0.04% TEMED. Stacking gels contained the same concentrations of SDS and APS, but 4.88% acrylamide, 125 mM Tris-Cl (pH 6.8), and 0.1% TEMED. As the running buffer, 1x Towbin buffer (24 mM Tris-Cl (no pH adjustment), 192 mM Gly, 0.1% SDS) was used, and SDS-PAGE was performed at 85 V for the stacking gel, and 135 V for the resolving gel. Semi-dry Western blotting was done using the Trans-Blot® SD Semi-Dry Transfer Cell (Bio-Rad Laboratories). Here, the SDS-gel was equilibrated in Transfer buffer (48 mM Tris-Cl (no pH adjustment); 39 mM Gly; 20% (v/v) methanol), and was sandwiched between two 3 mm Whatman® Blotting Papers soaked in Transfer buffer together with a polyvinylidene fluoride (PVDF) membrane with 0.45 µm pore size (Cat.-No. 10600023; GE Healthcare, Chicago, USA). The latter was pre-equilibrated in methanol. Blotting was performed for 90 minutes at 0.85 mA/cm² of membrane size, but using at least 60 mA. The Western blot membrane was subsequently blocked overnight on a rocking table in Tris-buffered saline containing Tween-20 (TBST) (150 mM NaCl; 20 mM Tris-Cl (pH 8.0); 0.1 % Tween-20) containing 3 to 5% of skim milk powder (Cat.-No. T145; Carl Roth). Note that electro-transfer of SPOT membranes differed from this procedure and is described in section 6.14.3.

6.10.3 Immunodetection

After overnight blocking, Western blots were incubated with primary antibodies (Tab. 7) under agitation for one hour at room temperature. Subsequently, the membrane was washed three times for 10 minutes in TBST, incubated with the secondary antibody for one hour (room temperature), and washed again at least six times for each 10 to 30 minutes. HRP signals were detected using ECL substrate of picogram level sensitivity (Cat.-Nos. 1862123 and 1862124; Thermo Fisher Scientific), or femtogram level sensitivity (Cat.-Nos. RPN2235V1 and -V2; GE Healthcare). Chemiluminescence was imaged with X-ray films (Fujifilm Super RX, Cat.-No. RF11; Hartenstein, Würzburg, Germany).

6.10.4 Total protein stains

As the loading control for Western blots, and to stain total proteins following analytic SDS-PAGE, Coomassie Brilliant Blue (CBB) (Cat.-No. 3074.1; Carl Roth) staining was performed. On a rocking table, Western blots were incubated in the CBB solution for up to 3 minutes, and SDS-polyacrylamide gels overnight, before destaining in an aqueous solution of 50% ethanol and 10% acetic acid. To stop destaining, gels and membranes were briefly incubated in distilled water.

6.10.5 Expression and purification of recombinant proteins from *E. coli*

Protein concentrations were determined following purifications using the BCA Protein Assay Kit (Cat.-No. 23225; Thermo Fisher Scientific), and measured with a plate-reader photospectrometer (Infinite F200 PRO; Tecan).

Tab. 7| Antibodies used for immunodetection. The Protein-A conjugate was used in combination with the anti-HA tag and anti-GFP primary antibodies following IP experiments using Anti-HA agarose to circumvent detection of IgG leached from the beads.

Epitope	Manufacturer	Name/Clone	Cat.-No.	Host	Dilution	Clonality
Primary antibodies						
HA tag	Covance	HA.11 Clone 16B12	MM2-101P	mouse	1:1,000	monoclonal
His tag	GE Healthcare	n/a	27-4710-01	mouse	1:3,000	monoclonal
Ub	Santa Cruz Biotechn.	P4D1	sc-8017	mouse	1:5,000	monoclonal
GFP	Clontech	Living Colors® JL-8	632381	mouse	1:1,000	monoclonal
cMyc	Sigma-Aldrich	n/a	C3956	rabbit	1:5,000	polyclonal
GST	Sigma-Aldrich	n/a	G7781	rabbit	1:10,000	polyclonal
HRP-coupled (secondary) antibodies						
rabbit IgG	Santa Cruz Biotechn.	n/a	sc-2004	goat	1:2,500	polyclonal
mouse IgG	Pierce	n/a	31437	goat	1:5,000	polyclonal
Native Ig	Novex	Protein A-HRP	101023	<i>S. aureus</i>	1:1,000	polyclonal

6.10.5.1 His⁸MBP-PRT1 and His⁸MBP-PRT7

E. coli BL21 (DE3) cells transformed with pVP16 vector containing 8xHis⁸MBP-PRT7, 8xHis⁸MBP-PRT1, or 8xHis⁸MBP-PRT1 mutant variants were grown in a culture of 200 ml LB medium including carbenicillin to OD₆₀₀ ≈ 1 before induction with 0.2 mM Isopropyl β-D-1-thiogalactopyranoside (IPTG). Protein was expressed at 20°C for 16 hours, and cells were subsequently harvested by centrifugation (4,000 RCF; 4°C; 10 min). The pellet was resuspended in Ni buffer (300 mM NaCl; 100 mM Tris-Cl, pH 8.0; 10% (v/v) glycerol; 0.25% (v/v) Tween-20), or Lysis-Equilibration-Wash (LEW) buffer (50 mM Na₂HPO₄; 300 mM NaCl; 1 mM DTT; pH 8.0 using NaOH), treated with lysozyme (1.2 mg/ml), and incubated on ice for up to one hour. Subsequently, cells were sonicated in the presence of 1 mM phenylmethanesulfonyl fluoride (PMSF) with a 3 mm titan sonotrode type MS73 (Cat.-No. 530703065; Gebr. Rettberg, Göttingen, Germany) applying the following settings: 2 min 40%, 10 min 60%, each 6 cycles. The lysate was cleared by centrifugation at 12,000 RCF, 4°C for 30 min. A 5 ml polypropylene column (Cat.-No. 34964; Qiagen, Hilden, Germany) was packed with 1 ml of Ni-NTA agarose (Cat.-No. 30230; Qiagen), and the beads were equilibrated in Ni buffer/LEW buffer. The cleared lysate was loaded onto the column and allowed to pass through three times by gravity flow. The beads were washed once with 5 ml of Ni buffer/LEW buffer, and once with Ni buffer/LEW buffer containing 20 mM imidazole (Cat.-No. 814223; Merck), before elution with 5 fractions à 500 µl of Ni buffer/LEW buffer containing 200 mM imidazole. The elution fractions were stored at -20°C until use.

6.10.5.2 ^{GST}PRT6¹⁻¹⁹³-HA

The UBR box of PRT6 (amino acids 1-193) was expressed as pDEST15::GST-PRT6¹⁻¹⁹³-HA from *E. coli* BL21-CodonPlus® (DE3)-RIL. Two batches of each 400 ml LB expression cultures containing carbenicillin were induced with 0.5 mM IPTG at OD₆₀₀ = 0.6, and protein was expressed overnight at 20°C. Following harvest, cell pellets were frozen for 30 min, and resuspended in each 15 ml of Lysis buffer (10 mM Na₂HPO₄; 1.8 mM KH₂PO₄; 2.7 mM KCl; 140 mM NaCl; 20% glycerol; 5 mM DTT; pH = 7.3). Suspensions were treated with 1 mg/ml lysozyme and 1 mM PMSF for one hour on ice and sonicated as described above for ^{His}MBP-tagged proteins. Subsequently, lysates were clarified by centrifugation at 14,800 RCF, 4°C, 30 min, and filtration with a 0.45 µm pore size filter unit. The cleared lysate was loaded onto a column containing a bead volume of 750 µl (corresponding to 1 ml of slurry) Protino Glutathione Agarose 4B (Cat.-No. 745500.10; Macherey-Nagel) equilibrated in lysis buffer. Binding was performed by slow rotation for 30 min at room temperature, and the column was subsequently washed twice with each 13 ml of lysis buffer. Protein was eluted with 4 ml of elution buffer (50 mM Tris-HCl, pH = 8; 10 mM glutathione), and finally concentrated to a final volume of 1 ml upon buffer exchange to lysis buffer using Amicon Ultra 30k concentrator columns (Cat.-No. C7715; Merck Millipore).

6.10.5.3 ^{His}ATE1

The ATE1 CDS was expressed in *E. coli* BL21-CodonPlus® (DE3)-RIL cells from pDest17 for N-terminal hexa-His (6His) fusion. An expression culture of 800 ml LB with carbenicillin was induced with 1 mM IPTG at OD₆₀₀ = 0.6 and cultivated at 18°C for 20 hours. The next day, the pelleted cells were resuspended in 30 ml of LEW buffer (see above), and the suspension was incubated on ice with 1.2 mg/ml of lysozyme for 30 min. After 20 min, PMSF was added at 1 mM. For sonication (5 min, 40%; 10 min, 60%; each 5 cycles), the suspension was split into two aliquots. The lysate was centrifuged at 4,000 crf and 4°C, 53 min, and the clear supernatant was transferred onto a Ni-NTA agarose column (see above) with a bead volume of 1 ml. Following washing steps using LEW buffer and LEW containing 20 mM imidazole, elution was performed at 40 mM imidazole in LEW in a total volume of 2.5 ml. The eluate was subjected to Amicon Ultra 30k filtration for buffer exchange to LEW storage buffer additionally containing 20% glycerol, and was concentrated to a final volume of 350 µl.

6.11 *In-vitro* autoubiquitination assays

Autoubiquitination assays *in vitro* were performed as described in Furlan et al. (2017), with some modifications. ^{His}MBP-PRT1 and ^{His}MBP-PRT7 proteins subjected to autoubiquitination assays were purified as described above, whereas ^{His}UBA1 (E1) and ^{His}UBC8 (E2) were obtained from M. Trujillo or A. Mot as purified recombinant proteins. Expression clones for ^{His}UBA1 and ^{His}UBC8 were cloned and provided by M. Trujillo. ^{His}MBP was obtained from A. Mot. In a reaction volume of 30 µl, purified E1 (40 nM), E2 (0.31 µM), and E3 (0.4 µM), or control proteins (1-2 µg) were combined as indicated in the experiment in the presence of ubiquitination buffer (26.7 mM Tris-Cl, pH 7.4; 50 mM KCl; 5 mM MgCl₂; 0.67 mM DTT; 2 mM ATP (Cat.-No. P0756S; New England Biolabs, Ipswich, USA); 2 µg Ub from bovine erythrocytes (Cat.-No. U6253; Sigma-Aldrich)). The mixture was incubated at 30°C for 3 hours, and the reaction was stopped by the addition of 10 µl of 5x SDS sample buffer, and incubation at

95°C for 5 minutes. After heat inactivation, the samples were directly subjected to SDS-PAGE and Western blotting.

6.12 X-peptide pull-down experiments

In a total volume of 250 μ l per sample, ^{His}MBP-PRT1 was diluted to 1.7 μ M in pull-down buffer (20 mM Tris-Cl, pH 7.4; 135 mM NaCl; 5 mM maltose; 1 mM DTT; 0.1% (v/v) Tween-20; 0.5% (w/v) skim milk powder) containing 20 pM synthetic peptides of the e^K-derived sequence (NH₂-)X-GSGAWLLPVSG-(PEG)-K-(biotin), with X being either Phe or Met. Synthetic peptides with C-terminal biotin were synthesized and provided by T. Grossmann and C. Müller. The solution was incubated at room temperature under rotation for 1.5 hours. Subsequently, samples were taken for input fractions, and the remaining solution was added to each 20 μ l bead volume of Pierce™ Avidin Agarose (Cat.-No. 20219; Thermo Fisher Scientific) equilibrated in pull-down buffer. Biotin-avidin association was permitted during incubation under rotation for 1 hour at room temperature. Following incubation, the beads were washed once with pull-down buffer, and eluted by addition of 30 μ l 3x SDS sample buffer and incubation at 96°C for 10 minutes.

6.13 *In-vitro* arginylation assays

In-vitro arginylation reactions using plant ATE1 were set up according to Wang et al. (2014), with a few modifications. 12-mer peptide substrates with C-terminal (PEG)-Lys-(biotin) functionalization were synthesized and provided by T. Grossmann and C. Müller. Peptide sequences were X-WAEENVPYTA (RIN4 ^{Δ 11}, with X = G, D), and X-GGAIISDFIPP (N-terminus ^{Δ 2} conserved in RAP2.2, RAP2.12, and HRE2; X = G, D, C, (O₃)-C). In a total reaction volume of 50 μ l, recombinant purified ^{His}ATE1 was provided at a concentration of 10 μ M in the reaction mixture composed of 50 mM HEPES, pH 7.5; 25 mM KCl; 15 mM MgCl₂; 1 mM (Fig. 49A) or 100 mM (Fig. 49B) DTT; 2.5 mM ATP (Cat.-No. P0756S; New England Biolabs); 0.6 mg/ml *E. coli* tRNA (Cat.-No. R1753; Sigma-Aldrich); 0.04 mg/ml *E. coli* aminoacyl-tRNA synthetase (Cat.-No. A3646; Sigma-Aldrich); 80 μ M (4 nCi/ μ l) ¹⁴C-Arg (Cat.-No. MC1243; Hartmann Analytic, Braunschweig, Germany); 50 μ M 12-mer peptide substrate. For combined PCO and ATE1 reactions, purified recombinant PCO enzymes with N-terminal 6His tag were provided by M. White and E. Flashman. Where applicable, PCOs were included in the reaction mixture at 1 μ M concentration. The mixture was incubated at 30°C for 16 to 40 hours. Following incubation, the samples were added to each 50 μ l bead slurry of Pierce™ Avidin Agarose (Cat.-No. 20219; Thermo Fisher Scientific) equilibrated in binding buffer (100 mM NaH₂PO₄; 150 mM NaCl; 0.1% Nonidet® P40 BioChemica), and were mixed with an additional 350 μ l of binding buffer. Binding was performed for 2 hours under slow rotation at room temperature, followed by four washing steps using each 700 μ l of binding buffer. For scintillation counting, the beads were resuspended in 4 ml of FilterSafe scintillation solution (Zinsser Analytic, Frankfurt, Germany), and counting was performed with a LS 6500 Multi-Purpose scintillation system (Beckman Coulter, Brea, USA).

6.14 SPOT peptide arrays

6.14.1 SPOT peptide array synthesis

A schematic of the principle of solid-phase Fmoc peptide synthesis is presented in Fig. 52. Synthesis of SPOT peptide membranes was performed using the SPOT robot system ResPep SL (Intavis, Köln, Germany) including the ResPep software (Intavis), and according to Gausepohl and Behn (2002), with minor changes (see below). The same synthesis protocol for application of the ResPep SL system was also more recently protocolled in Yim et al. (2015). A list of the used chemicals is provided in Tab. 8.

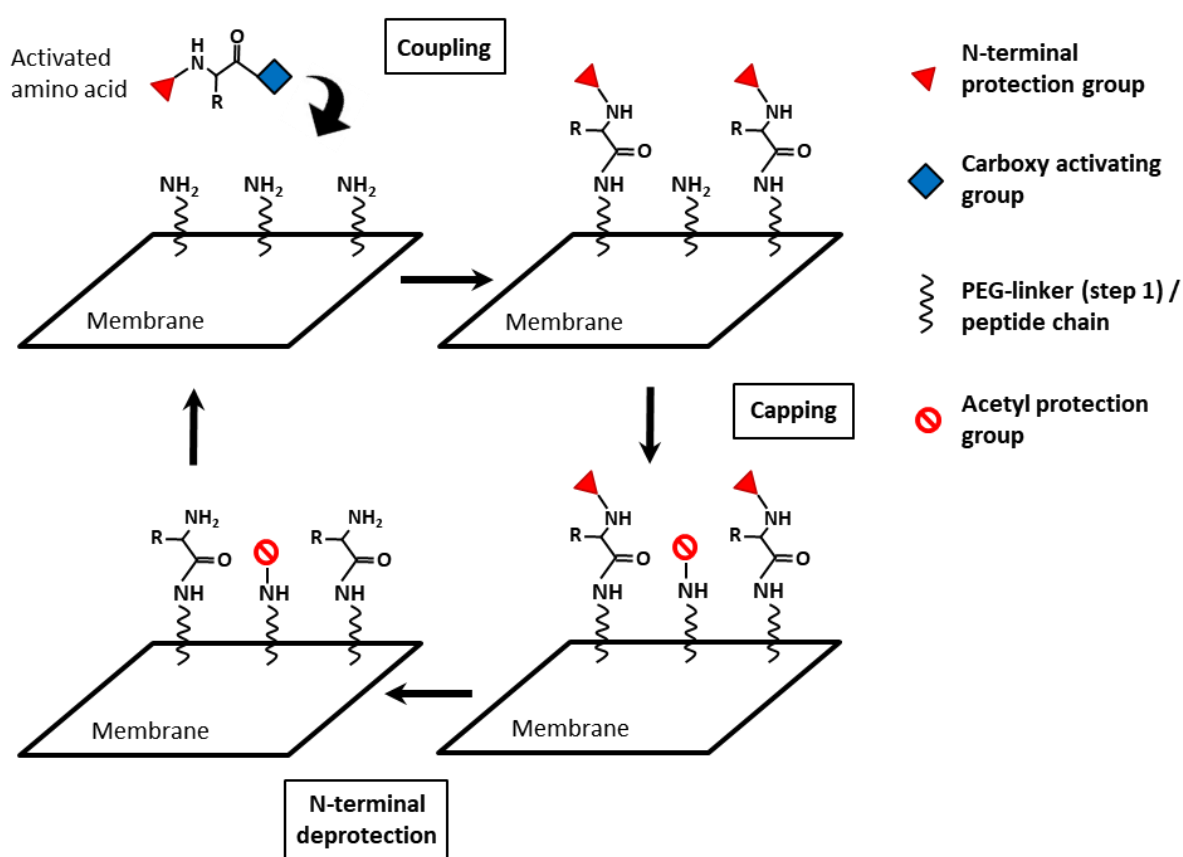


Fig. 52] The principle of SPOT solid-phase peptide synthesis. An amino acid with an activated carboxy group (i.e., HOBt ester) reacts with free amino groups presented by the membrane, or the previously coupled amino acid (**coupling**). In the next step, unreacted free N-termini are acetylated to prevent the synthesis of incorrect peptide sequences (**capping**). To enable for the next cycle of coupling, the N-terminal Fmoc protection group is removed using a mild base (**N-terminal deprotection**). This figure was modified from (Zander and Gausepohl, 2002).

The cellulose membrane was incubated in *N,N*-Dimethylformamide (DMF) overnight before synthesis. The ResPep spotter was programmed and equipped to conduct synthesis as follows:

Preactivation of Fmoc amino acids: Each 1 V of Fmoc amino acids (0.5 M in *N*-Methyl-2-pyrrolidone (NMP)) was mixed with 0.5 V hydroxybenzotriazole hydrate (HOBt) (1.1 M in NMP), and 0.5 V Diisopropylcarbodiimide (DIC) (1.1 M in NMP).

Synthesis cycles:

1. Coupling: Double coupling was performed in a SPOT volume of 0.18 to 0.22 μl (resulting in an individual spot diameter of 4 mm) with 10 min and 15 min coupling times for the first and second coupling reaction, respectively.

2. Capping: Free N-terminal amino groups were capped by dispensing of 2.4 ml of capping reagent (3% (v/v) acetic anhydride in NMP) to the membrane and reaction for 5 min.

3. Deprotection: Fmoc groups of coupled amino acids were removed by double dispensing of 100 μl of 20% (v/v) piperidine in DMF, with 5 minutes and 8 minutes reaction times for the first and second application, respectively.

The membrane was washed in between of capping and deprotection, as well as deprotection and coupling by each 8 washes with 9 ml of DMF, followed by 2 washes with 9 ml ethanol. Capping (i.e., N-acetylation) at the synthesis end was not performed to retain free N-termini.

Tab. 8 | Chemicals used for peptide array synthesis.

Purpose	Substance	Supplier	Cat.-No.
Membrane support	PEG derivatized cellulose membrane	Intavis	32.100
Amino acids	N- α -Fmoc-amino acids	Intavis	individual
Solvent/Wash	1-Methyl-2-pyrrolidone, peptide synthesis grade (NMP)	Carl Roth	P052.1
	1-Methyl-2-pyrrolidinone, biotech. grade, $\geq 99.7\%$ (NMP)	Sigma-Aldrich	494496
	N,N-Dimethylformamide, anhydrous, 99.8%	Sigma-Aldrich	227056
Wash	Ethanol $\geq 99.9\%$	Merck/VWR	1.11727
Storage of solvent	Molecular sieve 4 Å	Carl Roth	8471.2
Preactivation	DIC, purum, $\geq 98.0\%$ (GC) (N,N'-Diisopropylcarbodiimide)	Sigma-Aldrich	38370
	1-Hydroxybenzotriazole hydrate (HOBt), $\geq 97.0\%$ (T)	Sigma-Aldrich	54802
Capping	Acetic anhydride, 99.5%	Sigma-Aldrich	539996
Fmoc deprotection	Piperidine, $\geq 99.0\%$ (GC)	Sigma-Aldrich	P5881
Side-chain deprot.	Triisopropyl silane for synthesis	Sigma-Aldrich	841359

6.14.2 Side-chain deprotection

Removal of side-chain protection groups was performed manually according to Gausepohl and Behn (2002). Here, the membrane was incubated in a sealed polypropylene container in a mixture of 7.5 ml trifluoroacetic acid, 2.5 ml dichloromethane, 300 μl triisopropyl silane, and 200 μl water. Deprotection was conducted for 3 to 4 hours. Subsequently, the membrane was washed four times with 15 ml of dichloromethane (2 min per wash), subsequently four times for 2 min in each 15 ml DMF, and finally two times each 5 to 10 min in ethanol. For storage, the membrane was air-dried, sealed in plastic foil, and kept at -20°C until use. After use and stripping (see below), it was sealed again for storage at -20°C .

6.14.3 SPOT binding assays

SPOT assays were performed as outlined in Klecker and Dissmeyer (2016). Before each assay, the membrane was preactivated by incubation under agitation in methanol (10 minutes), followed by two short washes in ethanol, and equilibration in the assay buffer. Proteins bound to the membrane were subjected to electro-transfer using the 3-buffer semi-dry blot system described by Kyhse-Andersen (1984), for subsequent immunodetection (Fig. 53).

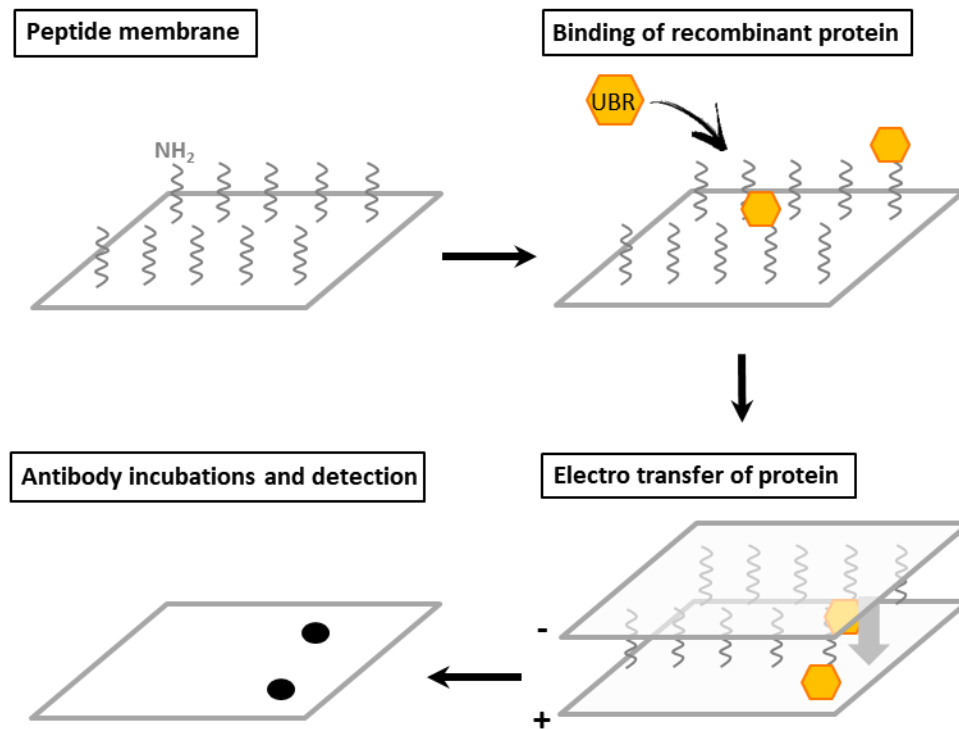


Fig. 53 | Procedure of binding assays using SPOT peptide arrays. A synthesized SPOT membrane bearing C-terminally coupled peptides with free N-termini (NH₂) is incubated with a solution of purified recombinant E3 (e.g., UBR box) in binding buffer. After binding, proteins are immobilized on a PVDF membrane by electro-transfer (Western blot). Immobilized proteins are detected by antibody incubations and HRP signal detection.

The 3-buffer blot system was assembled as follows: The SPOT membrane was briefly (max. 1 minute) equilibrated in Cathode buffer (25 mM Tris-BASE; 40 mM 6-aminocaproic acid; 0.01% (w/v) SDS; 20% (v/v) methanol; pH should be 9.4) just before blot assembly. A PVDF membrane (Cat.-No. 10600023; GE Healthcare) preactivated in methanol was equilibrated in Anode buffer I (30 mM Tris-BASE; 20% (v/v) methanol; pH should be 10.4). Together with the PVDF membrane, the SPOT membrane was sandwiched with the peptide-bound side facing the PVDF membrane between one 3 mm Whatman paper soaked with Cathode buffer (cathode (-) side; i.e., in contact with the SPOT membrane), and one 3 mm Whatman paper soaked with Anode buffer I on the anode (+) side (i.e., in contact with the PVDF membrane). A third layer of Whatman paper soaked with Anode buffer II (300 mM Tris-Cl, pH 10.4; 20% methanol) was placed between the anode and the blotting paper containing Anode buffer I. Blotting was performed for 30 min at 0.8 mA/cm² of SPOT membrane, but using at least 60 mA.

6.14.4 Binding conditions for SPOT assays using ^{His}MBP-PRT1

For PRT1 binding assays, the SPOT membrane was equilibrated in PRT1 binding buffer (20 mM Tris-Cl, pH 7.4; 135 mM NaCl; 0.1% (v/v) Tween-20), and blocked overnight in PRT1 binding buffer additionally containing 5 mM DTT and 10% (w/v) skim milk powder on a rocking table at 4°C. The next day, purified ^{His}MBP-PRT1 (or mutant variants) was diluted at 20 to 50 nM in 20 ml of PRT1 binding buffer containing 5 mM DTT, 10 mM maltose, and 0.075% (w/v) skim milk powder. The mixture was incubated under rotation for 10 to 20 min at room temperature, and subsequently transferred to a polyethylene box containing the SPOT membrane. Protein binding to the membrane was permitted during 2 to 4 hours at room temperature on a rocking platform. The membrane was subsequently washed three times each 10 to 20 minutes in PRT1 binding buffer containing 5 mM DTT and 10 mM maltose before performing Western blot.

6.14.5 Binding conditions for SPOT assays using the PRT6 UBR box

Proteins used to determine the binding properties of PRT6 on SPOT membranes were either GST-PRT6¹¹⁹⁻¹⁸⁹, a mutant variant of this construct containing an Ala-replacement at Asp-174 (both were provided as purified enzymes by H. Zhang and F. Theodoulou), or GST-PRT6¹⁻¹⁹³-HA (constructed, expressed, and purified as described above). In both cases, the SPOT membrane was equilibrated in PRT6 binding buffer (20 mM Tris-Cl, pH 8.0; 80 mM NaCl; 0.05% (v/v) Tween-20), and blocked overnight at 4°C in PRT6 binding buffer additionally containing 2.8 mM DTT and 7.5% (w/v) skim milk powder. Recombinant UBR protein was diluted to 100 nM in PRT6 binding buffer additionally containing 2.8 mM DTT, 5% (w/v) sucrose, and 0.5% (w/v) milk powder, and incubated under rotation for 5 min at room temperature. Protein was allowed to bind to the membrane for 2 to 3 hours at room temperature on a rocking platform. Subsequently, the membrane was washed three times each 10 minutes in PRT6 binding buffer (including 2.8 mM DTT and 5% (w/v) sucrose), and subjected to Western blotting.

6.14.6 SPOT membrane stripping

After each assay, bound protein was eluted from SPOT membranes using the membrane stripping protocol described in Leung et al. (2009). Here, the membrane was subsequently washed each three times for each 10 min in water, in stripping buffer A (8 M urea; 1% (w/v) SDS; 0.5% (v/v) β-mercaptoethanol), in stripping buffer B (50% (v/v) ethanol; 10% (v/v) acetic acid)), and in ethanol. Following stripping, the membrane was air-dried overnight.

6.15 Protoplast work

6.15.1 Protoplast preparation

Mesophyll protoplasts from *Arabidopsis* plants were prepared using the Tape-*Arabidopsis* Sandwich method previously described (Wu et al., 2009). In detail, 8 leaves per genotype were cut from 7- to 8

weeks-old plants grown on soil under short-day conditions. Leaves were immobilized to the desk with their upper surface (adaxial) using paper tape (Cat.-No. K25B; Hartenstein), and the lower epidermis (abaxial) was peeled off using Magic Tape (3M; Scotch®, Neuss, Germany). Leaves were transferred with the peeled side facing down into a petri dish (6 cm diameter) containing 5 ml of the protoplasting enzyme solution (0.4 M mannitol, 20 mM KCl, 20 mM MES (pH 5.7), 10 mM CaCl₂, 0.1% (w/v) bovine serum albumin (Cat.-No. 8076; Carl Roth), 1% (w/v) cellulase (Cat.-No. 16419; Serva Electrophoresis), 0.25% (w/v) macerozyme (Cat.-No. 28302; Serva Electrophoresis)). The petri dish containing enzyme solution and peeled leaves was placed on ice during the time of peeling, and was subsequently transferred to 19°C for dark incubation (no shaking). After three hours, residual protoplasts were released from the leaves by manual agitation of the individual leaves. The suspension containing protoplasts was transferred to cell culture tubes (Cat.-No. 163160; Greiner Bio-One, Kremsmünster, Austria), and subsequently kept on ice. Protoplasts were pelleted by centrifugation at 100 RCF, 4°C for 3 min. The supernatant was removed by inversion, and resuspended in 5 ml of ice-cold W5 solution (154 mM NaCl, 125 mM CaCl₂, 5 mM KCl, 5 mM glucose, 2 mM MES (pH 5.7)). In W5 solution, protoplasts were allowed to settle at the bottom of the vertically placed tubes during incubation on ice. After 20 to 30 minutes, W5 solution was removed using a pipet, and protoplasts were resuspended in 3 ml of ice-cold MMG solution (0.4 M mannitol, 15 mM MgCl₂, 4 mM MES (pH 5.7)). At this step, protoplasts were counted using a Fuchs-Rosenthal counting chamber, and cell density was adjusted to 3×10^5 cells per milliliter of suspension.

6.15.2 Maxi plasmid purification

Plasmid DNA used for transformation of *Arabidopsis* protoplasts was prepared from 500 ml of *E. coli* overnight cultures using the NucleoBond® kit PC500 (Cat.-No. 740574.25; Macherey-Nagel, Düren, Germany) according to the manufacturer's instructions for Maxi high-copy plasmid purification. Here, solutions were home-made according to the buffer compositions provided in the user manual. Following use, NucleoBond columns were washed with 3 column volumes of distilled water, stored at 4°C in 0.5 M HCl solution, and washed again with distilled water prior to re-use.

6.15.3 Protoplast transfection

For transient transformation, 5 to 10 µg of each plasmid DNA were prepared in a fresh cell culture tube per 100 µl of protoplasts to be transformed (except for pAM-PAT-proUBQ10::YFP and the mCherry expression vector, which were provided at 2 µg per 100 µl), with a maximum of 600 µl of protoplast suspension per tube. The protoplast suspension was added to the tubes and was mixed gently but thoroughly by inversion with 1.1 volumes of a solution containing 0.2 M mannitol, 0.1 M CaCl₂, and 40% (w/v) PEG MW-4000 (PEG-4000) (Cat.-No. 81242; Fluka, now: Sigma-Aldrich). The tubes were incubated vertically at room temperature (22°C) for 10 min, and subsequently mixed with 4.4 volumes of W5 solution. Protoplasts were centrifuged at 200 RCF for 1 minute, and the pellet was resuspended in 1 volume of W1 solution (0.5 M mannitol, 20 mM KCl, 4 mM MES (pH 5.7)). In the case of a cytokinin treatments of the protoplasts, W1 additionally contained 0.5 µM BA (Cat.-No. A7685,0001; AppliChem). Protoplasts were incubated overnight in the dark at 19°C for the expression of plasmid-encoded genes.

6.15.4 Cycloheximide and proteasome inhibitor treatments

For treating protoplasts with the translation inhibitor CHX (Cat.-No. sc-3508; Santa Cruz Biotechnology, Dallas, USA), aliquots of up to 200 μ l protoplast suspension were transferred to 2-ml reaction tubes after overnight expression. To reach 100 μ M working concentration, 0.72 μ l of a CHX stock solution (33.2 nM in ethanol, stored at -80°C) were added per 200 μ l of protoplast suspension. Mock treatment groups were mixed with the same volumes of ethanol. The mixtures were incubated without agitation in the dark for the indicated treatment durations, and protoplasts were subsequently centrifuged at 100 to 200 RCF and 4°C for 1 min. Pellets were frozen in liquid nitrogen for subsequent protein extraction or storage at -80°C .

To perform proteasome inhibitor treatments, a stock solution containing 100 mM MG-132 (Cat.-No. F1101; UBPBio, Oxfordshire, UK) in DMSO was stored at -80°C . A volume of 0.3 μ l of this stock solution, or of DMSO alone for mock treatments, was placed on the bottom of an empty 2-ml reaction tube per 180 μ l protoplast suspension to be treated, resulting in 50 μ M working concentrations. Using cut pipet tips, protoplasts transformed the evening before were added relatively quickly to prevent precipitation of MG-132. For indicated treatment times, protoplasts were incubated without agitation in the dark, subsequently pelleted, and frozen in liquid nitrogen. For combined CHX and MG-132 treatments (Fig. S15), MG-132 treatments were performed at least 30 minutes before starting CHX treatments.

6.15.5 Protein stability assays in protoplasts

Frozen protoplast pellets were prepared for SDS-PAGE either by Lyse & Load extraction, or by lysis with 3x SDS sample buffer (0.15 M Tris-Cl, pH 6.8; 30% (v/v) glycerol; 6% (w/v) SDS; 0.3 M DTT). For Lyse & Load buffer (see above) extraction (Fig. 29, 30, 31B, S14, S16), the protoplast pellets were resuspended using 1 volume of buffer per volume of the protoplast suspension before pelleting, and processed as described for seedling material. For extraction using 3x SDS sample buffer (Fig. 28, 29, 33, S18), the same volumes of 3x SDS sample buffer were applied to frozen protoplast pellets as explained for Lyse & Load buffer extraction. After thorough mixing, the samples were incubated at 95°C for 5 minutes before loading to SDS-gels. The experiment presented in Fig. S15 is an exception from this. Here, the frozen protoplast pellet derived from 180 μ l of protoplast suspension was resuspended in 116 μ l of RIPA buffer (see above), and incubated at 4°C and 850 rpm shaking for 1 hour. The soluble fraction was subsequently incubated for 15 min at 68°C with SDS sample buffer at a final strength of 1.5x, and the mixture was loaded onto an SDS-gel.

6.15.6 Co-immunoprecipitation in protoplasts

For the Co-IP experiment presented in Fig. 34, 450 μ l of protoplast suspension prepared from *prt1-1^{ts}* mutant plants were transfected per sample, using 45 μ g of plasmid DNA of each construct. After overnight expression, pelleting, and freezing in liquid nitrogen, protoplast pellets were each resuspended in 300 μ l of RIPA buffer with reduced detergent strength (i.e., 0.1% (v/v) Nonidet[®] P40

BioChemica; 0.05% (w/v) deoxycholate sodium salt). The samples were vortexed briefly and were shaken for 17 min at 750 rpm, 4°C. Cell debris was pelleted by centrifugation at 2,500 RCF, 4°C, 10 minutes. Supernatants were diluted using each 500 µl of RIPA buffer lacking any detergents, input fractions were taken, and the remaining solution was added to each 15 µl of GFP-Trap® Agarose beads (Cat.-No. gta-20, Chromotek, Planegg-Martinsried, Germany) equilibrated in RIPA buffer lacking detergents and protease inhibitors. After 1 hour 20 minutes of binding under slow rotation at 4°C, the beads were washed three times with each 800 µl of RIPA buffer lacking detergents and protease inhibitors, and eluted in each 55 µl of 2x SDS sample buffer by incubation at 68°C for 15 minutes. For SDS-PAGE, an input fraction corresponding to 12% (for GFP detection), and 4% (for detection of the HA-tag) of total inputs was loaded onto 10% acrylamide SDS-gels. Elution (i.e., IP) fractions were 30% (anti-GFP), and 46% (anti-HA tag) of total elution volumes.

For the experiment shown in Fig. S20, the procedure was the same as described above, but pelleting of cell debris following protein extraction was performed at 16,000 crf, and binding to GFP-Trap® beads was done for 3 hours and 15 min.

Fig. 35A presents an attempt to co-immunoprecipitate EIN2^{C-term}-YFP variants expressed from the *UBQ10* promoter and 3HA-PRT1^{C29A} expressed from the weak *EIN2* promoter. Here, 2.1 ml of protoplasts prepared from *prt1-1^{ts}* mutant plants were transfected per sample with 105 µg of each construct. Frozen protoplast pellets were extracted with each 800 µl of RIPA buffer containing 5 mM DTT, and reduced detergent strength (0.1% (v/v) Nonidet® P40 BioChemica; 0.05% (w/v) deoxycholate sodium salt), and shaking at 4°C and 950 rpm for 1 hour 15 min. IPs were performed using a bead volume of 7.5 µl of Anti-HA agarose (Cat.-No. A2095; Sigma-Aldrich) as described above for GFP-Trap® beads. Input fraction loaded to 10% acrylamide SDS-gels corresponded to 2.8% (anti-GFP), and 3.8% (anti-HA tag) of total inputs. IP fractions were 67% (anti-GFP), and 30% (anti-HA tag) of total eluate volumes.

Fig. 35B shows the result of an attempt to co-immunoprecipitate PRT1 variants transiently expressed in protoplasts from the weak *EIN2* promoter with stably expressed full-length EIN2-eGFP expressed from the native promoter. Here, plants of the transgenic *pSL34::proEIN2::EIN2-eGFP* genotype were protoplasted, and each 1.4 ml of protoplast suspension were transfected with 140 µg of either PRT1 plasmid (carrying either *genPRT1-3HA* or *3HA-PRT1^{C29A}* under control of *proEIN2*). Each sample was extracted using 800 µl of RIPA buffer (containing 2 mM DTT; 0.1% (v/v) Nonidet® P40 BioChemica; 0.05% (w/v) deoxycholate sodium salt) as described above, and the extracts were added to each 10 µl of bead volume of Anti-HA agarose. The samples were subsequently processed as described in this section for Fig. 35A, but only two washing steps were performed using each 550 µl of RIPA (no detergents; no protease inhibitor; 2 mM DTT). Input samples corresponded to 4.4% of total inputs, and IPs corresponded to 50% (anti-HA tag), and 45% (anti-GFP) of total eluate volumes.

6.16 Websites and software

Sequence information on the *Arabidopsis* genome was obtained from TAIR at www.arabidopsis.org.

Image processing was performed using Adobe Photoshop CS2 Version 9.0 and Microsoft PowerPoint Version 14.0.7232.5000 (a component of Microsoft Office Professional Plus 2010). To measure hypocotyl lengths, Fiji ("Fiji Is Just ImageJ" obtainable at <https://imagej.net/Fiji>) was employed.

DNA sequence analysis was done using Vector NTI Advance 11.5 (Invitrogen), whereas ClustalW Multiple sequence alignments were conducted using BioEdit 7.2.5 (Hall, 1999). An exception from this is the alignment presented in Fig. 27. Here, sequence alignments of putative EIN2 variants (UniProt Knowledgebase identifiers of the underlying sequences are presented in Tab. S8) were conducted using the full sequences recorded by UniProt with the Clustal Omega Multiple Sequence Alignment Tool at [<https://www.ebi.ac.uk/Tools/msa/clustalo/>], and manually curated. The cladogram was adapted from Liu et al. (2016a). Reverse complement DNA sequences were created using http://www.bioinformatics.org/sms/rev_comp.html, and sequences were formatted with the help of http://www.cellbiol.com/scripts/cleaner/dna_protein_sequence_cleaner.php. Protein domain assignments were adopted from the InterPro protein sequence analysis tool at <https://www.ebi.ac.uk/interpro>. Peptide properties were calculated using the Innovagen Peptide Property Calculator on <https://pepcalc.com/>.

For all PCRs, design of oligonucleotide primers was performed using the Primer3 web tool at <http://primer3.ut.ee/>, and primers were additionally checked for hairpin formation using the Oligo Calc web tool at <http://biotools.nubic.northwestern.edu/OligoCalc.html>.

As gene expression databases, *Arabidopsis* eFP Browser at www.bar.utoronto (Schmid et al., 2005; Winter et al., 2007), as well as the GENEVESTIGATOR® software (<https://genevestigator.com/gv/>) were employed. The chromosome map shown in Fig. S6 was created using the Chromosome Map Tool on TAIR, and the image was subsequently manually processed.

Statistical analyses were conducted using Microsoft Excel Version 14.0.7232.5000 (a component of Microsoft Office Professional Plus 2010) in combination with the “Real Statistics” Add-In obtainable at <http://www.real-statistics.com/free-download/>. Normality testing was performed using the Shapiro-Wilk Normality Test on <http://sdittami.altervista.org/shapirotest/ShapiroTest.html>. For Chi-square analysis, the Chi-square test calculator for a contingency table with multiple columns was used on the website <http://www.socscistatistics.com/tests/chisquare2/Default2.aspx> (2017/13/12).

7. References

- Aarts, M.G., Hodge, R., Kalantidis, K., Florack, D., Wilson, Z.A., Mulligan, B.J., Stiekema, W.J., Scott, R., and Pereira, A.** (1997). The Arabidopsis MALE STERILITY 2 protein shares similarity with reductases in elongation/condensation complexes. *Plant J.* **12**: 615–23.
- Aarts, M.G., Keijzer, C.J., Stiekema, W.J., and Pereira, A.** (1995). Molecular characterization of the CER1 gene of Arabidopsis involved in epicuticular wax biosynthesis and pollen fertility. *Plant Cell* **7**: 2115–27.
- Abbas, M., Berckhan, S., Rooney, D.J., Gibbs, D.J., Vicente Conde, J., Sousa Correia, C., Bassel, G.W., Marín-de la Rosa, N., León, J., Alabadí, D., Blázquez, M.A., and Holdsworth, M.J.** (2015). Oxygen sensing coordinates photomorphogenesis to facilitate seedling survival. *Curr. Biol.* **25**: 1483–8.
- Abozeid, A., Ying, Z., Lin, Y., Liu, J., Zhang, Z., and Tang, Z.** (2017). Ethylene Improves Root System Development under Cadmium Stress by Modulating Superoxide Anion Concentration in Arabidopsis thaliana. *Front. Plant Sci.* **8**: 1–15.
- Acosta, I.F., Laparra, H., Romero, S.P., Schmelz, E., Hamberg, M., Mottinger, J.P., Moreno, M.A., and Dellaporta, S.L.** (2009). Tasselseed1 Is a Lipoxygenase Affecting Jasmonic Acid Signaling in Sex Determination of Maize. *Science* **323**: 262–265.
- Alabadí, D., Gil, J., Blázquez, M.A., and García-Martínez, J.L.** (2004). Gibberellins Repress Photomorphogenesis in Darkness. *PLANT Physiol.* **134**: 1050–1057.
- Aloni, R., Aloni, E., Langhans, M., and Ullrich, C.I.** (2006). Role of auxin in regulating Arabidopsis flower development. *Planta* **223**: 315–328.
- Alonso, J.M. and Ecker, J.R.** (2001). The ethylene pathway: a paradigm for plant hormone signaling and interaction. *Sci. STKE* **2001**: re1.
- Alonso, J.M., Hirayama, T., Roman, G., Nourizadeh, S., and Ecker, J.R.** (1999). EIN2, a Bifunctional Transducer of Ethylene and Stress Responses in Arabidopsis. *Science* **284**: 2148–2152.
- Alonso, J.M. and Stepanova, A.N.** (2004). The Ethylene Signaling Pathway. *Science* **306**: 1513–1515.
- Amerik, A.Y. and Hochstrasser, M.** (2004). Mechanism and function of deubiquitinating enzymes. *Biochim. Biophys. Acta - Mol. Cell Res.* **1695**: 189–207.
- An, F. et al.** (2010a). Ethylene-induced stabilization of ETHYLENE INSENSITIVE3 and EIN3-LIKE1 is mediated by proteasomal degradation of EIN3 binding F-box 1 and 2 that requires EIN2 in Arabidopsis. *Plant Cell* **22**: 2384–401.
- An, H. and Harper, J.W.** (2018). Systematic analysis of ribophagy in human cells reveals bystander flux during selective autophagy. *Nat. Cell Biol.* **20**: 135–143.
- An, J.Y. et al.** (2012). UBR2 of the N-end rule pathway is required for chromosome stability via histone ubiquitylation in spermatocytes and somatic cells. *PLoS One* **7**: e37414.
- An, J.Y., Kim, E.-A., Jiang, Y., Zakrzewska, A., Kim, D.E., Lee, M.J., Mook-Jung, I., Zhang, Y., and Kwon, Y.T.** (2010b). UBR2 mediates transcriptional silencing during spermatogenesis via histone ubiquitination. *Proc. Natl. Acad. Sci. U. S. A.* **107**: 1912–1917.
- Apel, W., Schulze, W.X., and Bock, R.** (2010). Identification of protein stability determinants in chloroplasts. *Plant J.* **63**: 636–50.
- Aravind, L., Iyer, L.M., and Koonin, E. V.** (2003). Scores of RINGS but no PHDs in ubiquitin signaling. *Cell Cycle* **2**: 123–6.
- Aravind, L. and Koonin, E. V.** (2000). The U box is a modified RING finger - a common domain in ubiquitination. *Curr. Biol.* **10**: R132–4.
- Argyros, R.D., Mathews, D.E., Chiang, Y.-H., Palmer, C.M., Thibault, D.M., Etheridge, N., Argyros, D.A., Mason, M.G., Kieber, J.J., and Schaller, G.E.** (2008). Type B response regulators of

- Arabidopsis play key roles in cytokinin signaling and plant development. *Plant Cell* **20**: 2102–16.
- Ariizumi, T., Kawanabe, T., Hatakeyama, K., Sato, S., Kato, T., Tabata, S., and Toriyama, K.** (2008). Ultrastructural characterization of exine development of the transient defective exine 1 mutant suggests the existence of a factor involved in constructing reticulate exine architecture from sporopollenin aggregates. *Plant Cell Physiol.* **49**: 58–67.
- Ariizumi, T. and Toriyama, K.** (2011). Genetic Regulation of Sporopollenin Synthesis and Pollen Exine Development. *Annu. Rev. Plant Biol.* **62**: 437–460.
- von Arnim, A. and Deng, X.-W.** (1996). Light Control of Seedling Development. *Annu. Rev. Plant Physiol. Plant Mol. Biol.* **47**: 215–243.
- Asami, T., Min, Y.K., Nagata, N., Yamagishi, K., Takatsuto, S., Fujioka, S., Murofushi, N., Yamaguchi, I., and Yoshida, S.** (2000). Characterization of brassinazole, a triazole-type brassinosteroid biosynthesis inhibitor. *Plant Physiol.* **123**: 93–100.
- Ashikari, M., Sakakibara, H., Lin, S.Y., Yamamoto, T., Takashi, T., Nishimura, A., Angeles, E.R., Qian, Q., Kitano, H., and Matsuoka, M.** (2005). Cytokinin Oxidase Regulates Rice Grain Production 10.1126/science.1113373. *Science* **309**: 741–745.
- Astuti, R.I., Nasuno, R., and Takagi, H.** (2016). Nitric oxide signaling in yeast. *Appl. Microbiol. Biotechnol.*: 9483–9497.
- Axtell, M.J. and Staskawicz, B.J.** (2003). Initiation of {RPS2} Specified Disease Resistance in Arabidopsis It Is Coupled to the {AvrRpt2} Directed Elimination of {RIN4}. *Cell* **112**: 369–377.
- Aya, K., Ueguchi-Tanaka, M., Kondo, M., Hamada, K., Yano, K., Nishimura, M., and Matsuoka, M.** (2009). Gibberellin modulates anther development in rice via the transcriptional regulation of GAMYB. *Plant Cell* **21**: 1453–72.
- de Azevedo Souza, C., Kim, S.S., Koch, S., Kienow, L., Schneider, K., McKim, S.M., Haughn, G.W., Kombrink, E., and Douglas, C.J.** (2009). A novel fatty Acyl-CoA Synthetase is required for pollen development and sporopollenin biosynthesis in Arabidopsis. *Plant Cell* **21**: 507–25.
- Bachmair, A., Becker, F., and Schell, J.** (1993). Use of a reporter transgene to generate arabidopsis mutants in ubiquitin-dependent protein degradation. *Proc. Natl. Acad. Sci. U. S. A.* **90**: 418–21.
- Bachmair, A., Finley, D., and Varshavsky, A.** (1986). In vivo half-life of a protein is a function of its amino-terminal residue. *Science* **234**: 179–186.
- Bachmair, A. and Varshavsky, A.** (1989). The degradation signal in a short-lived protein. *Cell* **56**: 1019–32.
- Bacsa, B., Horváti, K., Bősze, S., Andrae, F., and Kappe, C.O.** (2008). Solid-phase synthesis of difficult peptide sequences at elevated temperatures: A critical comparison of microwave and conventional heating technologies. *J. Org. Chem.* **73**: 7532–7542.
- Bäumler, J., Riber, W., Klecker, M., Müller, L., Dissmeyer, N., Weig, A.R., Mastroph, A.** (2019). AtERF#111/ABR1 is a transcriptional activator involved in the wounding response. *Plant J. In press.*
- Bailey-Serres, J. and Voeselek, L.A.C.J.** (2008). Flooding Stress: Acclimations and Genetic Diversity. *Annu. Rev. Plant Biol.* **59**: 313–339.
- Bailly, V., Lauder, S., Prakash, S., and Prakash, L.** (1997). Yeast DNA repair proteins Rad6 and Rad18 form a heterodimer that has ubiquitin conjugating, DNA binding, and ATP hydrolytic activities. *J. Biol. Chem.* **272**: 23360–23365.
- Baker, R.T. and Varshavsky, A.** (1995). Yeast N-terminal amidase. A new enzyme and component of the N-end rule pathway. *J. Biol. Chem.* **270**: 12065–12074.
- Bakshi, A., Piya, S., Fernandez, J.C., Chervin, C., Hewezi, T., and Binder, B.M.** (2018). Ethylene Receptors Signal via a Noncanonical Pathway to Regulate Abscisic Acid Responses. *Plant Physiol.* **176**: 910–929.

- Balibrea Lara, M.E., Gonzalez Garcia, M.-C., Fatima, T., Ehneß, R., Lee, T.K., Proels, R., Tanner, W., and Roitsch, T.** (2004). Extracellular Invertase Is an Essential Component of Cytokinin-Mediated Delay of Senescence. *Plant Cell* **16**: 1276–1287.
- Balzi, E., Choder, M., Chen, W.N., Varshavsky, A., and Goffeau, A.** (1990). Cloning and functional analysis of the arginyl-tRNA-protein transferase gene ATE1 of *Saccharomyces cerevisiae*. *J. Biol. Chem.* **265**: 7464–71.
- Barlow, P., Luisi, B., Milner, A., Elliott, M., and Everett, R.** (1994). Structure of the C3HC4 domain by 1H-nuclear magnetic resonance spectroscopy. A new structural class of zinc-finger. *J. Mol. Biol.* **237**: 201–11.
- Bartel, B., Wüning, I., and Varshavsky, A.** (1990). The recognition component of the N-end rule pathway. *EMBO J.* **9**: 3179–89.
- Bartrina, I., Otto, E., Strnad, M., Werner, T., and Schmülling, T.** (2011). Cytokinin Regulates the Activity of Reproductive Meristems, Flower Organ Size, Ovule Formation, and Thus Seed Yield in *Arabidopsis thaliana*. *Plant Cell* **23**: 69–80.
- Bassham, D.C.** (2009). Function and regulation of macroautophagy in plants. *Biochim. Biophys. Acta - Mol. Cell Res.* **1793**: 1397–1403.
- Beaudoin, N., Serizet, C., Gosti, F., and Giraudat, J.** (2000). Interactions between abscisic acid and ethylene signaling cascades. *Plant Cell* **12**: 1103–1115.
- Becker, D., Boavida, L.C., Carneiro, J., Haury, M., and Feijo, A.** (2003). Transcriptional Profiling of *Arabidopsis* Tissues. *Society* **133**: 713–725.
- Bedinger, P.** (1992). The remarkable biology of pollen. *Plant Cell* **4**: 879–87.
- Begcy, K. and Dresselhaus, T.** (2018). Epigenetic responses to abiotic stresses during reproductive development in cereals. *Plant Reprod.*: 1–13.
- Bent, A.F., Innes, R.W., Ecker, J.R., and Staskawicz, B.J.** (1992). Disease Development in Ethylene-Insensitive *Arabidopsis thaliana* Infected with Virulent and Avirulent *Pseudomonas* and *Xanthomonas* Pathogens. *Mol. Plant-Microbe Interact.* **5**: 372.
- Bent, F. and Clough, S.** (1998). Floral dip: a simplified method for *Agrobacterium*-mediated transformation of *Arabidopsis*. *Plant J.* **16**: 735–743.
- Bentsink, L. and Koornneef, M.** (2008). Seed Dormancy and Germination. *Arab. B.* **6**: e0119.
- Bernoux, M., Timmers, T., Jauneau, A., Brière, C., de Wit, P.J.G.M., Marco, Y., and Deslandes, L.** (2008). RD19, an *Arabidopsis* cysteine protease required for RRS1-R-mediated resistance, is relocalized to the nucleus by the *Ralstonia solanacearum* PopP2 effector. *Plant Cell* **20**: 2252–64.
- Beyer, E.M.** (1976). A potent inhibitor of ethylene action in plants. *Plant Physiol.* **58**: 268–271.
- Bienko, M., Green, C.M., Sabbioneda, S., Crosetto, N., Matic, I., Hibbert, R.G., Begovic, T., Niimi, A., Mann, M., Lehmann, A.R., and Dikic, I.** (2010). Regulation of Translesion Synthesis DNA Polymerase η by Monoubiquitination. *Mol. Cell* **37**: 396–407.
- Bienvenut, W. V., Sumpton, D., Martinez, A., Lilla, S., Espagne, C., Meinel, T., and Giglione, C.** (2012). Comparative Large Scale Characterization of Plant versus Mammal Proteins Reveals Similar and Idiosyncratic *N*- α -Acetylation Features. *Mol. Cell. Proteomics* **11**: M111.015131.
- Binder, B.M., Kim, H.J., Mathews, D.E., Hutchison, C.E., Kieber, J.J., and Schaller, G.E.** (2018). A role for two-component signaling elements in the *Arabidopsis* growth recovery response to ethylene. *Plant Direct* **2**: e00058.
- Binder, B.M., Malley, R.C.O., Wang, W., Moore, J.M., Parks, B.M., Spalding, E.P., and Bleecker, A.B.** (2004a). *Arabidopsis* seedling growth response and recovery to ethylene. A kinetic analysis. *Plant Physiol.* **136**: 2913–2920.
- Binder, B.M., Mortimore, L.A., Stepanova, A.N., Ecker, J.R., and Bleecker, A.B.** (2004b). Short-term

- growth responses to ethylene in arabidopsis seedlings are EIN3/EIL1 independent. *Plant Physiol* **136**: 2921–2927.
- Bisson, M.M.A., Bleckmann, A., Allekotte, S., and Groth, G.** (2009). EIN2, the central regulator of ethylene signalling, is localized at the ER membrane where it interacts with the ethylene receptor ETR1. *Biochem. J.* **424**: 1–6.
- Bisson, M.M.A. and Groth, G.** (2010). New insight in ethylene signaling: Autokinase activity of ETR1 modulates the interaction of receptors and EIN2. *Mol. Plant* **3**: 882–889.
- Bisson, M.M.A. and Groth, G.** (2015). Targeting Plant Ethylene Responses by Controlling Essential Protein-Protein Interactions in the Ethylene Pathway. *Mol. Plant* **8**: 1165–1174.
- Bitá, C.E. and Gerats, T.** (2013). Plant tolerance to high temperature in a changing environment: scientific fundamentals and production of heat stress-tolerant crops. *Front. Plant Sci.* **4**: 1–18.
- Bleecker, A.B., Estelle, M.A., Somerville, C., and Kende, H.** (1988). Insensitivity to Ethylene Conferred by a Dominant Mutation in *Arabidopsis thaliana*. *Science* **241**: 1086–1089.
- Bleecker, A.B. and Kende, H.** (2000). Ethylene: A Gaseous Signal Molecule in Plants. *Annu. Rev. Cell Dev. Biol.* **16**: 1–18.
- Bonhomme, S., Grelon, M., Guerche, P., Horlow, C., and Vezon, D.** (1999). EMBO COURSE Practical Course on Genetic and Molecular Analysis of *Arabidopsis* Module 1 *Arabidopsis* gametogenesis.: 1–9.
- Book, A.J., Smalle, J., Lee, K.-H., Yang, P., Walker, J.M., Casper, S., Holmes, J.H., Russo, L.A., Buzinotti, Z.W., Jenik, P.D., and Vierstra, R.D.** (2009). The RPN5 subunit of the 26s proteasome is essential for gametogenesis, sporophyte development, and complex assembly in *Arabidopsis*. *Plant Cell* **21**: 460–78.
- Borg, M., Brownfield, L., and Twell, D.** (2009). Male gametophyte development: A molecular perspective. *J. Exp. Bot.* **60**: 1465–1478.
- Borges, F., Gardner, R., Lopes, T., Calarco, J.P., Boavida, L.C., Slotkin, R.K., Martienssen, R.A., and Becker, J.D.** (2012). FACS-based purification of *Arabidopsis* microspores, sperm cells and vegetative nuclei. *Plant Methods* **8**: 44.
- Bouchnak, I. and van Wijk, K.J.** (2019). N-Degron Pathways in Plastids. *Trends Plant Sci.*
- Bouquin, T., Meier, C., Foster, R., Nielsen, M.E., and Mundy, J.** (2001). Control of specific gene expression by gibberellin and brassinosteroid. *Plant Physiol.* **127**: 450–8.
- Braam, J.** (2013). In touch : plant responses to mechanical stimuli. *New Phytol.* **165**: 373–389.
- Brandstatter, I. and Kieber, J.J.** (1998). Two genes with similarity to bacterial response regulators are rapidly and specifically induced by cytokinin in *Arabidopsis*. *Plant Cell* **10**: 1009–19.
- Brenner, W.G., Romanov, G.A., Köllmer, I., Bürkle, L., and Schmölling, T.** (2005). Immediate-early and delayed cytokinin response genes of *Arabidopsis thaliana* identified by genome-wide expression profiling reveal novel cytokinin-sensitive processes and suggest cytokinin action through transcriptional cascades. *Plant J.* **44**: 314–333.
- Brower, C.S., Piatkov, K.I., and Varshavsky, A.** (2013). Neurodegeneration-Associated Protein Fragments as Short-Lived Substrates of the N-End Rule Pathway. *Mol. Cell*: 1–11.
- Browne, R.G., Iacuone, S., Li, S.F., Dolferus, R., and Parish, R.W.** (2018). Anther Morphological Development and Stage Determination in *Triticum aestivum*. *Front. Plant Sci.* **9**: 1–13.
- Brzobohaty, B., Moore, I., Kristoffersen, P., Bako, L., Campos, N., Schell, J., and Palme, K.** (1993). Release of active cytokinin by a beta-glucosidase localized to the maize root meristem. *Science* **262**: 1051–1054.
- Brzovic, P.S., Keeffe, J.R., Nishikawa, H., Miyamoto, K., Fox, D., Fukuda, M., Ohta, T., and Klevit, R.** (2003). Binding and recognition in the assembly of an active BRCA1/BARD1 ubiquitin-ligase complex. *Proc. Natl. Acad. Sci. U. S. A.* **100**: 5646–5651.

- Brzovic, P.S., Lissounov, A., Christensen, D.E., Hoyt, D.W., and Klevit, R.E.** (2006). A UbcH5/ubiquitin noncovalent complex is required for processive BRCA1-directed ubiquitination. *Mol. Cell* **21**: 873–880.
- Buchanan, B.B., Gruissem, W., and Jones, R.L.** (2002a). *Biochemistry and Molecular Biology of Plants*. Rockville, USA: American Society of Plant Physiologists, p. 1007.
- Buchanan, B.B., Gruissem, W., and Jones, R.L.** (2002b). Protein degradation. In *Biochemistry and Molecular Biology of Plants*. Rockville, USA: American Society of Plant Physiologists, pp. 447–454.
- Budhidarmo, R., Nakatani, Y., and Day, C.L.** (2012). RINGs hold the key to ubiquitin transfer. *Trends Biochem. Sci.* **37**: 58–65.
- Bürstenbinder, K., Möller, B., Plötner, R., Stamm, G., Hause, G., Mitra, D., and Abel, S.** (2017). The IQD Family of Calmodulin-Binding Proteins Links Calcium Signaling to Microtubules, Membrane Subdomains, and the Nucleus. *Plant Physiol.* **173**: 1692–1708.
- Cadwell, K., Coscoy, L., Martin, G.B., and Stebbins, C.E.** (2005). Ubiquitination on Nonlysine Residues by a Viral E3 Ubiquitin Ligase. *Science* **309**: 127–130.
- Caesar, K., Thamm, A.M.K., Witthöft, J., Elgass, K., Huppenberger, P., Grefen, C., Horak, J., and Harter, K.** (2011). Evidence for the localization of the Arabidopsis cytokinin receptors AHK3 and AHK4 in the endoplasmic reticulum. *J. Exp. Bot.* **62**: 5571–5580.
- Cai, Q., Yuan, Z., Chen, M., Yin, C., Luo, Z., Zhao, X., Liang, W., Hu, J., and Zhang, D.** (2014). Jasmonic acid regulates spikelet development in rice. *Nat. Commun.* **5**: 3476.
- Cai, W. and Zhang, D.** (2018). The role of receptor-like kinases in regulating plant male reproduction. *Plant Reprod.* **31**: 77–87.
- Calarco, J.P., Borges, F., Donoghue, M.T.A., Van Ex, F., Jullien, P.E., Lopes, T., Gardner, R., Berger, F., Feijó, J.A., Becker, J.D., and Martienssen, R.A.** (2012). Reprogramming of DNA methylation in pollen guides epigenetic inheritance via small RNA. *Cell* **151**: 194–205.
- Caldelari, D., Wang, G., Farmer, E.E., and Dong, X.** (2011). Arabidopsis *lox3 lox4* double mutants are male sterile and defective in global proliferative arrest. *Plant Mol. Biol.* **75**: 25–33.
- Calderón Villalobos, L.I.A. et al.** (2012). A combinatorial TIR1/AFB-Aux/IAA co-receptor system for differential sensing of auxin. *Nat. Chem. Biol.* **8**: 477–485.
- Calvo, S.E., Julien, O., Clauser, K.R., Shen, H., Kamer, K.J., Wells, J.A., and Mootha, V.K.** (2017). Comparative Analysis of Mitochondrial N-Termini from Mouse, Human, and Yeast. *Mol. Cell. Proteomics* **16**: 512–523.
- Canales, C., Bhatt, A.M., Scott, R., and Dickinson, H.** (2002). EXS, a putative LRR receptor kinase, regulates male germline cell number and tapetal identity and promotes seed development in Arabidopsis. *Curr. Biol.* **12**: 1718–1727.
- Capron, A., Okrész, L., and Genschik, P.** (2003a). First glance at the plant APC/C, a highly conserved ubiquitin-protein ligase. *Trends Plant Sci.* **8**: 83–9.
- Capron, A., Serralbo, O., Fülöp, K., Frugier, F., Parmentier, Y., Dong, A., Lecureuil, A., Guerche, P., Kondorosi, E., Scheres, B., and Genschik, P.** (2003b). The Arabidopsis anaphase-promoting complex or cyclosome: molecular and genetic characterization of the APC2 subunit. *Plant Cell* **15**: 2370–82.
- Cary, A.J., Liu, W., and Howell, S.H.** (1995). Cytokinin action is coupled to ethylene in its effects on the inhibition of root and hypocotyl elongation in Arabidopsis thaliana seedlings. *Plant Physiol.* **107**: 1075–1082.
- Cattaneo, P. and Hardtke, C.S.** (2017). BIG BROTHER uncouples cell proliferation from elongation in the arabidopsis primary root. *Plant Cell Physiol.* **58**: 1519–1527.
- Cecchetti, V., Altamura, M.M., Brunetti, P., Petrocelli, V., Falasca, G., Ljung, K., Costantino, P., and**

- Cardarelli, M.** (2013). Auxin controls arabidopsis anther dehiscence by regulating endothecium lignification and jasmonic acid biosynthesis. *Plant J.* **74**: 411–422.
- Cecchetti, V., Altamura, M.M., Falasca, G., Costantino, P., and Cardarelli, M.** (2008). Auxin regulates Arabidopsis anther dehiscence, pollen maturation, and filament elongation. *Plant Cell* **20**: 1760–74.
- Cecchetti, V., Celebrin, D., Napoli, N., Ghelli, R., Brunetti, P., Costantino, P., and Cardarelli, M.** (2017). An auxin maximum in the middle layer controls stamen development and pollen maturation in Arabidopsis. *New Phytol.* **213**: 1194–1207.
- Cecchetti, V., Pomponi, M., Altamura, M.M., Pezzotti, M., Marsilio, S., D’Angeli, S., Tornielli, G.B., Costantino, P., and Cardarelli, M.** (2004). Expression of rolB in tobacco flowers affects the coordinated processes of anther dehiscence and style elongation. *Plant J.* **38**: 512–25.
- Cha-Molstad, H. et al.** (2015). Amino-terminal arginylation targets endoplasmic reticulum chaperone BiP for autophagy through p62 binding. *Nat. Cell Biol.* **17**: 917–929.
- Cha-Molstad, H. et al.** (2017). P62/SQSTM1/Sequestosome-1 is an N-recognin of the N-end rule pathway which modulates autophagosome biogenesis. *Nat. Commun.* **8**.
- Chae, H.S., Faure, F., and Kieber, J.J.** (2003). The *eto1*, *eto2*, and *eto3* mutations and cytokinin treatment increase ethylene biosynthesis in Arabidopsis by increasing the stability of ACS protein. *Plant Cell* **15**: 545–559.
- Chandrasekharan, M.B., Huang, F., and Sun, Z.W.** (2010). Histone H2B ubiquitination and beyond: Regulation of nucleosome stability, chromatin dynamics and the trans-histone H3 methylation. *Epigenetics* **5**: 460–468.
- Chang, C.** (2016). Q and A: How do plants respond to ethylene and what is its importance? *BMC Biol.* **14**: 1–7.
- Chang, C., Kwok, S.F., Bleeker, A.B., and Meyerowitz, E.M.** (1993). Arabidopsis ethylene-response gene *ETR1*: Similarity of product to two-component regulators. *Science* **262**: 539–544.
- Chang, C. and Shockey, J.A.** (1999). The ethylene-response pathway: Signal perception to gene regulation. *Curr. Opin. Plant Biol.* **2**: 352–358.
- Chang, K.N. et al.** (2013). Temporal transcriptional response to ethylene gas drives growth hormone cross-regulation in Arabidopsis. *Elife* **2013**: 1–20.
- Chao, Q., Rothenberg, M., Solano, R., Roman, G., Terzaghi, W., and Eckert, J.R.** (1997). Activation of the Ethylene Gas Response Pathway in Arabidopsis by the Nuclear Protein ETHYLENE-INSENSITIVE3 and Related Proteins. *Cell* **89**: 1133–1144.
- Chapman, E.J. and Estelle, M.** (2009). Mechanism of Auxin-Regulated Gene Expression in Plants. *Annu. Rev. Genet.* **43**: 265–285.
- Chau, V., Tobias, J.W., Bachmair, A., Marriotr, D., Ecker, D.J., Gonda, D.K., and Varshavsky, A.** (1989). A Multiubiquitin Chain Is Confined to Specific Lysine in a Targeted Short-Lived Protein. *Science* **243**: 1576–1583.
- Che, P., Bussell, J.D., Zhou, W., Estavillo, G.M., Pogson, B.J., and Smith, S.M.** (2010). Signaling from the Endoplasmic Reticulum Activates Brassinosteroid Signaling and Promotes Acclimation to Stress in Arabidopsis. *Sci. Signal.* **3**: ra69–ra69.
- Chen, H., Huang, X., Gusmaroli, G., Terzaghi, W., Lau, O.S., Yanagawa, Y., Zhang, Y., Li, J., Lee, J.-H., Zhu, D., and Deng, X.W.** (2010a). Arabidopsis CULLIN4-Damaged DNA Binding Protein 1 Interacts with CONSTITUTIVELY PHOTOMORPHOGENIC1-SUPPRESSOR OF PHYA Complexes to Regulate Photomorphogenesis and Flowering Time. *Plant Cell* **22**: 108–123.
- Chen, H., Shen, Y., Tang, X., Yu, L., Wang, J., Guo, L., Zhang, Y., Zhang, H., Feng, S., Strickland, E., Zheng, N., and Deng, X.W.** (2006). Arabidopsis CULLIN4 Forms an E3 Ubiquitin Ligase with RBX1 and the CDD Complex in Mediating Light Control of Development. *Plant Cell* **18**: 1991–2004.

- Chen, L.Q. et al.** (2010b). Sugar transporters for intercellular exchange and nutrition of pathogens. *Nature* **468**: 527–532.
- Chen, Q.G. and Bleecker, A.B.** (1995). Analysis of ethylene signal-transduction kinetics associated with seedling-growth response and chitinase induction in wild-type and mutant arabidopsis. *Plant Physiol.* **108**: 597–607.
- Chen, R., Binder, B.M., Garrett, W.M., Tucker, M.L., Chang, C., and Cooper, B.** (2011a). Proteomic responses in *Arabidopsis thaliana* seedlings treated with ethylene. *Mol. Biosyst.* **7**: 2637–2650.
- Chen, S.-J., Wu, X., Wadas, B., Oh, J.-H., and Varshavsky, A.** (2017a). An N-end rule pathway that recognizes proline and destroys gluconeogenic enzymes. *Science* **355**: eaal3655.
- Chen, S., Jing, Y., Kang, X., Yang, L., Wang, D.L., Zhang, W., Zhang, L., Chen, P., Chang, J.F., Yang, X.M., and Sun, F.L.** (2017b). Histone H2B monoubiquitination is a critical epigenetic switch for the regulation of autophagy. *Nucleic Acids Res.* **45**: 1144–1158.
- Chen, W., Yu, X.-H., Zhang, K., Shi, J., De Oliveira, S., Schreiber, L., Shanklin, J., and Zhang, D.** (2011b). Male Sterile2 Encodes a Plastid-Localized Fatty Acyl Carrier Protein Reductase Required for Pollen Exine Development in *Arabidopsis*. *Plant Physiol.* **157**: 842–853.
- Chen, X., Goodwin, S.M., Boroff, V.L., Liu, X., and Jenks, M.A.** (2003). Cloning and characterization of the WAX2 gene of *Arabidopsis* involved in cuticle membrane and wax production. *Plant Cell* **15**: 1170–85.
- Chen, Y.C. and McCormick, S.** (1996). sidcar pollen, an *Arabidopsis thaliana* male gametophytic mutant with aberrant cell divisions during pollen development. *Development* **122**: 3243–3253.
- Chen, Y.F., Gao, Z., Kerris, R.J., Wang, W., Binder, B.M., and Schaller, G.E.** (2010c). Ethylene receptors function as components of high-molecular-mass protein complexes in *Arabidopsis*. *PLoS One* **5**.
- Chen, Y.F., Randlett, M.D., Findell, J.L., and Schaller, G.E.** (2002). Localization of the ethylene receptor ETR1 to the endoplasmic reticulum of *Arabidopsis*. *J. Biol. Chem.* **277**: 19861–19866.
- Cheng, C.Y., Mathews, D.E., Schaller, G.E., and Kieber, J.J.** (2013). Cytokinin-dependent specification of the functional megaspore in the *Arabidopsis* female gametophyte. *Plant J.* **73**: 929–940.
- Cheng, H., Qin, L., Lee, S., Fu, X., Richards, D.E., Cao, D., Luo, D., Harberd, N.P., and Peng, J.** (2004). Gibberellin regulates *Arabidopsis* floral development via suppression of DELLA protein function. *Development* **131**: 1055–1064.
- Cheng, H., Song, S., Xiao, L., Soo, H.M., Cheng, Z., Xie, D., and Peng, J.** (2009). Gibberellin acts through jasmonate to control the expression of MYB21, MYB24, and MYB57 to promote stamen filament growth in *Arabidopsis*. *PLoS Genet.* **5**: 20–22.
- Cheng, M.C., Kuo, W.C., Wang, Y.M., Chen, H.Y., and Lin, T.P.** (2017). UBC18 mediates ERF1 degradation under light–dark cycles. *New Phytol.* **213**: 1156–1167.
- Cheng, W.-H., Endo, A., Zhou, L., Penney, J., Chen, H.-C., Arroyo, A., Leon, P., Nambara, E., Asami, T., Seo, M., Koshiba, T., and Sheen, J.** (2002). A unique short-chain dehydrogenase/reductase in *Arabidopsis* glucose signaling and abscisic acid biosynthesis and functions. *Plant Cell* **14**: 2723–43.
- Cheng, Y., Dai, X., and Zhao, Y.** (2006). Auxin biosynthesis by the YUCCA flavin monooxygenases controls the formation of floral organs and vascular tissues in *Arabidopsis*. *Genes Dev.* **20**: 1790–1799.
- Cheong, Y.H., Chang, H.-S., Gupta, R., Wang, X., Zhu, T., and Luan, S.** (2002). Transcriptional profiling reveals novel interactions between wounding, pathogen, abiotic stress, and hormonal responses in *Arabidopsis*. *Plant Physiol.* **129**: 661–77.
- Chun, T., Aya, K., Asano, K., Yamamoto, E., Morinaka, Y., Watanabe, M., Kitano, H., Ashikari, M., Masuoka, M., and Tanaka-Ueguchi, M.** (2007). Gibberellin Regulates Pollen Viability and Pollen Tube Growth in Rice. *Plant Cell* **19**: 3876–88.

- Chini, A., Fonseca, S., Fernández, G., Adie, B., Chico, J.M., Lorenzo, O., García-Casado, G., López-Vidriero, I., Lozano, F.M., Ponce, M.R., Micol, J.L., and Solano, R.** (2007). The JAZ family of repressors is the missing link in jasmonate signalling. *Nature* **448**: 666–671.
- Chisholm, S.T., Dahlbeck, D., Krishnamurthy, N., Day, B., Sjolander, K., and Staskawicz, B.J.** (2005). Molecular characterization of proteolytic cleavage sites of the *Pseudomonas syringae* effector AvrRpt2. *Proc. Natl. Acad. Sci. U. S. A.* **102**: 2087–2092.
- Choe, S., Dilkes, B.P., Fujioka, S., Takatsuto, S., Sakurai, A., and Feldmann, K.A.** (1998). The DWF4 gene of *Arabidopsis* encodes a cytochrome P450 that mediates multiple 22 α -hydroxylation steps in brassinosteroid biosynthesis. *Plant Cell* **10**: 231–43.
- Choi, W.S., Jeong, B.-C., Joo, Y.J., Lee, M.-R., Kim, J., Eck, M.J., and Song, H.K.** (2010). Structural basis for the recognition of N-end rule substrates by the UBR box of ubiquitin ligases. *Nat. Struct. Mol. Biol.* **17**: 1175–81.
- Chory, J., Reinecke, D., Sim, S., Washburn, T., and Brenner, M.** (1994). A Role for Cytokinins in De-etiolation in *Arabidopsis* (det Mutants Have an Altered Response to Cytokinins). *Plant Physiol.* **104**: 339–347.
- Christensen, D.E., Brzovic, P.S., and Klevit, R.E.** (2007). E2-BRCA1 RING interactions dictate synthesis of mono- or specific polyubiquitin chain linkages. *Nat. Struct. Mol. Biol.* **14**: 941–948.
- Christians, M.J., Gingerich, D.J., Hansen, M., Binder, B.M., Kieber, J.J., and Vierstra, R.D.** (2009). The BTB ubiquitin ligases ETO1, EOL1 and EOL2 act collectively to regulate ethylene biosynthesis in *Arabidopsis* by controlling type-2 ACC synthase levels. *Plant J.* **57**: 332–345.
- Christians, M.J., Robles, L.M., Zeller, S.M., and Larsen, P.B.** (2008). The eer5 mutation, which affects a novel proteasome-related subunit, indicates a prominent role for the COP9 signalosome in resetting the ethylene-signaling pathway in *Arabidopsis*. *Plant J.* **55**: 467–477.
- Chung, T., Phillips, A.R., and Vierstra, R.D.** (2010). ATG8 lipidation and ATG8-mediated autophagy in *Arabidopsis* require ATG12 expressed from the differentially controlled ATG12A and ATG12B loci. *Plant J.* **62**: 483–493.
- Ciechanover, A., Wolin, S.L., Steitz, J. a, and Lodish, H.F.** (1985). Transfer RNA is an essential component of the ubiquitin- and ATP-dependent proteolytic system. *Proc. Natl. Acad. Sci. U. S. A.* **82**: 1341–5.
- Ciechanover, A., Elias, S., Heller, H., Ferber, S., and Hershko, A.** (1980a). Characterization of the Heat-stable Polypeptide of the ATP-dependent Proteolytic System. *J. Biol. Chem.* **255**: 8–11.
- Ciechanover, A., Ferber, S., Ganoth, D., Elias, S., Hershko, A., and Arfin, S.** (1988). Purification and Characterization of Arginyl-tRNA-Protein Transferase from Rabbit Reticulocytes. *J. Biol. Chem.* **263**: 11155–11167.
- Ciechanover, A., Heller, H., Elias, S., Haas, A.L., and Hershko, A.** (1980b). ATP-dependent conjugation of reticulocyte proteins with the polypeptide required for protein degradation. *Proc. Natl. Acad. Sci. U. S. A.* **77**: 1365–1368.
- Ciechanover, A., Hod, Y., and Rershkol, A.** (1978). A HEAT-STABLE POLYPEPTIDE COMPONENT OF AN ATP-DEPENDENT PROTEOLYTIC SYSTEM FROM RETICULOCYTES. *Biochem Biophys Res Commun.* **81**: 1100–1105.
- Clark, K.L., Larsen, P.B., Wang, X., and Chang, C.** (1998). Association of the *Arabidopsis* CTR1 Raf-like kinase with the ETR1 and ERS ethylene receptors. *Proc. Natl. Acad. Sci. U. S. A.* **95**: 5401–5406.
- Clarke, S.M., Cristescu, S.M., Miersch, O., Harren, F.J.M., Wasternack, C., and Mur, L.A.J.** (2009). Jasmonates act with salicylic acid to confer basal thermotolerance in *Arabidopsis thaliana*. *New Phytol.* **182**: 175–87.
- Clément, C.** (2001). Anther Plastids in Angiosperms. *Bot. Rev.* **67**: 54–73.
- Colombo, C. V, Rosano, G.L., Mogk, A., and Ceccarelli, E.A.** (2018). A Gatekeeper Residue Of ClpS1 From *Arabidopsis thaliana* Chloroplasts Determines Its Affinity Towards Substrates Of The

- Bacterial N-End Rule. *Plant Cell Physiol.* **59**: 624–636.
- Cooper, B.** (2013). Separation anxiety: an analysis of ethylene-induced cleavage of EIN2. *Plant Signal. Behav.* **8**: e24721.
- Corot, A., Roman, H., Douillet, O., Autret, H., Perez-Garcia, M.-D., Citerne, S., Bertheloot, J., Sakr, S., Leduc, N., and Demotes-Mainard, S.** (2017). Cytokinins and Abscisic Acid Act Antagonistically in the Regulation of the Bud Outgrowth Pattern by Light Intensity. *Front. Plant Sci.* **8**: 1–16.
- Cortleven, A., Ehret, S., Schmülling, T., and Johansson, H.** (2018). Ethylene-independent promotion of photomorphogenesis in the dark by cytokinin requires COP1 and the CDD complex. *J. Exp. Bot.*: 1–14.
- Cortleven, A. and Schmülling, T.** (2015). Regulation of chloroplast development and function by cytokinin. *J. Exp. Bot.* **66**: 4999–5013.
- Da Costa-Nunes, J.A. and Grossniklaus, U.** (2004). Unveiling the gene-expression profile of pollen. *Genome Biol.* **5**: 9–11.
- Cyr, D.M., Höhfeld, J., and Patterson, C.** (2002). Protein quality control: U-box-containing E3 ubiquitin ligases join the fold. *Trends Biochem. Sci.* **27**: 368–75.
- D’Agostino, I.B., Deruère, J., and Kieber, J.J.** (2000). Characterization of the Response of the Arabidopsis Response Regulator Gene Family to Cytokinin. *Plant Physiol.* **124**: 1706–1717.
- D’Agostino, I.B. and Kieber, J.J.** (1999). Molecular mechanisms of cytokinin action. *Curr. Opin. Plant Biol.* **2**: 359–64.
- Van Damme, P., Evjenth, R., Foyn, H., Demeyer, K., De Bock, P.-J., Lillehaug, J.R., Vandekerckhove, J., Arnesen, T., and Gevaert, K.** (2011). Proteome-derived peptide libraries allow detailed analysis of the substrate specificities of N(alpha)-acetyltransferases and point to hNaa10p as the post-translational actin N(alpha)-acetyltransferase. *Mol. Cell. Proteomics* **10**: M110.004580.
- Das, P.K., Shin, D.H., Choi, S.B., Yoo, S.D., Choi, G., and Park, Y. II** (2012). Cytokinins enhance sugar-induced anthocyanin biosynthesis in Arabidopsis. *Mol. Cells* **34**: 93–101.
- Davis, M.E. and Gack, M.U.** (2015). Ubiquitination in the antiviral immune response. *Virology* **479–480**: 52–65.
- Davydov, I. V. and Varshavsky, A.** (2000). RGS4 is arginylated and degraded by the N-end rule pathway in vitro. *J. Biol. Chem.* **275**: 22931–22941.
- Delessert, C., Wilson, I.W., Van Der Straeten, D., Dennis, E.S., and Dolferus, R.** (2004). Spatial and temporal analysis of the local response to wounding in Arabidopsis leaves. *Plant Mol. Biol.* **55**: 165–81.
- Deng, F., Guo, T., Lefebvre, M., Scaglione, S., Antico, C.J., Jing, T., Yang, X., Shan, W., and Ramonell, K.M.** (2017). Expression and regulation of ATL9, an E3 ubiquitin ligase involved in plant defense. *PLoS One* **12**: 1–18.
- Deng, Y., Dong, H., Mu, J., Ren, B., Zheng, B., Ji, Z., Yang, W.-C., Liang, Y., and Zuo, J.** (2010). *Arabidopsis* Histidine Kinase CKI1 Acts Upstream of HISTIDINE PHOSPHOTRANSFER PROTEINS to Regulate Female Gametophyte Development and Vegetative Growth. *Plant Cell* **22**: 1232–1248.
- Deng, Y., Humbert, S., Liu, J.-X., Srivastava, R., Rothstein, S.J., and Howell, S.H.** (2011). Heat induces the splicing by IRE1 of a mRNA encoding a transcription factor involved in the unfolded protein response in Arabidopsis. *Proc. Natl. Acad. Sci. U. S. A.* **108**: 7247–52.
- Deng, Y., Srivastava, R., Quilichini, T.D., Dong, H., Bao, Y., Horner, H.T., and Howell, S.H.** (2016). IRE1, a component of the unfolded protein response signaling pathway, protects pollen development in Arabidopsis from heat stress. *Plant J.* **88**: 193–204.
- Deshaies, R.J.** (1999). SCF and Cullin/Ring H2-based ubiquitin ligases. *Annu. Rev. Cell Dev. Biol.* **15**: 435–67.
- Deshaies, R.J. and Joazeiro, C.A.P.** (2009). RING Domain E3 Ubiquitin Ligases. *Annu. Rev. Biochem.*

- 78: 399–434.
- Dharmasiri, N., Dharmasiri, S., and Estelle, M.** (2005a). The F-box protein TIR1 is an auxin receptor. *Nature* **435**: 441–445.
- Dharmasiri, N., Dharmasiri, S., Weijers, D., Lechner, E., Yamada, M., Hobbie, L., Ehrismann, J.S., Jürgens, G., and Estelle, M.** (2005b). Plant Development Is Regulated by a Family of Auxin Receptor F Box Proteins. *Dev Cell* **9**: 109–19.
- Dieterle, M., Zhou, Y.C., Schäfer, E., Funk, M., and Kretsch, T.** (2001). EID1, an F-box protein involved in phytochrome A-specific light signaling. *Genes Dev.* **15**: 939–44.
- Disch, S., Anastasiou, E., Sharma, V.K., Laux, T., Fletcher, J.C., and Lenhard, M.** (2006). The E3 ubiquitin ligase BIG BROTHER controls Arabidopsis organ size in a dosage-dependent manner. *Curr. Biol.* **16**: 272–279.
- Dissmeyer, N., Rivas, S., and Graciet, E.** (2018). Life and death of proteins after protease cleavage: protein degradation by the N-end rule pathway. *New Phytol.* **218**: 929–935.
- Dissmeyer, N. and Schnittger, A.** (2011). Use of phospho-site substitutions to analyze the biological relevance of phosphorylation events in regulatory networks. In *Plant Kinases: Methods and Protocols*, Methods in Molecular Biology, N. Dissmeyer and A. Schnittger, eds (Springer Science+Business Media: Berlin), pp. 93–138.
- Ditzel, M. and Meier, P.** (2005). Ubiquitylation in apoptosis: DIAP1's (N)en(d)igma. *Cell Death Differ.* **12**: 1208–1212.
- Ditzel, M., Wilson, R., Tenev, T., Zachariou, A., Paul, A., Deas, E., and Meier, P.** (2003). Degradation of DIAP1 by the N-end rule pathway is essential for regulating apoptosis. *Nat. Cell Biol.* **5**: 467–73.
- Djanaguiraman, M., Perumal, R., Jagadish, S.V.K., Ciampitti, I.A., Welti, R., and Prasad, P.V. V** (2018). Sensitivity of sorghum pollen and pistil to high-temperature stress. *Plant. Cell Environ.* **41**: 1065–1082.
- Dobritsa, A.A., Shrestha, J., Morant, M., Pinot, F., Matsuno, M., Swanson, R., Moller, B.L., and Preuss, D.** (2009). CYP704B1 Is a Long-Chain Fatty Acid-Hydroxylase Essential for Sporopollenin Synthesis in Pollen of Arabidopsis. *Plant Physiol.* **151**: 574–589.
- Dobritzsch, S., Weyhe, M., Schubert, R., Dindas, J., Hause, G., Kopka, J., and Hause, B.** (2015). Dissection of jasmonate functions in tomato stamen development by transcriptome and metabolome analyses. *BMC Biol.* **13**: 1–18.
- Dohmen, R.J., Madura, K., Bartel, B., and Varshavsky, A.** (1991). The N-end rule is mediated by the UBC2(RAD6) ubiquitin-conjugating enzyme. *Proc. Natl. Acad. Sci. U. S. A.* **88**: 7351–5.
- Domitrovic, T., Fausto, A.K., Silva, T.D.F., Romanel, E., and Vaslin, M.F.S.** (2017). Plant arginyltransferases (ATEs). *Genet. Mol. Biol.* **40**: 253–260.
- Dong, C.H., Jang, M., Scharein, B., Malach, A., Rivarola, M., Liesch, J., Groth, G., Hwang, I., and Chang, C.** (2010). Molecular association of the Arabidopsis ETR1 ethylene receptor and a regulator of ethylene signaling, RTE1. *J. Biol. Chem.* **285**: 40706–40713.
- Dong, C.H., Rivarola, M., Resnick, J.S., Maggin, B.D., and Chang, C.** (2008). Subcellular co-localization of Arabidopsis RTE1 and ETR1 supports a regulatory role for RTE1 in ETR1 ethylene signaling. *Plant J.* **53**: 275–286.
- Dong, H. et al.** (2017a). Ubiquitylation activates a peptidase that promotes cleavage and destabilization of its activating E3 ligases and diverse growth regulatory proteins to limit cell proliferation in Arabidopsis. *Genes Dev.* **31**: 197–208.
- Dong, J., Ni, W., Yu, R., Deng, X.W., Chen, H., and Wei, N.** (2017b). Light-Dependent Degradation of PIF3 by SCFEBF1/2 Promotes a Photomorphogenic Response in Arabidopsis. *Curr. Biol.* **27**: 2420–2430.e6.

- Dong, J.G., Fernández-Maculet, J.C., and Yang, S.F.** (1992). Purification and characterization of 1-aminocyclopropane-1-carboxylate oxidase from apple fruit. *Proc. Natl. Acad. Sci. U. S. A.* **89**: 9789–9793.
- Dong, X., Hong, Z., Sivaramakrishnan, M., Mahfouz, M., and Verma, D.P.S.** (2005). Callose synthase (CalS5) is required for exine formation during microgametogenesis and for pollen viability in *Arabidopsis*. *Plant J.* **42**: 315–328.
- Dong, Y. et al.** (2017c). Sulfur availability regulates plant growth via glucose-TOR signaling. *Nat. Commun.* **8**: 1174.
- Dove, K.K. and Klevit, R.E.** (2017). RING-Between-RING E3s ligases: Emerging themes amid the variations Graphical abstract. *J Mol Biol.* **429**: 3363–3375.
- Drazic, A., Myklebust, L.M., Ree, R., and Arnesen, T.** (2016). The world of protein acetylation. *Biochim. Biophys. Acta - Proteins Proteomics* **1864**: 1372–1401.
- Drew, M.M.C.** (1997). Oxygen deficiency and root metabolism: Injury and acclimation under hypoxia and anoxia. *Annu. Rev. Plant Physiol. Plant Mol. Biol.* **48**: 223–250.
- Du, L., Jiao, F., Chu, J., Jin, G., Chen, M., and Wu, P.** (2007). The two-component signal system in rice (*Oryza sativa* L.): A genome-wide study of cytokinin signal perception and transduction. *Genomics* **89**: 697–707.
- Du, L., Li, N., Chen, L., Xu, Y., Li, Y., Zhang, Y., Li, C., and Li, Y.** (2014). The ubiquitin receptor DA1 regulates seed and organ size by modulating the stability of the ubiquitin-specific protease UBP15/SOD2 in *Arabidopsis*. *Plant Cell* **26**: 665–77.
- Dubois, M., Broeck, L. Van den, and Inzé, D.** (2018). The Pivotal Role of Ethylene in Plant Growth. *Trends Plant Sci.* **0**: 311–323.
- Duc, C. et al.** (2017). *Arabidopsis* ATRX Modulates H3.3 Occupancy and Fine-Tunes Gene Expression. *Plant Cell* **29**: 1773–1793.
- Dunker, A.K. et al.** (2001). Intrinsically disordered protein. *J.Mol.Graph.Model.* **19**: 26–59.
- Durbarry, A.** (2005). Male Germ Line Development in *Arabidopsis*. duo pollen Mutants Reveal Gametophytic Regulators of Generative Cell Cycle Progression. *Plant Physiol.* **137**: 297–307.
- Durrant, W.E., Rowland, O., Piedras, P., Hammond-Kosack, K.E., and Jones, J.D.G.** (2000). cDNA-AFLP Reveals a Striking Overlap in Race-Specific Resistance and Wound Response Gene Expression Profiles. *Plant Cell* **12**: 963–977.
- Earley, K.W., Haag, J.R., Pontes, O., Opper, K., Juehne, T., Song, K., and Pikaard, C.S.** (2006). Gateway-compatible vectors for plant functional genomics and proteomics. *Plant J.* **45**: 616–629.
- Ecker, J.R.** (1995). The ethylene signal transduction pathway in plants. *Science* **268**: 667–75.
- Eddins, M.J., Carlile, C.M., Gomez, K.M., Pickart, C.M., and Wolberger, C.** (2006). Mms2-Ubc13 covalently bound to ubiquitin reveals the structural basis of linkage-specific polyubiquitin chain formation. *Nat. Struct. Mol. Biol.* **13**: 915–920.
- Edelheit, O., Hanukoglu, A., and Hanukoglu, I.** (2009). Simple and efficient site-directed mutagenesis using two single-primer reactions in parallel to generate mutants for protein structure-function studies. *BMC Biotechnol.* **9**: 61.
- Eisenhaber, B., Chumak, N., Eisenhaber, F., and Hauser, M.-T.** (2007). The ring between ring fingers (RBR) protein family. *Genome Biol.* **8**: 209.
- Eldeeb, M.A. and Fahlman, R.P.** (2014). The anti-apoptotic form of tyrosine kinase Lyn that is generated by proteolysis is degraded by the N-end rule pathway. *Oncotarget* **5**: 2714–22.
- Eldeeb, M.A., Fahlman, R.P., Esmaili, M., and Ragheb, M.A.** (2018a). Regulating Apoptosis by Degradation: The N-End Rule-Mediated Regulation of Apoptotic Proteolytic Fragments in Mammalian Cells. *Int. J. Mol. Sci.* **19**.

- Eldeeb, M.A., Leitao, L.C.A., and Fahlman, R.** (2018b). Emerging Branches of the N-End Rule Pathways are Revealing the Sequence Complexities of N-Termini Dependent Protein Degradation . *Biochem Cell Biol* **96**: 289–294.
- Elias, S. and Ciechanover, A.** (1990). Post-translational addition of an Arginine Moiety to Acidic NH₂termini of proteins is required for their recognition by ubiquitin-protein ligase. *J. Biol. Chem.* **265**: 15511–15517.
- Ellis, C. and Turner, J.G.** (2002). A conditionally fertile *coi1* allele indicates cross-talk between plant hormone signalling pathways in *Arabidopsis thaliana* seeds and young seedlings. *Planta* **215**: 549–556.
- Ellison, C.T., Vandenbussche, F., Van Der Straeten, D., and Harmer, S.L.** (2011). XAP5 CIRCADIAN TIMEKEEPER Regulates Ethylene Responses in Aerial Tissues of *Arabidopsis*. *Plant Physiol.* **155**: 988–999.
- Elsasser, S., Gali, R.R., Schwikart, M., Larsen, C.N., Leggett, D.S., Müller, B., Feng, M.T., Tübing, F., Dittmar, G.A.G., and Finley, D.** (2002). Proteasome subunit Rpn1 binds ubiquitin-like protein domains. *Nat. Cell Biol.* **4**: 725–730.
- Erales, J. and Coffino, P.** (2014). Ubiquitin-independent proteasomal degradation. *Biochim. Biophys. Acta - Mol. Cell Res.* **1843**: 216–221.
- Erbse, A., Schmidt, R., Bornemann, T., Schneider-Mergener, J., Mogk, A., Zahn, R., Dougan, D.A., and Bukau, B.** (2006). ClpS is an essential component of the N-end rule pathway in *Escherichia coli*. *Nature* **439**: 753–756.
- Eriste, E., Norberg, A., Nepomuceno, D., Kuei, C., Kamme, F., Tran, D.-T., Strupat, K., Jörnvall, H., Liu, C., Lovenberg, T.W., and Sillard, R.** (2005). A novel form of neurotensin post-translationally modified by arginylation. *J. Biol. Chem.* **280**: 35089–97.
- Faden, F.** (2017). A simple technique for N-end rule-controlled conditional protein accumulation *in vivo*. Martin-Luther-Universität Halle-Wittenberg, Dissertation. urn:nbn:de:gbv:3:4-20678.
- Faden, F., Mielke, S., and Dissmeyer, N.** (2019). Modulating Protein Stability to Switch Toxic Protein Function On and Off in Living Cells. *Plant Physiol.* **179**: 929–942.
- Faden, F., Ramezani, T., Mielke, S., Almudi, I., Nairz, K., Froehlich, M.S., Höckendorff, J., Brandt, W., Hoehenwarter, W., Dohmen, R.J., Schnittger, A., and Dissmeyer, N.** (2016). Phenotypes on demand via switchable target protein degradation in multicellular organisms. *Nat. Commun.* **7**: 12202.
- Fan, L.M., Wang, Y.F., Wang, H., and Wu, W.H.** (2001). In vitro *Arabidopsis* pollen germination and characterization of the inward potassium currents in *Arabidopsis* pollen grain protoplasts. *J. Exp. Bot.* **52**: 1603–14.
- Feltham, R., Bettjeman, B., Budhidarmo, R., Mace, P.D., Shirley, S., Condon, S.M., Chunduru, S.K., McKinlay, M.A., Vaux, D.L., Silke, J., and Day, C.L.** (2011). Smac mimetics activate the E3 ligase activity of cIAP1 protein by promoting RING domain dimerization. *J. Biol. Chem.* **286**: 17015–17028.
- Ferreira, B.G., Falcioni, R., Guedes, L.M., Avritzer, S.C., Antunes, W.C., Souza, L.A., and Isaias, R.M.S.** (2017). Preventing False Negatives for Histochemical Detection of Phenolics and Lignins in PEG-Embedded Plant Tissues. *J. Histochem. Cytochem.* **65**: 105–116.
- Feng, G., Liu, G., and Xiao, J.** (2015). The *Arabidopsis* EIN2 restricts organ growth by retarding cell expansion. *Plant Signal. Behav.* **10**: e1017169.
- Feng, X.L., Ni, W.M., Elge, S., Mueller-Roeber, B., Xu, Z.H., and Xue, H.W.** (2006). Auxin flow in anther filaments is critical for pollen grain development through regulating pollen mitosis. *Plant Mol. Biol.* **61**: 215–226.
- Ferber, S. and Ciechanover, A.** (1987). Role of arginine-tRNA in protein degradation by the ubiquitin pathway. *Nature* **326**: 808–11.

- Fernández Gómez, J., Talle, B., and Wilson, Z.A.** (2015). Anther and pollen development: A conserved developmental pathway. *J. Integr. Plant Biol.* **57**: 876–891.
- Feys, B.J.F., Benedetti, C.E., Penfold, C.N., and Turner, J.G.** (1994). Arabidopsis Mutants Selected for Resistance To the Phytotoxin Coronatine Are Male-Sterile, Insensitive To Methyl Jasmonate, and Resistant To a Bacterial Pathogen. *Plant Cell* **6**: 751–759.
- Fiebig, A., Mayfield, J.A., Miley, N.L., Chau, S., Fischer, R.L., and Preuss, D.** (2000). Alterations in CER6, a gene identical to CUT1, differentially affect long-chain lipid content on the surface of pollen and stems. *Plant Cell* **12**: 2001–8.
- Finley, D.** (2009). Recognition and Processing of Ubiquitin-Protein Conjugates by the Proteasome. *Annu. Rev. Biochem.* **78**: 477–513.
- Firon, N., Nepi, M., and Pacini, E.** (2012). Water status and associated processes mark critical stages in pollen development and functioning. *Ann. Bot.* **109**: 1201–1213.
- Fluhr, R.** (1998). Ethylene perception: From two-component signal transducers to gene induction. *Trends Plant Sci.* **3**: 141–146.
- Fonseca, S., Chini, A., Hamberg, M., Adie, B., Porzel, A., Kramell, R., Miersch, O., Wasternack, C., and Solano, R.** (2009). (+)-7-iso-Jasmonoyl-L-isoleucine is the endogenous bioactive jasmonate. *Nat. Chem. Biol.* **5**: 344–350.
- Franchi, G.G., Nepi, M., Dafni, A., and Pacini, E.** (2002). Partially hydrated pollen: Taxonomic distribution, ecological and evolutionary significance. *Plant Syst. Evol.* **234**: 211–227.
- Franco-Zorrilla, J.M., Martín, A.C., Leyva, A., and Paz-Ares, J.** (2005). Interaction between Phosphate-Starvation, Sugar, and Cytokinin Signaling in Arabidopsis and the Roles of Cytokinin Receptors CRE1/AHK4 and AHK3. *PLANT Physiol.* **138**: 847–857.
- Frank, G., Pressman, E., Ophir, R., Althan, L., Shaked, R., Freedman, M., Shen, S., and Firon, N.** (2009). Transcriptional profiling of maturing tomato (*Solanum lycopersicum* L.) microspores reveals the involvement of heat shock proteins, ROS scavengers, hormones, and sugars in the heat stress response. *J. Exp. Bot.* **60**: 3891–3908.
- Freemont, P.S., Hanson, I.M., and Trowsdale, J.** (1991). A Novel Cysteine-Rich Sequence Motif. *Cell* **64**: 483–484.
- Friml, J., Wiśniewska, J., Benková, E., Mendgen, K., and Palme, K.** (2002). Lateral relocation of auxin efflux regulator PIN3 mediates tropism in Arabidopsis. *Nature* **415**: 806–9.
- Froger, A. and Hall, J.E.** (2007). Transformation of plasmid DNA into *E. coli* using the heat shock method. *J. Vis. Exp.*: 253.
- Fujioka, Y., Noda, N.N., Fujii, K., Yoshimoto, K., Ohsumi, Y., and Inagaki, F.** (2008). In vitro reconstitution of plant Atg8 and Atg12 conjugation systems essential for autophagy. *J. Biol. Chem.* **283**: 1921–1928.
- Fujita, H. and Syono, K.** (1996). Genetic Analysis of the Effects of Polar Auxin Transport Inhibitors on Root Growth in. *Plant Cell Physiol.* **37**: 1094–101.
- Furlan, G., Nakagami, H., Eschen-Lippold, L., Jiang, X., Majovsky, P., Kowarschik, K., Hoehenwarter, W., Lee, J., and Trujillo, M.** (2017). Changes in PUB22 Ubiquitination Modes Triggered by MITOGEN-ACTIVATED PROTEIN KINASE3 Dampen the Immune Response. *Plant Cell* **29**: 726–745.
- Gagne, J.M., Downes, B.P., Shiu, S.-H., Durski, A.M., and Vierstra, R.D.** (2002). The F-box subunit of the SCF E3 complex is encoded by a diverse superfamily of genes in Arabidopsis. *Proc. Natl. Acad. Sci. U. S. A.* **99**: 11519–11524.
- Gagne, J.M., Smalle, J., Gingerich, D.J., Walker, J.M., Yoo, S.-D., Yanagisawa, S., and Vierstra, R.D.** (2004). Arabidopsis EIN3-binding F-box 1 and 2 form ubiquitin-protein ligases that repress ethylene action and promote growth by directing EIN3 degradation. *Proc. Natl. Acad. Sci. U. S. A.* **101**: 6803–6808.

- Gajdošová, S. et al.** (2011). Distribution, biological activities, metabolism, and the conceivable function of cis-zeatin-type cytokinins in plants. *J. Exp. Bot.* **62**: 2827–2840.
- Galan, J.M. and Peter, M.** (1999). Ubiquitin-dependent degradation of multiple F-box proteins by an autocatalytic mechanism. *Proc. Natl. Acad. Sci. U. S. A.* **96**: 9124–9.
- Galuszka, P., Popelková, H., Werner, T., Frébortová, J., Pspíšilová, H., Mik, V., Köllmer, I., Schmülling, T., and Frébort, I.** (2007). Biochemical Characterization of Cytokinin Oxidases / Dehydrogenases from *Arabidopsis thaliana* Expressed in *Nicotiana tabacum* L. *J. Plant Growth Regul.* **26**: 255–267.
- Gamble, R.L., Coonfield, M.L., and Schaller, G.E.** (1998). Histidine kinase activity of the ETR1 ethylene receptor from *Arabidopsis*. *Proc. Natl. Acad. Sci. U. S. A.* **95**: 7825–9.
- Gao, Z., Chen, Y.F., Randlett, M.D., Zhao, X.C., Findell, J.L., Kieber, J.J., and Schaller, G.E.** (2003). Localization of the Raf-like Kinase CTR1 to the Endoplasmic Reticulum of *Arabidopsis* through Participation in Ethylene Receptor Signaling Complexes. *J. Biol. Chem.* **278**: 34725–34732.
- Gao, Z. and Schaller, G.E.** (2009). The role of receptor interactions in regulating ethylene signal transduction. *Plant Signal. Behav.* **4**: 1152–3.
- Gao, Z., Wen, C.K., Binder, B.M., Chen, Y.F., Chang, J., Chiang, Y.H., Kerris, R.J., Chang, C., and Schaller, G.E.** (2008). Heteromeric interactions among ethylene receptors mediate signaling in *Arabidopsis*. *J. Biol. Chem.* **283**: 23801–23810.
- Garzón, M., Eifler, K., Faust, A., Scheel, H., Hofmann, K., Koncz, C., Yephremov, A., and Bachmair, A.** (2007). PRT6/At5g02310 encodes an *Arabidopsis* ubiquitin ligase of the N-end rule pathway with arginine specificity and is not the CER3 locus. *FEBS Lett.* **581**: 3189–3196.
- Gausepohl, H. and Behn, C.** (2002). Automated Synthesis of Solid-Phase Bound Peptides. In *Peptide Arrays on Membrane Supports*, J. Koch and M. Mahler, eds (Springer Berlin Heidelberg: Berlin, Heidelberg), pp. 55–68.
- Gendreau, E., Traas, J., Desnos, T., Grandjean, O., Caboche, M., and Höfte, H.** (1997). Cellular basis of hypocotyl growth in *Arabidopsis thaliana*. *Plant Physiol.* **114**: 295–305.
- Geraats, B.P.J., Bakker, P.A.H.M., and van Loon, L.C.** (2002). Ethylene Insensitivity Impairs Resistance to Soilborne Pathogens in Tobacco and *Arabidopsis thaliana*. *Mol. Plant-Microbe Interact.* **15**: 1078–1085.
- Ghassemian, M., Nambara, E., Cutler, S., Kawaide, H., Kamiya, Y., and McCourt, P.** (2000). Regulation of abscisic acid signaling by the ethylene response pathway in *Arabidopsis*. *Plant Cell* **12**: 1117–26.
- Gibbs, D.J.** (2015). Emerging Functions for N-Terminal Protein Acetylation in Plants. *Trends Plant Sci.* **20**: 599–601.
- Gibbs, D.J. et al.** (2014a). Nitric Oxide Sensing in Plants Is Mediated by Proteolytic Control of Group VII ERF Transcription Factors. *Mol. Cell* **53**: 369–379.
- Gibbs, D.J. et al.** (2018). Oxygen-dependent proteolysis regulates the stability of angiosperm polycomb repressive complex 2 subunit VERNALIZATION 2. *Nat. Commun.* **9**: 5438.
- Gibbs, D.J., Bacardit, J., Bachmair, A., and Holdsworth, M.J.** (2014b). The eukaryotic N-end rule pathway: Conserved mechanisms and diverse functions. *Trends Cell Biol.* **24**: 603–611.
- Gibbs, D.J., Conde, J.V., Berckhan, S., Prasad, G., Mendiondo, G.M., and Holdsworth, M.J.** (2015). Group VII Ethylene Response Factors Coordinate Oxygen and Nitric Oxide Signal Transduction and Stress Responses in Plants. *Plant Physiol.* **169**: 23–31.
- Gibbs, D.J., Lee, S.C., Md Isa, N., Gramuglia, S., Fukao, T., Bassel, G.W., Correia, C.S., Corbineau, F., Theodoulou, F.L., Bailey-Serres, J., and Holdsworth, M.J.** (2011). Homeostatic response to hypoxia is regulated by the N-end rule pathway in plants. *Nature* **479**: 415–418.
- Gibson, S.I., Laby, R.J., and Kim, D.** (2001). The sugar-insensitive 1 (*sis1*) mutant of *Arabidopsis* is

- allelic to ctr1. *Biochem. Biophys. Res. Commun.* **280**: 196–203.
- Gifford, E.M. and Foster, A.S.** (1989). *Morphology and evolution of vascular plants* / Ernest M. Gifford, Adriance S. Foster 3rd ed. (WH Freeman and Company: San Francisco, USA).
- Giglione, C., Fieulaine, S., and Meinnel, T.** (2015). N-terminal protein modifications: Bringing back into play the ribosome. *Biochimie* **114**: 134–146.
- Gil, P., Dewey, E., Friml, J., Zhao, Y., Snowden, K.C., Putterill, J., Palme, K., Estelle, M., and Chory, J.** (2001). BIG: a calossin-like protein required for polar auxin transport in *Arabidopsis*. *Genes Dev* **15**: 1985–1997.
- Girod, P.A., Carpenter, T.B., van Nocker, S., Sullivan, M.L., and Vierstra, R.D.** (1993). Homologs of the essential ubiquitin conjugating enzymes UBC1, 4, and 5 in yeast are encoded by a multigene family in *Arabidopsis thaliana*. *Plant J.* **3**: 545–52.
- Giuntoli, B., Shukla, V., Maggiorelli, F., Giorgi, F.M., Lombardi, L., Perata, P., and Licausi, F.** (2017). Age-dependent regulation of ERF-VII transcription factor activity in *Arabidopsis thaliana*. *Plant. Cell Environ.*: 2333–2346.
- Gladkova, C., Maslen, S.L., Skehel, J.M., and Komander, D.** (2018). Mechanism of parkin activation by PINK1. *Nature* **559**: 410–414.
- Glotzer, M., Murray, A.W., and Kirschner, M.W.** (1991). Cyclin is degraded by the ubiquitin pathway. *Nature* **349**: 132–8.
- Goldberg, R.B., Beals, T.P., and Sanders, P.M.** (1993). Anther Development : Basic Principles and Practical Applications. *Plant Cell* **5**: 1217–1229.
- Goldstein, G., Scheid, M., Hammerling, U., Schlesinger, D.H., Niall, H.D., and Boyse, E.A.** (1975). Isolation of a polypeptide that has lymphocyte-differentiating properties and is probably represented universally in living cells. *Proc. Natl. Acad. Sci. U. S. A.* **72**: 11–15.
- Gonda, D.K., Bachmair, A., Wüning, I., Tobias, J.W., Lane, W.S., and Varshavsky, A.** (1989). Universality and structure of the N-end rule. *J. Biol. Chem.* **264**: 16700–16712.
- González-Lamothe, R., Tsitsigiannis, D.I., Ludwig, A.A., Panicot, M., Shirasu, K., and Jones, J.D.G.** (2006). The U-box protein CMPG1 is required for efficient activation of defense mechanisms triggered by multiple resistance genes in tobacco and tomato. *Plant Cell* **18**: 1067–83.
- Goslin, K., Eschen-Lippold, L., Naumann, C., Linster, E., Sorel, M., Klecker, M., de Marchi, R., Kind, A., Wirtz, M., Lee, J., Dismeyer, N., and Graciet, E.** (2019). Differential N-end Rule Degradation of RIN4/NOI Fragments Generated by the AvrRpt2 Effector Protease. *Plant Physiol.* **180**: 2272–2289.
- Graciet, E., Mesiti, F., and Wellmer, F.** (2010). Structure and evolutionary conservation of the plant N-end rule pathway. *Plant J.* **61**: 741–751.
- Graciet, E., Walter, F., Maoileidigh, D.O., Pollmann, S., Meyerowitz, E.M., Varshavsky, A., and Wellmer, F.** (2009). The N-end rule pathway controls multiple functions during *Arabidopsis* shoot and leaf development. *Proc. Natl. Acad. Sci. U. S. A.* **106**: 13618–13623.
- Gray, W.M., del Pozo, J.C., Walker, L., Hobbie, L., Risseuw, E., Banks, T., Crosby, W.L., Yang, M., Ma, H., and Estelle, M.** (1999). Identification of an SCF ubiquitin-ligase complex required for auxin response in *Arabidopsis thaliana*. *Genes Dev.* **13**: 1678–91.
- Green, M.C., Monser, K.P., and Clem, R.J.** (2004). Ubiquitin protein ligase activity of the anti-apoptotic baculovirus protein Op-IAP3. *Virus Res.* **105**: 89–96.
- Grefen, C., Donald, N., Hashimoto, K., Kudla, J., Schumacher, K., and Blatt, M.R.** (2010). A ubiquitin-10 promoter-based vector set for fluorescent protein tagging facilitates temporal stability and native protein distribution in transient and stable expression studies. *Plant J.* **64**: 355–365.
- Grefen, C., Städele, K., Růžička, K., Obrdlík, P., Harter, K., and Horák, J.** (2008). Subcellular localization and in vivo interactions of the *Arabidopsis thaliana* ethylene receptor family

- members. *Mol. Plant* **1**: 308–320.
- Grienenberger, E., Kim, S.S., Lallemand, B., Geoffroy, P., Heintz, D., Souza, C. de A., Heitz, T., Douglas, C.J., and Legrand, M.** (2010). Analysis of TETRAKETIDE α -PYRONE REDUCTASE function in *Arabidopsis thaliana* reveals a previously unknown, but conserved, biochemical pathway in sporopollenin monomer biosynthesis. *Plant Cell* **22**: 4067–83.
- Griffiths, J., Murase, K., Rieu, I., Zentella, R., Zhang, Z.-L., Powers, S.J., Gong, F., Phillips, A.L., Hedden, P., Sun, T., and Thomas, S.G.** (2006). Genetic characterization and functional analysis of the GID1 gibberellin receptors in *Arabidopsis*. *Plant Cell* **18**: 3399–414.
- Grigoryeva, S., Stewart, A.E., Kwon, Y.T., Arfin, S.M., Bradshaw, R.A., Jenkins, N.A., Copeland, N.G., and Varshavsky, A.** (1996). A mouse amidase specific for N-terminal asparagine: The gene, the enzyme, and their function in the N-end rule pathway. *J. Biol. Chem.* **271**: 28521–28532.
- Groll, M., Bajorek, M., Köhler, A., Moroder, L., Rubin, D.M., Huber, R., Glickman, M.H., and Finley, D.** (2000). A gated channel into the proteasome core particle. *Nat. Struct. Biol.* **7**: 1062–1067.
- Groll, M., Ditzel, L., Löwe, J., Stock, D., Bochtler, M., Bartunik, H., and Huber, R.** (1997). Structure of 20S proteasome from yeast at 2.4 Å resolution. *Nature* **386**: 463–471.
- de Groot, R.J., Rümmerapf, T., Kuhn, R.J., Strauss, E.G., and Strauss, J.H.** (1991). Sindbis virus RNA polymerase is degraded by the N-end rule pathway. *Proc. Natl. Acad. Sci. U. S. A.* **88**: 8967–71.
- Grove, M.D., Spencer, G.F., Rohwedder, W.K., Mandava, N., Worley, J.F., Warthen, J.D., Steffens, G.L., Flippen-Anderson, J.L., and Cook, J.C.** (1979). Brassinolide, a plant growth-promoting steroid isolated from *Brassica napus* pollen. *Nature* **281**: 216–217.
- Gu, T., Mazzurco, M., Sulaman, W., Matias, D.D., and Goring, D.R.** (1998). Binding of an arm repeat protein to the kinase domain of the S-locus receptor kinase. *Proc. Natl. Acad. Sci. U. S. A.* **95**: 382–7.
- Gu, Y. and Innes, R.W.** (2012). The KEEP ON GOING Protein of *Arabidopsis* Regulates Intracellular Protein Trafficking and Is Degraded during Fungal Infection. *Plant Cell* **24**: 4717–4730.
- Guan, Y.-F., Huang, X.-Y., Zhu, J., Gao, J.-F., Zhang, H.-X., and Yang, Z.-N.** (2008). RUPTURED POLLEN GRAIN1, a Member of the MtN3/saliva Gene Family, Is Crucial for Exine Pattern Formation and Cell Integrity of Microspores in *Arabidopsis*. *Plant Physiol.* **147**: 852–863.
- Guo, H. and Ecker, J.R.** (2003). Plant Responses to Ethylene Gas Are Mediated by SCFEBF1/EBF2-Dependent Proteolysis of EIN3 Transcription Factor. *Cell* **115**: 667–677.
- Guo, X., Lu, W., Ma, Y., Qin, Q., and Hou, S.** (2013). The BIG gene is required for auxin-mediated organ growth in *Arabidopsis*. *Planta* **237**: 1135–1147.
- Gusti, A., Baumberger, N., Nowack, M., Pusch, S., Eisler, H., Potuschak, T., De Veylder, L., Schnittger, A., and Genschik, P.** (2009). The *Arabidopsis thaliana* F-box protein FBL17 is essential for progression through the second mitosis during pollen development. *PLoS One* **4**: e4780.
- Gutierrez-Marcos, J.F. and Dickinson, H.G.** (2012). Epigenetic reprogramming in plant reproductive lineages. *Plant Cell Physiol.* **53**: 817–823.
- Guzmán, P. and Ecker, J.R.** (1990). Exploiting the triple response of *Arabidopsis* to identify ethylene-related mutants. *Plant Cell* **2**: 513–23.
- Haas, A.L., Bright, P.M., and Jackson, V.E.** (1988). Functional diversity among putative E2 isozymes in the mechanism of ubiquitin-histone ligation. *J. Biol. Chem.* **263**: 13268–75.
- Haas, A.L. and Rose, I.A.** (1982). The mechanism of ubiquitin activating enzyme. A kinetic and equilibrium analysis. *J. Biol. Chem.* **257**: 10329–10337.
- Haas, A.L., Warms, J. V., Hershko, A., and Rose, I.A.** (1982). Ubiquitin-activating enzyme. Mechanism and role in protein-ubiquitin conjugation. *J. Biol. Chem.* **257**: 2543–8.
- Haglund, K., Sigismund, S., Polo, S., Szymkiewicz, I., Di Fiore, P.P., and Dikic, I.** (2003). Multiple

- monoubiquitination of RTKs is sufficient for their endocytosis and degradation. *Nat. Cell Biol.* **5**: 461–466.
- Hakenjos, J.P., Richter, R., Dohmann, E.M.N., Katsiarimpa, A., Isono, E., and Schwechheimer, C.** (2011). MLN4924 Is an Efficient Inhibitor of NEDD8 Conjugation in Plants. *Plant Physiol.* **156**: 527–536.
- Hall, A.E. and Bleecker, A.B.** (2003). Analysis of combinatorial loss-of-function mutants in the Arabidopsis ethylene receptors reveals that the *ers1 etr1* double mutant has severe developmental defects that are EIN2 dependent. *Plant Cell* **15**: 2032–2041.
- Hall, A.E., Findell, J., Schaller, G., Sisler, E., and Bleecker, A.B.** (2000). Ethylene perception by the ERS1 protein in Arabidopsis. *Plant Physiol.* **123**: 1449–58.
- Hall, B.P., Shakeel, S.N., Amir, M., Haq, N.U., Qu, X., and Schaller, G.E.** (2012). Histidine Kinase Activity of the Ethylene Receptor ETR1 Facilitates the Ethylene Response in Arabidopsis. *Plant Physiol.* **159**: 682–695.
- Hall, T.A.** (1999). BioEdit: A User-Friendly Biological Sequence Alignment Editor and Analysis Program for Windows 95/98/NT. *Nucleic Acids Symp. Ser.* **41**: 95–98.
- Hamilton, A.J., Bouzayen, M., and Grierson, D.** (1991). Identification of a tomato gene for the ethylene-forming enzyme by expression in yeast. *Proc. Natl. Acad. Sci. U. S. A.* **88**: 7434–7437.
- Han, S., Cho, H., Noh, J., Qi, J., Jung, H.-J., Nam, H., Lee, S., Hwang, D., Greb, T., and Hwang, I.** (2018). BIL1-mediated MP phosphorylation integrates PXY and cytokinin signalling in secondary growth. *Nat. Plants* **4**: 605–614.
- Hanahan, D.** (1983). Studies on transformation of *Escherichia coli* with plasmids. *J. Mol. Biol.* **166**: 557–80.
- Hanna, J., Leggett, D.S., and Finley, D.** (2003). Ubiquitin Depletion as a Key Mediator of Toxicity by Translational Inhibitors. *Mol. Cell. Biol.* **23**: 9251–9261.
- Hansen, M., Chae, H.S., and Kieber, J.J.** (2009). Regulation of ACS protein stability by cytokinin and brassinosteroid. *Plant J.* **57**: 606–614.
- Hartig, K. and Beck, E.** (2006). Crosstalk between auxin, cytokinins, and sugars in the plant cell cycle. *Plant Biol.* **8**: 389–396.
- Hartig, K. and Beck, E.** (2005). Endogenous cytokinin oscillations control cell cycle progression of tobacco BY-2 cells. *Plant Biol.* **7**: 33–40.
- Harvey, R.B.** (1928). ETHYLENE IS A RIPENER OF FRUITS AND VEGETABLES. *Science* **67**: 421–422.
- Hatfield, P.M., Gosink, M.M., Carpenter, T.B., and Vierstra, R.D.** (1997). The ubiquitin-activating enzyme (E1) gene family in Arabidopsis thaliana. *Plant J.* **11**: 213–226.
- Hattori, Y. et al.** (2009). The ethylene response factors SNORKEL1 and SNORKEL2 allow rice to adapt to deep water. *Nature* **460**: 1026–1030.
- Hause, B., Demus, U., Teichmann, C., Parthier, B., and Wasternack, C.** (1996). Developmental and tissue-specific expression of JIP-23, a jasmonate-inducible protein of barley. *Plant Cell Physiol.* **37**: 641–9.
- He, J.-X., Gendron, J.M., Sun, Y., Gampala, S.S.L., Gendron, N., Sun, C.Q., and Wang, Z.-Y.** (2005). BZR1 is a transcriptional repressor with dual roles in brassinosteroid homeostasis and growth responses. *Science* **307**: 1634–8.
- Hearn, T.J., Marti Ruiz, M.C., Abdul-Awal, S.M., Wimalasekera, R., Stanton, C.R., Haydon, M.J., Theodoulou, F.L., Hannah, M.A., and Webb, A.A.R.** (2018). BIG Regulates Dynamic Adjustment of Circadian Period in Arabidopsis thaliana. *Plant Physiol.* **178**: 358–371.
- Hedhly, A., Hormaza, J.I., and Herrero, M.** (2009). Global warming and sexual plant reproduction. *Trends Plant Sci.* **14**: 30–36.
- Hellmann, H. and Estelle, M.** (2002). Plant development: regulation by protein degradation. *Science*

- 297: 793–797.
- Hershko, A.** (1988). Ubiquitin-mediated Protein Degradation. *J Biol Chem* **263**: 15237–15240.
- Hershko, A. and Ciechanover, A.** (1992). The Ubiquitin System for Protein Degradation. *Annu. Rev. Biochem.* **61**: 761–807.
- Hershko, A., Heller, H., Elias, S., and Ciechanover, A.** (1983). Components of Ubiquitin-Protein Ligase System. *J. Biol. Chem.* **258**: 8206–8214.
- Heslop-Harrison, J.** (1962). Origin of Exine. *Nature* **195**: 1069.
- Higuchi, M. et al.** (2004). In planta functions of the Arabidopsis cytokinin receptor family. *Proc. Natl. Acad. Sci. U. S. A.* **101**: 8821–8826.
- Hilpert, K., Winkler, D.F., and Hancock, R.E.** (2007). Peptide arrays on cellulose support: SPOT synthesis, a time and cost efficient method for synthesis of large numbers of peptides in a parallel and addressable fashion. *Nat. Protoc.* **2**: 1333–1349.
- Hinojosa, L., Matanguihan, J.B., and Murphy, K.M.** (2018). Effect of high temperature on pollen morphology, plant growth and seed yield in quinoa (*Chenopodium quinoa* Willd.). *J. Agron. Crop Sci.*: 33–45.
- Hinz, M., Wilson, I.W., Yang, J., Buerstenbinder, K., Llewellyn, D., Dennis, E.S., Sauter, M., and Dolferus, R.** (2010). Arabidopsis RAP2.2: An Ethylene Response Transcription Factor That Is Important for Hypoxia Survival. *Plant Physiol.* **153**: 757–772.
- Hoecker, U.** (2005). Regulated proteolysis in light signaling. *Curr. Opin. Plant Biol.* **8**: 469–476.
- Hoege, C., Pfander, B., Moldovan, G.L., Pyrowolakis, G., and Jentsch, S.** (2002). RAD6- dependent DNA repair is linked to modification of PCNA by ubiquitin and SUMO. *Nature* **419**: 135–141.
- Hoeller, D., Crosetto, N., Blagoev, B., Raiborg, C., Tikkanen, R., Wagner, S., Kowanetz, K., Breitling, R., Mann, M., Stenmark, H., and Dikic, I.** (2006). Regulation of ubiquitin-binding proteins by monoubiquitination. *Nat. Cell Biol.* **8**: 163–169.
- Hoernstein, S.N.W., Mueller, S.J., Fiedler, K., Schuelke, M., Vanselow, J.T., Schuessele, C., Lang, D., Nitschke, R., Igloi, G.L., Schlosser, A., and Reski, R.** (2016). Identification of Targets and Interaction Partners of Arginyl-tRNA Protein Transferase in the Moss *Physcomitrella patens*. *Mol. Cell. Proteomics* **15**: 1808–22.
- Hofmann, R.M. and Pickart, C.M.** (1999). Noncanonical MMS2-encoded ubiquitin-conjugating enzyme functions in assembly of novel polyubiquitin chains for DNA repair. *Cell* **96**: 645–653.
- Holman, T.J. et al.** (2009). The N-end rule pathway promotes seed germination and establishment through removal of ABA sensitivity in Arabidopsis. *Proc. Natl. Acad. Sci. U. S. A.* **106**: 4549–54.
- Honys, D. and Twell, D.** (2004). Transcriptome analysis of haploid male gametophyte development in Arabidopsis. *Genome Biol.* **5**: R85.1-R.85.13.
- Hoppe, T., Cassata, G., Barral, J.M., Springer, W., Hutagalung, A.H., Epstein, H.F., and Baumeister, R.** (2004). Regulation of the myosin-directed chaperone UNC-45 by a novel E3/E4-multiubiquitylation complex in *C. elegans*. *Cell* **118**: 337–349.
- Horstman, A., Tonaco, I.A.N., Boutilier, K., and Immink, R.G.H.** (2014). A Cautionary note on the use of split-YFP/BiFC in plant protein-protein interaction studies. *Int. J. Mol. Sci.* **15**: 9628–9643.
- Hou, B., Lim, E.K., Higgins, G.S., and Bowles, D.J.** (2004). N-glycosylation of cytokinins by glycosyltransferases of Arabidopsis thaliana. *J. Biol. Chem.* **279**: 47822–47832.
- Hsieh, K. and Huang, A.H.C.** (2007). Tapetosomes in Brassica tapetum accumulate endoplasmic reticulum-derived flavonoids and alkanes for delivery to the pollen surface. *Plant Cell* **19**: 582–96.
- Hu, J. et al.** (2008). Potential sites of bioactive gibberellin production during reproductive growth in Arabidopsis. *Plant Cell* **20**: 320–36.

- Hu, L., Xu, J., Xie, X., Zhou, Y., Tao, P., Li, H., Han, X., Wang, C., Liu, J., Xu, P., Neculai, D., and Xia, Z. (2017). Oligomerization-primed coiled-coil domain interaction with Ubc13 confers processivity to TRAF6 ubiquitin ligase activity. *Nat. Commun.* **8**.
- Hu, R.G., Brower, C.S., Wang, H., Davydov, I. V., Sheng, J., Zhou, J., Yong, T.K., and Varshavsky, A. (2006). Arginyltransferase, its specificity, putative substrates, bidirectional promoter, and splicing-derived isoforms. *J. Biol. Chem.* **281**: 32559–32573.
- Hu, R.G., Sheng, J., Qi, X., Xu, Z., Takahashi, T.T., and Varshavsky, A. (2005). The N-end rule pathway as a nitric oxide sensor controlling the levels of multiple regulators. *Nature* **437**: 981–986.
- Hua, J., Chang, C., Sun, Q., and Meyerowitz, E.M. (1995). Ethylene insensitivity conferred by Arabidopsis EPS gene. *Science* **269**: 1712–1714.
- Hua, J. and Meyerowitz, E.M. (1998). Ethylene responses are negatively regulated by a receptor gene family in Arabidopsis thaliana. *Cell* **94**: 261–271.
- Hua, J., Sakai, H., Nourizadeh, S., Chen, Q.G., Bleecker, A.B., Ecker, J.R., and Meyerowitz, E.M. (1998). EIN4 and ERS2 are members of the putative ethylene receptor gene family in Arabidopsis. *Plant Cell* **10**: 1321–1332.
- Hua, Z. and Vierstra, R.D. (2011). The Cullin-RING Ubiquitin-Protein Ligases. *Annu. Rev. Plant Biol.* **62**: 299–334.
- Huang, A., Hibbert, R.G., De Jong, R.N., Das, D., Sixma, T.K., and Boelens, R. (2011). Symmetry and asymmetry of the RING-RING dimer of Rad18. *J. Mol. Biol.* **410**: 424–435.
- Huang, H., Gao, H., Liu, B., Qi, T., Tong, J., Xiao, L., Xie, D., and Song, S. (2017a). Arabidopsis MYB24 Regulates Jasmonate-Mediated Stamen Development. *Front. Plant Sci.* **8**: 1–8.
- Huang, H., Liu, B., Liu, L., and Song, S. (2017b). Jasmonate action in plant growth and development. *J. Exp. Bot.* **68**: 1349–1359.
- Huang, S., Cerny, E., Qi, Y., Bhat, D., Aydt, C.M., Hanson, D.D., Malloy, K.P., and Ness, L.A. (2003a). Transgenic Studies on the Involvement of Cytokinin and Gibberellin in Male Development. *Plant Physiol.* **131**: 1270–1282.
- Huang, Y., Li, H., Hutchison, C.E., Laskey, J., and Kieber, J.J. (2003b). Biochemical and functional analysis of CTR1, a protein kinase that negatively regulates ethylene signaling in Arabidopsis. *Plant J.* **33**: 221–233.
- Huang, Y., Minaker, S., Roth, C., Huang, S., Hieter, P., Lipka, V., Wiermer, M., and Li, X. (2014). An E4 Ligase Facilitates Polyubiquitination of Plant Immune Receptor Resistance Proteins in Arabidopsis. *Plant Cell* **26**: 485–496.
- Hülkamp, M., Kopczak, S.D., Horejsi, T.F., Kihl, B.K., and Pruitt, R.E. (1995). Identification of genes required for pollen-stigma recognition in Arabidopsis thaliana. *Plant J.* **8**: 703–14.
- Humbard, M.A., Surkov, S., De Donatis, G.M., Jenkins, L.M., and Maurizi, M.R. (2013). The N-degradome of Escherichia coli: Limited proteolysis in vivo generates a large pool of proteins bearing N-degrons. *J. Biol. Chem.* **288**: 28913–28924.
- Hutchison, C.E., Li, J., Argueso, C., Gonzalez, M., Lee, E., Lewis, M.W., Maxwell, B.B., Perdue, T.D., Schaller, G.E., Alonso, J.M., Ecker, J.R., and Kieber, J.J. (2006). The Arabidopsis histidine phosphotransfer proteins are redundant positive regulators of cytokinin signaling. *Plant Cell* **18**: 3073–87.
- Hwang, C.-S., Shemorry, A., and Varshavsky, A. (2010a). N-terminal acetylation of cellular proteins creates specific degradation signals. *Science* **327**: 973–7.
- Hwang, C.-S., Shemorry, A., and Varshavsky, A. (2010b). Supplemental information. *Science* **327**: 973–977.
- Hwang, I., Chen, H.-C., and Sheen, J. (2002). Two-component signal transduction pathways in Arabidopsis. *Plant Physiol.* **129**: 500–15.

- Hwang, I. and Sheen, J.** (2001). Two-component circuitry in Arabidopsis cytokinin signal transduction. *Nature* **413**: 383–389.
- Ibañez, C. et al.** (2018). Brassinosteroids Dominate Hormonal Regulation of Plant Thermomorphogenesis via BZR1. *Curr. Biol.*: 1–8.
- Ibañez, C., Poeschl, Y., Peterson, T., Bellstädt, J., Denk, K., Gogol-Döring, A., Quint, M., and Delker, C.** (2017). Ambient temperature and genotype differentially affect developmental and phenotypic plasticity in Arabidopsis thaliana. *BMC Plant Biol.* **17**: 1–14.
- Ichihashi, Y., Kawade, K., Usami, T., Horiguchi, G., Takahashi, T., and Tsukaya, H.** (2011). Key Proliferative Activity in the Junction between the Leaf Blade and Leaf Petiole of Arabidopsis. *Plant Physiol.* **157**: 1151–1162.
- Ichihashi, Y. and Tsukaya, H.** (2015). Behavior of Leaf Meristems and Their Modification. *Front. Plant Sci.* **6**: 1–8.
- Ikeda, F. et al.** (2011). SHARPIN forms a linear ubiquitin ligase complex regulating NF- κ B activity and apoptosis. *Nature* **471**: 637–641.
- Imaizumi, T.** (2005). F-Box protein mediates cyclic degradation of a repressor of CONSTANS. *Science* **309**: 293–297.
- Imamura, A., Hanaki, N., Nakamura, A., Suzuki, T., Taniguchi, M., Kiba, T., Ueguchi, C., Sugiyama, T., and Mizuno, T.** (1999). Compilation and characterization of Arabidopsis thaliana response regulators implicated in His-Asp phosphorelay signal transduction. *Plant Cell Physiol.* **40**: 733–42.
- Inobe, T., Fishbain, S., Prakash, S., and Matouschek, A.** (2011). Defining the geometry of the two-component proteasome degron. *Nat. Chem. Biol.* **7**: 161–167.
- Dello Iorio, R. et al.** (2008). A Genetic Framework for the Control of Cell Division and Differentiation in the Root Meristem. *Science* **322**: 1380–1384.
- Dello Iorio, R., Linhares, F.S., Scacchi, E., Casamitjana-Martinez, E., Heidstra, R., Costantino, P., and Sabatini, S.** (2007). Cytokinins Determine Arabidopsis Root-Meristem Size by Controlling Cell Differentiation. *Curr. Biol.* **17**: 678–682.
- Isayenkov, S., Mrosk, C., Stenzel, I., Strack, D., and Hause, B.** (2005). Suppression of allene oxide cyclase in hairy roots of Medicago truncatula reduces jasmonate levels and the degree of mycorrhization with Glomus intraradices. *Plant Physiol.* **139**: 1401–10.
- Ishida, K., Yamashino, T., Yokoyama, A., and Mizuno, T.** (2008). Three type-B response regulators, ARR1, ARR10 and ARR12, play essential but redundant roles in cytokinin signal transduction throughout the life cycle of Arabidopsis thaliana. *Plant Cell Physiol.* **49**: 47–57.
- Ishiguro, S., Kawai-Oda, A., Ueda, J., Nishida, I., and Okada, K.** (2001). The DEFECTIVE IN ANTHHER DEHISCENCE gene encodes a novel phospholipase A1 catalyzing the initial step of jasmonic acid biosynthesis, which synchronizes pollen maturation, anther dehiscence, and flower opening in Arabidopsis. *Plant Cell* **13**: 2191–2209.
- Ito, T., Ng, K.-H., Lim, T.-S., Yu, H., and Meyerowitz, E.M.** (2007). The homeotic protein AGAMOUS controls late stamen development by regulating a jasmonate biosynthetic gene in Arabidopsis. *Plant Cell* **19**: 3516–29.
- Ito, T., Wellmer, F., Yu, H., Das, P., Ito, H., Alves-Ferreira, M., Riechmann, J.L., and Meyerowitz, E.M.** (2004). The homeotic protein AGAMOUS controls microsporogenesis by regulation of SPOROCTELESS. *Nature* **430**: 356–360.
- Ito, Y. and Kurata, N.** (2006). Identification and characterization of cytokinin-signalling gene families in rice. *Gene* **382**: 57–65.
- Itoh, H., Matsuoka, M., and Steber, C.M.** (2003). A role for the ubiquitin-26S-proteasome pathway in gibberellin signaling. *Trends Plant Sci.* **8**: 492–497.

- Izhaki, A., Borochoy, A., Zamski, E., and Weiss, D. (2002). Gibberellin regulates post-microsporogenesis processes in petunia anthers. *Physiol. Plant.* **115**: 442–447.
- Jacobsen, S.E. and Olszewski, N.E. (1991). Characterization of the Arrest in Anther Development Associated with Gibberellin Deficiency of the gib-1 Mutant of Tomato. *Plant Physiol.* **97**: 409–414.
- Jarret, D.A., Morris, J., Cullen, D.W., Gordon, S.L., Verrall, S.R., Milne, L., Hedley, P.E., Allwood, J.W., Brennan, R.M., and Hancock, R.D. (2018). A Transcript and Metabolite Atlas of Blackcurrant Fruit Development Highlights Hormonal Regulation and Reveals the Role of Key Transcription Factors. *Front. Plant Sci.* **9**: 1–22.
- Jegadeesan, S., Beery, A., Altahan, L., Meir, S., Pressman, E., and Firon, N. (2018). Ethylene production and signaling in tomato (*Solanum lycopersicum*) pollen grains is responsive to heat stress conditions. *Plant Reprod.*: 1–17.
- Jenks, M.A., Tuttle, H.A., Eigenbrode, S.D., and Feldmann, K.A. (1995). Leaf Epicuticular Waxes of the Eceriferum Mutants in Arabidopsis. *Plant Physiol.* **108**: 369–377.
- Jentsch, S., McGrath, J.P., and Varshavsky, A. (1987). The yeast DNA repair gene RAD6 encodes a ubiquitin-conjugating enzyme. *Nature* **329**: 131–4.
- Jessen, D., Olbrich, A., Knüfer, J., Krüger, A., Hoppert, M., Polle, A., and Fulda, M. (2011). Combined activity of LACS1 and LACS4 is required for proper pollen coat formation in Arabidopsis. *Plant J.* **68**: 715–726.
- Jewell, J.B. and Browse, J. (2016). Epidermal jasmonate perception is sufficient for all aspects of jasmonate-mediated male fertility in Arabidopsis. *Plant J.* **85**: 634–47.
- Ji, C.H. et al. (2019). The N-Degron Pathway Mediates ER-phagy. *Mol. Cell.*
- Jia, G., Liu, X., Owen, H.A., and Zhao, D. (2008). Signaling of cell fate determination by the TPD1 small protein and EMS1 receptor kinase. *Proc. Natl. Acad. Sci. U. S. A.* **105**: 2220–2225.
- Jiang, Y. et al. (2016). The arginylation branch of the N-end rule pathway positively regulates cellular autophagic flux and clearance of proteotoxic proteins. *Autophagy* **12**: 2197–2212.
- Jin, H., Pang, L., Fang, S., Chu, J., Li, R., and Zhu, Z. (2018). High ambient temperature antagonizes ethylene-induced exaggerated apical hook formation in etiolated Arabidopsis seedlings. *Plant. Cell Environ.* **3**: 1–11.
- Joazeiro, C.A.P. and Weissman, A.M. (2000). RING finger proteins: mediators of ubiquitin ligase activity. *Cell* **102**: 549–552.
- Johansen, T. and Lamark, T. (2011). Selective autophagy mediated by autophagic adapter proteins. *Autophagy* **7**: 279–296.
- Johnson, K.A., Sistrunk, M.L., Polisensky, D.H., and Braam, J. (1998). Arabidopsis thaliana Responses to Mechanical Stimulation Do Not Require ETR1 or EIN2. *Plant Physiol.* **116**: 643–649.
- Johnston, J.A., Johnson, E.S., Waller, P.R., and Varshavsky, A. (1995). Methotrexate inhibits proteolysis of Dihydrofolate reductase by the N-end rule pathway. *J. Biol. Chem.* **270**: 8172–8178.
- Jones, J.S., Weber, S., and Prakash, L. (1988a). The *Saccharomyces cerevisiae* RAD18 gene encodes a protein that contains potential zinc finger domains for nucleic acid binding and a putative nucleotide binding sequence. *Nucleic Acids Res.* **16**: 7119–31.
- Jones, L.H., Martinková, H., Strnad, M., and Hanke, D.E. (1996). Occurrence of aromatic cytokinins in oil palm (*Elaeis guineensis* Jacq.). *J. Plant Growth Regul.* **15**: 39–49.
- Jones, M.G., Fish, N., and Lindsey, K. (1988b). Plant tissue culture. *Methods Mol. Biol.* **4**: 499–517.
- Josse, E.M. and Halliday, K.J. (2008). Skotomorphogenesis: The Dark Side of Light Signalling. *Curr. Biol.* **18**: R1144–R1146.
- Ju, C. et al. (2012). CTR1 phosphorylates the central regulator EIN2 to control ethylene hormone

- signaling from the ER membrane to the nucleus in *Arabidopsis*. *Proc. Natl. Acad. Sci. U. S. A.* **109**: 19486–91.
- Ju, C. and Chang, C.** (2012). Advances in ethylene signalling: protein complexes at the endoplasmic reticulum membrane. *AoB Plants* **2012**: pls031–pls031.
- Ju, C., Van De Poel, B., Cooper, E.D., Thierer, J.H., Gibbons, T.R., Delwiche, C.F., and Chang, C.** (2015). Conservation of ethylene as a plant hormone over 450 million years of evolution. *Nat. Plants* **1**: 1–7.
- Jun, S.H., Han, M.J., Lee, S., Seo, Y.S., Kim, W.T., and An, G.** (2004). OsEIN2 is a positive component in ethylene signaling in rice. *Plant Cell Physiol.* **45**: 281–289.
- Jura, N., Scotto-Lavino, E., Sobczyk, A., and Bar-Sagi, D.** (2006). Differential modification of Ras proteins by ubiquitination. *Mol. Cell* **21**: 679–687.
- Kakimoto, T.** (1996). CK11, a histidine kinase homolog implicated in cytokinin signal transduction. *Science* **274**: 982–985.
- Kakimoto, T.** (2001). Identification of plant cytokinin biosynthetic enzymes as dimethylallyl diphosphate:ATP/ADP isopentenyltransferases. *Plant Cell Physiol.* **42**: 677–85.
- Kamiyoshihara, Y., Tieman, D.M., Huber, D.J., and Klee, H.J.** (2012). Ligand-Induced Alterations in the Phosphorylation State of Ethylene Receptors in Tomato Fruit. *Plant Physiol.* **160**: 488–497.
- Karimi, M., Bleys, A., Vanderhaeghen, R., and Hilson, P.** (2007). Building Blocks for Plant Gene Assembly. *Plant Physiol.* **145**: 1183–1191.
- Kats, I., Khmelinskii, A., Kschonsak, M., Huber, F., Knieß, R.A., Bartosik, A., and Knop, M.** (2018). Mapping Degradation Signals and Pathways in a Eukaryotic N-terminome. *Mol Cell* **70**: 488–501.e5.
- Katsir, L., Chung, H.S., Koo, A.J., and Howe, G.A.** (2008a). Jasmonate signaling: a conserved mechanism of hormone sensing. *Curr. Opin. Plant Biol.* **11**: 428–435.
- Katsir, L., Schillmiller, A.L., Staswick, P.E., He, S.Y., and Howe, G.A.** (2008b). COI1 is a critical component of a receptor for jasmonate and the bacterial virulence factor coronatine. *Proc. Natl. Acad. Sci. U. S. A.* **105**: 7100–7105.
- Katzmann, D.J., Babst, M., and Emr, S.D.** (2001). Ubiquitin-dependent sorting into the multivesicular body pathway requires the function of a conserved endosomal protein sorting complex, ESCRT-I. *Cell* **106**: 145–155.
- Kazuo Hosoda, Aya Imamura, Etsuko Katoh, Tomohisa Hatta, Mari Tachiki, Hisami Yamada, Takeshi Mizuno, and Toshimasa Yamazakia** (2002). Molecular structure of the GARP family of plant Myb-related DNA binding motifs of the *Arabidopsis* response regulators. *Plant Cell* **14**: 2015–2029.
- Kepinski, S. and Leyser, O.** (2005). The *Arabidopsis* F-box protein TIR1 is an auxin receptor. *Nature* **435**: 446–451.
- Kieber, J.J. et al.** (1993). CTR1, a Negative Regulator of the Ethylene Pathway in *Arabidopsis*, Encodes a Member of the Raf Family of Protein Kinases. *Cell* **72**: 427–441.
- Kim, D.-Y., Scalf, M., Smith, L.M., and Vierstra, R.D.** (2013a). Advanced Proteomic Analyses Yield a Deep Catalog of Ubiquitylation Targets in *Arabidopsis*. *Plant Cell* **25**: 1523–1540.
- Kim, H.J., Chiang, Y.-H., Kieber, J.J., and Schaller, G.E.** (2013b). SCF-KMD controls cytokinin signaling by regulating the degradation of type-B response regulators. *Proc. Natl. Acad. Sci. U. S. A.* **110**: 10028–33.
- Kim, H.J., Oh, S.A., Brownfield, L., Hong, S.H., Ryu, H., Hwang, I., Twell, D., and Nam, H.G.** (2008). Control of plant germline proliferation by SCFFBL17 degradation of cell cycle inhibitors. *Nature* **455**: 1134–1137.
- Kim, H.K., Kim, R.R., Oh, J.H., Cho, H., Varshavsky, A., and Hwang, C.S.** (2014). The N-terminal

- methionine of cellular proteins as a degradation signal. *Cell* **156**: 158–169.
- Kim, J.-M., Seok, O.-H., Ju, S., Heo, J.-E., Yeom, J., Kim, D.-S., Yoo, J.-Y., Varshavsky, A., Lee, C., and Hwang, C.-S.** (2018a). Formyl-methionine as an N-degron of a eukaryotic N-end rule pathway. *Science* **0174**: eaat0174.
- Kim, J., Patterson, S.E., and Binder, B.M.** (2013c). Reducing jasmonic acid levels causes ein2 mutants to become ethylene responsive. *FEBS Lett.* **587**: 226–230.
- Kim, K.-W., Franceschi, V.R., Davin, L.B., and Lewis, N.G.** (2006). Beta-glucuronidase as reporter gene: advantages and limitations. *Methods Mol. Biol.* **323**: 263–73.
- Kim, S.H., Kwon, C., Lee, J.H., and Chung, T.** (2012). Genes for plant autophagy: Functions and interactions. *Mol. Cells* **34**: 413–423.
- Kim, S.S. et al.** (2010). *LAP6/POLYKETIDE SYNTHASE A* and *LAP5/POLYKETIDE SYNTHASE B* Encode Hydroxyalkyl α -Pyrone Synthases Required for Pollen Development and Sporopollenin Biosynthesis in *Arabidopsis thaliana*. *Plant Cell* **22**: 4045–4066.
- Kim, S.T., Lee, Y.J., Tasaki, T., Hwang, J., Kang, M.J., Yi, E.C., Kim, B.Y., and Kwon, Y.T.** (2018b). The N-recognin UBR4 of the N-end rule pathway is required for neurogenesis and homeostasis of cell surface proteins. *PLoS One* **13**: e0202260.
- Kim, S.T., Lee, Y.J., Tasaki, T., Mun, S.R., Hwang, J., Kang, M.J., Ganipiseti, S., Yi, E.C., Kim, B.Y., and Kwon, Y.T.** (2018c). The N-recognin UBR4 of the N-end rule pathway is targeted to and required for the biogenesis of the early endosome. *J. Cell Sci.* **131**: jcs217646.
- Kim, S.T., Tasaki, T., Zakrzewska, A., Yoo, Y.D., Sung, K.S., Kim, S.H., Cha-Molstad, H., Hwang, J., Kim, K.A., Kim, B.Y., and Kwon, Y.T.** (2013d). The N-end rule proteolytic system in autophagy. *Autophagy* **9**: 1100–1103.
- Kim, S.Y., Hong, C.B., and Lee, I.** (2001). Heat Shock Stress Causes Stage-specific Male Sterility in *Arabidopsis thaliana*. *J. Plant Res.* **114**: 301–307.
- Kim, T.-W., Hwang, J.-Y., Kim, Y.-S., Joo, S.-H., Chang, S.C., Lee, J.S., Takatsuto, S., and Kim, S.-K.** (2005). *Arabidopsis* CYP85A2, a cytochrome P450, mediates the Baeyer-Villiger oxidation of castasterone to brassinolide in brassinosteroid biosynthesis. *Plant Cell* **17**: 2397–412.
- Kinoshita-Tsujimura, K. and Kakimoto, T.** (2011). Cytokinin receptors in sporophytes are essential for male and female functions in *Arabidopsis thaliana*. *Plant Signal. Behav.* **6**: 66–71.
- Kircher, S. and Schopfer, P.** (2012). Photosynthetic sucrose acts as cotyledon-derived long-distance signal to control root growth during early seedling development in *Arabidopsis*. *Proc. Natl. Acad. Sci. U. S. A.* **109**: 11217–11221.
- Klecker, M. and Dissmeyer, N.** (2016). Peptide Arrays for Binding Studies of E3 Ubiquitin Ligases. *Methods Mol Biol.* **1450**: 85–94.
- Klionsky, D.J.** (2007). Autophagy: from phenomenology to molecular understanding in less than a decade. *Nat Rev Mol Cell Biol.* **8**: 931–937.
- Klionsky, D.J. and Ohsumi, Y.** (1999). Vacuolar import of proteins and organelles from the cytoplasm. *Annu. Rev. Cell Dev. Biol.* **15**: 1–32.
- Koegl, M., Hoppe, T., Schlenker, S., Ulrich, H.D., Mayer, T.U., and Jentsch, S.** (1999). A novel ubiquitination factor, E4, is involved in multiubiquitin chain assembly. *Cell* **96**: 635–644.
- Komander, D. and Rape, M.** (2012). The Ubiquitin Code. *Annu. Rev. Biochem.* **81**: 203–229.
- Koops, P., Pelsler, S., Ignatz, M., Klose, C., Marrocco-Selden, K., and Kretsch, T.** (2011). EDL3 is an F-box protein involved in the regulation of abscisic acid signalling in *Arabidopsis thaliana*. *J. Exp. Bot.* **62**: 5547–5560.
- Koornneef, M., Hanhart, C.J., and Thiel, F.** (1989). A genetic and phenotypic description of eceriferum mutants in *Arabidopsis thaliana*. *J. Hered.* **80**: 118–122.
- Koornneef, M. and Stam, P.** (1992). Genetic analysis. In *Methods in Arabidopsis Research*, C. Koncz,

- N. Chua, and J. Schell, eds (World Scientific, New Jersey), pp. 83–99.
- Koren, I., Timms, R.T., Kula, T., Xu, Q., Li, M.Z., and Elledge, S.J.** (2018). The Eukaryotic Proteome Is Shaped by E3 Ubiquitin Ligases Targeting C-Terminal Degrons. *Cell* **173**: 1622–1635.e14.
- Korver, R.A., Koevoets, I.T., and Testerink, C.** (2018). Out of Shape During Stress: A Key Role for Auxin. *Trends Plant Sci.* **23**: 783–793.
- Kraft, E., Bostick, M., Jacobsen, S.E., and Callis, J.** (2008). ORTH/VIM proteins that regulate DNA methylation are functional ubiquitin E3 ligases. *Plant J.* **56**: 704–715.
- Kraft, E., Stone, S.L., Ma, L., Su, N., Gao, Y., Lau, O.-S., Deng, X.-W., and Callis, J.** (2005). Genome Analysis and Functional Characterization of the E2 and RING-Type E3 Ligase Ubiquitination Enzymes of Arabidopsis. *PLANT Physiol.* **139**: 1597–1611.
- Kurakawa, T., Ueda, N., Maekawa, M., Kobayashi, K., Kojima, M., Nagato, Y., Sakakibara, H., and Kyojuka, J.** (2007). Direct control of shoot meristem activity by a cytokinin-activating enzyme. *Nature* **445**: 652–655.
- Kurepa, J., Li, Y., Perry, S.E., and Smalle, J.A.** (2014). Ectopic expression of the phosphomimic mutant version of Arabidopsis response regulator 1 promotes a constitutive cytokinin response phenotype. *BMC Plant Biol.* **14**: 28.
- Kurepa, J., Walker, J.M., Smalle, J., Gosink, M.M., Davis, S.J., Durham, T.L., Sung, D.Y., and Vierstra, R.D.** (2003). The small ubiquitin-like modifier (SUMO) protein modification system in Arabidopsis. Accumulation of sumo1 and -2 conjugates is increased by stress. *J. Biol. Chem.* **278**: 6862–6872.
- Kuroha, T., Tokunaga, H., Kojima, M., Ueda, N., Ishida, T., Nagawa, S., Fukuda, H., Sugimoto, K., and Sakakibara, H.** (2009). Functional Analyses of LONELY GUY Cytokinin-Activating Enzymes Reveal the Importance of the Direct Activation Pathway in Arabidopsis. *Plant Cell* **21**: 3152–3169.
- Kuromori, T., Ito, T., Sugimoto, E., and Shinozaki, K.** (2011). Arabidopsis mutant of AtABCG26, an ABC transporter gene, is defective in pollen maturation. *J. Plant Physiol.* **168**: 2001–2005.
- Kushwah, S. and Laxmi, A.** (2014). The interaction between glucose and cytokinin signal transduction pathway in Arabidopsis thaliana. *Plant. Cell Environ.* **37**: 235–53.
- Kwon, D.H., Park, O.H., Kim, L., Jung, Y.O., Park, Y., Jeong, H., Hyun, J., Kim, Y.K., and Song, H.K.** (2018). Insights into degradation mechanism of N-end rule substrates by p62/SQSTM1 autophagy adapter. *Nat. Commun.* **9**: 3291.
- Kwon, Y., Oh, J.E., Noh, H., Hong, S.W., Bhoo, S.H., and Lee, H.** (2011). The ethylene signaling pathway has a negative impact on sucrose-induced anthocyanin accumulation in Arabidopsis. *J. Plant Res.* **124**: 193–200.
- Kwon, Y.T., Balogh, S. a, Davydov, I. V, Kashina, A.S., Yoon, J.K., Xie, Y., Gaur, A., Hyde, L., Denenberg, V.H., and Varshavsky, A.** (2000). Altered activity, social behavior, and spatial memory in mice lacking the NTAN1p amidase and the asparagine branch of the N-end rule pathway. *Mol. Cell. Biol.* **20**: 4135–4148.
- Kwon, Y.T., Kashina, A.S., and Varshavsky, A.** (1999). Alternative splicing results in differential expression, activity, and localization of the two forms of arginyl-tRNA-protein transferase, a component of the N-end rule pathway. *Mol. Cell. Biol.* **19**: 182–193.
- Kwon, Y.T., Kashina, A.S., Davydov, I. V., Hu, R.-G., An, J.Y., Seo, J.W., Du, F., and Varshavsky, A.** (2002). An Essential Role of N-Terminal Arginylation in Cardiovascular Development. *Science* **297**: 96–99.
- Kwon, Y.T., Reiss, Y., Fried, V.A., Hershko, A., Yoon, J.K., Gonda, D.K., Sangan, P., Copeland, N.G., Jenkins, N.A., and Varshavsky, A.** (1998). The mouse and human genes encoding the recognition component of the N-end rule pathway. *Proc. Natl. Acad. Sci. U. S. A.* **95**: 7898–7903.
- Kwon, Y.T., Xia, Z., An, J.Y., Tasaki, T., Davydov, I. V, Seo, J.W., Sheng, J., Xie, Y., and Varshavsky, A.** (2003). Female lethality and apoptosis of spermatocytes in mice lacking the UBR2 ubiquitin

- ligase of the N-end rule pathway. *Mol. Cell. Biol.* **23**: 8255–71.
- Kwon, Y.T., Xia, Z., Davydov, I. V, Lecker, S.H., and Varshavsky, A.** (2001). Construction and analysis of mouse strains lacking the ubiquitin ligase UBR1 (E3alpha) of the N-end rule pathway. *Mol. Cell. Biol.* **21**: 8007–21.
- Kyhse-Andersen, J.** (1984). Electrophoretic transfer of multiple gels: a simple apparatus without buffer tank for rapid transfer of proteins from polyacrylamide to nitrocellulose. *J. Biochem. Biophys. Methods* **10**: 203–9.
- Lalanne, E. and Twell, D.** (2002). Genetic Control of Male Germ Unit Organization in Arabidopsis. *Plant Physiol.* **129**: 865–875.
- Lämke, J. and Bäurle, I.** (2017). Epigenetic and chromatin-based mechanisms in environmental stress adaptation and stress memory in plants. *Genome Biol.* **18**: 1–11.
- Lander, G.C., Estrin, E., Matyskiela, M.E., Bashore, C., Nogales, E., and Martin, A.** (2012). Complete subunit architecture of the proteasome regulatory particle. *Nature* **482**: 186–191.
- Lando, D., Gorman, J.J., Whitelaw, M.L., and Peet, D.J.** (2003). Oxygen-dependent regulation of hypoxia-inducible factors by prolyl and asparaginyl hydroxylation. *Eur. J. Biochem.* **270**: 781–790.
- Lange, P.F. and Overall, C.M.** (2013). Protein TAILS: When termini tell tales of proteolysis and function. *Curr. Opin. Chem. Biol.* **17**: 73–82.
- Larkindale, J.** (2002). Protection against Heat Stress-Induced Oxidative Damage in Arabidopsis Involves Calcium, Abscisic Acid, Ethylene, and Salicylic Acid. *Plant Physiol.* **128**: 682–695.
- Lauwers, E., Erpapazoglou, Z., Haguenaer-Tsapis, R., and André, B.** (2010). The ubiquitin code of yeast permease trafficking. *Trends Cell Biol.* **20**: 196–204.
- Lauwers, E., Jacob, C., and Andre, B.** (2009). K63-linked ubiquitin chains as a specific signal for protein sorting into the multivesicular body pathway. *J. Cell Biol.* **185**: 493–502.
- Laxmi, A., Paul, L.K., Raychaudhuri, A., Peters, J.L., and Khurana, J.P.** (2006). Arabidopsis cytokinin-resistant mutant, *cnr1*, displays altered auxin responses and sugar sensitivity. *Plant Mol. Biol.* **62**: 409–425.
- Lebendiker, M. and Danieli, T.** (2014). Production of prone-to-aggregate proteins. *FEBS Lett.* **588**: 236–246.
- Lechtenberg, B.C., Rajput, A., Sanishvili, R., Dobaczewska, M.K., Ware, C.F., Mace, P.D., and Riedl, S.J.** (2016). Structure of a HOIP/E2~ubiquitin complex reveals RBR E3 ligase mechanism and regulation. *Nature* **529**: 546–550.
- Lee, H.Y., Chen, Y.C., Kieber, J.J., and Yoon, G.M.** (2017). Regulation of the turnover of ACC synthases by phytohormones and heterodimerization in Arabidopsis. *Plant J.* **91**: 491–504.
- Lee, H.Y. and Yoon, G.M.** (2018). Regulation of Ethylene Biosynthesis by Phytohormones in Etiolated Rice (*Oryza sativa* L.) Seedlings. *Mol. Cells* **41**: 311–319.
- Lee, K.-E., Heo, J.-E., Kim, J.-M., and Hwang, C.-S.** (2016). N-Terminal Acetylation-Targeted N-End Rule Proteolytic System: The Ac/N-End Rule Pathway. *Mol. Cells* **39**: 169–178.
- Lee, M.J., Tasaki, T., Moroi, K., An, J.Y., Kimura, S., Davydov, I. V, and Kwon, Y.T.** (2005). RGS4 and RGS5 are in vivo substrates of the N-end rule pathway. *Proc. Natl. Acad. Sci. U. S. A.* **102**: 15030–5.
- Legge, G.B., Martinez-Yamout, M.A., Hambly, D.M., Trinh, T., Lee, B.M., Dyson, H.J., and Wright, P.E.** (2004). ZZ domain of CBP: An unusual zinc finger fold in a protein interaction module. *J. Mol. Biol.* **343**: 1081–1093.
- Leggett, D.S., Hanna, J., Borodovsky, A., Crosas, B., Schmidt, M., Baker, R.T., Walz, T., Ploegh, H., and Finley, D.** (2002). Multiple Associated Proteins Regulate Proteasome Structure and Function. *Mol. Cell* **10**: 495–507.

- Lehman, A., Black, R., and Ecker, J.R.** (1996). HOOKLESS1, an Ethylene Response Gene, Is Required for Differential Cell Elongation in the Arabidopsis Hypocotyl. *Cell* **85**: 183–194.
- Lei, M., Zhu, C., Liu, Y., Karthikeyan, A.S., Bressan, R.A., Raghothama, K.G., and Liu, D.** (2011). Ethylene signalling is involved in regulation of phosphate starvation-induced gene expression and production of acid phosphatases and anthocyanin in Arabidopsis. *New Phytol.* **189**: 1084–1095.
- Leivar, P., Monte, E., Oka, Y., Liu, T., Carle, C., Castillon, A., Huq, E., and Quail, P.H.** (2008). Multiple Phytochrome-Interacting bHLH Transcription Factors Repress Premature Seedling Photomorphogenesis in Darkness. *Curr. Biol.* **18**: 1815–1823.
- Lemus, L. and Goder, V.** (2014). Regulation of Endoplasmic Reticulum-Associated Protein Degradation (ERAD) by Ubiquitin. *Cells* **3**: 824–847.
- Letham, D.S.** (1973). Cytokinins from Zea mays. *Phytochemistry* **12**: 2445–2455.
- Leung, G.C., Murphy, J.M., Briant, D., and Sicheri, F.** (2009). Characterization of Kinase Target Phosphorylation Consensus Motifs Using Peptide SPOT Arrays. In *Peptide Microarrays, Methods in Molecular Biology*, pp. 187–195.
- Li, D.-D., Xue, J.-S., Zhu, J., and Yang, Z.-N.** (2017a). Gene Regulatory Network for Tapetum Development in Arabidopsis thaliana. *Front. Plant Sci.* **8**: 1–14.
- Li, F. and Vierstra, R.D.** (2012). Autophagy: A multifaceted intracellular system for bulk and selective recycling. *Trends Plant Sci.* **17**: 526–537.
- Li, J., Nagpal, P., Vitart, V., McMorris, T.C., and Chory, J.** (1996). A role for brassinosteroids in light-dependent development of Arabidopsis. *Science* **272**: 398–401.
- Li, J., Nam, K.H., Vafeados, D., and Chory, J.** (2001a). BIN2, a new brassinosteroid-insensitive locus in Arabidopsis. *Plant Physiol* **127**: 14–22.
- Li, L., Li, C., and Howe, G.A.** (2001b). Genetic Analysis of Wound Signaling in Tomato. Evidence for a Dual Role of Jasmonic Acid in Defense and Female Fertility. *Plant Physiol.* **127**: 1414–1417.
- Li, L., Nelson, C.J., Trösch, J., Castleden, I., Huang, S., and Millar, A.H.** (2017b). Protein Degradation Rate in *Arabidopsis thaliana* Leaf Growth and Development. *Plant Cell* **29**: 207–228.
- Li, L., Zhao, Y., McCaig, B.C., Wingerd, B.A., Wang, J., Whalon, M.E., Pichersky, E., and Howe, G.A.** (2004). The tomato homolog of CORONATINE-INSENSITIVE1 is required for the maternal control of seed maturation, jasmonate-signaled defense responses, and glandular trichome development. *Plant Cell* **16**: 126–43.
- Li, M., Tang, D., Wang, K., Wu, X., Lu, L., Yu, H., Gu, M., Yan, C., and Cheng, Z.** (2011). Mutations in the F-box gene LARGER PANICLE improve the panicle architecture and enhance the grain yield in rice. *Plant Biotechnol. J.* **9**: 1002–1013.
- Li, Q., Zheng, J., Li, S., Huang, G., Skilling, S.J., Wang, L., Li, L., Li, M., Yuan, L., and Liu, P.** (2017c). Transporter-Mediated Nuclear Entry of Jasmonoyl-Isoleucine Is Essential for Jasmonate Signaling. *Mol. Plant* **10**: 695–708.
- Li, W., Ma, M., Feng, Y., Li, H., Wang, Y., Ma, Y., Li, M., An, F., and Guo, H.** (2015). EIN2-Directed Translational Regulation of Ethylene Signaling in Arabidopsis. *Cell* **163**: 670–683.
- Li, X.** (2011). Arabidopsis Pollen Tube Germination. *BIO-PROTOCOL* **1**.
- Li, Y., Zhang, L., Li, D., Liu, Z., Wang, J., Li, X., and Yang, Y.** (2016). The Arabidopsis F-box E3 ligase RIFP1 plays a negative role in abscisic acid signalling by facilitating ABA receptor RCAR3 degradation. *Plant Cell Environ.* **39**: 571–582.
- Li, Y., Zheng, L., Corke, F., Smith, C., and Bevan, M.W.** (2008). Control of final seed and organ size by the DA1 gene family in Arabidopsis thaliana. *Genes Dev.* **22**: 1331–1336.
- Liao, C.-J., Lai, Z., Lee, S., Yun, D.J., and Mengiste, T.** (2016). Arabidopsis HOOKLESS1 regulates responses to pathogens and abscisic acid through interaction with MED18 and acetylation of

- WRKY33 and ABI5 chromatin. *Plant Cell* **28**: tpc.00105.2016.
- Licausi, F., Van Dongen, J.T., Giuntoli, B., Novi, G., Santaniello, A., Geigenberger, P., and Perata, P.** (2010). HRE1 and HRE2, two hypoxia-inducible ethylene response factors, affect anaerobic responses in *Arabidopsis thaliana*. *Plant J.* **62**: 302–315.
- Licausi, F., Kosmacz, M., Weits, D. a, Giuntoli, B., Giorgi, F.M., Voeselek, L. a C.J., Perata, P., and van Dongen, J.T.** (2011). Oxygen sensing in plants is mediated by an N-end rule pathway for protein destabilization. *Nature* **479**: 419–22.
- Liebermann, M.** (1979). Biosynthesis and Action of Ethylene. *Annu. Rev. Plant Physiol.* **30**: 533–591.
- Liew, C.W., Sun, H., Hunter, T., and Day, C.L.** (2010). RING domain dimerization is essential for RNF4 function. *Biochem. J.* **431**: 23–29.
- Lin, C.-C. et al.** (2019). Regulatory cascade involving transcriptional and N-end rule pathways in rice under submergence. *Proc. Natl. Acad. Sci. U. S. A.* **116**: 3300–3309.
- Lin, H.C., Yeh, C.W., Chen, Y.F., Lee, T.T., Hsieh, P.Y., Rusnac, D. V., Lin, S.Y., Elledge, S.J., Zheng, N., and Yen, H.C.S.** (2018). C-Terminal End-Directed Protein Elimination by CRL2 Ubiquitin Ligases. *Mol. Cell* **70**: 602-613.e3.
- Linster, E. et al.** (2015). Downregulation of N-terminal acetylation triggers ABA-mediated drought responses in *Arabidopsis*. *Nat. Commun.* **6**: 7640.
- Liu, H. and Nonomura, K.-I.** (2016). A wide reprogramming of histone H3 modifications during male meiosis I in rice is dependent on the Argonaute protein MEL1. *J. Cell Sci.* **129**: 3553–3561.
- Liu, J. et al.** (2008). Targeted Degradation of the Cyclin-Dependent Kinase Inhibitor ICK4/KRP6 by RING-Type E3 Ligases Is Essential for Mitotic Cell Cycle Progression during *Arabidopsis* Gametogenesis. *Plant Cell* **20**: 1538–1554.
- Liu, X., Huang, J., Parameswaran, S., Ito, T., Seubert, B., Auer, M., Rymaszewski, A., Jia, G., Owen, H.A., and Zhao, D.** (2009). The SPOROCTELESS/NOZZLE Gene Is Involved in Controlling Stamen Identity in *Arabidopsis*. *Plant Physiol.* **151**: 1401–1411.
- Liu, X.C. and Dickinson, H.G.** (1989). Cellular energy levels and their effect on male cell abortion in cytoplasmically male sterile lines of *Petunia bybrida*. *Sex Plant Reprod* **2**: 167–172.
- Liu, Y., Yang, K., Wei, X., and Wang, X.** (2016a). Revisiting the phosphatidylethanolamine-binding protein (PEBP) gene family reveals cryptic FLOWERING LOCUS T gene homologs in gymnosperms and sheds new light on functional evolution. *New Phytol.* **212**: 730–744.
- Liu, Y.J. et al.** (2016b). Degradation of the separase-cleaved Rec8, a meiotic cohesin subunit, by the n-end rule pathway. *J. Biol. Chem.* **291**: 7426–7438.
- Lohrmann, J. and Harter, K.** (2002). Plant Two-Component Signaling Systems and the Role of Response Regulators. *PLANT Physiol.* **128**: 363–369.
- Lomin, S.N., Yonekura-Sakakibara, K., Romanov, G.A., and Sakakibara, H.** (2011). Ligand-binding properties and subcellular localization of maize cytokinin receptors. *J. Exp. Bot.* **62**: 5149–5159.
- Lorick, K.L., Jensen, J.P., Fang, S., Ong, A.M., Hatakeyama, S., and Weissman, A.M.** (1999). RING fingers mediate ubiquitin-conjugating enzyme (E2)-dependent ubiquitination. *Proc. Natl. Acad. Sci. U. S. A.* **96**: 11364–11369.
- Lucas, X. and Ciulli, A.** (2017). Recognition of substrate degrons by E3 ubiquitin ligases and modulation by small-molecule mimicry strategies. *Curr. Opin. Struct. Biol.* **44**: 101–110.
- Lupas, A.N. and Koretke, K.K.** (2003). Bioinformatic analysis of ClpS, a protein module involved in prokaryotic and eukaryotic protein degradation. *J. Struct. Biol.* **141**: 77–83.
- Lupi, A.C.D., Lira, B.S., Gramegna, G., Trench, B., Alves, F.R.R., Demarco, D., Peres, L.E.P., Purgatto, E., Freschi, L., and Rossi, M.** (2019). *Solanum lycopersicum* GOLDEN 2-LIKE 2 transcription factor affects fruit quality in a light- and auxin-dependent manner. *PLoS One* **14**: 1–22.
- Ma, B., Zhou, Y., Chen, H., He, S.-J., Huang, Y.-H., Zhao, H., Lu, X., Zhang, W.-K., Pang, J.-H., Chen, S.-**

- Y., and Zhang, J.-S.** (2018a). Membrane protein MHZ3 stabilizes OsEIN2 in rice by interacting with its Nramp-like domain. *Proc. Natl. Acad. Sci. U. S. A.* **115**: 2520–2525.
- Ma, H.** (2005). Molecular Genetic Analyses of Microsporogenesis and Microgametogenesis in Flowering Plants. *Annu. Rev. Plant Biol.* **56**: 393–434.
- Ma, Y. et al.** (2018b). Disrupted Genome Methylation in Response to High Temperature Has Distinct Affects on Microspore Abortion and Anther Indehiscence. *Plant Cell* **30**: tpc.00074.2018.
- MacGurn, J.A., Hsu, P.-C., and Emr, S.D.** (2012). Ubiquitin and Membrane Protein Turnover: From Cradle to Grave. *Annu. Rev. Biochem.* **81**: 231–259.
- Mähönen, A.P., Bishopp, A., Higuchi, M., Nieminen, K.M., Kinoshita, K., Törmäkangas, K., Ikeda, Y., Oka, A., Kakimoto, T., and Helariutta, Y.** (2006). Cytokinin signaling and its inhibitor AHP6 regulate cell fate during vascular development. *Science* **311**: 94–98.
- Majovsky, P., Naumann, C., Lee, C.W., Lassowskat, I., Trujillo, M., Dissmeyer, N., and Hoehenwarter, W.** (2014). Targeted proteomics analysis of protein degradation in plant signaling on an LTQ-Orbitrap mass spectrometer. *J. Proteome Res.* **13**: 4246–4258.
- Von Malek, B., Van Der Graaff, E., Schneitz, K., and Keller, B.** (2002). The Arabidopsis male-sterile mutant *dde2-2* is defective in the ALLENE OXIDE SYNTHASE gene encoding one of the key enzymes of the jasmonic acid biosynthesis pathway. *Planta* **216**: 187–192.
- Mallory, A.C., Bartel, D.P., and Bartel, B.** (2005). MicroRNA-directed regulation of Arabidopsis AUXIN RESPONSE FACTOR17 is essential for proper development and modulates expression of early auxin response genes. *Plant Cell* **17**: 1360–75.
- Mandaokar, A., Thines, B., Shin, B., Markus Lange, B., Choi, G., Koo, Y.J., Yoo, Y.J., Choi, Y.D., Choi, G., and Browse, J.** (2006). Transcriptional regulators of stamen development in Arabidopsis identified by transcriptional profiling. *Plant J.* **46**: 984–1008.
- Mandel, M. and Higa, A.** (1970). Calcium-dependent bacteriophage DNA infection. *J. Mol. Biol.* **53**: 159–62.
- Maor, R., Jones, A., Nühse, T.S., Studholme, D.J., Peck, S.C., and Shirasu, K.** (2007). Multidimensional Protein Identification Technology (MudPIT) Analysis of Ubiquitinated Proteins in Plants. *Mol. Cell. Proteomics* **6**: 601–610.
- de Marchi, R. et al.** (2016). The N-end rule pathway regulates pathogen responses in plants. *Sci. Rep.* **6**: 26020.
- Mariani, C. and Wolters-Arts, M.** (2000). Complex waxes. *Plant Cell* **12**: 1795–8.
- Marín, I.** (2010). Diversification and Specialization of Plant RBR Ubiquitin Ligases. *PLoS One* **5**: e11579.
- Marsch-Martínez, N., Ramos-Cruz, D., Irepan Reyes-Olalde, J., Lozano-Sotomayor, P., Zúñiga-Mayo, V.M., and De Folter, S.** (2012). The role of cytokinin during Arabidopsis gynoecia and fruit morphogenesis and patterning. *Plant J.* **72**: 222–234.
- Mascarenhas, J.P.** (1990). Gene activity during pollen development. *Annu. Rev. Plant Biol.* **41**: 317–338.
- Mason, M.G., Mathews, D.E., Argyros, D.A., Maxwell, B.B., Kieber, J.J., Alonso, J.M., Ecker, J.R., and Schaller, G.E.** (2005). Multiple type-B response regulators mediate cytokinin signal transduction in *Arabidopsis*. *Plant Cell* **17**: 3007–3018.
- Matsumoto, G., Wada, K., Okuno, M., Kurosawa, M., and Nukina, N.** (2011). Serine 403 phosphorylation of p62/SQSTM1 regulates selective autophagic clearance of ubiquitinated proteins. *Mol. Cell* **44**: 279–289.
- Matta-Camacho, E., Kozlov, G., Li, F.F., and Gehring, K.** (2010). Structural basis of substrate recognition and specificity in the N-end rule pathway. *Nat. Struct. Mol. Biol.* **17**: 1182–7.
- Mauney, J.K., Hillman, W.S., Miller, C.O., Skoog, F., Clayton, R.A., and Strong, F.M.** (1952). Bioassay,

- Purification, and Properties of a Growth Factor from Coconut. *Physiol. Plant.* **5**: 485–497.
- Maxwell, P.H., Wiesener, M.S., Chang, G.W., Clifford, S.C., Vaux, E.C., Cockman, M.E., Wykoff, C.C., Pugh, C.W., Maher, E.R., and Ratcliffe, P.J.** (1999). The Tumour Suppressor Protein VHL Targets Hypoxia Inducible Factors for Oxygen Dependent Proteolysis. *Nature* **399**: 271–275.
- Mayerhofer, H., Panneerselvam, S., and Mueller-Dieckmann, J.** (2012). Protein kinase domain of CTR1 from *Arabidopsis thaliana* promotes ethylene receptor cross talk. *J. Mol. Biol.* **415**: 768–779.
- McConn, M. and Browse, J.** (1996). The Critical Requirement for Linolenic Acid Is Pollen Development, Not Photosynthesis, in an *Arabidopsis* Mutant. *Plant Cell* **8**: 403–416.
- McCormick, S.** (2004). Control of male gametophyte development. *Plant Cell* **16 Suppl**: S142–S153.
- McCormick, S.** (1993). Male Gametophyte Development. *Plant Cell* **5**: 1265–1275.
- McDaniel, B.K. and Binder, B.M.** (2012). Ethylene receptor 1 (ETR1) is sufficient and has the predominant role in mediating inhibition of ethylene responses by silver in *Arabidopsis thaliana*. *J. Biol. Chem.* **287**: 26094–26103.
- McNellis, T.W. and Deng, X.W.** (1995). Light control of seedling morphogenetic pattern. *Plant Cell* **7**: 1749–61.
- Meierhofer, D., Wang, X., Huang, L., and Kaiser, P.** (2008). Quantitative analysis of global ubiquitination in HeLa cells by mass spectrometry. *J. Proteome Res* **7**: 4566–4576.
- Meinke, D.W., Cherry, J.M., Dean, C., Rounsley, S.D., and Koornneef, M.** (1998). *Arabidopsis thaliana*: a model plant for genome analysis. *Science* **282**: 662, 679–82.
- Melnykov, A., Chen, S.-J., and Varshavsky, A.** (2019). Gid10 as an alternative N-recognition of the Pro/N-degron pathway. *Proc. Natl. Acad. Sci. U. S. A.* **116**: 15914–15923.
- Mendonzo, G.M., Gibbs, D.J., Szurman-Zubrzycka, M., Korn, A., Marquez, J., Szarejko, I., Maluszynski, M., King, J., Axcell, B., Smart, K., Corbineau, F., and Holdsworth, M.J.** (2016). Enhanced waterlogging tolerance in barley by manipulation of expression of the N-end rule pathway E3 ligase PROTEOLYSIS6. *Plant Biotechnol. J.* **14**: 40–50.
- Merchante, C., Alonso, J.M., and Stepanova, A.N.** (2013). Ethylene signaling: Simple ligand, complex regulation. *Curr. Opin. Plant Biol.* **16**: 554–560.
- Merchante, C., Brumos, J., Yun, J., Hu, Q., Spencer, K.R., Enríquez, P., Binder, B.M., Heber, S., Stepanova, A.N., and Alonso, J.M.** (2015). Gene-specific translation regulation mediated by the hormone-signaling molecule EIN2. *Cell* **163**: 684–97.
- Mesihovic, A., Iannaccone, R., Firon, N., and Fragkostefanakis, S.** (2016). Heat stress regimes for the investigation of pollen thermotolerance in crop plants. *Plant Reprod.* **29**: 93–105.
- Miller, C.O., Skoog, F., Okumura, F.S., Von Saltza, M.H., and Strong, F.M.** (1956). Isolation, Structure and Synthesis of Kinetin, a Substance Promoting Cell Division. *J. Am. Chem. Soc.* **78**: 1375–1380.
- Miller, C.O., Skoog, F., Von Saltza, M.H., and Strong, F.M.** (1955). KINETIN, A CELL DIVISION FACTOR FROM DEOXYRIBONUCLEIC ACID 1. *J. Am. Chem. Soc.* **77**: 1392–1392.
- Mimnaugh, E.G., Chen, H.Y., Davie, J.R., Celis, J.E., and Neckers, L.** (1997). Rapid deubiquitination of nucleosomal histones in human tumor cells caused by proteasome inhibitors and stress response inducers: effects on replication, transcription, translation, and the cellular stress response. *Biochemistry* **36**: 14418–29.
- Min, L., Li, Y., Hu, Q., Zhu, L., Gao, W., Wu, Y., Ding, Y., Liu, S., Yang, X., and Zhang, X.** (2014). Sugar and Auxin Signaling Pathways Respond to High-Temperature Stress during Anther Development as Revealed by Transcript Profiling Analysis in Cotton. *Plant Physiol.* **164**: 1293–1308.
- Miura, K., Jin, J.B., Lee, J., Yoo, C.Y., Stirm, V., Miura, T., Ashworth, E.N., Bressan, R.A., Yun, D.-J., and Hasegawa, P.M.** (2007). SIZ1-Mediated Sumoylation of ICE1 Controls CBF3/DREB1A Expression and Freezing Tolerance in *Arabidopsis*. *Plant Cell* **19**: 1403–1414.

- Miyase, S., Tomita, K., Inoue, H., Suzuki, K., Yamaizumi, M., Watanabe, K., and Tateishi, S.** (2004). Differential Regulation of Rad18 through Rad6-dependent Mono- and Polyubiquitination. *J. Biol. Chem.* **280**: 515–524.
- Miyazaki, J.H. and Yang, S.F.** (1987). The methionine salvage pathway in relation to ethylene and polyamine biosynthesis. *Physiol. Plant.* **69**: 366–370.
- Mogk, A., Schmidt, R., and Bukau, B.** (2007). The N-end rule pathway for regulated proteolysis: prokaryotic and eukaryotic strategies. *Trends Cell Biol.* **17**: 165–172.
- Mok, D.W. and Mok, M.C.** (2001). Cytokinin Metabolism and Action. *Annu. Rev. Plant Physiol. Plant Mol. Biol.* **52**: 89–118.
- Monte, E., Amador, V., Russo, E., Martínez-García, J., and Prat, S.** (2003). PHOR1: A U-Box GA Signaling Component with a Role in Proteasome Degradation? *J. Plant Growth Regul.* **22**: 152–162.
- Moon, J., Parry, G., and Estelle, M.** (2004). The ubiquitin-proteasome pathway and plant development. *Plant Cell* **16**: 3181–95.
- Moore, B., Zhou, L., Rolland, F., Hall, Q., Cheng, W.-H., Liu, Y.-X., Hwang, I., Jones, T., and Sheen, J.** (2003). Role of the Arabidopsis glucose sensor HXK1 in nutrient, light, and hormonal signaling. *Science* **300**: 332–6.
- Morant, M., Jørgensen, K., Schaller, H., Pinot, F., Møller, B.L., Werck-Reichhart, D., and Bak, S.** (2007). CYP703 is an ancient cytochrome P450 in land plants catalyzing in-chain hydroxylation of lauric acid to provide building blocks for sporopollenin synthesis in pollen. *Plant Cell* **19**: 1473–87.
- Morett, E. and Bork, P.** (1999). A novel transactivation domain in parkin. *Trends Biochem. Sci.* **24**: 229–31.
- Mot, A.C., Prell, E., Klecker, M., Naumann, C., Faden, F., Westermann, B., and Dismeyer, N.** (2018). Real-time detection of N-end rule-mediated ubiquitination via fluorescently labeled substrate probes. *New Phytol.* **217**: 613–624.
- Mothes, K. and Engelbrecht, L.** (1963). On the activity of a kinetin-like root factor. *Life Sci.* **11**: 852–857.
- Moussatche, P. and Klee, H.J.** (2004). Autophosphorylation activity of the Arabidopsis ethylene receptor multigene family. *J. Biol. Chem.* **279**: 48734–48741.
- Müller, B. and Sheen, J.** (2007). Arabidopsis cytokinin signaling pathway. *Sci. STKE* **2007**: cm5.
- Müller, B. and Sheen, J.** (2008). Cytokinin and auxin interaction in root stem-cell specification during early embryogenesis. *Nature* **453**: 1094–1097.
- Müller, C.J., Larsson, E., Spíchal, L., and Sundberg, E.** (2017). Cytokinin-auxin crosstalk in the gynoecial primordium ensures correct domain patterning. *Plant Physiol.* **175**: pp.00805.2017.
- Mustroph, A., Fukao, T., Bailey-Serres, J., Lee, S.C., Yaghoubi-Masihi, A., Yang, H., Ma, K., Zanetti, M.E., and Oosumi, T.** (2010). Cross-Kingdom Comparison of Transcriptomic Adjustments to Low-Oxygen Stress Highlights Conserved and Plant-Specific Responses. *Plant Physiol.* **152**: 1484–1500.
- Mustroph, A., Holtan, H.E., Bailey-Serres, J., Jang, C.J.H., Repetti, P.P., Galbraith, D.W., Girke, T., and Zanetti, M.E.** (2009). Profiling transcriptomes of discrete cell populations resolves altered cellular priorities during hypoxia in Arabidopsis. *Proc. Natl. Acad. Sci. U. S. A.* **106**: 18843–18848.
- Nagashima, Y., Mishiba, K.-I., Suzuki, E., Shimada, Y., Iwata, Y., and Koizumi, N.** (2011). Arabidopsis IRE1 catalyses unconventional splicing of bZIP60 mRNA to produce the active transcription factor. *Sci. Rep.* **1**: 29.
- Nagpal, P., Ellis, C.M., Weber, H., Ploense, S.E., Barkawi, L.S., Guilfoyle, T.J., Hagen, G., Alonso, J.M., Cohen, J.D., Farmer, E.E., Ecker, J.R., and Reed, J.W.** (2005). Auxin response factors ARF6

- and ARF8 promote jasmonic acid production and flower maturation. *Development* **132**: 4107–4118.
- Nakano, T., Suzuki, K., Fujimura, T., and Shinshi, H.** (2006). Genome-Wide Analysis of the ERF Gene Family. *Plant Physiol.* **140**: 411–432.
- Narayanan, S., Prasad, P.V.V., and Welti, R.** (2018). Alterations in wheat pollen lipidome during high day and night temperature stress. *Plant Cell Environ.* **41**: 1749–1761.
- Naumann, C.** (2017). Identifizierung und Charakterisierung neuer Substrate des N-end rule pathways in *Arabidopsis thaliana*. Martin-Luther-Universität Halle-Wittenberg, Dissertation. urn:nbn:de:gbv:3:4-20154.
- Naumann, C., Mot, A.C., and Dissmeyer, N.** (2016). Generation of Artificial N-end Rule Substrate Proteins In Vivo and In Vitro. *Methods Mol. Biol.* **1450**: 55–83.
- Navarro, L. et al.** (2004). The Transcriptional Innate Immune Response to g22. Interplay and Overlap with Avr Gene-Dependent Defense Responses and Bacterial Pathogenesis. *Plant Physiol.* **135**: 1113–1128.
- Neljubov, D.** (1901). Über die horizontale Nutation der Stengel von *Pisum sativum* und einiger anderer Pflanzen. Beihefte zum Bot. Zentralblatt: 128–129.
- Nelson, D.C., Lasswell, J., Rogg, L.E., Cohen, M.A., and Bartel, B.** (2000). FKF1, a clock controlled gene that regulates the transition of flowering in *Arabidopsis*. *Cell* **101**: 331–340.
- Nelson, D.C., Scaffidi, A., Dun, E.A., Waters, M.T., Flematti, G.R., Dixon, K.W., Beveridge, C.A., Ghisalberti, E.L., and Smith, S.M.** (2011). F-box protein MAX2 has dual roles in karrikin and strigolactone signaling in *Arabidopsis thaliana*. *Proc. Natl. Acad. Sci. U. S. A.* **108**: 8897–8902.
- Nemhauser, J.L., Mockler, T.C., and Chory, J.** (2004). Interdependency of brassinosteroid and auxin signaling in *Arabidopsis*. *PLoS Biol.* **2**: E258.
- Netien, G., Beauchesne, G., and Mentzer, C.** (1951). Influence du lait de maïs sur la croissance des tissus de carotte in vitro. *Comp. Rendus L'Acad. Des Sci.* **233**: 92–98.
- Ni, W., Xu, S.L., Tepperman, J.M., Stanley, D.J., Maltby, D.A., Gross, J.D., Burlingame, A.L., Wang, Z.Y., and Quail, P.H.** (2014). A mutually assured destruction mechanism attenuates light signaling in *Arabidopsis*. *Science* **344**: 1160–1164.
- Nieminen, K. et al.** (2008). Cytokinin signaling regulates cambial development in poplar. *Proc. Natl. Acad. Sci. U. S. A.* **105**: 20032–20037.
- Nishimura, C., Ohashi, Y., Sato, S., Kato, T., Tabata, S., and Ueguchi, C.** (2004). Histidine Kinase Homologs That Act as Cytokinin Receptors Possess Overlapping Functions in the Regulation of Shoot and Root Growth in *Arabidopsis*. *Plant Cell* **16**: 1365–1377.
- Nishimura, K., Asakura, Y., Friso, G., Kim, J., Oh, S. -h., Rutschow, H., Ponnala, L., and van Wijk, K.J.** (2013). ClpS1 Is a Conserved Substrate Selector for the Chloroplast Clp Protease System in *Arabidopsis*. *Plant Cell* **25**: 2276–2301.
- Nishito, Y., Hasegawa, M., Inohara, N., and Núñez, G.** (2006). MEX is a testis-specific E3 ubiquitin ligase that promotes death receptor-induced apoptosis. *Biochem. J.* **396**: 411–417.
- Niu, Y. and Xiang, Y.** (2018). An Overview of Biomembrane Functions in Plant Responses to High-Temperature Stress. *Front. Plant Sci.* **9**: 1–18.
- Noh, B., Murphy, A.S., and Spalding, E.P.** (2001). Multidrug Resistance-like Genes of *Arabidopsis* Required for Auxin Transport and Auxin-Mediated Development. *Plant Cell* **13**: 2441–2454.
- Nonomura, K.-I., Morohoshi, A., Nakano, M., Eiguchi, M., Miyao, A., Hirochika, H., and Kurata, N.** (2007). A germ cell specific gene of the ARGONAUTE family is essential for the progression of premeiotic mitosis and meiosis during sporogenesis in rice. *Plant Cell* **19**: 2583–94.
- Nørholm, M.H.H.** (2010). A mutant Pfu DNA polymerase designed for advanced uracil-excision DNA engineering. *BMC Biotechnol.* **10**: 21.

- Notenboom, V., Hibbert, R.G., van Rossum-Fikkert, S.E., Olsen, J. V., Mann, M., and Sixma, T.K.** (2007). Functional characterization of Rad18 domains for Rad6, ubiquitin, DNA binding and PCNA modification. *Nucleic Acids Res.* **35**: 5819–30.
- Nowack, M.K., Grini, P.E., Jakoby, M.J., Lafos, M., Koncz, C., and Schnittger, A.** (2006). A positive signal from the fertilization of the egg cell sets off endosperm proliferation in angiosperm embryogenesis. *Nat. Genet.* **38**: 63–67.
- O'Malley, R.C., Rodriguez, F.I., Esch, J.J., Binder, B.M., O'Donnell, P., Klee, H.J., and Bleecker, A.B.** (2005). Ethylene-binding activity, gene expression levels, and receptor system output for ethylene receptor family members from Arabidopsis and tomato. *Plant J.* **41**: 651–659.
- Oh, E., Zhu, J.Y., Bai, M.Y., Arenhart, R.A., Sun, Y., and Wang, Z.Y.** (2014). Cell elongation is regulated through a central circuit of interacting transcription factors in the Arabidopsis hypocotyl. *Elife* **2014**: 1–19.
- Oh, E., Zhu, J.Y., and Wang, Z.Y.** (2012). Interaction between BZR1 and PIF4 integrates brassinosteroid and environmental responses. *Nat. Cell Biol.* **14**: 802–809.
- Oh, S.A., Park, J.H., Lee, G.I., Paek, K.H., Park, S.K., and Nam, H.G.** (1997). Identification of three genetic loci controlling leaf senescence in Arabidopsis thaliana. *Plant J* **12**: 527–535.
- Ohi, M.D., Vander Kooi, C.W., Rosenberg, J.A., Chazin, W.J., and Gould, K.L.** (2003). Structural insights into the U-box, a domain associated with multi-ubiquitination. *Nat. Struct. Biol.* **10**: 250–255.
- Ohsumi, Y.** (2001). Molecular dissection of autophagy: two ubiquitin-like systems. *Nat Rev Mol Cell Biol* **2**: 211–216.
- Okamoto, T., Tsurumi, S., Shibasaki, K., Obana, Y., Takaji, H., Oono, Y., and Rahman, A.** (2008). Genetic Dissection of Hormonal Responses in the Roots of Arabidopsis Grown under Continuous Mechanical Impedance. *Plant Physiol.* **146**: 1651–1662.
- Ossowski, S., Schneeberger, K., Lucas-Iledó, J.I., Clark, R.M., Shaw, R.G., Weigel, D., Lynch, M., and Warthmann, N.** (2010). The rate and molecular spectrum of spontaneous mutations in Arabidopsis thaliana Supporting Online Material. *Science* **327**: 92–95.
- Osterlund, M.T., Hardtke, C.S., Ning, W., and Deng, X.W.** (2000). Targeted destabilization of HY5 during light-regulated development of Arabidopsis. *Nature* **405**: 462–466.
- Ozkan, E., Yu, H., and Deisenhofer, J.** (2005). Mechanistic insight into the allosteric activation of a ubiquitin-conjugating enzyme by RING-type ubiquitin ligases. *Proc. Natl. Acad. Sci. U. S. A.* **102**: 18890–18895.
- Pacini, E., Franchi, G.G., and Hesse, M.** (1985). The Tapetum: Its Form, Function, and Possible Phylogeny in Embryophyta. *Pl. Syst. Evol.* **149**: 155–185.
- Pacini, E., Guarnieri, M., and Nepi, M.** (2006). Pollen carbohydrates and water content during development, presentation, and dispersal: A short review. *Protoplasma* **228**: 73–77.
- Pankiv, S., Clausen, T.H., Lamark, T., Brech, A., Bruun, J.A., Outzen, H., Øvervatn, A., Bjørkøy, G., and Johansen, T.** (2007). p62/SQSTM1 binds directly to Atg8/LC3 to facilitate degradation of ubiquitinated protein aggregates by autophagy*[S]. *J. Biol. Chem.* **282**: 24131–24145.
- Pareek, A., Singh, A., Kumar, M., Kushwaha, H.R., Lynn, A.M., and Singla-Pareek, S.L.** (2006). Whole-Genome Analysis of Oryza sativa Reveals Similar Architecture of Two-Component Signaling Machinery with Arabidopsis. *PLANT Physiol.* **142**: 380–397.
- Parish, R.W. and Li, S.F.** (2010). Death of a tapetum: A programme of developmental altruism. *Plant Sci.* **178**: 73–89.
- Parish, R.W., Phan, H.A., Iacuone, S., and Li, S.F.** (2012). Tapetal development and abiotic stress: A centre of vulnerability. *Funct. Plant Biol.* **39**: 553–559.
- Park, J.H., Halitschke, R., Kim, H.B., Baldwin, I.T., Feldmann, K.A., and Feyereisen, R.** (2002). A

- knock-out mutation in allene oxide synthase results in male sterility and defective wound signal transduction in *Arabidopsis* due to a block in jasmonic acid biosynthesis. *Plant J.* **31**: 1–12.
- Park, S.K., Howden, R., and Twell, D.** (1998). The *Arabidopsis thaliana* gametophytic mutation *geminipollen1* disrupts microspore polarity, division asymmetry and pollen cell fate. *Development* **125**: 3789–3799.
- Parsons, K., Nakatani, Y., and Nguyen, M.D.** (2015). P600/UBR4 in the central nervous system. *Cell. Mol. Life Sci.* **72**: 1149–1160.
- Paszowski, J. and Grossniklaus, U.** (2011). Selected aspects of transgenerational epigenetic inheritance and resetting in plants. *Curr. Opin. Plant Biol.* **14**: 195–203.
- Pavri, R., Zhu, B., Li, G., Trojer, P., Mandal, S., Shilatifard, A., and Reinberg, D.** (2006). Histone H2B Monoubiquitination Functions Cooperatively with FACT to Regulate Elongation by RNA Polymerase II. *Cell* **125**: 703–717.
- Payasi, A. and Sanwal, G.G.** (2010). Ripening of Climacteric Fruits and Their Control. *J. Food Biochem.* **34**: 679–710.
- Pearce, S., Ferguson, A., King, J., and Wilson, Z.A.** (2015). FlowerNet: A Gene Expression Correlation Network for Anther and Pollen Development. *Plant Physiol.* **167**: 1717–1730.
- Peng, J., Schwartz, D., Elias, J.E., Thoreen, C.C., Cheng, D., Marsischky, G., Roelofs, J., Finley, D., and Gygi, S.P.** (2003). A proteomics approach to understanding protein ubiquitination. *Nat. Biotechnol.* **21**, 921–926 Hitch. A. L., Auld, K., Gygi, S. P., Silver, P. A **100**: 12735–12740.
- Peng, Y., Chen, L., Lu, Y., Wu, Y., Dumenil, J., Zhu, Z., Bevan, M.W., and Li, Y.** (2015). The Ubiquitin Receptors DA1, DAR1, and DAR2 Redundantly Regulate Endoreduplication by Modulating the Stability of TCP14/15 in *Arabidopsis*. *Plant Cell* **27**: 649–662.
- Penninckx, I.A., Thomma, B.P., Buchala, A., Métraux, J.P., and Broekaert, W.F.** (1998). Concomitant activation of jasmonate and ethylene response pathways is required for induction of a plant defensin gene in *Arabidopsis*. *Plant Cell* **10**: 2103–13.
- Pernisova, M., Klima, P., Horak, J., Valkova, M., Malbeck, J., Soucek, P., Reichman, P., Hoyerova, K., Dubova, J., Friml, J., Za;zimalova, E., and Hejatko, J.** (2009). Cytokinins modulate auxin-induced organogenesis in plants via regulation of the auxin efflux. *Proc. Natl. Acad. Sci. U. S. A.* **106**: 3609–3614.
- Peth, A., Besche, H.C., and Goldberg, A.L.** (2009). Ubiquitinated Proteins Activate the Proteasome by Binding to Usp14/Ubp6, which Causes 20S Gate Opening. *Mol. Cell* **36**: 794–804.
- Pfleger, C.M. and Kirschner, M.W.** (2000). The KEN box: An APC recognition signal distinct from the D box targeted by Cdh1. *Genes Dev.* **14**: 655–665.
- Piatkov, K.I., Brower, C.S., and Varshavsky, A.** (2012a). The N-end rule pathway counteracts cell death by destroying proapoptotic protein fragments. *Proc. Natl. Acad. Sci. U. S. A.* **109**: E1839–E1847.
- Piatkov, K.I., Colnaghi, L., Békés, M., Varshavsky, A., and Huang, T.T.** (2012b). The Auto-Generated Fragment of the Usp1 Deubiquitylase Is a Physiological Substrate of the N-End Rule Pathway. *Mol. Cell*: 926–933.
- Pickart, C.M.** (2001). Echanisms nderlying ubiquitination. *Annu. Rev. Biochem.* **70**: 503–33.
- Pickart, C.M. and Fushman, D.** (2004). Polyubiquitin chains: Polymeric protein signals. *Curr. Opin. Chem. Biol.* **8**: 610–616.
- Pickart, C.M. and Rose, I.A.** (1985). Functional-Heterogeneity of Ubiquitin Carrier Proteins. *J. Biol. Chem.* **260**: 1573–1581.
- Piffanelli, P., Ross, J.H.E., and Murphy, D.J.** (1998). Biogenesis and function of the lipidic structures of pollen grains. *Sex. Plant Reprod.* **11**: 65–80.
- Piffanelli, P., Ross, J.H.E., and Murphy, D.J.** (1997). Intra- and extracellular lipid composition and

- associated gene expression patterns during pollen development in *Brassica napus*. *Plant J.* **11**: 549–562.
- Pils, B. and Heyl, A.** (2009). Unraveling the Evolution of Cytokinin Signaling. *Plant Physiol.* **151**: 782–791.
- Pischke, M.S., Jones, L.G., Otsuga, D., Fernandez, D.E., Drews, G.N., and Sussman, M.R.** (2002). An *Arabidopsis* histidine kinase is essential for megagametogenesis. *Proc. Natl. Acad. Sci. U. S. A.* **99**: 15800–5.
- Planchet, E., Jagadis Gupta, K., Sonoda, M., and Kaiser, W.M.** (2005). Nitric oxide emission from tobacco leaves and cell suspensions: rate limiting factors and evidence for the involvement of mitochondrial electron transport. *Plant J.* **41**: 732–743.
- Plasman, K., Van Damme, P., and Gevaert, K.** (2013). Contemporary positional proteomics strategies to study protein processing. *Curr. Opin. Chem. Biol.* **17**: 66–72.
- Podlešáková, K., Zalabák, D., Čudejová, M., Plíhal, O., Szüčová, L., Doležal, K., Spíchal, L., Strnad, M., and Galuszka, P.** (2012). Novel cytokinin derivatives do not show negative effects on root growth and proliferation in submicromolar range. *PLoS One* **7**.
- Van de Poel, B. et al.** (2012). Targeted Systems Biology Profiling of Tomato Fruit Reveals Coordination of the Yang Cycle and a Distinct Regulation of Ethylene Biosynthesis during Postclimacteric Ripening. *Plant Physiol.* **160**: 1498–1514.
- Ponting, C.P., Blake, D.J., Davies, K.E., Kendrick-Jones, J., and Winder, S.J.** (1996). ZZ and TAZ: new putative zinc fingers in dystrophin and other proteins. *Trends Biochem Sci.* **21**: 11–13.
- Potuschak, T., Lechner, E., Parmentier, Y., Yanagisawa, S., Grava, S., Koncz, C., and Genschik, P.** (2003). EIN3-Dependent Regulation of Plant Ethylene Hormone Signaling by Two *Arabidopsis* F Box Proteins. *Cell* **115**: 679–689.
- Potuschak, T., Stary, S., Schlögelhofer, P., Becker, F., Nejinskaia, V., and Bachmair, A.** (1998). PRT1 of *Arabidopsis thaliana* encodes a component of the plant N-end rule pathway. *Proc. Natl. Acad. Sci. U. S. A.* **95**: 7904–8.
- Poyurovsky, M. V., Priest, C., Kentsis, A., Borden, K.L.B., Pan, Z.Q., Pavletich, N., and Prives, C.** (2007). The Mdm2 RING domain C-terminus is required for supramolecular assembly and ubiquitin ligase activity. *EMBO J.* **26**: 90–101.
- del Pozo, J.C. and Estelle, M.** (1999). The *Arabidopsis* cullin AtCUL1 is modified by the ubiquitin-related protein RUB1. *Proc. Natl. Acad. Sci. U. S. A.* **96**: 15342–7.
- Pressman, E., Peet, M.M., and Pharr, D.M.** (2002). The effect of heat stress on tomato pollen characteristics is associated with changes in carbohydrate concentration in the developing anthers. *Ann. Bot.* **90**: 631–6.
- Preuss, D., Lemieux, B., Yen, G., and Davis, R.W.** (1993). A conditional sterile mutation eliminates surface components from *Arabidopsis* pollen and disrupts cell signaling during fertilization. *Genes Dev.* **7**: 974–985.
- Price, J., Laxmi, A., St Martin, S.K., and Jang, J.-C.** (2004). Global transcription profiling reveals multiple sugar signal transduction mechanisms in *Arabidopsis*. *Plant Cell* **16**: 2128–50.
- Printsev, I., Yen, L., Sweeney, C., and Carraway, K.L.** (2014). Oligomerization of the Nrdp1 E3 ubiquitin ligase is necessary for efficient autoubiquitination but not ErbB3 ubiquitination. *J. Biol. Chem.* **289**: 8570–8578.
- Procissi, A., De Laissardière, S., Férault, M., Vezon, D., Pelletier, G., and Bonhomme, S.** (2001). Five gametophytic mutations affecting pollen development and pollen tube growth in *Arabidopsis thaliana*. *Genetics* **158**: 1773–1783.
- Punwani, J.A. and Kieber, J.J.** (2010). Localization of the *Arabidopsis* histidine phosphotransfer proteins is independent of cytokinin. *Plant Signal. Behav.* **5**: 896–898.

- Pusch, S., Dissmeyer, N., and Schnittger, A.** (2011). Bimolecular-fluorescence complementation assay to monitor kinase-substrate interactions in vivo. *Methods Mol. Biol.* **779**: 245–57.
- Qi, T., Huang, H., Song, S., and Xie, D.** (2015). Regulation of Jasmonate-Mediated Stamen Development and Seed Production by a bHLH-MYB Complex in Arabidopsis. *Plant Cell* **27**: 1620–33.
- Qiao, H., Chang, K.N., Yazaki, J., and Ecker, J.R.** (2009). Interplay between ethylene, ETP1/ETP2 F-box proteins, and degradation of EIN2 triggers ethylene responses in Arabidopsis. *Genes Dev.* **23**: 512–521.
- Qiao, H., Shen, Z., Huang, S.-S.C., Schmitz, R.J., Urich, M.A., Briggs, S.P., and Ecker, J.R.** (2013). Response to perspective: “separation anxiety: an analysis of ethylene-induced cleavage of EIN2”. *Plant Signal. Behav.* **8**.
- Qiao, H., Shen, Z., Huang, S. -s. C., Schmitz, R.J., Urich, M.A., Briggs, S.P., and Ecker, J.R.** (2012). Processing and Subcellular Trafficking of ER-Tethered EIN2 Control Response to Ethylene Gas. *Science* **338**: 390–393.
- Qu, X., Hall, B.P., Gao, Z., and Schaller, G.E.** (2007). A strong constitutive ethylene-response phenotype conferred on Arabidopsis plants containing null mutations in the ethylene receptors ETR1 and ERS1. *BMC Plant Biol.* **7**: 1–15.
- Qu, X. and Schaller, G.E.** (2004). Requirement of the Histidine Kinase Domain for Signal Transduction by the Ethylene Receptor ETR1. *PLANT Physiol.* **136**: 2961–2970.
- Quilichini, T.D., Douglas, C.J., and Lacey Samuels, A.** (2014). New views of tapetum ultrastructure and pollen exine development in Arabidopsis thaliana. *Ann. Bot.* **114**: 1189–1201.
- Rahmati Ishka, M., Brown, E., Weigand, C., Tillett, R.L., Schlauch, K.A., Miller, G., and Harper, J.F.** (2018). A comparison of heat-stress transcriptome changes between wild-type Arabidopsis pollen and a heat-sensitive mutant harboring a knockout of cyclic nucleotide-gated cation channel 16 (cngc16). *BMC Genomics* **19**: 1–19.
- Rai, M.I., Wang, X., Thibault, D.M., Kim, H.J., Bombyk, M.M., Binder, B.M., Shakeel, S.N., and Schaller, G.E.** (2015). The ARGOS gene family functions in a negative feedback loop to desensitize plants to ethylene. *BMC Plant Biol.* **15**: 1–14.
- Rai, R. and Kashina, A.** (2005). Identification of mammalian arginyltransferases that modify a specific subset of protein substrates. *Proc. Natl. Acad. Sci. U. S. A.* **102**: 10123–10128.
- Rai, R., Wong, C.C.L., Xu, T., Leu, N.A., Dong, D.W., Guo, C., McLaughlin, K.J., Yates, J.R., and Kashina, A.** (2008). Arginyltransferase regulates alpha cardiac actin function, myofibril formation and contractility during heart development. *Development* **135**: 3881–3889.
- Ramon, M., Rolland, F., and Sheen, J.** (2008). Sugar Sensing and Signaling. *Arab. B.* **6**: e0117.
- Ranaweera, R.S. and Yang, X.** (2013). Auto-ubiquitination of Mdm2 enhances its substrate ubiquitin ligase activity. *J. Biol. Chem.* **288**: 18939–18946.
- Rao, H., Uhlmann, F., Nasmyth, K., and Varshavsky, A.** (2001). Degradation of a cohesin subunit by the N-end rule pathway is essential for chromosome stability. *Nature* **410**: 955–9.
- Rashotte, A.M., Carson, S.D.B., To, J.P.C., and Kieber, J.J.** (2003). Expression Profiling of Cytokinin Action in Arabidopsis. *Plant Physiol.* **132**: 1998–2011.
- Ray, S., Zhao, Y., Jamaluddin, M., Edeh, C.B., Lee, C., and Brasier, A.R.** (2014). Inducible STAT3 NH2 terminal mono-ubiquitination promotes BRD4 complex formation to regulate apoptosis. *Cell. Signal.* **26**: 1445–1455.
- Redig, P., Shaul, O., Inzé, D., Van Montagu, M., and Van Onckelen, H.** (1996). Levels of endogenous cytokinins, indole-3-acetic acid and abscisic acid during the cell cycle of synchronized tobacco BY-2 cells. *FEBS Lett.* **391**: 175–180.
- Reed, J.W., Wu, M.-F., Reeves, P.H., Hodgens, C., Yadav, V., Hayes, S., and Pierik, R.** (2018). Three

- Auxin Response Factors Promote Hypocotyl Elongation. *Plant Physiol.* **178**: 864–875.
- Reiland, S., Messerli, G., Baerenfaller, K., Gerrits, B., Endler, A., Grossmann, J., Gruissem, W., and Baginsky, S.** (2009). Large-scale Arabidopsis phosphoproteome profiling reveals novel chloroplast kinase substrates and phosphorylation networks. *Plant Physiol.* **150**: 889–903.
- Reiss, Y. and Hershko, A.** (1990). Affinity Purification Protein Substrates of Ubiquitin-Protein Ligase on Immobilized. *J. Biol. Chem.* **265**: 3685–3690.
- Reiss, Y., Kaim, D., and Hershko, A.** (1988). Specificity of binding of NH₂-terminal residue of proteins to ubiquitin-protein ligase. Use of amino acid derivatives to characterize specific binding sites. *J. Biol. Chem.* **263**: 2693–8.
- Resnick, J.S., Wen, C.-K., Shockey, J.A., and Chang, C.** (2006). REVERSION-TO-ETHYLENE SENSITIVITY1, a conserved gene that regulates ethylene receptor function in Arabidopsis. *Proc. Natl. Acad. Sci. U. S. A.* **103**: 7917–22.
- Riber, W., Müller, J.T., Visser, E.J.W., Sasidharan, R., Voeselek, L. a C.J., and Mustroph, A.** (2015). The greening after extended darkness1 is an N-end rule pathway mutant with high tolerance to submergence and starvation. *Plant Physiol.* **167**: 1616–29.
- Richard, C., Lescot, M., and Veylder, L. De** (2002). Effect of auxin, cytokinin, and sucrose on cell cycle gene expression in. *Pharmacia*: 167–176.
- Riefler, M., Novak, O., Strnad, M., and Schmülling, T.** (2006). Arabidopsis Cytokinin Receptor Mutants Reveal Functions in Shoot Growth, Leaf Senescence, Seed Size, Germination, Root Development, and Cytokinin Metabolism. *Plant Cell* **18**: 40–54.
- Rieu, I., Twell, D., and Firon, N.** (2017). Pollen Development at High Temperature: From Acclimation to Collapse. *Plant Physiol.* **173**: 1967–1976.
- Rieu, I., WoltersArts, M., Derksen, J., Mariani, C., and Weterings, K.** (2003). Ethylene regulates the timing of anther dehiscence in tobacco. *Planta* **217**: 131–137.
- Riley, B.E. et al.** (2013). Structure and function of Parkin E3 ubiquitin ligase reveals aspects of RING and HECT ligases. *Nat. Commun.* **4**: 1–9.
- Riou-Khamlichi, C., Menges, M., Healy, J.M.S., and Murray, J.A.H.** (2002). Sugar Control of the Plant Cell Cycle: Differential Regulation of Arabidopsis D-Type Cyclin Gene Expression. *Mol. Cell. Biol.* **20**: 4513–4521.
- Rodríguez, F.I., Esch, J.J., Hall, A.E., Binder, B.M., Eric Schaller, G., and Blecker, A.B.** (1999). A copper cofactor for the ethylene receptor ETR1 from Arabidopsis. *Science* **283**: 996–998.
- Roman-Hernandez, G., Grant, R.A., Sauer, R.T., and Baker, T.A.** (2009). Molecular basis of substrate selection by the N-end rule adaptor protein ClpS. *Proc. Natl. Acad. Sci. U. S. A.* **106**: 8888–8893.
- Roman, G., Lubarsky, B., Kieber, J.J., Rothenberg, M., and Ecker, J.R.** (1995). Genetic analysis of ethylene signal transduction in Arabidopsis thaliana: five novel mutant loci integrated into a stress response pathway. *Genetics.* **139**: 1393–409.
- Romanov, G.A., Lomin, S.N., and Schmülling, T.** (2018). Cytokinin signaling: from the ER or from the PM? That is the question! *New Phytol.* **218**: 41–53.
- Van Rosmalen, M., Krom, M., and Merckx, M.** (2017). Tuning the Flexibility of Glycine-Serine Linkers to Allow Rational Design of Multidomain Proteins. *Biochemistry* **56**: 6565–6574.
- Routaboul, J.M., Skidmore, C., Wallis, J.G., and Browse, J.** (2012). Arabidopsis mutants reveal that short-and long-term thermotolerance have different requirements for trienoic fatty acids. *J. Exp. Bot.* **63**: 1435–1443.
- Rowland, E., Kim, J., Bhuiyan, N.H., and van Wijk, K.J.** (2015). The Arabidopsis Chloroplast stromal N-terminome; complexities of N-terminal protein maturation and stability. *Plant Physiol.* **169**: pp.01214.2015.
- Russell, S.D.** (1992). Double Fertilization. *Int Rev Cytol.* **140**: 357–388.

- Rutley, N. and Twell, D. (2015). A decade of pollen transcriptomics. *Plant Reprod.* **28**: 73–89.
- Ruzicka, K., Simaskova, M., Duclercq, J., Petrasek, J., Zazimalova, E., Simon, S., Friml, J., Van Montagu, M.C.E., and Benkova, E. (2009). Cytokinin regulates root meristem activity via modulation of the polar auxin transport. *Proc. Natl. Acad. Sci. U. S. A.* **106**: 4284–4289.
- Saha, S. and Kashina, A. (2011). Posttranslational arginylation as a global biological regulator. *Dev. Biol.* **358**: 1–8.
- Saha, S., Wong, C.C.L., Xu, T., Namgoong, S., Zebroski, H., Yates, J.R., and Kashina, A. (2011). Arginylation and methylation double up to regulate nuclear proteins and nuclear architecture in vivo. *Chem. Biol.* **18**: 1369–1378.
- Sakai, H., Aoyama, T., and Oka, A. (2000). Arabidopsis ARR1 and ARR2 response regulators operate as transcriptional activators. *Plant J.* **24**: 703–11.
- Sakai, H., Honma, T., Aoyama, T., Sato, S., Kato, T., Tabata, S., and Oka, A. (2001). ARR1, a transcription factor for genes immediately responsive to cytokinins. *Science* **294**: 1519–21.
- Sakai, H., Hua, J., Chen, Q., Chang, C., Medrano, L., Bleecker, A., and Meyerowitz, E. (1998). ETR2 is an ETR1-like gene involved in ethylene signaling in *Arabidopsis*. *Proc. Natl. Acad. Sci. U. S. A.* **95**: 5812–5817.
- Sakata, T., Oshino, T., Miura, S., Tomabechi, M., Tsunaga, Y., Higashitani, N., Miyazawa, Y., Takahashi, H., Watanabe, M., and Higashitani, A. (2010). Auxins reverse plant male sterility caused by high temperatures. *Proc. Natl. Acad. Sci. U. S. A.* **107**: 8569–8574.
- Samach, A., Klenz, J.E., Kohalmi, S.E., Risseuw, E., Haughn, G.W., and Crosby, W.L. (1999). The *UNUSUAL FLORAL ORGANS* gene of *Arabidopsis thaliana* is an F-box protein required for normal patterning and growth in the floral meristem. *Plant J.* **20**: 433–445.
- Sanders, P.M., Bui, A.Q., Weterings, K., McIntire, K.N., Hsu, Y.C., Lee, P.Y., Truong, M.T., Beals, T.P., and Goldberg, R.B. (1999). Anther developmental defects in *Arabidopsis thaliana* male-sterile mutants. *Sex. Plant Reprod.* **11**: 297–322.
- Sanders, P.M., Lee, P.Y., Biesgen, C., Boone, J.D., Beals, T.P., Weiler, E.W., and Goldberg, R.B. (2000). The arabidopsis DELAYED DEHISCENCE1 gene encodes an enzyme in the jasmonic acid synthesis pathway. *Plant Cell* **12**: 1041–61.
- Santolini, J., André, F., Jeandroz, S., and Wendehenne, D. (2017). Nitric oxide synthase in plants: Where do we stand? *Nitric Oxide - Biol. Chem.* **63**: 30–38.
- Sasaki, A., Itoh, H., Gomi, K., Ueguchi-Tanaka, Miyako Ishiyama, K., Kobayashi, Masatomo Jeong, D.-H., An, G., Kitano, H., Ashikari, M., and Matsuoka, M. (2003). Accumulation of Phosphorylated Repressor for Gibberellin Signaling in an F- box Mutant. *Science*. **299**: 1896–1899.
- Sasidharan, R., Hartman, S., Liu, Z., Martopawiro, S., Sajeev, N., van Veen, H., Yeung, E., and Voeselek, L.A.C.J. (2018). Signal Dynamics and Interactions during Flooding Stress. *Plant Physiol.* **176**: 1106–1117.
- Sato, S., Kamiyama, M., Iwata, T., Makita, N., Furukawa, H., and Ikeda, H. (2006). Moderate increase of mean daily temperature adversely affects fruit set of *Lycopersicon esculentum* by disrupting specific physiological processes in male reproductive development. *Ann. Bot.* **97**: 731–738.
- Sato, T. and Theologis, A. (1989). Cloning the mRNA encoding 1-aminocyclopropane-1-carboxylate synthase, the key enzyme for ethylene biosynthesis in plants. *Proc. Natl. Acad. Sci. U. S. A.* **86**: 6621–6625.
- Savatin, D. V., Gramegna, G., Modesti, V., and Cervone, F. (2014). Wounding in the plant tissue: the defense of a dangerous passage. *Front. Plant Sci.* **5**: 1–11.
- Saxena, K.B. and Hingane, A.J. (2015). Male Sterility Systems in Major Field Crops and Their Potential Role in Crop Improvement. In *Plant Biology and Biotechnology* (Springer India: New Delhi), pp.

- 639–656.
- Schaller, F., Biesgen, C., Müssig, C., Altmann, T., and Weiler, E.W.** (2000). 12-oxophytodienoate reductase 3 (OPR3) is the isoenzyme involved in jasmonate biosynthesis. *Planta* **210**: 979–984.
- Schaller, G.E. and Binder, B.M.** (2017). Inhibitors of Ethylene Biosynthesis and Signaling. *Methods Mol. Biol.* **1573**: 223–235.
- Schaller, G.E. and Bleecker, A.B.** (1995). Ethylene-Binding Sites Generated in Yeast Expressing the Arabidopsis ETR1 Gene. *Science* **270**: 1809–1811.
- Scharein, B., Voet-van-Vormizeele, J., Harter, K., and Groth, G.** (2008). Ethylene signaling: Identification of a putative ETR1-AHP1 phosphorelay complex by fluorescence spectroscopy. *Anal. Biochem.* **377**: 72–76.
- Scheepens, J.F., Frei, E.S., Armbruster, G.F.J., and Stöcklin, J.** (2012). Pollen dispersal and gene flow within and into a population of the alpine monocarpic plant *Campanula thyrsoidea*. *Ann. Bot.* **110**: 1479–1488.
- Scheffner, M., Huibregtse, J.M., and Howley, P.M.** (1994). Identification of a human ubiquitin-conjugating enzyme that mediates the E6-AP-dependent ubiquitination of p53. *Proc. Natl. Acad. Sci. U. S. A.* **91**: 8797–801.
- Scheffner, M., Huibregtse, J.M., Vierstra, R.D., and Howley, P.M.** (1993). The HPV-16 E6 and E6-AP complex functions as a ubiquitin-protein ligase in the ubiquitination of p53. *Cell* **75**: 495–505.
- Schellingen, K., Van Der Straeten, D., Vandenbussche, F., Prinsen, E., Remans, T., Vangronsveld, J., and Cuypers, A.** (2014). Cadmium-induced ethylene production and responses in *Arabidopsis thaliana* rely on ACS2 and ACS6 gene expression. *BMC Plant Biol.* **14**: 214.
- Schiefthaler, U., Balasubramanian, S., Sieber, P., Chevalier, D., Wisman, E., and Schneitz, K.** (1999). Molecular analysis of NOZZLE, a gene involved in pattern formation and early sporogenesis during sex organ development in *Arabidopsis thaliana*. *Proc. Natl. Acad. Sci. U. S. A.* **96**: 11664–11669.
- Schmid, M., Davison, T.S., Henz, S.R., Pape, U.J., Demar, M., Vingron, M., Schölkopf, B., Weigel, D., and Lohmann, J.U.** (2005). A gene expression map of *Arabidopsis thaliana* development. *Nat. Genet.* **37**: 501–506.
- Schmidt, R., Zahn, R., Bukau, B., and Mogk, A.** (2009). ClpS is the recognition component for *Escherichia coli* substrates of the N-end rule degradation pathway. *Mol. Microbiol.* **72**: 506–517.
- Schmülling, T., Werner, T., Riefler, M., Krupková, E., and Bartrina Y Manns, I.** (2003). Structure and function of cytokinin oxidase/dehydrogenase genes of maize, rice, *Arabidopsis* and other species. *J. Plant Res.* **116**: 241–252.
- Schuenemann, V.J., Kralik, S.M., Albrecht, R., Spall, S.K., Truscott, K.N., Dougan, D.A., and Zeth, K.** (2009). Structural basis of N-end rule substrate recognition in *Escherichia coli* by the ClpAP adaptor protein ClpS. *EMBO Rep.* **10**: 508–514.
- Schuessele, C., Hoernstein, S.N.W., Mueller, S.J., Rodriguez-Franco, M., Lorenz, T., Lang, D., Igloi, G.L., and Reski, R.** (2016). Spatio-temporal patterning of arginyl-tRNA protein transferase (ATE) contributes to gametophytic development in a moss. *New Phytol.* **209**: 1014–1027.
- Schütze, K., Harter, K., and Chaban, C.** (2009). Bimolecular fluorescence complementation (BiFC) to study protein-protein interactions in living plant cells. *Methods Mol. Biol.* **479**: 189–202.
- Schwager, K.M., Calderon-Villalobos, L.I. a, Dohmann, E.M.N., Willige, B.C., Knierer, S., Nill, C., and Schwechheimer, C.** (2007). Characterization of the VIER F-BOX PROTEINE genes from *Arabidopsis* reveals their importance for plant growth and development. *Plant Cell* **19**: 1163–1178.
- Schwark, A. and Schierle, J.** (1992). Interaction of Ethylene and Auxin in the Regulation of Hook Growth I The Role of Auxin in Different Growing Regions of the Hypocotyl Hook of *Phaseolus vulgaris*. *J. Plant Physiol.* **140**: 562–570.

- Scott, R.A. and Liverman, J.L.** (1956). Promotion of Leaf Expansion by Kinetin and Benzylaminopurine. *Plant Physiol.* **31**: 321–322.
- Scott, R.J., Spielman, M., and Dickinson, H.G.** (2004). Stamen Structure and Function. *Plant Cell* **16**: S46 LP-S60.
- Shakeel, S.N., Gao, Z., Amir, M., Chen, Y.F., Rai, M.I., Haq, N.U., and Schaller, G.E.** (2015). Ethylene regulates levels of ethylene receptor/CTR1 signaling complexes in *Arabidopsis thaliana*. *J. Biol. Chem.* **290**: 12415–12424.
- Sheard, L.B. et al.** (2010). Jasmonate perception by inositol-phosphate-potentiated COI1-JAZ co-receptor. *Nature* **468**: 400–407.
- Shemorry, A., Hwang, C.S., and Varshavsky, A.** (2013). Control of Protein Quality and Stoichiometries by N-Terminal Acetylation and the N-End Rule Pathway. *Mol. Cell* **50**: 540–551.
- Shi, H., Liu, R., Xue, C., Shen, X., Wei, N., Deng, X.W., and Zhong, S.** (2016a). Seedlings Transduce the Depth and Mechanical Pressure of Covering Soil Using COP1 and Ethylene to Regulate EBF1/EBF2 for Soil Emergence. *Curr. Biol.* **26**: 139–149.
- Shi, H., Shen, X., Liu, R., Xue, C., Wei, N., Deng, X.W., and Zhong, S.** (2016b). The Red Light Receptor Phytochrome B Directly Enhances Substrate-E3 Ligase Interactions to Attenuate Ethylene Responses. *Dev. Cell* **39**: 597–610.
- Shi, J., Cui, M., Yang, L., Kim, Y.J., and Zhang, D.** (2015). Genetic and Biochemical Mechanisms of Pollen Wall Development. *Trends Plant Sci.* **20**: 741–753.
- Shi, J., Drummond, B., Wang, H., Archibald, R.L., and Habben, J.E.** (2016c). Maize and *Arabidopsis* ARGOS proteins interact with ethylene receptor signaling complex, supporting a regulatory role for ARGOS in ethylene signal transduction. *Plant Physiol.* **171**: pp.00347.2016.
- Shi, Y., Tian, S., Hou, L., Huang, X., Zhang, X., Guo, H., and Yang, S.** (2012). Ethylene Signaling Negatively Regulates Freezing Tolerance by Repressing Expression of *CBF* and Type-A *ARR* Genes in *Arabidopsis*. *Plant Cell* **24**: 2578–2595.
- Shimizu-Sato, S., Tanaka, M., and Mori, H.** (2009). Auxin-cytokinin interactions in the control of shoot branching. *Plant Mol. Biol.* **69**: 429–435.
- Singh, D.P., Jermakow, A.M., and Swain, S.M.** (2002). Gibberellins Are Required for Seed Development and Pollen Tube Growth in *Arabidopsis*. *Plant Cell* **14**: 3133–47.
- Skirycz, A., Claeys, H., De Bodt, S., Oikawa, A., Shinoda, S., Andriankaja, M., Maleux, K., Eloy, N.B., Coppens, F., Yoo, S.-D., Saito, K., and Inzé, D.** (2011). Pause-and-Stop: The Effects of Osmotic Stress on Cell Proliferation during Early Leaf Development in *Arabidopsis* and a Role for Ethylene Signaling in Cell Cycle Arrest. *Plant Cell* **23**: 1876–1888.
- Skoog, F. and Miller, C.O.** (1957). Chemical regulation of growth and organ formation in plant tissues cultured in vitro. *Symp. Soc. Exp. Biol.* **11**: 118–30.
- Smalle, J., Haegman, M., Kurepa, J., Van Montagu M, M. Van, and Straeten, D. V** (1997). Ethylene can stimulate *Arabidopsis* hypocotyl elongation in the light. *Proc. Natl. Acad. Sci. U. S. A.* **94**: 2756–61.
- Smalle, J. and Vierstra, R.D.** (2004). the Ubiquitin 26S Proteasome Proteolytic Pathway. *Annu. Rev. Plant Biol.* **55**: 555–590.
- Smith, D.M., Chang, S.C., Park, S., Finley, D., Cheng, Y., and Goldberg, A.L.** (2007). Docking of the Proteasomal ATPases' Carboxyl Termini in the 20S Proteasome's α Ring Opens the Gate for Substrate Entry. *Mol. Cell* **27**: 731–744.
- Smyth, D.R., Bowman, J.L., and Meyerowitz, E.M.** (1990). Early flower development in *Arabidopsis*. *Plant Cell* **2**: 755–67.
- Soffer, R.L. and Hoehlinshi, H.** (1969). Enzymic modification of proteins. I. General characteristics of the arginine-transfer reaction in rabbit liver cytoplasm. *J. Mol. Biol.* **43**: 163–175.

- Solano, R., Stepanova, A., Chao, Q., and Ecker, J.R.** (1998). Nuclear events in ethylene signaling: a transcriptional cascade mediated by ETHYLENE-INSENSITIVE3 and ETHYLENE-RESPONSE-FACTOR1. *Genes Dev.* **12**: 3703–3714.
- Somers, D.E., Schultz, T.F., Milnamow, M., and Kay, S.A.** (2000). ZEITLUPE encodes a novel clock associated PAS protein from Arabidopsis. *Cell* **101**: 319–329.
- Song, S., Huang, H., Gao, H., Wang, J., Wu, D., Liu, X., Yang, S., Zhai, Q., Li, C., Qi, T., and Xie, D.** (2014). Interaction between MYC2 and ETHYLENE INSENSITIVE3 Modulates Antagonism between Jasmonate and Ethylene Signaling in Arabidopsis. *Plant Cell* **26**: 263–279.
- Song, S., Qi, T., Huang, H., Ren, Q., Wu, D., Chang, C., Peng, W., Liu, Y., Peng, J., and Xie, D.** (2011). The Jasmonate-ZIM Domain Proteins Interact with the R2R3-MYB Transcription Factors MYB21 and MYB24 to Affect Jasmonate-Regulated Stamen Development in Arabidopsis. *Plant Cell* **23**: 1000–1013.
- Song, S., Qi, T., Huang, H., and Xie, D.** (2013). Regulation of stamen development by coordinated actions of jasmonate, auxin, and gibberellin in arabidopsis. *Mol. Plant* **6**: 1065–1073.
- Sorensen, A.M., Kröber, S., Unte, U.S., Huijser, P., Dekker, K., and Saedler, H.** (2003). The Arabidopsis aborted microspores (ams) gene encodes a MYC class transcription factor. *Plant J.* **33**: 413–423.
- Spanu, P., Reinhardt, D., and Boller, T.** (1991). Analysis and cloning of the ethylene-forming enzyme from tomato by functional expression of its mRNA in *Xenopus laevis* oocytes. *EMBO J.* **10**: 2007–13.
- Spíchal, L., Rakova, N.Y., Riefler, M., Mizuno, T., Romanov, G.A., Strnad, M., and Schmölling, T.** (2004). Two cytokinin receptors of Arabidopsis thaliana, CRE1/AHK4 and AHK3, differ in their ligand specificity in a bacterial assay. *Plant Cell Physiol.* **45**: 1299–1305.
- Spitzer, C., Schellmann, S., Sabovljevic, A., Shahriari, M., Keshavaiah, C., Bechtold, N., Herzog, M., Muller, S., Hanisch, F.-G., and Hulskamp, M.** (2006). The Arabidopsis elch mutant reveals functions of an ESCRT component in cytokinesis. *Development* **133**: 4679–4689.
- Van Staden, J., Cook, E.L., and Noodén, L.D.** (1988). Cytokinins and Senescence. In *Senescence and Aging in Plants* (Elsevier), pp. 281–328.
- Stary, S., Yin, X., Potuschak, T., Schlögelhofer, P., Nizhynska, V., and Bachmair, A.** (2003). PRT1 of Arabidopsis is a ubiquitin protein ligase of the plant N-end rule pathway with specificity for aromatic amino-terminal residues. *Plant Physiol.* **133**: 1360–6.
- Stegmann, M., Anderson, R.G., Ichimura, K., Pecenkova, T., Reuter, P., Zarsky, V., McDowell, J.M., Shirasu, K., and Trujillo, M.** (2012). The Ubiquitin Ligase PUB22 Targets a Subunit of the Exocyst Complex Required for PAMP-Triggered Responses in Arabidopsis. *Plant Cell* **24**: 4703–4716.
- Stein, B.J., Grant, R.A., Sauer, R.T., and Baker, T.A.** (2016). Structural Basis of an N-Degron Adaptor with More Stringent Specificity. *Structure* **24**: 232–242.
- Stewart, J.L., Maloof, J.N., and Nemhauser, J.L.** (2011). PIF genes mediate the effect of sucrose on seedling growth dynamics. *PLoS One* **6**: 1–8.
- Stewart, M.D., Ritterhoff, T., Klevit, R.E., and Brzovic, P.S.** (2016). E2 enzymes: More than just middle men. *Cell Res.* **26**: 423–440.
- Stieglitz, H.** (1977). Role of p-1 , 3-Glucanase in Postmeiotic Microspore Release. *Developmental Biol.* **57**: 87–97.
- Stintzi, A. and Browse, J.** (2000). The Arabidopsis male-sterile mutant, opr3, lacks the 12-oxophytodienoic acid reductase required for jasmonate synthesis. *Proc. Natl. Acad. Sci. U. S. A.* **97**: 10625–10630.
- Stone, S.L., Anderson, E.M., Mullen, R.T., and Goring, D.R.** (2003). ARC1 is an E3 ubiquitin ligase and promotes the ubiquitination of protein during the rejection of self-incompatible Brassica pollen. *Plant Cell* **15**: 885–898.

- Stone, S.L., Arnoldo, M.A., and Goring, D.R.** (1999). A breakdown of Brassica self-incompatibility in ARC1 antisense transgenic plants. *Science* **286**: 1729–1731.
- Stone, S.L., Hauksdóttir, H., Troy, A., Herschleb, J., Kraft, E., and Callis, J.** (2005). Functional analysis of the RING-type ubiquitin ligase family of Arabidopsis. *Plant Physiol.* **137**: 13–30.
- De Storme, N. and Geelen, D.** (2014). The impact of environmental stress on male reproductive development in plants: biological processes and molecular mechanisms. *Plant. Cell Environ.* **37**: 1–18.
- Van Der Straeten, D., Djudzman, A., Van Caeneghem, W., Smalle, J., and Van Montagu, M.** (1993). Genetic and physiological analysis of a new locus in Arabidopsis that confers resistance to 1-Aminocyclopropane-1-Carboxylic Acid and ethylene and specifically affects the ethylene signal transduction pathway. *Plant Physiol.* **102**: 401–408.
- Van der Straeten, D., Rodrigues-Pousada, R.A., Villarroyel, R., Hanley, S., Goodman, H.M., and Van Montagu, M.** (1992). Cloning, genetic mapping, and expression analysis of an Arabidopsis thaliana gene that encodes 1-aminocyclopropane-1-carboxylate synthase. *Proc. Natl. Acad. Sci. U. S. A.* **89**: 9969–9973.
- Van der Straeten, D., Van Wiemeersch, L., Goodman, H.M., and Van Montagu, M.** (1990). Cloning and sequence of two different cDNAs encoding 1-aminocyclopropane-1-carboxylate synthase in tomato. *Proc. Natl. Acad. Sci. U. S. A.* **87**: 4859–63.
- Street, I.H., Aman, S., Zubo, Y., Ramzan, A., Wang, X., Shakeel, S.N., Kieber, J.J., and Schaller, G.E.** (2015). Ethylene Inhibits Cell Proliferation of the Arabidopsis Root Meristem. *Plant Physiol.* **169**: 338–350.
- Strnad, M.** (1997). The aromatic cytokinins. *Physiol. Plant.* **101**: 674–688.
- Su, W. and Howell, S.H.** (1992). A single genetic locus, *Ckr1*, defines *Arabidopsis* mutants in which root growth is resistant to low concentrations of cytokinin. *Plant Physiol.* **99**: 1569–1574.
- Su, Y.-T., Gao, C., Liu, Y., Guo, S., Wang, A., Wang, B., Erdjument-Bromage, H., Miyagi, M., Tempst, P., and Kao, H.-Y.** (2013). Monoubiquitination of filamin B regulates vascular endothelial growth factor-mediated trafficking of histone deacetylase 7. *Mol. Cell. Biol.* **33**: 1546–60.
- Su, Y.H., Liu, Y.B., and Zhang, X.S.** (2011). Auxin-cytokinin interaction regulates meristem development. *Mol. Plant* **4**: 616–625.
- Sugiyama, N., Nakagami, H., Mochida, K., Daudi, A., Tomita, M., Shirasu, K., and Ishihama, Y.** (2008). Large-scale phosphorylation mapping reveals the extent of tyrosine phosphorylation in Arabidopsis. *Mol. Syst. Biol.* **4**.
- Sullivan, M.L., Carpenter, T.B., and Vierstra, R.D.** (1994). Homologues of wheat ubiquitin-conjugating enzymes--TaUBC1 and TaUBC4 are encoded by small multigene families in Arabidopsis thaliana. *Plant Mol. Biol.* **24**: 651–661.
- Sun, J., Niu, Q.-W., Tarkowski, P., Zheng, B., Tarkowska, D., Sandberg, G., Chua, N.-H., and Zuo, J.** (2003). The Arabidopsis AtIPT8/PGA22 gene encodes an isopentenyl transferase that is involved in de novo cytokinin biosynthesis. *Plant Physiol.* **131**: 167–76.
- Sun, M.X., Huang, X.Y., Yang, J., Guan, Y.F., and Yang, Z.N.** (2013). Arabidopsis RPG1 is important for primexine deposition and functions redundantly with RPG2 for plant fertility at the late reproductive stage. *Plant Reprod.* **26**: 83–91.
- Suryadinata, R., Roesley, S.N.A., Yang, G., and Šarčević, B.** (2014). Mechanisms of generating polyubiquitin chains of different topology. *Cells* **3**: 674–689.
- Suzuki, H., Chiba, T., Suzuki, T., Fujita, T., Ikenoue, T., Omata, M., Furuichi, K., Shikama, H., and Tanaka, K.** (2000a). Homodimer of two F-box proteins betaTrCP1 or betaTrCP2 binds to IkappaBalpha for signal-dependent ubiquitination. *J. Biol. Chem.* **275**: 2877–2884.
- Suzuki, T., Sakurai, K., Imamura, A., Nakamura, A., Ueguchi, C., and Mizuno, T.** (2000b). Compilation and Characterization of Histidine-Containing Phosphotransmitters Implicated in His-to-Asp

- Phosphorelay in Plants: AHP Signal Transducers of *Arabidopsis thaliana*. *Biosci. Biotechnol. Biochem.* **64**: 2486–2489.
- Svenning, S., Lamark, T., Krause, K., and Johansen, T.** (2011). Plant NBR1 is a selective autophagy substrate and a functional hybrid of the mammalian autophagic adapters NBR1 and p62/SQSTM1. *Autophagy* **7**: 993–1010.
- Swarup, R., Perry, P., Hagenbeek, D., Van Der Straeten, D., Beemster, G.T.S., Sandberg, G., Bhalerao, R., Ljung, K., and Bennett, M.J.** (2007). Ethylene upregulates auxin biosynthesis in *Arabidopsis* seedlings to enhance inhibition of root cell elongation. *Plant Cell* **19**: 2186–96.
- Szekeres, M., Németh, K., Koncz-Kálmán, Z., Mathur, J., Kauschmann, A., Altmann, T., Rédei, G.P., Nagy, F., Schell, J., and Koncz, C.** (1996). Brassinosteroids rescue the deficiency of CYP90, a cytochrome P450, controlling cell elongation and de-etiolation in *Arabidopsis*. *Cell* **85**: 171–182.
- Tait, S.W.G., De Vries, E., Maas, C., Keller, A.M., D'Santos, C.S., and Borst, J.** (2007). Apoptosis induction by Bid requires unconventional ubiquitination and degradation of its N-terminal fragment. *J. Cell Biol.* **179**: 1453–1466.
- Takatsuka, H., Umeda-Hara, C., and Umeda, M.** (2015). Cyclin-dependent kinase-activating kinases CDKD;1 and CDKD;3 are essential for preserving mitotic activity in *Arabidopsis thaliana*. *Plant J.* **82**: 1004–1017.
- Takei, K., Sakakibara, H., and Sugiyama, T.** (2001). Identification of Genes Encoding Adenylate Isopentenyltransferase, a Cytokinin Biosynthesis Enzyme, in *Arabidopsis thaliana*. *J. Biol. Chem.* **276**: 26405–26410.
- Takei, K., Ueda, N., Aoki, K., Kuromori, T., Hirayama, T., Shinozaki, K., Yamaya, T., and Sakakibara, H.** (2004a). AtIPT3 is a key determinant of nitrate-dependent cytokinin biosynthesis in *Arabidopsis*. *Plant Cell Physiol.* **45**: 1053–1062.
- Takei, K., Yamaya, T., and Sakakibara, H.** (2004b). *Arabidopsis* CYP735A1 and CYP735A2 encode cytokinin hydroxylases that catalyse the biosynthesis of trans-Zeatin. *J. Biol. Chem.* **279**: 41866–41872.
- Takemoto, D. and Jones, D.A.** (2005). Membrane Release and Destabilization of *Arabidopsis* RIN4 Following Cleavage by *Pseudomonas syringae* AvrRpt2. *Mol. Plant-Microbe Interact.* **18**: 1258–1268.
- Talloji, P.** (2011). Identification of novel components and links in ubiquitin dependent protein degradation pathways of *Arabidopsis thaliana*. Universität zu Köln, Dissertation. urn:nbn:de:hbz:38-49238.
- Tan, S.T. and Xue, H.W.** (2014). Casein Kinase 1 Regulates Ethylene Synthesis by Phosphorylating and Promoting the Turnover of ACS5. *Cell Rep.* **9**: 1692–1703.
- Tan, X., Calderon-Villalobos, L.I.A., Sharon, M., Zheng, C., Robinson, C. V., Estelle, M., and Zheng, N.** (2007). Mechanism of auxin perception by the TIR1 ubiquitin ligase. *Nature* **446**: 640–645.
- Tanaka, Y., Suzuki, T., Yamashino, T., and Mizuno, T.** (2004). Comparative Studies of the AHP Histidine-containing Phosphotransmitters Implicated in His-to-Asp Phosphorelay in *Arabidopsis thaliana*. *Biosci. Biotechnol. Biochem.* **68**: 462–465.
- Taniguchi, M., Kiba, T., Sakakibara, H., Ueguchi, C., Mizuno, T., and Sugiyama, T.** (1998). Expression of *Arabidopsis* response regulator homologs is induced by cytokinins and nitrate. *FEBS Lett.* **429**: 259–262.
- Tasaki, T., Mulder, L.C.F., Iwamatsu, A., Lee, M.J., Davydov, I. V., Varshavsky, A., Muesing, M., and Kwon, Y.T.** (2005). A family of mammalian E3 ubiquitin ligases that contain the UBR box motif and recognize N-degrons. *Mol Cell Biol* **25**: 7120–7136.
- Tasaki, T., Sriram, S.M., Park, K.S., and Kwon, Y.T.** (2012). The N-end rule pathway. *Annu. Rev. Biochem.* **81**: 261–89.
- Tasaki, T., Zakrzewska, A., Dudgeon, D.D., Jiang, Y., Lazo, J.S., and Kwon, Y.T.** (2009). The substrate

- recognition domains of the N-end rule pathway. *J. Biol. Chem.* **284**: 1884–95.
- Tateishi, K., Omata, M., Tanaka, K., and Chiba, T.** (2001). The NEDD8 system is essential for cell cycle progression and morphogenetic pathway in mice. *J. Cell Biol.* **155**: 571–579.
- Thines, B., Katsir, L., Melotto, M., Niu, Y., Mandaokar, A., Liu, G., Nomura, K., He, S.Y., Howe, G.A., and Browse, J.** (2007). JAZ repressor proteins are targets of the SCFCO11 complex during jasmonate signalling. *Nature* **448**: 661–665.
- Thomma, B.P.H.J., Eggermont, K., Tierens, K.F.M., and Broekaert, W.F.** (1999). Requirement of functional ethylene-insensitive 2 gene for efficient resistance of Arabidopsis to infection by *Botrytis cinerea*. *Plant Physiol.* **121**: 1093–1101.
- Thompson, A.R., Doelling, J.H., Suttangkakul, A., and Vierstra, R.D.** (2005). Autophagic Nutrient Recycling in Arabidopsis Directed by the ATG8 and ATG12 Conjugation Pathways. *Plant Physiol.* **138**: 2097–2110.
- Thrower, J.S.** (2000). Recognition of the polyubiquitin proteolytic signal. *EMBO J.* **19**: 94–102.
- Timms, R.T., Zhang, Z., Rhee, D.Y., Harper, J.W., Koren, I., and Elledge, S.J.** (2019). A glycine-specific N-degron pathway mediates the quality control of protein N-myristoylation. *Science* **365**: eaaw4912.
- To, J.P.C., Deruère, J., Maxwell, B.B., Morris, V.F., Hutchison, C.E., Ferreira, F.J., Schaller, G.E., and Kieber, J.J.** (2007). Cytokinin regulates type-A Arabidopsis Response Regulator activity and protein stability via two-component phosphorelay. *Plant Cell* **19**: 3901–14.
- To, J.P.C., Haberer, G., Ferreira, F.J., Deruère, J., Mason, M.G., Schaller, G.E., Alonso, J.M., Ecker, J.R., and Kieber, J.J.** (2004). Type-A Arabidopsis response regulators are partially redundant negative regulators of cytokinin signaling. *Plant Cell* **16**: 658–71.
- Tobias, J.W., Shrader, T.E., Rocap, G., and Varshavsky, A.** (1991). The N-end rule in bacteria. *Science* **254**: 1374–1377.
- Townsend, A., Bastin, J., Gould, K., Brownlee, G., Andrew, M., Coupar, B., Boyle, D., Chan, S., and Smith, G.** (1988). Defective presentation to class I-restricted cytotoxic T lymphocytes in vaccinia-infected cells is overcome by enhanced degradation of antigen. *J. Exp. Med.* **168**: 1211–24.
- Travella, S., Klimm, T.E., and Keller, B.** (2006). RNA Interference-Based Gene Silencing as an Efficient Tool for Functional Genomics in Hexaploid Bread Wheat. *PLANT Physiol.* **142**: 6–20.
- Trempe, J., Sauvé, V., Grenier, K., Seirafi, M., Tang, M.Y., Nagar, B., Fon, E.A., and Gehring, K.** (2013). Structure of Parkin Reveals. *Science* **340**: 1451–1455.
- Trujillo, M.** (2017). News from the PUB: plant U-box type E3 ubiquitin ligases. *J. Exp. Bot.*: 1–14.
- Trujillo, M., Ichimura, K., Casais, C., and Shirasu, K.** (2008). Negative Regulation of PAMP-Triggered Immunity by an E3 Ubiquitin Ligase Triplet in Arabidopsis. *Curr. Biol.* **18**: 1396–1401.
- Tsiatsiani, L., Timmerman, E., De Bock, P.-J., Vercammen, D., Stael, S., van de Cotte, B., Staes, A., Goethals, M., Beunens, T., Van Damme, P., Gevaert, K., and Van Breusegem, F.** (2013). The Arabidopsis METACASPASE9 Degradome. *Plant Cell* **25**: 2831–2847.
- Tsuchisaka, A. and Theologis, A.** (2004a). Heterodimeric interactions among the 1-amino-cyclopropane-1-carboxylate synthase polypeptides encoded by the Arabidopsis gene family. *Proc. Natl. Acad. Sci. U. S. A.* **101**: 2275–80.
- Tsuchisaka, A. and Theologis, A.** (2004b). Unique and overlapping expression patterns among the Arabidopsis 1-amino-cyclopropane-1-carboxylate synthase gene family members. *Plant Physiol.* **136**: 2982–3000.
- Tsukada, M. and Ohsumi, Y.** (1993). Isolation and characterization of autophagy-defective mutants of *Saccharomyces cerevisiae*. *FEBS Lett.* **333**: 169–74.
- Turek, I., Tischer, N., Lassig, R., and Trujillo, M.** (2018). Multi-tiered pairing selectivity between E2

- ubiquitin-conjugating enzymes and E3 ligases. *J. Biol. Chem.* **293**: 16324–16336.
- Twell, D.** (1992). Use of a nuclear-targeted beta-glucuronidase fusion protein to demonstrate vegetative cell-specific gene expression in developing pollen. *Plant J* **2**: 887–892.
- Vandenbussche, F., Petrasek, J., Zadnikova, P., Hoyerova, K., Pesek, B., Raz, V., Swarup, R., Bennett, M., Zazimalova, E., Benkova, E., and Van Der Straeten, D.** (2010). The auxin influx carriers AUX1 and LAX3 are involved in auxin-ethylene interactions during apical hook development in *Arabidopsis thaliana* seedlings. *Development* **137**: 597–606.
- Vanhaeren, H., Nam, Y.-J., De Milde, L., Chae, E., Storme, V., Weigel, D., Gonzalez, N., and Inzé, D.** (2017a). Forever Young: The Role of Ubiquitin Receptor DA1 and E3 Ligase BIG BROTHER in Controlling Leaf Growth and Development. *Plant Physiol.* **173**: 1269–1282.
- Vanhaeren, H., Nam, Y.-J., De Milde, L., Chae, E., Storme, V., Weigel, D., Gonzalez, N., and Inzé, D.** (2017b). Forever Young: The Role of Ubiquitin Receptor DA1 and E3 Ligase BIG BROTHER in Controlling Leaf Growth and Development. *Plant Physiol.* **173**: 1269–1282.
- Vanneste, S. and Friml, J.** (2009). Auxin: A Trigger for Change in Plant Development. *Cell* **136**: 1005–1016.
- Varshavsky, A.** (2019). N-degron and C-degron pathways of protein degradation. *Proc. Natl. Acad. Sci. U. S. A.* **116**: 358–366.
- Varshavsky, A.** (1991). Naming a Targeting Signal. *Cell* **64**: 13–15.
- Varshavsky, A.** (1996). The N-end rule: functions, mysteries, uses. *Proc. Natl. Acad. Sci. U. S. A.* **93**: 12142–12149.
- Varshavsky, A.** (1992). The N-End Rule. *Cell* **69**: 725–735.
- Varshavsky, A.** (2011). The N-end rule pathway and regulation by proteolysis. *Protein Sci.* **20**: 1298–1345.
- Varshavsky, A.** (2017). The Ubiquitin System, Autophagy, and Regulated Protein Degradation. *Annu. Rev. Biochem.* **86**: 123–128.
- Varshavsky, A.** (2005). Ubiquitin fusion technique and related methods. *Methods Enzymol.* **399**: 777–799.
- Vaseva, I.I., Qudeimat, E., Potuschak, T., Du, Y., Genschik, P., Vandenbussche, F., and Van Der Straeten, D.** (2018). The plant hormone ethylene restricts *Arabidopsis* growth via the epidermis. *Proc. Natl. Acad. Sci. U. S. A.* **115**: E4130–E4139.
- van der Veen, A.G. and Ploegh, H.L.** (2012). Ubiquitin-Like Proteins. *Annu. Rev. Biochem.* **81**: 323–357.
- Veillet, F., Gaillard, C., Coutos-Thévenot, P., and La Camera, S.** (2016). Targeting the AtCWIN1 Gene to Explore the Role of Invertases in Sucrose Transport in Roots and during *Botrytis cinerea* Infection. *Front. Plant Sci.* **7**: 1–20.
- Venne, A.S., Solari, F.A., Faden, F., Paretti, T., Dissmeyer, N., and Zahedi, R.P.** (2015). An improved workflow for quantitative N-terminal charge-based fractional diagonal chromatography (ChaFRADIC) to study proteolytic events in *Arabidopsis thaliana*. *Proteomics* **15**: 2458–2469.
- Verma, R., Aravind, L., Oania, R., McDonald, W.H., Yates, J.R., Koonin, E. V., and Deshaies, R.J.** (2002). Role of Rpn11 metalloprotease in deubiquitination and degradation by the 26S proteasome. *Science* **298**: 611–615.
- Ververidis, P. and John, P.** (1991). Complete recovery in vitro of ethylene-forming enzyme activity. *Phytochemistry* **30**: 725–727.
- Vicente, J. et al.** (2019). Distinct branches of the N-end rule pathway modulate the plant immune response. *New Phytol.* **221**: 988–1000.
- Vierstra, R.D.** (1993). Protein Degradation in Plants. *Annu. Rev. Plant Physiol. Plant Mol. Biol.* **44**: 385–410.

- Vierstra, R.D.** (2012). The Expanding Universe of Ubiquitin and Ubiquitin-Like Modifiers. *Plant Physiol.* **160**: 2–14.
- Vierstra, R.D.** (2009). The ubiquitin-26S proteasome system at the nexus of plant biology. *Nat. Rev. Mol. Cell Biol.* **10**: 385–397.
- Voesenek, L.A.C.J., Harren, F.J.M., Bogemann, G.M., Blom, C.W.P.M., and Reuss, J.** (1990). Ethylene Production and Petiole Growth in Rumex Plants Induced by Soil Waterlogging: The Application of a Continuous Flow System and a Laser Driven Intracavity Photoacoustic Detection System. *PLANT Physiol.* **94**: 1071–1077.
- Voet-Van-Vormizeele, J. and Groth, G.** (2008). Ethylene controls autophosphorylation of the histidine kinase domain in ethylene receptor ETR1. *Mol. Plant* **1**: 380–387.
- Vogel, J.P., Schuerman, P., Woeste, K., Brandstatter, I., and Kieber, J.J.** (1998a). Isolation and characterization of Arabidopsis mutants defective in the induction of ethylene biosynthesis by cytokinin. *Genetics* **149**: 417–427.
- Vogel, J.P., Woeste, K.E., Theologis, A., and Kieber, J.J.** (1998b). Recessive and dominant mutations in the ethylene biosynthetic gene ACS5 of Arabidopsis confer cytokinin insensitivity and ethylene overproduction, respectively. *Proc. Natl. Acad. Sci. U. S. A.* **95**: 4766–4771.
- Voges, D., Zwickl, P., and Baumeister, W.** (1999). the 26S Proteasome: a Molecular Machine Designed for Controlled. *Annu. Rev. Biochem.* **68**: 1015–1068.
- Vogler, F., Schmalzl, C., Enghart, M., Bircheneder, M., and Sprunck, S.** (2014). Brassinosteroids promote Arabidopsis pollen germination and growth. *Plant Reprod.* **27**: 153–167.
- Vögtle, F.N., Wortelkamp, S., Zahedi, R.P., Becker, D., Leidhold, C., Gevaert, K., Kellermann, J., Voos, W., Sickmann, A., Pfanner, N., and Meisinger, C.** (2009). Global Analysis of the Mitochondrial N-Proteome Identifies a Processing Peptidase Critical for Protein Stability. *Cell* **139**: 428–439.
- Vreeburg, R.A.M., Benschop, J.J., Peeters, A.J.M., Colmer, T.D., Ammerlaan, A.H.M., Staal, M., Elzenga, T.M., Staals, R.H.J., Darley, C.P., McQueen-Mason, S.J., and Voesenek, L.A.C.J.** (2005). Ethylene regulates fast apoplastic acidification and expansin A transcription during submergence-induced petiole elongation in Rumex palustris. *Plant J.* **43**: 597–610.
- Wadas, B., Piatkov, K.I., Brower, C.S., and Varshavsky, A.** (2016). Analyzing N-terminal arginylation through the use of peptide arrays and degradation assays. *J. Biol. Chem.* **291**: 20976–20992.
- Walbot, V. and Egger, R.L.** (2016). Pre-Meiotic Anther Development: Cell Fate Specification and Differentiation. *Annu. Rev. Plant Biol.* **67**: 365–395.
- Walsh, C.K. and Sadanandom, A.** (2014). Ubiquitin chain topology in plant cell signaling: a new facet to an evergreen story. *Front. Plant Sci.* **5**: 1–6.
- Wan, L., Xia, X., Hong, D., Li, J., and Yang, G.** (2010). Abnormal vacuolization of the tapetum during the tetrad stage is associated with male sterility in the recessive genic male sterile brassica napus L. line 9012A. *J. Plant Biol.* **53**: 121–133.
- Wang, G.L., Jiang, B.H., Rue, E.A., and Semenza, G.L.** (1995). Hypoxia-inducible factor 1 is a basic-helix-loop-helix-PAS heterodimer regulated by cellular O₂ tension. *Proc. Natl. Acad. Sci. U. S. A.* **92**: 5510–5514.
- Wang, H., Lu, Y., Jiang, T., Berg, H., Li, C., and Xia, Y.** (2013a). The Arabidopsis U-box/ARM repeat E3 ligase AtPUB4 influences growth and degeneration of tapetal cells, and its mutation leads to conditional male sterility. *Plant J.* **74**: 511–523.
- Wang, H., Piatkov, K.I., Brower, C.S., and Varshavsky, A.** (2009a). Glutamine-Specific N-Terminal Amidase, a Component of the N-End Rule Pathway. *Mol. Cell* **34**: 686–695.
- Wang, J., Han, X., Saha, S., Xu, T., Rai, R., Zhang, F., Wolf, Y.I., Wolfson, A., Yates, J.R., and Kashina, A.** (2011a). Arginyltransferase is an ATP-independent self-regulating enzyme that forms distinct functional complexes in vivo. *Chem. Biol.* **18**: 121–130.

- Wang, J., Han, X., Wong, C.C.L., Cheng, H., Aslanian, A., Xu, T., Leavis, P., Roder, H., Hedstrom, L., Yates, J.R., and Kashina, A. (2014). Arginyltransferase ATE1 catalyzes midchain arginylation of proteins at side chain carboxylates in vivo. *Chem. Biol.* **21**: 331–337.
- Wang, J., Pejaver, V.R., Dann, G.P., Wolf, M.Y., Kellis, M., Huang, Y., Garcia, B.A., Radivojac, P., and Kashina, A. (2018a). Target site specificity and in vivo complexity of the mammalian arginylome. *Sci. Rep.* **8**: 16177.
- Wang, K., Guo, Z.-L., Zhou, W.-T., Zhang, C., Zhang, Z.-Y., Lou, Y., Xiong, S.-X., Yao, X., Fan, J.-J., Zhu, J., and Yang, Z.-N. (2018b). The regulation of sporopollenin biosynthesis genes for rapid pollen wall formation. *Plant Physiol.* **178**: pp.00219.2018.
- Wang, K.H., Roman-Hernandez, G., Grant, R.A., Sauer, R.T., and Baker, T.A. (2008a). The Molecular Basis of N-End Rule Recognition. *Mol. Cell* **32**: 406–414.
- Wang, K.L.-C., Yoshida, H., Lurin, C., and Ecker, J.R. (2004). Regulation of ethylene gas biosynthesis by the Arabidopsis ETO1 protein. *Nature* **428**: 945–50.
- Wang, K.L., Li, H., and Ecker, J.R. (2002a). Ethylene Biosynthesis and Signaling Networks. *Plant Cell* **14**: 131–152.
- Wang, S.Y., Adams, D.O., and Lieberman, M. (1982). Recycling of 5'-Methylthioadenosine-Ribose Carbon Atoms into Methionine in Tomato Tissue in Relation to Ethylene Production. *Plant Physiol* **70**: 117–121.
- Wang, W., Hall, A.E., O'Malley, R., and Bleecker, A.B. (2003). Canonical histidine kinase activity of the transmitter domain of the ETR1 ethylene receptor from *Arabidopsis* is not required for signal transmission. *Proc. Natl. Acad. Sci. U. S. A.* **100**: 352–357.
- Wang, W., Wang, L., Chen, C., Xiong, G., Tan, X.Y., Yang, K.Z., Wang, Z.C., Zhou, Y., Ye, D., and Chen, L.Q. (2011b). Arabidopsis CSLD1 and CSLD4 are required for cellulose deposition and normal growth of pollen tubes. *J. Exp. Bot.* **62**: 5161–5177.
- Wang, X., Herr, R.A., Chua, W.J., Lybarger, L., Wiertz, E.J.H.J., and Hansen, T.H. (2007). Ubiquitination of serine, threonine, or lysine residues on the cytoplasmic tail can induce ERAD of MHC-I by viral E3 ligase mK3. *J. Cell Biol.* **177**: 613–624.
- Wang, X., Jin, C., Tang, Y., Tang, L.Y., and Zhang, Y.E. (2013b). Ubiquitination of tumor necrosis factor receptor-associated factor 4 (TRAF4) by smad ubiquitination regulatory factor 1 (Smurf1) regulates motility of breast epithelial and cancer cells. *J. Biol. Chem.* **288**: 21784–21792.
- Wang, X., Li, W., Piqueras, R., Cao, K., Deng, X.W., and Wei, N. (2009b). Regulation of COP1 nuclear localization by the COP9 signalosome via direct interaction with CSN1. *Plant J.* **58**: 655–667.
- Wang, Y., Wu, Y., Yu, B., Yin, Z., and Xia, Y. (2017). EXTRA-LARGE G PROTEINs Interact with E3 Ligases PUB4 and PUB2 and Function in Cytokinin and Developmental Processes. *Plant Physiol.* **173**: 1235–1246.
- Wang, Y., Zhang, W.-Z., Song, L.-F., Zou, J.-J., Su, Z., and Wu, W.-H. (2008b). Transcriptome Analyses Show Changes in Gene Expression to Accompany Pollen Germination and Tube Growth in Arabidopsis. *Plant Physiol.* **148**: 1201–1211.
- Wang, Z.Y., Nakano, T., Gendron, J., He, J., Chen, M., Vafeados, D., Yang, Y., Fujioka, S., Yoshida, S., Asami, T., and Chory, J. (2002b). Nuclear-localized BZR1 mediates brassinosteroid-induced growth and feedback suppression of brassinosteroid biosynthesis. *Dev. Cell* **2**: 505–513.
- Wanner, G. (2010). *Mikroskopisch-botanisches Praktikum*. 2nd ed., Stuttgart, Germany: Georg Thieme Verlag KG.
- Wauer, T. and Komander, D. (2013). Structure of the human Parkin ligase domain in an autoinhibited state. *EMBO J.* **32**: 2099–2112.
- Wedemeyer, W.J., Welker, E., and Scheraga, H.A. (2002). Proline cis-trans isomerization and protein folding. *Biochemistry* **41**: 14637–14644.

- Wei, N., Kwok, S.F., von Arnim, A.G., Lee, A., McNellis, T.W., Piekos, B., and Deng, X.W.** (1994). Arabidopsis COP8, COP10, and COP11 genes are involved in repression of photomorphogenic development in darkness. *Plant Cell* **6**: 629–43.
- Weiser, A.A., Or-Guil, M., Tapia, V., Leichsenring, A., Schuchhardt, J., Frömmel, C., and Volkmer-Engert, R.** (2005). SPOT synthesis: Reliability of array-based measurement of peptide binding affinity. *Anal. Biochem.* **342**: 300–311.
- Weissman, A.M.** (2001). Themes and variations on ubiquitylation. *Nat. Rev. Mol. Cell Biol.* **2**: 169–78.
- Weits, D.A., Giuntoli, B., Kosmacz, M., Parlanti, S., Hubberten, H.-M., Riegler, H., Hoefgen, R., Perata, P., van Dongen, J.T., and Licausi, F.** (2014). Plant cysteine oxidases control the oxygen-dependent branch of the N-end-rule pathway. *Nat. Commun.* **5**: 1–10.
- Weits, D.A., Kunkowska, A.B., Kamps, N.C.W., Portz, K.M.S., Packbier, N.K., Nemeček, Z., Gailloch, C., Lohmann, J.U., Pedersen, O., van Dongen, J.T., and Licausi, F.** (2019). An apical hypoxic niche sets the pace of shoot meristem activity. *Nature*.
- Wen, R., Newton, L., Li, G., Wang, H., and Xiao, W.** (2006). Arabidopsis thaliana UBC13: Implication of error-free DNA damage tolerance and Lys63-linked polyubiquitylation in plants. *Plant Mol. Biol.* **61**: 241–253.
- Wen, X., Zhang, C., Ji, Y., Zhao, Q., He, W., An, F., Jiang, L., and Guo, H.** (2012). Activation of ethylene signaling is mediated by nuclear translocation of the cleaved EIN2 carboxyl terminus. *Cell Res.* **22**: 1613–6.
- Wenzel, D.M., Lissounov, A., Brzovic, P.S., and Klevit, R.E.** (2011). UBC7 reactivity profile reveals parkin and HHARI to be RING/HECT hybrids. *Nature* **474**: 105–108.
- Werner, T., Köllmer, I., Bartrina, I., Holst, K., and Schmülling, T.** (2006). New insights into the biology of cytokinin degradation. *Plant Biol.* **8**: 371–381.
- Werner, T., Motyka, V., Laucou, V., Smets, R., Onckelen, H. Van, and Schmülling, T.** (2003). Cytokinin-deficient transgenic Arabidopsis plants show functions of cytokinins in the regulation of shoot and root. *Plant Cell* **15**: 2532–2550.
- Werner, T., Motyka, V., Strnad, M., and Schmülling, T.** (2001). Regulation of plant growth by cytokinin. *Proc. Natl. Acad. Sci. U. S. A.* **98**: 10487–10492.
- White, M.D. et al.** (2017). Plant cysteine oxidases are dioxygenases that directly enable arginyl transferase-catalysed arginylation of N-end rule targets. *Nat. Commun.* **8**: 14690.
- White, M.D., Kamps, J.J.A.G., East, S., Taylor Kearney, L.J., and Flashman, E.** (2018). The plant cysteine oxidases from Arabidopsis thaliana are kinetically tailored to act as oxygen sensors. *J. Biol. Chem.* **293**: 11786–11795.
- Wiborg, J., O’Shea, C., and Skriver, K.** (2008). Biochemical function of typical and variant *Arabidopsis thaliana* U-box E3 ubiquitin-protein ligases. *Biochem. J.* **413**: 447–457.
- Wickson, M. and Thimann, K. V.** (1958). The Antagonism of Auxin and Kinetin in Apical Dominance. *Physiol. Plant.* **11**: 62–74.
- Wijeratne, A.J., Zhang, W., Sun, Y., Liu, W., Albert, R., Zheng, Z., Oppenheimer, D.G., Zhao, D., and Ma, H.** (2007). Differential gene expression in Arabidopsis wild-type and mutant anthers: Insights into anther cell differentiation and regulatory networks. *Plant J.* **52**: 14–29.
- Wilkinson, K.D., Urban, M.K., and Haas, A.L.** (1980). Ubiquitin is the ATP-dependent proteolysis factor I of rabbit reticulocytes. *J. Biol. Chem.* **255**: 7529–7532.
- Willems, A.R., Schwab, M., and Tyers, M.** (2004). A hitchhiker’s guide to the cullin ubiquitin ligases: SCF and its kin. *Biochim. Biophys. Acta - Mol. Cell Res.* **1695**: 133–170.
- Willems, P., Ndash, E., Jonckheere, V., Stael, S., Sticker, A., Martens, L., Van Breusegem, F., Gevaert, K., and Van Damme, P.** (2017). N-terminal Proteomics Assisted Profiling of the Unexplored Translation Initiation Landscape in Arabidopsis thaliana. *Mol. Cell. Proteomics* **16**: 1064–1080.

- Williams, C., Van Den Berg, M., Sprenger, R.R., and Distel, B.** (2007). A conserved cysteine is essential for Pex4p-dependent ubiquitination of the peroxisomal import receptor Pex5p. *J. Biol. Chem.* **282**: 22534–22543.
- Wilson, Z.A., Morroll, S.M., Dawson, J., Swarup, R., and Tighe, P.J.** (2001). The Arabidopsis MALE STERILITY1 (MS1) gene is a transcriptional regulator of male gametogenesis, with homology to the PHD-finger family of transcription factors. *Plant J.* **28**: 27–39.
- Wilson, Z.A., Song, J., Taylor, B., and Yang, C.** (2011). The final split: The regulation of anther dehiscence. *J. Exp. Bot.* **62**: 1633–1649.
- Winter, D., Vinegar, B., Nahal, H., Ammar, R., Wilson, G. V., and Provart, N.J.** (2007). An “electronic fluorescent pictograph” Browser for exploring and analyzing large-scale biological data sets. *PLoS One* **2**: 1–12.
- Woeste, K.E., Vogel, J.P., and Kieber, J.J.** (1999a). Factors regulating ethylene biosynthesis in etiolated Arabidopsis thaliana seedlings. *Physiol. Plant.* **105**: 478–484.
- Woeste, K.E., Ye, C., and Kieber, J.J.** (1999b). Two Arabidopsis mutants that overproduce ethylene are affected in the posttranscriptional regulation of 1-aminocyclopropane-1-carboxylic acid synthase. *Plant Physiol.* **119**: 521–530.
- Wolters-Arts, M., Lush, W.M., and Mariani, C.** (1998). Lipids are required for directional pollen-tube growth. *Nature* **392**: 818–821.
- Wong, C.C.L., Xu, T., Rai, R., Bailey, A.O., Yates, J.R., Wolf, Y.I., Zebroski, H., and Kashina, A.** (2007). Global analysis of posttranslational protein arginylation. *PLoS Biol.* **5**: 2231–2242.
- Worley, C.K., Ling, R., and Callis, J.** (1998). Engineering in vivo instability of firefly luciferase and Escherichia coli ??-glucuronidase in higher plants using recognition elements from the ubiquitin pathway. *Plant Mol. Biol.* **37**: 337–347.
- Wu, F.H., Shen, S.C., Lee, L.Y., Lee, S.H., Chan, M.T., and Lin, C.S.** (2009). Tape-arabidopsis sandwich - A simpler arabidopsis protoplast isolation method. *Plant Methods* **5**: 1–10.
- Wu, H. and Yang, M.** (2005). Reduction in vacuolar volume in the tapetal cells coincides with conclusion of the tetrad stage in Arabidopsis thaliana. *Sex. Plant Reprod.* **18**: 173–178.
- Wu, S.S., Platt, K. a, Ratnayake, C., Wang, T.W., Ting, J.T., and Huang, A.H.** (1997). Isolation and characterization of neutral-lipid-containing organelles and globuli-filled plastids from Brassica napus tapetum. *Proc. Natl. Acad. Sci. U. S. A.* **94**: 12711–12716.
- Wulfetange, K., Lomin, S.N., Romanov, G.A., Stolz, A., Heyl, A., and Schmulling, T.** (2011). The Cytokinin Receptors of Arabidopsis Are Located Mainly to the Endoplasmic Reticulum. *Plant Physiol.* **156**: 1808–1818.
- Xia, T., Li, N., Dumenil, J., Li, J., Kamenski, A., Bevan, M.W., Gao, F., and Li, Y.** (2013). The Ubiquitin Receptor DA1 Interacts with the E3 Ubiquitin Ligase DA2 to Regulate Seed and Organ Size in Arabidopsis. *Plant Cell* **25**: 3347–3359.
- Xia, Z., Webster, A., Du, F., Piatkov, K., Ghislain, M., and Varshavsky, A.** (2008). Substrate-binding sites of UBR1, the ubiquitin ligase of the N-end rule pathway. *J. Biol. Chem.* **283**: 24011–28.
- Xie, D.-X., Feys, B.F., James, S., Nieto-Rostro, M., and Turner, J.G.** (1998). COI1: An Arabidopsis Gene Required for Jasmonate-Regulated Defense and Fertility. *Science* **280**: 1091–1094.
- Xie, M., Chen, H., Huang, L., O’Neil, R.C., Shokhirev, M.N., and Ecker, J.R.** (2018). A B-ARR-mediated cytokinin transcriptional network directs hormone cross-regulation and shoot development. *Nat. Commun.* **9**: 1–13.
- Xie, Q., Guo, H.S., Dallman, G., Fang, S., Weissman, A.M., and Chua, N.H.** (2002). SINAT5 promotes ubiquitin-related degradation of NAC1 to attenuate auxin signals. *Nature* **419**: 167–170.
- Xing, S., Quodt, V., Chandler, J., Höhmann, S., Berndtgen, R., and Huijser, P.** (2013). SPL8 Acts Together with the Brassinosteroid-Signaling Component BIM1 in Controlling Arabidopsis

- thaliana Male Fertility. *Plants* **2**: 416–428.
- Xu, A., Zhang, W., and Wen, C.K.** (2014). ENHANCING CTR1-10 ETHYLENE RESPONSE2 is a novel allele involved in CONSTITUTIVE TRIPLE-RESPONSE1-mediated ethylene receptor signaling in Arabidopsis. *BMC Plant Biol.* **14**: 1–13.
- Xu, F. et al.** (2015). Two N-Terminal Acetyltransferases Antagonistically Regulate the Stability of a Nod-Like Receptor in Arabidopsis. *Plant Cell* **27**: 1547–1562.
- Xu, L., Liu, F., Lechner, E., Genschik, P., Crosby, W.L., Peng, W., Huang, D., and Xie, D.** (2002). The SCF-COI1 Ubiquitin-Ligase Complexes Are Required for Jasmonate Response in Arabidopsis. *Society* **14**: 1919–1935.
- Xu, P., Duong, D.M., Seyfried, N.T., Cheng, D., Xie, Y., Robert, J., Rush, J., Hochstrasser, M., Finley, D., and Peng, J.** (2009). Quantitative Proteomics Reveals the Function of Unconventional Ubiquitin Chains in Proteasomal Degradation. *Cell* **137**: 133–145.
- Yadav, V., Molina, I., Ranathunge, K., Castillo, I.Q., Rothstein, S.J., and Reed, J.W.** (2014). ABCG Transporters Are Required for Suberin and Pollen Wall Extracellular Barriers in Arabidopsis. *Plant Cell* **26**: 3569–3588.
- Yamagami, T., Tsuchisaka, A., Yamada, K., Haddon, W.F., Harden, L.A., and Theologis, A.** (2003). Biochemical diversity among the 1-amino-cyclopropane-1-carboxylate synthase isozymes encoded by the Arabidopsis gene family. *J. Biol. Chem.* **278**: 49102–49112.
- Yamaguchi, N., Suzuki, M., Fukaki, H., Morita-Terao, M., Tasaka, M., and Komeda, Y.** (2007). CRM1/BIG-mediated auxin action regulates Arabidopsis inflorescence development. *Plant Cell Physiol.* **48**: 1275–90.
- Yamasaki, H. and Sakihama, Y.** (2000). Simultaneous production of nitric oxide and peroxonitrite by plant nitrite reductase: in vitro evidence for the NR-dependent formation of reactive nitrogen species. *FEBS Lett.* **462**: 89–92.
- Yan, J., Zhang, C., Gu, M., Bai, Z., Zhang, W., Qi, T., Cheng, Z., Peng, W., Luo, H., Nan, F., Wang, Z., and Xie, D.** (2009). The Arabidopsis CORONATINE INSENSITIVE1 protein is a jasmonate receptor. *Plant Cell* **21**: 2220–36.
- Yan, Y., Christensen, S., Isakeit, T., Engelberth, J., Meeley, R., Hayward, A., Emery, R.J.N., and Kolomiets, M. V.** (2012). Disruption of *OPR7* and *OPR8* Reveals the Versatile Functions of Jasmonic Acid in Maize Development and Defense. *Plant Cell* **24**: 1420–1436.
- Yan, Y., Stolz, S., Chételat, A., Reymond, P., Pagni, M., Dubugnon, L., and Farmer, E.E.** (2007). A downstream mediator in the growth repression limb of the jasmonate pathway. *Plant Cell* **19**: 2470–83.
- Yanagawa, Y., Sullivan, J.A., Komatsu, S., Gusmaroli, G., Suzuki, G., Yin, J., Ishibashi, T., Saijo, Y., Rubio, V., Kimura, S., Wang, J., and Deng, X.W.** (2004). Arabidopsis COP10 forms a complex with DDB1 and DET1 in vivo and enhances the activity of ubiquitin conjugating enzymes. *Genes Dev.* **18**: 2172–2181.
- Yanagisawa, S., Yoo, S.D., and Sheen, J.** (2003). Differential regulation of EIN3 stability by glucose and ethylene signalling in plants. *Nature* **425**: 521–525.
- Yang, C.W., Gonzalez-Lamothe, R., Ewan, R.A., Rowland, O., Yoshioka, H., Shenton, M., Ye, H., O'Donnell, E., Jones, J.D., and Sadanandom, A.** (2006). The E3 ubiquitin ligase activity of arabidopsis PLANT U-BOX17 and its functional tobacco homolog ACRE276 are required for cell death and defense. *Plant Cell* **18**: 1084–1098.
- Yang, J., Tian, L., Sun, M.-X., Huang, X.-Y., Zhu, J., Guan, Y.-F., Jia, Q.-S., and Yang, Z.-N.** (2013). AUXIN RESPONSE FACTOR17 Is Essential for Pollen Wall Pattern Formation in Arabidopsis. *Plant Physiol.* **162**: 720–731.
- Yang, P., Fu, H., Walker, J., Papa, C.M., Smalle, J., Ju, Y.M., and Vierstra, R.D.** (2004). Purification of the Arabidopsis 26 S proteasome: Biochemical and molecular analyses revealed the presence of

- multiple isoforms. *J. Biol. Chem.* **279**: 6401–6413.
- Yang, S.F. and Hoffman, N.E.** (1984). Ethylene Biosynthesis and its Regulation in Higher Plants. *Annu. Rev. Plant Physiol.* **35**: 155–189.
- Yang, W.-C., Ye, D., Xu, J., and Sundaresan, V.** (1999). The SPOROCTELESS gene of Arabidopsis is required for initiation of sporogenesis and encodes a novel nuclear protein. *Genes Dev.* **13**: 2108–2117.
- Yao, X., Tian, L., Yang, J., Zhao, Y.N., Zhu, Y.X., Dai, X., Zhao, Y., and Yang, Z.N.** (2018). Auxin production in diploid microsporocytes is necessary and sufficient for early stages of pollen development. *PLoS Genet.* **14**: 1–19.
- Yau, R. and Rape, M.** (2016). The increasing complexity of the ubiquitin code. *Nat. Cell Biol.* **18**: 579–586.
- Ye, Q., Zhu, W., Li, L., Zhang, S., Yin, Y., Ma, H., and Wang, X.** (2010). Brassinosteroids control male fertility by regulating the expression of key genes involved in Arabidopsis anther and pollen development. *Proc. Natl. Acad. Sci. U. S. A.* **107**: 6100–6105.
- Ye, Y. and Rape, M.** (2009). Building ubiquitin chains: E2 enzymes at work. *Nat. Rev. Mol. Cell Biol.* **10**: 755–764.
- Yee, D. and Goring, D.R.** (2009). The diversity of plant U-box E3 ubiquitin ligases: From upstream activators to downstream target substrates. *J. Exp. Bot.* **60**: 1109–1121.
- Yim, S., Khare, D., Kang, J., Hwang, J.U., Liang, W., Martinoia, E., Zhang, D., Kang, B., and Lee, Y.** (2016). Postmeiotic development of pollen surface layers requires two Arabidopsis ABCG-type transporters. *Plant Cell Rep.* **35**: 1863–1873.
- Yim, Y.Y., Betke, K., and Hamm, H.** (2015). Using peptide arrays created by the SPOT method for defining protein-protein interactions. *Methods Mol. Biol.* **1278**: 307–20.
- Yin, C.-C. et al.** (2015). Ethylene Responses in Rice Roots and Coleoptiles Are Differentially Regulated by a Carotenoid Isomerase-Mediated Abscisic Acid Pathway. *Plant Cell* **27**: 1061–1081.
- Yin, Q. et al.** (2009). E2 interaction and dimerization in the crystal structure of TRAF6. *Nat. Struct. Mol. Biol.* **16**: 658–666.
- Yoon, G.M. and Kieber, J.J.** (2013). 14-3-3 regulates 1-aminocyclopropane-1-carboxylate synthase protein turnover in Arabidopsis. *Plant Cell* **25**: 1016–28.
- Yoshida, H., Nagata, M., Saito, K., Kevin, W.L.C., and Ecker, J.R.** (2005). Arabidopsis ETO1 specifically interacts with and negatively regulates type 2 1-aminocyclopropane-1-carboxylate synthases. *BMC Plant Biol.* **5**: 1–13.
- Yoshida, H., Wang, K.L.C., Chang, C.M., Mori, K., Uchida, E., and Ecker, J.R.** (2006). The ACC synthase TOE sequence is required for interaction with ETO1 family proteins and destabilization of target proteins. *Plant Mol. Biol.* **62**: 427–437.
- Yoshida, S., Ito, M., Callis, J., Nishida, I., and Watanabe, A.** (2002). A delayed leaf senescence mutant is defective in arginyl-tRNA : protein arginyltransferase , a component of the N-end rule pathway in Arabidopsis. *Plant J.* **32**: 129–137.
- Yu, F., Lou, L., Tian, M., Li, Q., Ding, Y., Cao, X., Wu, Y., Belda-Palazon, B., Rodriguez, P.L., Yang, S., and Xie, Q.** (2016). ESCRT-I Component VPS23A Affects ABA Signaling by Recognizing ABA Receptors for Endosomal Degradation. *Mol. Plant* **9**: 1570–1582.
- Yu, H., Ito, T., Zhao, Y., Peng, J., Kumar, P., and Meyerowitz, E.M.** (2004). Floral homeotic genes are targets of gibberellin signaling in flower development. *Proc. Natl. Acad. Sci. U. S. A.* **101**: 7827–7832.
- Yu, J., Han, J., Kim, Y.-J., Song, M., Yang, Z., He, Y., Fu, R., Luo, Z., Hu, J., Liang, W., and Zhang, D.** (2017). Two rice receptor-like kinases maintain male fertility under changing temperatures. *Proc. Natl. Acad. Sci. U. S. A.* **114**: 12327–12332.

- Yu, J. and Wen, C.K.** (2013). Arabidopsis aux1rcr1 mutation alters AUXIN RESISTANT1 targeting and prevents expression of the auxin reporter DR5:GUS in the root apex. *J. Exp. Bot.* **64**: 921–933.
- Yu, Y. and Huang, R.** (2017). Integration of Ethylene and Light Signaling Affects Hypocotyl Growth in Arabidopsis. *Front. Plant Sci.* **08**: 2012–2017.
- Yu, Y., Wang, J., Zhang, Z., Quan, R., Zhang, H., Deng, X.W., Ma, L., and Huang, R.** (2013). Ethylene Promotes Hypocotyl Growth and HY5 Degradation by Enhancing the Movement of COP1 to the Nucleus in the Light. *PLoS Genet.* **9**.
- Yuan, L., Liu, Z., Song, X., Johnson, C., Yu, X., and Sundaresan, V.** (2016). The CKI1 Histidine Kinase Specifies the Female Gametic Precursor of the Endosperm. *Dev. Cell* **37**: 34–46.
- Yudina, Z., Roa, A., Johnson, R., Biris, N., de Souza Aranha Vieira, D.A., Tshiperson, V., Reszka, N., Taylor, A.B., Hart, P.J., Demeler, B., Diaz-Griffero, F., and Ivanov, D.N.** (2015). RING Dimerization Links Higher-Order Assembly of TRIM5 α to Synthesis of K63-Linked Polyubiquitin. *Cell Rep.* **12**: 788–797.
- Zamariola, L., De Storme, N., Tiang, C.L., Armstrong, S.J., Franklin, F.C.H., and Geelen, D.** (2013). SGO1 but not SGO2 is required for maintenance of centromere cohesion in Arabidopsis thaliana meiosis. *Plant Reprod.* **26**: 197–208.
- Zander, N. and Gausepohl, H.** (2002). Chemistry of Fmoc Peptide Synthesis on Membranes. In *Peptide Arrays on Membrane Supports*, J. Koch and M. Mahler, eds (Springer Berlin Heidelberg: Berlin, Heidelberg), pp. 23–39.
- Zeng, L.R., Park, C.H., Venu, R.C., Gough, J., and Wang, G.L.** (2008). Classification, expression pattern, and E3 Ligase Activity Assay of Rice U-box-containing proteins. *Mol. Plant* **1**: 800–815.
- Zhan, H., Xiong, H., Wang, S., and Yang, Z.N.** (2018). Anther Endothecium-Derived Very-Long-Chain Fatty Acids Facilitate Pollen Hydration in Arabidopsis. *Mol. Plant* **11**: 1101–1104.
- Zhang, F., Patel, D.M., Colavita, K., Rodionova, I., Buckley, B., Scott, D.A., Kumar, A., Shabalina, S.A., Saha, S., Chernov, M., Osterman, A.L., and Kashina, A.** (2015a). Arginylation regulates purine nucleotide biosynthesis by enhancing the activity of phosphoribosyl pyrophosphate synthase. *Nat. Commun.* **6**: 7517.
- Zhang, F., Saha, S., and Kashina, A.** (2012a). Arginylation-dependent regulation of a proteolytic product of talin is essential for cell-cell adhesion. *J. Cell Biol.* **197**: 819–836.
- Zhang, F., Wang, L., Ko, E.E., Shao, K., and Qiao, H.** (2018a). Histone deacetylases SRT1 and SRT2 interact with ENAP1 to mediate ethylene-induced transcriptional repression. *Plant Cell* **30**: tpc.00671.2017.
- Zhang, F., Wang, L., Qi, B., Zhao, B., Ko, E.E., Riggan, N.D., Chin, K., and Qiao, H.** (2017a). EIN2 mediates direct regulation of histone acetylation in the ethylene response. *Proc. Natl. Acad. Sci. U. S. A.* **114**: 201707937.
- Zhang, H., Deery, M.J., Gannon, L., Powers, S.J., Lilley, K.S., and Theodoulou, F.L.** (2015b). Quantitative proteomics analysis of the Arg/N-end rule pathway of targeted degradation in Arabidopsis roots. *Proteomics* **15**: 2447–2457.
- Zhang, H., Gannon, L., Hassall, K.L., Deery, M.J., Gibbs, D.J., Holdsworth, M.J., van der Hoorn, R.A.L., Lilley, K.S., and Theodoulou, F.L.** (2018b). N-terminomics reveals control of Arabidopsis seed storage proteins and proteases by the Arg/N-end rule pathway. *New Phytol.* **218**: 1106–1126.
- Zhang, H., Gannon, L., Jones, P.D., Rundle, C.A., Hassall, K.L., Gibbs, D.J., Holdsworth, M.J., and Theodoulou, F.L.** (2018c). Genetic interactions between ABA signalling and the Arg/N-end rule pathway during Arabidopsis seedling establishment. *Sci. Rep.* **8**: 1–12.
- Zhang, L., Fairall, L., Goult, B.T., Calkin, A.C., Hong, C., Millard, C.J., Tontonoz, P., and Schwabe, J.W.R.** (2011a). The IDOL-UBE2D complex mediates sterol-dependent degradation of the LDL receptor. *Genes Dev.* **25**: 1262–1274.

- Zhang, L., Li, Z., Quan, R., Li, G., Wang, R., and Huang, R. (2011b). An AP2 Domain-Containing Gene, ESE1, Targeted by the Ethylene Signaling Component EIN3 Is Important for the Salt Response in Arabidopsis. *Plant Physiol.* **157**: 854–865.
- Zhang, L., Zhao, Y.-L., Gao, L.-F., Zhao, G.-Y., Zhou, R.-H., Zhang, B.-S., and Jia, J.-Z. (2012b). TaCKX6-D1, the ortholog of rice OsCKX2, is associated with grain weight in hexaploid wheat. *New Phytol.* **195**: 574–584.
- Zhang, R.-X. et al. (2019). BIG regulates stomatal immunity and jasmonate production in Arabidopsis. *New Phytol.* **222**: 335–348.
- Zhang, S.-S., Yang, H., Ding, L., Song, Z.-T., Ma, H., Chang, F., and Liu, J.-X. (2017b). Tissue-Specific Transcriptomics Reveals an Important Role of the Unfolded Protein Response in Maintaining Fertility upon Heat Stress in Arabidopsis. *Plant Cell* **29**: 1007–1023.
- Zhang, S., Wang, S., Lv, J., Liu, Z., Wang, Y., Ma, N., and Meng, Q. (2017c). SUMO E3 Ligase SISIZ1 Facilitates Heat Tolerance in Tomato. *Plant Cell Physiol.* **59**: 58–71.
- Zhang, W., Sun, Y., Timofejeva, L., Chen, C., Grossniklaus, U., and Ma, H. (2006). Regulation of Arabidopsis tapetum development and function by DYSFUNCTIONAL TAPETUM1 (DYT1) encoding a putative bHLH transcription factor. *Development* **133**: 3085–3095.
- Zhang, Y., Liu, Z., Wang, J., Chen, Y., Bi, Y., and He, J. (2015c). Brassinosteroid is required for sugar promotion of hypocotyl elongation in Arabidopsis in darkness. *Planta* **242**: 881–893.
- Zhang, Y., Liu, Z., Wang, L., Zheng, S., Xie, J., and Bi, Y. (2010). Sucrose-induced hypocotyl elongation of Arabidopsis seedlings in darkness depends on the presence of gibberellins. *J. Plant Physiol.* **167**: 1130–1136.
- Zhang, Z., Hu, M., Feng, X., Gong, A., Cheng, L., and Yuan, H. (2017d). Proteomes and Phosphoproteomes of Anther and Pollen: Availability and Progress. *Proteomics* **17**: 1–12.
- Zhang, Z., Ren, J.-S., Clifton, I.J., and Schofield, C.J. (2004). Crystal Structure and Mechanistic Implications of 1-Aminocyclopropane-1-Carboxylic Acid Oxidase—The Ethylene-Forming Enzyme. *Chem. Biol.* **11**: 1383–1394.
- Zhao, C. et al. (2017). Temperature increase reduces global yields of major crops in four independent estimates. *Proc. Natl. Acad. Sci. U. S. A.* **114**: 9326–9331.
- Zhao, D.-Z., Wang, G.-F., Speal, B., and Ma, H. (2002). The EXCESS MICROSPOROCTES1 gene encodes a putative leucine-rich repeat receptor protein kinase that controls somatic and reproductive cell fates in the Arabidopsis anther. *Genes Dev.* **16**: 2021–2031.
- Zhao, J., Bai, W., Zeng, Q., Song, S., Zhang, M., Li, X., Hou, L., Xiao, Y., Luo, M., Li, D., Luo, X., and Pei, Y. (2015). Moderately enhancing cytokinin level by down-regulation of GhCKX expression in cotton concurrently increases fiber and seed yield. *Mol. Breed.* **35**: 60.
- Zhao, Y. (2010). Auxin Biosynthesis and Its Role in Plant Development. *Annu Rev Plant Biol* **61**: 49–64.
- Zhao, Y., Christensen, S.K., Fankhauser, C., Cashman, J.R., Cohen, J.D., Weigel, D., and Chory, J. (2001). A role for flavin monooxygenase-like enzymes in auxin biosynthesis. *Science* **291**: 306–309.
- Zheng, N., Wang, P., Jeffrey, P.D., and Pavletich, N.P. (2000). Structure of a c-Cbl–Ubch7 Complex: RING Domain Function in Ubiquitin-Protein Ligases. *Cell* **102**: 533–539.
- Zheng, Y., Cui, X., Su, L., Fang, S., Chu, J., Gong, Q., Yang, J., and Zhu, Z. (2017). Jasmonate inhibits COP1 activity to suppress hypocotyl elongation and promote cotyledon opening in etiolated Arabidopsis seedlings. *Plant J.* **90**: 1144–1155.
- Zhong, S., Shi, H., Xue, C., Wang, L., Xi, Y., Li, J., Quail, P.H., Deng, X.W., and Guo, H. (2012). A molecular framework of light-controlled phytohormone action in arabidopsis. *Curr. Biol.* **22**: 1530–1535.
- Zhou, J. et al. (2018). Regulation of *Arabidopsis* brassinosteroid receptor BRI1 endocytosis and

- degradation by plant U-box PUB12/PUB13-mediated ubiquitination. *Proc. Natl. Acad. Sci. U. S. A.*: 201712251.
- Zhou, L., Jang, J.C., Jones, T.L., and Sheen, J.** (1998). Glucose and ethylene signal transduction crosstalk revealed by an *Arabidopsis* glucose-insensitive mutant. *Proc. Natl. Acad. Sci. U. S. A.* **95**: 10294–9.
- Zhu, J.Y., Li, Y., Cao, D.M., Yang, H., Oh, E., Bi, Y., Zhu, S., and Wang, Z.Y.** (2017). The F-box Protein KIB1 Mediates Brassinosteroid-Induced Inactivation and Degradation of GSK3-like Kinases in *Arabidopsis*. *Mol. Cell* **66**: 648-657.e4.
- Zinn, K.E., Tunc-Ozdemir, M., and Harper, J.F.** (2010). Temperature stress and plant sexual reproduction: Uncovering the weakest links. *J. Exp. Bot.* **61**: 1959–1968.
- Zuñiga-Mayo, V.M., Baños-Bayardo, C.R., Díaz-Ramírez, D., Marsch-Martínez, N., and De Folter, S.** (2018). Conserved and novel responses to cytokinin treatments during flower and fruit development in *Brassica napus* and *Arabidopsis thaliana*. *Sci. Rep.* **8**: 1–10.
- Zuñiga-Mayo, V.M., Reyes-Olalde, J.I., Marsch-Martinez, N., and de Folter, S.** (2014). Cytokinin treatments affect the apical-basal patterning of the *Arabidopsis* gynoecium and resemble the effects of polar auxin transport inhibition. *Front. Plant Sci.* **5**: 1–8.
- Zürcher, E., Liu, J., Di Donato, M., Geisler, M., and Müller, B.** (2016). Plant development regulated by cytokinin sinks. *Science* **353**: 1027–1030.
- Zwirn, P., Stary, S., Luschnig, C., and Bachmair, A.** (1997). *Arabidopsis thaliana* RAD6 homolog AtUBC2 complements UV sensitivity, but not N-end rule degradation deficiency, of *Saccharomyces cerevisiae* rad6 mutants. *Curr. Genet.* **32**: 309–314.

8. Acknowledgments

This work would not have been possible without the initiation and support by Dr. Nico Dissmeyer, as well as the help and guidance by Prof. Ingo Heilmann. I also want to sincerely thank the referees of my thesis.

I am particularly grateful to Dr. Dissmeyer for constant backup, confidence, and encouragement for trying new approaches. I also thank all members of the Dissmeyer lab, especially Dr. Frederik Faden, Dr. Christin Naumann, Pavel Reichman, and Dr. Augustin Mot, for a pleasant and motivating working environment, for scientific discussions, technical support, and for doing an endless number of favors. This also addresses the members of the neighboring group, especially Dr. Giulia Furlan and Kathrin Kowarschik. To all of them, I also owe thanks for sharing plasmids, proteins, and materials. Tribute is also due to all members of the SEB department for sharing knowledge and materials, and I want to particularly thank Dr. Lennart Eschen-Lippold in this context.

For scientific advice, guidance, and discussions, as well as for shared materials and technical support, I greatly thank Prof. Marco Trujillo, Prof. Bettina Hause, and Dr. Debora Gasperini. For constant scientific support and shared plant lines, I thank Dr. Thomas Potuschak, and I thank Prof. Paul E. Grini for scientific discussions and contributions. I also appreciate the extensive scientific advice provided by Dr. Ivan Acosta.

I am grateful to Emily Flashman and Mark White for initializing combined PCO and ATE1 experiments, for providing recombinant proteins, for helpful discussions, and for a very pleasant and fruitful collaboration. For the provision of biotinylated synthetic peptides and a gratifying collaboration, I thank Prof. Tom Grossmann and Dr. Carolin Müller. For initializing SPOT assay experiments with UBR^{PRT6} and for providing recombinant proteins, I want to thank Prof. Frederica Theodoulou and Dr. Hongtao Zhang. I am grateful to Dr. Katharina Bürstenbinder and Jakob Quegwer for sharing plant lines. I want to express my gratitude to Prof. Angelika Mustroph and Judith Bäuml for providing plasmids and for an enjoyable collaboration. My thanks are due to Prof. Mike Schutkowski and Prof. Claus Wasternack for helpful discussions and advices. For technical and scientific support, as well as for comments on the manuscript, I like to thank Dr. Christian Behn. I would like to acknowledge Prof. Yoshihisa Ikeda and Prof. Markus Grebe for providing plant lines. Petra Majovsky, Domenika Thieme, and Dr. Wolfgang Hoehenwarter are acknowledged for mass spectrometry services and for sharing materials and efforts for SPOT peptide synthesis. For scientific discussions and support, I would also like to thank Dr. Carla Ibañez. I would like to thank Hagen Stellmach and Ramona Schubert for help with microscopy and embeddings. I want to heartily thank my husband, Dr. Till Klecker, for scientific and mental support, and for comments on the manuscript.

I am grateful to the German Research Foundation (Deutsche Forschungsgemeinschaft, DFG) for funding this work via grant DI 1794/3-1 awarded to N. Dissmeyer, and I thank the Leibniz Association, the ScienceCampus Halle – Plant-based Bioeconomy, and the Leibniz Institute of Plant Biochemistry (IPB) at Halle, Germany, for further funding awarded to N. Dissmeyer. I want to thank The Society for Experimental Biology (SEB) for financing my travel to and attendance at the SEB's Annual Meeting 2015 in Prague.

9. Appendix

9.1 Supplemental Figures and Tables

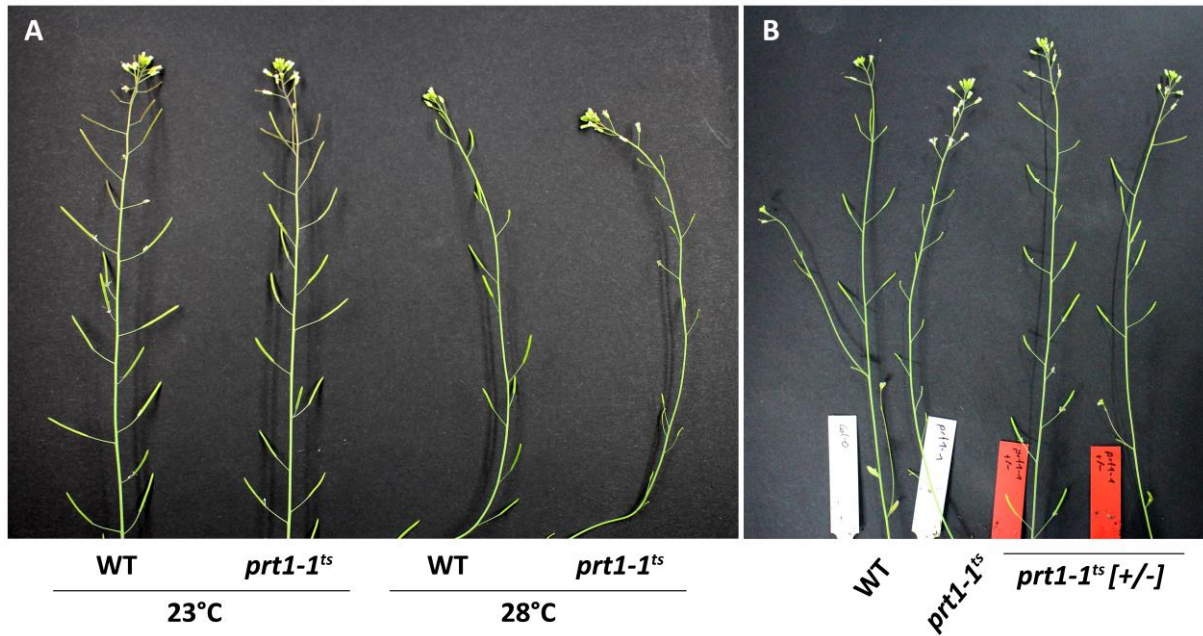


Fig. S1| Silique formation of WT and *prt1-1^{ts}* mutant lines at control and elevated temperature. Stems of the main inflorescences from plants grown at 55-65 percent relative air humidity are shown. **A**, Plants were germinated under short day 22-23°C conditions for ten days and subsequently transferred to a long day light regime and the indicated temperature condition. Pictures were taken at comparable developmental stages for 23°C and 28°C grown plants. **B**, Plants were germinated as in A, and transferred to 28°C long day conditions after 10 days. Stems of WT, *prt1-1^{ts}* mutant, and *prt1-1^{ts}* heterozygous (*prt1-1^{ts} [+/-]*) plants are shown.

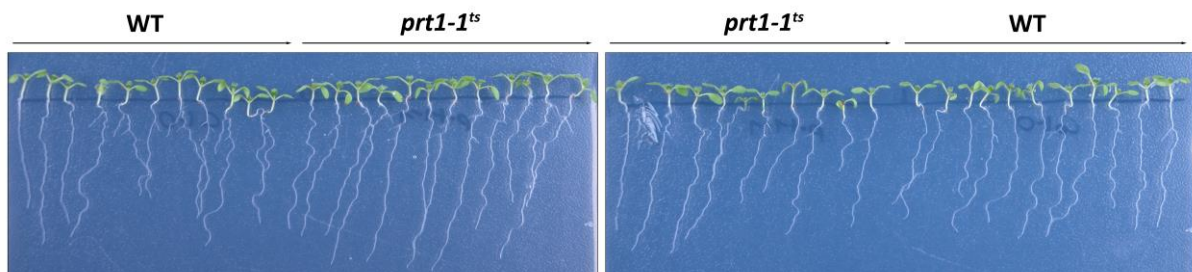


Fig. S2| Seedling morphology of WT and *prt1-1^{ts}* mutant plants at 28°C. Seedlings were surface sterilized, sowed on 1/2 strength MS plates and stratified for 3 days at 4°C. Subsequently, plates were transferred to 28°C long day (16/8) conditions and were grown for 6 days.

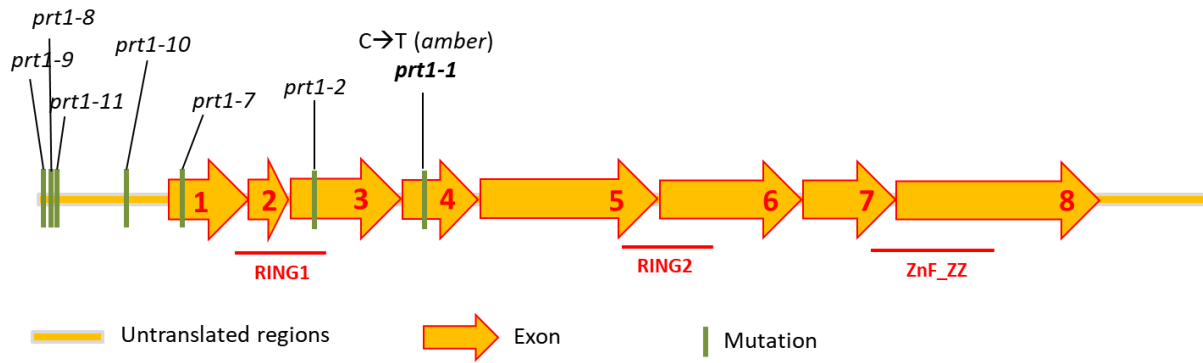


Fig. S3| Exon structure and polymorphisms of the *PRT1* transcript. All indicated mutations refer to T-DNA insertion sites, except for the single base pair substitution in *prt1-1*. **ZnF_ZZ**, ZZ -type Zn finger.

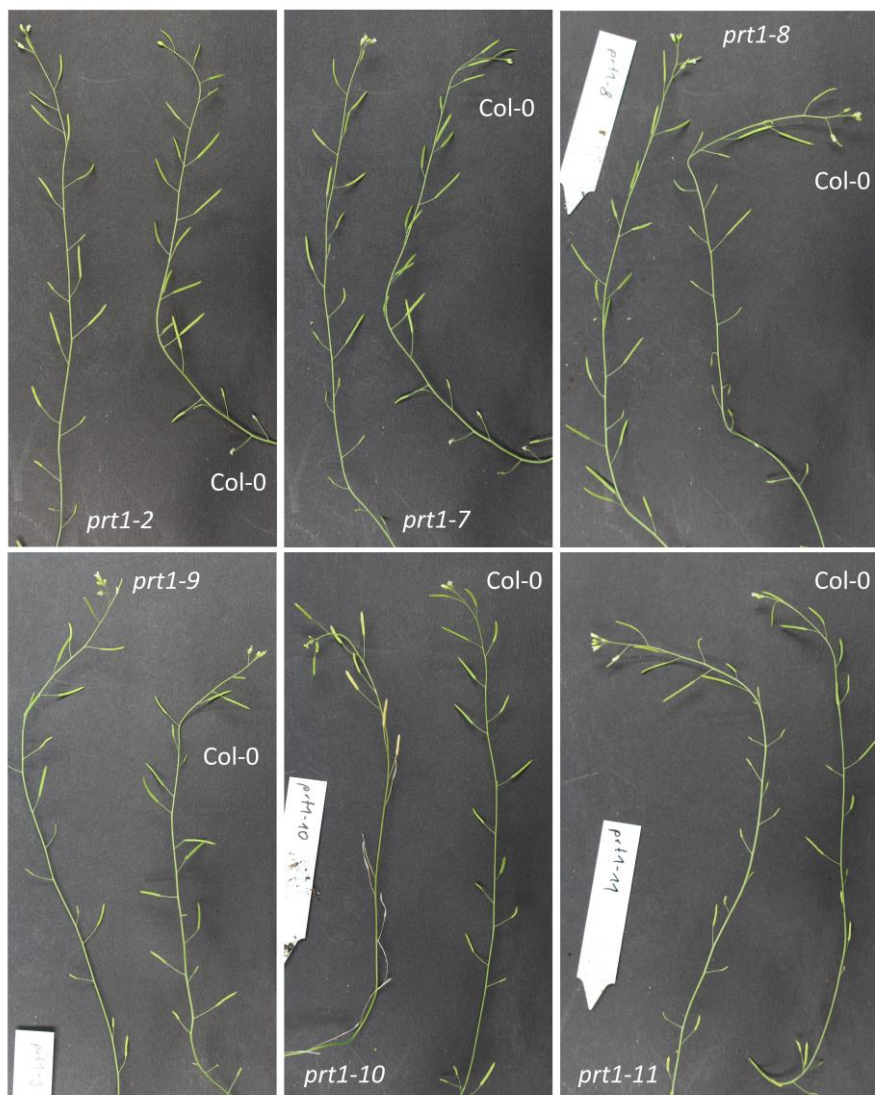


Fig. S4| Silique formation of the main inflorescence stem of *PRT1* T-DNA insertion lines at 28°C and a WT plant of the ecotype Col-0. Plants were germinated under short day conditions at control temperature (22-23°C) and 55-65 percent relative air humidity, and grown for ten days before transfer to a long day light regime and 28°C at the same humidity. Col-0 is the ecotype background of the *prt1-1* line, as well as of *prt1-2*, *prt1-7*, *prt1-9*, and *prt1-11*, whereas *prt1-8* is in the *Ler*, and *prt1-10* is in the *Ws-4* ecotype.

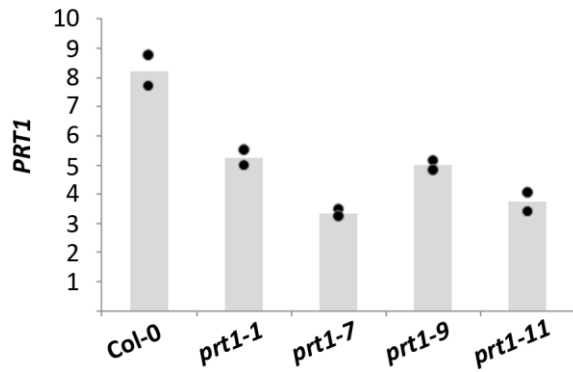


Fig. S5 | Transcript levels of *PRT1* in mutant lines and the WT ecotype Col-0. Transcript levels of *PRT1* in leaf samples of rosette plants were calculated relative to *PP2A*. Bars represent the means of two technical replicates from one experiment. Data points are the values of each technical replicate. Col-0 is the ecotype background of all lines. **RTL**, Relative transcript level ($10^{2^{\Delta\Delta CT}}$).

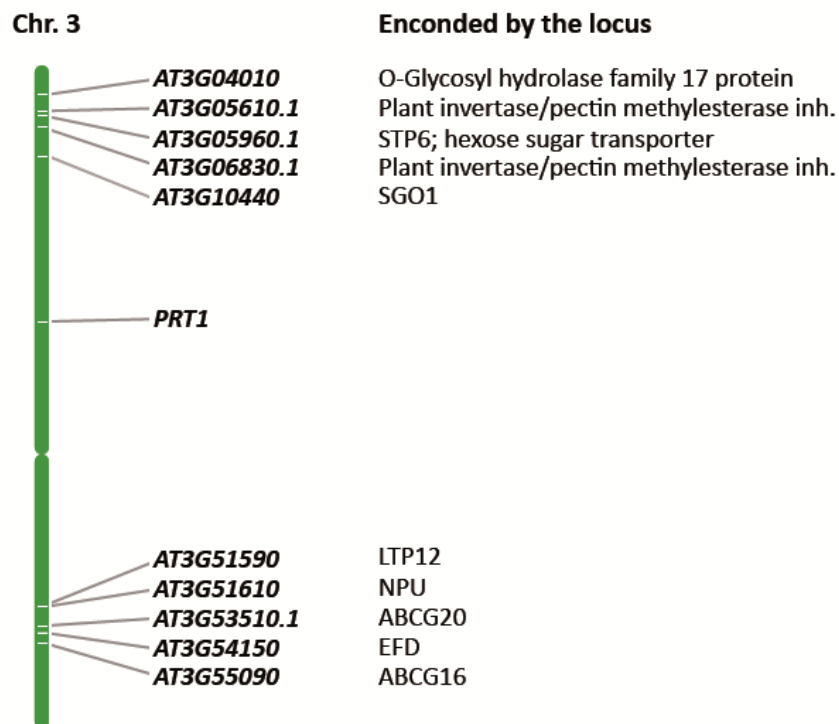


Fig. S6 | Map of chromosome 3 including selected genes in roughly 36 cM distance from the *PRT1* locus. *AT3G04010*, *AT3G05610.1*, and *AT3G06830.1* are expressed predominantly during pollen stages. STP6 may play a role during late pollen maturation (TAIR). SGO1 protects meiotic centromere cohesion and mutants show defects in gametogenesis (Zamariola et al., 2013). The promoter of *LIPID TRANSFER PROTEIN 12* (LTP12) is active exclusively in the tapetum during microspore development (TAIR). *NO PRIMEXINE AND PLASMA MEMBRANE UNDULATION* (NPU) encodes a membrane protein involved in pollen development (TAIR). ABCG20 and ABCG16 are implicated in pollen coat formation (see discussion). EXINE FORMATION DEFECTIVE (EFD) is required for callose wall and primexine formation (TAIR). The depicted loci are highlighted in Tab. S1.

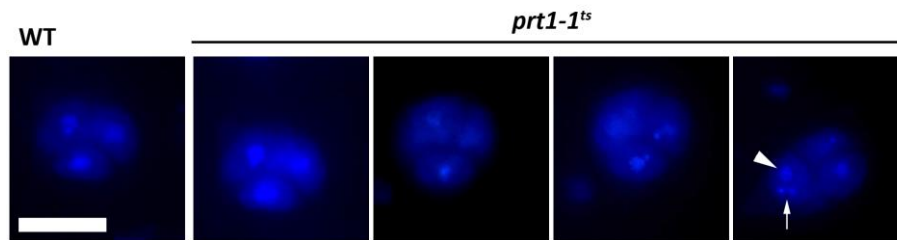


Fig. S7 | Microsporocytes of WT and *prt1-1^{ts}* grown at 28°C following DAPI and Aniline blue staining. The experiment was performed and images were captured by P. Grini. Anthers from flowers of meiotic to post-meiotic anther stages were isolated and squeezed between microscope slides. Preparations were covered with staining solution (PBS containing 2.5 µg/ml DAPI; 0.1 mg/ml Aniline blue; 0.1% (v/v) Tween-20; 5% (v/v) DMSO). The suspension was sealed and incubated for 1 hour in the dark before microscopy of the whole mount preparation. The arrowhead indicates the vegetative nucleus of a (postmeiotic) tricellular microspore of *prt1-1^{ts}*, and the arrow points at the two generative nuclei of the same microspore. All images are the same magnifications. Scale bar: 20 µm.

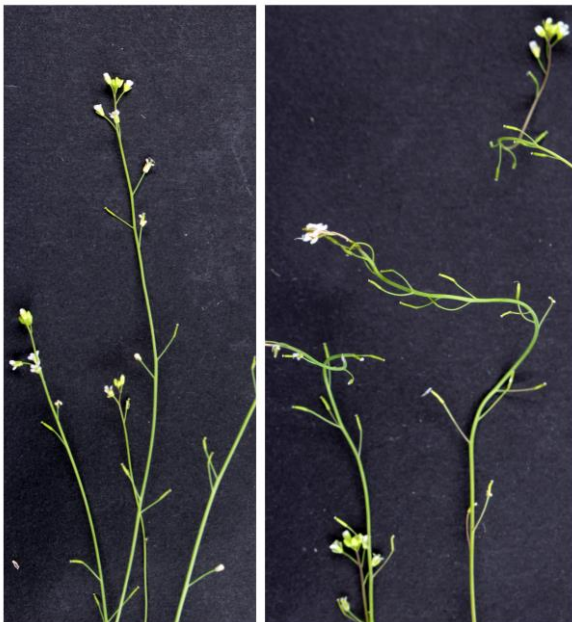


Fig. S8 | Inflorescences of *prt1-1^{ts}* grown at 28°C in a water-saturated ambient air. Plants were grown at 28°C from the 10-day seedling stage and were covered with transparent bags at the time of first flower production in order to create an environment of high air humidity. Silique formation was assessed after additional ten days. No siliques were formed on any of the four replicate plants and representative stems were photographed.

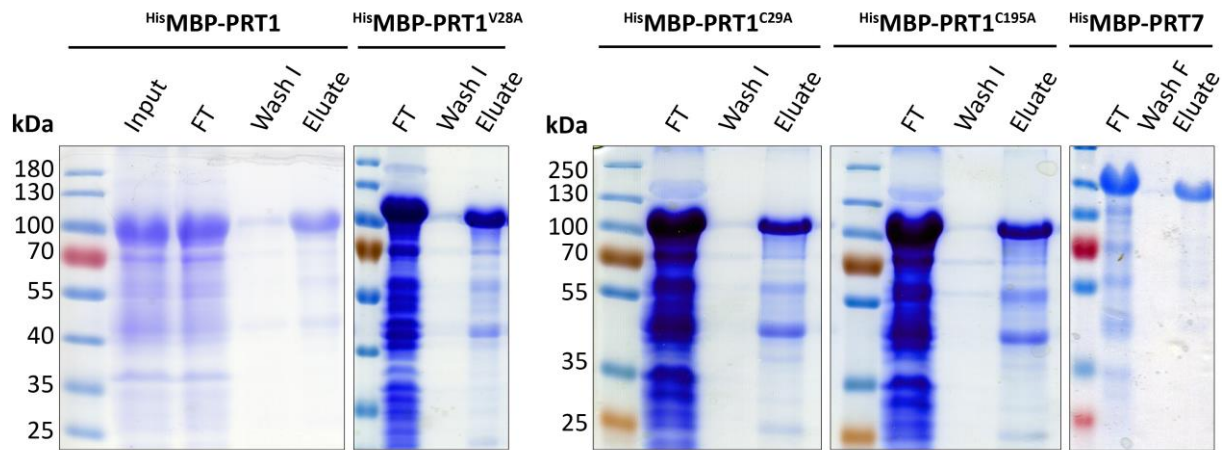


Fig. S9| Purifications of HisMBP-fused recombinant proteins. Ni-NTA based protein purifications were analyzed by CBB staining after 10-percent acrylamide SDS-PAGE. Fractions are bacterial lysate input (^{His}MBP-PRT1^{WT}, left panel) and/or column flow-through (FT), a sample of the first or final wash fractions (Wash I and Wash F, respectively), and the eluates which were directly subjected to *in-vitro* assays. The calculated protein sizes are 92 kDa for ^{His}MBP-PRT1 variants, and 96.5 kDa for ^{His}MBP-PRT7.

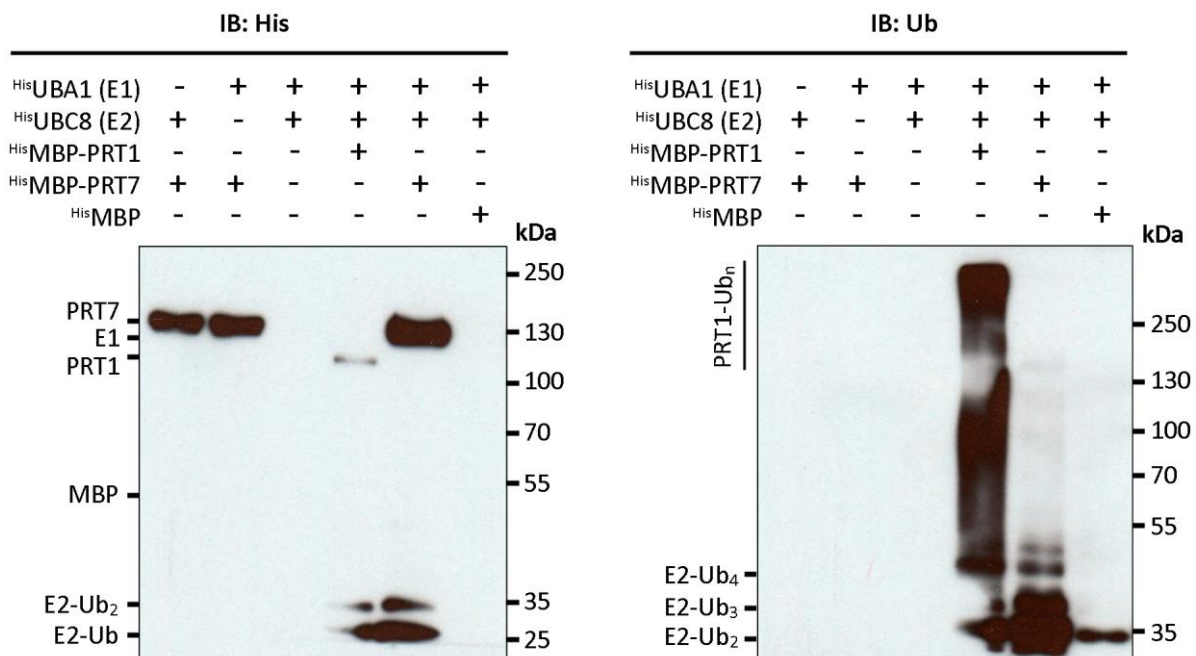


Fig. S10| Autoubiquitination assays of PRT1 and PRT7. Recombinantly expressed and purified ^{His}MBP-fusion proteins of PRT1 or PRT7 were subjected to an autoubiquitination reaction engaging ^{His}UBA1 and ^{His}UBC8 as the E1 and E2 enzymes, respectively. All reactions were performed in the presence of ATP and Ub. The results were analyzed by immunoblotting using antibodies against the His-tag (left panel), or Ub (right panel). Expected protein sizes: ^{His}UBA1: 123 kDa; ^{His}UBC8: 19 kDa; ^{His}E2-Ub: 27,5 kDa; ^{His}E2-Ub₂: 36 kDa; ^{His}MBP: 46 kDa (was not detected); ^{His}MBP-PRT1: 92 kDa; ^{His}MBP-PRT7: 96.5 kDa.

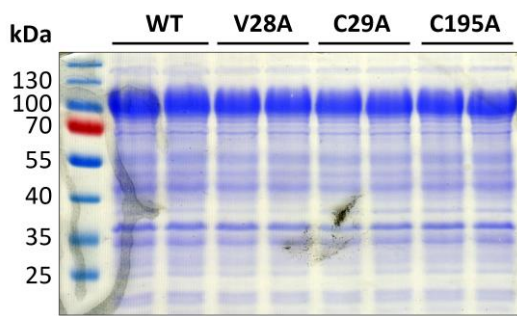


Fig. S11 | Expression of ^{His}MBP-PRT1 protein variants in *E. coli*. Whole-cell bacterial fractions after overnight expression were subjected to 10 percent acrylamide SDS-PAGE and CBB staining. All protein variants have a calculated molecular weight of 92 kDa.

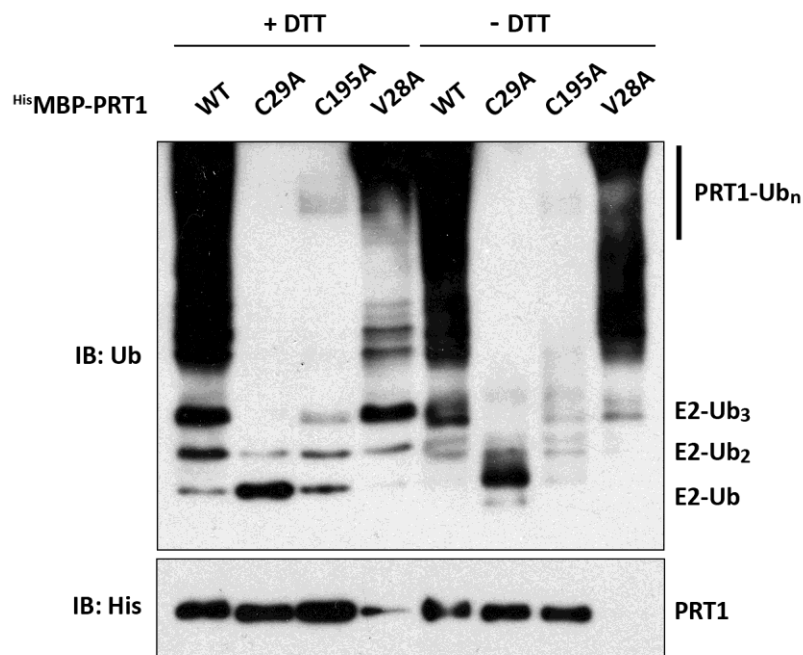


Fig. S12 | Sensitivity of Ub-products from the ^{His}MBP-PRT1 autoubiquitination reaction towards reducing conditions. Autoubiquitination reactions with ^{His}MBP-PRT1 variants were performed in the presence of ^{His}UBA1, ^{His}UBC8, Ub, and ATP, and reactions were subjected to SDS-PAGE following denaturation with a sample buffer that either contained 0.5 M DTT (+ DTT), or lacked reducing agents (- DTT). Immunodetections with antibodies against Ub (IB: Ub), or the His tag (IB: His) are shown. Note that species of intermediate molecular weight produced by ^{His}MBP-PRT1^{V28A} are increased upon non-reducing sample preparation (IB: Ub). However, the protein concentration of this variant was also lower in this experiment than for the other PRT1 variants (IB: His).

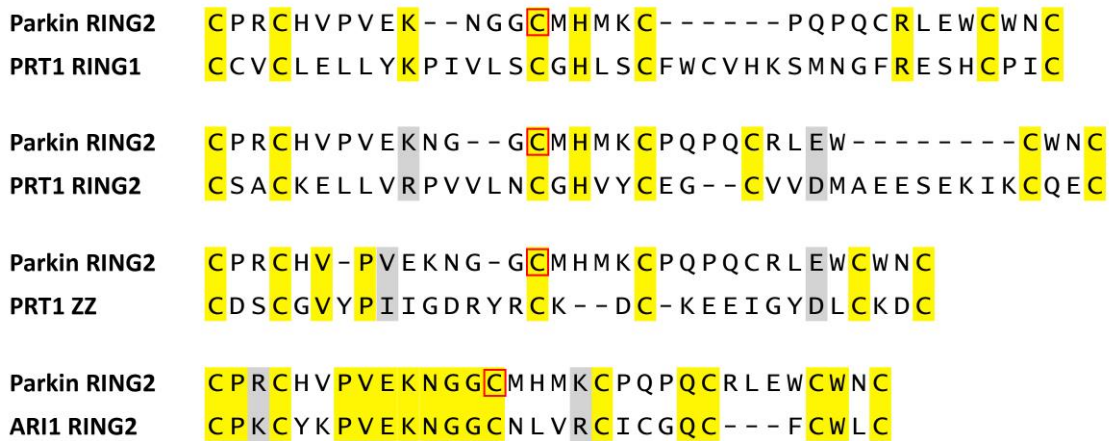


Fig. S13 | Alignments of the PRT1 Zn finger domains with RING2 from the human RBR E3 ligase parkin. Conserved residues are highlighted in yellow. Conservation of an amino acid with similar properties is indicated by grey color. The catalytic Cys-431 of parkin is marked with a red box. An alignment of the RING2 domains from parkin and the plant RBR E3 ligase ARI1 (AT4G34370) is shown for comparison.

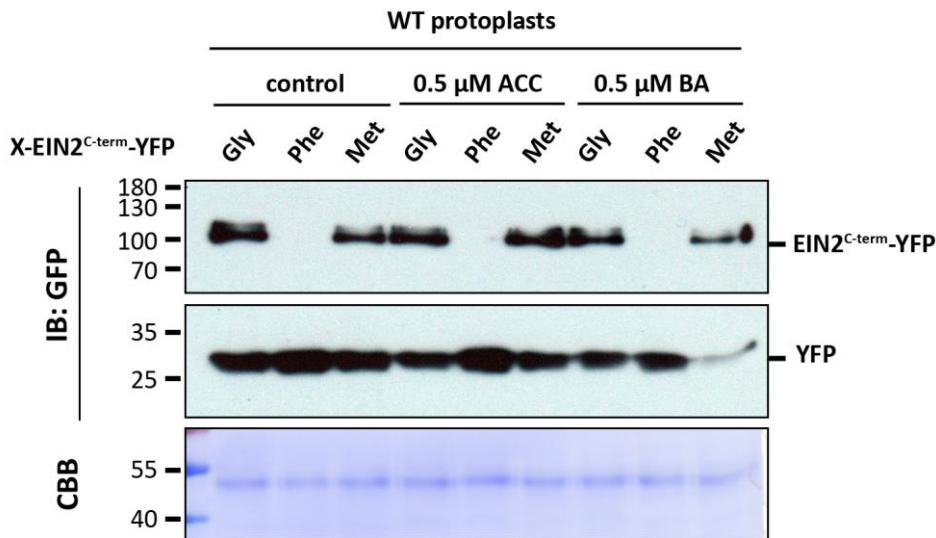


Fig. S14 | Stability and Ub excision efficiency of EIN2^{C-term}-YFP constructs in *Arabidopsis* protoplasts. Variants of X-EIN2^{C-term}-YFP, where X denotes the first amino acid (Phe in the WT sequence) which was replaced by Gly or Met, were co-expressed with YFP alone as a control in *Arabidopsis* protoplasts and analyzed by immunodetections with the anti-GFP antibody. While Gly- and Phe-starting variants were generated via the UFT (i.e., as N-terminal Ub-fusions), Met-EIN2^{C-term}-YFP was expressed as a simple ORF. During overnight expression, protoplasts were incubated in a solution containing either 0.5 μM ACC, 0.5 μM BA, or no additives. EIN2^{C-term}-YFP is expected at 98 kDa, YFP at 27.4 kDa. Protein migration was compared to the PageRuler™ (Thermo Fisher Scientific).

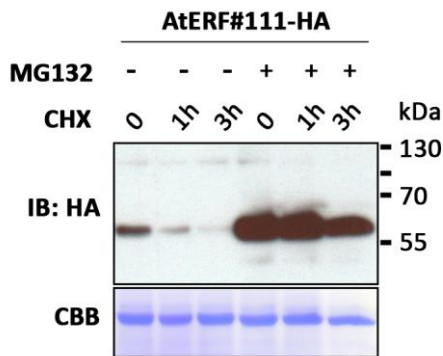


Fig. S15| Proteasome inhibitor treatment in *Arabidopsis* protoplasts. A target of Ub-depending degradation (AtERF#111) was expressed from the *p35S* promoter in *Arabidopsis* protoplasts, and protoplasts were subjected to a medium containing 50 μ M of the proteasome inhibitor (MG132), or a control treatment, in combination with a CHX chase following overnight expression. Protein levels were analyzed using the anti-HA antibody. The expression clone was provided by J. Bäumlner and A. Mustroph. This Western blot was included in a manuscript that was accepted for publication in *The Plant Journal* (Bäumlner et al., 2019).

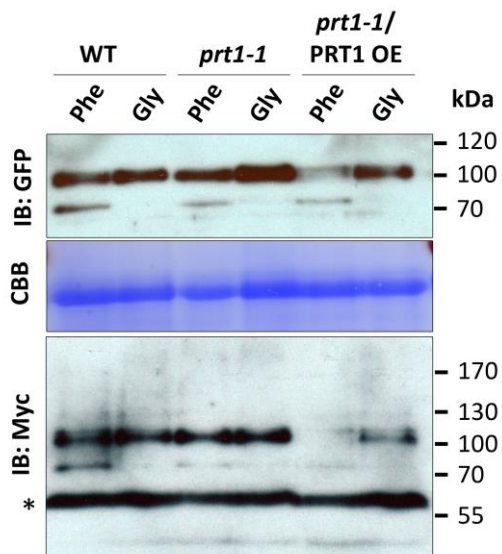


Fig. S16| Detection and stability of EIN2^{C-term}-Myc-YFP^C. *Arabidopsis* protoplasts of WT or *prt1-1^{ts}* mutant background were transfected with Phe- or Gly-exposing variants of EIN2⁶⁴⁷⁻¹²⁹⁴-Myc-YFP^C encoded as Ub-fusion constructs, with YFP^C referring the C-terminal half of YFP. In the last two lanes, 3HA-PRT1 was co-transfected. All constructs were expressed under control of the *UBQ10* promoter. Immunoblots were analyzed using antibodies against GFP or the Myc-tag. X-EIN2⁶⁴⁷⁻¹²⁹⁴-Myc-YFP^C has a calculated molecular weight of 85.8 kDa. The asterisk indicates a cross-reaction of the anti-Myc antibody.

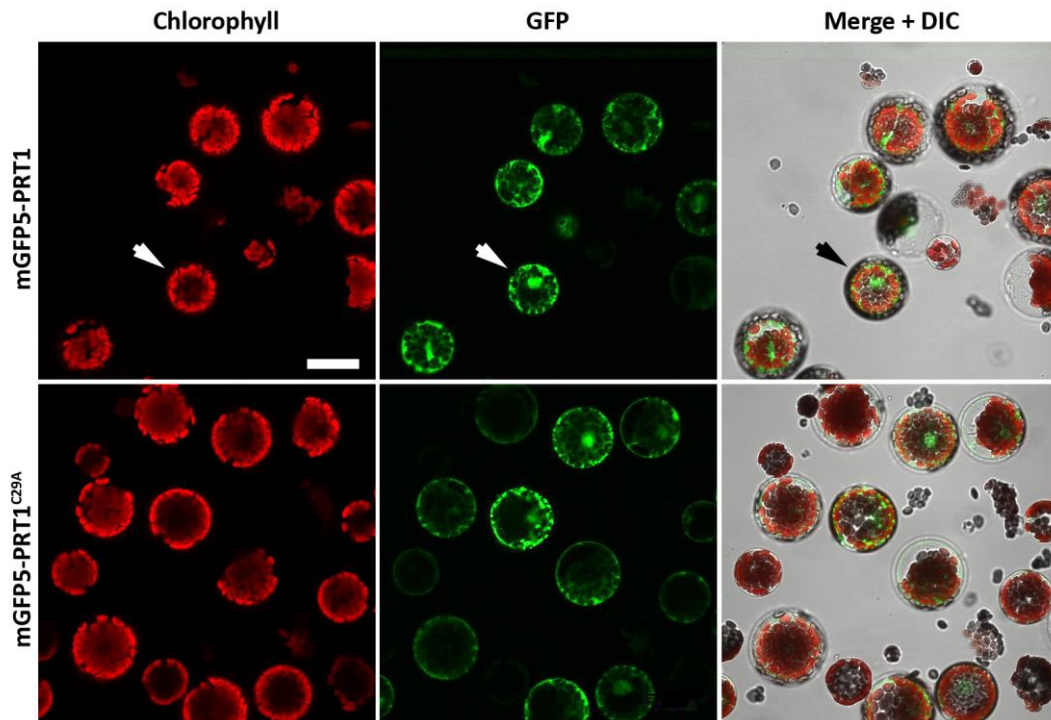


Fig. S17| *Arabidopsis* protoplasts transiently expressing N-terminally GFP-tagged PRT1. Protoplasts of the *prt1-1^{ts}* genotype were transfected with plasmids for expression of *mGFP5-PRT1* or *mGFP5-PRT1^{C29A}*. An overview of several protoplasts from each sample is presented. A magnification of the protoplast indicated with an arrowhead is shown in Fig. 31. Scale bar: 33 μ m.

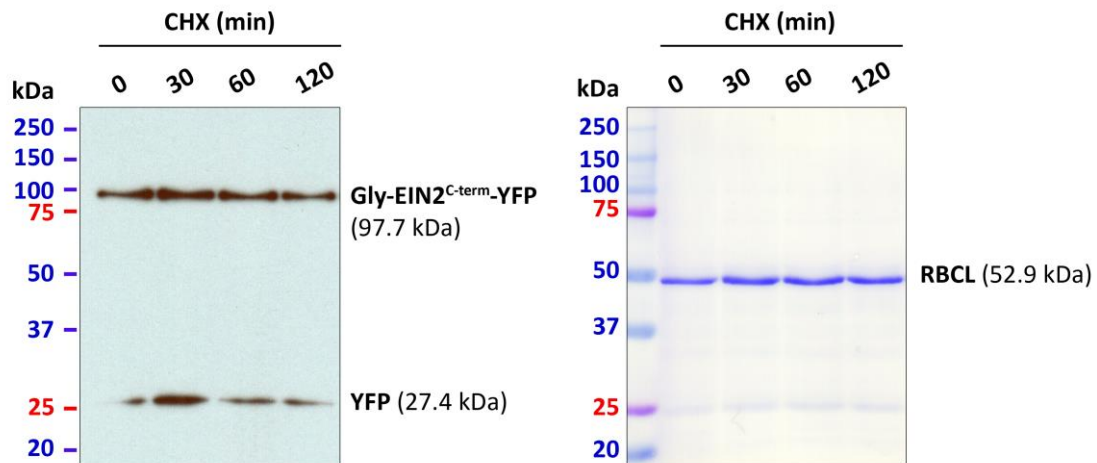


Fig. S18| Apparent molecular weight of $EIN2^{C-term}$ -YFP in comparison to an alternative protein standard. *Gly-EIN2⁶⁴⁷⁻¹²⁹⁴-YFP* was expressed as an N-terminal Ub fusion, and YFP alone was co-expressed in *Arabidopsis* protoplasts of the WT genotype. After overnight expression, protoplasts were subjected to a CHX pulse, and chase samples were analyzed by SDS-PAGE and immunoblot using the anti-GFP antibody (left panel). Protein migration was compared to the Bio-Rad Precision Plus Protein™ Dual Color Standard (Cat. # 161-0394). The corresponding CBB stain of the membrane is shown in the right panel. Notably, while the $EIN2^{C-term}$ -YFP construct and YFP alone migrate as expected from the calculated molecular weight when compared to the protein marker, this standard gives rise to size discrepancies with the large subunit of RuBisCO (RBCL).

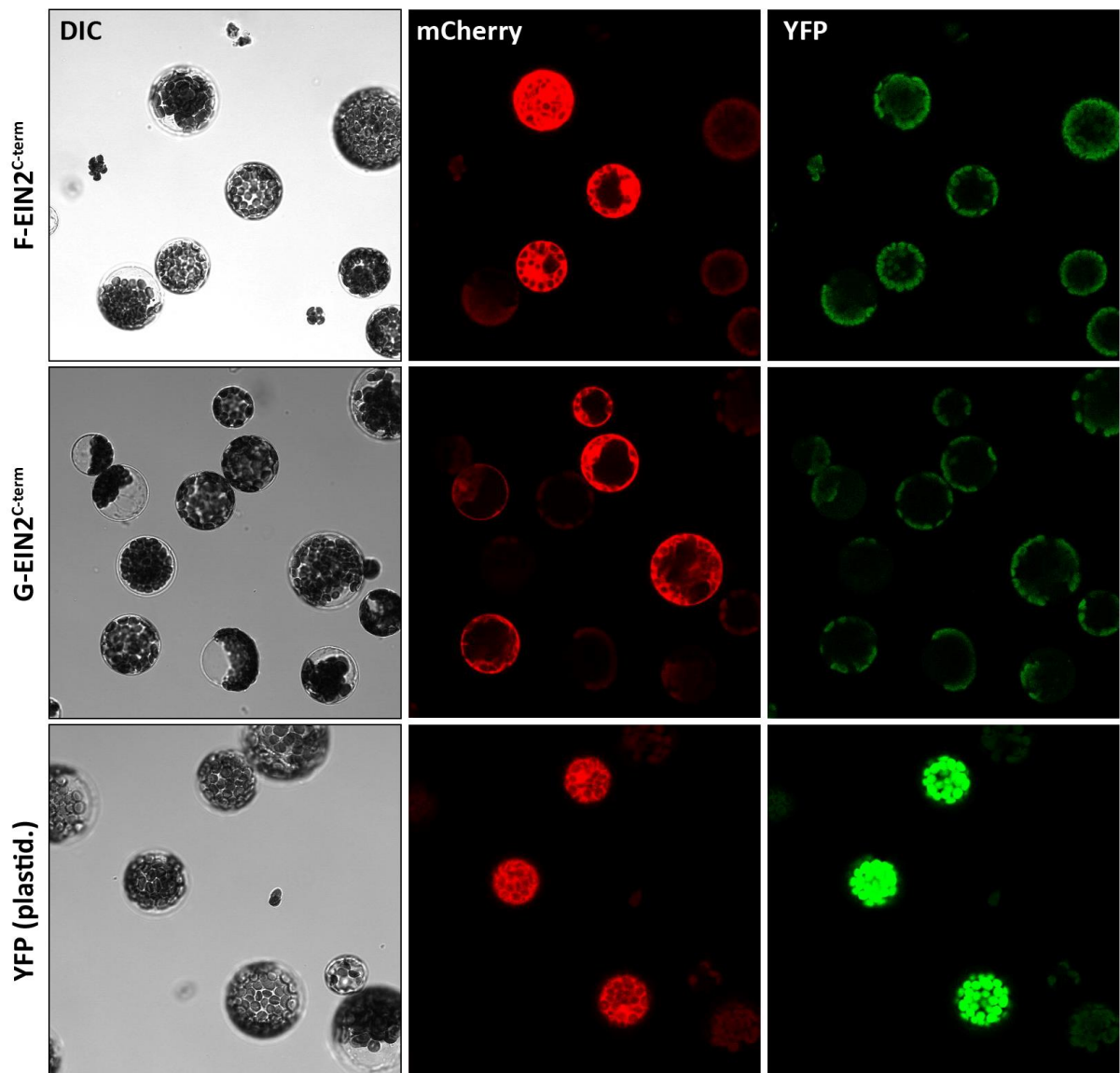


Fig. S19 | BiFC assay to test for a physical interaction of EIN2^{C-term} and PRT1 in *Arabidopsis* protoplasts. Gly- or Phe-initiated variants of EIN2⁶⁴⁷⁻¹²⁹⁴ were expressed as N-terminal 3HA-Ub^{K29,48R} fusions, and C-terminal 3HA-YFP^C-fusions, with YFP^C referring to the C-terminal half of YFP. In both cases, PRT1-YFP^N, containing the N-terminal half of YFP, was co-expressed, as well as an mCherry-expressing vector for cytoplasmic and nuclear localization as a transformation control (kindly provided by G. Furlan and M. Trujillo). As a positive control for YFP signal, full-length YFP for plastidial localization was co-expressed with mCherry.

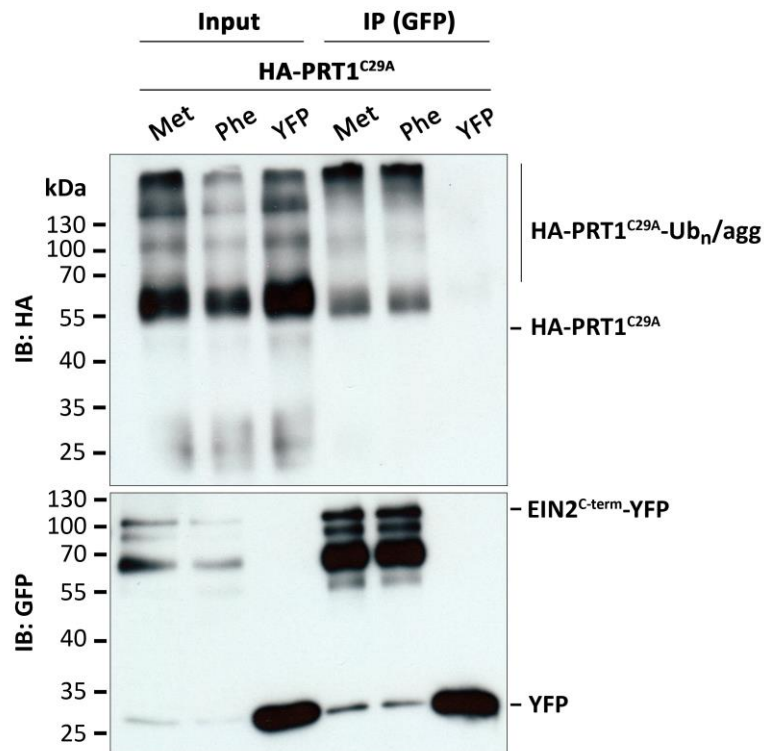


Fig. S20 | Co-IP of EIN2^{C-term}-YFP and 3HA-PRT1^{C29A} from *Arabidopsis* protoplasts. EIN2^{C-term}-YFP was expressed in *Arabidopsis* protoplasts of the *prt1-1^{ts}* mutant genotype either as a Ub-fusion construct to expose N-terminal Phe, or as a regular ORF where Phe-1 was replaced by Met. As a control, YFP alone was transfected instead of EIN2^{C-term}-YFP. All samples were co-transfected with 3HA-PRT1^{C29A}, and all constructs were under control of the *UBQ10* promoter. IP was performed after overnight expression using the GFP-trap, and samples were analyzed by immunoblotting using antibodies against the HA- or GFP-tag. 3HA-PRT1^{C29A} has a molecular weight of 50 kDa, EIN2^{C-term}-YFP is expected at 98 kDa, and YFP at 27 kDa. A smear starting about 8 kDa higher than calculated for native 3HA-PRT1^{C29A} was detected using the anti-HA-tag antibody and might correspond to ubiquitinated, or aggregated species (Ub_n/agg). EIN2^{C-term}-YFP normally migrates with an apparent molecular weight of ~110 kDa in comparison to the PageRuler™ (Thermo Fisher Scientific). Fragmentation was observed within this experiment for EIN2^{C-term}-YFP likely due to extended denaturation treatment prior to PAGE.

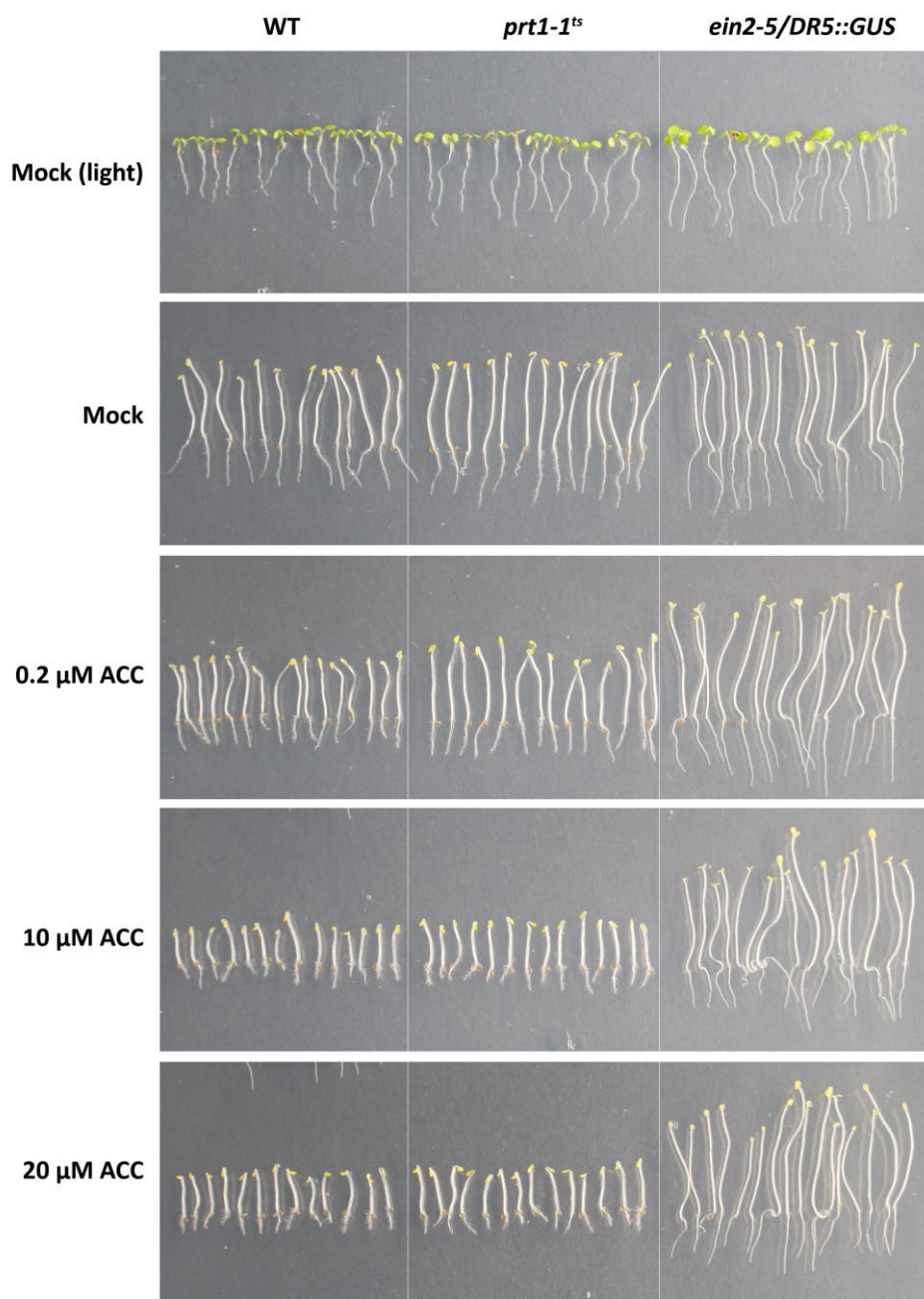


Fig. S21 | Dose response of *prt1-1^{ts}* and *ein2-5* to ACC during germination in the dark. Seedlings of the indicated genotypes were subjected to the triple response assay within an experiment corresponding to the one shown in Fig. 36. Representative seedlings were arranged for photography. For the assay, seeds were aligned on agar medium containing 0.5 percent sucrose and the indicated concentrations of ACC, stratified for 5 days, transferred to growth temperature and light for 6 hours, and subsequently dark incubated for additional 4 days. The light control group shown in the first row was kept under illuminated conditions. Representative seedlings were arranged for photography.

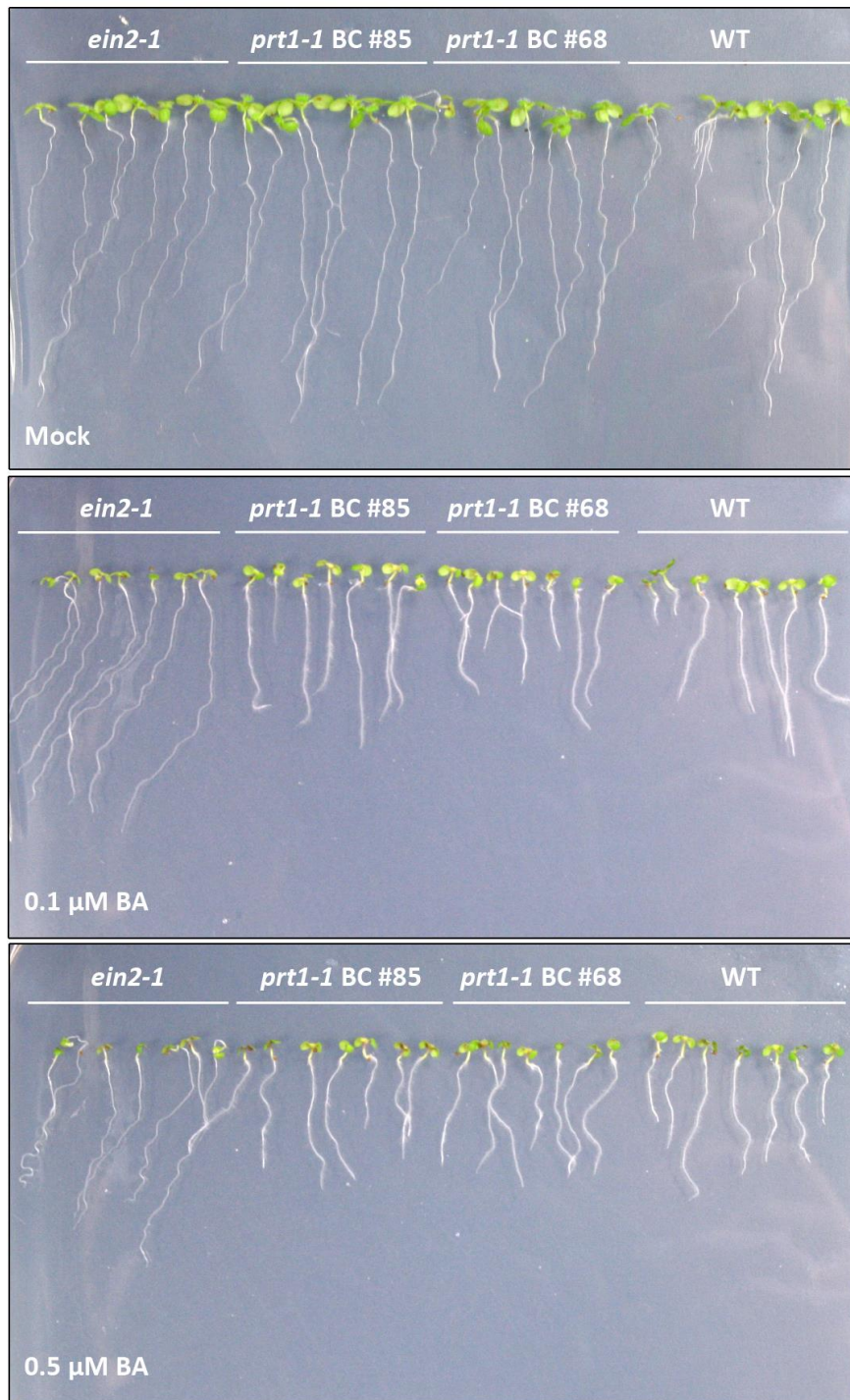


Fig. S22 | Sensitivity of *prt1-1* backcross lines towards cytokinin in the light. Root growth inhibition by BA was assayed for WT seedlings in comparison to two backcross (BC) lines homozygous for the *prt1-1* allele which were both able to produce seeds at 28°C. Seeds were placed on sugar-supplemented agar medium containing 0.1 μM BA (cytokinin), 0.5 μM BA, or a mock solution (0.006% DMSO). After stratification for 5 days, plates were transferred to 22°C conditions where the plants were grown for 8 days under a long-day light regime (16/8).

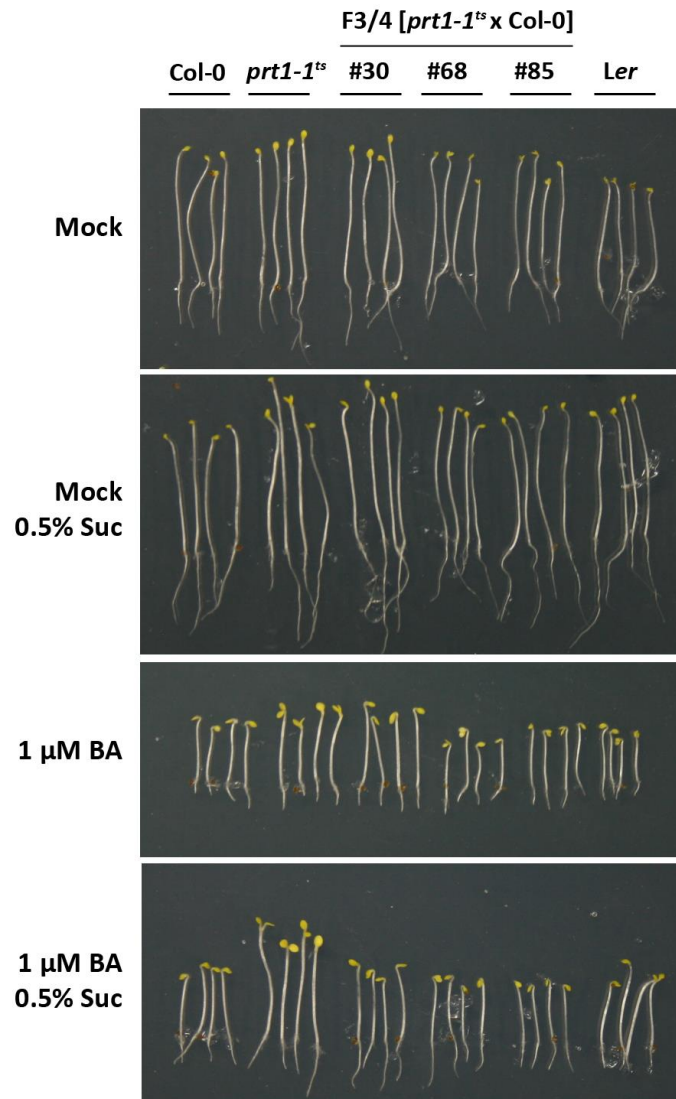


Fig. S23 | Triple response to cytokinin of *prt1-1^{ts}* and backcross lines in the presence and absence of additional sucrose in the medium. Seeds were placed on agar-containing medium supplemented with 1 μ M BA, or a mock solution (0.006% DMSO), in the presence or absence of 0.5% sucrose. Genotypes are WT of the two ecotypes Col-0 and *Ler*, *prt1-1^{ts}*, and three lines derived from a *prt1-1^{ts}* backcross: Line #30 (F3 was used) has the WT PRT1 locus and is sterile at 28°C (compare to Fig. 8), #68 and #85 (both F4) are homozygous for *prt1-1*, but produce WT-like siliques at 28°C. Note: Seeds of Col-0, #68, and #85 were produced in parallel, whereas *Ler*, *prt1-1^{ts}*, and #30 were derived from another, older seed batch. Representative seedlings from the assay were aligned for photography.

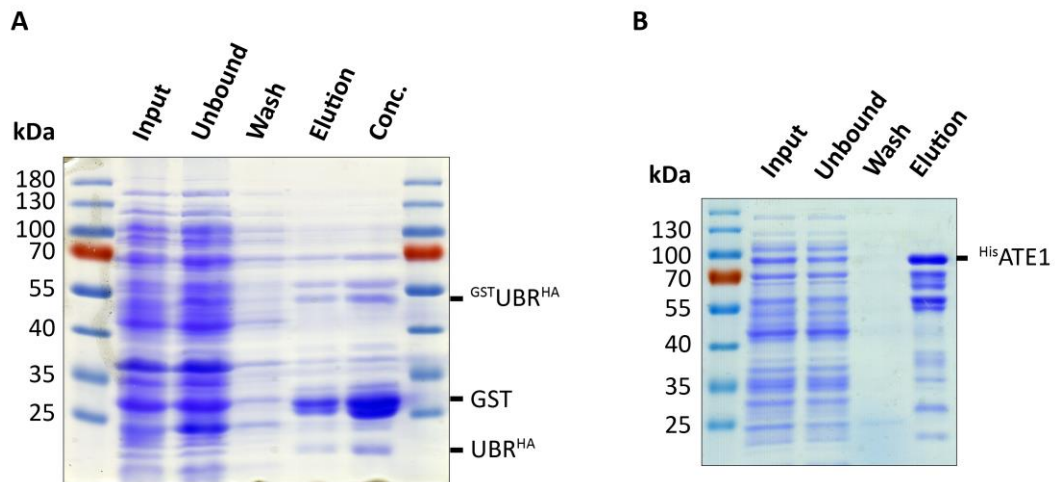


Fig. S24| Purifications of recombinant $\text{GSTUBR}^{\text{HA}}$ and HisATE1 proteins from *E. coli*. Protein purifications were analyzed by CBB staining after SDS-PAGE (10 percent acrylamide). **A**, $\text{GSTUBR}^{\text{HA}}$ (i.e., $\text{GSTPRT6}^{1-193}\text{-HA}$) was purified via glutathione agarose. Input and unbound bacterial lysate fractions are depicted together with a fraction of the first wash step, the elution, and a sample of the protein solution after Amicon® Ultra buffer exchange and concentration. **B**, HisATE1 was purified via Ni-NTA agarose. Fractions as in A, but elution fraction is after buffer exchange and concentration. The identity of ATE1 was confirmed by mass spectrometry performed by P. Majovsky, Domenika Thieme¹, and W. Hoehenwarter (data not shown). This piece of data was published in White et al. (2017).

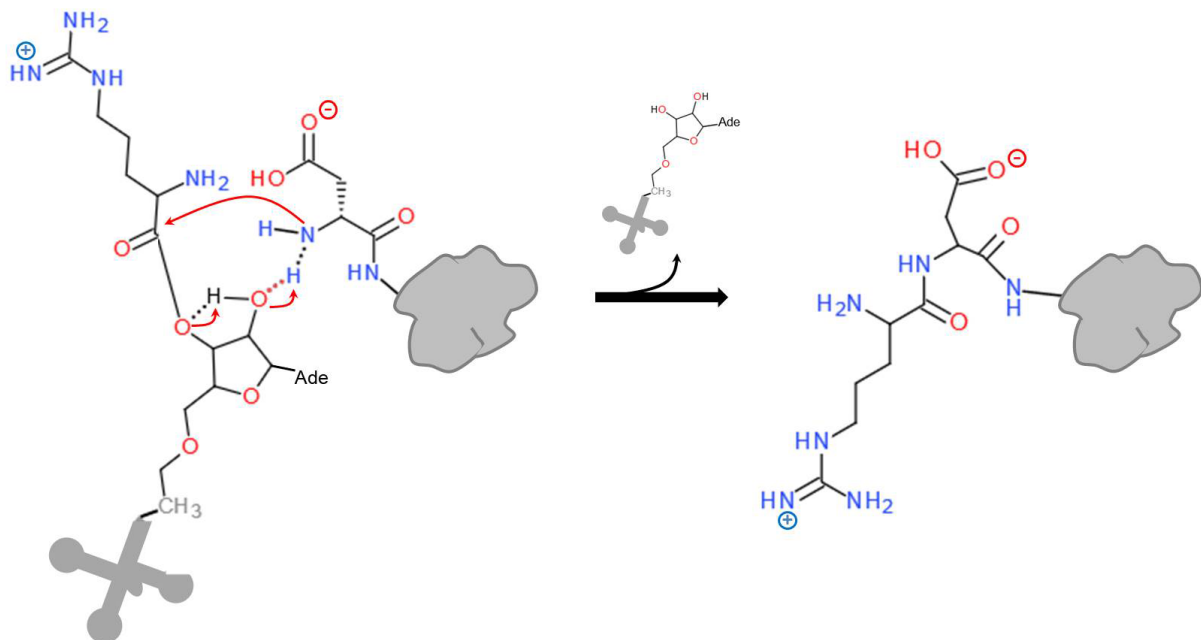


Fig. S25| Proposed mechanism of the ATE reaction modified from (Wang et al., 2014).

¹ Leibniz Institute of Plant Biochemistry, 06120 Halle (Saale), Germany

Tab. S1 | Genes in ~36 cM distance from PRT1 (AT3g24800; Chr. 3; 9,056,300 bp) with annotation to male gametogenesis.
Genes depicted in Fig. S6 are highlighted in red

AGI	Description [selection]
Chr. 3 range from 1 to 2,600,000 bp	
AT3G01130	unknown protein; EXPRESSED IN: male gametophyte, pollen tube.
AT3G01240.1	unknown protein; EXPRESSED DURING: L mature pollen stage, M germinated pollen stage, 4 anthesis, C globular stage, petal differentiation and expansion stage.
AT3G01250.1	unknown protein; EXPRESSED DURING: L mature pollen stage, M germinated pollen stage, 4 anthesis, C globular stage, petal differentiation and expansion stage.
AT3G01620.1	beta-1,4-N-acetylglucosaminyltransferase family protein; EXPRESSED DURING: L mature pollen stage, M germinated pollen stage, [...].
AT3G01620.1	beta-1,4-N-acetylglucosaminyltransferase family protein; EXPRESSED DURING: L mature pollen stage, M germinated pollen stage, [...].
AT3G03080.1	Zinc-binding dehydrogenase family protein; EXPRESSED DURING: L mature pollen stage, M germinated pollen stage, [...].
AT3G03430.1	Calcium-binding EF-hand family protein; EXPRESSED DURING: L mature pollen stage, M germinated pollen stage, 4 anthesis, [...].
AT3G04010	O-Glycosyl hydrolases family 17 protein; EXPRESSED DURING: L mature pollen stage, LP.06 six leaves visible, M germinated pollen stage, [...].
AT3G04200.1	RmlC-like cupins superfamily protein; EXPRESSED DURING: L mature pollen stage, [...].
AT3G04943.1	LCR41, encodes a member of a family of small, secreted, cysteine rich protein with sequence similarity to the PCP (pollen coat protein) gene family.
AT3G04945.1	LCR18; encodes a member of a family of small, secreted, cysteine rich protein with sequence similarity to the PCP (pollen coat protein) gene family.
AT3G05140	ROP binding protein kinases 2 (RBK2); EXPRESSED DURING: L mature pollen stage, M germinated pollen stage, 4 anthesis.
AT3G05150.1	Major facilitator superfamily protein; EXPRESSED DURING: L mature pollen stage, M germinated pollen stage, 4 anthesis, petal differentiation and expansion stage.
AT3G05165	Major facilitator superfamily protein; EXPRESSED IN: male gametophyte, pollen tube; EXPRESSED DURING: L mature pollen stage, M germinated pollen stage.
AT3G05530.1	Encodes RPT5a (Regulatory Particle 5a), one of the six AAA-ATPases of the proteasome regulatory particle. Essential for gametophyte development.
AT3G05610.1	Plant invertase/pectin methylesterase inhibitor superfamily; EXPRESSED DURING: L mature pollen stage, M germinated pollen stage, 4 anthesis, [...].
AT3G05960.1	STP6; encodes a hexose sugar transporter that is expressed in pollen. STP6 may play a role during late pollen maturation or pollen tube germination.
AT3G06830.1	Plant invertase/pectin methylesterase inhibitor superfamily; EXPRESSED DURING: L mature pollen stage, M germinated pollen stage, 4 anthesis, [...].
AT3G07070.1	Protein kinase superfamily protein; EXPRESSED DURING: L mature pollen stage, M germinated pollen stage, 4 anthesis.
AT3G07610.2	IBM1; likely encodes a protein with histone H3mK9 demethylation activity. ibm1 mutants have morphological defects, including faulty pollen development.
AT3G07970.1	QRT2; Required for pollen separation during normal development. In qrt mutants, pollen grains are released in tetrads.

Tab. S1 | Continued.**Chr. 3 range from 18,907,719 – 21,303,020 bp**

AT3G51590	LTP12; promoter is active exclusively in the tapetum during the uninucleate microspore and bicellular pollen stages.
AT3G51610	Encodes a membrane protein NO PRIMEXINE AND PLASMA MEMBRANE UNDULATION (NPU).
AT3G52000	serine carboxypeptidase-like 36 (scpl36); EXPRESSED DURING: L mature pollen stage, M germinated pollen stage.
AT3G52080.1	Encodes a cation:proton exchanger expressed in pollen.
AT3G52560	MMZ4/UEV1D encodes a protein that may play a role in DNA damage responses; only family member whose transcripts are detected in pollen.
AT3G53510.1	ABCG20; belongs to a clade of five Arabidopsis thaliana ABCG half-transporters.
AT3G53670.2	Unknown protein; EXPRESSED IN: sperm cell, male gametophyte, pollen tube; EXPRESSED DURING: L mature pollen stage, M germinated pollen stage.
AT3G53750	ACT3; member of the Actin gene family. Expressed in mature pollen.
AT3G54150	EFD; encodes a DNA methyltransferase required for pollen exine formation and male fertility via the regulation of callose wall and primexine formation.
AT3G54240	Alpha/beta-Hydrolases superfamily protein. EXPRESSED DURING: L mature pollen stage, M germinated pollen stage, 4 anthesis.
AT3G54420	EP3; encodes an EP3 chitinase; the gene is also expressed in mature pollen.
AT3G08445	Novel transcribed region; detected in carpel, receptacle, leaf, light-grown seedling, flower, pollen, aerial.
AT3G55090	ABCG16; belongs to a clade of five Arabidopsis thaliana ABCG half-transporters; required for synthesis of an intact pollen wall.
AT3G55200	SAP130a; encodes a spliceosomal protein; RNAi lines display low pollen viability.
AT3G55220	SAP130b; encodes a spliceosomal protein; RNAi lines display low pollen viability.
AT3G55610	P5CS2; encodes delta 1-pyrroline-5-carboxylate synthetase B. Mutants are defective in pollen development.
AT3G08565	Novel transcribed region; detected in root, carpel, receptacle, dark-grown seedling, light-grown seedling, flower, pollen, aerial.
AT3G57510	Encodes ADPG1, a polygalacturonase protein involved in silique and anther dehiscence.

Important candidates outside of the calculated range on chr. 3

AT3G10440	SGO1; encodes a protein that protects meiotic centromere cohesion.
AT3G11170	FAD7; chloroplastic enzyme responsible for the synthesis of 16:3 and 18:3 fatty acids.
AT3G11980	MS2; MALE STERILITY 2, FATTY ACID REDUCTASE 2
AT3G54650	F BOX-LIKE17, FBL17

Tab. S2 | Transcript levels relative to the transcript of PP2A (RTL = $1000 * 2^{[-ACT]}$) from anthers of WT and *prt1-1^{ts}* grown at 28°C.

RTL values, Exp. #1		YUC2	YUC6	OPR3	DAD1	LOX3	MYB21	MYB24	ARR4	ARR5	ARR6	EIN3	ETR2	ABCG1	SWEET8	HXK1
Col-0	RTL	257.03	71.30	3810.55	12.17	375.01	36378.14	44477.38	2666.60	254.37	505.23	28148.77	132.59	3031.43	209.50	3877.16
		312.08	74.33	4563.05	9.23	410.37	31669.01	36631.17	2818.64	265.17	568.41	29960.71	153.36	2584.71	261.52	3260.29
<i>prt1-1^{ts}</i>	RTL	225.31	17.34	5696.20	42.99	559.61	40574.46	65458.11	1827.66	615.57	1132.88	13177.46	90.87	5388.93	104.57	4062.87
		297.30	16.63	5979.40	48.70	559.61	37336.12	58586.65	2056.23	619.85	1231.14	15670.72	126.74	5502.17	98.24	3464.15
RTL values, Exp. #2		YUC2	YUC6	OPR3	DAD1	LOX3	MYB21	MYB24	ARR4	ARR5	ARR6	EIN3	ETR2	ABCG1	SWEET8	HXK1
Col-0	RTL	349.90	47.86	4740.37	44.97	401.93	29548.23	59507.52	4873.64	491.41	1342.57	40085.26	98.41	2557.97	410.37	3305.80
		433.77	63.59	5445.26	60.16	471.39	32785.82	59096.47	4242.75	549.05	1459.02	43865.05	144.09	2897.88	399.15	2897.88
<i>prt1-1^{ts}</i>	RTL	308.85	33.38	5917.55	113.83	776.47	40364.08	69310.40	3149.23	734.58	1641.48	15189.47	124.57	4453.69	215.39	2897.88
		335.64	20.26	7594.74	97.73	861.55	39533.40	63778.58	3422.38	694.96	1687.63	16392.91	141.12	4707.63	296.27	2877.87

Tab. S3| Oligonucleotide primers used for genotyping.

Name	Sequence (5'-3')	Plant line
prt1-1_fw	CAGAGGAAGAGCAAGAACGAGAAT	<i>prt1-1</i>
prt1-1_rev	CCACCTTCTGTTTATCTACAC	
PRT1_UTR_fw	CCGAAAAGCAAAAGCTATC	<i>prt1-2, prt1-7</i>
PRT1_Exon3_rev	TCTTCTTATGAGCAAGTGGGTACA	<i>prt1-2, prt1-7, prt1-9</i>
SALK_LB	GCGTGGACCGCTTGCTGCAACTCTCTCAGG	<i>prt1-2, prt1-11</i>
SALK_LB2	CCAAACTGGAACAACACTCAACCCTATCTC	<i>prt1-2</i>
RB_SALK	CTCCGCTCATGATCAGATTGTCGTTTCCCG	
SAIL_LB1	GCCTTTTCAGAAATGGATAAATAGCCTTGCTTCC	<i>prt1-7, prt1-9</i>
PRT1_upstream_fw	TCTACCCTTATATGGCATGGCA	<i>prt1-9, prt1-11</i>
PRT1_Exon1_rev	GGCAAACGCAGCAGAGAAAT	
ein2-1_dCAPS_fw	CCAGAGGAAAGAGAGTTGGATGTAAGTACTCTACCGCT	<i>ein2-1</i>
ein2-1_dCAPS_rev	CGCCATCTTTGTTTCAACAATCAGATCC	
ein2-5_wt_fw	GTCCTGCATGACTTCTCG	<i>ein2-5</i>
ein2-5_rev	CCAAGTATGCTTTACCCTG	
ein2-5_del_fw	GTCGTCCTGCTCTGAAGA	
EIN2_Exon7_fw	GTGATTGATCCGGCGTTCTC	<i>p35S::EIN2-eGFP</i>
eGFP_rev	GCTGAACTTGTGGCCGTTTA	

Tab. S4| Primers used for cloning. For gateway cloning, *attB1*- (GGGGACAAGTTTGTACAAAAAAGCAGGCTTA) and *attB2*- (GGGGACCACTTTGTACAAGAAAGCTGGGTA) sites were attached at the primer 5' ends of sense (fw) and antisense (rev) primers, respectively.

Name	Sequence (5'-3')	Construct
proPRT1_fw	GGGGCGCGCCAAATATCAGGATGCAGTTC	pAM-PAT-proPRT1 ^{ΔCTCT} -GW
proPRT1_rev	CCCTCGAGATTGTTATCGCAAGAGAGAGA	
proATL9_fw	GGGGCGCGCCGAGCTTTTAGATCAACGAT	pAM-PAT-proATL9-GW
proATL9_rev	CCCTCGAGTTGAAGATCATCGTATGGAA	
proEIN2_fw	GGGGCGCGCCAGGAGAAAGAGGGGTCGAGA	pAM-PAT-proEIN2-GW
proEIN2_rev	CCCTCGAGCTAAATCTATCTGATAATATAATTACTC	
proUBQ10_fw	GGGGCGCGCCATTTAAATAGTCTAG	pAM-PAT-ProUBQ10 GW
proUBQ10_rev	CCCCTCGAGGCTGTTAATCAGAAAAAC	
PRT1_kozak_ss	GCTTAGCCGCATGGGAATGGCCGAACTATGAAAGATATTA	pEN-kozak-PRT1 by C. Naumann
PRT1new_as	<i>attB2</i> -TTCTGTGCTTGATGACTCATTAGAAG	
Fw_HA	ATGGGATCCTACCCATACGATG	pEN-3HA-PRT1
Rev_HA-PRT1	TCGGCCATAGCACCAGCACCAGCGTAATC	
Fw_attB1-HA	<i>attB1</i> -ATGGGATCCTACCCATACG	
Fw_PRT1	CTGGTGCTATGGCCGAACTATGAAAGATA	
Rev_PRT1+stop	TCATTCTGTGCTTGATGACTCAT	pEN-3HA-PRT1
Rev_attB2-PRT1	<i>attB2</i> -TCATTCTGTGCTTGATGACTC	pEN-GFP-PRT1
attB1_mGFP5_fw	attB1-ATGGTAGATCTGACTAGTAAAGGAG	pEN-GFP-PRT1
mGFP5_rev	GTTTCGGCCATGCTAGCTTTGTATAGTTCATCCATG	
GFP-PRT1_fw	CAAAGCTAGCATGGCCGAACTATGAAAGATATTA	
genPRT1-HAT_fw	CAAGCACAGAAGGAGGAGGAGGAATGGGATCCTACCCATACGAT	pEN-genPRT1-3HA
HA-genPRT1_rev	TCCTCCTCTTCTGTGCTTGATGACTCATTAGA	
attB1-genPRT1_fw	<i>attB1</i> -ACGGCGGTGGATATTGGC	
attB2-HAT_rev	<i>attB2</i> -TCAAGCGTAATCTGGAACGTC	

attB1_Ub	<i>attB1</i> -ATGCAGATCTTCGTCAAGACG	pEN-Ub ^{K29,48R} -EIN2 ^{C-term} -Myc pEN-Ub-EIN2 ^{C-term} -YFP
EIN2-myc_rev	GAACTTCC ACC CAA TGA TCC GTA CGC AG	
EIN2_myc_fw	CG GAT CAT TGG GT GGA AGT TCA TTT CAT TTG GAG AG	
attB2_Myc_noS	<i>attB2</i> -AAGATCCTCCTCAGAAATCAACTT	pEN-Ub ^{K29,48R} -EIN2 ^{C-term} -Myc
Ub_fw	ATGCAGATCTTCGTCAAGACG	
Myc_rev	AAGATCCTCCTCAGAAATCAACTT	
Kozak-HAT_fw	GCCGCCACCATGGGATCCTACCCATACGATG	
HAT_rev_1	CGAAGATCTGCATGATTTACGGGTTGGGGTTTC	
Ubiq_fw	CGTGAAATCATGCAGATCTTCGTCAAGACG	
EIN2-KpnI-Ascl_rev	GGGGCGCGCCAACCAGCACCGGTACCACCCAATGA-TCCGTACGCAG	pEN-3HA-Ub ^{K29,48R} -EIN2 ^{C-term} -KpnI-Ascl
attB1_Kozak	<i>attB1</i> -GCCGCCACCATGGGATCCTACC	
attB2_EIN2	<i>attB2</i> -GGGGCGCGCCAACCAGCACC	
GAGA-HAT_fw	GGGGTACCGGTGCTGGTGCTATGGGATCCTACCCATACGATG	pEN-3HA-Ub ^{K29,48R} -EIN2 ^{C-term} -3HA
HAT_rev2	GTGGCGCGCGTAGCGTAATCTGGAACGTCGTATG	
ss_UBQ_EIN2	TTAGAGGTGGGTTCCGCAGCTTAAGTGGGG	
YFP-EIN2_rev	CTAGGCACCACACCCAATGATCCGTACGCAG	
as_UBQ_EIN2	AGCTGCGGAACCCACCTCTAAGTCTTAAGACAAGATG	pEN-Ub-EIN2 ^{C-term} -YFP
EIN2-YFP_fw	GATCATTGGGTGTGGTGCCTAGGGTGAGC	
attB2-YFP	<i>attB2</i> -TCACTTGTACAGCTCGTCCATGC	pEN-Ub-EIN2 ^{C-term} -YFP pEN-Met-EIN2 ⁶⁴⁷⁻¹²⁹⁴ -YFP pEN-YFP
attB1-Met-EIN2	<i>attB1</i> -ATGCGCAGCTTAAGTGGGGAAGGG	pEN-Met-EIN2 ⁶⁴⁷⁻¹²⁹⁴ -YFP
PRT7_CDS_fw	AGAGAATCTTTATTTTCAGGGTATGGCATCTGGTGTTC	
PRT7-attB2	<i>attB2</i> -TCACTCCATCCTTTTACG	pEN-TEV-PRT7
adapter_TEV	<i>attB1</i> -GAGAATCTTTATTTTCAG	
ATE1_pos2_ss	<i>attB1</i> -ATGTCTTTGAAAAACGATGCGAGT	
ATE1_as	<i>attB2</i> -TCAGTTGATTTACATACCACTTCTCTC	pEN-ATE1 by C. Naumann
attB1-YFP	<i>attB1</i> -ATGGTGGTGCCTAGGGTGAGCAAG	pEN-YFP

Tab. S5| Primers used for site-directed mutagenesis.

Name	Sequence (5'-3')	Site changed	Change
PRT1_V28A_fw	CGATCAATTTCTCTGCTGCGGTGCCTGGAACCTCTTTACAA	PRT1 Val-28 to Ala	GTT → GCG
PRT1_V28A_rev	TTGTAAAGAAGTTCAGGCACGCGCAGCAGAGAAATTGATCG		
PRT1_C29A_fw	CTCTGCTGCGTTGCTCTGGAACCTCTTTACAAGC	PRT1 Cys-29 to Ala	TGC → GCT
PRT1_C29A_rev	GCTTGTAAGAAGTTCAGAGCAACGCAGCAGAG		
PRT1_C195A_fw	GCTCTGTTTCAGCAGCTAAGGAGCTGCTTGTACG	PRT1 Cys-195 to Ala	TGT → GCT
PRT1_C195A_rev	CGTACAAGCAGCTCCTTAGCTGCTGAACAGAGC		
EIN2_F646G_fw	GACTTAGAGGTGGGGTTCGAGCTTAAGTGGGG	EIN2 Phe-646 to Gly	TTC → GGT
EIN2_F646G_rev	CCCCACTTAAGCTGCGACCCACCTCTAAGTC		

Tab. S6| Primers used for semi-quantitative RT-PCR. The sequence of the *attB1*-site is GGGGACAAGTTTGTACAAAAAAGCAGGCTTA.

Name	Sequence (5'-3')	Target
PRT1_UTR_fw	CCGCAAAAGCAAAGCTATC	endog. <i>PRT1</i> (Fig. 19, left panel)
PRT1_FL_rev	TCATTCTGTGCTTGATGACTCA	
Fw_PRT1	CTGGTGCTATGGCCGAAACTATGAAAGATA	endog. <i>PRT1</i> (Fig. 19, right panel)
PRT1_rev	TCATTCTGTGCTTGATGACTCATTAG	endog. <i>PRT1</i> (Fig. 19, right panel); <i>3HA-PRT1</i>
Fw_HA	ATGGGATCCTACCCATACGATG	<i>3HA-PRT1</i>
attB1_mGFP5_fw	<i>attB1</i> -ATGGTAGATCTGACTAGTAAAGGAG	<i>GFP-PRT1</i> ^{C29A}
PRT1_Exon3_rev	TCTTCTTATGAGCAAGTGGGTACA	
TUB2_fw	CAGTACCGTTCCCTCACAGT	<i>TUB2</i>
TUB2_rev	TCACCTTCTTCATCCGAGT	

Tab. S7| Primers used for qPCR. Sense (ss) and antisense (as) primers are listed.

Target	Sequence (5'-3')		Target	Sequence (5'-3')	
<i>PRT1</i> (AT3G24800)	CACGGTCTCCTCAGTTCTG	ss	<i>YUC2</i> (AT4G13260)	AGCCTGCTCAAGTGGTTTCC	ss
	CCCTTCCTCGCCTTCATCTG	as		CCGATCCGTGTACCAAGAA	as
<i>HXK1</i> (AT4G29130)	CGGTGGCTGTTTTGGTTGTT	ss	<i>DAD1</i> (AT2G44810)	AAGCAAGGCACGAAGTTTCT	ss
	CGGAGTCGCACAATCCTCTT	as		CTCCACGCTCTCTGTATCC	as
<i>SWEET8</i> (AT5G40260)	GCACCAGCAAGACTTTCTG	ss	<i>ARR4</i> (AT1G10470)	GGATTCTCTCCGCGTTAT	ss
	GACCGTAAAACACCCACAACA	as		CCTCATCTTCTGCCGTCGAA	as
<i>MYB21</i> (AT3G27810)	GCTCCGGTGGCTGAACTATC	ss	<i>ARR5</i> (AT3G48100)	GAGGTTTTGCGTCCCGAGAT	ss
	GACCACCTGTTCCCACTT	as		CGCTCGATGAACTTCCGATCA	as
<i>MYB24</i> (AT5G40350)	TCAGGAGATGCAGAGGTGAGA	ss	<i>ARR6</i> (AT5G62920)	GTTCACTCGCAGCTCAAACG	ss
	TGGCGAGAGAGTTCCAAACA	as		AGCTGGCGAGAATCATCAGT	as
<i>LOX3</i> (AT1G17420)	TCAACACGCCGCTCTAAACT	ss	<i>ETR2</i> (AT3G23150)	GAACCGGCAGTTACACGTA	ss
	GGATTAACCGCCGATCAAC	as		AGCACCACCACTTCAAACGA	as
<i>YUC6</i> (AT5G25620)	CTACCCGACGAAGCAACAGT	ss	<i>EIN3</i> (AT3G20770)	GCAACAGTTCCAGCTTGTG	ss
	CGCCACATCCAAGGTTTTTC	as		TGCTGCATTCCATCCATCGT	as
<i>OPR3</i> (AT2G06050)	CGTGGTTGGCATGCTCAATA	ss	<i>PP2A</i> (AT1G13320)	GACCGGAGCCAAGTAGGAC	ss
	GCCTTCCAGACTCTGTTTGC	as		AAAATTGGTAACTTTTCCAGCA	as
<i>ABCG1</i> (AT2G39350)	CCGTCATCACCGTACCCAAA	ss			
	GGATTCACCGCCGAAACTA	as			

Tab. S8| EIN2 protein sequences used for conservation analysis. The table presents UniProt Knowledgebase (KB) identifiers of the putative and *bona fide* EIN2 protein sequences used for EIN2 alignments presented in Fig. 27.

UniProtKB ID	Species
Q9S814	<i>Arabidopsis thaliana</i>
R0FM89	<i>Capsella rubella</i>
M4CZ92	<i>Brassica rapa subsp. pekinensis</i>
A0A0R5P8Z6	<i>Carica papaya</i>
A0A0D2QWS0	<i>Gossypium raimondii</i>
A0A067EIG6	<i>Citrus sinensis</i>
B9S0K3	<i>Ricinus communis</i>
A0A2K2A1B2	<i>Populus trichocarpa</i>
K7KFT2	<i>Glycine max</i>
V7D0R4	<i>Phaseolus vulgaris</i>
B3GN62	<i>Medicago truncatula</i>
A0A0A0KH67	<i>Cucumis sativus</i>
D1M862	<i>Prunus persica</i>
F6HR32	<i>Vitis vinifera</i>
Q6Q2C1	<i>Solanum lycopersicum</i>
A0A0J8B2A2	<i>Beta vulgaris subsp. vulgaris</i>
A0A2G5D2B6	<i>Aquilegia coerulea</i>
A0A1D6MFG0	<i>Zea mays</i>
K3ZQ33	<i>Setaria italica</i>
Q0D8I9	<i>Oryza sativa subsp. japonica</i>
A0A2K1J8Y5	<i>Physcomitrella patens subsp. patens</i>

9.2 List of publications

9.2.1 Publications with contributions from this work

Bäumler J, Riber W, **Klecker M**, Müller L, Dissmeyer N, Weig AR, Mustroph A. (2019) AtERF#111/ABR1 is a transcriptional activator involved in the wounding response. The manuscript is accepted for publication in "The Plant Journal".

Goslin K, Eschen-Lippold L, Naumann C, Linster E, Sorel M, **Klecker M**, de Marchi R, Kind A, Wirtz M, Lee J, Dissmeyer N, Graciet E (2019). Differential N-end rule degradation of RIN4/NOI fragments generated by the AvrRpt2 effector protease. *Plant Physiol.* 180(4):2272-2289. doi: 10.1104/pp.19.00251

Mot AC, Prell E, **Klecker M**, Naumann C, Faden F, Westermann B, Dissmeyer N. (2018) Real-time detection of N-end rule-mediated ubiquitination via fluorescently labeled substrate probes. *New Phytol.* 217(2):613-624. doi: 10.1111/nph.14497

White MD, **Klecker M**, Hopkinson RJ, Weits DA, Mueller C, Naumann C, O'Neill R, Wickens J, Yang J, Brooks-Bartlett JC, Garman EF, Grossmann TN, Dissmeyer N, Flashman E. (2017) Plant cysteine oxidases are dioxygenases that directly enable arginyl transferase-catalysed arginylation of N-end rule targets. *Nat Commun.* 23;8:14690. doi: 10.1038/ncomms14690

Dong H, Dumenil J, Lu FH, Na L, Vanhaeren H, Naumann C, **Klecker M**, Prior R, Smith C, McKenzie N, Saalbach G, Chen L, Xia T, Gonzalez N, Seguela M, Inze D, Dissmeyer N, Li Y, Bevan MW. (2017) Ubiquitylation activates a peptidase that promotes cleavage and destabilization of its activating E3 ligases and diverse growth regulatory proteins to limit cell proliferation in *Arabidopsis*. *Genes Dev.* 31(2):197-208. doi: 10.1101/gad.292235.116

Publications in journals without peer-review process:

Klecker M, Dissmeyer N. (2016) Peptide Arrays for Binding Studies of E3 Ubiquitin Ligases. *Methods Mol Biol.* 1450:85-94. doi: 10.1007/978-1-4939-3759-2_7

9.2.2 Further publications

Klecker M, Gasch P, Peisker H, Dörmann P, Schlicke H, Grimm B, Mustroph A (2014). A Shoot-Specific Hypoxic Response of *Arabidopsis* Sheds Light on the Role of the Phosphate-Responsive Transcription Factor PHOSPHATE STARVATION RESPONSE1. *Plant Physiol.* 165(2):774-790. doi: 10.1104/pp.114.237990

Ibañez C, Delker C, Martinez C, Bürstenbinder K, Janitza P, Lippmann R, Ludwig W, Sun H, James GV, **Klecker M**, Grossjohann A, Schneeberger K, Prat S, Quint M (2018). Brassinosteroids Dominate Hormonal Regulation of Plant Thermomorphogenesis via BZR1. *Curr Biol.* 2018 Jan 22;28(2):303-310.e3. doi: 10.1016/j.cub.2017.11.077

9.3 Persönliche Daten

Name: Maria Katharina Klecker, geb. Bongartz
Geburtsdatum und -ort: 03.10.1986 in Marburg, Deutschland
Familienstand: verheiratet mit Till Klecker
Staatsangehörigkeit: Deutschland

Beruflicher Werdegang

02/2018 – heute Wissenschaftliche Mitarbeiterin am Lehrstuhl für Pflanzenphysiologie, Universität Bayreuth

12/2012 – 12/2017 Doktorandin im Fachbereich Pflanzenbiochemie im Labor von Dr. Nico Dissmeyer, Leibniz-Institut für Pflanzenbiochemie, Halle (Saale)
Titel der Dissertation: „The substrate specificity of N-end rule components from *Arabidopsis thaliana*“

07/2012 Externe freie Mitarbeit für die Redaktion „bild der wissenschaft“, Leinfelden

04/2012 – 10/2012 Wissenschaftliche Mitarbeit im Labor von Prof. Dr. Angelika Mustroph, Lehrstuhl für Pflanzenphysiologie, Universität Bayreuth

11/2011 – 01/2012 Nebentätigkeit als wissenschaftliche Mitarbeiterin im Labor von Prof. Dr. Angelika Mustroph, Lehrstuhl für Pflanzenphysiologie, Universität Bayreuth

11/2008 – 04/2009 Arbeit als wissenschaftliche Hilfskraft im Labor von Prof. Dr. Stephan Clemens, Lehrstuhl für Pflanzenphysiologie, Universität Bayreuth

07/2006 – 09/2006 Freie Mitarbeit in der Redaktion der regionalen Tageszeitung „Neue Westfälische“ in Höxter

Bildungsweg

10/2009 – 09/2011 Studium der Biochemie und molekularen Biologie an der Universität Bayreuth
Abschluss: *Master of Science*; Note: ausgezeichnet (1,1)
Masterarbeit am Lehrstuhl für Pflanzenphysiologie
Betreuerin: Prof. Dr. Angelika Mustroph

10/2006 – 09/2009	Studium der Biologie mit molekularer Ausrichtung an der Universität Bayreuth Abschluss: <i>Bachelor of Science</i> ; Note: gut (2,1) Bachelorarbeit am Lehrstuhl für Pflanzenphysiologie Betreuer: Prof. Dr. Stephan Clemens
1997 – 2006	Gymnasium Brede in Brakel, Abschluss: Abitur (Gesamtnote: 1,6)
1994 – 1997	Katholische Grundschule Lühtringen
1993 – 1994	Grundschule Haid-Bad Wurzach

9.4 Erklärung

Ich habe diese Arbeit selbständig und ohne fremde Hilfe verfasst und keine anderen als die angegebenen Quellen und Hilfsmittel benutzt. Wörtlich oder inhaltlich wiedergegebene Textstellen sind als Zitate kenntlich gemacht. Alle Abbildungen wurden von mir eigenständig erstellt und bearbeitet, bei nachempfundenen Abbildungen ist die Quelle genannt.

Ich habe nicht versucht, diese Arbeit in der gegenwärtigen oder einer anderen Fassung bei einer anderen Fakultät einzureichen. Ich habe bisher keinen vergeblichen Promotionsversuch unternommen.

Ich bin nicht vorbestraft und es ist kein Ermittlungsverfahren gegen mich eingeleitet.

Bayreuth, 26.08.2019

(Maria Klecker)